Vol. 186, August 31, 1986
Complete in one issue

ISSN 0003-2670

ANALYTICA CHIMICA ACTA

International journal devoted to all branches of analytical chemistry

ELSEVIER

ANALYTICA CHIMICA ACTA

International journal devoted to all branches of analytical chemistry
Revue internationale consacrée à tous les domaines de la chimie analytique
Internationale Zeitschrift für alle Gebiete der analytischen Chemie

PUBLICATION SCHEDULE FOR 1986

	J	F	M	A	M	J	J	A	S	O	N	D
Analytica Chimica Acta	179	180	181	182	183	184	185	186	187	188 189	190	191

Scope. *Analytica Chimica Acta* publishes original papers, short communications, and reviews dealing with ever aspect of modern chemical analysis both fundamental and applied.

Submission of Papers. Manuscripts (three copies) should be submitted as designated below for rapid and efficien handling:

Papers from the Americas to: Professor Harry L. Pardue, Department of Chemistry, Purdue University, West Lafayette IN 47907, U.S.A.

Papers from all other countries to: Dr. A. M. G. Macdonald, Department of Chemistry, The University, P.O. Box 363 Birmingham B15 2TT, England. Papers dealing particularly with computer techniques to: Professor J. T. Clerc Universität Bern, Pharmazeutisches Institut, Baltzerstrasse 5, CH-3012 Bern, Switzerland.

Submission of an article is understood to imply that the article is original and unpublished and is not being considere for publication elsewhere. Upon acceptance of an article by the journal, authors will be asked to transfer the copyrigh of the article to the publisher. This transfer will ensure the widest possible dissemination of information.

Information for Authors. Papers in English, French and German are published. There are no page charges Manuscripts should conform in layout and style to the papers published in this Volume. Authors should consul Vol. 170 for detailed information. Reprints of this information are available from the Editors or from: Elsevier Editoria Services Ltd., Mayfield House, 256 Banbury Road, Oxford OX2 7DH (Great Britain).

Reprints. Fifty reprints will be supplied free of charge. Additional reprints (minimum 100) can be ordered. An orde form containing price quotations will be sent to the authors together with the proofs of their article.

Advertisements. Advertisement rates are available from the publisher.

Subscriptions. Subscriptions should be sent to: Elsevier Science Publishers B.V., Journals Department, P.O. Bo 211, 1000 AE Amsterdam, The Netherlands. Tel: 5803 911, Telex: 18582.

Publication. *Analytica Chimica Acta* appears in 13 volumes in 1986. The subscription for 1986 (Vols. 179–191) i Dfl. 2730.00 plus Dfl. 312.00 (p.p.h.) (total approx. US $1192.94). All earlier volumes (Vols. 1–178) except Vols. 2 and 28 are available at Dfl. 231.00 (US $90.59), plus Dfl. 15.00 (US $5.88) p.p.h., per volume.

Our p.p.h. (postage, packing and handling) charge includes surface delivery of all issues, except to subscribers in th U.S.A., Canada, Japan, Australia, New Zealand, P.R. China, India, Israel, South Africa, Malaysia, Thailand, Singapore South Korea, Taiwan, Pakistan, Hong Kong, Brazil, Argentina and Mexico, who receive all issues by air deliver (S.A.L. — Surface Air Lifted) at no extra cost. For the rest of the world, airmail and S.A.L. charges are available upor request.

Claims for issues not received should be made within three months of publication of the issues. If not they cannot b honoured free of charge.

For further information, or a free sample copy of this or any other Elsevier Science Publishers journal, readers in th U.S.A. and Canada can contact the following address: Elsevier Science Publishing Co. Inc., Journal Information Center, 52 Vanderbilt Avenue, New York, NY 10017, U.S.A., Tel: (212) 916-1250.

JOURNAL OF CONTAMINANT HYDROLOGY

This international journal publishes scientific articles pertaining to the contamination of groundwater, thus providing a common forum for a diverse group of scientists involved in investigations of groundwater contamination. Emphasis will be on investigations of the physical, chemical, and biological processes that influence the behavior of organic and inorganic contaminants in both the unsaturated (vadose) and the saturated zones. Articles on contamination of surface water will not be included unless they specifically deal with the link between surface and groundwater.

The scope of the journal will cover a wide range of topics, including experimental investigations of contaminant sorption, diffusion, transformation, volatilization, and transport in the unsaturated and saturated zones; characterization of soil and aquifer properties, but only as they influence contaminant behavior; development and testing of mathematical models of contaminant behavior; innovative techniques for restoration of contaminated sites; and development of new tools or techniques for monitoring the extent of soil and groundwater contamination.

Call for papers!

Authors are invited to submit manuscripts (3 copies) to the Editorial Office, Journal of Contaminant Hydrology, P.O. Box 1930, 1000 BX Amsterdam, The Netherlands.
A detailed Guide for Authors is available on request.
Fifty reprints of each article published are supplied free of charge.

There are no page charges.

Subscription Information
1986: Volume 1 (4 issues)
US $ 99.50 / Dfl. 254.00 including postage

A free sample copy is available on request

ELSEVIER SCIENCE PUBLISHERS
P.O. Box 211, 1000 AE Amsterdam, The Netherlands
52 Vanderbilt Avenue, New York, NY 10017, USA

ANALYTICA CHIMICA ACTA
VOL. 186 (1986)


RESPECT COPYRIGHT
BERNE
CONVENTION
100 YEARS
1886-1986
ENCOURAGE CREATIVITY

ANALYTICA CHIMICA ACTA

International journal devoted to all branches of analytical chemistry

ELSEVIER Amsterdam–Oxford–New York–Tokyo

Anal. Chim. Acta, Vol. 186 (1986)

0003-2670/86/$03.5

Analytica Chimica Acta, 186 (1986) 1—9
Elsevier Science Publishers B.V., Amsterdam — Printed in The Netherlands

CARBON-FIBER MICRO-ELECTRODES AS SUBSTRATES FOR MERCURY FILMS

J. GOŁAŚ[a] and JANET OSTERYOUNG*

Department of Chemistry, State University of New York at Buffalo, Buffalo, NY 14214 (U.S.A.)

(Received 22nd January 1986)

SUMMARY

Conditions for mercury deposition at a cylindrical carbon-fiber micro-electrode are examined. A better construction of electrode body with a means of holding the fiber is described. Data obtained in thiocyanate and acetate buffer solutions suggest that in order to obtain linear dependence of the square-wave stripping peak on the mercury concentration, the deposit should not exceed a few monolayers. The surface inhomogeneity of the carbon fibers was confirmed by electron microscopy. The codeposition of lead(II) with mercury(II) is described; the square-wave stripping peak increased linearly with lead concentration up to 4 μM. Cyclic staircase voltammograms showed enhanced response to lead(II) at a mercury-coated fiber.

Several papers have been published recently on different types of carbon fiber micro-electrodes [1—4]. Edmonds [5] has reviewed this and related work in the context of the properties of the carbon fibers. These fibers can be used either directly as carbon electrodes or as a base material for mercury-film electrodes. Although the results obtained with carbon fibers are still sometimes difficult to compare with each other, because of variability of the starting material and different pretreatment procedures, the increasing volume of experimental data followed by some theoretical considerations [6, 7] is bringing these materials closer to general practical applications. Three types of carbon-fiber electrodes have been used: (1) the exposed single fiber with cylindrical geometry, (2) single fibers or arrays of fibers embedded in an insulator and having disk geometry, and (3) brushes, or arrays of exposed fibers. The first two seem to offer the best possibilities as voltammetric electrodes. Behavior of these electrodes depends on dimensions and shapes and also on the properties of the material. Diffusion and convection are difficult to control or reproduce with the brush configuration [2].

Procedures for fabricating carbon-fiber micro-electrodes are improving [1, 8, 9], which should encourage and simplify further investigations. This paper

---

[a]Permanent address: Academy of Mining and Metallurgy, Institute of Material Science, 30-059 Krakow, Poland.

0003-2670/86/$03.50

describes an improvement over a previous procedure for making exposed carbon-fiber micro-electrodes [9]. The main aim is to indicate limitations of exposed fibers for mercury deposition and for in situ deposition of lead. Relations between the properties of the apparent film of lead amalgam and the resulting cyclic voltammograms of lead are also presented.

Although relatively long (ca. 8—10 mm) cylindrical carbon fiber electrodes may seem to be more fragile and less practical than corresponding disk electrodes, they have in fact several advantages. They are much less sensitive to imperfect seal between electrode and insulator than are disk electrodes, because the integrated current density in the vicinity of the seal is a minute fraction of the total. Non-planar diffusion at an exposed fiber depends on the radius of the fiber rather than its length, so that electrode area and properties of cylindrical diffusion can be controlled independently, again in contrast to the disk. In particular, the length of the fiber can be adjusted to give the desired total current for a given type of experiment. Finally, the exposed fiber electrodes make it possible to investigate the properties of the surface of the cylinder as an electrode, which might be different from those of the cross-section.

EXPERIMENTAL

Instrumentation and reagents

An electrolytic cell (IBM) was used along with a three-electrode system in which carbon fiber, platinum and saturated calomel electrodes were used as working, counter and reference electrodes, respectively. Two voltammetric techniques were used: square-wave voltammetry (s.w.v.) and staircase voltammetry (s.c.v.). All voltammetric measurements were made with a computer-controlled potentiostat based on a Digital Equipment Corp. PDP-8/e minicomputer [10]. Some additional coulometric measurements were done with an EG&G PARC Model 173 potentiostat and with Model 179 digital coulometer.

Reagents were of analytical grade, and distilled water passed through a Millipore Milli-Q purification system was used for preparation of the solutions. The following solutions were used as supporting electrolytes: 0.1 M potassium thiocyanate (pH 2.5; acidified with nitric acid), acetate buffer (1.25 M potassium acetate/1.7 M acetic acid, pH 4.6) and 0.1 M potassium nitrate. The proper amounts of 0.05 M mercury(II) nitrate and 0.01 M lead nitrate were added to the chosen supporting electrolyte from Eppendorf pipets.

Solutions were purged with argon for about 7 min before each experiment; after purging, the argon flow was directed over the solution. All experiments were run in quiet solutions without stirring. From previous experience, stirring during deposition causes the fiber to move, which worsens reproducibility of stripping measurements.

Construction and preliminary tests of electrodes

The working electrodes were made from carbon fibers of 8-μm diameter (AESAR, Johnson Matthey). The procedure for making the electrode involves sealing the fiber into a matrix of tygon and heat-shrinkable tubing [7]. Gentle heating of the tip of the electrode with a soldering iron melts the inner tygon tube and shrinks the outer tube about the fiber and molten tygon. The main change from the preliminary procedure [9] is the teflon body and glass support, as shown in Fig. 1. This body allows very quick replacement of the fiber in the case of damage and improves protection against breakage by providing an additional support which holds the tip of the fiber.

It should be noted that fibers, even from the same manufacturer, differ in the smoothness of their surface. There are also different shapes of cross-sections (e.g., AESAR fibers are circular whereas Celion GY-70 is bilobal). An electron micrograph of AESAR carbon fibers is presented in Fig. 2. The surface is randomly covered with small dimples which did not disappear after pretreatment. The standard pretreatment procedure included cleaning in a solution of Alconox detergent in an ultrasonic bath, rinsing with water, cleaning again in nitric acid/water (1 + 4) solution in the ultrasonic bath, rinsing with water, and finally drying. The last step was a moderate electro-oxidation at +0.3 V for 1 min.

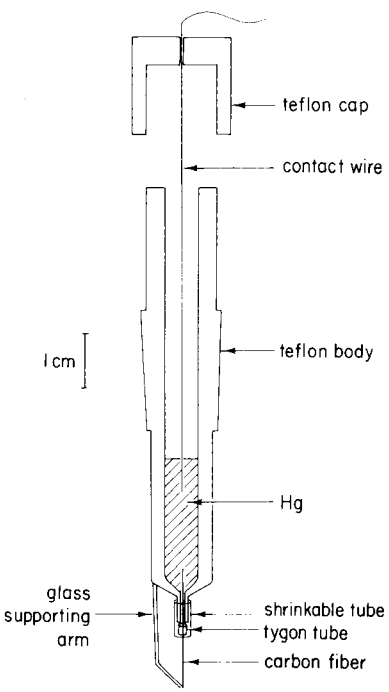

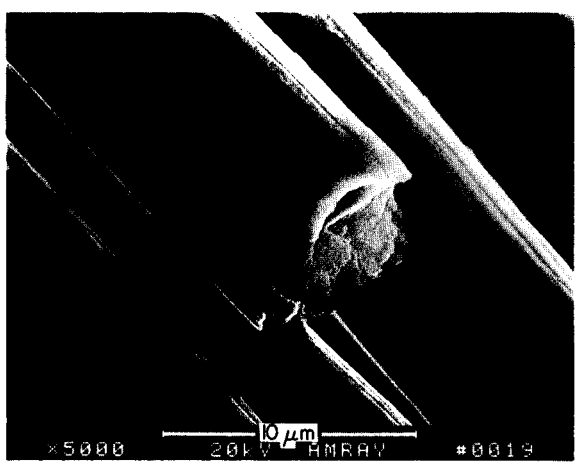

Fig. 1. Schematic drawing of the cylindrical carbon-fiber micro-electrode.

Fig. 2. Electron microscope picture of a bunch of the AESAR carbon fibers.

In principle, after cleaning, one could select the proper part of the best-looking fiber by microscopic examination, but this procedure would be too time-consuming to yield practical electrodes. Furthermore, there is considerable uncertainty regarding what properties might be desirable to optimize performance in voltammetric experiments. A series of experiments was done on different fibers to examine the quantitative variability from fiber to fiber. Four carbon fibers were used for deposition of mercury and the resulting square-wave anodic stripping voltammograms were compared for four deposition times (10, 20, 40, 100 s), two deposition potentials (—0.6, —1.0 V) and several concentrations of mercury(II) in the range 1—80 μM in 0.1 M thiocyanate. Although the results for each particular fiber were reproducible for deposition for a given time and concentration of Hg(II) (usually three repeated scans gave identical curves) different results were obtained for different fibers. For illustration, representative data are presented in Table 1. These results suggest that the heterogeneous appearance of the surfaces shown in Fig. 2 actually relates to differences in surface properties which affect electrochemical behavior.

Based on this preliminary series of experiments, one of those electrodes was chosen for further investigations. This was the carbon-fiber microelectrode of length 9.06 mm (by microscopic measurement) and area of 0.228 mm^2. This electrode was then successfully used for several months without any damage. All of the following data were obtained for this one electrode.

RESULTS AND DISCUSSION

Mercury has been deposited on carbon fiber surfaces but it has not been established how much mercury can be deposited quantitatively. Following previous results [9], the conditions for mercury deposition were investigated more carefully in three different electrolytes, potassium thiocyanate, acetate buffer and potassium nitrate. The results in the first two supporting electrolytes are discussed together because they are qualitatively the same, whereas the nature of the mercury deposition in potassium nitrate is more complex.

TABLE 1

Peak current density for square-wave anodic-stripping voltammograms[a]

E_d (V)	i_p/A (μA mm^{-2}) for areas (mm^2) of			
	0.265	0.279	0.164	0.228[b]
—0.6	33.32	21.33	46.16	44.96
—1.0	132.23	75.98	153.35	116.01

[a]Solution, 80 μm Hg(II) in 0.1 M KSCN; deposition time, 40 s; square-wave parameters, ΔE_s = 4 mV, E_{sw} = 25 mV, f = 100 Hz. The four different electrodes are identified by their areas. [b]This electrode was taken for further investigations.

A series of depositions was run at E_d = —1.0 V for deposition times (t_d) of 10, 20, 40 or 100 s in the 1—80 μM range of Hg(II) concentration. The observed dependences of anodic-stripping peak current density on mercury concentration in 0.1 M thiocyanate and in acetate buffer are shown in Figs. 3 and 4, respectively.

At sufficiently low concentrations of Hg(II) or short deposition times, the stripping peak current depends linearly on the concentration of Hg(II), but at higher concentrations or longer times, the dependence is less strong. This is more obvious for 0.1 M thiocyanate, in which the stripping peaks were usually approximately three times larger than for acetate buffer under the same conditions. As a result, in 0.1 M thiocyanate, the curves (Fig. 3B) become non-linear at concentrations smaller than those of Fig.4B.

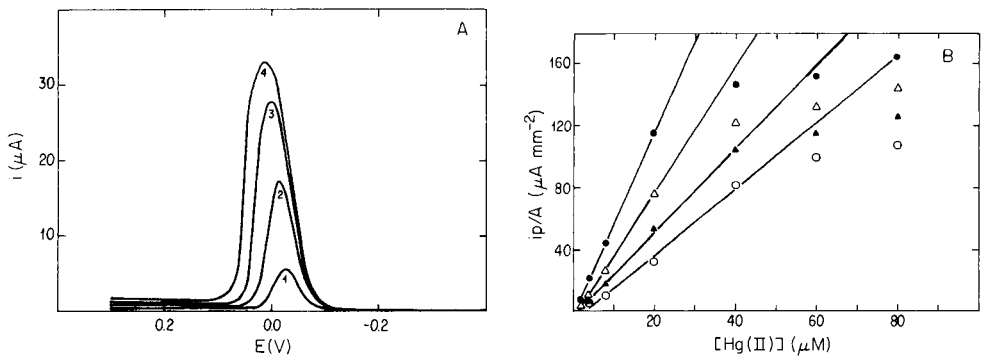

Fig. 3. (A) Anodic-stripping square-wave voltammograms of mercury in 0.1 M KSCN at pH 2.5. Square-wave parameters: E_{sw} = 24 mV, ΔE_s = 4 mV, f = 100 Hz. E_d = —1.0 V, t_d = 40 s. [Hg(II)]: (1) 8; (2) 20; (3) 40; (4) 80 μM. (B) Dependence of the peak current density on Hg(II) concentration for varied deposition times: (○) 10; (▲) 20; (△) 40; (●) 100 s. Other conditions as in (A).

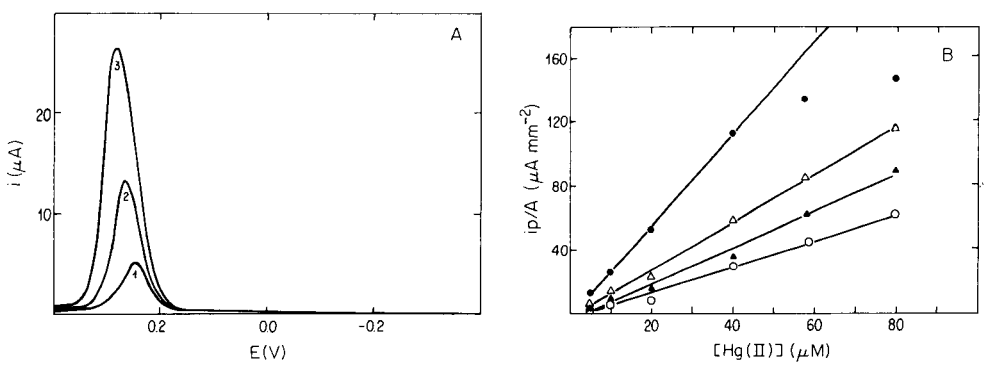

Fig. 4. (A) Anodic-stripping square wave voltammograms of mercury in 1.25/1.7 M acetate buffer pH 4.6. [Hg(II)]: (1) 20; (2) 40; (3) 80 μM. Other conditions as in Fig. 3A. (B) Dependence of the peak current density on mercury concentration for varied deposition times: (○) 10, (▲) 20, (△) 40, (●) 100 s.

In order to estimate the amount of deposited mercury at which this effect starts, the charge consumed during each deposition was measured. There was no sharp boundary between the linear and non-linear ranges. The boundary region was defined as that in the range of conditions between 40 μM Hg(II) with 10-s deposition and 20 μM Hg(II) with 100-s deposition. The mean values for five replicate measurements were Q = 4.37 μC (S_x = 0.34 μC) for 20 μM Hg(II), and Q = 0.99 μC (S_x = 0.02 μC) for 40 μM Hg(II). It is well known that deposits of mercury on carbon substrates are not coherent films but rather exist as collections of puddles or droplets. Such deposits were observed on carbon-fiber electrodes. However, bearing this in mind, it is still useful to calculate the effective film thicknesses corresponding to these charges. Using l = 9.06 mm and r = 4 μm, the critical range of thickness of the deposit corresponding to these charges is 3—14 Å. With a value of 1.44 Å as the atomic radius of Hg, these numbers suggest that the stripping peak current depends linearly on coverage only up to a few monolayers.

At higher coverages, reproducibility of the anodic stripping peak worsens, the peak becomes wider and flatter, and even the peak area (which should be proportional to total charge) does not depend linearly on deposition time. The latter point is shown in Fig. 5. Examples were taken of two different concentrations of Hg(II) and two different deposition times. As can be seen, for values of $i_p w_{1/2}/A$ (peak current density times width at half height) in the range 5—10 μA V mm^{-2}, the dependence on deposition time decreases. This range of values again corresponds to an average thickness of several angstroms, agreeing with the results of Figs. 3 and 4. The same trends, characterized by the same critical numbers, occurred in acetate buffer. Therefore, this effect is due to the surface of the carbon fiber itself, and is not due only to the special characteristics of thiocyanate.

Similar experiments were done in 0.1 M potassium nitrate. Some typical anodic-stripping voltammograms are shown in Fig. 6. Peak current is linear

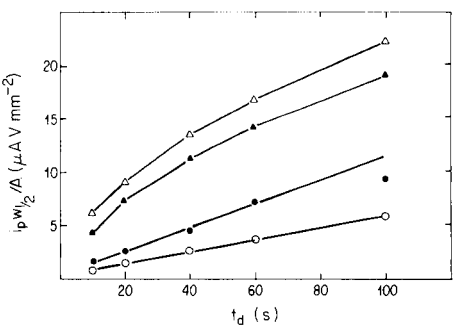

Fig. 5. Dependence of peak area on deposition time in the anodic-stripping square-wave voltammetry of mercury in 0.1 M KSCN. Curves: (○) 20 μM Hg(II), E_d = —0.6 V; (●) 20 μM Hg(II), E_d = —1.0 V; (▲) 80 μM Hg(II), E_d = —0.6 V; (△) 80 μM Hg(II), E_d = —1.0 V. Peak area approximated as height times width at half height, $w_{1/2}$.

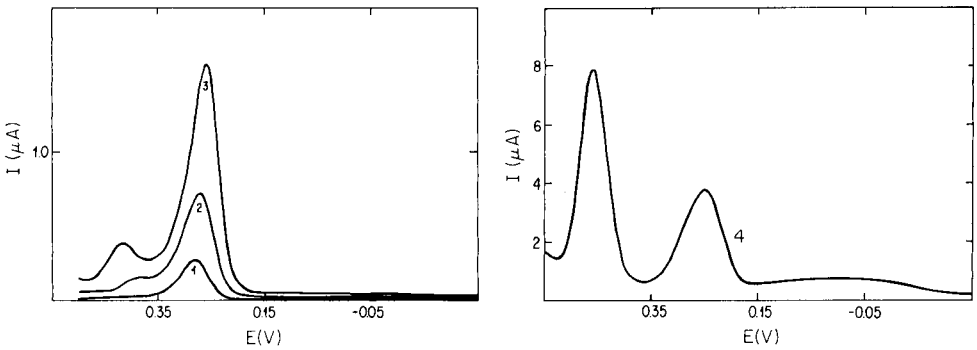

Fig. 6. Anodic-stripping square-wave voltammograms of mercury in 0.1 M KNO_3. [Hg(II)]: (1) 8; (2) 20; (3) 40; (4) 160 μM. Other conditions as Fig. 3A.

with concentration of Hg(II) up to the concentrations at which the second peak appears. But the currents are 10—20-fold smaller than those obtained in thiocyanate or acetate solution. The results are qualitatively the same with added nitric acid (pH $\geqslant$ 2.5). Clearly, the deposition of mercury is hindered and the stripping process is complicated in this medium. The equilibrium constant for the reaction of Hg^{2+} with mercury to form Hg_2^{2+} is 88 [11]. Equilibrium for this reaction is established rapidly, so in the vicinity of the electrode when mercury is present, the major form in solution should be Hg_2^{2+}. Thiocyanate, acetate, and nitrate all form insoluble salts of the composition Hg_2X_2. In the case of thiocyanate, the Hg(II) oxidation state is stabilized by formation of $Hg(SCN)_4^{2-}$. The equilibrium constant for the reaction $Hg_2(SCN)_2(s) + 2SCN^- = Hg(SCN)_4^{2-} + Hg$ is 1 l mol^{-1} [11], and therefore in 0.1 M thiocyanate one would expect no precipitation of $Hg_2(SCN)_2$ in the presence of mercury for concentrations of Hg(II) less than 0.01 M. For acetate, again HgX_4^{2-} is the predominant form, and the equilibrium constant for the disproportionation reaction is sufficiently large that no precipitate should form [11—13]. Nitrate is quite different. The solubility product of $Hg_2(NO_3)_2 \cdot 2H_2O(s)$ estimated from enthalpy values [11] is given by $\log K = -57$ $(mol\ l^{-1})^3$, but it is well known that $Hg_2(NO_3)_2$ is quite soluble in slightly acidic aqueous solution. Stabilization of Hg(II) by complex formation is negligible [14]. Therefore, the undesirable behavior of mercury deposits in nitrate media appears to be due to the presence of Hg(I).

Anodic stripping of codeposited lead

The following series of experiments was done to test the range of conditions suitable for in situ codeposition of lead. The solution was 0.1 M thiocyanate (pH 2.5) with 40 μM Hg(II). Deposition was done without stirring for 60 s at —0.6 V. The nominal thickness of the mercury deposit under these conditions is 18 Å. After deposition, anodic square-wave voltammograms were obtained with E_{sw} = 25 mV, ΔE_s = 6 mV, and f = 100 Hz. The electrode

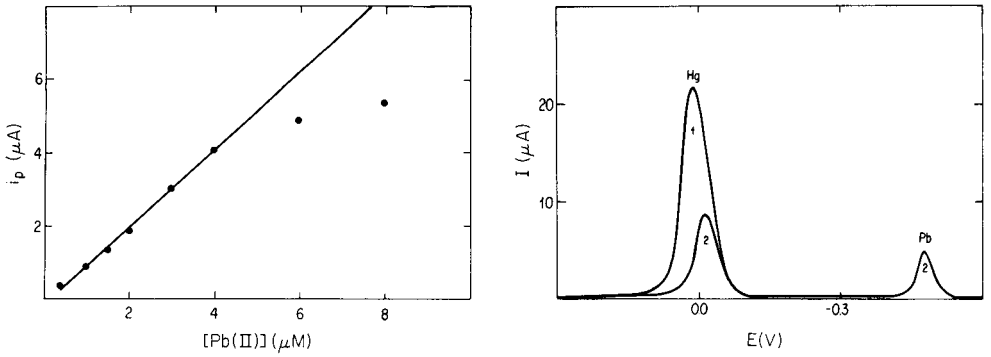

Fig. 7. Dependence of peak height on concentration of lead in the anodic-stripping square-wave voltammetry of lead codeposited with mercury. (E_d = —0.6 V; t_d = 60 s; E_{sw} = 24 mV, ΔE_s = 4 mV, f = 100 Hz; 0.1 K KSCN, pH 2.5, 40 μM Hg(II). Straight line fitted to linear portion; correlation coefficient = 0.9992.)

Fig. 8. Anodic-stripping square-wave voltammograms: (1) mercury; (2) mercury/lead amalgam. (2.5 μM Pb(II); other conditions as Fig. 7).

was conditioned before each deposition for 1 min at +0.3 V. The procedure was repeated for varied concentrations of lead. Anodic-stripping peak current increased linearly with concentration of lead up to 4 μM (Fig. 7). However, at 1 μM Pb(II), the anodic stripping peak for mercury was diminished and shifted to more negative potential, and this effect was systematically more pronounced, the higher the concentration of Pb(II). An example is shown in Fig. 8. The solubility of lead in mercury is 0.013 mol Pb/mol Hg. The molar ratio of lead to mercury in the amalgam under the conditions of this experiment, assuming deposition is diffusion-controlled, is just the concentration ratio, [Pb(II)]/[Hg(II)]. In the present case with 40 μM Hg(II), saturation should occur for ⩾0.5 μM Pb(II). The first diminution in the mercury stripping peak was observed at 1 μM Pb(II). It is well established that saturation must be avoided to obtain acceptable results for anodic stripping voltammetry [15—17]. In the present case, the calibration curve remained linear up to a concentration of about eight times the saturation value. For concentrations of Pb(II) greater than about 8 μM (ca. 15 times the saturation value), broader anodic-stripping peaks were obtained between —0.4 and —0.5 V and no peak was obtained for stripping of mercury. This effect has been reported previously for cadmium [9].

Finally, a few observations are presented on the practical use of mercury-coated carbon-fiber electrodes. Figure 9 presents two cyclic staircase voltammograms, both obtained in thiocyanate solution with 40 μM Hg(II) and 1.2 mM Pb(II). Curve 1 (Fig. 9) was obtained at a clean fiber, whereas curve 2 was obtained at a mercury-coated fiber (deposit thickness of ca. 95 Å). The voltammogram is improved dramatically by the presence of the mercury deposit. Presently, there is no theoretical basis for treating this problem,

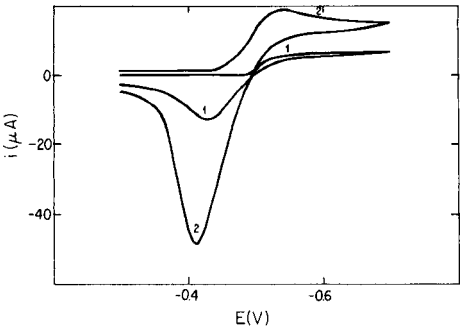

Fig. 9. Cyclic staircase voltammograms (sweep rate 0.8 V s^{-1}): (1) no previous mercury deposition; (2) mercury deposited at —0.3 V. Apparent thickness of the deposit, ca. 95 Å; 0.1 M KSCN, pH 2.5, 0.04 mM Hg(II), 1.2 mM Pb(II).

which involves aspects of cylindrical diffusion, nucleation and growth, and films. However, the practical implications for developing quantitative methods suggest that this phenomenon should be examined in much greater detail.

This work was supported in part by the Office of Naval Research.

REFERENCES

1 M. R. Cushman, B. G. Bennett and C. W. Anderson, Anal. Chim. Acta, 130 (1981) 323.
2 G. Schultze and W. Frenzel, Anal. Chim. Acta, 159 (1984) 95.
3 M. A. Dayton, J. C. Brown, K. J. Stutts and R. M. Wightman, Anal. Chem., 52 (1980) 946.
4 V. J. Jennings and J. E. Morgan, Analyst, 110 (1985) 121.
5 T. E. Edmonds, Anal. Chim. Acta, 175 (1985) 1.
6 K. Aoki, K. Honda, K. Tokuda and H. Matsuda, J. Electroanal. Chem., 182 (1985) 267.
7 K. Aoki, K. Honda, K. Tokuda and H. Matsuda, J. Electroanal. Chem., 186 (1985) 79.
8 J. L. Ponchon, R. Cespuglio, F. Gonon, M. Jouvet and J. F. Pujol, Anal. Chem., 51 (1979) 1483.
9 J. Gołaś and J. Osteryoung, Anal. Chim. Acta, 181 (1986) 211.
10 T. R. Brumleve, J. J. O'Dea, R. A. Osteryoung and J. Osteryoung, Anal. Chem., 53 (1981) 702.
11 A. J. Bard, R. Parsons and J. Jordan (Eds.), Standard Potentials in Aqueous Solution, International Union of Pure and Applied Chemistry, M. Dekker, New York, 1985.
12 D. D. Perrin (Ed.), Stability Constants of Metal-ion Complexes: Part B. Organic Ligands, IUPAC Chemical Data Series No. 22, Pergamon, Oxford, 1979.
13 J. Kragten, Atlas of Metal—Ligand Equilibria in Aqueous Solution, Ellis Horwood, Chichester, 1978.
14 R. M. Smith and A. E. Martell, Critical Stability Constants, Vol. 4: Inorganic Complexes, Plenum, New York, 1976.
15 M. T. Kozlovskii, A. J. Zebreva and V. P. Gladyshev, Amalgamy i ikh Primienene, Alma-Ata, 1971.
16 Z. Stojek, B. Stepnik, Z. Kublik, J. Electroanal. Chem., 74 (1976) 277.
17 T. R. Copeland and R. K. Skogerboe, Anal. Chem., 46 (1974) 1257A.

Analytica Chimica Acta, 186 (1986) 11—19
Elsevier Science Publishers B.V., Amsterdam — Printed in The Netherlands

PRECONCENTRATION OF TRANQUILIZERS BY ADSORPTION/EXTRACTION AT A WAX-IMPREGNATED GRAPHITE ELECTRODE

TAFEEDAH B. JARBAWI
Department of Chemistry, Birzeit University, Birzeit, P.O. Box 14 (West Bank/Israel)
WILLIAM R. HEINEMAN*
Department of Chemistry, University of Cincinnati, Cincinnati, OH 45221 (U.S.A.)
(Received 9th July (1985)

SUMMARY

The tranquilizers promethiazine, diethazine, trifluoperazine, fluphenazine and clozapin adsorb at the surface and extract into the wax-impregnated graphite electrode (WIGE) as shown by chronocoulometry. Extraction/adsorption at the electrode serves as a preconcentration step which improves the limit of detection for the drugs by differential pulse voltammetry. A 15-min preconcentration gave a linear range of 10^{-4}—5×10^{-8} M with a detection limit of 5×10^{-9} M for clozapin in pH 7 phosphate buffer. The determination of tranquilizers in urine and plasma required no preliminary treatment; the detection limits were 5×10^{-8} M in urine and 10^{-7} M in plasma. Plasma measurements were made at a WIGE covered with a Spectrapor membrane to prevent electrode fouling by protein adsorption.

The good detection limits of differential pulse voltammetry have frequently prompted its use for the determination of drugs in pharmaceutical preparations [1]. The detection limits for such organic compounds can be improved by preconcentrating the electroactive species at the electrode by adsorption at the electrode/solution interface, extraction into the electrode, or a combination of these two phenomena [2, 3]. Although the concept of preconcentration by electrochemical extraction into a microelectrode is the basis of the widely used technique of anodic stripping voltammetry for metal ions [4, 5], extraction into an electrode has not been widely applied in electroanalysis for organic compounds. Kuwana and French [6] first demonstrated the concept of oxidatively stripping an organic compound that is dissolved in a carbon-paste electrode. Extraction of other compounds into carbon paste has since been observed and exploited for improving detection limits by a particular electroanalytical technique [7]. Adsorption on the electrode surface has also been investigated as a means of preconcentrating the sample [8—12].

During development of the technique of thin-layer differential pulse voltammetry [13], a surprisingly low detection limit (5×10^{-9} M) was observed

0003-2670/86/$03.50

for the tranquilizer, chlorpromazine, at a wax-impregnated graphite electrode (WIGE) [2]. This detection limit was subsequently attributed to adsorption of chlorpromazine at the electrode interface and extraction into the wax [3]. Chronocoulometry proved to be an effective technique for investigating the adsorbed and extracted material.

This paper describes the electrochemical behavior of several tranquilizers (promethiazine, diethazine, trifluoperazine, fluphenazine, and clozapin) at the WIGE. These phenothiazines are known to adsorb on various surfaces including biological membranes where they affect osmotic permeability [14, 15]. The purpose of this work was to investigate a class of drugs to determine the generality of preconcentration at the WIGE.

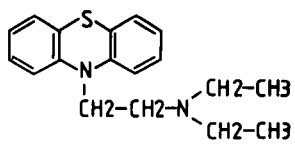

Diethazine

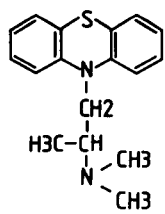

Promethiazine

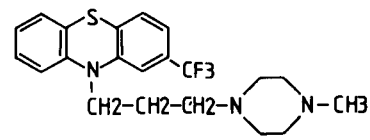

Trifluoperazine

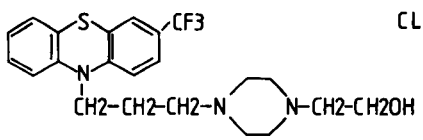

Fluphenazine

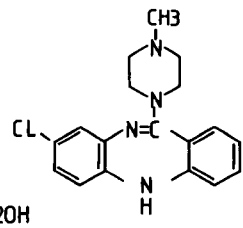

Clozapin

EXPERIMENTAL

Apparatus and reagents

Instrumentation, preparation of the WIGE and the electrochemical cell have been previously described [3]. All potentials cited here are relative to the saturated calomel electrode.

Clozapin, promethiazine, diethazine, trifluoperazine and fluphenazine were obtained from Professor Gaston J. Patriarche (Institute de Pharmacie, Université Libre de Bruxelles). Phosphate and acetate buffers were prepared from reagent-grade dipotassium hydrogenphosphate, potassium dihydrogenphosphate and sodium acetate (Fisher Scientific Company). Plasma was provided by the University Hospital. Spectrapor membrane tubing (Spectrum Medical Industries) with a molecular-weight cutoff of 12,000—14,000 was used to prevent fouling of the WIGE by proteins in plasma.

Procedure

No preliminary treatment of the urine or plasma samples was applied. For urine samples, the drug was preconcentrated into the WIGE by simply dipping the electrode into a stirred sample for a specified period of time. The electrode was then removed from the urine, rinsed, blotted dry and transferred to pH 7 or pH 4 buffer where the differential pulse voltammogram was recorded.

Two procedures were followed for determining the tranquilizers in plasma. The first procedure is the same as that followed for urine samples. In the second procedure, the WIGE surface was wrapped in Spectrapor membrane tubing. The electrode with the membrane coating was dipped in a plasma sample for 40 min. The electrode was removed from the sample, the membrane removed, and the electrode was rinsed, blotted dry and then immersed in pH 7 or pH 4 buffer where a differential pulse voltammogram was recorded.

RESULTS AND DISCUSSION

Differential pulse voltammetry

Well-defined differential pulse voltammograms were obtained for the oxidation of all the tranquilizers studied. In pH 7 phosphate buffer, clozapin, diethazine and promethiazine showed peak potentials of 350 mV, 560 mV and 610 mV, respectively. In pH 4 acetate buffer, trifluoperazine and fluphenazine gave peak potentials of 700 mV and 670 mV, respectively.

The peak current for the oxidation wave of each tranquilizer was optimized by systematic variation of modulation amplitude (pulse height), pulse width and scan rate. The effect of modulation amplitude at different scan rates on the peak current of clozapin, which exhibits behavior representative of all the drugs, is shown in Fig. 1. The effect of variations in pulse width at a 2 mV s^{-1} scan rate and a 100 mV modulation amplitude was to decrease sensitivity with increasing pulse width (0.5, 1.0 and 2.0 s). Maximum sensitivity for all of the drugs was obtained with a large pulse height (100 mV) of short duration (0.5 s) at a slow scan rate (2 mV s^{-1}).

The accumulation of the tranquilizers is easily seen from differential pulse voltammograms at a WIGE that has been immersed in a tranquilizer solution for increasing periods of time, as illustrated in Fig. 2 for the oxidation of clozapin in phosphate buffer, pH 7. A plot of peak current vs. preconcentration time from Fig. 2 is shown in Fig. 3. Accumulation in the electrode occurs at a significant rate for the first 15 min, after which time the rate drops significantly. A disproportionately large value of peak current is obtained after 1 min relative to the currents obtained at longer extraction times. This is attributed to an initial accumulation of clozapin by adsorption at the interface with subsequent accumulation by diffusion into the wax. The surface-adsorbed species would exhibit greater sensitivity because no diffusion to the interface is required for oxidation. Thus, the initial enhance-

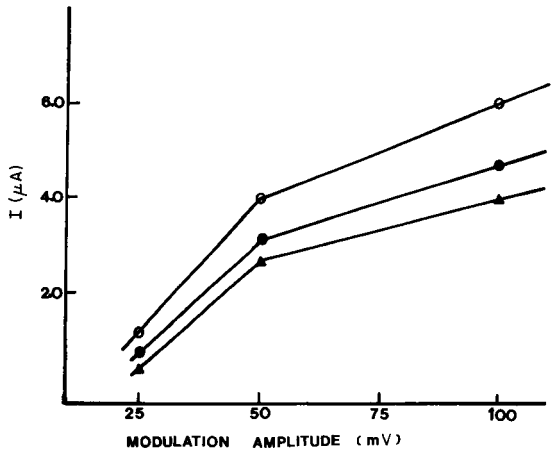

Fig. 1. Effect of modulation amplitude on peak current for 10 μM clozapin in phosphate buffer pH 7.00 at the WIGE. Scan rates: (▲) 10; (●) 5; (○) 2 mV s^{-1}.

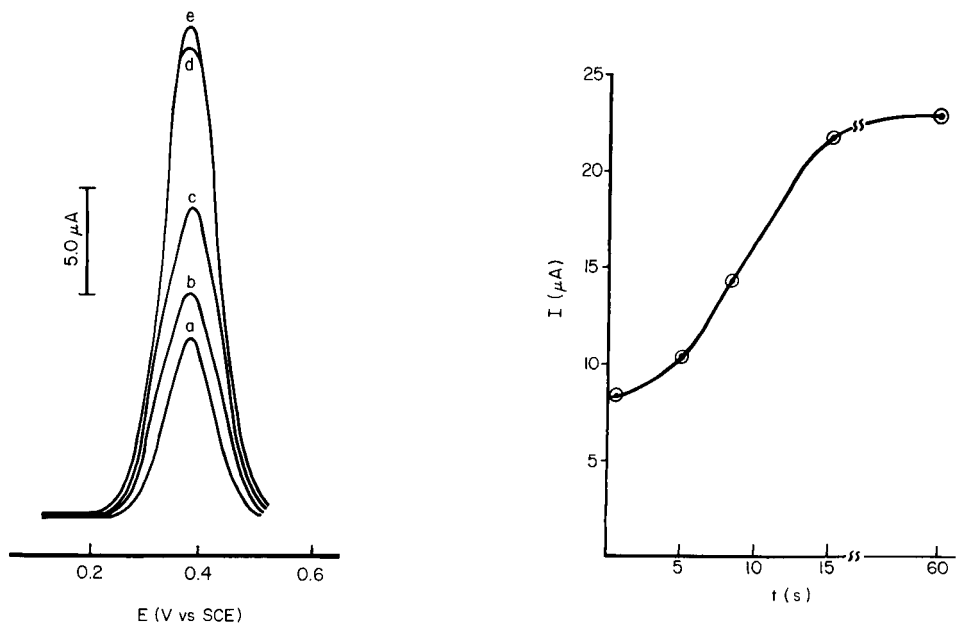

Fig. 2. Differential pulse voltammograms at a WIGE after soaking in 10 μM clozapin/phosphate buffer pH 7 for different times: (a) 1, (b) 5, (c) 8, (d) 15, (e) 60 min. Voltammograms recorded in phosphate buffer after rinsing the WIGE with distilled water. Scan rate 2 mV s^{-1}, modulation amplitude 100 mV, clock time 0.5 s.

Fig. 3. Peak current vs. time plot from data in Fig. 2.

ment in peak current is due primarily to adsorption, which occurs rapidly, and subsequent enhancement is due primarily to diffusion into the wax. Approximately 15 min is required for sufficient clozapin to diffuse into the wax to satisfy the partition coefficient for the distribution of clozapin between the aqueous phase and the wax phase. Deposition times longer than 15 min give a relatively small enhancement in peak current for this concentration of clozapin. This general behavior is representative of the other tranquilizers.

Well-defined voltammograms were obtained in the raw urine samples. Figure 4 shows a typical differential pulse voltammogram of diethazine in urine.

Standard plots

Standard plots were obtained for standard solutions of clozapin, diethazine and promethiazine in phosphate buffer pH 7. Because of solubility considerations, standard plots were obtained for standard solutions of trifluoperazine and fluphenazine in acetate buffer pH 4 rather than phosphate buffer pH 7.

A linear relationship between peak height and concentration from 5×10^{-8} to 10^{-4} M with a detection limit of 5×10^{-9} M was obtained for clozapin with a deposition time of 15 min. A negative deviation from linearity was exhibited by solutions of concentration greater than 10^{-4} M. For this deposition time, saturation of the WIGE by the tranquilizer occurs for solutions of such high concentration. These concentrations can be accommodated by resorting to shorter deposition times. Longer deposition times can be used to achieve lower detection limits, although the improvement is not substantial. For example, increasing the deposition time from 15 min to 10 h improves the detection limit for clozapin to 10^{-10} M.

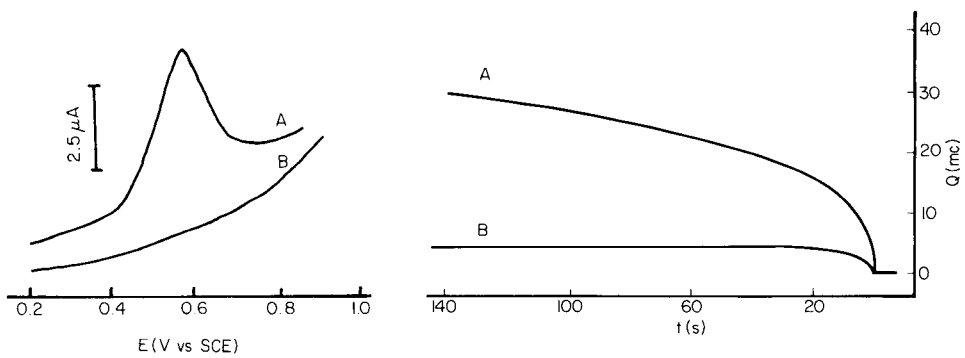

Fig. 4. Differential pulse voltammograms: (A) 10 μM diethazine in urine; (B) blank urine. Voltammograms recorded in phosphate buffer after rinsing the WIGE with distilled water. Preconcentration time, 15 min.

Fig. 5. Charge/time curves for potential step from 0.2 to 0.57 V vs. SCE: (A) WIGE soaked in 10 μM clozapin for 15 min, rinsed with distilled water and immersed in phosphate buffer; (B) WIGE unexposed to clozapin and immersed in buffer.

The linear range of diethazine and promethiazine was from 5×10^{-7} to 10^{-4} M with a detection limit of 5×10^{-8} M. The same linear range and detection limit were obtained for the trifluoperazine and fluphenazine in acetate buffer pH 4. Least-squares data for the standard plots are in Table 1.

Biological samples

The detection limit for all of these drugs in urine is about 5×10^{-8} M with a deposition time of 15 min.

The determination of the drugs at a WIGE that was immersed directly in blood plasma was precluded by protein adsorption on the electrode surface. Although voltammetric waves for the drugs were observable at a protein-fouled electrode, the limit of detection was restricted to about 10^{-5} M. Covering the electrode with a membrane that passes the drugs to the electrode surface but prevents access of protein proved to be an effective means of allowing the direct determination of drugs in plasma. A Spectrapor membrane was suitable for this purpose. The sensitivity was diminished by the restriction in diffusion to the electrode. Nonetheless, direct measurements could be made with a detection limit of about 10^{-7} M for all of the drugs. In order to achieve this detection limit, the preconcentration time was extended to 40 min because of the restricted diffusion of drug through the membrane.

The generally poor selectivity of voltammetric techniques can pose difficulties in the analysis of urine and plasma samples which contain oxidizable substances such as uric acid. The WIGE offers a means of improving selectivity by means of selective preconcentration at the electrode. Species that do not absorb on, or extract into, the electrode are removed by rinsing prior to the recording of the voltammogram. For example, no interference was observed from uric acid.

Chronocoulometry

Previous studies on chlorpromazine at the WIGE showed the preconcentration of chlorpromazine to be a result of both adsorption of the drug at the electrode interface and extraction into the electrode itself [3]. The extrac-

TABLE 1

Linear least-squares data for standard plots for tranquilizers[a]

Buffer	Tranquilizer	Slope	Intercept	Correlation coefficient	Standard error of estimate
Phosphate pH 7	Clozapin	0.382 ± 0.005	3.17 ± 0.025	0.994	0.051
	Promethiazine	0.534 ± 0.007	3.70 ± 0.031	0.993	0.038
	Diethazine	0.479 ± 0.004	3.32 ± 0.028	0.995	0.026
Acetate pH 4	Trifluoperazine	0.477 ± 0.008	3.24 ± 0.035	0.994	0.041
	Fluphenazine	0.772 ± 0.003	4.88 ± 0.028	0.995	0.026

[a]Based on 3 runs for each calibration plot. Deposition time is 15 min.

tion is presumably by diffusion into the wax, which fills the voids in the carbon material. Chronocoulometry at an electrode into which a drug has been preconcentrated is a good technique for distinguishing adsorbed material from material that has diffused into the interior of the electrode and, consequently, must diffuse back to the surface for electro-oxidation.

The extent of adsorption and extraction of each of the phenothiazines was quantified by chronocoulometry. A charge/time curve was recorded after a WIGE had been soaked for 15 min in a solution of the drug, rinsed with distilled water and transferred to supporting electrolyte. Curve A in Fig. 5 shows the clozapin charge/time curve for a potential step from 200 to 570 mV; curve B shows results of a potential step for a WIGE that was not exposed to clozapin. The integrated Cottrell equation [16] can be applied to determine the surface concentration of adsorbed species

$$Q = 2\pi^{-1/2} nFAD^{1/2} Ct^{1/2} + Q_{ads} + Q_{d.l.}$$

where D and C are the diffusion coefficient and concentration of clozapin in the WIGE, respectively; other terms have their usual meanings. Plots of Q vs. $t^{1/2}$ for clozapin and supporting electrolyte are shown in Fig. 6. Correcting the intercept of curve A for $Q_{d.l.}$, as indicated by the curve B intercept, gives a surface concentration for adsorbed clozapin of 1.1×10^{-7} mol cm^{-2} and a slope of 0.196 cm^2 s^{-1}. The slope is directly proportional to the diffusion coefficient and concentration of clozapin in the WIGE. The linearity of the Q vs. $t^{1/2}$ plot confirms the diffusion-controlled nature of the oxidation of clozapin which has been extracted into the WIGE. Figure 7 shows Q vs. $t^{1/2}$

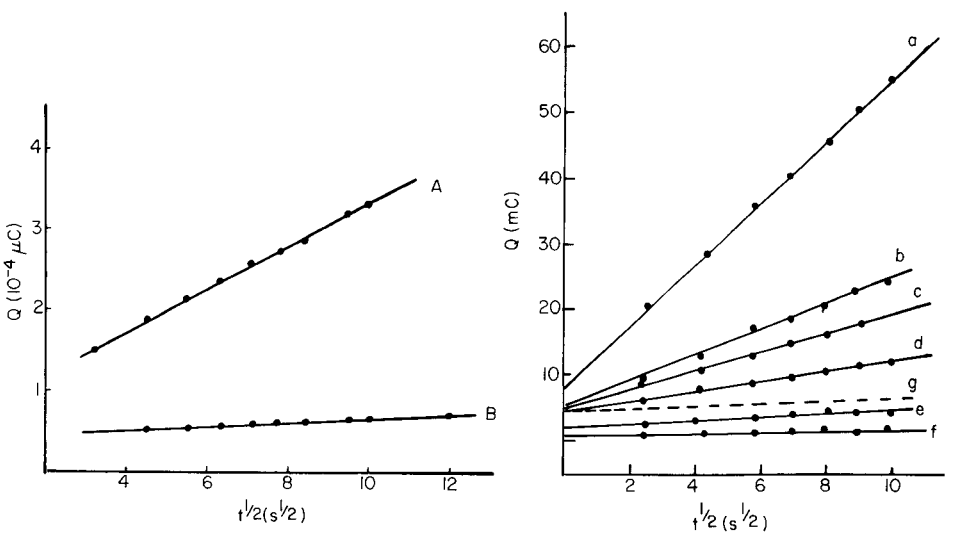

Fig. 6. Charge vs. $t^{1/2}$ plots from data in Fig. 5.

Fig. 7. Charge vs. $t^{1/2}$ plots for various concentrations of clozapin after 15-min deposition times at the WIGE: (a) 5×10^{-4}; (b) 5×10^{-5}; (c) 1×10^{-5}; (d) 5×10^{-6}; (e) 1×10^{-6} M clozapin; (f) blank phosphate buffer pH 7 at WIGE and graphite electrode; (g) 5×10^{-5} M clozapin at graphite electrode after 15-min deposition time.

TABLE 2

Slope of the $Q/t^{1/2}$ plots and surface concentration of adsorbed drugs at the WIGE after deposition for 15 min in 5×10^{-5} M solutions

Buffer	Tranquilizer	Slope ($mC\ s^{-1}$)	Surface concentration ($mol\ cm^{-2}$)
Phosphate pH 7	Clozapin	0.198	1.1×10^{-7}
	Diethazine	0.195	8.8×10^{-8}
	Promethiazine	0.162	6.5×10^{-8}
Acetate pH 4	Trifluoperazine	0.113	5×10^{-8}
	Fluphenazine	0.076	3×10^{-8}

plots for various concentrations of clozapin (5×10^{-4}—1×10^{-6} M) in phosphate buffer pH 7 at a deposition time of 15 min. The slopes of these lines increase with increasing concentration, which indicates that the concentration of clozapin in the WIGE after extraction depends on its concentration in the solution into which the WIGE is dipped. The charge intercept also increases with increasing concentration. Thus, the overall electroanalytical response for a WIGE dipped in a solution of clozapin and then transferred into supporting electrolyte represents contributions from both adsorbed and extracted clozapin that are concentration-dependent.

The slope of the $Q/t^{1/2}$ plot for a WIGE dipped into a 5×10^{-5} M clozapin solution depended on the deposition time. The slope increased with deposition time up to about 15 min, at which point it essentially reached a plateau. This is analogous to the behavior observed for the peak anodic current for differential pulse voltammetry as shown in Fig. 3. Similar results were obtained for lower concentrations. However, a similar experiment on a more concentrated solution of clozapin (5×10^{-4} M) showed no measurable effect of deposition time on slope. The maximum extraction is evidently achieved very rapidly (less than about 60 s) at this concentration level.

Clozapin was found to adsorb on a graphite electrode without wax impregnation. Figure 7 shows $Q/t^{1/2}$ plots for graphite in a phosphate buffer alone (line f) and after immersion for 15 min in 5×10^{-5} M clozapin in phosphate buffer (line g). The two lines are parallel, indicating that clozapin adsorbs at the surface of graphite. However, the absence of a time-dependent ($t^{1/2}$) charge response indicates that clozapin does not "extract" into the graphite electrode as it does into the WIGE.

All of the drugs investigated showed charge/time behavior that is similar to that described above for clozapin. Table 2 shows the surface concentration of the adsorbed drugs at the WIGE and the slopes of their $Q/t^{1/2}$ plots.

T. B. J. acknowledges financial support from Birzeit University. W. R. H. acknowledges financial support provided by NSF Grant CHE-8217045.

REFERENCES

1 M. A. Brooks, in P. T. Kissinger and W. R. Heineman (Eds.), Laboratory Techniques in Electroanalytical Chemistry, Dekker, New York, 1984, pp. 569—609.
2 T. J. Jarbawi, W. R. Heineman and G. J. Patriarche, Anal. Chim. Acta, 125 (1981) 57.
3 T. J. Jarbawi and W. R. Heineman, Anal. Chim. Acta, 13 (1982) 359.
4 W. R. Heineman, H. B. Mark, Jr., J. A. Wise and D. A. Roston, in P. T. Kissinger and W. R. Heineman (Eds.), Laboratory Techniques in Electroanalytical Chemistry, Dekker, New York, 1984, pp. 569—609.
5 J. Wang, Stripping Analysis: Principles, Instrumentation, and Applications, VCH, Deerfield Beach, FL, 1985.
6 T. Kuwana and W. G. French, Anal. Chem., 36 (1964) 241.
7 J. Wang and B. A. Freiha, Anal. Chem., 56 (1984) 849.
8 R. Kalvoda, Anal. Chim. Acta, 138 (1982) 11.
9 J. Wang and B. A. Freiha, Anal. Chim. Acta, 154 (1983) 82.
10 H. Y. Cheng, L. Falat and R. L. Li, Anal. Chem., 54 (1982) 1384.
11 J. Wang, D. B. Luo, P. A. M. Farias and J. S. Mahmond, Anal. Chem., 57 (1985) 158.
12 J. Wang, M. Bonakdar and C. Morgan, Anal. Chem., 58 (1986) 1024.
13 T. P. DeAngelis, R. E. Bond, E. E. Brooks and W. R. Heineman, Anal. Chem., 49 (1977) 1792.
14 H. Nogami, T. Nagai and N. Namba, Chem. Pharm. Bull., 18 (1970) 1643.
15 A. R. Freeman and M. A. Spirtes, Biochem. Pharmacol., 12 (1963) 1237.
16 F. C. Anson, Anal. Chem., 38 (1966) 54.

Analytica Chimica Acta, 186 (1986) 21—30
Elsevier Science Publishers B.V., Amsterdam — Printed in The Netherlands

DETERMINATION OF SOME QUINOXALINE-*N*-DIOXIDE DERIVATIVES BY ADSORPTIVE STRIPPING VOLTAMMETRY

VĚRA STARÁ and MILOSLAV KOPANICA*

UNESCO Laboratory of Environmental Electrochemistry at the J. Heyrovský Institute of Physical Chemistry and Electrochemistry, Czechoslovak Academy of Sciences, Jilská 16, 110 00 Prague 1 (Czechoslovakia)

(Received 8th October 1985)

SUMMARY

Some derivatives of quinoxaline-*N*-dioxides, which are used as growth promoters in animals (Carbadox, Cyadox, Olaquindox), can be determined at nanomolar concentrations by stripping voltammetry from a static mercury drop electrode after adsorptive accumulation on the electrode surface. With differential pulse voltammetry, in 0.1 M sodium perchlorate with 5% (v/v) dimethylformamide, the detection limit for Cyadox is 3×10^{-10} mol l^{-1} after accumulation for 300 s in stirred solution; detection limits are 2×10^{-9} mol l^{-1} (180 s accumulation) for Carbadox and 7×10^{-9} mol l^{-1} (60 s accumulation) for Olaquindox. The relative standard deviations are 0.85% for Cyadox (4×10^{-9} mol l^{-1}), 0.54% for Carbadox (2×10^{-8} mol l^{-1}) and 0.95% for Olaquindox (2×10^{-8} mol l^{-1}). Surfactants interfere.

Some derivatives of quinoxaline-*N*-dioxides are used as growth promoters in calves, pigs, etc. Because these compounds can be toxic to man [1], methods are required for the determination of small amounts of these substances in animal feeds and in organ and tissue samples. The methods used mostly involve u.v. spectrophotometry and gas or liquid chromatography with different detection modes. The quinoxaline-*N*-dioxides are polarographically active [2, 3] and thus polarographic methods, usually differential pulse polarography (d.p.p.), are applied for their determination [4—7]. The detection limits of these methods are frequently inadequate.

To increase the sensitivity of such determinations, the voltammetric behaviour of these compounds was examined so that conditions could be established for their adsorptive stripping determination. The compounds studied were Cyadox (I), Carbadox (II), Olaquindox (III), the *N*-cyanomethylamide of 3-methylquinoxaline-1,4-dioxide-2-carboxylic acid (IV) and quinoxaline-2-carboxylic acid (V).

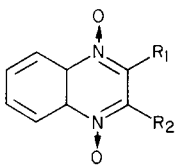

I: $R_1 = -CH{=}N-NHCOCH_2CN$; $R_2 = H$
II: $R_1 = -CH{=}N-NHCOOCH_3$; $R_2 = H$
III: $R_1 = -CONHCH_2CH_2OH$; $R_2 = CH_3$
IV: $R_1 = -CONHCH_2CN$; $R_2 = CH_3$

0003-2670/86/$03.50

EXPERIMENTAL

Equipment and method

The polarographic analyzer (PA-4; Laboratorní přístroje, Prague) was used in the three-electrode configuration; a static mercury drop electrode (SMDE-1; Laboratorní přístroje, Prague) served as the working electrode, a saturated calomel electrode (SCE) as the reference electrode and a platinum wire as the auxiliary electrode. Dissolved oxygen was removed from the tested solutions by argon.

The electrocapillary curves were measured by using the method of interrupted convection [8]; the capillary used had an inner diameter of 65 μm and a drop time of 65 s.

Voltammetric measurements with preconcentration of the analyte were done with the SMDE operated in the hanging mercury drop electrode mode with stirred solutions (mechanical stirrer) during the preconcentration step and a 10-s rest period before the polarization was started.

Reagents

The substances Cyadox (I), Carbadox (II) and Olaquindox (III) were products of the Research Institute of Pharmacy and Biochemistry, Prague; all contained more than 99.8% of the active substance according to the producer. The quinoxaline-2-carboxylic acid (V) was prepared in the Research Center of Biofactors, Prague (96% of the active substance). The *N*-cyanomethylamide of 3-methylquinoxaline-1,4-dioxide-2-carboxylic acid (IV) was 99% pure (Lachema, Brno). Solutions of Cyadox and Carbadox (10^{-3} mol l^{-1}) were prepared by dissolution in *N*,*N*-dimethylformamide (DMF) and used for three days, kept in the dark in a refrigerator; solutions of other substances were prepared identically each day. Less concentrated solutions were prepared by dilution with the electrolyte used.

The DMF was purified by distillation and kept at 6°C. All other solutions were prepared from reagent-grade chemicals; twice-distilled water (quartz apparatus) was used throughout.

RESULTS AND DISCUSSION

Voltammetric behaviour of some derivatives of quinoxaline-N-*dioxides*

In acidic and neutral media, the quinoxaline-*N*-dioxides are polarographically reduced in two steps [2, 3]:

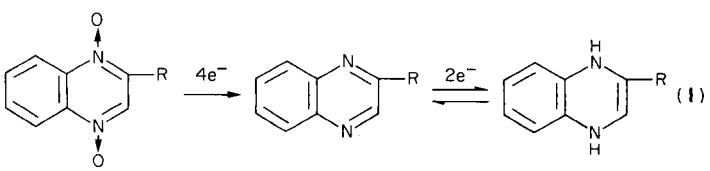

A third wave appears on the polarogram if R is polarographically active and another wave corresponding to the reaction of the mercury salt formed was

observed for some derivatives [6]. Voltammetric measurements at the hanging mercury drop electrode (HMDE) with d.c. techniques gave results corresponding to the published polarographic data. All studied substances (with the exception of substance V) yielded two reduction peaks, which correspond to the reduction processes given in Reaction 1. The peak potential values (E_p) depended on the pH of the supporting electrolyte: two reduction peaks (corresponding to the step-wise reduction of the two N → O groups) were obtained in acidic media (pH 1—3); at higher pH values, the reduction of N → O groups proceeded in one step. Basic voltammetric data (peak potential values E_{p1} and E_{p2} corresponding to the reduction of the N → O groups and to the reduction of the quinoxaline ring, respectively, together with the ratio of the corresponding peak current values i_{p1} and i_{p2}) are summarized in Table 1. The values of the peak current ratio i_{p1}/i_{p2} given in Table 1 for compounds I, II and III result from the number of electrons involved in the two reduction processes (Reaction 1); in the case of compound IV, the value of the i_{p1}/i_{p2} ratio is irregular because the reduction of the N → O groups proceeded in two overlapping peaks. Examination of the cyclic voltammograms of the compounds studied (except for quinoxaline-2-carboxylic acid) showed not only the described cathodic peaks but also an anodic peak corresponding to the reversible reduction of the quinoxaline ring (Reaction 1). The value of the anodic peak current depended on the range of polarization of the HMDE. When the cyclic voltammogram was recorded in the range from 0 to —1.0 V, the anodic peak was higher than when the HMDE was polarized over the range from 0 to —1.50 V. The peak current vs. scan rate (20—200 mV s^{-1}) dependence for compounds I, II, III and IV was found to be linear for both cathodic and anodic peaks.

It was also found that the peak currents of all these recorded peaks increased when the HMDE was kept for a definite period of time (accumulation time t_{acc}) at zero potential (vs. SCE) or in open circuit, before the polarization scan was started (Fig. 1). The enhancement of the peak currents depended on the duration of the accumulation period t_{acc} and on the potential E_{acc} at which the HMDE was kept during t_{acc} before polarization was started.

TABLE 1

Peak potentials and peak currents for quinoxaline derivatives in 0.05 M $NaClO_4$/0.05 M Britton-Robinson buffer supporting electrolyte solutions

Compound	pH of the supporting electrolyte	E_{p1} (V)	E_{p2} (V)	i_{p1}/i_{p2}
Cyadox (I)	6.5	—0.53	—0.62	2:1
Carbadox (II)	6.5	—0.55	—0.68	2:1
Olaquindox (III)	2.5	—0.14	—0.33	2:1
IV	6.5	—0.46	—0.74	0.3:1
V	2.5	—	—0.24	—

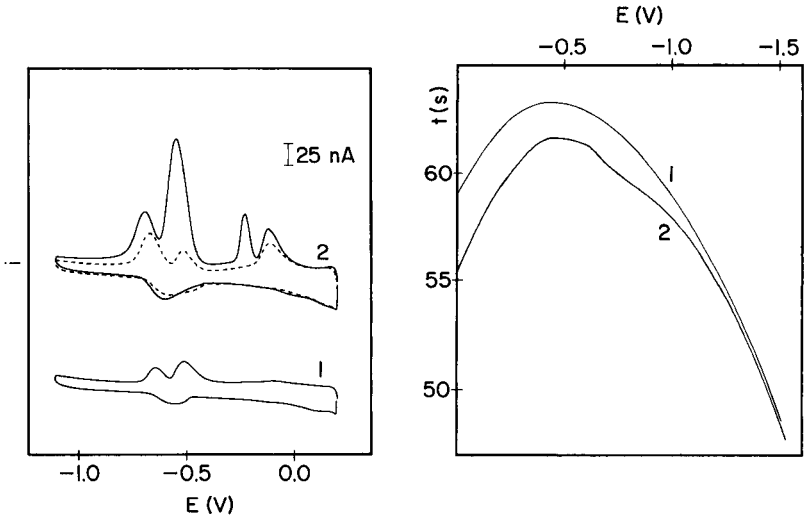

Fig. 1. Cyclic voltammograms of Cyadox: (1) without accumulation period; (2) 15-s accumulation at +0.20 V; (---) second scan with identical drop without accumulation. Conditions: 2×10^{-6} mol l^{-1} Cyadox in 0.1 M $NaClO_4$ with 5% (v/v) DMF; SMDE polarized from +0.20 to −1.20 V at 50 mV s^{-1}.

Fig. 2. Electrocapillary curve of Cyadox. Conditions: (1) 0.1 M $NaClO_4$ with 5% (v/v) DMF; (2) 1×10^{-6} mol l^{-1} Cyadox in 0.1 M $NaClO_4$ with 5% (v/v) DMF; capillary inner diameter 65 μm; drop time (open circuit) 65 s.

Maximum enhancement occurred when E_{acc} was +0.20 V, and a shift of E_{acc} to more negative potentials caused a gradual decrease of the measured current. Besides the reduction peaks given Table 1, a peak situated at more positive potential (−0.15 V at pH 6.5 for Cyadox) became more distinct when the accumulation period was applied (Fig. 1). Because the substances I, II, III and IV form compounds with mercury, this peak corresponds to the cathodic stripping voltammetric (c.s.v.) response of the quinoxaline-*N*-dioxides [6].

These findings indicated that the compounds studied were accumulated on the electrode by adsorption in the form of their mercury compounds. This was supported by measurement of the electrocapillary curves. Electrocapillary curves of the compounds I, II, III and IV were found to have a shape similar to that given in Fig. 2, which corresponds to the dependence of the drop time on the applied potential for Cyadox in 0.1 M sodium perchlorate containing 5% (v/v) DMF. The course of these curves can be interpreted as follows: relatively strong adsorption of these compounds on the mercury/solution interface occurs in the potential range between 0 and −0.40 V, a desorption process occurs at ca. −1.50 V and faradaic processes occur in the range between −0.50 and −0.80 V. Furthermore, the increasing difference between the surface tensions of mercury in the pure electrolyte, and in electrolyte containing these compounds at the more positive potentials

(—0.10—0 V), corresponds to the usual shape of electrocapillary curves of species which form compounds with mercury and adsorb on the mercury electrode, as reported, e.g., for cysteine [9].

The effect of adsorption was also observed on the recordings of repeated cyclic voltammograms measured with identical electrodes in the range from 0 to —1.20 V. In the case of Cyadox, when no accumulation period was applied, the height of the more positive peak (E_{p1} = —0.53 V) decreased by 20% in the second scan and in further scans remained practically constant, whereas the height of the more negative peak (E_{p2} = —0.62 V) increased by ca. 15% in the second scan and then remained constant. When a 20-s accumulation period at 0 V was applied, the height of the more positive peak decreased by 90% in the second scan, whereas the height of the more negative peak decreased under these conditions by 20%. Similar results were obtained with the other compounds studied, with the exception of quinoxaline-2-carboxylic acid.

The results obtained (i.e., the dependence of the enhancement of the reduction peak currents, i_p, on the accumulation potential and accumulation time, the linear dependences of the peak current on scan rate, the nature of the cyclic voltammograms and the shape of the electrocapillary curves) verify that adsorption processes are involved in the voltammetric reduction of the compounds studied. The observed phenomena can therefore be explained as follows: under the conditions given in Table 1, substances I, II, III and IV form compounds with mercury and are adsorbed on the HMDE surface:

$$X + Hg \xrightarrow{dep} HgX_{ads};\ HgX_{ads} + n\,e^- \xrightarrow{strip} Hg + X_{ads}$$

where X is a quinoxaline derivative (I, II, III or IV) and the subscript ads means the adsorbed species. In the following cathodic polarization step, the adsorbed species undergo reduction according to Reaction 1. The product of the N → O group reduction is adsorbed on the electrode surface and desorption takes place at ca. —1.50 V. The studied compounds thus exhibit both c.s.v. response [10] and adsorptive stripping voltammetric response [11], which both permit highly sensitive modes of determination.

Voltammetric behaviour of quinoxaline-2-carboxylic acid

Compared with quinoxaline-*N*-dioxides, the voltammetric behaviour of quinoxaline-2-carboxylic acid (V) is simple. The cyclic voltammogram of this compound showed one cathodic (E_{pc} = —0.24 V) and one anodic (E_{pa} = —0.22 V) peak, of practically identical heights at pH 2.5. Repeated cyclic voltammograms showed a slow decrease of the height of both the cathodic and anodic peaks over ten consecutive scans done at 1-min intervals. A slightly less pronounced accumulation effect was observed in acidic media; at most, the peak current was trebled with short accumulation periods (10—20 s) and longer accumulation times resulted in decreases of the measured current.

Analytical application

In the investigation of the analytical use of the described phenomena, differential pulse voltammetry (d.p.v.; pulse rate 5 s^{-1}, pulse duration 100 ms, interval between pulses 100 ms, polarization rate 20 mV s^{-1}) was applied. Compounds I, II, III and IV yielded reduction peaks in 0.02 M Britton-Robinson buffer (pH 4—7)/0.05 M $NaClO_4$ solutions containing 5% (v/v) DMF. These peaks corresponded to those given in Table 1, accompanied by a peak in the potential region —0.10 to —0.20 V corresponding to the reaction of the mercury compound. Accumulation at +0.20 V or with open circuit produced a significant enhancement of the reduction peak current as shown in Fig. 3 for compound I. When the d.p.v. mode was applied, the ratio of the peak currents i_{p1}/i_{p2} did not correspond to the value given in Table 1;

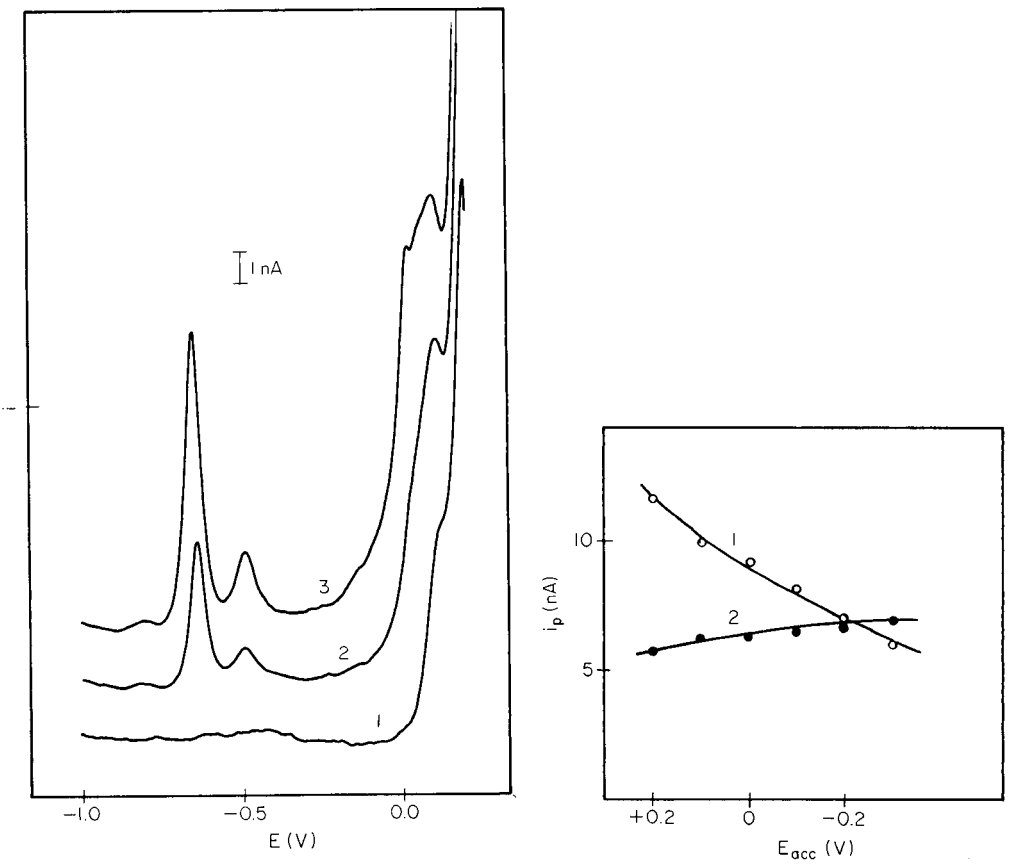

Fig. 3. D.p.v. curves of Cyadox at different accumulation times: (1) 0 s; (2) 60 s; (3) 120 s. Conditions: 5 × 10^{-9} mol l^{-1} Cyadox in 0.1 M $NaClO_4$ with 5% (v/v) DMF, polarization rate 20 mV s^{-1}, pulse amplitude —25 mV, accumulation potential +0.20 V.

Fig. 4. Dependence of peak current on accumulation potential: (1) for 2 × 10^{-8} mol l^{-1} Cyadox; (2) for 2 × 10^{-8} mol l^{-1} Carbadox. Conditions: 0.1 M $NaClO_4$ with 5% (v/v) DMF, accumulation time 10 s.

the more negative peak was always higher. The probable reason is that the electrode process corresponding to the more negative peak (E_{p2}) is reversible (reduction of the quinoxaline ring, Reaction 1). Because of lower background currents and higher sensitivities, use of the differential pulse mode and measurement of the more negative reduction peak (E_{p2}) was found preferable for analytical applications.

Influence of pH and solvent on the accumulation process

Examination of the effect of hydrogen ion concentration on the accumulation process showed that maximum peak currents occurred in the range pH 5.0—7.0. In the case of Olaquindox, however, it was necessary to use more acidic solutions because of the lower stability of Olaquindox in neutral or slightly acidic media. No difference was observed in measurements with an accumulation period in buffered (Britton-Robinson buffer) or unbuffered (0.1 M $NaClO_4$) electrolytes. The presence of DMF in the supporting electrolyte influenced the adsorptive stripping voltammetric determination. Experiments with varied DMF concentrations (5—30% v/v) showed that 5% DMF in the electrolyte was sufficient to keep the compounds studied in soluble form and to obtain the maximally enhanced currents.

Influence of accumulation potential and accumulation time

With most of the compounds, maximal current enhancement was obtained at relatively positive accumulation potentials (+0.2 to —0.1 V) or with open circuit in stirred solutions. A shift of the E_{acc} to more negative values increased the i_p values in the case of Carbadox. In contrast, a remarkable decrease in the i_p values and a shift of the E_p value to more negative potential were observed in the case of Cyadox (Fig. 4). In these experiments with Cyadox, it was further observed that two overlapping peaks of the mercury compound (E_p = —0.15 V) were formed when the accumulation potential was +0.20 V, while with accumulation potentials of +0.1 to —0.3 V, only one mercury compound peak was obtained, the height of which decreased at more negative E_{acc} values. When the accumulation potential was —0.10 V, the current related to the mercury compound corresponded to only 10% of that obtained at E_{acc} = +0.2 V (total current of both overlapping peaks). Different results were obtained in the measurement of the i_p vs. E_{acc} dependence of Carbadox; the mercury compound (E_p = —0.1 V) gave only one peak, the height of which corresponded to ca. 30% of that of the reduction of the quinoxaline ring and did not change with varied accumulation potentials. With compounds III—V, the i_p vs. E_{acc} plots were similar to that of Cyadox, but the decrease of i_p with more negative accumulation potential was less pronounced.

From these results, it can be concluded that in the case of Cyadox the mercury compound formed probably plays the predominant role in the adsorption process, whereas with Carbadox the role of the mercury compound is less significant in the accumulation process; the optimum accumula-

tion potential is close to the electrocapillary value, as in the case of chemical adsorption of neutral species. Obviously, the measurement of the mercury compound peak (c.s.v. response) has little analytical value because the signal is either lower than that from reduction of the adsorbed species (Carbadox) or varies significantly when longer accumulation times are applied, and two overlapping peaks are obtained (Cyadox). The splitting of the peak and non-linearity of the corresponding dependence of the peak current on analyte concentration (at high analyte concentration or when long accumulation intervals are applied) has been observed in the c.s.v. of some mercury compounds. This effect has been attributed to some reaction between the compound determined and mercury(I) and mercury(II) and to the fact that only the first layer of the mercury compound bound to the electrode surface is electrochemically active [10, 12].

As generally holds in adsorption stripping voltammetry, the peak currents (corresponding to reduction of the N → O groups and to reduction of the quinoxaline ring) increased with prolonged accumulation time, practically linearly at low concentrations of the studied compounds [11, 13]. The length of the accumulation time must be selected carefully, depending on the analyte concentration, to avoid saturation of the electrode surface [11, 13]. With compounds I—V, the longest accumulation times applied were as follows: up to 300 s for 10^{-10} mol l^{-1} Cyadox, up to 180 s for 10^{-9} mol l^{-1} Carbadox, up to 60 s for 10^{-8} mol l^{-1} Olaquindox, and 20 s for 10^{-8} mol l^{-1} IV or V.

Dependence of the peak current on concentration and reproducibility

The reduction peak current vs. concentration dependences were linear over wide concentration ranges. Table 2 summarizes the results of the regression analysis of the peak current vs. concentration dependences of compounds I—V. The data given in Table 2 were calculated from the results obtained with the longest possible accumulation time, as given in the table. In the determination of higher concentrations, shorter accumulation times

TABLE 2

Peak current vs. concentration dependences

Compound	Linear range i_p vs. conc. (mol l^{-1})	Slope[a] (nA $nmol^{-1}$)	Detection limit (mol l^{-1})	Maximum t_{acc} (s)	E_{acc} (V)
Cyadox	5×10^{-10}—3×10^{-7}	0.62(0.9998)	3×10^{-10}	300	+0.20
Carbadox	4×10^{-9}—5×10^{-7}	0.26(0.9996)	2×10^{-9}	180	+0.20
Olaquindox	8×10^{-9}—1×10^{-6}	0.05(0.9990)	7×10^{-9}	60	—[b]
IV	5×10^{-9}—5×10^{-7}	0.10(0.9992)	4×10^{-9}	20	+0.10
V	1×10^{-8}—1×10^{-7}	0.13(0.9991)	8×10^{-9}	20	—[b]

[a]Slope of the regression line with the correlation coefficient in parentheses. [b]Open circuit.

would be needed. The detection limits presented correspond to signal/noise ratios of 4. In all cases, the peak currents correspond to the reduction of the quinoxaline ring (peak potential E_{p2}, Table 1).

The reproducibility of the results was tested by ten successive measurements of 4×10^{-9} mol l^{-1} Cyadox and 2×10^{-8} mol l^{-1} solutions of compounds II, III, IV and V with automatic control of the accumulation times, provided by the instrument used. Relative standard deviations obtained in these experiments were 0.85% for Cyadox, 0.54% for Carbadox, 0.95% for Olaquindox, 0.70% for the quinoxaline-2-carboxylic acid and 1.9% for compound IV. Such precision data were obtained provided that the measurements of Carbadox, Cyadox and quinoxaline-2-carboxylic acid were completed within 90 min after mixing the sample solution with the supporting electrolyte solution, or in the case of compounds III and IV within 20 min. These time requirements are imposed by the limited stability of dilute solutions of compounds III and IV.

The influence of mercury in the cell was tested in two sets of measurements, without and with mercury (15 g) at the bottom of the cell. In both cases, identical results were obtained in successive measurements during 90 min (Carbadox, Cyadox and compound V) or during 20 min (compounds III and IV). These data indicate that mercury, present in the cell from dislodging of the drops, does not affect the precision of determinations for these compounds.

Influence of the supporting electrolyte concentration

In some determinations based on adsorptive stripping voltammetry, the supporting electrolyte concentration had a significant influence on the peak current enhancement [13]. With the compounds studied here, no effect was observed when the concentration of the supporting electrolyte was varied in the range 10^{-3}—10^{-1} M. The accumulation effect was, however, suppressed when more concentrated electrolyte solution was used; in 1 M supporting electrolyte, the peak current decreased by ca. 40%.

Interferences

The presence of chloride, which exhibits a well defined c.s.v. response, did not affect the reduction peaks of compounds I—V unless chloride was present in $>10^5$-fold molar excess, when the peaks became distorted. As expected, the interfering effect of surface-active substances such as gelatin or Triton X-100 is more serious because of competition for the adsorption sites. The presence of 10^{-3}% Triton X-100 in the analyzed solution caused a decrease in the peak current. With the studied compounds (at a concentration of 10^{-8} mol l^{-1}), the decrease of the peak current corresponded to more than 60% of the peak current recorded in the absence of the surfactant. This interference was reduced by shortening the accumulation time, but this increased the detection limit, of course. To eliminate the interfering effect of surfactants, it was necessary to apply a separation procedure. Good results

(99% recovery) were attained with Cyadox and Carbadox when a molecular-exclusion separation was used (Sephadex G-25 column with 5 mm i.d., 60 mm long, flow rate 0.5 ml min^{-1}) with 0.1 M sodium perchlorate containing 5% (v/v) DMF as eluent.

Analysis of veterinary samples

The method based on adsorptive accumulation of these quinoxaline derivatives was applied for the determination of Cyadox, Carbadox and Olaquindox in the extracts of feed mixtures, animal urine and blood plasma without separation of surfactants. The results of these determinations were in good agreement with the results obtained by polarography (feed mixtures) and radiochemical methods. Detailed procedures will be published elsewhere. The main advantage of the proposed mode of determination is its high sensitivity and precision. Because quinoxaline-2-carboxylic acid (V) is supposed to be the final product of the metabolism of Carbadox [4], the voltammetric determination of this compound may find application in the analysis of animal tissues and organs.

REFERENCES

1 Toxicology data on Carbadox and its metabolites, Pfizer, Brussels, 1975.
2 Y. Kidami, K. Ohira and H. Koike, J. Pharm. Soc., Jpn., 93 (1973) 157.
3 N. K. Dutt and G. S. Sanyal, Fresenius Z. Anal. Chem., 258 (1973) 107.
4 I. Šestáková and P. Škarka, Biol. Chem. Vet., 14 (1978) 15.
5 I. Šestáková, P. Škarka and O. Manoušek, Biol. Chem. Vet., 16 (1980) 29.
6 P. Škarka and I. Šestáková, Biol. Chem. Vet., 16 (1980) 403.
7 I. Šestáková and P. Škarka, Biol. Chem. Vet., 18 (1982) 311, 20 (1984) 559.
8 L. Novotný and I. Smoler, J. Electroanal. Chem., 146 (1983) 183.
9 C. A. Mairesse-Ducarmois, G. J. Patriarche and J. L. Vandenbalck, Anal. Chim. Acta, 71 (1974) 165.
10 T. M. Florence, J. Electroanal. Chem., 97 (1979) 219.
11 R. Kalvoda, Anal. Chim. Acta, 162 (1984) 197.
12 M. T. Stankovich and A. J. Bard, J. Electroanal. Chem., 75 (1977) 487.
13 J. Wang, Am. Lab., May 1985, p. 41.

Analytica Chimica Acta, 186 (1986) 31—38
Elsevier Science Publishers B.V., Amsterdam — Printed in The Netherlands

DETERMINATION OF TRACES OF STREPTOMYCIN AND RELATED ANTIBIOTICS BY ADSORPTIVE STRIPPING VOLTAMMETRY

JOSEPH WANG* and JAWAD S. MAHMOUD

Department of Chemistry, New Mexico State University, Las Cruces, NM 88003 (U.S.A.)

(Received 25th February 1986)

SUMMARY

Adsorptive stripping voltammetry provides sensitive determinations of trace amounts of the saccharide-related antibiotics, streptomycin, erythromycin and novobiocin. A static mercury drop electrode is immersed in a stirred alkaline solution of the drug for a fixed time (60—300 s) at a suitable potential, and the adsorbed species is then stripped in the linear-scan or differential-pulse mode. The preconcentration potentials and stripping peak potentials (vs. Ag/AgCl) are, respectively, —1.2 V and —1.58 V for streptomycin, —0.9 V and —1.2 V for erythromycin, and —1.0 V and —1.38 V for novobiocin. The interfacial behavior is discussed. Short preconcentration periods suffice to quantify streptomycin, novobiocin, and erythromycin down to the 7×10^{-10} M, 2.5×10^{-9} M, and 1.3×10^{-8} M levels, respectively. Streptomycin added to urine can be quantified after simple dilution.

Streptomycin is a trisaccharide derivative that is important in tuberculosis therapy and the treatment of other infections such as tularemia and plague. The electrochemical reduction of streptomycin, involving the aliphatic aldehyde group, has been exploited for polarographic measurements of the drug [1—3]. The use of alkaline medium is required because of the negative redox potential and the diminishing response at lower pH levels. With d.c. polarography, millimolar and submillimolar concentrations of streptomycin can be quantified [1, 2], while differential pulse polarography permits detection of micromolar levels [3].

Presented here is a very sensitive adsorptive stripping voltammetric procedure for quantifying traces of streptomycin, and the related saccharide antibiotics novobriocin and erythromycin. Adsorptive stripping voltammetry is now well-established for trace measurements for numerous electroactive compounds that adsorb reproducibly onto an electrode surface [4]. The adsorption of streptomycin, novobiocin and erythromycin is sufficiently pronounced that immersing the static mercury drop electrode in the stirred sample solution for a few minutes allows convenient quantitation of these antibiotics at the nanomolar concentration level, as described below.

0003-2670/86/$03.50

EXPERIMENTAL

A PAR 264A voltammetric analyzer with a PAR 303A static mercury drop electrode and other equipment were used as described previously [5].

Stock solutions (1×10^{-4} M) of the different antibiotics (Sigma) were prepared daily by dissolution in deionized water (streptomycin, erythromycin) or acetone (novobiocin). Supporting electrolytes were 0.01 M sodium hydroxide for streptomycin, phosphate buffer pH 7.4 for novobiocin, and borate buffer pH 11.6 for erythromycin. Urine samples were obtained from healthy volunteers.

The supporting electrolyte solution (10 ml) was added to the cell and degassed with nitrogen for 8 min. The preconcentration potential was applied to the working electrode for a selected time, while the solution was stirred at 400 rpm. The stirring was then stopped, and after a 15-s rest period, a negative-going scan was initiated, with simultaneous recording of the resulting voltammogram. After background voltammograms had been recorded, aliquots of the antibiotic standard were introduced, and the absorptive stripping cycle was repeated with a new drop. All data were obtained at room temperature.

RESULTS AND DISCUSSION

Streptomycin

Figure 1 shows repetitive cyclic voltammograms for 2.5×10^{-6} M streptomycin in 0.01 M sodium hydroxide. Stirring the solution for 1 min at −1.20 V prior to the first scan (scan 1) yielded large cathodic peaks because

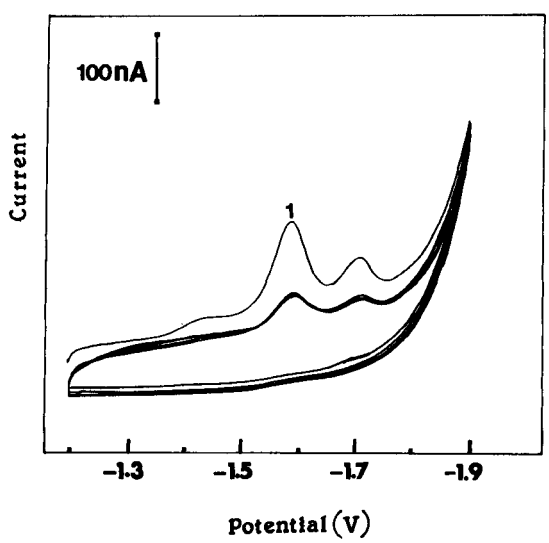

Fig. 1. Repetitive cyclic voltammograms for 2.5×10^{-6} M streptomycin in 0.01 M NaOH, after 1-min stirring at −1.20 V. Scan rate, 50 mV s^{-1}.

of reduction of the accumulated streptomycin. No peaks were observed in the anodic branch. Subsequent repetitive scans yielded substantially smaller cathodic peaks that represent the response of the species in solution (i.e., rapid desorption of the product). For a 1×10^{-6} M solution, full surface coverage was achieved after stirring for 60 s. The charge was estimated to be 3.65 μC by cutting and weighing the recorded peaks. For quantitative purposes, the peak at −1.58 V is most useful. The peak current at saturation increased linearly as the potential scan rate was increased from 5 to 200 mV s^{-1}. The corresponding log (peak current) vs. log (scan rate) had a slope of 1.03. A slope of 1.00 is expected for an ideal reaction of surface species.

The spontaneous adsorption of streptomycin can be used as an effective preconcentration step prior to the voltammetric quantitation of the drug. Figure 2 shows linear-scan voltammograms for 1×10^{-8} M streptomycin after different preconcentration times. Although quantitation at this level is not feasible without preconcentration (curve a), well-defined peaks were observed following preconcentration (curves b—d). The longer the preconcentration time, the more streptomycin is adsorbed, and the larger the peak current (see below). A detection limit near 7×10^{-10} M is estimated based on the signal-to-noise characteristics (S/N = 3) of the response following 300-s preconcentration (curve d). Compared to previous voltammetric procedures for streptomycin [3], the adsorptive stripping procedure lowers the detection limit by four orders of magnitude. Also shown in Fig. 2 are plots of peak current vs. preconcentration time at different streptomycin levels. For the 1×10^{-8} M solution (curve A), the peak current increases linearly with preconcentration time (slope, 3.06 nA min^{-1}; intercept, 0.042 nA; correlation coefficient, 0.999). For the 2.5×10^{-8} M and 5×10^{-8} M solutions, deviations from

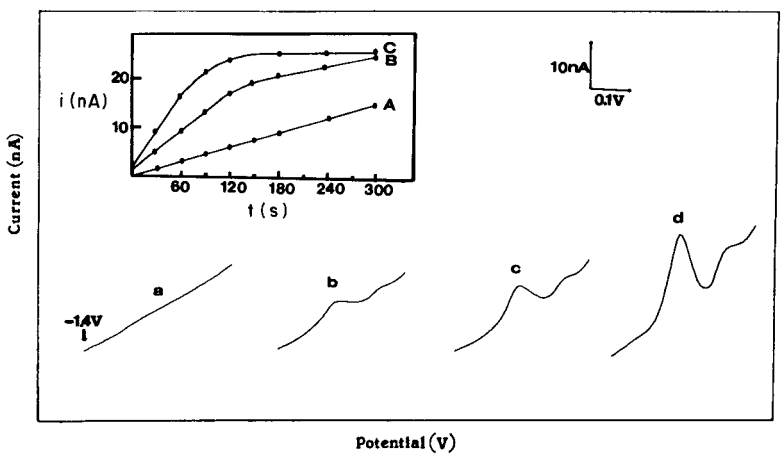

Fig. 2. Effect of preconcentration period on the stripping voltammogram for 1×10^{-8} M streptomycin in 0.01 M NaOH. Preconcentration period: (a) 0, (b) 60, (c) 120, (d) 300 s. Inset are the current/time plots at different concentrations: (A) 1×10^{-8} M; (B) 2.5×10^{-8} M; (C) 5×10^{-8} M. Other conditions as in Fig. 1.

linearity are observed as full surface coverage is approached, i.e., at periods longer than 120 and 90 s, respectively.

The adsorptive stripping response strongly depends on the electrolyte concentration (Fig. 3, curve a). Maximum peak height occurs with 0.01 M sodium hydroxide. The effect of the preconcentration potential on the streptomycin peak current was examined over the range −0.2 to −1.4 V (Fig. 3, curve b). Optimal conditions are obtained at −1.2 V. Electrocapillary measurements were done for a 2×10^{-4} M streptomycin solution (not shown). The surface tension (drop time) of the DME was decreased relative to the blank solution over the range −0.3 to −1.3 V. These results indicate significant adsorption over a wide potential range, as was indicated also from curve (b) of Fig. 3.

Forced convection during the preconcentration period affects the stripping peak current by increasing the rate of transport of streptomycin molecules to the electrode surface. For example, a 4-fold peak enhancement was obtained for a stirred (400 rpm) solution compared with a quiescent one (1×10^{-7} M streptomycin, preconcentration for 60 s). The differential-pulse cathodic stripping response was compared to that obtained in corresponding linear-scan stripping measurements. Although both stripping modes yielded significant peak current enhancement compared to the response without preconcentration, the linear-scan mode offers improved performance in terms of sensitivity and speed. This mode was used throughout.

Quantitative evaluation was based on the dependence of the peak current on the streptomycin concentration. Figure 4 shows voltammograms for solutions of increasing streptomycin concentration, from 2×10^{-8} M to 1×10^{-7} M, after preconcentration for 30 s. Well-defined stripping peaks were observed over this concentration range. In contrast, the corresponding responses from the solution (dotted lines) are not useful for quantitative work. The calibration plots obtained at different preconcentration times are also shown. For 30-s preconcentration (plot B), the response is linear for the entire range (slope, 1.50 nA/10^{-8} M; intercept, 0.55 nA; correlation coef-

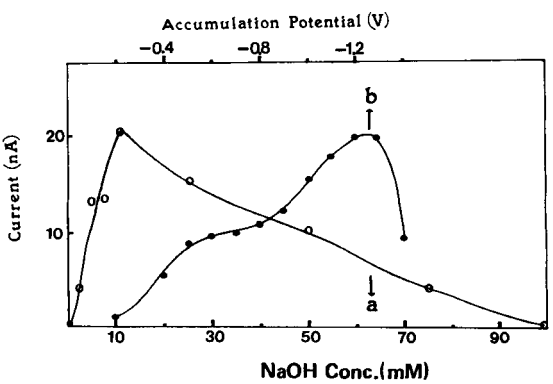

Fig. 3. Effects of (a) NaOH concentration, and (b) preconcentration potential, on the streptomycin peak current. Streptomycin concentration: (a) 5×10^{-8} M; (b) 1×10^{-7} M. Preconcentration time: (a) 60; (b) 30 s. Other conditions as in Fig. 1.

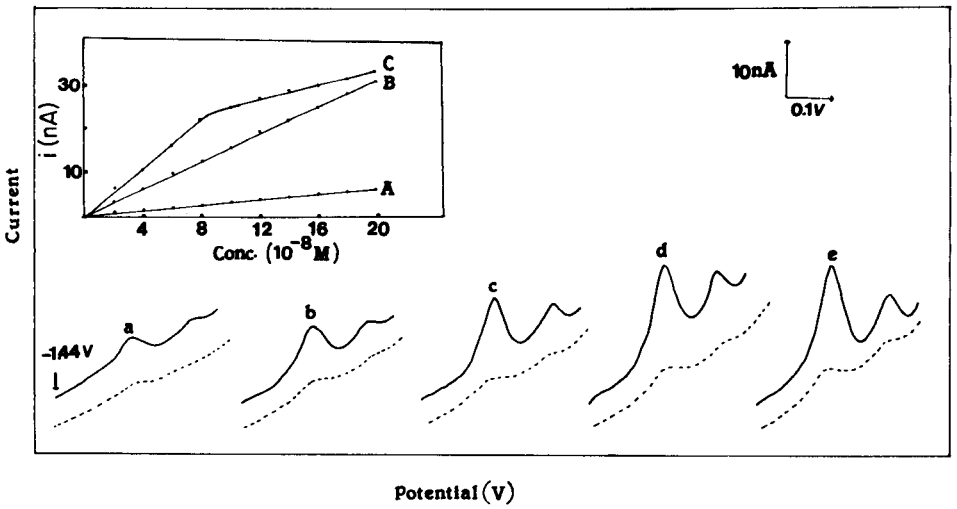

Fig. 4. Stripping voltammograms obtained for solutions containing 2—10 × 10^{-8} M streptomycin concentration (curves a—e). Preconcentration period, 30 s; other conditions as in Fig. 1. Dotted lines represent the response without preconcentration. Inset are the calibration plots after different preconcentration times: (A) 0, (B) 30, (C) 60 s.

ficient, 0.999). The 60-s plot (plot C) deviates from linearity as expected: the slope of the initial linear portion is 2.56 nA/10^{-8} M; intercept, 0.72 nA; correlation coefficient, 0.998. The reproducibility was estimated by ten successive measurements on a stirred 4 × 10^{-8} M streptomycin solution (60-s preconcentration); the mean peak current was 18.1 nA with a range of 16.6—18.9 nA, and a relative standard deviation of 5.1%.

Various species that are likely in biological samples can influence the preconcentration or measurement steps. Therefore, the effects of possible interferences on the adsorptive stripping response of 1 × 10^{-7} M streptomycin were evaluated (conditions as in Fig. 1). Additions of 15 μg ml^{-1} albumin or camphor did not affect the streptomycin response. As expected, gelatin caused significant (90%) depression of the peak current. Zinc (2 μg ml^{-1}) produced an overlapping peak (at −1.35 V); this interference was also reported for differential-pulse measurements but was removed with EDTA [3].

Data for streptomycin in a diluted urine sample are illustrated in Fig. 5. The sensitivity of the adsorptive stripping procedure permits assays of untreated urine samples containing micromolar concentrations of streptomycin, after sample dilution to minimize matrix effects (curve b). In contrast, no response is observed in the corresponding voltammogram without preconcentration (curve c), or in the unspiked sample (curve a). Urine samples collected from different volunteers yielded response characteristics similar to those shown in Fig. 5. It may be possible to apply the method to urine samples containing lower levels of the drug, or to other body fluids, by using a clean-up procedure instead of the dilution step.

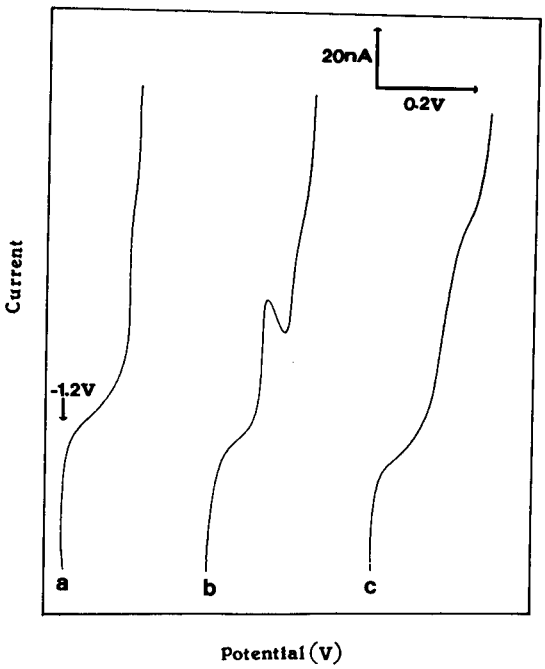

Fig. 5. Voltammograms for a urine sample: (a) control urine (diluted, 1:20 with 0.01 M NaOH); (b, c) urine with 1×10^{-6} M streptomycin added (and diluted 1:20 with 0.01 M NaOH). Preconcentration time: (a, b) 60 s; (c) 0 s. Other conditions as in Fig. 1.

Quantitation of novobiocin and erythromycin

Little has been published on the voltammetric behavior and quantitation of the saccharide-related antibiotics, novobiocin and erythromycin [3], despite their increasing pharmaceutical utility. Adsorptive stripping voltammetry permits quantitation of these drugs down to the nanomolar concentration level. For example, 5×10^{-8} M novobiocin can be quantified after a short preconcentration period (Fig. 6A); the response without preconcentration does not permit quantitation. The redox process of this glycoside (used for treatment of various bacterial infections) probably involves the reaction of the quinone group. A detection limit of 2.5×10^{-9} M is estimated based on the signal-to-noise characteristics (S/N = 3) of the adsorptive stripping peak at −1.38 V.

Various electrolytes were screened to find the optimal conditions for novobiocin (5×10^{-7} M) after a 30-s preconcentration. No response was observed in acetate buffer (pH 4.8), but peak current enhancements (relative to no preconcentration) of 3.2, 6.0, 8.6, and 10.5 were obtained in borate buffer (pH 10.4), 0.1 M ammonium acetate, 0.01 M sodium hydroxide, and 0.05 M phosphate buffer (pH 7.4), respectively. The phosphate buffer was used because it also offered the best signal-to-background characteristics. A preconcentration potential of −1.0 V yielded the most useful response; pre-

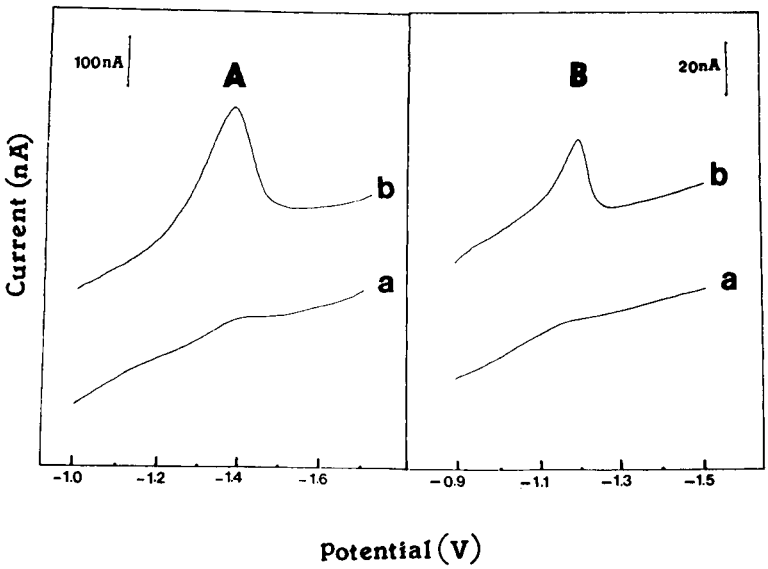

Fig. 6. Voltammograms for (A) 5×10^{-8} M novobiocin and (B) 2×10^{-7} M erythromycin, (a) without and (b) with preconcentration. For curves (b), preconcentration time and potential: (A) 240 s at —1.0 V; (B) 120 s at —0.9 V. Conditions: (A) 0.05 M phosphate buffer pH 7.4, differential-pulse stripping with 5 mV s^{-1} scan rate and 50-mV pulse amplitude; (B) 0.025 M borate buffer pH 11.6, linear-scan stripping with 50 mV s^{-1} scan rate.

concentration potentials of —0.4 V to - 1.0 V were checked. The differential-pulse waveform was preferred over the linear-scan mode because it offered improved response characteristics.

The dependence of peak height on novobiocin concentration was evaluated for a series of eight samples (5×10^{-8} M increments) with a 60-s preconcentration step and other conditions as for Fig. 6A. The resulting calibration plot reflected the adsorption isotherm. For conditions of low surface coverage, i.e., concentration lower than 2×10^{-7} M, linear dependence was observed (slope of the linear portion, 1.61 nA/10^{-8} M; intercept, 0.86 nA; correlation coefficient, 0.999). Curvature (toward the concentration axis) was observed at higher concentrations. Thus, calibration plots should be used for quantitation. For a 5×10^{-8} M novobiocin solution, the peak current increased linearly with the preconcentration time over the entire range (0—240 s) examined (slope, 0.096 nA s^{-1}).

In addition to novobiocin and streptomycin, the adsorptive stripping method yields substantial improvements in sensitivity for erythromycin, a streptomyces species containing a large lactone ring. A short preconcentration period (120 s) yields a well-defined stripping peak (at —1.2 V) that allows convenient quantitation of 2×10^{-7} M erythromycin (Fig. 6B). A detection limit of 1.3×10^{-8} M erythromycin is estimated based on the signal-to-noise characteristics of the adsorptive stripping voltammogram.

A 0.025 M boric acid solution (adjusted to pH 11.6 with sodium hydroxide) yielded the best response characteristics and peak-current enhancement among six alkaline electrolytes examined. A preconcentration potential of —0.9 V and the linear scan mode yielded the most useful results and were used for erythromycin quantitation.

Nonlinear dependences were observed when the erythromycin peak current was plotted against concentration or preconcentration time. For a series of eight 2×10^{-7} M increments, the calibration plot was linear up to 1×10^{-6} M (slope, 9.76 nA/10^{-7} M; intercept, 0.47 nA; correlation coefficient, 0.997; 60-s preconcentration; other conditions as in Fig. 6B). The time-dependence plot exhibited linearity up to 120 s (slope of 0.30 nA s^{-1}; intercept, —0.27 nA; correlation coefficient, 0.996; 2×10^{-7} M erythromycin; other conditions as in Fig. 6B).

This work was supported by the National Institute of Health, Grant No. GM30912-02.

REFERENCES

1 G. B. Levy, P. Schwed and J. W. Sackett, J. Am. Chem. Soc., 68 (1946) 528.
2 L. Doan and B. E. Riedel, Can. Pharm. J. Sci., 96 (1963) 109.
3 H. Siegerman, in A. J. Bard (Ed.), Electroanalytical Chemistry, Vol. 11, M. Dekker, New York, 1979, p. 291.
4 See, e.g., J. Wang, Am. Lab., 17(5) (1985) 41.
5 J. Wang, P. A. Farias and J. S. Mahmoud, Anal. Chim. Acta, 172 (1985) 57.

Analytica Chimica Acta, 186 (1986) 39—47
Elsevier Science Publishers B.V., Amsterdam — Printed in The Netherlands

DETERMINATION OF TRACES OF PURINE BY CATHODIC STRIPPING VOLTAMMETRY AT THE HANGING COPPER AMALGAM DROP ELECTRODE

STEFAN GŁODOWSKI, RENATA BILEWICZ and ZENON KUBLIK*
Department of Chemistry, University of Warsaw, Pasteura 1, Warsaw 02093 (Poland)
(Received 9th January 1986)

SUMMARY

In the presence of purine, the copper(II)/copper(Hg) couple splits into copper(II)/copper(I) and copper(I)/copper(Hg) couples, which form two well-separated systems of peaks under voltammetric conditions. The copper(I)/purine complex adsorbs on the electrode surface and can be deposited on the electrode surface by electroreduction of copper(II) ions at the HMDE or by electro-oxidation of the hanging copper amalgam drop electrode (HCADE). The deposit can be stripped either cathodically or anodically over the pH range 2—9. The cathodic stripping variant at the HCADE, in solution with pH 2, offers the best results, with linear response for the range 5×10^{-9}—1.5×10^{-7} mol dm^{-3} purine after an accumulation time of 3 min. The detection limit found with the HMDE in the presence of copper(II) ions is higher.

Cathodic stripping voltammetry (c.s.v.) at mercury electrodes has been successfully exploited for the determination of traces of many organic compounds [1, 2]. Paleček and co-workers [3, 4] have shown that traces of purine derivatives can also be determined; some purine bases react with mercury to form sparingly soluble compounds on the electrode surface, but the c.s.v. stripping peaks of purines so obtained are located quite close to the mercury dissolution potential and can be severely masked under certain conditions.

For several analytes, it has been shown that accumulation on the electrode surface in the form of a compound with copper ions, shifts the location of the stripping peaks towards more negative potentials than the stripping peaks of the corresponding mercury compounds. Effects of this type have been observed with the hanging copper amalgam drop electrode (HCADE) [5], a copper amalgam film electrode [6], and with a hanging mercury drop electrode (HMDE) in the presence of Cu(II) ions in solution [5, 7].

The aim of the present work was to assess the possibilities of the HCADE and the HMDE for determining traces of purine by stripping techniques. According to Florence [1] and Paleček [3, 4], purine did not yield a c.s.v. peak at the HMDE. Under polarographic conditions, purine is electro-reduced in two irreversible stages [8]. Additional anodic signals corresponding to the

0003-2670/86/$03.50

re-oxidation of unstable products of electro-reduction were observed by Elving et al. [9] in cyclic voltammetry. There are at least some adsorption effects. Tensammetric and electrocapillary studies by Dryhurst and Elving [10] showed that in moderately acidic solutions purine is adsorbed at the mercury electrode surface at about the electrocapillary maximum.

EXPERIMENTAL

Voltammetric curves were recorded with a Radelkis OH-105 polarograph and differential pulse voltammograms with a Unitra PP04 pulse polarograph connected with a Kabid-Press 6801 X-Y recorder. A conventional three-electrode cell was used. The reference electrode was a saturated calomel electrode (SCE) and all the potentials reported here are referred to this electrode; the counter electrode was a platinum foil (ca. 2 cm^2). The indicating electrode was the HMDE [11] or the HCADE. For the latter, the container of the HMDE was filled with a saturated copper amalgam, prepared by dissolving copper foil in mercury. The concentration of copper in the amalgam was determined on the basis of the Ševčik-Randles equation from the height of the copper dissolution peak. The copper concentration in the amalgam was 3.3×10^{-3} mol dm^{-3} unless otherwise stated. Surface areas of the HMDE and the HCADE were 2.4 mm^2. The quantity of electricity passed during recording of the stripping peaks was calculated from the peak areas.

A stock 1×10^{-3} mol dm^{-3} solution of purine (International Enzymes) was prepared daily. Aliquots of this solution were added to the deaerated supporting electrolyte from a microsyringe. All other chemicals were of reagent grade. Water was distilled thrice. Before voltammetry, the solutions were deoxygenated by passing argon for 10 min. Most experiments were done at room temperature (20 ± 2°C). Calibration plots were constructed from measurements under thermostated conditions (20 ± 0.1°C). During the accumulation step, the solutions were stirred magnetically; the subsequent quiescent period was 30 s.

RESULTS

Cyclic voltammetry

Figure 1 compares the cyclic voltammetric curves obtained with the HMDE and the HCADE for acetate-buffered solution containing 2×10^{-5} mol dm^{-3} purine. With the HMDE, there are two irreversible cathodic peaks, in accordance with earlier polarographic [8] and voltammetric [9] results. There is no evidence of reaction between purine and mercury, also in agreement with earlier results [3, 4]. At the HCADE, however, these irreversible cathodic peaks are accompanied by a semi-reversible system of peaks around −0.4 V. The shape of the cathodic peak in curve B indicates that the copper/purine complex produced during the anodic scan accumulates on the electrode surface.

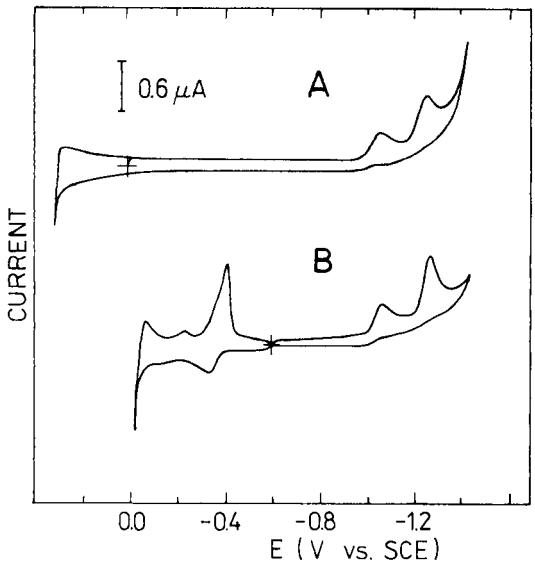

Fig. 1. Cyclic voltammetric curves for 2×10^{-5} mol dm^{-3} purine: (A) at the HMDE; (B) at the HCADE. Acetate buffer, pH 4.8; scan rate 4 V min^{-1}.

Figure 2 illustrates the influence of pH on the cyclic voltammograms obtained at the HMDE and HCADE. The curves obtained at the HMDE show no signals that could be interpreted as a reaction between purine and mercury, whereas reactions proceed over the entire pH range tested with the

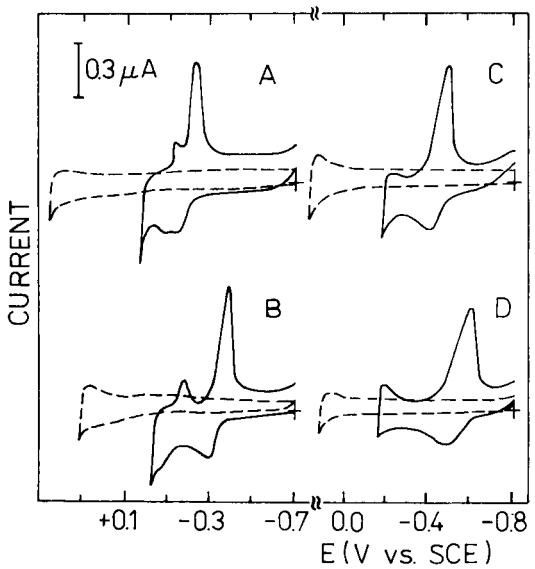

Fig. 2. Effect of pH on the cyclic voltammetric curves for 2×10^{-5} mol dm^{-3} purine: (---) at the HMDE; (—) at the HCADE. Buffer: (A) 0.1 mol dm^{-3} $LiClO_4$, pH 2; (B) acetate, pH 4.8; (C) phosphate, pH 7.0; (D) borate, pH 9.2. Scan rate 4 V min^{-1}.

HCADE. In acidic solutions, the main peaks are accompanied by a small additional system at slightly more positive potential. At higher pH, only the larger peaks remain, shifted towards more negative potentials. The location of the cathodic peak on the potential axis (in mV) as a function of pH can be described by the relation $E_p^c = -132 - 49$ pH, which is valid over the pH range 2—9.2. Below pH 1, the main peaks are seriously affected by the currents corresponding to the formation and reduction of Cu(II) ions. The occurrence of additional voltammetric peaks as shown in curves A and B is sometimes explained on the basis of the Wopschall and Shain theory [12] of adsorption processes. However, in the present case, such an explanation cannot be satisfactory. The peak splitting occurred on the curves obtained for markedly smaller concentration of purine, where the amount of deposited material was much lower than the amount needed to cover the electrode surface with a monolayer of deposit. It is more probable that the peak splitting reflects the occurrence of a multistage electrode process. When such a problem is studied, it is better to work not with a high concentration of copper amalgam but with a low concentration of Cu(II) ions in solution.

Figure 3 shows the influence of purine on the curves of the Cu(II)/Cu(Hg) system obtained at the HMDE in the presence of Cu(II) ions; the absence of the high concentration of copper in amalgam extends the useful potential range to more positive potentials. The dashed curves obtained in the absence of purine correspond to the reversible two-electron Cu(II)/Cu(Hg) process. The addition of 2×10^{-5} mol dm^{-3} purine changes the cyclic voltammogram. Peak c_2 (Fig. 3A) corresponding to the electro-reduction of aquated copper-(II), decreases and the cathodic peaks c_1 and c_3 appear on the cyclic curve. The abrupt decay of peak c_3 indicates that this peak is related to reduction of the adsorbed substance. Similar changes appeared on the anodic branch of the cyclic curve; the anodic peak a_1 is much sharper than the other peaks. Reversal of the scan direction at point X produced peak a_1, i.e., peaks a_1 and c_1 correspond to the same couple. Increased concentrations of purine increased the heights of peaks c_1, c_3, a_1 and a_3 but decreased the heights of the peaks c_2 and a_2. It is apparent that purine affects the copper(II)/copper(Hg) couple similarly to ammonia [13], i.e. the single two-electron process is split into two one-electron processes. When the potential scan was stopped at point X for several minutes, the height of peaks a_1 or c_3 increased, i.e. at this potential the copper(I)/purine complex is accumulated on the electrode surface. At pH 4.8 (Fig. 3), the a_1/c_1 peaks shifted to more positive potentials and the c_3/a_3 peaks to more negative potentials. In neutral solution, the c_1/a_1 peaks were masked by the mercury dissolution current.

Stripping voltammetry

Figure 4 shows a comparison of stripping curves for 2×10^{-7} mol dm^{-3} purine obtained under different experimental conditions; curves A, A′ and A″ were obtained at the HCADE and curves B and B′ at the HMDE with copper(II) ions in solution. In both cases, the copper(I)/purine complex was

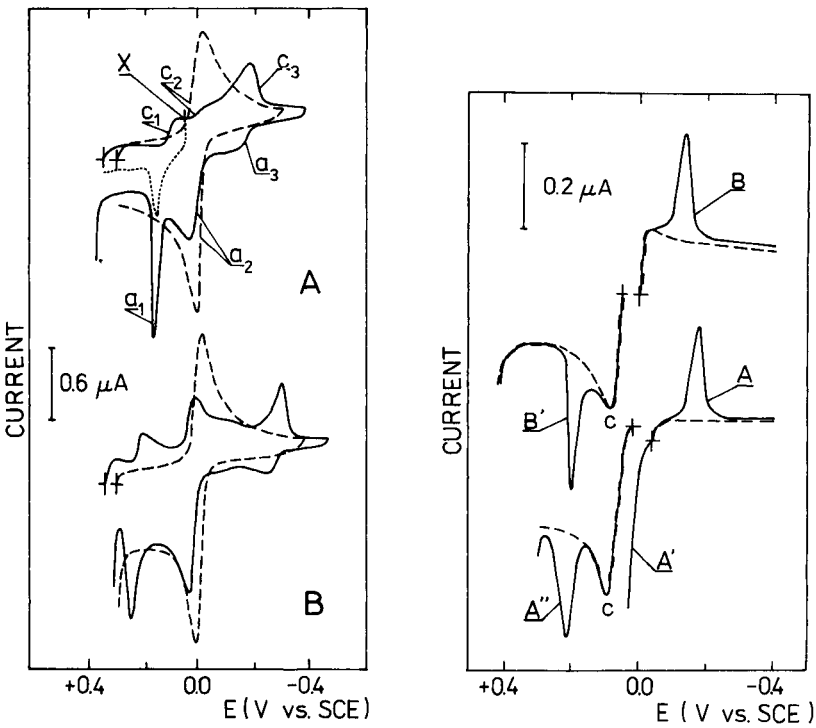

Fig. 3. The influence of purine on the cyclic voltammetric curves of the system Cu(II)/Cu(Hg) obtained at the HMDE. Solutions: (A) 0.1 mol dm^{-3} $LiClO_4$, pH 2; (B) acetate buffer, pH 4.8; (---) 1×10^{-4} mol dm^{-3} Cu(II); (—) 1×10^{-4} mol dm^{-3} Cu(II) + 2×10^{-5} mol dm^{-3} purine. (· · ·) Obtained with voltage scan reversed at point X; scan rate 2 V min^{-1}.

Fig. 4. (A, A″) Cathodic (A) and anodic (A′, A″) stripping curves at the HCADE with saturated (A, A′) and 1.4×10^{-4} mol dm^{-3} (A″) copper amalgam. (B, B′) Cathodic (B) and anodic (B′) stripping curves at the HMDE in presence of 3×10^{-5} mol dm^{-3} Cu(II) ions. Conditions: 0.1 mol dm^{-3} $LiClO_4$, pH 2; 2×10^{-7} mol dm^{-3} purine; 1-min accumulation at the potentials marked by +; scan rate 2 V min^{-1}. (---) Background currents. Peak C is explained in the text.

deposited on the electrode in the accumulation step. After accumulation, the electrode was polarized either towards negative potentials (curves A and B) or towards positive potentials (curves A′, A″ and B′). The background currents (dashed curves) are lowest and flattest with the amalgam electrodes. The enhanced background current in case B is caused by reduction of copper(II) ions. A decreased copper(II) ion concentration would decrease not only the background current but also the purine stripping peak.

In principle, case B′ should also produce a small flat background current because copper(II) ions cannot be oxidized. However, in practice, some copper(II) is reduced to copper amalgam during the accumulation and oxidation of this amalgam produces the harmful peak C. A shift of the accumulation potential to more positive values decreases peak C, but then the stripping

peak also diminishes. In case A', the background current is significant because of copper dissolution from the saturated copper amalgam, and the stripping peak of purine is completely masked. A decrease in the copper concentration in the amalgam decreases the copper dissolution current; curve A'' obtained under such conditions shows that the stripping peak of purine is then better separated from peak C. Comparison of the different modes of obtaining the stripping peaks for purine indicates that c.s.v. at the HCADE offers the best conditions for determining the traces of purine. The height of the stripping peaks of purine depends on the concentration of copper in the amalgam or copper(II) ions in solution. For small amounts of copper or copper(II) ions, the effect is significant, but when the ratio of the copper to the purine concentrations exceeds 100, further increase in the copper concentration has, in practice, no influence.

Variations in pH of the solution from 2 to 9 led to a systematic shift of the stripping peak to more negative potentials; the peak shape deteriorated and its height decreased by about 50%. Nevertheless, in borate buffer solution, the plot of i_p vs. purine concentration was linear over the range 2×10^{-8}—1×10^{-7} mol dm^{-3}. However, the best signals were obtained in acidic solution with pH 2.

The accumulation potential has a marked effect on the height of the stripping peak; the optimum potential must be found experimentally for each set of conditions studied. The height of the cathodic stripping peak obtained at the HCADE from 1×10^{-7} mol dm^{-3} purine at pH 2 remained constant provided that the accumulation potential was 140—180 mV more positive than the potential of the stripping peak.

Figure 5 illustrates the shapes of the cathodic stripping peaks obtained for very low concentrations of purine. For 5×10^{-9} mol dm^{-3} purine, the strip-

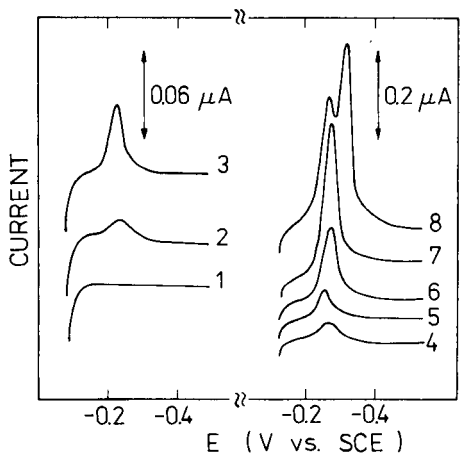

Fig. 5. Cathodic stripping curves obtained at the HCADE in 0.1 mol dm^{-3} $LiClO_4$ solution, pH 2, containing different concentrations of purine: (1) 0; (2) 5×10^{-9}; (3) 2×10^{-8}; (4) 5×10^{-8}; (5) 1×10^{-7}; (6) 2×10^{-7}; (7) 4×10^{-7}; (8) 8×10^{-7} mol dm^{-3}. Accumulation at —0.1 V: (1—3) 3 min; (4—8) 1 min. Scan rate 2 V min^{-1}.

ping peak is small but still useful; at 8×10^{-7} mol dm^{-3} purine, the peak splits. Plot A (Fig. 6) shows the dependence of the peak height on purine concentration; at the higher purine concentrations, the peak height becomes constant, at a value corresponding to the formation of a monolayer of the copper(I)/purine deposit. The quantity of electricity involved in the formation of the monolayer was 31 ± 2 μC cm^{-2}. The dependence of the stripping peak height on the accumulation time is shown in Fig. 6 (curve B); for accumulation times exceeding 3 min, the peak attains a constant height though its width increases slightly. The quantity of electricity involved in the formation of the highest peak was 34 μC cm^{-2}, but the value obtained on the basis of the plot 6A is probably more reliable.

The calibration plot obtained for 3-min accumulation times was linear over the range 5×10^{-9}—1.5×10^{-7} mol dm^{-3} purine with a correlation coefficient 0.9979. The relative standard deviation for eight measurements of 1×10^{-7} mol dm^{-3} purine was 4.1%.

The copper(I)/purine complex accumulated on the HCADE can also be stripped by differential-pulse voltammetry. The differential-pulse stripping peaks at pH 2 for different concentrations of purine were about twice the height of those obtained by the conventional technique, but this advantage cannot be properly exploited because the background currents obtained by the pulse mode were poorly defined.

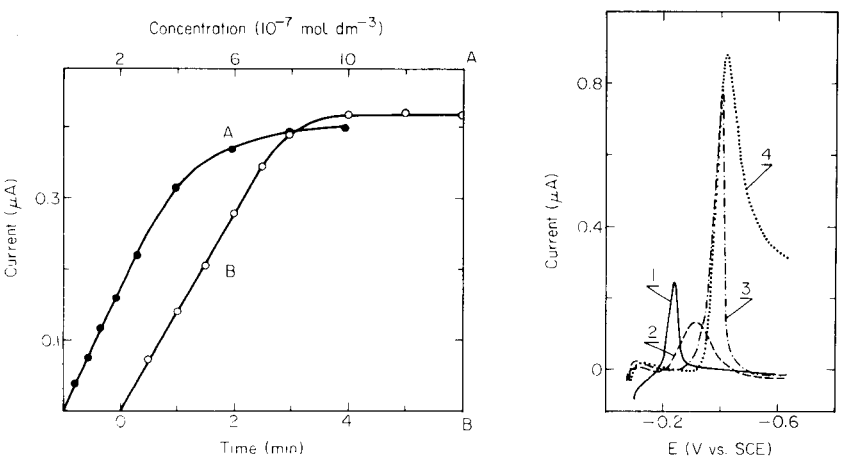

Fig. 6. Plots of the stripping peak height against: (A) concentration of purine for 1-min accumulation; (B) accumulation time for 1.5×10^{-7} mol dm^{-3} purine. Conditions: 0.1 mol dm^{-3} $LiClO_4$, pH 2; accumulation potential —0.1 V; scan rate 2 V min^{-1}.

Fig. 7. (1—3) Cathodic stripping peaks obtained after 1-min accumulation for: (1) 2×10^{-7} mol dm^{-3} purine; (2) 1×10^{-6} mol dm^{-3} iodide; (3) 1×10^{-6} mol dm^{-3} thiocyanate; (4) electro-reduction peak of 1×10^{-4} mol dm^{-3} lead(II). Conditions: 0.1 mol dm^{-3} $LiClO_4$ at pH 2, HCADE, scan rate 2 V min^{-1}.

Interferences

In general, purine and its derivatives are a very stable class of compounds [14], but certain purine bases react with mercury under open circuit conditions [3]. In the present work, solutions of purine (pH 2) were left for 2 h in contact with the copper amalgam under moderate stirring conditions, and the stripping peaks were found to have unchanged height. Accordingly, no special precautions were taken to prevent contact of the solution with the detached mercury or copper amalgam droplets.

The cathodic stripping peaks of the copper(I)/purine complex were not affected by common components of supporting electrolytes such as sulphate or nitrate at concentrations of 0.2 mol dm^{-3}, or phosphate at <0.05 mol dm^{-3}. The presence of chloride ions increased the height of the stripping peak and decreased its width; with increasing concentrations of chloride, the anodic limit and the stripping peak shifted toward more negative potentials but the stripping peak shifted more slowly and so became distorted. In solutions containing 2×10^{-7} mol dm^{-3} purine, interference occurred with $\geqslant 0.1$ mol dm^{-3} chloride; for lower purine concentrations, less chloride was tolerated.

Figure 7 shows the peaks of several substances which may affect the stripping peak for purine; these curves were obtained separately for each component. Traces of lead(II) ions occur frequently as contaminants, but it is apparent from the positions of the peaks in Fig. 7 that at pH 2 even significant concentrations of lead(II) ions will not affect the stripping peak of purine. However, in less acidic solutions, the overlap of the peaks is significant.

Generally, the formation of mixed deposits is harmful in cathodic stripping determinations. Significant interferences occurred when cathodic stripping curves were recorded for purine in the presence of thiocyanate or iodide. In particular cases, it may be possible to avoid such interfering effects if the accumulation potentials can be made sufficiently negative to prevent deposition of the component with most positive accumulation potential. Unfortunately, the stripping peak of the copper(I)/purine complex is located at the most positive potential and so the influence of iodide and thiocyanate cannot be avoided in this manner.

DISCUSSION

The copper amalgam electrode offers a new approach to the cathodic stripping voltammetry [5, 6], widening the possibilities of this technique. For example, traces of thiocyanate cannot be determined by stripping from the HMDE but can be determined successfully at the HCADE [5]. Similarly, traces of benzotriazole cannot be determined at the HMDE in presence of chloride but can be determined at a copper amalgam film electrode [6]. The present work confirms the advantages of the HCADE in c.s.v. Traces of purine do not give any c.s.v. signal at the HMDE but do give a signal at the HCADE over a wide region of pH from 2 to 9.

The results presented show clearly that purine is accumulated on the electrode surface as a copper(I)/purine complex. The quantity of electricity involved in the formation of a monolayer of this complex is 31 ± 2 μC cm^{-2}. This value is markedly lower than the values reported for other copper(I) deposits, e.g., 113 μC cm^{-2} [5] for copper(I) iodide and 60 or 70 μC cm^{-2} [15] for the first and second monolayers of copper(I) thiocyanate, respectively. Obviously, the deposited copper(I)/purine complex covers a much larger surface area than the inorganic copper(I) molecules.

In principle, a compound deposited on the electrode surface in an intermediate oxidation state can be electro-reduced or electro-oxidized, i.e., it can be exploited analytically by cathodic or anodic stripping voltammety. The results presented above showed that the advantages of the cathodic or anodic stripping depend on the oxidation state of the substrate used in the accumulation step. For cathodic stripping, it is better to prepare the deposit by oxidation, whereas for anodic stripping it is better to prepare the deposit by reduction of the ions added to the solution.

This work was done as part of the Project MR I 32 and CPBP.01.17.

REFERENCES

1 T. M. Florence, J. Electroanal. Chem., 97 (1979) 219.
2 K. Z. Brainina, Bioelectrochem. Bioenerg., 8 (1981) 479.
3 E. Paleček, Anal. Biochem., 108 (1980) 129.
4 E. Paleček, Anal. Lett., 13 (1980) 331. E. Paleček, F. Jelen, Mac AnH Hung and J. Lasovsky, Bioelectrochem. Bioenerg., 8 (1981) 621.
5 R. Bilewicz and Z. Kublik, Anal. Chim. Acta, 123 (1981) 201; 171 (1985) 205.
6 M. Donten and Z. Kublik, Anal. Chim. Acta, 185 (1986) 209.
7 U. Forsman, J. Electroanal. Chem., 111 (1980) 325; 122 (1981) 215; Anal. Chim. Acta, 146 (1983) 71.
8 D. L. Smith and P. J. Elving, J. Am. Chem. Soc., 84 (1962) 1412.
9 P. J. Elving, S. J. Pace and J. E. O'Reilly, J. Am. Chem. Soc., 95 (1973) 647.
10 G. Dryhurst and P. J. Elving, Talanta, 16 (1969) 855.
11 W. Kemula and Z. Kublik, Anal. Chim. Acta, 18 (1958) 104.
12 R. H. Wopschall and I. Shain, Anal. Chem., 39 (1967) 1527, 1535,1514.
13 M. Stackelberg and H. Freyhold, Z. Elektrochem., (1940) 120.
14 G. Dryhurst, Electrochemistry of Biological Molecules, Academic Press, New York, 1977, p. 77.
15 R. Bilewicz and Z. Kublik, J. Electroanal. Chem., 195 (1985) 137.

Analytica Chimica Acta, 186 (1986) 49—56
Elsevier Science Publishers B.V., Amsterdam — Printed in The Netherlands

DETERMINATION OF TIN IN THE ng g^{-1} RANGE BY DIFFERENTIAL PULSE POLAROGRAPHY

G. WEBER

Institut für Spektrochemie und Angewandte Spektroskopie, Bunsen-Kirchhoff-Str. 11, D-4600 Dortmund 1 (Federal Republic of Germany)

(Received 6th March 1986)

SUMMARY

A sensitive determination method of tin by differential pulse polarography is described. Addition of tropolone to acetate supporting electrolyte at about pH 4.7 provides a 30-fold signal enhancement, giving a sensitivity comparable to that obtained in anodic stripping voltammetry, but without the need for enrichment by pre-electrolysis. The response is linear over more than three orders of magnitude (1 ng ml^{-1}—5 μg ml^{-1} Sn), allowing measurements within a wide concentration range without changes in sample preparation or measuring conditions. Large amounts of Ti, W, Cr or Mo interfere, but can be removed completely by pre-separation of tin based on extraction with tropolone/toluene and back-extraction into the supporting electrolyte. Results for tin in water and fruit juice are consistent with those obtained by other techniques.

The tin contents of environmental and biological samples cover a wide range, reaching from μg g^{-1} quantities in canned foods down to ng g^{-1} and even pg g^{-1} quantities in water or urine [1]. The most important methods for the determination of tin, especially in the low ng g^{-1} range, are electrothermal atomic absorption spectrometry (a.a.s.) and differential-pulse anodic stripping voltammetry (d.p.a.s.v.). Electrothermal a.a.s., however, suffers from a very narrow linear range and from matrix interferences, which can cause high background signals or even loss of tin during the ashing step. An example of the interferences in voltammetry is overlap of the peaks of tin and lead; a special supporting electrolyte [2, 3] or measuring technique [4, 5] is needed to overcome this difficulty. Further, the necessary pre-electrolysis is time-consuming and is influenced by many factors. This electrochemical enrichment step can be avoided in some cases by the addition of organic complexing agents, which enhance the sensitivity in differential pulse polarography. The enhancement effect can be explained by adsorption and catalytic reduction of the metal chelate at the electrode surface. Examples of this mechanism are nickel and cobalt determinations by differential pulse polarography after addition of dimethylglyoxime [6, 7], or the determination of nickel as dithiocarbamate [8]. Signal enhancement in the voltammetric determination of tin after addition of methylene blue has also been reported [9], but only in combination with an anodic stripping process.

0003-2670/86/$03.50

In the present work, tropolone is used for signal enhancement in the differential-pulse polarographic determination of tin. Tropolone is a widely used complexing agent, which is suitable for the extraction and enrichment of traces of tin [10] and can also be determined by polarography.

EXPERIMENTAL

Equipment and solutions

All measurements were made with a Metrohm Polarecord E-506 with Metrohm VA-Stand E-655. The working conditions were as follows: dropping mercury working electrode with a Ag/AgCl/KCl (3 M) reference electrode and a platinum auxiliary electrode; drop time 1 s; scan rate 4 mV s^{-1}; pulse height 50 mV. The supporting electrolyte was a 0.2 M sodium acetate/acetic acid buffer of pH 4.7, containing 10 mg of tropolone in 100 ml (8.2×10^{-4} M).

Tropolone (98%) was purchased from Janssen Chimica (Beerse, Belgium). Organotin compounds (mono-, di-, and tri-butyltin chlorides) were obtained from Schering (Bergkamen, F.R.G.). All other chemicals were of Merck p.a. quality.

Procedures

General procedures. Optimization of buffer and tropolone concentrations was done by variation of the buffer concentration from 0.01 M to 1.0 M, pH from 3.5 to 6.0, and tropolone concentration from 4×10^{-7} M to 2.5×10^{-3} M. For optimization and interference studies, polarograms were recorded in the range 0 V to −1.2 V. For quantitative work, polarograms were recorded only from −0.6 V to −0.9 V. Tin was determined by the standard addition technique by means of the peak at −0.72 V.

Analyses of water and fruit juice. Water was digested by u.v. photolysis [11] at pH 1. Fruit juice was digested with a mixture of nitric and sulfuric acids. Tin was determined directly or after pre-separation by the following procedure.

Pre-separation of tin. The aqueous sample (20 ml) was mixed in a separatory funnel with 8 ml of hydrobromic acid (47%) and extracted with 8 ml of tropolone in toluene (50 mg in 100 ml) for 10 min. After back-extraction of the organic layer with 20 ml of the supporting electrolyte for 10 min, tin was determined directly in the aqueous layer.

Parallel determinations by electrothermal a.a.s. and a.c.a.s.v. were done as in previously reported procedures [12].

RESULTS AND DISCUSSION

Two polarographic signals are obtained for tin in 0.2 M acetate buffer of pH 4.7, one at −0.26 V and the other at −0.58 V. Tropolone is reduced at −1.1 V in the same medium. In Fig. 1, tin signals with and without the addition of tropolone are compared. Tropolone enhances the sensitivity by a

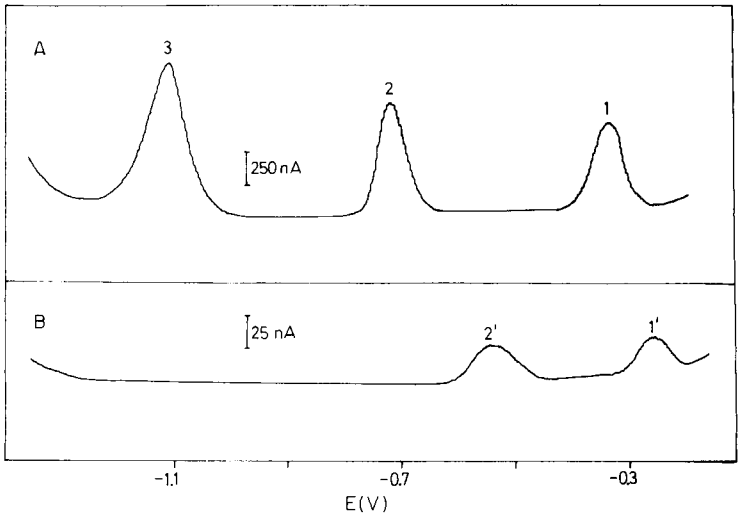

Fig. 1. Polarograms of 5 μg ml^{-1} tin in acetate buffer with (A) and without (B) addition of tropolone: (1, 2) tin peaks in 0.2 M acetate buffer containing 50 mg l^{-1} tropolone; (1', 2') corresponding peaks without tropolone; (3) tropolone peak.

factor of 30. There is also a shift of the peak potentials to more negative values, indicating complexation of tin by tropolone. Although both tin peaks are enhanced, only the one at —0.72 V was used for quantitative work because of its better reproducibility and fewer interferences.

Figure 2 shows the electrocapillary curves for acetate buffer with and without addition of tropolone. The surface tension is lowered by tropolone and the maximum effect occurs between —0.6 V and —0.8 V; thus, it can be concluded that tropolone is adsorbed onto the electrode surface. The signal enhancement can be explained by this adsorption and catalytic reduction of the tin/tropolone chelate at the electrode surface, similarly to the nickel/dimethylglyoxime system [6, 7].

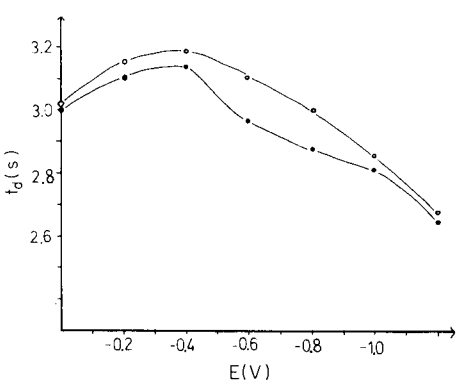

Fig. 2. Electrocapillary curves of the supporting electrolyte: (○) without tropolone; (●) with 0.001 M tropolone.

Influence of electrolyte composition on tin signals

Figure 3 illustrates the dependence of the peak current on buffer concentration, pH and tropolone concentration. Buffer concentration has no appreciable effect on peak current in the range 0.1—0.5 M. At higher concentrations, the peak height decreases slowly and measurements become less reproducible. Buffer concentrations of less than 0.1 M have inadequate buffering capacity and therefore are not suitable, despite the slightly enhanced sensitivity. Use of ammonium acetate instead of sodium acetate has no significant effect. For pH >4.5, the peak height is independent of pH. For pH <4.5, there is a decrease of peak height with decreasing pH. There is also a linear decrease of the peak potential with increasing pH, indicating the involvement of protons in the electrochemical process. A pH of 4.7 provided the most reproducible results (with regard to peak potential and peak current). The influence of tropolone concentration was tested for a 1 μg ml^{-1} solution of tin (8.4 × 10^{-6} M). A tropolone concentration of at least 1 × 10^{-4} M is needed to give full sensitivity. This corresponds to a 20-fold molar excess of tropolone. Further increase in tropolone concentration has little influence on the sensitivity. Maximum sensitivity is obtained for 8.2 × 10^{-4} M (10 mg/100 ml).

Influence of measuring conditions

Measurements also were made by a.c. polarography, but the results were not satisfactory. Use of other types of electrodes (SMDE or HMDE) had no positive effect, except for the low ng g^{-1} range, in which measurements at the HMDE resulted in better baseline stability and in slightly enhanced sensitivity. There was, however, no increase in sensitivity when the solution was stirred or when a potential was applied prior to the measurement.

Calibration graphs

Differential-pulse polarographic measurements at the DME gave a linear relationship between peak current and tin concentration in the range 1 ng ml^{-1} to 5 μg ml^{-1}. Regression analysis (N = 16) gave the equation: I_P = 0.164 (±0.002) × C + 3.95 (±2.93) with I_P in nA and C in ng ml^{-1} (s_{xy} = 9.4 and r = 0.9995). The relative standard deviation of measurements at the 100 ng ml^{-1} level was s_r = 1.9% (N = 6).

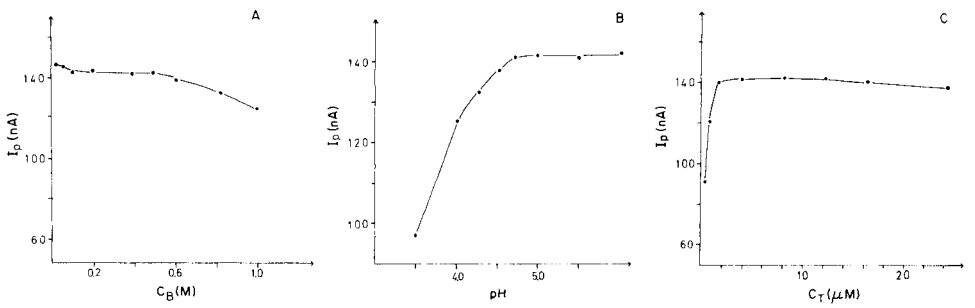

Fig. 3. Effects of solution components on peak current: (A) buffer concentration (C_B); (B) pH; (C) tropolone concentration (C_T).

For concentrations >5 μg ml^{-1}, the sensitivity decreased, because the excess of tropolone became less than 20-fold. Increasing the tropolone concentration enables the linear range to be extended to at least 10 μg ml^{-1}. The determination of low levels of tin is limited by reagent blanks, which are of the order of 1 ng ml^{-1}. It can be estimated from the sensitivity of the method, that purification of reagents, especially of tropolone, should give a limit of detection of about 0.1 ng ml^{-1}. Figure 4 shows typical polarograms of tin in the low ng g^{-1} range.

Determination of organotin compounds

In some matrices, tin is present not only as inorganic tin but also in the form of organotin compounds, which are used, for example, as stabilizing additives for plastics or as biocidal agents [1]. Tetraalkyltin compounds cannot be determined by polarography, but mono-, di- and tri-alkyl derivatives of tin are reduced at different potentials and can be determined simultaneously [13].

In the acetate/tropolone supporting electrolyte, the peak potential of monobutyltin is similar to that of inorganic tin. The dibutyltin signal is well separated from this peak (—100 mV). The peak potential of tributyltin is only 20 mV more negative than that of dibutyltin and therefore simultaneous determination of these two species is impossible. Clearly, tributyltin does not form a strong complex with tropolone. The shifts in peak potentials for the mono- and di-butyltins, compared to acetate buffer without tropolone,

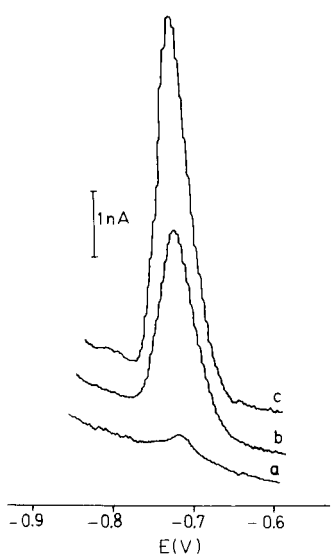

Fig. 4. Typical d.p. polarograms of tin: (a) blank; (b) 5 ng ml^{-1}; (c) 10 ng ml^{-1}.

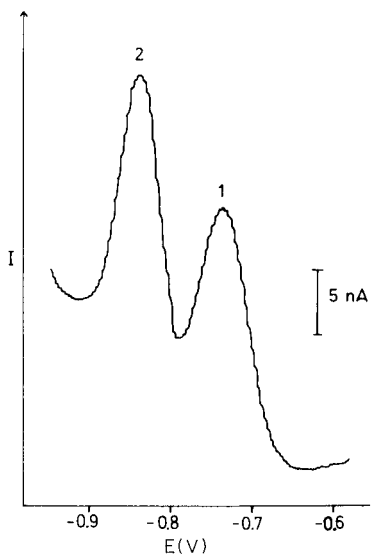

Fig. 5. Determination of organotin compounds: (1) monobutyltin trichloride (500 ng ml^{-1} as tin), (2) dibutyltin dichloride (400 ng ml^{-1} as tin).

are −220 mV and −140 mV, respectively, whereas that for tributyltin is only −40 mV. This means that the shifted dibutyltin peak and the tributyltin peak overlap. Mono- and dibutyltin compounds can be determined simultaneously, which is illustrated in Fig. 5. In contrast to inorganic tin, the signal enhancement of organotin compounds by tropolone is only by a factor of about 2, giving a limit of detection of about 20 ng ml^{-1} (as tin). One advantage of this method, is, however, that the sensitivity for dibutyltin is better than that for monobutyltin. With the above-mentioned method [13], the sensitivity decreases in the order mono- > di- > tri-organotin.

Interferences of other elements

The recoveries of 100 ng ml^{-1} tin after addition of 100 μg (50-fold excess) of different elements are listed in Table 1. If these elements are reduced within the potential range 0 V to −1.0 V, the peak potentials of the corresponding signals are also listed. Overlap with the tin peak at −0.72 V occurs only in the cases of nickel and indium, but this interference is removed simply by adding EDTA to the solution. The nickel and indium peaks vanish completely because of complex formation with EDTA, but the tin peak is not affected. Addition of EDTA also prevents the interference of aluminum, which suppresses the tin signal by complex formation with tropolone. Large amounts of iron or gallium interfere because of precipitation at pH 4.7, but the tin peak can still be quantified. Only the sensitivity is slightly decreased. Large amounts of Cr, Mo, W, V or Ti result in unstable baselines or even peak overlap, because the peak potentials of these elements are quite close to

TABLE 1

Recovery of 100 ng ml^{-1} tin after addition of other elements

Element	Amount (μg)	E_p (V)	Tin recovery (%)	Element	Amount (μg)	E_p (V)	Tin recovery (%)
Al	100	—	4	Mg	100	—	98
Al	100[a]	—	96	Mn	100	—	95
As	100	—	100	Mo	100	−0.52	99
Be	100	—	100	Ni	100	−0.81	—[c]
Bi	100	−0.30	99	Ni	100[b]	—	98
Ca	100	—	99	Pb	100	−0.44	97
Cd	100	−0.57	98	Sb	100	−0.62	97
Co	100	—	96	Te	100	−0.18	98
Cr	100	—	102	Ti	50	−0.85	94
Cu	100	−0.15	101	Tl	100	−0.41	96
Fe	100	—	100	V	100	—	90
Ga	100	—	97	V	50	—	95
In	100	−0.71	—[c]	W	20	−0.8	92
In	100[b]	—	100	Zn	100	—	96

[a]With 2.5 mg EDTA added. [b]With 0.6 mg EDTA added. [c]Peak overlap.

that of tin. This interference is severe in the case of tungsten and titanium, which can be tolerated only in 10- and 25-fold amounts, respectively.

Pre-separation of tin

A solution of tropolone in organic solvents can be used to extract tin from aqueous media containing hydrobromic acid [10]. When toluene is used as solvent under optimized conditions (see Experimental), the recovery of tin is 95—100%. The solubility of tropolone in both organic and aqueous solvents offers the possibility of back-extraction into an aqueous medium. The supporting electrolyte can be used for this purpose without changes. After back-extraction and degassing with nitrogen, polarographic measurement of tin is possible directly in the electrolyte solution. The overall recovery of tin (extraction and back-extraction) is 81% without, and 91% with, centrifugation for phase separation.

This separate procedure completely removes the interferences of W, V, Mo, Cr, Ti and also those of Ni, In and Al. Matrix effects caused by high salt concentrations (e.g., after digestion steps) are also prevented. Additionally, this procedure can be used for enrichment of tin by extraction from large volumes and back-extraction into smaller volumes. Moreover, it has been shown [12] that tin can be extracted from some matrices (e.g., water) without preceding digestion steps. However, polarographic measurements are possible only if no interfering organic molecules are co-extracted.

Determination of tin in water and fruit juice

For comparison of the proposed method with the electrothermal a.a.s. and alternating-current a.s.v. methods, water from the river Rhine (collected at Duisburg) and canned fruit juice were analyzed. As can be seen from Table 2, there is good agreement between the results of the three different methods. These analyses were repeated with direct application of the pre-separation method (extraction and back-extraction), because digestion of the matrix is the most time-consuming step of the whole procedure. For water, this was possible and a value of 13.0 ng ml^{-1} was obtained, which is in good agreement with the result after digestion by u.v. photolysis. For fruit

TABLE 2

Analyses of water and fruit juice

Sample	Sn found (ng ml^{-1})		
	A.a.s.	A.s.v.	This method
River Rhine (at Duisburg)	13.1 ± 0.8	12.0 ± 0.5	12.3 ± 0.7
Fruit juice (pineapple)	680 ± 21	695 ± 15	668 ± 13

juice, the extraction of tin is possible, but polarographic measurements after back-extraction are impossible because of interfering organic substances.

REFERENCES

1 G. Weber, Fresenius Z. Anal. Chem., 321 (1985) 217.
2 E. Desimoni, F. Palmisano and L. Sabbatini, Anal. Chem., 52 (1980) 1889.
3 S. Glodowski and Z. Kublik, Anal. Chim. Acta, 115 (1980) 51.
4 S. Dogan, G. Nembrini and W. Haerdi, Anal. Chim. Acta, 130 (1981) 385.
5 P. Kiekens, R. M. H. Verbeeck, H. Donche and E. Temmerman, Anal. Chim. Acta, 127 (1981) 251.
6 C. J. Flora and E. Nieboer, Anal. Chem., 52 (1980) 1013.
7 J. Weinzierl and F. Umland, Fresenius Z. Anal. Chem., 312 (1982) 608.
8 M. Uto, Y. Itoh and M. Sugawara, Fresenius Z. Anal. Chem., 321 (1985) 68.
9 L. G. Petrova, V. I. Ignatov and E. Y. Neiman, Zh. Anal. Khim., 33 (1978) 1949.
10 H. A. Meinema, T. Burger-Wiersma, G. Versluis-deHaan and E. C. Gevers, Environ. Sci. Technol., 12 (1978) 288.
11 P. Burba and P. G. Willmer, Fresenius Z. Anal. Chem., 311 (1982) 222.
12 G. Weber, Fresenius Z. Anal. Chem., 322 (1985) 311.
13 K. Hasebe, Y. Yamamoto and T. Kambara, Fresenius Z. Anal. Chem., 310 (1982) 234.

Analytica Chimica Acta, 186 (1986) 57—69
Elsevier Science Publishers B.V., Amsterdam — Printed in The Netherlands

THE MECHANISMS OF PRECONCENTRATION AND VOLTAMMETRIC BEHAVIOUR OF URANIUM(VI) AT GLASSY CARBON ELECTRODES MODIFIED BY TRIOCTYLPHOSPHINE OXIDE

K.-H. LUBERT* and M. SCHNURRBUSCH

Akademie der Wissenschaften der DDR, Forschungsstelle für Chemische Toxikologie, Permoserstrasse 15, 7050 Leipzig (German Democratic Republic)

(Received 24th June 1985)

SUMMARY

Uranium(VI) ($\geqslant 10^{-5}$ M) can be determined at glassy carbon (GC) electrodes modified with a multilayer of trioctylphosphine oxide (TOPO) in a two-step procedure involving preconcentration at the electrode at potentials near 0 V vs. SCE and stripping in a cathodic scan. Various voltammetric and capacity measurements were made in attempts to elucidate the mechanisms and kinetics of the processes. The uranium(VI) is preconcentrated by reaction with the TOPO in which GC surface groups participate. During the cathodic stripping step, preconcentrated uranium(VI) amplifies the reduction current of GC surface functional groups, so that the electrode reaction can be considered as mediated electron transfer. The rate-determining steps are the diffusion of the analyte in the solution during preconcentration and charge transfer in the bulk of the multilayer during stripping. The acetate buffer used affects the reaction in a complicated manner which is discussed in detail.

Electroanalytical procedures for the determination of traces of metal ions or metal-containing species often include preconcentration of the analyte at the electrode as the first step. This preconcentration can be achieved by electrodeposition or, in the case of metals which are insoluble in mercury, with the aid of organic complexing agents or complex-forming groups of modified solid electrodes. In recent years, many examples have been reported for adsorptive preconcentration of metal ions at mercury electrodes [1—10], and for their preconcentration on carbon paste electrodes modified by complex-forming groups [11—14] or a cation-exchange resin [15], as well as modified platinum [16, 17] and modified glassy carbon (GC) electrodes [18—21].

One example of the analytical utilization of modified solid electrodes is the determination of uranium(VI) at GC electrodes modified by trioctylphosphine oxide (TOPO), first described by Izutsu et al. [18]. This procedure has many advantages [19], particularly its good selectivity; its sensitivity and its low detection limit permit determinations in the 10^{-8} M range even when

*Address for correspondence: Akademie der Wissenschaften der DDR, Zentralinstitut für Isotopen- und Strahlenforschung, Permoserstrasse 15, DDR-7050 Leipzig, German Democratic Republic.

0003-2670/86/$03.50

the less sensitive linear voltammetry is used for detection [19]. The applicability of the procedure for determining very low uranium contents in natural waters has been demonstrated [19, 22]. However, the mechanism of the preconcentration and the electrode reaction of uranium(VI) at the TOPO-modified GC surface are almost completely unknown.

The characteristic feature of analytical applications of modified electrodes is the accumulation of the analyte by means of a selective reaction with molecules attached to the electrode surface or with surface functionalities. Aspects concerning the mechanism and kinetics of such reactions are rarely discussed, although there are several points of interest. First, the role of surface functionalities in the electrode reaction as well as in modifying the GC surface is of special interest. The existence of various groups on GC surfaces and their significance for all reactions occurring there are generally accepted [23—28], but the nature and concentration of different groups are not known in detail and depend on the method of manufacture and on the electrochemical history of the electrode. At least two different types of bonded oxygen have been discussed [23, 29] and the occurrence of acidic surface groups has been concluded from the pH-dependent response of GC electrodes [30—33]. Several authors suppose that quinoid-like groups or a redox couple similar to quinone/hydroquinone exist on GC surfaces [24, 28] and reactions of surface functionalities are often utilized for chemical modifications of GC electrodes [34].

The second feature is that accumulation reactions take place at a multilayered surface so that transport of the reacting species to the reactive site is important. Thus, in addition to elucidating the single steps of the reaction, the role of the phase or interface boundary at which the single steps occur must be considered. Thirdly, experimental results [19] indicate that the reduction of uranium(VI) at TOPO-coated GC is involved with redox reactions of GC surface groups. The question thus arises if catalysis plays a role in the reaction. For these reasons, the mechanism of the reaction of uranium(VI) at TOPO-multilayer-coated GC electrodes is discussed here in some detail, based on earlier experimental findings [19] and on some new results from voltammetric and capacity measurements. Finally, a reaction scheme is proposed which is in agreement with the experimental data and which may contribute to obtaining insight into the general pathways of these accumulation reactions.

EXPERIMENTAL

Electrodes and their preparation

The disk electrode had a commercially available GC electrode rod (5-mm diameter; VEB Elektrokohle Lichtenberg, Berlin) inserted in a PTFE tube. The electrode was fixed in a rotating holder (Radiometer).

Before use, the GC was polished with an aluminium oxide suspension and then thoroughly rinsed with distilled water and ethanol. The GC surface was coated by injecting TOPO from a microlitre syringe onto it whilst the

electrode was immersed (with the GC uppermost) in a thermostatted bath held at >55°C (TOPO m.p. = 55°C). Unless otherwise stated, 20 μl of a methanolic or ethanolic TOPO solution (5×10^{-3} M) was placed on the GC surface. The electrode was left in the thermostat for 10—20 min. Complete coating of the GC surface was checked microscopically.

Instruments, reagents and solutions

The voltammograms were recorded with a multifunctional polarograph (GWP 673; Zentrum für Wissenschaftlichen Gerätebau, Akademie der Wissenschaften der DDR) and the capacity of the electrode was measured with an impedance bridge (frequency 1.6 kHz). The glass cell was equipped with a platinum wire counter electrode and a saturated calomel reference electrode (SCE), the latter being connected to the cell via a salt bridge. All potentials are referred to the SCE.

Solutions were deaerated with oxygen-free nitrogen and voltammograms were recorded while a nitrogen blanket was maintained. All reagents, except TOPO, were of analytical-reagent grade. The TOPO was from Ferak (Berlin). The pH was adjusted with acetic acid and sodium acetate as required. Triple-distilled water was used. The uranium stock solution was 5×10^{-3} M in uranyl acetate.

Procedures

Preconcentration was done with rotation of the electrode alone or with rotation and agitation of the solution with nitrogen. Unless indicated otherwise, the electrode potential during the preconcentration was 0 V vs. SCE. After a rest time of 30 s, the voltammogram was recorded beginning at the preconcentration potential. In general, the scan rate was 1 V min^{-1}.

RESULTS

TOPO-coated GC electrodes in uranium-free solutions

Figure 1 shows cyclic voltammograms of the TOPO-coated electrode in acetate-buffered solutions equilibrated with nitrogen (curve a) or air (curve b); in the potential range from about −0.6 V to −1.0 V, some reduction occurs. The hydrogen wave in the same electrolyte shifted by 0.2—0.3 V to more negative potentials after coating of the electrode with TOPO, in contrast to GC electrodes modified with quinolin-8-ol, where the hydrogen wave was found to be shifted in the positive direction.

The capacity of bare GC electrodes increased sharply immediately after the electrode had been polished with alumina, and then decreased slowly at a rate depending on the surface roughness, the duration of contact with air, and the composition of the electrolyte solution. After 20—40 min, the capacity approached a constant value, which could be measured (in acetate buffer, 0.1 M HAc + 0.1 M NaAc) at 1.6 kHz with an error of about 5%. These capacity values for a GC electrode (5-mm diameter) are shown in

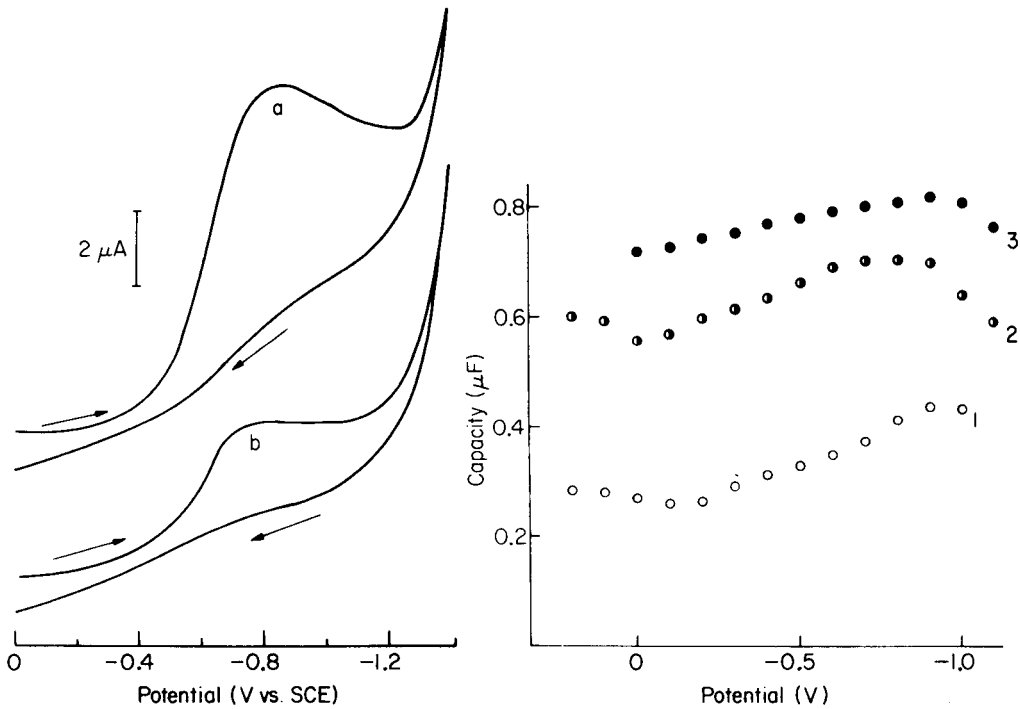

Fig. 1. Cyclic voltammograms of the TOPO-coated GC electrode in 0.3 M acetate buffer equilibrated with (a) air or (b) nitrogen.

Fig. 2. Capacity of the electrode at 1.6 kHz in acetate buffer (0.1 M HAc + 0.1 M NaAc). Curves: (1) bare GC; (2) TOPO-coated GC in uranium-free solution; (3) after preconcentration of 1×10^{-6} M uranyl acetate for 30 min.

Fig. 2 (curve 1). When this electrode was coated with TOPO as described above, its capacity increased to about twice the capacity of the uncoated electrode (curve 2). The capacity of the coated electrode after preconcentration of uranium(VI) for 30 min is also shown (curve 3).

TOPO-coated GC electrodes in uranium-containing solutions

When uranium(VI) (2×10^{-6} M) was preconcentrated from acetate buffer at different rotation rates of the electrode, the peak current obtained in the following cathodic scan was found to depend linearly on the square root of the rotation rate in the range 0—45 $\text{min}^{-1/2}$, the peak current increasing from 3.0 to 6.8 μA. The influence of the electrode potential used during the preconcentration [19] was confirmed; the peak currents decreased linearly as the potential was varied from +0.2 V to −0.4 V and then decreased suddenly (Fig. 3). Further, the differential coefficient di_p/dE_{preconc}, which indicates the dependence of peak currents on the preconcentration potential, increased

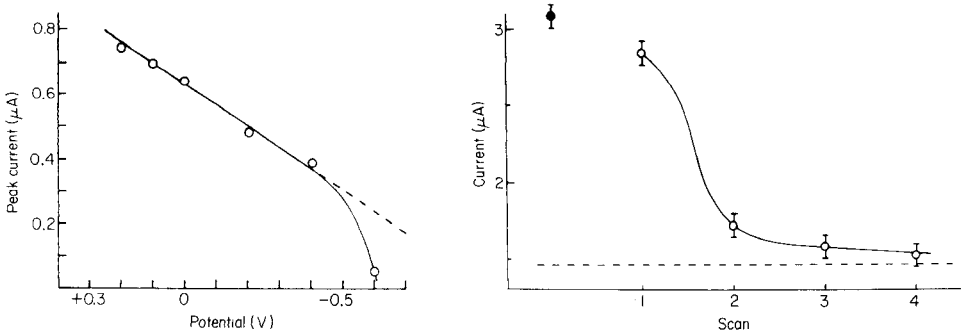

Fig. 3. Dependence of peak currents on the preconcentration potential. Conditions: 1×10^{-7} M uranyl ion, 0.1 M KCl/acetate buffer at pH 5.6, preconcentration for 10 min.

Fig. 4. (○) Decrease of peak current after solution exchange on successive scans; (●) peak current without solution exchange for comparison. The dashed line indicates the uranium-free solution. Conditions: 2×10^{-6} M uranyl ion, 50 μl of TOPO solution on GC, acetate buffer, 5-min preconcentration.

with the uranium content of the solution, for instance in the range 0—5×10^{-7} M uranyl ion from 0.3 to 1.1 $\mu A\ V^{-1}$ after preconcentration for 10 min.

In further tests, the preconcentration was done in the usual manner and then the uranium-containing solution was replaced by the base electrolyte without added uranium. The peak currents obtained in the following scans (nos. 2—4) after renewed preconcentration (under the same conditions) decreased very quickly (Fig. 4) and approached the limit of the uranium-free solution. Because of the very thick TOPO layer applied, the currents were considerably lower than in other cases.

As reported earlier [19], the peak currents depended on pH in acetate-buffered solutions containing 0.5 M KCl, reaching a maximum around pH 5.2. In further tests, the effect of varying the buffer concentration at a nearly constant pH of 4.5 was studied. Enhancement of the concentrations of acetate and acetic acid from 0.005 M to 0.1 M results in the doubling of the stripping peak currents.

Figure 5 shows the voltammograms obtained in the presence of 5×10^{-6} M permanganate and 8×10^{-7} M uranyl acetate after preconcentration for 5 min. As can be seen, the cathodic part of the voltammograms is influenced by permanganate, but to a considerably smaller extent than by uranium(VI), indicating the selectivity of the procedure for uranyl ion.

Cyclic voltammograms for different scan rates (v) are given in Fig. 6, to illustrate the slow decrease of the current after the peak maximum. The log i_p/log v plot from these data had a slope of 0.62 ± 0.03 in the investigated range from 0.1 to 2.5 V min^{-1}.

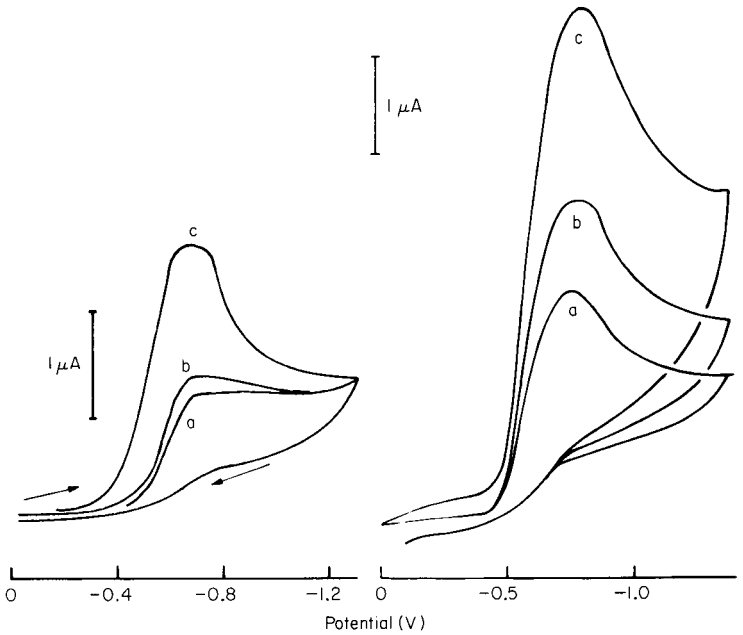

Fig. 5. Voltammograms of TOPO-coated GC electrodes in presence of permanganate and U(VI): (a) 0.5 M KCl, pH 4.0; (b) a + 5 × 10^{-6} M permanganate; (c) b + 8 × 10^{-7} M uranyl ion after a 5-min preconcentration.

Fig. 6. Cyclic voltammograms for different scan rates after preconcentration of 4 × 10^{-7} M uranyl ion for 5 min. Scan rate: (a) 0.5; (b) 1.0; (c) 2.5 V min^{-1}.

DISCUSSION

TOPO coating

The reduction of oxidizing agents (Fig. 1) as well as GC surface groups occurs at TOPO-coated GC in the same potential range as the reduction of surface functionalities at bare GC [23, 25]. Surface groups seem to be involved in these reactions, analogously to reduction of oxygen on carbon and graphite [35].

The potential-independent increase of the electrode capacity after the electrode has been coated with TOPO (Fig. 2) could be caused by polarization of GC surface groups and/or dissociation of such groups induced by TOPO molecules. The shifting of the hydrogen wave to more negative potentials after the GC has been coated with TOPO, and the well-known interaction of tertiary phosphine oxides with protons and acids to give hydrogen-bonded complexes or hydroxyphosphonium salts [36], suggest interaction (at least of the first layer) of TOPO molecules with acidic surface groups. The phosphine oxide could be attached to the electrode surface by hydrogen bonds or by electrostatic forces (if the strongly polar P—O group causes dissociation of surface groups):

$R_3PO + H{-}R^* \rightleftharpoons R_3PO \ldots H{-}R^*$

$R_3PO + H{-}R^* \rightleftharpoons [R_3PO{-}H]^+ (R^*)^-$

where the asterisks indicate surface functional groups. These reactions would occur immediately at the GC surface, but at the interface between the TOPO layer and the electrolyte solution (and possibly within the TOPO layer), the reactions with components of the base electrolyte would be

$R_3PO + H^+ \rightleftharpoons R_3PO \ldots H^+$

$R_3PO + HAc \rightleftharpoons [R_3PO{-}H]^+ Ac^-$.

The TOPO coatings used had surface concentrations of 3.8—12.5 $\times$ 10^{-7} mol cm^{-2}. Provided that the areas of the TOPO molecules in the coatings are of the same order as the value measured at mercury electrodes [37], the thickness of the TOPO layers used can be estimated as about 10^{-4} cm. An approximation based on the density of solid TOPO (ca. 1 g cm^{-3}) gives a layer thickness of 1.5—5 $\times$ 10^{-4} cm for the concentrations mentioned.

The two-step procedure

The reaction of uranium(VI) at the TOPO-coated GC was investigated under the conditions applied for trace determinations [19]. The uranium(VI) concentrations used were low ($\leqslant 10^{-6}$ M) and the two-step procedure was applied, i.e., preconcentration at potentials where cathodic reduction cannot occur and then voltammetric detection. As reported previously [19], peak currents increase linearly with the concentration of uranium(VI) (c) and the preconcentration time, t_{pr}, if $c \times t_{pr}$ is less than about 8×10^{-6} mol l^{-1} min $\approx$ 5×10^{-7} mol cm^{-3} s, and approach a limit for greater $c \times t_{pr}$, values, indicating that only a limited amount of uranium(VI) can be preconcentrated. If diffusion of the analyte is the rate-determining step in the preconcentration (see below), the preconcentrated amount n_{pr} can be roughly estimated by $n_{pr} \approx A D c t_{pr}/\delta$, where D is the diffusion coefficient of uranyl ions in the solution (ca. 10^{-5} cm^2 s^{-1}), δ is the thickness of the diffusion layer (ca. 10^{-3} cm for strongly stirred solutions) and A is the electrode area (ca. 0.2 cm^2). Thus, $n_{pr} \approx 2 \times 10^{-3}$ c t_{pr}, if c is given in mol cm^{-3} and t in seconds. The upper limit of n_{pr} is estimated to be about 10^{-8} mol. The maximum amount of uranium(VI) which can reach the electrode (or the TOPO layer) by diffusion during time t in unstirred solution cannot exceed the amount of the analyte in the thin layer adjacent to the electrode surface (with thickness x and area A). As $x \approx (Dt)^{1/2}$, this amount n_{diff} can be estimated from $n_{diff} \leqslant A\ c\ (Dt)^{1/2}$. Uranium(VI) is reduced at the electrode used in the potential range from —0.5 to —1.0 V, which corresponds to t = 10—60 s at scan rates of 0.5—2.5 V min^{-1}. With the above approximate values of D and A, and t = 10 s or 60 s, $n_{diff} \leqslant (2{-}5) \times 10^{-3}$ c. Thus, $n_{diff}/n_{pr} \leqslant (1{-}2.5)/t_{pr}$. It is concluded that the amount of analyte diffusing during the cathodic scan from the solution to the electrode can be neglected if preconcentration is done for 2 min or longer. This is confirmed by comparing the peak currents obtained with and without medium exchange (Fig. 4).

Preconcentration

During the preconcentration time, a defined fraction of the analyte is transferred from the 50 ml of electrolyte solution to the TOPO layer. From the above considerations, the concentration of uranium(VI) in the TOPO layer can be estimated as $10^{-(4\pm1)}$ mol cm^{-3}.

The effects of the preconcentration potential on stripping peak currents, including the behaviour for more negative potentials (see Results), seems to indicate participation of GC surface reactions in the preconcentration. As pointed out by Laser and Ariel [23], reduced GC surface groups are oxidized during the whole anodic scan, whereas they are reduced predominantly near the cathodic scan reverse point at ca. −0.5 V. During the preconcentration of uranium(VI), reduced surface functionalities seem also to be oxidized to some extent, depending on preconcentration time and potential. At potentials more negative than −0.4 V, reduced surface groups cannot be oxidized, and the currents observed after preconcentration at such potentials are very small (Fig. 3).

The differential coefficient di_p/dE_{pr} increases with the uranium content of the solution (see Results) and the capacity of the TOPO-coated GC electrode increases after preconcentration of uranyl ion (Fig. 2). The influence of the uranium content on the differential coefficient indicates a potential-dependent reaction with participation of uranium(VI). These features indicate that the preconcentrated uranium(VI) is situated, at least to some extent, immediately at the electrode surface and is not uniformly distributed in the TOPO layer. Although all details of the preconcentration mechanism are not yet fully understood, the following reactions seems probable (in the potential range of about +0.5 to −0.5 V): (1) diffusion of uranyl ions to the interface between the TOPO layer and the electrolyte solution; (2) reaction of uranyl with phosphine oxide at this interface boundary with participation of protons or acids

$$R_3PO{-}H^+ + UO_2^{2+} \rightleftharpoons R_3PO{-}UO_2^{2+} + H^+ \qquad (1)$$

(3) transport of the uranium(VI) species and charge transport through the TOPO layer; (4) surface reaction of uranyl ions, probably with participation of GC surface groups, surface-bonded TOPO and protons; and (5) re-oxidation of surface groups. Interactions between these single steps are to be expected.

The linear dependence of peak currents on the square root of the rotation rate during the preconcentration (see Results) indicates that the diffusion of uranium(VI) to the TOPO layer/solution interface is the rate-determining step of the preconcentration. But the re-oxidation of surface groups is also slow at naked GC electrodes [23], and at poly(vinylbenzoquinone)-coated platinum the oxidation rate is slower than the rate of reduction [38].

Reduction of uranium(VI) at TOPO-coated glassy carbon

Zittel and Miller [39] reported that uranyl ions are reduced at uncoated GC in 0.5 M sulphuric acid at about −0.12 V. It was found here that in

acetate buffer at pH 4.6, this reduction occurs near —0.4 V at bare GC, whereas at TOPO-coated GC electrodes, preconcentrated uranium(VI) yields a reduction current in the potential range of —0.5 to —1.0 V (see Fig. 6) with the peak maximum near —0.75 V. Two peaks at about —0.4 V and —0.75 V were observed when the GC surface was not completely coated by TOPO.

In the potential range from —0.5 to —1.0 V, oxidized surface groups are reduced at bare GC as well as at TOPO-coated GC (Fig. 1). When uranyl ion has been preconcentrated in the TOPO layer, the reduction current of surface groups seems to be amplified; the measured current can be divided into two contributions, the current i_0 obtained without uranium(VI) and a "catalytic" contribution i_c. [It should be noted that i_c is not identical with Δi but $i_0 = \Delta i(c_{U(VI)} = 0)$ and $i_c = \Delta i(c_{U(VI)} > 0) - i_0$.] From theoretical considerations [40] and earlier results [41], such behaviour is expected in cases of redox catalysis or mediated electron transfer at modified electrodes, where an immobilized redox couple acts as electron carrier between the electrode and the substrate, which would otherwise undergo a slow reaction at the naked electrode. In the case under discussion, the immobilized redox couple comprises the functional groups on the GC surface and the substrate is the (preconcentrated) uranium(VI). During the cathodic scan the following reactions occur at the electrode:

$$R^*_{ox} + H^+ + e^- \rightarrow H{-}R^*_{red} \qquad (2a)$$

$$(2)H{-}R^*_{red} + U(VI) \rightarrow (2)R^*_{ox} + U(IV) + \ldots \qquad (2b)$$

As pointed out by Murray [34], the substrate becomes reduced at a potential near that of the reduction of the immobilized redox couple, if the second reaction is fast.

Immobilization of a redox couple at the electrode is usually achieved by coating the electrode with a polymer which contains redox functional groups or by incorporating a redox couple into an inert polymer layer. That groups on the GC surface are also able to catalyse slow electrode reactions (e.g., the oxidation of NADH) was shown by Čenas et al. [42] and Falat and Cheng [43]. In the case under discussion, the electrode is coated by a relatively thick layer of an inert monomer, in contrast to the known examples of catalysis at redox-modified (or pretreated) electrodes. As estimated above, only the substrate in the TOPO layer reacts at the electrode during the cathodic scan because of the high substrate concentration in this layer as well as its thickness.

The reduction peaks at TOPO-coated GC are not symmetrical (cf. Fig. 6); the currents decrease slowly after the peak maximum, and the tailing is more pronounced for faster scan rates (Fig. 6) and for greater uranium concentrations in the TOPO layer. The log—log plot of peak current, i_p, vs. scan rate, v, had a slope of 0.62 ± 0.03 (see Results). Laviron and coworkers [44, 45] described a multilayer model corresponding to "space-distributed redox-modified electrodes" and predicted the observed dependence of i_p on $v^{0.6}$ for

moderate scan rates, when the electrode reaction is controlled by the "bulk reaction", i.e., charge diffusion in the bulk of the multilayer is the rate-determining step. At high and low scan rates, i_p varied linearly with v. The tailing of peak currents has been predicted [45] and experimentally confirmed [46].

The present experimental findings suggest that the electrode reaction is governed by diffusion in the TOPO layer, although some assumptions made by Laviron [44] such as facile counter-ion migration and homogeneous distribution of electroactive centres are certainly not satisfied. On the contrary, the fact that increasing acetate buffer concentration increases the peak currents found (see Results) suggests that the acetate buffer participates in the slow transport processes inside the TOPO layer. The tests with medium exchange showed that the cathodic reduction yields a product without catalytic activity. It is considered that uranium of lower valency is formed (Eqn. 2b) which cannot be oxidized during the following preconcentration, usually done at 0 V, because it was shown that uranium(IV) is oxidized at TOPO-coated GC only at potentials more positive than +0.5 V.

Influence of pH and buffer concentration

Any redox reactions of acidic surface groups during the preconcentration and the cathodic scan are certainly pH-dependent. The decrease of peak currents at low pH (see Results) can be attributed to a shift of the equilibrium of reaction (1) to the left, which reduces the amount of preconcentrated uranium(VI); the decrease at pH > 5 may be due to hydrolysis of uranyl ions. A small shift of E_p to more negative potentials was observed for higher pH (cf. Fig. 7, [19]).

However, the pH of the buffer influences the reactions in a rather complicated manner. A log–log plot of the peak current Δi_p against the buffer concentration (c_p) in the range 0.005 M to 0.1 M (with 1:1 ratios of acetate and

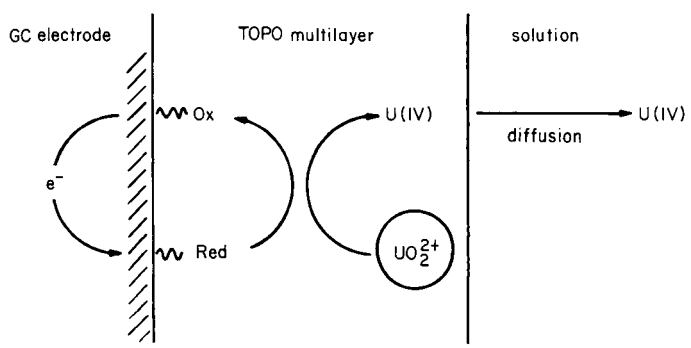

Fig. 7. Scheme of the mediated electron transfer of TOPO-coated GC; Red and Ox are the reduced and oxidized states of the GC surface functional groups; preconcentrated U(VI) is encircled.

acetic acid), for 2×10^{-6} M uranyl ion had a slope of 0.20 ± 0.02. In uranium-free solutions, the influence of the buffer concentration could be neglected. The increased peak currents for more concentrated buffer solutions could be caused by increased preconcentration of uranium(VI) or by some "catalysis" of the electrode reaction during the cathodic scan by the buffer. Acetate catalyses the electrode reaction of the benzoquinone/hydroquinone couple at mercury electrodes [47—49]; thus, it is possible that acetate also catalyses redox reactions of functional groups, e.g., quinone-like groups [24, 28], on the GC surface. The preconcentrated amount of uranium(VI) could, however, be enhanced by the buffer in various ways. First, all components of the acetate buffer seem to be present in the TOPO layer; protons as well as acetic acid can be bonded by phosphine oxides [36] and the acetic acid bonded can dissociate in the usual manner in the TOPO phase. Such dissociation and the buffering capacity in the TOPO layer will be changed for different buffer concentrations in the solution. Reaction 1, for example, would be facilitated by higher buffer concentrations. Further, the amount of acidic groups at the GC surface could be influenced by the buffer concentration at this interface, and the concentration of uranium(VI) in the TOPO layer and at the TOPO/GC interface could be enhanced by the complexing ability of acetate for uranyl ions [50].

Conclusions

The experimental findings allow at least qualitative conclusions concerning the nature of TOPO-coated electrodes, and the mechanism and kinetics of the reaction with uranyl ion. The phosphine oxide seems to be bonded to the GC surface by acidic surface groups; the electrode is indeed chemically modified and not simply coated. The TOPO coating, however, comprises several hundred monolayers, as estimated from its thickness. The potential-dependence of the preconcentration indicates that this step involves an electrode reaction during which uranium(VI) is bound at the electrode surface as well as in the bulk TOPO layer; the preconcentration cannot be considered as simple extraction of uranyl ions by the TOPO. A characteristic feature of the preconcentration step is the simultaneous preconcentration of the analyte and reoxidation of GC surface groups. The reaction rate seems to be governed by slow diffusion transport of uranium(VI) in the solution.

Preconcentrated uranium(VI) reacts at the TOPO-coated GC electrode in that potential range in which surface functionalities are reduced. The reduction currents of surface groups are amplified by uranium(VI) depending on its concentration in the TOPO-multilayer. The electrode reaction can thus be considered as a mediated electron transfer [34] and can be represented by the scheme shown in Fig. 7. The two-step procedure and the thick TOPO layers are advantageous for analytical purposes because slow diffusion of the analyte in the solution is thus separated from the electrode reaction. The very complex nature of the reactions occurring is evident from the observed experimental dependences, e.g., the complicated influence of the buffer.

This paper was presented in part at Euroanalysis V, Krakow, August, 1984.

REFERENCES

1 C. J. Flora and E. Nieboer, Anal. Chem., 52 (1980) 1013.
2 H. Sawamoto, J. Electroanal. Chem., 113 (1980) 301.
3 H. Pihlar, P. Valenta and H. W. Nürnberg, Fresenius Z. Anal. Chem., 307 (1981) 337.
4 V. Gemmer-Čolos, H. Tuss, D. Saur and R. Neeb, Fresenius Z. Anal. Chem., 307 (1981) 347.
5 R. Kalvoda, Anal. Chim. Acta, 138 (1982) 11.
6 H. Sawamoto, J. Electroanal. Chem., 147 (1983) 279.
7 A. Meyer and R. Neeb, Fresenius Z. Anal. Chem., 315 (1983) 118.
8 M. Schnurrbusch, K.-H. Lubert and A. Thomas, Z. Chem., 23 (1983) 194.
9 N. Khac Lam, R. Kalvoda and M. Kopanica, Anal. Chim. Acta, 154 (1983) 79.
10 H. Braun and M. Metzger, Fresenius Z. Anal. Chem., 318 (1984) 321.
11 H. Monien and K. Zinke, Fresenius Z. Anal. Chem., 250 (1970) 178.
12 A. Narayanan and R. Neeb, Fresenius Z. Anal. Chem., 269 (1974) 344.
13 G. T. Cheek and R. F. Nelson, Anal. Lett., A11 (1978) 393.
14 H. Monien, U. Gerlach and P. Jacob, Fresenius Z. Anal. Chem., 306 (1981) 136.
15 J. Wang, B. Greene and C. Morgan, Anal. Chim. Acta, 158 (1984) 15.
16 J. A. Cox and M. Majda, Anal. Chim. Acta, 118 (1980) 271.
17 J. A. Cox and P. J. Kulesza, Anal. Chim. Acta, 154 (1983) 71.
18 K. Izutsu, T. Nakamura and T. Oku, Nippon Kagaku Kaishi, (1980) 1656.
19 K.-H. Lubert, M. Schnurrbusch and A. Thomas, Anal. Chim. Acta, 144 (1982) 123.
20 K. Izutsu, T. Nakamura, R. Takizawa and H. Hanawa, Anal. Chim. Acta, 149 (1983) 147.
21 T. Miwa, L.-T. Jin and A. Mizuike, Anal. Chim. Acta, 160 (1984) 135.
22 K. Izutsu, T. Nakamura and T. Ando, Anal. Chim. Acta, 152 (1983) 285.
23 D. Laser and M. Ariel, J. Electroanal. Chem., 52 (1974) 291.
24 R. E. Panzer and P. J. Elving, Electrochim. Acta, 20 (1975) 635.
25 L. Bjelica, R. Parsons and R. M. Reeves, Croat. Chem. Acta, 53 (1980) 211.
26 H. Gunasingham and B. Fleet, Analyst, 107 (1982) 896.
27 R. C. Engstrom, Anal. Chem., 54 (1982) 2310.
28 J. Schreurs, J. van den Berg, A. Wonders and E. Barendrecht, Recl. Trav. Chim. Pays-Bas, 103 (1984) 251.
29 L. Dunsch and R. Naumann, Z. Chem., 14 (1974) 31.
30 J. Doležal and K. Štulik, J. Electroanal. Chem., 17 (1968) 87.
31 A. Dodson and V. J. Jennings, Anal. Chim. Acta, 72 (1974) 205.
32 T. Evans and T. Kuwana, Anal. Chem., 49 (1977) 1632.
33 H. Gunasingham and B. Fleet, Analyst, 108 (1983) 316.
34 R. W. Murray, in A. J. Bard (Ed.), Electroanalytical Chemistry, Vol. 13, Dekker, New York, 1984, p. 191.
35 E. Yeager, Electrochim. Acta, 29 (1984) 1527 (and references therein).
36 H. R. Hays and D. J. Peterson, in G. M. Kosolapoff and L. Maier (Eds.), Organic Phosphorus Compounds, Vol. 3, Wiley-Interscience, New York, 1972, p. 341.
37 A. Anastopoulos, P. Karabinas and D. Jannakondakis, J. Electroanal. Chem., 127 (1981) 219.
38 B. Lionel Funt and P. M. Hoang, J. Electroanal. Chem., 154 (1983) 229.
39 H. E. Zittel and F. J. Miller, Anal. Chem., 37 (1965) 200.
40 C. P. Andrieux and J. M. Saveant, J. Electroanal. Chem., 93 (1978) 163.
41 C. Degrand and L. L. Miller, J. Am. Chem. Soc., 102 (1980) 5728.
42 N. Čenas, J. Rozgaite, A. Pocius and A. Kulys, J. Electroanal. Chem., 154 (1983) 121.
43 L. Falat and H.-Y. Cheng, J. Electroanal. Chem., 157 (1983) 393.

44 E. Laviron, J. Electroanal. Chem., 112 (1980) 1.
45 E. Laviron, L. Roullier and C. Degrand, J. Electroanal. Chem., 112 (1980) 11.
46 C. Degrand and L. L. Miller, J. Electroanal. Chem., 117 (1981) 267.
47 W. Lorenz and K.-H. Lubert, Z. Phys. Chem. (Leipzig), 241 (1969) 285.
48 K.-H. Lubert, Thesis, Leipzig, 1973.
49 W. Lorenz and G. Salié, J. Electroanal. Chem., 80 (1977) 1.
50 Ch. Miyake and H. W. Nürnberg, J. Inorg. Nucl. Chem., 29 (1967) 2411.

Analytica Chimica Acta, 186 (1986) 71—80
Elsevier Science Publishers B.V., Amsterdam — Printed in The Netherlands

MEMBRANE-DIALYZER INJECTION LOOP FOR ENHANCING THE SELECTIVITY OF ANION-RESPONSIVE LIQUID-MEMBRANE ELECTRODES IN FLOW SYSTEMS
Part 1. A Sensing System for NO_x and Nitrite

GLENN B. MARTIN and M. E. MEYERHOFF*
Department of Chemistry, University of Michigan, Ann Arbor, Michigan 48109 (U.S.A.)
(Received 23rd January 1986)

SUMMARY

A general approach for enhancing the selectivity of anion-responsive liquid-membrane electrodes is described. The method is based on use of the receptor channel of a flow-through dialyzer unit as the injection loop in a flow-injection system. An appropriate membrane in the dialyzer prevents ionic interferents from reaching an inselective electrode in the final flow stream. The concept is demonstrated by developing a highly selective semi-automated method for the determination of dissolved NO_x or nitrite at levels greater than 5 μM. Nitrogen dioxide is trapped across a teflon membrane in the dialyzer and converted to nitrate by a buffered peroxide recipient solution. This solution is injected and carried to a tubular nitrate electrode. The final selectivity and detection capabilities of this gas-sensing arrangement are examined and compared to those of the nitrate electrode alone and more conventional sensing systems based on pH electrodes. A dialyzer unit with wider channels improves the efficiency of gas transfer and thus the detection capabilities of the system.

In recent years, potentiometric ion-selective liquid (or polymer) membrane electrodes have found wide use in various fields. While highly-selective devices based on neutral carriers exist for accurate determinations of cations (e.g., K^+, Na^+, Ca^{2+}, etc. [1]), relatively few liquid membrane systems are known to exhibit selective response to given anions [2—4]. Indeed, most anion-sensitive liquid electrodes reported to date use relatively inselective ion-exchangers as the active membrane components (e.g., Aliquat-336 and other quaternary ammonium species); the resulting electrodes usually show selectivity patterns in accordance with the Hofmeister series [5, 6], i.e., organic anions > $HClO_4^-$ > SCN^- > I^- > NO_3^- > Br^- > Cl^- > HCO_3^-. This sequence is based on the relative lipophilicity of the anions and thus their partition coefficients into the organic membranes. As a result, the applications of such electrodes have been rather limited. In this and the following paper, a novel approach is described which should enhance the utility of these electrodes when used as detectors in flow-injection analysis (f.i.a.). In this paper, the development of a new, highly selective NO_x/nitrite sensing system is described. It is based on a relatively inselective nitrate polymer-membrane electrode.

0003-2670/86/$03.50

Several liquid-membrane electrodes for nitrate have been suggested [7—12]. The most useful devices are based on poly(vinyl chloride) (PVC) membranes incorporating tridodecylhexadecylammonium nitrate or tris(4,7-diphenyl-1,10-phenanthroline)nickel(II) as the ion-exchanging component. While selectivity over lipophilic anions is generally poor, these electrodes have been used successfully to determine nitrate in samples which do not contain large amounts of such interferents [13, 14] and also to determine nitrogen oxides after their oxidation to nitrate, usually with hydrogen peroxide [15, 16]. Several companies offer a gas-sensing electrode for the determination of the nitrogen oxides (NO_x). This sensor is analogous to the conventional Severinghaus pCO_2 gas sensor in that NO_x diffuses through an outer gas-permeable membrane and alters the pH of a thin electrolyte film in contact with a glass pH electrode [17]. Such a sensor can be used to determine anionic nitrite in solution by acidifying the samples [18—20]. Again, though useful in certain instances, this NO_x sensor displays rather poor selectivity relative to other acidic gases, or anions which can be converted to these gases by acidification of the sample [20] (e.g., sulfite, hydrogencarbonate, acetate, etc.). During progress on this work, a promising new liquid-membrane nitrite-selective electrode was reported which appears to offer rather high selectivity over many interfering anions [4].

It has been demonstrated [21] that an extremely selective sensing arrangement for ammonia gas can be developed by using a dialyzer unit in conjunction with a flow-through polymer-membrane ammonium-ion-selective electrode. In that work, the electrode used was not very selective for ammonium ions but the addition of the upstream gas-permeable membrane rendered the resulting system completely selective for ammonia over potassium and other common interferents. In the present paper, this basic concept is extended by developing a system which uses a relatively inselective anion-responsive electrode as the detector. Because of the selectivity deficiencies of the present NO_x and nitrate sensors described above, a novel system for NO_x determinations based on existing nitrate electrodes was thought to be a suitable model for illustrating the potential of this general approach to developing more practical potentiometric systems.

Figure 1 outlines the flow instrument and chemistry underlying the proposed NO_x/nitrite sensing system. A variation introduced here which was not present in the earlier work [21] is the use of the upper channel of the gas dialyzer unit as an injection loop in a flow-injection mode. This variation offers improvements in detection limits compared to operating the recipient stream on a continuous basis; if lower detection limits are required, a larger volume of sample can be passed through the lower channel of the dialyzer and the analyte gas can be continuously trapped in a small static volume of recipient solution (within the upper channel of the dialyzer unit) prior to injection to the electrode. It will be shown that this NO_x-sensing arrangement can be used to detect nitrite with significantly greater selectivity than existing NO_x sensors. Further, the dialysis/flow-injection method of operation

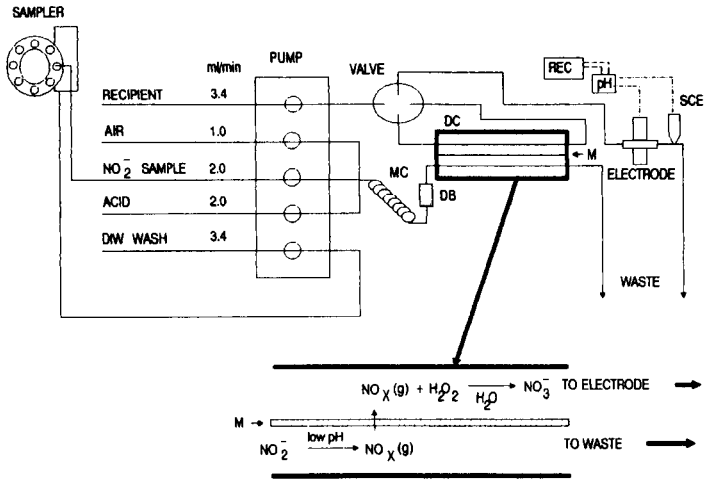

Fig. 1. Schematic diagram of the semi-automated dialyzer/flow-injection instrument for detection of NO_x/nitrite: (DC) dialysis chamber; (MC) mixing coil; (M) microporous membrane; (pH) pH/mV meter; (REC) strip-chart recorder; (SCE) saturated calomel electrode; (DB) tubular debubbler.

does indeed yield superior sensitivity over analogous systems in which the recipient stream flows continuously through the dialyzer.

EXPERIMENTAL

Apparatus

Figure 1 is a schematic diagram of the semi-automated flow system. A Rainin (Woburn, MA) peristaltic pump was used to deliver the sample (2.0 ml min^{-1}), acid (2.0 ml min^{-1}), air (1.0 ml min^{-1}), and recipient (3.4 ml min^{-1}) streams through the system. A Rheodyne model 5020 4-way rotary injection valve was used to control the recipient/carrier stream flow. A Technicon Sampler II served as the autosampler, and was operated with a throughput rate of 30 samples per hour, at a 1:1 sample:wash ratio (for 1-min sample times). Potentiometric measurements were made with a Fisher Accumet pH Meter (Model 620) and recorded on a Fisher Recordall Series 5000 strip-chart recorder. All potentials were measured vs. a saturated calomel reference electrode (SCE) placed downstream from the working electrode.

To improve the efficiency of gas transfer, a modified gas dialyzer unit was machined from plexiglas (termed the wide-channel unit here). Each channel of this unit had a greater surface-to-volume ratio than the commercially available dialyzers used previously [21] (26.4 cm^{-1} rather than 16.3 cm^{-1}). Figure 2 illustrates the design and dimensions of this modified unit. To reduce movement of the membrane and uneven solution flow caused by variable pressure within the dialyzer, each channel contains two support ribs to

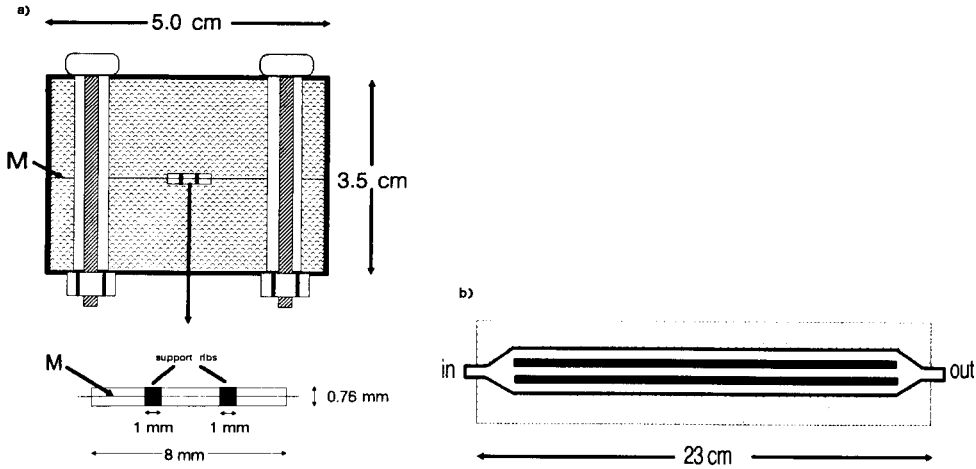

Fig. 2. (a) Normal and expanded end-on view of the wide-channel dialyzer; (M) microporous membrane. (b) Expanded top view of each channel of the dialyzer.

hold the gas-permeable membrane securely in place. For all experiments reported here, the dialyzer was fitted with a microporous polytetrafluoroethylene membrane (0.2 μm pore size; W. L. Gore Associates, Elkton, MD).

Reagents

All chemicals used were of analytical-reagent grade. Standard solutions and buffers were prepared with distilled or reverse osmosis-deionized water. The nitrate exchanger was obtained from Corning. *o*-Nitrophenyl octyl ether (Fluka), and PVC powder (Scientific Polymer Products, Ontario, NY) were used. The final nitrite-sensing system utilized a 0.005 M phosphate buffer, pH 2.8, containing 0.1 wt.% hydrogen peroxide and 1 μM nitrate, as the recipient/carrier stream.

Preparation and characterization of the tubular flow-through nitrate electrode

The tubular nitrate-sensitive electrode was fabricated from 0.89-mm i.d. PVC tubing in a manner similar to that described for the preparation of potassium electrodes [22]. In this case, however, the casting solution contained 30% PVC, 65% *o*-nitrophenyl octyl ether, and 5% of the Corning nitrate exchanger (all by weight). The membrane components were dissolved in enough tetrahydrofuran to form a viscous solution. A solution containing 0.05 M sodium nitrate and 0.05 M sodium chloride saturated with silver chloride, was used as the internal reference solution. The electrode was tested for nitrate response with continuously flowing nitrate standards prepared in the recipient/carrier buffer passing directly through the electrode. The resulting steady-state response was evaluated by measuring the change in potential from the baseline value (potential when only recipient stream buffer flows

through the electrode). The change in potential (ΔE) was then plotted vs. the logarithm of the nitrate concentration. This method showed that the detection limit for nitrate in the recipient/carrier buffer was 1 μM.

Evaluation of final membrane dialyzer/flow-injection arrangement

In these studies, standard solutions of nitrite or other anions were placed in the autosampler. Within the system, the samples are acidified with 0.5 M phosphoric acid and segmented by air bubbles. The sample plug then enters a mixing coil where NO_x is generated (from nitrite). Before entering the mixing coil, the sample stream is debubbled using a tubular debubbler [23]. At the moment the sample plug begins to enter the dialyzer, the rotary injection valve controlling the flow of the recipient/carrier stream is turned so that this stream bypasses the dialyzer unit. Five seconds after the end of the sample plug exits the dialyzer (65 s after sample enters the dialyzer for a 1-min sampling time), the rotary valve is positioned so that the recipient stream plug, contained in the upper channel of the dialyzer, is injected through the electrochemical cell and on to waste. The sample stream goes immediately to waste after exiting the dialyzer. Calibration and selectivity data were obtained by measuring the resulting peak height (in mV) for each sample.

RESULTS AND DISCUSSION

Characterization of the nitrate electrode

Table 1 includes the selectivity coefficients of the Corning PVC membrane electrode for nitrate reported by Davies et al. [24]. This membrane does not exhibit high selectivity over many other anions, especially those which are more lipophilic than nitrate. A similar selectivity pattern was observed for the tubular flow-through nitrate electrode used here. Operating in the flowing system, the electrode exhibited near-Nernstian response (slopes of 55—60 mV/pNO_3) down to 10 μM nitrate when the 0.005 M phosphate buffer at pH 2.8 was used as the background electrolyte. The membrane components utilized in the Orion nitrate electrode [8] offer similar selectivity and response to nitrate when incorporated into the tubular flow-through design and could be used, if desired, in place of the Corning membrane exchanger.

Characterization of the membrane dialyzer/flow injection system for NO_x/nitrite

Effect of dialyzer geometry. When acidified nitrite samples are allowed to flow through the lower channel of the dialyzer, the NO_x generated diffuses through the microporous teflon membrane into the recipient solution contained within the upper channel. This solution traps the NO_x by oxidation to nitrate, thereby maintaining a gradient of NO_x across the membrane. Subsequent injection of the recipient buffer results in the potentiometric response by the nitrate-sensitive electrode to the final concentration of nitrate trapped

TABLE 1

Comparison of apparent selectivity coefficients (K_{ij}^{pot})

Anion	Apparent selectivity coefficients[a]		
	This work		Previous work [24]
	pH electrode	Nitrate electrode	
NO_2^-	1	1	0.066
HCO_3^-	5×10^{-3}	5×10^{-5}	—
F^-	5×10^{-2}	2×10^{-4}	8.7×10^{-4}
Cl^-	5×10^{-2}	5×10^{-5}	5.0×10^{-3}
Br^-	5×10^{-5}	5×10^{-5}	—
I^-	—	—	17
$CH_3CO_2^-$	3×10^{-2}	5×10^{-5}	—
$HOC(CH_2CO_2H)_2CO_2^-$	5×10^{-5}	5×10^{-5}	—
NO_3^-	5×10^{-5}	5×10^{-5}	1.0
SO_3^{2-}	0.17	6×10^{-2}	—
SO_4^{2-}	—	—	1×10^{-5}
ClO_3^-	—	—	1.66
ClO_4^-	—	—	800

[a]Separate solutions method using interferent concentration of 0.1 M.

in the upper channel of the dialyzer. To improve the detection capabilities of the system, the modified wide-channel dialyzer unit was fabricated which had a greater surface-to-volume ratio than the commercially available dialyzers (see Experimental). Figure 3 illustrates how the response of the system depends on the dialyzer geometry. Under exactly the same flow conditions and sampling times, the use of the modified dialyzer results in greater mass

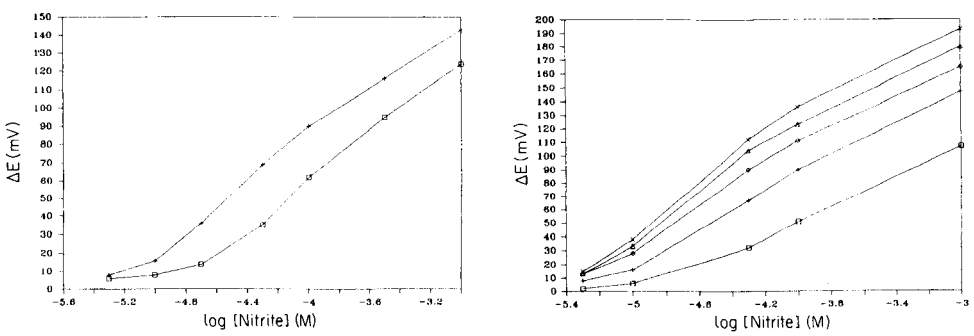

Fig. 3. Comparison of potentiometric response of the dialyzer/flow-injection system for NO_x/nitrite with the conventional (□) and modified (+) dialyzers. Sampling time, 1 min.

Fig. 4. Effect of sampling time on the response of the dialyzer/flow-injection system for NO_x/nitrite: (□) 1 min (continuous flow); (+) 1 min (f.i.a.); (◇) 2 min (f.i.a.); (△) 3 min (f.i.a.); (×) 4 min (f.i.a.).

transfer of NO_x between the two streams. This occurs because decreasing the depth of the two streams limits the aqueous diffusion-layer factor in the flux equation governing mass transfer [25]. Based on the results shown in Fig. 3, it appears that the efficiency of gas transfer is improved to a greater extent at lower pNO_x than at higher values. Thus, the wide-channel dialyzer offers the advantage of better detection capabilities without a concomitant decrease in sample throughput. Neither reproducibility nor wash-out times were adversely affected by replacing the commercial dialyzer with the wide-channel design.

Choice of recipient/trapping solution

Two methods of trapping NO_x in the recipient stream are possible: an oxidative trap in which nitrite is converted to nitrate, or a high-pH buffer trap which forces the equilibrium of the $2NO_2^- + H_2O = NO_3^- + NO_2^- + 2H^+$ reaction to the right. The high-pH trap was tested first by using 0.05 M Tris-phosphate, pH 8.5, as the recipient solution. This method gave very poor response to the nitrite standards, probably because of the inherent potentiometric response of the electrode to the high concentration of phosphate, and the differences in response of the electrode to nitrate and nitrite. The latter effect contributes because in this buffer-trap mode half of the total nitrogen oxide species is converted to nitrite, for which the membrane electrode has a selectivity coefficient of only 0.066 [24].

For the oxidizing trap, three different oxidants ($KMnO_4$, $K_2Cr_2O_7$, and H_2O_2) were examined, all in a phosphate buffer at low pH. Both permanganate and dichromate proved to be major interferents. Hydrogen peroxide did not interfere, and was the most effective in oxidizing and trapping the NO_x. Consequently, a phosphate buffer containing hydrogen peroxide was chosen as the carrier/trapping solution. Optimization of this buffer involved studying the effect of buffer strength, pH and peroxide concentration. In general, it was found that lower pH and more dilute buffer concentrations resulted in better detection limits toward nitrite. However, requirements for the nitrate electrode to operate in solutions above pH 2.5 [24] and electrode noise problems associated with low ionic strength impose a practical lower limit on these two parameters. In addition, it was found that 0.1 wt.% hydrogen peroxide in the recipient buffer was sufficient for the conversion of nitrite to nitrate in the concentration range of interest (i.e., 5—100 μM). Surprisingly, significant increases in the peroxide concentration decreased the response of the system, particularly at low nitrite levels. Based on these observations, a 0.005 M phosphate buffer, pH 2.8, containing 0.1% hydrogen peroxide and 1 μM potassium nitrate was used. The addition of nitrate speeded the return to baseline and improved the magnitude of the response at lower nitrite levels; various workers have shown for the determination of many other analytes in flow-injection systems that addition of a low concentration of analyte to the carrier stream improves the responses at low levels.

Dependence of response on sampling time

Figure 4 shows a plot of the response vs. sampling time of the nitrite-sensing system. The longer the sampling time, the greater the potentiometric response for a given nitrite concentration. The increased sensitivity obtained with the injection-loop approach is readily observed when contrasted to the response obtained when the system is operated in a continuous-flow mode (i.e., recipient/carrier stream continuously pumped through the upper channel of dialyzer). The injection loop effectively concentrates the NO_x from the large volume of the sample plug into the much smaller recipient volume. This preconcentration step explains the increased detection capabilities of the membrane dialyzer/flow-injection arrangement. Figure 5 shows a typical strip-chart recording of the response obtained when standards of nitrite are introduced into the system using a 1 min sampling time. Peak potentials (measurement off baseline) for replicate standard samples (n = 4) were generally reproducible to within 2.5 mV whereas absolute peak potentials (measurement off chart zero) were more reproducible (<1 mV), particularly at nitrite levels >50 μM. This difference in precision is due to a small but constant negative drift in the baseline potential of the tubular nitrate electrode when operated on a continuous basis in the presence of nitrate.

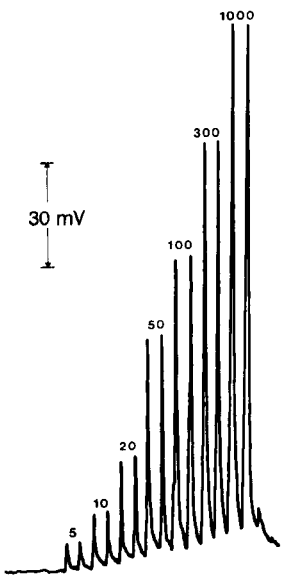

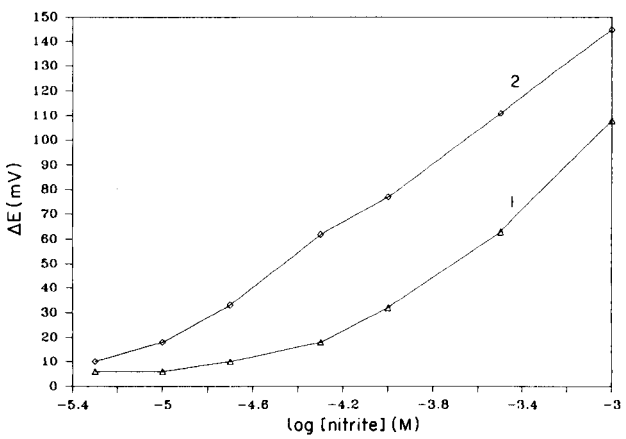

Fig. 5. Typical strip-chart recording obtained with the NO_x/nitrite sensing system with a 1-min (f.i.a.) sampling time and standard nitrite solutions. Numbers on the peaks refer to concentration (μM).

Fig. 6. Comparison of potentiometric response to nitrite obtained with the dialyzer/flow-injection system (1-min sampling time) and different electrodes: (1) pH electrode; (2) nitrate-sensitive electrode.

Comparison of the nitrate and pH electrodes as detectors in the dialyzer/flow-injection system

To compare the proposed system with the conventional NO_x sensing approach, which utilizes a pH electrode behind a gas-permeable membrane [17], the nitrate-sensitive electrode was replaced by a tubular polymer pH electrode [26], and the recipient/trapping solution was changed to 0.01 M sodium nitrite, which is the recommended fill solution for the static NO_x sensors [17]. The response to nitrite standards and other potential interfering anions was then determined. As shown in Fig. 6, when the same sampling times and flow parameters are used, the detection limits for nitrite are about one order of magnitude lower when the nitrate-sensitive electrode is used as the detector. The detection limits found for the flow-through pH-sensing mode are similar to those obtained with the conventional static gas-sensing designs [20].

Table 1 compares the apparent selectivity coefficients of the two detection systems with those reported earlier for the nitrate electrode alone [24]. The superior selectivity of the gas sensing system based on the nitrate-sensitive electrode is due to the ability of the nitrate-responsive membrane to discriminate against anionic forms of the various acidic gases. All the volatile acids tested, or their respective anions, gave response with the system based on the pH electrode while only sulfite yielded any significant response when the nitrate electrode was used. The actual selectivity over sulfite is even better than indicated in Table 1 because the selectivity coefficients listed were determined for fixed interferent concentrations of 0.1 M; at sulfite levels <1 mM, there was essentially no potentiometric response when 0.1% hydrogen peroxide was used because of the oxidation of SO_2 to sulfate in the recipient stream. The nitrate-sensitive electrode has high selectivity over sulfate but only marginal selectivity over hydrogensulfite (the major form of sulfite in the recipient solution based on $pK_a = 7.2$). Thus, SO_2 levels approaching the concentration of oxidant in the recipient stream will be completely oxidized to undetectable sulfate, whereas above this oxidant concentration, excess diffusing SO_2 will form more detectable hydrogensulfite.

Conclusions

Under optimized conditions, the semi-automated dialyzer/flow-injection system provides a throughput of 30 samples per hour with good selectivity for nitrite over many common anions. The system exhibits good precision and detection limits and should prove useful for the direct determination of nitrite as NO_x in a variety of samples. It appears that the use of this dialyzer/flow-injection concept could be applied advantageously to detect other species for which a membrane can separate the analyte in some detectable form from possible interferents. Such a system is reported for salicylate in the following paper [27].

The authors are grateful to the National Institutes of Health for supporting this work (grant GM-28882-05).

REFERENCES

1 D. Ammann, W. E. Morf, P. Anker, P. C. Meier, E. Pretsch and W. Simon, Ion-Sel. Electrode Rev., 5 (1983) 3.
2 H. B. Herman and G. A. Rechnitz, Science, 184 (1974) 1074.
3 J. A. Greenberg and M. E. Meyerhoff, Anal. Chim. Acta, 141 (1982) 57.
4 P. Schulthess, D. Ammann, B. Kräutler, C. Caderas, R. Stepánek and W. Simon, Anal. Chem., 57 (1985) 1397.
5 F. Hofmeister, Arch. Exp. Pathol. Pharmakol., 24 (1888) 247.
6 W. E. Morf, The Principles of Ion-Selective Electrodes and of Membrane Transport, Elsevier, Amsterdam, 1981, Chap. 11.
7 W. M. Wise, U.S. Patent No. 3,671,413, June 20, 1972.
8 J. W. Ross, U.S. Patent No. 3,483,112, December 9, 1969.
9 T. N. Dobbelstein and W. Diehl, Talanta, 16 (1969) 1341.
10 J. Senkyr and J. Petr, J. Chem. Listy, 73 (1979) 1097.
11 A. V. Gordievskii, V. S. Shterman, A. Ya. Syrchenkov, N. I. Savvin and A. F. Zhuker, Zh. Anal. Khim., 27 (1972) 772.
12 H. J. Nielson and E. H. Hansen, Anal. Chim. Acta, 85 (1976) 1.
13 J. A. Burman and G. Johansson, Anal. Chim. Acta, 80 (1975) 215.
14 See, e.g., K. Cammann, Working with Ion-selective Electrodes, 2nd edn., Springer-Verlag, Berlin, 1979, p. 168.
15 G. P. Morie, C. J. Ledford and C. A. Glover, Anal. Chim. Acta, 60 (1972) 397.
16 See, e.g., J. Koryta and K. Štulík, Ion-selective Electrodes, 2nd edn., Cambridge University Press, Cambridge, 1983, p. 185.
17 M. Riley, in A. K. Covington (Ed.), Ion-Selective Electrode Methodology, Vol. II, CRC Press, Boca Raton, 1979, Chap. 1.
18 S. Sherken, AOAC J., 59 (1976) 971.
19 M. A. Tabatabai, Comm. Soil Sci. Plant Anal., 5—6 (1974) 569.
20 S. S. M. Hassan and F. S. Tados, Anal. Chem., 57 (1985) 162.
21 Y. M. Fraticelli and M. E. Meyerhoff, Anal. Chem., 53 (1981) 992.
22 P. M. Kovach and M. E. Meyerhoff, J. Chem. Educ., 60 (1983) 766.
23 G. B. Martin, H. K. Cho and M. E. Meyerhoff, Anal. Chem., 56 (1984) 2612.
24 J. E. W. Davies, G. J. Moody and J. D. R. Thomas, Anal. Chim. Acta, 97 (1972) 87.
25 W. E. van der Linden, Anal. Chim. Acta, 151 (1983) 359.
26 W. N. Opdycke, S. J. Parks and M. E. Meyerhoff, Anal. Chim. Acta, 155 (1983) 11.
27 Q. Chang and M. E. Meyerhoff, Anal. Chim. Acta, 186 (1986) 81.

Analytica Chimica Acta, 186 (1986) 81—90
Elsevier Science Publishers B.V., Amsterdam — Printed in The Netherlands

MEMBRANE-DIALYZER INJECTION LOOP FOR ENHANCING THE SELECTIVITY OF ANION-RESPONSIVE LIQUID-MEMBRANE ELECTRODES IN FLOW SYSTEMS
Part 2. A Selective Sensing System for Salicylate

QINLIN CHANG[a] and M. E. MEYERHOFF*
Department of Chemistry, University of Michigan, Ann Arbor, Michigan 48109 (U.S.A.)
(Received 23rd January 1986)

SUMMARY

An electrode-based flow-injection system suitable for the direct determination of salicylic acid is described. The system utilizes a tubular polymer membrane electrode based on manganese(III) tetraphenylporphyrin chloride to sense salicylate ions formed in a recipient buffer solution held within the upper channel of a flow-through membrane dialyzer assembly. Samples containing salicylic acid are manually introduced into the lower channel of the dialysis unit, in which a thin silicone rubber membrane separates the two channels. The analyte is trapped across the membrane as salicylate ions within a static layer of an appropriate recipient buffer. After a fixed trapping time, the recipient plug is flushed to the electrode in a conventional flow-injection manner. Peak potentials observed are logarithmically related to the salicylic acid concentrations in the original sample. Without the dialysis unit, the electrode response to salicylate is nearly Nernstian over the range 2×10^{-6}—10^{-2} M. In the complete flow/dialysis system, near Nernstian response was achieved for 10^{-4}—10^{-2} M salicylate with a 2-min trapping time. Detection limits can be altered by changing the trapping time. Anionic salicylate can be determined by acidifying the sample. The resulting system offers very high selectivity for salicylate (as salicylic acid) over most inorganic and organic anions normally found in blood. Preliminary studies demonstrate the practical application of this system for the determination of salicylate in serum.

As described in the preceding paper [1], initial efforts to utilize membrane dialyzers with potentiometric polymer-membrane electrodes in flow arrangements have focused on designing highly selective detection systems for gases (e.g., NO_x [1], NH_3 [2], and CO_2 [3]). In these cases, the gas-permeable membrane served to screen out ionic species within the samples which would otherwise interfere with the working electrode. This paper describes how this approach can be used for the detection of neutral organic molecules. The development of an electrode-based flow-injection system suitable for the direct determination of salicylic acid in complex samples is reported.

The determination of salicylate in blood is an important diagnostic test for the detection and prevention of aspirin abuse among patients with chronic

[a]On leave from Sichuan College of Chemical Engineering, Zigong, Sichuan, China.

0003-2670/86/$03.50

pain conditions or in cases of accidental aspirin overdose involving children. Indeed, while therapeutic blood-salicylate concentrations rarely rise above 1.5 mM, levels above 2.2 mM are considered toxic [4]. The classical spectrophotometric method for detecting salicylate in blood involves the formation of a complex between salicylate and excess of iron(III) ions [5]. Although relatively simple and fast, this method is subject to many interferences from substances which also form colored complexes with iron(III) [5]. Anion-selective liquid-membrane electrodes based on lipophilic ion-exchangers (e.g., Aliquat-336) recently have been proposed for the assay of aspirin in tablets after hydrolysis of the acetylsalicylic acid to salicylate [6]. Unfortunately, these sensors generally suffer significant interference from a wide range of other anionic species (Hofmeister pattern [7]) and thus cannot be utilized for direct measurements in blood where chloride levels are quite high (98—109 mM [8]).

In earlier work [9], it was observed that commercial carbon dioxide sensors equipped with silicone-rubber gas-permeable membranes displayed rather large responses toward salicylate and other organic anions in acidic solutions. This interference results from the ability of salicylic acid to permeate the silicone-rubber membrane and alter the pH of the internal electrolyte layer in contact with a glass pH electrode. Such interference was not observed when microporous teflon membranes were used in place of silicone rubber. These observations suggested that under certain conditions, potentiometric gas-sensing configurations could be useful for detecting relatively large neutral molecules as well as gases. However, because the membrane diffusion rates of the larger organic compounds are considerably slower than those of gases, long response times and even more sluggish recovery times (from high concentration to low) preclude the use of conventional static gas-sensor designs for such purposes.

In the present work, the concept of using a membrane dialyzer as a sample loop in an electrode-based flow-injection arrangement solves this problem by separating the selective molecular dialysis from the down-stream potentiometric sensor. Further improvements in selectivity for one acid over another can be achieved by using a more discriminating indicator electrode as the detector. A schematic diagram of the system designed for salicylate is shown in Fig. 1. A fresh plug of internal recipient buffer is used for each measurement. As illustrated, the upper channel of the dialyzer serves as the injection loop of a conventional flow-injection set-up. Unlike the preceding NO_x system [1], the bottom channel of the dialyzer serves as a second loop into which the test sample is loaded manually as a static plug. Figure 2 shows an expanded view of the dialysis chamber as well as the chemical and physical processes involved. After a fixed trapping time, the solution in the upper channel is flushed to the electrode and the salicylate levels are detected potentiometrically. It will be shown that the use of this membrane-dialyzer/flow-injection arrangement substantially improves the effective selectivity of the polymer membrane electrode such that salicylate can be determined directly in serum.

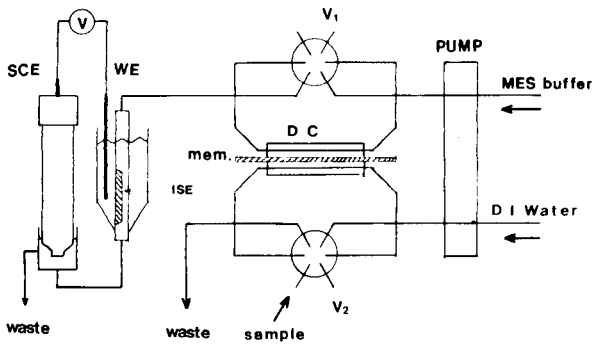

Fig. 1. Schematic diagram of the dialyzer/flow injection set-up for determining salicylic acid; (ISE) tubular PVC ion-selective membrane; (WE) working electrode unit for potentiometric measurements; (SCE) saturated calomel reference electrode; (V) pH/mV meter; (DC) dialysis chamber; (mem) silicone rubber membrane; (V_1, V_2) flow-injection valves.

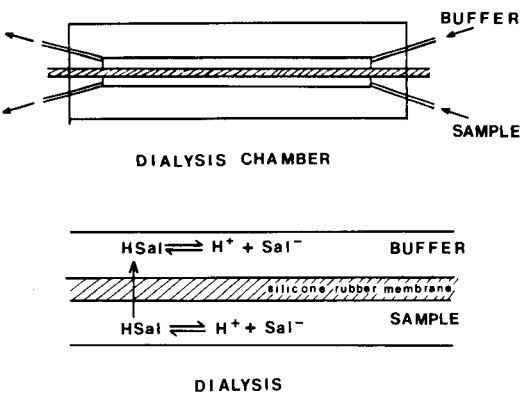

Fig. 2. Expanded view of the membrane-dialyzer unit and outline of the processes which take place therein.

EXPERIMENTAL

Apparatus

A schematic diagram of the final flow-injection system is shown in Fig. 1. An AutoAnalyzer proportioning pump, model-1 (Technicon) was used to deliver the carrier solution (3.2 ml min^{-1}) and a water wash (3.2 ml min^{-1}) through the membrane dialyzer. The dialysis unit was a special wide-channel type identical to that used in the preceding report [1]. The unit was fitted with a 0.1-mm thick vinyl-methyl silicone rubber membrane (SciMed Life System, Minneapolis, MN). For all the data reported here, the dialysis chamber was submerged in a water bath maintained at 25°C. Two Rheodyne (model 5020) 4-way rotary injection valves (V_1 and V_2) were used to introduce the sample and control the dialysis times. All potentiometric measurements were made with a Beckman model 4500 Digital Altex pH/mV meter and recorded on a Heath-Schlumberger strip-chart recorder.

Reagents

All chemicals were reagent grade. Standard and buffer solutions were prepared with distilled-deionized water.

4-Morpholine-ethanesulfonic acid (MES) was obtained from Aldrich. The materials used in electrode preparation were Aliquat-336 (trioctylmethylammonium chloride; Aldrich), dibutyl sebacate and dioctyl phthalate (Eastman-Kodak) and poly(vinyl chloride) powder (PVC; Scientific Polymer Products, Ontario, NY). The manganese(III) tetraphenylporphyrin chloride (MnTPPCl) used to prepare the porphyrin-based salicylate electrode was a gift from Professor John Groves, Princeton University.

For the porphyrin-based electrode system, 0.05 M MES/sodium hydroxide buffer, pH 6.5, was used as both the carrier and recipient solution in preliminary characterization studies. For serum measurements, a 0.1 M MES/sodium hydroxide buffer, pH 6.5, was used. In studies with the Aliquat-based salicylate electrode, a 0.05 M Tris(hydroxymethyl)aminomethane/phosphoric acid buffer, pH 8.0, served as the carrier and recipient solution.

Preparation and characterization of tubular flow-through salicylate electrodes

Two types of salicylate-sensitive electrodes were investigated. Both were fabricated with 0.89 mm i.d. PVC tubing in a manner similar to that described for preparation of potassium electrodes [10]. One simplification in the design involved threading the tubular electrode through the small open end of a plastic Finnpipette tip to form a compartment in which the internal reference solution and Ag/AgCl electrode can be placed. The tight fit of the electrode tubing within the small opening of the pipette tip formed a natural seal. Once filled with internal reference solution, a piece of Parafilm was used to seal the top of the assembly to prevent slow evaporation of the internal solution.

The Aliquat 336-based electrodes were prepared by using the casting solution described by Choi and Fung [6] for fabrication of their salicylate-responsive electrode. A 0.1 M sodium chloride solution containing 0.01 M sodium salicylate and saturated with silver chloride was used as the internal reference fill. The MnTPPCl-based salicylate electrode was prepared with the following casting solution: 1.2 mg of MnTPPCl, 30 mg of PVC powder, and 60 μl of dibutyl sebacate, all dissolved in 1 ml of freshly distilled tetrahydrofuran. A 0.05 M MES/sodium hydroxide buffer, pH 6.5, containing 0.01 M sodium salicylate and 0.1 M sodium chloride was used as the internal reference solution.

Evaluation of polymer-membrane electrodes. Before the final dialyzer/flow-injection system was used, both of the tubular salicylate electrodes were evaluated for response toward salicylate, as well as other anions. This was accomplished by using the appropriate carrier-stream buffer solution for each of the electrodes and directly loading standard solutions of sodium salicylate or other anion salts (prepared in the working buffer) into the flow-

injection loop provided by the top channel of the dialyzer. The loop was loaded manually by suction with a syringe. This direct-injection mode enabled the performance of the electrodes to be evaluated without changing the working parameters of the final system (e.g., flow rates, pressures and dispersion). Calibration and selectivity data were obtained by measuring the peak height (ΔE, from the baseline) of the potentiometric signals and plotting these values vs. the logarithm of the anion concentration.

Evaluation of final membrane-dialyzer/flow-injection arrangement

In these studies, standard solutions of salicylate or other anions were prepared in 0.05 M sulfuric acid. Before introduction of the sample through the valve (V_2 in Fig. 1), both valves were turned to the load position. Thus, in the V_1 loop, a fresh segment of recipient buffer solution was stopped within the dialyzer channel. The standard solutions were then loaded by suction through valve V_2 into the lower channel of the dialyzer. The total volume of the loop V_2 was 0.68 ml (including connecting tubing), and use of 2 ml of sample ensured that the loop was completely flushed of the previous solution and that the lower dialyzer channel was completely filled with sample. The sample remained in the chamber for a fixed time (2 min in most experiments). At the end of this period, both valves were turned to the "inject" position and the recipient plug passed through the tubular electrode to waste. At the same time, the sample solution was flushed from loop V_2. Calibration and selectivity data were obtained by measuring the peak height (ΔE) for each sample as described above.

Procedure for salicylate in serum

Some unidentified outdated plasma was obtained from the Department of Public Health, Washtenaw County, Michigan. This frozen plasma was thawed, centrifuged to remove any particulate matter, and then stored at 5°C until use. Preliminary measurements indicated that the plasma did not contain any measurable salicylate. Thus, it provided a suitable serum-like matrix in which to prepare standards. These standards were prepared by spiking various aliquots of plasma with known amounts of sodium salicylate. Calibration curves were obtained by injecting 1:5 dilutions (1 part sample and 4 parts acid) of these standards (in 0.05 M sulfuric acid) into the dialyzer/flow-injection system.

Recoveries were studied on a serum sample drawn from one of the authors who did not previously ingest aspirin. Again, this serum sample initially had an insignificant concentration of salicylate as measured with the electrode-based instrument. Aliquots of this serum sample were spiked with different levels of salicylate. The spiked samples were then diluted 1:5 with acid and the resulting peak potentials were recorded and compared to a two-point working curve prepared with the plasma-based standards.

RESULTS AND DISCUSSION

Responses of the electrodes based on MnTPPCl and Aliquat-336

In preliminary studies with the membrane dialyzer system, Aliquat-336 was used as the active membrane component in the salicylate-sensitive polymer electrode described by Choi and Fung [6]. However, results from these feasibility experiments indicated that in order to obtain adequate detection limits for serum, impractically long trapping times would be required. This was due to the relatively poor response of the Aliquat membrane to salicylate in the flow system (see Fig. 3) in combination with a 3—4% salicylate transfer efficiency within the dialyzer (based on acceptable trapping times, e.g., 2 min). Consequently, the possibility of using other ion-exchangers or carriers was investigated to obtain a polymeric salicylate electrode with better detection capabilities.

Separate studies in this laboratory with conventional polymer-electrode designs had indicated that membranes based on MnTPPCl responded to salicylate at very low concentrations when MES buffer, pH 6.5, was used as the background electrolyte. The response of a tubular flow-through design in which the polymer membrane was prepared with MnTPPCl was then directly compared with the response to salicylate of the Aliquat system. From Fig. 3, it is evident that the porphyrin-based membrane offers a significant improvement in detection limits while maintaining a nearly Nernstian slope (typically 60—64 mV/decade) over a wide concentration range (2×10^{-6}—10^{-2} M). Fresh MnTPPCl-based electrodes often had even higher slopes (e.g., 70—80 mV) but this super-Nernstian behavior usually disappeared after the first day of use. It should be noted that the data shown in Fig. 3 were obtained with the same flow-injection set-up, but with different background electrolyte buffers (carrier solutions). Separate experiments indicated that these background electrolyte buffers yielded the optimum response to salicylate

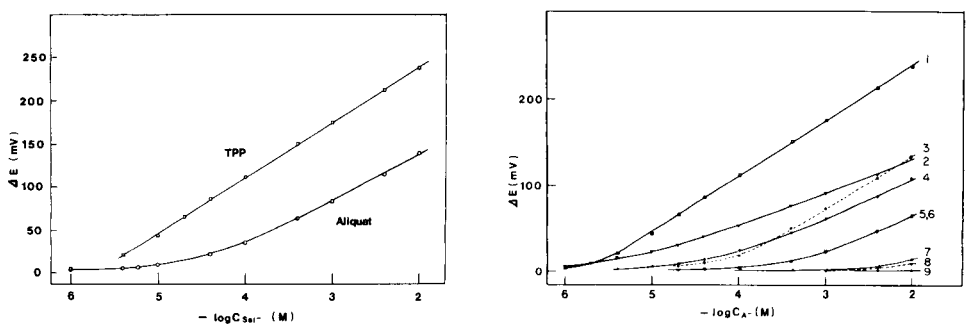

Fig. 3. Responses of the electrodes based on MnTPPCl and Aliquat-336 to salicylate in appropriate buffers in the f.i.a. arrangement.

Fig. 4. Response of the MnTPPCl membrane to various anionic species in MES/NaOH buffer, pH 6.5: (1) salicylate; (2) ClO_4^-; (3) acetylsalicylate; (4) benzoate; (5) Cl^-; (6) Br^-; (7) lactate; (8) HCO_3^-; (9) oxalate.

for the respective electrode systems (i.e., the Aliquat-based electrode had much worse detection limits when evaluated in the 0.05 M MES/sodium hydroxide, pH 6.5, than in the Tris buffer). Based on these experiments, the porphyrin electrode was used in all subsequent studies.

Aside from improved detection capabilities, the MnTPPCl-based membrane also exhibited an interesting selectivity pattern toward other anionic species. Figure 4 shows the potentiometric response of this membrane to salicylate as well as other inorganic and organic ions in the flow system. It was found that most of the response to acetylsalicylic acid was due to the presence of salicylate in the standards as a result of hydrolysis of the test compound in the pH 6.5 MES/sodium hydroxide buffer. Overall, the response pattern closely resembles, but is not identical to, the Hofmeister sequence most often observed for anion-responsive liquid-membrane electrodes based on ion-exchangers [7]. For example, response to bromide and chloride is essentially the same, yet the Hofmeister sequence predicts greater response to bromide. In addition, response slopes for certain anions (e.g., perchlorate) are considerably sub-Nernstian over a rather wide concentration range. Further, in separate experiments (not shown), it was found that the MnTPPCl membrane has a rather large response to hydroxide even at hydroxide levels approaching 10^{-9} M. This mandates the use of a relatively strong buffer when this electrode is applied. While the exact mechanism of ion extraction and transport by the MnTPPCl within the membrane is not clear, it is believed that the porphyrin behaves as an ion-exchanger or neutral carrier (depending on whether the fifth axial ligand is neutral or anionic) to which salicylate can coordinate as a sixth axial ligand with the manganese center. Recent studies by Schulthess et al. [11] on a new membrane electrode for nitrite based on the use of a Vitamin B_{12} derivative support this hypothesis.

While the MnTPPCl electrode displayed desirable detection limits and an unusual selectivity pattern, its useful lifetime was much less than that of the Aliquat-based electrodes. Indeed, with constant use over a 1-week period, the baseline potential continuously became less positive, and detection limits for salicylate gradually became poorer. Therefore, the MnTPPCl membrane was typically replaced every 7—10 days.

Response characteristics and selectivity of the dialyzer/flow-injection system for salicylic acid

When acidified salicylate samples are loaded into the lower channel of the dialyzer, the salicylic acid molecule partitions into the silicone rubber (Fig. 2) and diffuses through the membrane. This process is aided by the buffer trap (MES/sodium hydroxide, pH 6.5) provided by the fresh recipient solution in the upper channel. This solution traps the salicylic acid as salicylate, thereby maintaining a large chemical potential gradient of salicylic acid across the membrane. Figure 5 shows a typical strip-chart recording obtained with this system for aqueous salicylic acid standards and a 2-min trapping time. It can be seen that, despite the manual operation of the valves, reproducibility of

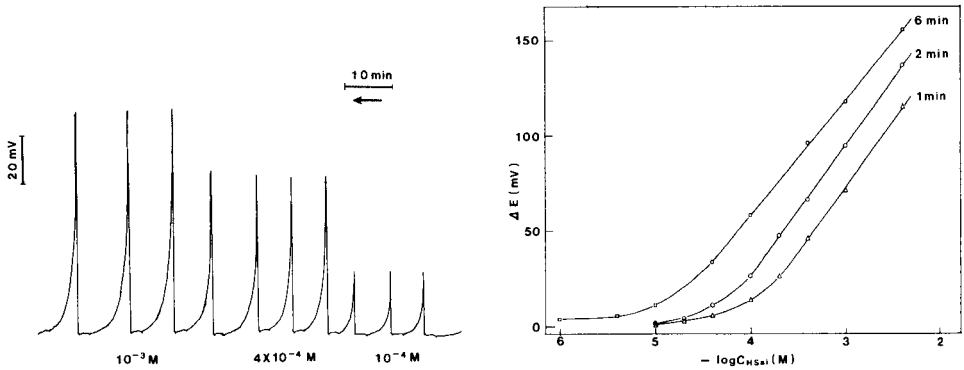

Fig. 5. Typical strip-chart recording obtained from the dialyzer/flow-injection arrangement for replicate injections of aqueous salicylic acid standards using 2-min trapping times.

Fig. 6. Effect of trapping time (1—6 min) on the response of the dialyzer/flow-injection arrangement to salicylic acid.

the peak heights is good (standard deviations for triplicate injections of the same standards are typically about 1.4 mV). However, it can also be seen that the baseline recovery time after each sample injection is rather long. These tailing peaks are caused by the reservoir of salicylic acid left behind in the silicone membrane (which continues to leach out even after injection) as well as the inherently slow recovery times of the porphyrin-based membrane. The latter was observed in the direct-injection experiments undertaken to characterize the tubular membrane electrode and can be attributed to a high association constant between the salicylate anions and the porphyrin within the membrane.

Naturally, for given salicylic acid concentrations, the magnitude of the potentiometric response was governed by the trapping time. Figure 6 shows how the detection limits of the system can be improved by using a longer trapping period. For the 2-min trapping time used in much of this work, the efficiency of salicylic acid transfer from the sample to the recipient solution was calculated to be typically 4—7%, based on prior direct-injection calibration of the salicylate electrode. This trapping efficiency increased when the dialyzer was maintained at higher temperatures; however, elevated temperatures tended to cause outgassing of the solutions and bubble problems. Thus, all experiments were done with the dialyzer thermostatted at 25°C. At this temperature, there usually is a slight increase in dialysis efficiency with increasing concentration of salicylic acid and this effect causes somewhat super-Nernstian behavior in the final sensing arrangement (e.g., slopes are generally 64—70 mV/decade) even when the tubular MnTPPCl electrode itself has Nernstian response properties. This type of behavior has been observed previously with gas sensing dialyzer systems [2, 12].

The selectivity of the final membrane-dialyzer/flow-injection arrangement

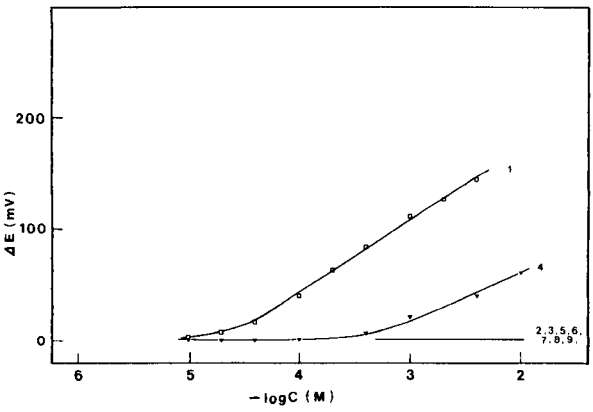

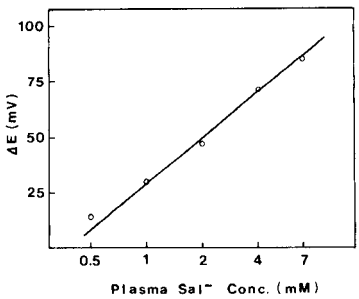

Fig. 7. Potentiometric response of the dialyzer/flow-injection arrangement to various species in acid using a 2-min trapping time. Numbers refer to the anions in Fig. 4.

Fig. 8. Calibration curve obtained for plasma-based salicylate standards. (Plotted as concentration of salicylate in plasma prior to dilution with acid.)

is excellent. As shown in Fig. 7, most of the inorganic and organic ions tested yielded no response at 10^{-2} M concentrations. Even higher levels of chloride (10^{-1} M) also resulted in negligible potentiometric response. Comparison of these results with those in Fig. 4 clearly illustrates how the silicone-rubber membrane effectively eliminates anionic interferences for those species which cannot permeate this membrane. For example, perchlorate, which is a major interferent with the porphyrin-membrane electrode alone (see Fig. 4) apparently does not get through the silicone-rubber membrane, at least not during the 2-min trapping period. Among the organic acids tested, only benzoic acid represents a significant interference, although the system is more responsive to salicylic acid by a factor of nearly 60. In this case, the selectivity pattern closely parallels that obtained by direct injection through the membrane electrode because both species probably diffuse through the silicone rubber membrane at nearly the same rate. Thus, in practice, ultimate selectivity is dictated by the kinetics of transfer through the silicone membrane and the intrinsic response of the detecting electrode toward the anionic form of the species.

Salicylate in serum

Preliminary efforts to determine the salicylate content of serum samples with aqueous salicylate standards proved difficult. Recovery studies with salicylate-spiked serum consistently yielded recoveries between 60 and 70% despite the fact that the samples were first diluted 1:5 with acid prior to being loaded into the membrane dialyzer. Clearly, the protein content of the serum was affecting the efficiency of salicylic acid transfer across the silicone-rubber membrane. To overcome this matrix effect, salicylate standards were

TABLE 1

Summary of salicylate results for serum

Salicylate conc. (mM)				
Added	Found[a,b]		Recovery (%)	
	Day 1	Day 2	Day 1	Day 2
1.00	0.96	1.01	96	101
2.00	1.72	1.96	86	98
4.00	4.22	3.59	105	90

[a]From a 2-point calibration made before test. [b]Values are the average of two determinations.

prepared in a plasma matrix. Figure 8 shows a typical working curve obtained with these standards. It can be seen that the plot is linear over the range of salicylate concentrations required for blood measurements [4]. A two-point calibration in this range was used in a further recovery study of spiked serum samples. Table 1 shows that recoveries ranged from 86 to 105% for two separate experiments. In view of the uncertainties associated with manual control of the trapping time as well as the time needed for manual loading of the sample, these results are considered satisfactory so that the proposed method can be used to estimate salicylate concentrations in serum. Fully automated arrangements would obviously provide better precision.

The authors gratefully acknowledge the National Institutes of Health for supporting this work (Grant GM-28882-05).

REFERENCES

1 G. B. Martin and M. E. Meyerhoff, Anal. Chim. Acta, 186 (1986) 71.
2 Y. M. Fraticelli and M. E. Meyerhoff, Anal. Chem., 53 (1981) 992.
3 W. N. Opdycke, S. J. Parks and M. E. Meyerhoff, Anal. Chim. Acta, 155 (1983) 11.
4 R. V. Blanke, in N. W. Teitz (Ed.), Fundamentals of Clinical Chemistry, Saunders, Philadelphia, 1976, Chap. 21.
5 P. Trinder, Biochem. J., 57 (1954) 301.
6 K. K. Choi and K. W. Fung, Anal. Chim. Acta, 138 (1982) 385.
7 W. E. Morf, The Principles of Ion-Selective Electrodes and of Membrane Transport, Elsevier, Amsterdam, 1981, Chap. 11.
8 N. Weissman and V. J. Pileggi, in R. J. Henry, D. C. Cannon and J. W. Winkelman (Eds.), Clinical Chemistry, Principles and Technics, Harper and Row, Hagerstown, MD, 1974, Chap. 19.
9 R. K. Kobos, S. J. Parks and M. E. Meyerhoff, Anal. Chem., 54 (1982) 1976.
10 P. M. Kovach and M. E. Meyerhoff, J. Chem. Educ., 60 (1983) 766.
11 P. Schulthess, D. Ammann, B. Kräutler, C. Caderas, R. Stepánek and W. Simon, Anal. Chem., 57 (1985) 1397.
12 H. L. Lee and M. E. Meyerhoff, Analyst, 110 (1985) 371.

Analytica Chimica Acta, 186 (1986) 91—100
Elsevier Science Publishers B.V., Amsterdam — Printed in The Netherlands

BIPOLAR PULSE CONDUCTOMETRIC DETECTION OF ENZYME REACTIONS IN FLOW-INJECTION SYSTEMS
Urea in Serum and Urine

DOUGLAS TAYLOR[a] and TIMOTHY A. NIEMAN*
School of Chemical Sciences, University of Illinois, Urbana, IL 61801 (U.S.A.)
(Received 11th November 1985)

SUMMARY

Conductometric monitoring of enzymatic reactions in a flow-injection system is described. Two conductance cells are used and the responses are manipulated automatically to provide a differential signal. The hydrolysis of urea, catalyzed by urease, is used as an example to illustrate the technique. Blood serum and urine control standards are used to assess the precision and accuracy. The conductometric method is shown to be equal to, or better than existing methods for urea with regard to detection limits (0.1 mM in urine, 0.01 mM in serum), working range, precision (3% RSD), accuracy, and sample preparation. The method has a sample throughput of 20 h^{-1}.

There has been a steady increase in the applications of flow-injection methods because of its speed, ease of automation, increased reproducibility and reagent conservation [1]. The common detectors for flow-injection systems are u.v.-visible photometers, ion-selective electrodes and electrochemical cells. Conductance can be very sensitive [2], but conductometry is generally not selective and has been little used for monitoring reactions in flowing streams. Usually some other process must be coupled with conductance to give the needed selectivity.

Enzyme/substrate reactions are some of the most selective reactions known [3]. Especially for clinical chemistry, a significant number of these reactions has been incorporated into flow-injection systems. There are many enzyme/substrate reactions which can cause a change in the ionic strength of the solution under investigation, and this change in ionic strength can be monitored by conductance measurements. Examination of tabulations of enzymes and the reactions that they catalyze [4] indicates a variety of oxidoreductases, hydrolases, and lyases which are candidates for conductance monitoring. Some of these reactions have been followed by conductance, e.g., those with amino acid oxidase, lipase, elastase, asparaginase, urease, adenosine deaminase, and lysine decarboxylase [5, 6]. For example, urease catalyzes the hydrolysis

[a]Present address: Lederle Laboratories, Process Research and Development, Building 110, Room 614, Pearl River, NY 10965, U.S.A.

0003-2670/86/$03.50

of urea to ammonia (weak base) and carbonic acid (weak acid); the ammonia and carbonic acid then react to yield ammonium and hydrogen carbonate ions in the presence of a buffer, B:

$$HB + Urea + 2H_2O \xrightarrow[pH\ 7]{Urease} 2NH_4^+ + HCO_3^- + B^- \quad (1)$$

Reactions which release only a weak acid, such as conversion of glucose to gluconic acid as catalyzed by glucose oxidase, can also be monitored if the buffer used is neutral or positively charged in its basic form, e.g., Tris [tris-(hydroxymethyl)-aminomethane] [7]. Release of just a weak base, most often ammonia, can also be monitored if the buffer is neutral or negatively charged in its acidic form (e.g., phosphate).

Assays based on conductometric monitoring of enzyme/substrate reactions are usually rate methods in order to discriminate against differences in background conductivity from one sample to the next. For a given sample, the background signal will remain constant but the signal caused by the analyte increases with time as the reaction proceeds. Use of a rate method requires that at least two measurements of the conductance be made at different times. Adapting a rate method to flow injection is desirable because of the sensitivity and selectivity possible by combining conductance and enzymes, and the convenience of flow-injection systems.

Urea is a very common analyte in clinical and agricultural applications [8, 9]. Numerous methods have been developed to determine urea; because of the specificity of urease for urea [10], many of these methods have been based on enzymatic hydrolysis [7, 11—15], one or both of the hydrolysis products being monitored. Usually the ammonium ion is detected, either by further reaction to form a colored or fluorescent product, or by ion-selective electrodes [11—14, 16]; because ammonia is often present in natural samples, these methods can suffer from interferences and give incorrect values. Present conductometric methods for urea monitor the rate of production of the ionic products from the nonionic urea in the enzymatic reaction and are done in batch mode to allow measurement of the extent of reaction at different times [7, 15].

This paper describes the principles involved in adapting a conductometric method to a flow-injection system. The hydrolysis of urea catalyzed by urease is used as an example. The method is applied to the determination of urea in urine and serum and compared to presently available methods with respect to sample throughput, sample preparation, dynamic working range, and precision.

EXPERIMENTAL

Instrumentation and reagents

The computer-controlled bipolar-pulse conductance (BICON) instrument used has been described in detail [17]. Of importance for this work, the instrument has a multiplexed input to make measurements on multiple cells.

The conductance cells were made from two pieces of plexiglas with platinum rods (1.0-mm diameter) for electrodes. The design was based on previous work on conductance flow cell design [18]. The electrodes were polished flush with the plexiglas surface. The two plexiglas halves were separated by a teflon spacer 0.38 mm thick. The electrode faces were directly opposite each other when the cell was assembled. The total cell volume was approximately 30 μl.

The basic arrangement is shown in Fig. 1. For the present work, it is necessary to make conductance measurements at different extents of reaction, therefore multiple cells are necessary. Cell 1 monitors background ions before reaction with the enzyme. Cell 2 monitors the sum of product and background ions after reaction. The difference between cell 1 and 2 is proportional to the concentration of the ions created in the enzyme column, which in turn is proportional to the amount of urea present in solution. The instrument was used in the voltage pulse mode with 1-V pulse height and 10-μs pulse width. The conductance reading from cell 2 was output to a chart recorder. The peak areas on each cell and the difference between were displayed at a terminal.

Urease was covalently bound to controlled-pore glass (CPG) and contained in a plexiglas column (3.2-mm i.d. $\times$ 57-mm long) capped with nylon end fittings with 1/4—28 couplings. The caps had 20-μm stainless steel frits to contain the CPG. Enough enzyme was immobilized on the CPG to cause complete reaction of at least 10 mM urea in the 39 s required to pass through the column. This means that the method is not a rate method but rather a differential equilibrium method because the reaction is either 0 or 100% complete as long as the sample concentration is $\leqslant$10 mM. By taking the difference between measurements at two different extents of reaction, one still maintains freedom from interference by substances with fixed concentrations.

The flow system consisted of a Rainin Rabbit peristaltic pump (0.7 ml min^{-1}), A Rheodyne model 5020 injector with 70-μl injection loop, and 0.8-mm i.d. teflon tubing with 1/4—28 connectors.

The urease (E.C. 3.5.1.5) was from Sigma (type IX). Analytical-grade urea, $NaH_2PO_4 \cdot H_2O$, $Na_4P_2O_7 \cdot 10H_2O$ and NaCl (Mallinckrodt) were used as

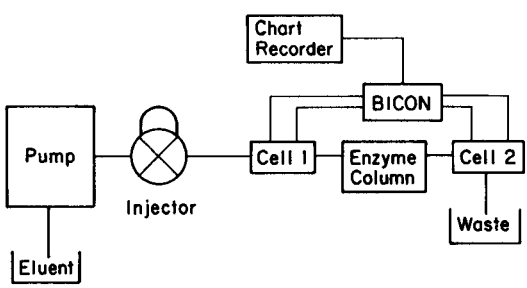

Fig. 1. Block diagram of the flow system.

received. Solutions were made with water purified in a Continental/Millipore Milli-Q water treatment system. Aqueous urea standards were stable for 1 week if refrigerated when not in use.

Enzyme immobilization scheme

The enzyme was immobilized on the CPG by using a modification of a procedure developed by Klopf and Nieman [19]. A 0.5-g quantity of CPG (Electronucleonics, 25-nm pore diameter, 125—177-μm particle diameter) was washed with concentrated nitric acid, filtered, washed with water, and then silanized by reacting at 90°C for 3 h with (3-aminopropyl)triethoxysilane in 0.05 M acetate buffer at pH 5.0. Approximately 0.5 ml of the silane was added to 30 ml of the buffer which had reached the reaction temperature. The CPG was then filtered and washed on a sintered glass filter. To the silanized CPG, 1 ml of glutaraldehyde (25%) and 1 ml of 0.1 M pyrophosphate buffer, pH 7.0, were added. The mixture was kept at room temperature for 2.5 h. For the first 30 min, the reaction proceeded under vacuum to reduce the partial pressure of oxygen. The CPG was again filtered and washed. Urease was attached by placing the CPG in a filter flask and adding 10 ml of enzyme solution which contained 10 mg ml^{-1} of urease in 0.1 M pyrophosphate buffer at pH 7.0. The reaction temperature was 4°C. Again for the first 30 min, the reaction proceeded under vacuum. The CPG was left in contact with the enzyme solution for approximately 24 h in a refrigerator. The last step was to filter and wash the CPG and store it in phosphate buffer (0.1 M, pH 7).

Measurement procedure

The order of injection was sodium chloride solutions for cell calibration, then the urea standards, and finally the urine or serum samples. Typically, three injections were made for each solution and the measurements for those replicate injections were averaged. The cell response curves were calculated and then the corrected area differences for the standards and samples were calculated. The concentrations of the samples were obtained using the least-squares line from the corrected area difference vs. urea concentrations as the working curve. When urine was the sample of interest, the carrier stream was 20 mM phosphate buffer at pH 7.3 and the sodium chloride concentrations were 0—10 mM. Thus, the cell calibration curves approximated the true plot of conductance vs. concentration in the region of the sample background ion concentration (approximately 4 mM). When serum was the sample, the carrier was 2.0 mM and the sodium chloride solutions only covered the range 2.5—3.5 mM. In this case, the calibration curves represented the tangent to the true conductance vs. concentration curves in the concentration range expected from the background ions. The urea standards for the serum trials contained 3.0 mM sodium chloride so that the cell calibration curves would be accurate for the standards as well as the unknowns. The need for sodium chloride is explained later. All urea and

sodium chloride standards contained phosphate buffer at 25 mM for the urine work and 2.5 mM for the serum work. The lower buffer concentration was used with serum because the analyte concentration range was lower than with urine. Lowering the background concentration kept the signal-to-background ratio the same for each type of sample.

Sample treatment for urine and serum

Urine controls (Urichem Level I, lot 484-024; Fisher Diagnostics) were reconstituted as directed with water. The samples were then diluted 100-fold. The diluted samples also contained 25 mM phosphate buffer, pH 7.3. Dilutions of 1200 and 1500 were also used. The Somogyi-Nelson method for deproteinization [20] was evaluated but caused the pH of the samples to change so drastically that the enzyme reaction did not proceed well. Also, the method is much more time-consuming (20 vs. 2 min/sample for the dilute and inject method) and troublesome so its use was discontinued. For the within-day reproducibility studies, five different dilutions were prepared from the same bottle of reconstituted urine. Between-day samples came from different bottles but all were from the same lot. The reconstituted urine was stable for at least a week if kept refrigerated. Dilutions of the reconstituted urine were made fresh daily.

The serum controls (Moni-Trol ES Level II, lot PTS-102; American Dade) were reconstituted with the carbonate diluent supplied by the manufacturer. The serum was then filtered using a centrifugal filtration process (Centrifree; Amicon). Approximately 1 ml of serum was placed in each of the filtration units. The samples were centrifuged for 1.5 h to obtain about 0.5 ml of colorless filtrate. The filtrate was then diluted 50-fold. The diluted samples also contained 2.5 mM phosphate buffer, pH 7.3. No other sample treatment was applied. The filtrate and diluted samples were only stable for one day.

RESULTS AND DISCUSSION

Initial column check

The column was first checked to see if an acceptable working curve for urea was possible. This was accomplished by making a set of aqueous urea standards with concentrations between 0.1 and 10 mM in 10 mM phosphate buffer at pH 7. The carrier stream was water initially and cell 1 was not in the system at this time. Injections of each standard plus a buffer blank were made and the heights of the resulting peaks were measured. A log-log plot of the peak height of a standard minus the peak height of the blank against the urea concentration was linear from 0.5 to 10 mM. Peaks from the most concentrated standards were 5—6 min wide at the baseline, but peaks for lower concentrations or for injections of other electrolytes were only 2 min wide. This tailing was probably due to absorption of urea [21], or perhaps ammonia, on the beads of the column. The phenomenon could be avoided if the ionic

strength of the carrier was made high enough. In this case, use of 20 mM phosphate buffer in the carrier was sufficient. The sample buffer concentration was also increased to 25 mM. The buffer concentration of the blank and the samples was made greater than that of the carrier stream to assure that a positive peak would be seen on cell 1 because the program could not detect negative peaks.

The efficiency of the column was also checked. This was done by comparing the areas from injections of a strong electrolyte with those from aqueous urea standards. Equation 1 shows that for each urea molecule, two positive and two negative ions are added to the solution. A 1 mM solution of urea, after hydrolysis, should give the same signal as 2 mM sodium chloride if the hydrolysis reaction goes to completion and if Na^+ and NH_4^+ show the same conductance, and if HCO_3^-, B^- and Cl^- show the same conductance. This was in fact what was seen and demonstrated that the column was 100% efficient at converting urea to ammonium and hydrogencarbonate ions under the conditions tested (flow rate 0.7 ml min^{-1}, maximum concentration of 10 mM).

Cell calibration

Cell calibration is needed because the two cells will not give the same response to the same number of ions (Fig. 2). As a result, two samples with the same urea concentration but different background ionic strengths would not give the same response. To account for this dissimilar response, the two cell response curves must be rotated and translated into coincidence. By injecting solutions of a strong electrolyte, at varying concentrations, response curves can be calculated. Normally, the response curve is taken as the least-squares line calculated from the area vs. concentration data from injections of strong electrolyte. However, the conductance vs. concentration curve is not truly linear. This non-linearity can be accounted for in two ways. If the background ion concentrations found in the samples cover only a small range, such as in biological samples, then the response curve can be adequately

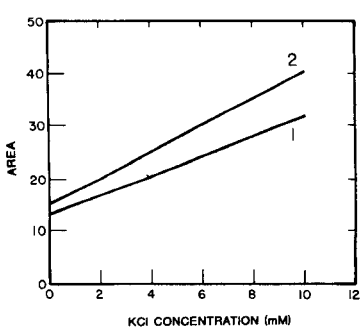

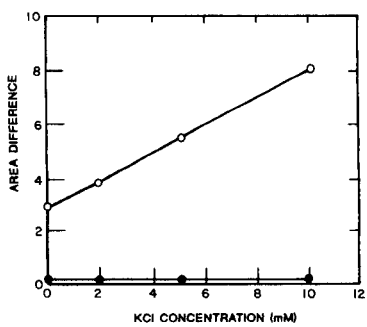

Fig. 2. Uncorrected calibration curves: (1) for cell 1; (2) for cell 2.

Fig. 3. Calibration check using KCl injections: (○) uncorrected areas; (●) corrected areas.

approximated by a straight line over a short concentration range. The least-squares line will be the tangent to the conductance vs. concentration curve. In this case, the standards should also have a background ion concentration at about the mid-point of the range covered by the strong electrolyte standards. This ensures that the cell correction curves are valid for the urea standards. The alternative is to cover a large range of concentrations with strong electrolyte injections and to use regression to fit the data to a non-linear equation such as conductance = constant $- b(\text{concentration})^{1/2}$. This would make the rotation and translation into coincidence more complex, but would be better for situations in which the background ion concentrations are not similar from sample to sample. With most biological samples (blood, urine, etc.) the background matrix is very similar between samples.

If straight lines are used to describe the cell responses, then the following equation can be used to translate and rotate them into coincidence.

$$\text{Corrected area difference} = (Y_2 - B_2) - (Y_1 - B_1)M_2/M_1 \quad (2)$$

where Y_i is an area reading on cell i, B_i and M_i are the slope and intercept for the cell response curve for cell i. By using this equation, the corrected area difference will be zero if no reaction occurs between cell 1 and cell 2, regardless of the background ionic strength of the sample. Figure 3 shows two working curves; one is the uncorrected area difference vs. concentration, and the other is the corrected area difference vs. concentration for injections of potassium chloride. Because no reaction occurred between cell 1 and cell 2, the corrected area difference should be zero. This was used as a check of the correction equation. As a second check, samples of 3 mM urea, with and without 5 mM NaCl, were compared. The cell response curves were calculated from injections of sodium chloride. The uncorrected area differences were 10.29 and 12.04 for 3 mM urea without and with 5 mM NaCl, respectively. However, the corrected area differences agreed within 1.3% experimental error and were 9.25 and 9.38 for the two solutions.

Performance characteristics

The detection limit (signal-to-noise ratio of 2) depended on the experimental conditions used. When the measurement was done with a blank buffer concentration of 25 mM, the detection limit was 0.1 mM. When the blank concentration was decreased to 2.5 mM, the detection limit decreased to 0.01 mM. Typical reproducibility for multiple injections of the same solution was 3% relative standard deviation (RSD). The sample throughput was 20 h^{-1} and the peak widths were near 2 min at the baseline. Figure 4 shows a typical urea working curve. The diameter of the points represents the error bars for ± one standard deviation. The expected range of urea concentrations in urine, after dilution by 100, is also given. The conductometric method is similar to other methods with regard to detection limits, dynamic range and precision. Because of the possibility of changing the background buffer concentration, the dynamic range and detection limits are actually better than those of most methods. The conductance method, because of the specificity of the enzyme, has no interferences.

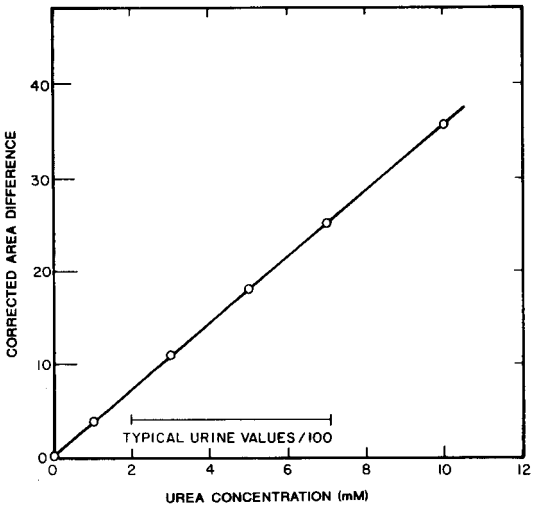

Fig. 4. Urea working curve.

The choice of background buffer strength depends on the concentrations of analyte expected. Because the reaction being monitored releases a weak acid and base, the buffer should have enough capacity to prevent significant pH changes (>0.5 pH units). Changes in pH may change the enzyme activity or may change the degree of ionization of the products, thus causing non-linear calibration. The matrix of the sample may also have some bearing on the choice of buffer concentration. The buffer should be more concentrated than any buffers in the sample, again so that the pH is not greatly changed. When in doubt, the pH of an unknown should be checked and matched to an aqueous standard.

Air bubbles in the flow cells must be avoided. The bubbles cause changes in the flow pattern within the cell and affect sample dispersion which will change the area measurement. Also, the bubbles cause additional tailing of the peak. This tailing is possibly due to ammonia going into the gas phase and then slowly dissolving back into solution. The tailing effect was not seen when sodium chloride was injected, even with a bubble in the cell. If the cell is taken apart to get rid of a bubble, then the system needs to be recalibrated.

Application to urine and blood serum

Results from injections of urine controls are given in Table 1. The reported and found values show excellent agreement for the 1/100 dilution. The relative standard deviation of five separate assay values indicated within-day precision of 2.5%. Results on four successive days were 3.46, 3.52, 3.37, and 3.45 mM, corresponding to 1.8% RSD. There is no difference between the day-to-day and within-day precision values based on the *F*-test at the 95% confidence level.

Results for dilutions of 1/500 and 1/200 are also given in Table 1. As the dilution factor gets higher, results become increasingly worse. This is probably

TABLE 1

Results for urea in urine and serum control samples

Solution	Concentration ±2 SD (mM)	
	Reported[a]	Found
Fisher Urichem Control/100	3.46 ± 0.36	3.46 ± 0.36[b]
Fisher Urichem Control/200	1.73	1.96
Fisher Urichem Control/500	0.692	0.877
Monitrol II Serum Control	18.6 ± 1.07	18.4 ± 1.35[c]

[a]From data provided by the manufacturer. [b]Average of results from five separate dilutions with twice the pooled standard deviation (roughly a 95% confidence interval). [c]Average of four injections on duplicate samples from the same lot.

due to errors in the correction procedure. The cell correction curves approximate the true conductance vs. concentration curves best at the 1/100 dilution range. The curves are not accurate for lower concentrations of background ions. It was coincidental that the background ion concentrations were in the proper range with the 1/100 dilutions. This would indicate that the best method for calculating the cell response curves is the one used for serum if the background ion concentrations are within a narrow range. In this case, only a small portion of the conductance vs. concentration curve is approximated, the range where the background ion concentration is expected to be. If the background ion concentration is unknown, then an approximate value for the analyte concentration can be obtained by using sodium chloride concentrations which cover a larger range, as was done in this case.

The results in Table 1 for serum show that the conductometric method compares well with the method used by the supplier. The precision is similar to that in the urine trials. The serum trials indicated the need for accurate cell correction curves. Originally, 0—5 mM solutions of sodium chloride were used. Results from these experiments yielded urea concentrations which were too high because the equations for the cell response curves did not approach the true cell response curves in the concentration range of the background ions. However, the expected range of background ions is very narrow and well characterized in serum [22]; thus when the sodium chloride concentrations used encompassed just this narrow range, the cell correction curves accurately reflected the true response of the cells and the serum values became more in line with the manufacturer's reported values.

The conductometric method is similar to other methods in terms of detection limits (0.1 mM in urine, 0.01 mM in serum), working range (0.01—10 mM) and precision, both within-run (2.5%) and day-to-day (1.8%). The conductometric flow-injection method is rather slow in sample throughput relative to many flow-injection methods but it is not unrealistic compared with the typical sample throughput of 50 h^{-1} for other flow-injection methods for urea. The method is equal to or superior to other methods in the areas of interferences and ease of sample preparation.

Conclusions

The use of compound-specific enzyme/substrate reactions in flow injection with conductometric monitoring can be extended in two ways. Other ion-producing enzyme reactions could be used, e.g., the deamination of histidine catalyzed by histidine ammonia lyase (E.C. 4.3.1.3). Two sequential enzyme reactors could be applied, the second reactor serving to produce ions from the product of the first. For example, if the first reactor contained creatinase (E.C. 3.5.3.3), which catalyzes the hydrolysis of creatine to sarcosine and urea, the urea produced could be detected as outlined in this paper. The conductometric flow-injection technique could thus be extended to several dozen enzyme/substrate systems.

REFERENCES

1 H. Mottola, Anal. Chem., 53 (1981) 1312A.
2 D. A. MacInnes, The Principles of Electrochemistry, Dover Publications, New York, 1961, Chaps. 3, 18.
3 P. Carr and L. D. Bowers, Immobilized Enzymes in Analytical and Clinical Chemistry, Wiley, New York, 1980, Chap. 4.
4 Enzyme Nomenclature, 1978 International Union of Biochemistry, Nomenclature Committee, Academic Press, New York, 1979.
5 A. J. Lawrence and G. R. Moores, Eur. J. Biochem., 24 (1972) 538.
6 C. Ballot, B. Saizonou-Manika, C. Mealot, G. Favre-Bonvin and J. M. Wallach, Anal. Chim. Acta, 163 (1984) 305.
7 M. Hanss, C. Policard and J. Pre, Ann. Biol. Clin., 35 (1977) 343.
8 A. L. Lehninger, Biochemistry, 2nd edn., Worth Publishers, New York, 1975, pp. 831, 840, 846.
9 D. E. Menconi, Anal. Chem., 57 (1985) 1790.
10 J. B. Sumner, in J. B. Sumner and K. Myrback (Eds.), The Enzymes, Vol. 1, Academic Press, New York, 1951, Chap. 24.
11 K. Warren, N. P. Kubasik, B. B. Bridy, H. E. Sine and J. P. D'Souza, Clin. Chem., 26 (1980) 133.
12 J. Georges, Clin. Chem., 25 (1979) 1888.
13 K. Begum and H. Mottola, Anal. Biochem., 142 (1984) 1.
14 M. Werner, R. J. Mohrbocher, C. Riendiau, E. Murador and S. Cambiaghi, Clin. Chem., 25 (1979) 20.
15 M. Shephard and C. G. Fraser, Clin. Chem., 25 (1979) 1350.
16 G. Johansson and L. Ogren, Anal. Chim. Acta, 84 (1976) 23.
17 R. F. Geiger, Ph.D. Thesis, University of Illinois, 1983.
18 D. Taylor and T. A. Nieman, Anal. Chim. Acta, 159 (1984) 397.
19 L. L. Klopf and T. A. Nieman, Anal. Chem., 57 (1985) 46.
20 D. C. Williams, G. F. Huff and W. R. Seitz, Clin. Chem., 22 (1976) 372.
21 R. E. Adams and P. W. Carr, Anal. Chem., 50 (1978) 944.
22 K. Dien and C. Lentner (Eds.), Scientific Tables, 7th edn., Geigy Pharmaceuticals, Ardsley, 1970, pp. 564, 565.

Analytica Chimica Acta, 186 (1986) 101—113
Elsevier Science Publishers B.V., Amsterdam — Printed in The Netherlands

POSITIVE- AND NEGATIVE-ION CHEMICAL IONIZATION GAS CHROMATOGRAPHY/MASS SPECTROMETRY OF POLYNUCLEAR AROMATIC HYDROCARBONS

SUSAN A. BROTHERTON[a] and WILSON M. GULICK, Jr.*

Department of Chemistry and Chemical Engineering, Michigan Technological University, Houghton, Michigan 49931 (U.S.A.)

(Received 23rd May 1985)

SUMMARY

Four groups of isomeric polynuclear aromatic hydrocarbons (PAH) were examined by gas chromatography/mass spectrometry (GC/MS) using positive-ion chemical ionization and negative-ion chemical ionization with a variety of reagent gases in order to evaluate the utility of each; differentiation of isomers was the ultimate goal. Hydrogen positive-ion chemical ionization (PICI) yielded different spectra for all but one isomer pair while retaining sensitivity comparable to electron-impact mass spectrometry. Several experimental conditions in the negative-ion mode afforded distinctly different spectra for isomeric PAH, but often sensitivities were reduced. The thirteen model compounds divided approximately into three classes according to the types and extent of reactions of the molecular anion. Class 1 gave as good sensitivity as hydrogen PICI; class 2 gave isomer-dependent spectra, but reduced sensitivity; class 3 gave no isomer differentiation, but greatly enhanced sensitivity.

Determinations of polycyclic aromatic hydrocarbons (PAH) are complicated by the occurrence of isomers that are often difficult to separate even when capillary-column gas chromatography is used. Mass spectra of isomers under electron impact (EI) or methane positive-ion chemical ionization (PICI) conditions are nearly always indistinguishable [1]. This survey was undertaken to evaluate chemical ionization techniques that might afford advantages over EI without sacrifice of sensitivity. Because conditions were sought which could be used in a routine service laboratory, no special adaptations or optimizations were attempted. Several sets of results suggest that the conditions used offer substantial potential for determinations of polynuclear aromatic hydrocarbons.

Lee, Hites and their co-workers [2—4] showed that some isomer differentiation occurs with positive ions generated in mixtures of argon and methane. Competition between charge transfer and proton transfer leads to $(M + H)^+/M^+$ ratios which correlate with differences in ionization potentials of the isomeric PAH. In one report [3], the argon/methane ratio in the ion source

[a]Present address: EMS Laboratories, Inc., Indianapolis, Indiana, U.S.A.

0003-2670/86/$03.50

was adjusted to obtain $(M + H)^+/M^+ = 1.6$ for naphthalene; more recently [4], 15% methane in argon was selected. It is well known that the ionic composition of an argon/methane mixture depends on the source pressure as well as the mixing ratio [5]. Negative-ion chemical ionization (NICI) mass spectra have been investigated by Hunt and Sethi [6] who found that isomer differences could be seen when oxygen was used as reactant gas; however, filament lifetime was severely shortened. Dougherty et al. [7] examined the negative-ion spectra of a number of PAH using isobutane and isobutane doped with oxygen. Isomer differentiation was not obtained, but several mass peaks were assigned to species which resulted from oxygen incorporation. More recently, methane/nitrous oxide mixtures have been used to distinguish isomeric PAH from the abundances of the adducts $(M + OH)^-$, $(M - H + NO)^-$ and $(M - H + N_2O)^-$ [8], and some methane NICI results have been reported [9, 10].

The thirteen compounds grouped by molecular weight in Tables 1 and 2 were chosen as models for this survey because they span a convenient molecular weight range for gas chromatography and offer realistic instances of difficult separations. Data are compared for positive-ion spectra obtained in five reactant gases and negative-ion data obtained in eight gases. Isomer differentiation was observed in a number of these experiments and individual

TABLE 1

Summary of positive-ion data[a]

Compound	CH_4	C_4H_{10}/O_2	Ar/CH_4	H_2	N_2/N_2O
M.w. 178					
Phenanthrene	(M) 20 (M + H) 100 (M + 29) 20 (M + 41) 5	(M) 40 (M + H) 100 (M + 41) 10 (M + 43) 10 (M + 57) tr	(M) 100 (M + H) 40 (M + 15) 5 (M + 29) 20 (M + 41) tr	(M) 40 (M + H) 100	(M) 100 (M + H)
Anthracene	(M) 35 (M + H) 100 (M + 29) 20 (M + 41) 5	(M) 20 (M + H) 100 (M + 43) 5 (M + 57) tr	(M) 100 (M + H) 30 (M + 15) tr (M + 29) 15	(M) 100 (M + H) 95	(M) 100 (M + H)
M.w. 202					
Fluoranthene	(M) 20 (M + H) 100 (M + 15) tr (M + 29) 20 (M + 41) 5	(M) 20 (M + H) 100 (M + 41) 5 (M + 43) 10 (M + 57) 20	(M) 100 (M + H) 40 (M + 15) 10 (M + 29) 20	(M) 50 (M + H) 100	(M) 100 (M + H)
Pyrene	(M) 40 (M + H) 100 (M + 29) 30 (M + 41) 5	(M) 35 (M + H) 100 (M + 43) 10 (M + 57) 5	(M) 100 (M + H) 35 (M + 15) tr (M + 29) 15 (M + 41) tr	(M) 95 (M + H) 100	(M) 100 (M + H)

TABLE 1 (continued)

Compound	CH_4	C_4H_{10}/O_2	Ar/CH_4	H_2	N_2/N_2O
M.w. 228					
Benz(a)-anthracene	(M) 40 (M + H) 100 (M + 29) 20 (M + 41) tr	(M) 20 (M + H) 100 (M + 43) 5 (M + 57) tr	(M) 100 (M + H) 35 (M + 15) tr (M + 29) 15	(M) 100 (M + H) 100	(M) 100 (M + H) 30
Chrysene	(M) 30 (M + H) 100 (M + 29) 20 (M + 41) 5	(M) 30 (M + H) 100 (M + 43) 10 (M + 57) tr	(M) 100 (M + H) 50 (M + 15) 5 (M + 29) 20 (M + 41) tr	(M) 70 (M + H) 100	(M) 100 (M + H) 30
Triphenylene	(M) 30 (M + H) 100 (M + 29) 30 (M + 41) 10	(M) 20 (M + H) 100 (M + 43) 10 (M + 57) 5	(M) 100 (M + H) 45 (M + 15) 5 (M + 29) 20 (M + 41) tr	(M) 60 (M + H) 100	(M) 100 (M + H) 30
Tetracene	(M) 60 (M + H) 100 (M + 29) 20	(M) 40 (M + H) 100 (M + 43) 10 (M + 57) 10	(M) 100 (M + H) 30 (M + 15) tr (M + 29) 10	(M) 100 (M + H) 65 (M + 2H) 50 (M + 3H) 70	(M) 100 (M + H) 30
M.w. 252					
Benzo(b)-fluoranthene	(M) 30 (M + H) 100 (M + 15) tr (M + 29) 25 (M + 41) 5	(M) 20 (M + H) 100 (M + 57) 10	(M) 100 (M + H) 40 (M + 15) 5 (M + 29) 20 (M + 41) tr	(M) 70 (M + H) 100	(M) 100 (M + H) 30
Benzo(k)-fluoranthene	(M) 40 (M + H) 100 (M + 29) 25 (M + 41) 5	(M) 25 (M + H) 100 (M + 57) 10	(M) 100 (M + H) 40 (M + 15) 5 (M + 29) 20	(M) 85 (M + H) 100	(M) 100 (M + 1) 25*
Benzo(e)pyrene	(M) 40 (M + H) 100 (M + 29) 30 (M + 41) 5	(M) 20 (M + H) 100 (M + 43) tr (M + 57) 10	(M) 100 (M + H) 35 (M + 15) 5 (M + 29) 20	(M) 95 (M + H) 100	(M) 100 (M + H) 30
Benzo(a)pyrene	(M) 50 (M + H) 100 (M + 29) 10 (M + 41) tr	(M) 30 (M + H) 100 (M + 57) 10	(M) 100 (M + H) 35 (M + 15) tr (M + 29) 10	(M) 100 (M + H) 70	(M) 100 (M + 1) 25*
Perylene	(M) 60 (M + H) 100 (M + 29) 20	(M) 40 (M + H) 100 (M + 57) 10	(M) 100 (M + H) 30 (M + 15) 5 (M + 29) 10	(M) 100 (M + H) 70	(M) 100 (M + H) 30

[a]Data are presented in the format (ion)% relative abundance; tr. ⩽ 2% relative abundance. Data are not corrected for carbon-13. Peaks asterisked have intensities within ±5% of the carbon-13 isotope contribution.

TABLE 2

Summary of negative-ion data[a]

Compound	CH_4	C_4H_{10}/O_2	Ar/CH_4	H_2	N_2/N_2O	CO_2	CO	N_2/COS
M.w. 178								
Phenanthrene	(M − H) 100	(M − H) 100	(M − H) 100	(M − H) 100	(M − 2H) 30 (M − H) 20	(M + 2H) 66 (M + 3) 9*	(M) 8 (M + 2H) 100 (M + 3) 14*	(S_5) 100
	(M) 15* (M + H) 80	(M) 15* (M + H) 25	(M) 50 (M + H) 40	(M) 50 (M + H) 30		(M + 15) 32 (M + 30) 100 (M + 31) 17*	(M + 15) 7 (M + 30) 69 (M + 31) 14*	(M) 0.7
		(M + 15) 35	(M + 14) 20		(M + 15) 100	(M + 42) 16 (M + 43) 6	(M + 43) 22	
Anthracene	(M − H) 10	(M − H) 40		(M − H) 10		(M) 100 (M + 1) 16*	(M) 100 (M + 1) 16*	
	(M) 100 (M + H) 35	(M) 100 (M + 1) 15*	(M) 100 (M + 1) 15*	(M) 100 (M + H) 25	(M) 100 (M + H) 15 (M + 15) 50	(M + 2) 2 (M + 15) 2 (M + 30) 19	(M + 2) tr	(S_5) 63
		(M + 15) 10			(M + 29) 15			(M) 100 (M + 1) 14*
M.w. 202								
Fluoranthene	(M) 100 (M + 1) 20*	(M − H) 100	(M) 100 (M + 1) 20* (M + 14) 5	(M) 100 (M + 1) 20*	(M) 100 (M + 1) 20* (M + 15) 5	(M) 100 (M + 1) 16* (M + 2) tr	(M) 100 (M + 1) 17* (M + 2) tr	(S_5) 20 (M) 100 (M + 1) 16*
		(M) 85 (M + H) 65 (M + 15) 65						
Pyrene	(M − H) 40 (M) 40 (M + H) 100 (M + 15) tr	(M − H) 100 (M) 90 (M + H) 65 (M + 15) 70	(M − 2H) 45 (M − H) 100 (M) 50 (M + H) 70 (M + 14) 15	(M − H) 100 (M) 70 (M + H) 70	(M − 2H) 20 (M − H) 10 (M) 10 (M + 15) 100	(M) 100 (M + 1) 20* (M + 2H) 11 (M + 15) 39 (M + 30) 49 (M + 31) 11 (M + 34) 21 (M + 38) 10	(M) 100 (M + 1) 19* (M + 2H) 4 (M + 15) 4 (M + 30) 5 (M + 43) 9	(S_5) 100 (M) 13 (M + 1) 2
M.w. 228								
Benz(a)-anthracene	(M) 100 (M + H) 25 (M + 14) 5	(M) 100 (M + 1) 20* (M + 15) 15	(M) 100 (M + 1) 20* (M + 15) 5	(M) 100 (M + 1) 20*	(M) 100 (M + 1) 15* (M + 15) 40 (M + 31) 10	(M) 100 (M + 1) 20* (M + 2) 2* (M + 30) 6	(M) 100 (M + 1) 19* (M + 2) 2* (M + 43) tr	(S_5) 20 (M) 100 (M + 1) 20* (M + 2) 2*

Chrysene		(M − 2H) 15	(M − 2H) 80		(M − 2H) 20	(M − 2H) 8	(M − 2H) 76	(S_5) 100
							(M − H) 22	
	(M − H) 100	(M − H) 100	(M − H) 100	(M − H) 100	(M − H) 15	(M + 2H) 100	(M) 10	(M) 1.3
						(M + 3) 13*	(M + H) 13	
	(M) 20*	(M) 30	(M) 50	(M) 20*	(M) 5	(M + 15) 76	(M + 2H) 100	
						(M + 16) 17*	(M + 3) 19*	
	(M + H) 95	(M + H) 40	(M + H) 45	(M + H) 35		(M + 30) 44	(M + 15) 19	
							(M + 16) 22	
							(M + 24) 16	
							(M + 28) 31	
	(M + 2) 15*	(M + 15) 60	(M + 13) 30		(M + 15) 100	(M + 42) 26	(M + 30) 16	
			(M + 14) 20			(M + 43) 11	(M + 43) 95	
							(M + 44) 17*	
Triphenylene		(M − 2H) 20	(M − 2H) 100		(M − 2H) 40			
	(M − H) 100	(M − H) 100	(M − H) 70	(M − H) 100	(M − H) 25			
	(M) 20*	(M) 40	(M) 30	(M) 25	(M) 5			
	(M + H) 95	(M + H) 35	(M + H) 20	(M + H) 30		—	—	-
	(M + 2) 20*	(M + 2H) 5	(M + 2H) 5					
	(M + 15) 5	(M + 15) 35	(M + 13) 15		(M + 15) 100			
Tetracene	(M) 100	(M) 100	(M) 100	(M) 100	(M) 100			
	(M + H) 50	(M + H) 40	(M + 1) 20*	(M + H) 50	(M + 1) 20*	—	—	—
				(M + 2H) 25	(M + 16) 40			
	(M + 14) 15	(M + 15) 40	(M + 14) tr	(M + 17) 25				
M.w. 252								
Benzo(b)-fluoranthene	(M) 100	(M) 100	(M) 100	(M) 100	(M) 100	(M) 100	(M) 100	(S_5) 3
						(M + 1) 23*	(M + 1) 21*	
	(M + 1) 25*	(M + 1) 25*	(M + 1) 25*	(M + 1) 25*	(M + 1) 25*	(M + 2) 2*	(M + 2) 2*	(M) 100
								(M + 1) 21*
								(M + 2) 2*
Benzo(k)-fluoranthene	(M) 100	(M) 100	(M) 100	(M) 100	(M) 100	(M) 100	(M) 100	(S_5) 13
						(M + 1) 21*	(M + 1) 22*	
	(M + 1) 25*	(M + 1) 25*	(M + 1) 25*	(M + 1) 25*	(M + 1) 25*	(M + 2) 2*	(M + 2) 2*	(M) 100
								(M + 1) 21*
								(M + 2) 2*
Benzo(e)-pyrene			(M − 2H) 50		(M − 2H) 20			
	(M − H) 45	(M − H) 70	(M − H) 40	(M − H) 100	(M − H) 15			
	(M) 100	(M) 20	(M) 40	(M) 90	(M) 20			
	(M + H) 100	(M + H) 5	(M + H) 25	(M + H) 70	(M + H) 60			
					(M + 2) 15*	—	—	—
	(M + 14) 80	(M + 15) 100	(M + 14) 100		(M + 14) 20			
					(M + 15) 100			

TABLE 2 (continued)

Compound	CH_4	C_4H_{10}/O_2	Ar/CH_4	H_2	N_2/N_2O	CO_2	CO	N_2/COS
Benzo(a)-pyrene	(M) 100 (M + 1) 25*	(M) 100 (M + 1) 25*	(M) 100 (M + 1) 25*	(M) 100 (M + 1) 25*	(M) 100 (M + 1) 25*	(M) 100 (M + 1) 23* (M + 2) 2*	(M) 100 (M + 1) 22* (M + 2) 2*	(S_5) 3 (M) 100 (M + 1) 22* (M + 2) 2*
Perylene	(M) 100 (M + H) 30 (M + 14) 50	(M) 100 (M + 1) 20* (M + 15) tr	(M) 100 (M + 1) 25* (M + 14) 100	(M) 100 (M + 1) 25* (M + 17) 5	(M) 100 (M + 1) 20* (M + 13) 15 (M + 14) 15	—	—	—

[a]Data presented in the format (ion)% relative abundance; tr. ⩽2% relative abundance. Data are not corrected for carbon-13. Peaks asterisked have intensities within ±5% of the carbon-13 isotope contribution.

compounds, or groups of related compounds, showed enhanced sensitivity under various conditions. In the PICI mode, hydrogen produced the overall best combination of isomer differentiation and response. The best individual sensitivities, however, were obtained in the NICI mode, but the variation among compounds was extremely large.

EXPERIMENTAL

Chemicals and gases

The PAH listed in the tables were obtained from commercial sources (ChemServices, West Chester, PA; Eastman Kodak, Rochester, NY; Nanogens, Watsonville, CA; and Supelco, Bellefonte, PA) and used as received. The compounds were dissolved in toluene (Burdick and Jackson, Muskegon, MI) to make solutions containing two to five components each. Concentrations were chosen to permit injection of 2—200 ng of each component depending upon the mass spectral sensitivity under a particular set of ionization conditions. Flame-ionization gas chromatography showed no interfering impurities. All gases were obtained from Matheson (Joliet, IL) or Liquid Air Corp. (San Francisco, CA). Gas mixtures were prepared assuming ideal gas behavior by addition of the pure constituents to an evacuated tank.

Instrumentation and methods

The gas chromatography/mass spectrometry (GC/MS) system was a Hewlett-Packard 5985-B with negative-ion option and "Answer" software. The GC/MS was modified so that the capillary GC column could be inserted directly into the ion source. Reactant gases were also plumbed directly into the source through a Whitey micrometering valve.

Chromatography. All chromatography was done using splitless injection and helium carrier gas at head pressure 12 psig. The column used throughout was a 25-m × 0.32-mm i.d. fused silica capillary coated with SE-54 (J & W Scientific, Rancho Cordova, CA). Column temperature was held at 50° for 3 min and then increased at 10° min^{-1} to 250°.

Mass spectrometry. The mass spectrometer was in use for routine work, not dedicated to this research. It was tuned in the EI mode using H-P "Autotune" and then in the CI mode using methane at 0.2 torr. The ion-source temperature was maintained at 200° throughout all experiments and the electron energy was 150 eV for all positive-ion spectra. Decafluorotriphenylphosphine (DFTPP) was run through the GC as a final check of mass axis calibration and sensitivity. Reactant gas was then changed and DFTPP was run again to monitor system performance. Pressure, as monitored by a thermocouple probe inserted into the source, was adjusted to obtain maximum ionization for phenanthrene introduced through the GC column. All CI-source pressures were in the range 0.1—0.4 torr. Within that range, pressure seemed to have relatively little effect on sensitivity except with argon/methane, for which response peaked sharply at 0.15 torr. Reactant gas iden-

tity and source pressure were the only parameters which differed from one set of experiments to another.

In the NICI experiments, 70-eV electron energy was used. Source parameters were optimized with methane present at 0.4 torr using the H-P procedure. Final sensitivity and mass calibration checks were done with DFTPP and when reactant gas was changed, its pressure was adjusted for maximum ionization of phenanthrene. Except for nitrogen/carbonyl sulfide and carbon dioxide, which were run at 0.1 torr and CO, run at 0.2 torr, broad sensitivity maxima were found in the pressure range 0.4—0.8 torr. In several of the plasmas, Cl^- and Cl_2^- were prominent and identified from their isotope ratios. The source of chlorine is presumed to be intermittent use of the instrument for polychlorinated biphenyls.

Each experiment was done at least twice with the instrument freshly tuned; no significant spectral differences were observed. Total ion chromatograms were spot-checked for consistent mass spectra across GC peaks without discovery of significant spectral dependence on analyte concentration in the source.

RESULTS AND DISCUSSION

Positive-ion results are summarized in Table 1 and negative-ion data are in Table 2. Because in no case did extensive fragmentation occur, only the *m/z* regions near the molecular ions are reported. Tables 3 and 4 summarize, respectively, positive- and negative-ion response factors, which are given to

TABLE 3

Positive-ion response factors[a]

Compound	EI[b]	CH_4	Ar/CH_4[c]	C_4H_{10}/O_2[d]	H_2	N_2/N_2O[e]
Phenanthrene	21	8.0	22	10	25	38
Anthracene	18	8.0	20	50	14	18
Fluoranthene	17	5.0	13	24	19	13
Pyrene	22	4.5	16	9.0	20	22
Benz(a)anthracene	15	3.0	9.0	28	13	11
Chrysene	19	2.0	8.0	6.0	16	12
Triphenylene	12	0.5	10	14	10	6.0
Tetracene[f]	10	1.0	1.5	3.0	0.1	0.8
Benzo(b)fluoranthene	4.0	5.0	8.0	8.0	36	4.0
Benzo(k)fluoranthene	12	2.0	5.0	3.0	37	3.0
Benzo(e)pyrene	10	0.5	6.0	10	14	5.0
Benzo(a)pyrene	2.0	4.0	5.0	6.0	31	1.4
Perylene	25	1.3	2.0	4.0	2.0	2.0

[a]Precision estimated as ± 10%; data normalized to benzo(e)pyrene (EI) = 10. [b]Electron-impact data at 70 eV for reference. [c]Argon/methane, 95:5 ratio. [d]Isobutane/oxygen, 98.6:1.4 ratio. [e]Nitrogen/nitrous oxide, 9:1 ratio. [f]Some decomposition of tetracene is suspected, so response factors may be artificially small.

TABLE 4

Negative-ion response factors[a]

Compound	CH_4	Ar/CH_4[b]	C_4H_{10}/O_2[c]	H_2	N_2/N_2O[d]	CO_2	CO	N_2/COS[e]
Phenanthrene	6.0	2.0	1.5	0.6	0.6	0.4	0.6	0.03
Anthracene	31	33	4.0	11	1.0	3.5	4.3	0.6
Fluoranthene	13×10^2	17×10^2	37	1.2×10^2	6.0	13	22	2.5
Pyrene	10	4.0	5.0	1.0	1.0	0.2	0.8	0.6
Benz(a)anthracene	34	72	5.0	30	1.0	7	7	2.6
Chrysene	7.0	5.0	4.5	3.5	0.5	0.4	0.4	0.1
Triphenylene	4.0	19	1.0	3.0	0.2	—	—	—
Tetracene[f]	2.0	12	10	3.0	0.4	—	—	—
Benzo(b)-fluoranthene	7.0×10^2	20×10^2	1.6×10^2	7.5×10^2	20×10^2	18	30	15
Benzo(k)-fluoranthene	15×10^2	2.9×10^2	19×10^2	6.0×10^2	25×10^2	24	28	22
Benzo(e)pyrene	6.0	19	3.0	5.0	0.3	—	—	—
Benzo(a)pyrene	3.8×10^2	24×10^2	96	6.0×10^2	15×10^2	14	19	12
Perylene	13	36	12	1.3×10^2	1.5	—	—	—

[a]Precision estimated as ± 10%; data normalized as in Table 3 to benzo(e)pyrene (EI) = 10. [b]Argon/methane, 95:5 ratio. [c]Isobutane/oxygen, 98.6:1.4 ratio. [d]Nitrogen/nitrous oxide, 9:1 ratio. [e]Nitrogen/carbonyl sulfide, 5:1 ratio. [f]Some decomposition of tetracene is suspected, so response factors may be artificially small.

only two significant figures because manual sample injection is not a highly precise technique. Response factor is defined here as total counts (total abundance) excluding plasma ions, per nanogram of compound injected.

Positive-ion chemical ionization

Methane, isobutane/oxygen, and argon/methane all gave similar results in PICI. Methane spectra all showed an $(M + H)^+$ base peak, differed in molecular ion abundance (20—60%), and had ions at $(M + 29)^+$ and $(M + 41)^+$ from addition of $C_2H_5^+$ and $C_3H_5^+$. While in principle the differences in abundance of the molecular ion might form a basis of isomer identification, this was found to be insufficiently reproducible. Similar results were obtained with isobutane/oxygen except for the appearance of the heavier addition ion, $(M + 57)^+$, $(C_4H_9)^+$. In contrast to previous results [2, 3], with argon/methane and our source conditions, charge transfer from Ar^+ was dominant and gave the molecular ion as the base peak in each spectrum; it is unlikely that the isomers could be distinguished. Simonsick and Hites [4] refined this method and concluded that an internal standard is required to overcome variations caused by differences in ion source contamination.

Spectra obtained with nitrogen/nitrous oxide were very similar to EI spectra. They showed only M^+ and $(M + 1)^+$ because this mixture functions as a charge-exchange reagent without significant production of addition ions. Addition of H^+ from traces of water produces intensity at M + 1 slightly greater than the carbon-13 contribution in all but three cases. As can be seen from the data in Table 3, each of these PICI techniques gives generally poorer sensitivity than EI, particularly with the higher-molecular-weight compounds.

Hydrogen provided both the best isomer differentiation and the most consistent sensitivity which was similar to that of EI; the notable exception was tetracene but sample decomposition may have been a factor in that case. Only the isomer pair benzo(a)pyrene/perylene gave identical spectra in hydrogen; however, spectra of benzo(k)fluoranthene and benzo(e)pyrene were too similar to permit positive identification. The hydrogen source pressure was 0.2 torr, a condition under which an abundant [11] reactant ion is H_3^+, which has a low proton affinity and is known to function as both a Brønsted acid and a charge-exchange reagent. One concludes, therefore, that the proton-acceptor properties of the isomers studied here differ to an exploitable extent. The repeatability of these spectral differences was examined using a separate solution which contained equal amounts of fluoranthene, pyrene, and chrysene. Four replicate experiments at the 100-ng per component level were done. In every spectrum, $(M + 1)^+$ was the base peak and the abundance of M^+ was always greater for pyrene than for fluoranthene. The relative standard deviations of the relative abundances of M^+ for the three compounds were 11.6, 6.3, and 7.6%, respectively. Because, in addition, the total ion chromatogram obtained with hydrogen was exceptionally clean and free from noise, hydrogen PICI should be a useful method for screening PAH unknowns.

Negative-ion chemical ionization

In contrast to the PICI results, these model compounds exhibited three major ionization patterns in NICI. Class 1 compounds, anthracene, fluoranthene, benz(a)anthracene, tetracene and perylene, with one exception had the molecular anion as base peak. Class 2 compounds, phenanthrene, pyrene, chrysene, triphenylene and benzo(e)pyrene, showed more variation in ionization. The molecular anion was the base peak only for pyrene in carbon dioxide or monoxide, and benzo(e)pyrene in methane; the $(M - H)^-$ anion was most frequently the base peak in these spectra. The two benzofluoranthenes and benzo(a)pyrene, class 3, yielded only M^- and isotope peaks. This present result for benzo(e)pyrene is in contrast to the reported [10] failure to find ionization for that compound in methane NICI, a comparison which exemplifies the irreproducibility of NICI recently discussed [12].

Formulae were assigned (Table 2) to ions only when an obvious transfer of one or two hydrogens occurred. Ions $(M + 14)^-$ and $(M + 15)^-$ occurred frequently. These have been attributed [6, 7] to $(M - 2H + O)^-$ and $(M - H + O)^-$, respectively, and the enhanced response of the electron-capture detector to PAH when oxygen-doped carrier gas is used was presumed [13] to be due to O_2^- attack on the PAH. Recent work [14] with CD_4 has shown, however, that several nitrogen heterocycles give $(M + 14)^-$, which is $(M + CH_2)^-$. The present data show $(M + 14)^-$ most frequently in argon/methane or methane alone, while $(M + 15)^-$ dominates in reactant gases which contain oxygen. This observation suggests that while $(M + 14)^-$ may result from CH_2 addition, $(M + 15)^-$ is likely to be an oxygen adduct. These adducts appear

to result from reaction of the molecular anion or a fragment anion with molecular oxygen because no oxygen ions such as O_2^-, O^-, or RO^- were detected in the hydrocarbon-based reactant gas plasmas, including the oxygen-doped isobutane. The hydrogen plasma contained observable OH^-, but only the tetracene and perylene spectra showed an anion representing addition of 17 mass units. Because H^- has a large proton affinity, it can abstract H^+ as well as form adducts; indeed, both $(M - H)^-$ and $(M + H)^-$ are present in some spectra and the spectra of class 2 compounds are dominated by these ions. They are much less prominent in spectra of class 1 compounds which have the molecular anion as base peak; only the anthracene spectrum showed detectable $(M - H)^-$.

When the reactant gas was nitrogen/nitrous oxide, both O^- and NO^- were observed in the plasma. Class 2 compounds appear to be more reactive toward the strong gas-phase base [15], O^-, than class 1 compounds. The former show loss of one and two hydrogen atoms and have $(M - H + O)^-$ as base peak, while the latter have M^- as base peak and show additions only and no hydrogen abstraction. Only in this gas mixture did several compounds show adduct ions which were attributed to Cl^- contamination (see above) of the source.

Spectra obtained with CO_2 and CO as moderating gases were quite similar to one another, but distinct from those obtained in other gases. Spectra of class 1 compounds contained the molecular anion as base peak and some small amounts of $(M - H + O)^-$ and $(M - 2H + 2O)^-$. Class 2 compounds gave very different spectra in which the molecular anion was weak or absent (except for pyrene for which M^- was the base) and $(M + 2H)^-$ was prominent, along with adduct ions which result from addition of one or more oxygen atoms and loss of one or several hydrogens. The ions $(M + 44)^-$, $(M + 43)^-$ and $(M + 42)^-$ may result from addition of the elements of CO_2, and loss of 0—2 hydrogens. Other adducts are difficult to identify. The CO_2 plasma contains ions at m/z = 60 (CO_3^-), 68 and 112; the CO plasma shows m/z = 126 and 148. Both plasmas contain a prominent ion at m/z = 168 which could be $C_6O_6^-$; the average abundance of mass 169 is consistent with this interpretation. As well as forming adducts, these carbon-oxygen species may be responsible for hydrogen abstraction.

Carbonyl sulfide was examined in hope of generating S^- or a related base softer than O^-, which might react more selectively. A 5:1 mixture of nitrogen and carbonyl sulfide gave a plasma which contained polysulfide anions from S_2^- to S_6^- and small amounts of CO^- and COS^-. The intensities of the peaks at two mass units higher clearly distinguished the sulfide ions from SO_{2x}^- which have the same nominal mass. Only the molecular anion and its isotope peaks were observed for any of the PAH in this reactant gas and no addition of any sulfur species was detected. Because the sulfur species capture electrons preferentially and greatly reduce the response of the PAH (Table 4), these are not useful conditions.

The fact that these PAH exhibit three different patterns of ionization in

NICI should be of use for their identification; however, the response factors differ by more than 10^4, which reduces the generality of the method and may lead to misinterpretations of results from impure samples. For example, Dougherty et al. [7] reported only an ion at m/z = 252 $(M + 24)^-$ for triphenylene in isobutane, a result which they were unable to explain. Data in Tables 2 and 4 suggest that while triphenylene gives a distinct NICI spectrum in oxygen-doped isobutane, its response is very much smaller than that for any of the compounds in class 3. Inadvertent contamination of triphenylene with one of those compounds could lead to the anomalous result and would exemplify the high selectivity of NICI to which Dougherty [12] has recently referred.

Class 3 compounds form very stable anions and, in each reactant gas tested, give uniformly the greatest response but no isomer differentiation under any of these conditions. Isomer differentiation for compounds of classes 1 and 2 is enhanced by N_2/N_2O, CO_2, and CO, but at the price of sharply reduced responses. Isobutane doped with oxygen gives disappointing response factors, as does hydrogen. The former result is surprising in view of the enhancement of sensitivity of electron capture GC [14] when similar oxygen doping is used. In NICI, argon/methane appears to be a good compromise, although several compounds give slightly larger response factors in methane itself; both assist isomer identification to about the same extent. As shown in Table 4, different individual PAH respond best under different experimental conditions; for example, perylene in hydrogen gives a response enhanced by nearly an order of magnitude above any other conditions we examined.

The response factors given here can be compared approximately with those reported for methane/nitrous oxide NICI [8]; data were reported for nine of the same compounds examined here. The methane/nitrous oxide NICI produced responses which were substantially larger than those found for any of our conditions for five compounds and substantially smaller for four others. A utilitarian comparison can be made on the basis of the amount of substance required; this was stated to be 1 to 2 ng [8]. For all but one PAH, this level can be achieved in hydrogen PICI, where it is estimated that about 100 pg can be detected. [A conservative estimate of signal-to-noise ratio was made from two total ion chromatograms in hydrogen. The average number of counts in the base peak for three PAH, as measured at the maxima in the TIC, was compared with the average total counts between peaks. Although other PAH were also present, fluoranthene, pyrene, and chrysene were chosen for this comparison because of their nearly identical response factors; $S/N > 300$ were obtained with the PAH at 100 ng and the electron multiplier at two thirds maximum voltage.] In NICI, class 3 compounds can be detected at the 10-pg level, although isomer differentiation is not achieved. Class 1 compounds show responses similar to that of hydrogen PICI, and class 2 compounds are somewhat less responsive.

In summarizing results from a number of experimental conditions and

comparing them to similar results from other laboratories, our aims are to enlarge the basis for choice of methods for identifying or quantifying PAH and to call attention to potential problem areas. Although hydrogen PICI appears advantageous for screening PAH, individual compounds or groups of compounds show enhanced responses under various conditions. One of these may be the method of choice depending upon particular need and analyte composition.

This work was abstracted in part from the M.S. Thesis of S.A.B., November 1983, and was presented in part at the 31st Annual Conference on Mass Spectrometry and Allied Topics, Boston, Massachusetts in May 1983.

REFERENCES

1 M. L. Lee, M. V. Novotny and K. D. Bartle, Analytical Chemistry of Polycyclic Aromatic Hydrocarbons, Academic Press, New York, 1981.
2 M. L. Lee and R. A. Hites, J. Am. Chem. Soc., 99 (1977) 2008.
3 M. L. Lee, D. L. Vassilaros, W. S. Pipkin and W. L. Sorensen, Trace Organic Analysis: A New Frontier in Analytical Chemistry, National Bureau of Standards, Washington, DC, 1978; Nat. Bur. Stand. Spec. Publ., 519 (1978) 731.
4 W. J. Simonsick, Jr. and R. A. Hites, Anal. Chem., 56 (1984) 2749.
5 D. P. Beggs, Hewlett-Packard Application Note AN 176-19.
6 D. F. Hunt and S. K. Sethi, in M. L. Gross (Ed.), High Performance Mass Spectrometry — Chemical Applications, American Chemical Society, Washington, DC, 1978; ACS Symp. Ser., 70 (1978) 150.
7 R. C. Dougherty, S. V. Howard and J. D. Wander, in N. L. Richards and B. L. Jackson (Eds.), Carcinogenic Polynuclear Aromatics in the Marine Environment, U.S. Environmental Protection Agency, Washington, DC, 1982; EPA-600/9-82-013, pp. 14—25.
8 M. Oehme, Anal. Chem., 55 (1983) 2290.
9 Y. Iida and S. Daishima, Chem. Lett., (1983) 273.
10 M. V. Buchanan and G. Olerich, Org. Mass Spectrom., 19 (1984) 486.
11 J. A. Michnowicz, Hewlett-Packard Application Note AN 176-13. D. P. Beggs, Hewlett-Packard Application Note AN 176-18.
12 R. C. Dougherty, 33rd Annual Conference on Mass Spectrometry and Allied Topics, San Diego, CA, May 1985, Abstracts, p. 85.
13 D. A. Miller, K. Skogerboe and E. P. Grimsrud, Anal. Chem., 53 (1981) 464.
14 D. Stockl and H. Budzikiewicz, Org. Mass Spectrom., 17 (1982) 376.
15 A. P. Bruins, A. J. Ferrier-Corriea, A. G. Harrison, K. R. Jennings and R. K. Mitchum, Adv. Mass Spectrom., 7A (1978) 355.

Analytica Chimica Acta, 186 (1986) 115—122
Elsevier Science Publishers B.V., Amsterdam — Printed in The Netherlands

ELECTRON PARAMAGNETIC RESONANCE SPECTROSCOPY IN STUDIES OF THE CHEMICAL STATES OF MANGANESE IN PARTICULATE SUBSTANCES IN RIVER WATERS AND OF THE REDUCTION OF MANGANESE BY TANNERY EFFLUENTS

TETSUHIKO YOSHIMURA*, TOMIO OZAKI and TOSHIHIDE OKUNO

The Environmental Science Institute of Hyogo Prefecture, Yukihira-cho, Suma-ku, Kobe 654 (Japan)

(Received 3rd January 1986)

SUMMARY

The chemical states of manganese(II) species in particulate substances in river water, with and without the influence of tannery effluents, were investigated by the use of electron paramagnetic resonance (e.p.r.) spectroscopy. In the e.p.r. spectra of the particulate substances in river water, the six-line signal characteristic of Mn(II) was distinctly observed. The relative intensity of the Mn(II) signal was found to be higher in the lower reaches of a river, and especially below tannery effluent inflows, suggesting that manganese in river water is reduced by natural and artificially added organic compounds. It is shown that the reduction of manganese in river sediments and manganese dioxide by tannery effluents can afford an insoluble Mn(II) species at pH 11 and a soluble Mn(II) species at pH 7.

Manganese is indispensable to all organisms. Both manganese deficiency and excessive intake are deleterious for biological systems [1—3]. A knowledge of the transfer and the chemical states of manganese in river water is essential to an understanding of the manganese cycle in soil/water/plant/animal relationships.

Manganese within the pH range of natural waters is present as manganese(II) in solution and manganese(III) and (IV) in suspended solids [4, 5]. The mechanisms of oxidation of manganese(II) by dissolved oxygen and reduction of manganese(III) and (IV) by dissolved organic substances have been investigated [6—10]. These studies showed that the oxidation and reduction are affected by various inorganic and organic substances, the pH of the water, and sunlight. Sunda et al. [7] first observed the photoreduction of manganese oxides by dissolved organic substances (humic substances) in sea water. Stone and Morgan [5, 6] recently showed that the reduction and dissolution of Mn(III) and (IV) oxide suspensions by various organic compounds resembling natural materials proceeded by surface complex formation prior to electron transfer.

The manganese(II) ion has five unpaired 3*d*-electrons and is readily observed by electron paramagnetic resonance (e.p.r.) spectroscopy, not only at

0003-2670/86/$03.50

room temperature but also at lower temperatures. The e.p.r. spectra of aqueous manganese(II) solutions with six hyperfine lines can be observed at quite low manganese concentrations and are sensitive to various complexing agents; thus the spectra can be used to determine the concentration of manganese(II) and to elucidate the chemical states of manganese(II) [11]. The mechanisms of manganese(II) binding to humic and fulvic acids from a soil and to dissolved yellow organic substances in a natural water have been investigated by e.p.r. spectroscopy [12—14].

Tannery effluents contain a large number of organic substances including proteins and lipids and their denatured compounds, as well as inorganic species such as calcium, sodium, chromium and iron. The effluents have a wide range of pH values but are mainly highly alkaline [15]. Thus, the chemical states of various metal ions in river water near a tannery waste effluent may be markedly affected.

In the present work, the chemical states of manganese are qualitatively investigated in particulate substances from river water in the absence and presence of tannery effluents, by the use of e.p.r. spectroscopy. The reduction of manganese in river sediments and manganese dioxide by tannery effluents is also studied.

EXPERIMENTAL

Apparatus and chemicals

The e.p.r. measurements were made with a JES-ME-3X spectrometer with 100-kHz field modulation, at room temperature (ca. 20°C) and at liquid nitrogen temperature (77 K). The instrument conditions were calibrated with a Takeda-Riken frequency counter (TR-5211A), and 1,1-diphenyl-2-picrylhydrazyl (DPPH) radical powder (g = 2.0036) and manganese(II) in magnesium oxide (ΔH_{3-4} = 86.9 G) as standards. The second-derivative display was obtained by the use of 80-Hz field modulations. Manganese was determined separately with a Hitachi 170-30 atomic absorption spectrometer.

Manganese dioxide was purchased from Wako Pure Chemical Industries. All other chemicals were obtained as the purest available grade and were used as received.

Procedures

Water and sediment samples as well as tannery effluents were collected from stations in Hyogo Prefecture. Water samples and tannery effluents were filtered through 0.4-μm pore diameter membrane filters (Nuclepore Corp.). The particulate substances retained by the filter were washed with water from a Milli-Q system (Millipore). The particulate and dissolved substances were treated with concentrated nitric/perchloric acids and nitric acid/hydrogen peroxide, respectively, and evaporated to dryness. The residues were dissolved in 0.1 M hydrochloric acid and the solutions thus obtained were used for atomic absorption spectrometry (a.a.s.) [16]. Sediment samples were

extracted with concentrated nitric/hydrochloric acids by heating and evaporating to dryness; the residues were dissolved in 0.1 M hydrochloric acid, and used for a.a.s. [16].

Reductions with tannery effluents were examined as follows. The chemical composition of the particulate substances in tannery effluent used was found to be 35.1% C, 5.3% H, 3.9% N, 1.3% Cr, and 1.4% Fe. The untreated tannery effluent had a pH of 11; to adjust to pH 7, 0.1 M hydrochloric acid was added. Manganese dioxide and a river sediment with a high manganese content (point no. 2 of the Muko River, see Table 2) were each ground to a fine powder. The powders (2 mg MnO_2 or 10 mg of sediment) were each suspended in 0.1 ml of tannery effluent, both at pH 11 and pH 7, in filtered effluent at pH 11, and in pure water. These eight suspensions were transferred to an e.p.r. quartz tube and sealed. Measurements at 77 K were made immediately after sample preparation and after standing under laboratory conditions for one week, one month, and three months.

RESULTS AND DISCUSSION

Manganese in river water

Table 1 lists the manganese concentrations ($\mu g\ l^{-1}$) in the dissolved and particulate fractions from several river waters, as well as the ratio of manganese in the particulate fractions to total manganese. Metal concentrations in fresh waters are known to depend markedly on sampling conditions such as location, time and season [16]. The manganese concentrations in Table 1 vary from station to station. It is clear, however, that a large portion of manganese is included in the particulate fractions at the sampling points of the Hayashida River where the tannery effluents flow in. This may result from manganese binding or adsorption, or both, on the various insoluble organic substances in tannery effluents and from the formation of insoluble manganese compounds (e.g., $Mn(OH)_2$) under the extreme chemical conditions.

TABLE 1

Manganese concentrations in the dissolved and particulate fractions from river water

Sampling station		Mn conc. ($\mu g\ l^{-1}$)		Ratio particulate/total
River	Point no.	Dissolved	Particulate	
Hayashida	1[a]	2.4	11	0.82
	2[a]	2.6	77	0.97
	3[a]	5.5	21	0.79
	4[a]	3.3	35	0.91
Otsumo	1[b]	80	22	0.22
Kako	1[b]	5.7	46	0.89

[a]Downstream from the inflow of a tannery effluent. [b]Lower reaches of the river, not affected by tannery effluent.

The particulate substances in the river water at four sampling points on the Hayashida River exhibited similar e.p.r. spectra (at 77 K) whether wet or dry. Further, those in the dried state exhibited similar spectra at room temperature and 77 K. The 77 K spectrum for those at sampling point no. 3 is typical (Fig. 1). The signal (g = 4.3) around 1500 G could result from high-spin iron(III) at the center of a distorted tetrahedron [17, 18]. The broad signal ranging from 2500 to 4500 G could be mainly from chromium(III), which is present in tannery effluents at high concentration. The six-line signal overlapping with the chromium(III) signal is likely to be the characteristic signal of manganese(II) with a nuclear spin of 5/2. Figure 1 also shows a sharp intense signal at g = 2.005, which may be due to an unidentified radical. When the sample was heated in air at about 200°C for 1 h, the intensity of this signal was decreased by about 40% in the e.p.r. spectra both at room temperature and at 77 K; prolonged heating caused no further intensity change. The iron(III) and manganese(II) signals, but not the chromium(III) signal were observed in the particulates from rivers other than those affected by tannery effluents.

Figure 2 shows the expanded spectrum of the manganese(II) signal in Fig. 1 as well as its second derivative. Almost the same spectra were also observed in the particulates in the river waters unaffected by tannery effluents. The absorption line located at the lowest magnetic field among the six

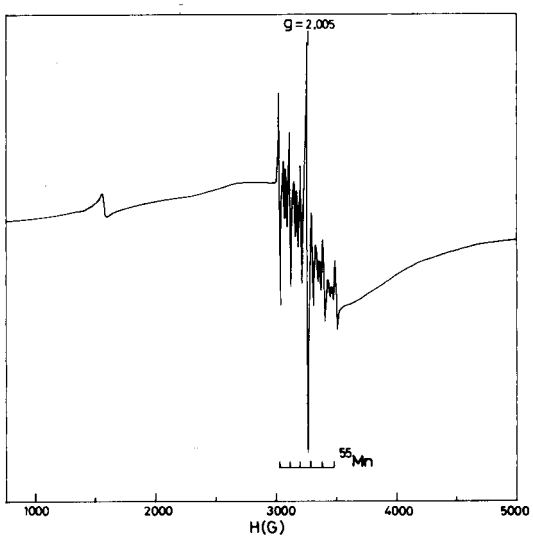

Fig. 1. The e.p.r. spectrum of dried particulate matter in river water at sampling point no. 3, Hayashida River, measured at 77 K. Instrument settings: modulation frequency and amplitude, 100 kHz and 5 G; microwave frequency and power, 9.184 GHz and 10 mW.

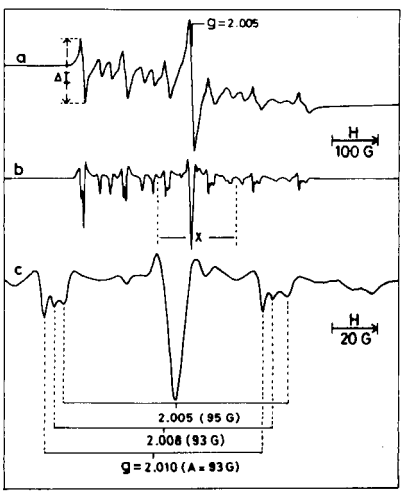

Fig. 2. Expanded e.p.r. spectra of manganese(II) in Fig. 1: (a) first derivative; (b) second derivative; (c) expanded second derivative of the region marked X in (b). (Instrument settings as in Fig. 1.)

lines is the most intense (Fig. 2, curve a). The intense forbidden hyperfine lines were characteristically observed in addition to the normal six lines. It is clearer in the second-derivative display (Fig. 2, curves b, c) that this manganese(II) signal consists of three components with different e.p.r. parameters (g and A values). This signal with three components was maintained even after prolonged heating in air at ca. 200°C.

It should be noted that the e.p.r.-detectable manganese(II) is not the total manganese(II) in the sample because there are manganese(II) compounds in which the six-line signal is so markedly broadened that it virtually disappears [12, 19]. Although the concentration of e.p.r.-detectable manganese(II) in solids cannot be determined because of the absence of an appropriate standard material, the relative intensity ratio can be estimated from the e.p.r. intensity and the total manganese concentration. The e.p.r. intensity was estimated from the peak-to-peak height (ΔI in Fig. 2, curve a) for the line at the lowest field, and total manganese was determined by a.a.s. In Table 2, the ratios of e.p.r.-detectable manganese(II) to total manganese are represented by defining the ratio at sampling point 1 on the Muko River as unity. That point, with a total manganese content of 3.5 $\mu g\ mg^{-1}$ in the sediment, is located near the source of the river and cannot be appreciably polluted by organic substances. As shown in Table 2, the relative intensity of e.p.r.-detectable manganese(II) is higher downstream, especially where the water is affected by tannery effluents, than upstream.

Reduction by tannery effluents

It has been demonstrated that natural waters contain various organic reductants and that manganese(III) and (IV), and iron(III) compounds in

TABLE 2

Ratios of e.p.r.-detectable manganese(II) to total manganese in particulates and sediments

Sampling station		Ratio e.p.r.-detectable/total
River	Point no.	
Particulate substances		
Hayashida	1[a]	120
	2[a]	70
	3[a]	290
	4[a]	90
Otsumo	1[b]	20
Kako	1[b]	60
Sediments		
Hayashida	4[a]	60
Muko	1[c]	1[d]
	2[c]	0

[a,b]See footnotes to Table 1. [c]Near source of river. [d]The ratio at point 1 on the Muko river is defined as unity.

natural waters can be reduced by such substances [5—7, 20, 21]. Tannery effluents also contain organic compounds with thiol and hydroxyl groups. The reduction of the manganese in river sediments and of manganese dioxide by the tannery effluents was examined by e.p.r. spectroscopy. The sediment used for the reduction experiment contained a high concentration of manganese (1.8 μg mg^{-1}) and had no manganese(II) e.p.r. signal. None of the eight suspensions investigated (see Experimental) exhibited a six-line manganese(II) signal at 77 K immediately after sample preparation. Furthermore, the four suspensions of manganese dioxide or the sediment in the filtrate from tannery effluents, or in pure water, did not exhibit such a spectrum even after standing for three months.

As is shown in Fig. 3, however, two suspensions of manganese dioxide in unfiltered tannery effluents at pH 11 and pH 7, after standing for three months, exhibited a distinct six-line manganese(II) signal. The signal at pH 11 consisted of two components with different e.p.r. parameters. Both suspensions were filtered through a 0.4-μm filter. The filtrate at pH 11 gave no e.p.r. signal but the precipitate had a signal identical to curve (a) in Fig. 3. The filtrate at pH 7 had a signal identical to that in curve (b) in Fig. 3 and the precipitate gave no manganese(II) signal. The sediment suspended in a tannery effluent at pH 7 after standing for three months had a spectrum essentially identical with curve (b) in Fig. 3, while that at pH 11 gave no manganese(II) signal.

Spectra (a) in Figs. 2 and 3 resemble each other, though an intense radical signal is absent in spectrum (a) of Fig. 3. Spectrum (b) in Fig. 3 closely resembles the spectrum of manganese(II) species such as $[Mn(H_2O)_6]^{2+}$ solution frozen in Sephadex [22], subcellular fractions of organs from mice treated with manganese(II) chloride [23], and manganese(II) ions in borate glasses [24].

These results indicate that the reduction of manganese dioxide by the tannery effluents can afford insoluble manganese(II) compounds similar to those found in river water at high alkalinity and soluble manganese(II) species

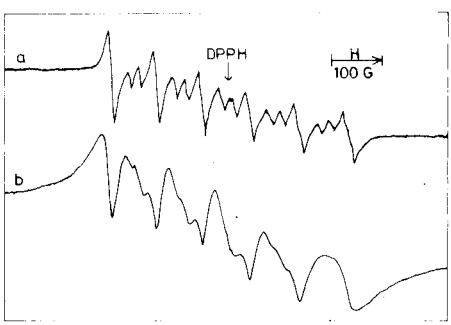

Fig. 3. The e.p.r. spectra of manganese(II) obtained after the reduction of manganese dioxide by tannery effluents: (a) pH 11; (b) pH 7. E.p.r. parameters estimated from the second derivatives: (a) g_1 = 2.009, A_1 = 94 G; g_2 = 2.005, A_2 = 96 G; (b) g = 2.009, A = 93 G. (Instrument settings as in Fig. 1.)

at pH 7. It seems likely that the reduction at high alkalinity takes place much more slowly than at pH 7. No reduction of manganese dioxide by the filtrate of tannery effluents at pH 11 was observed, thus the particulate fraction may contribute considerably to the reduction under highly alkaline conditions.

It has been reported that although chromium(III) is oxidized by manganese dioxide [25, 26], this reaction is inhibited by other substances in natural waters [25]. This oxidation can be expected to accompany the reduction of manganese(IV) to manganese(II). Because the tannery effluents used here contain high concentrations of chromium(III), the reduction of manganese dioxide by chromium(III) may not be negligible. This reduction, however, will be ineffective in the formation of manganese(II) species in tannery effluents because the effluents contain a large concentration of organic reductants. Furthermore, the reduction of manganese dioxide by micro-organisms in tannery effluents is possible, though its effectiveness is not known.

We express our gratitude to Mr. K. Ashida of the Environmental Science Institute of Hyogo Prefecture for donating the samples of river sediments.

REFERENCES

1 E. J. Underwood, Trace Elements in Human and Animal Nutrition, 3rd edn., Academic Press, New York, 1971, p. 177.
2 J. J. R. Frausto da Silva and R. J. P. Williams, Struct. Bonding, 29 (1976) 67.
3 G. D. Lawrence and D. T. Sawyer, Coord. Chem. Rev., 27 (1978) 173.
4 P. N. Linnik and B. I. Nabivanets, Hydrobiol. J., 13 (1977) 91.
5 A. T. Stone and J. J. Morgan, Environ. Sci. Technol., 18 (1984) 450.
6 A. T. Stone and J. J. Morgan, Environ. Sci. Technol., 18 (1984) 617.
7 W. G. Sunda, S. G. Huntsman and G. R. Harvey, Nature (London), 301 (1983) 234.
8 D. E. Wilson, Geochim. Cosmochim. Acta, 44 (1980) 1311.
9 M. A. Kessick and J. J. Morgan, Environ. Sci. Technol., 9 (1975) 157.
10 W. Sung and J. J. Morgan, Geochim. Cosmochim. Acta, 45 (1981) 2377.
11 W. G. Bryson, D. P. Hubbard, B. M. Peake and J. Simpson, Anal. Chim. Acta, 77 (1975) 107.
12 R. W. Gaver, F. P. Milanovich and R. L. Ward, J. Environ. Sci. Health, A11 (1976) 743.
13 D. S. Gamble, M. Schnitzer and D. S. Skinner, Can. J. Soil. Sci., 57 (1977) 47.
14 M. B. McBride, Soil Sci., 126 (1978) 200.
15 S. A. J. Shivas, J. Am. Leather Chem. Assoc., 73 (1978) 370.
16 A. E. Greenberg, J. J. Connors and D. Jenkins (Eds.), Standard Methods, 15th edn., American Public Health Association, Washington, 1980.
17 T. Caster, G. S. Newell, W. C. Holton and C. P. Slichter, J. Chem. Phys., 32 (1960) 668.
18 N. Senesi, S. M. Griffith and M. Schnitzer, Geochim. Cosmochim. Acta, 41 (1977) 969.
19 G. H. Reed and W. J. R. Ray, Biochemistry, 10 (1971) 3190.
20 C. J. Miles and P. L. Brezonik, Environ. Sci. Technol., 15 (1981) 1089.
21 R. K. Skogerboe and S. A. Wilson, Anal. Chem., 53 (1981) 228.
22 G. H. Reed and M. Cohn, J. Biol. Chem., 247 (1972) 3073.

23 H. Sakurai, M. Nishida and T. Yoshimura, Inorg. Chim. Acta, 66 (1982) L17.
24 H. W. Wijn and R. F. Balderen, J. Chem. Phys., 46 (1967) 1381.
25 D. C. Schroeder and G. F. Lee, Water Air Soil Pollut., 4 (1975) 355.
26 R. Bartett and B. James, J. Environ. Qual., 8 (1979) 31.

Analytica Chimica Acta, 186 (1986) 123—130
Elsevier Science Publishers B.V., Amsterdam — Printed in The Netherlands

QUANTITATIVE PHOTOACOUSTIC SPECTROMETRY
Determination of Copper(II) and Iron(III) Complexed on Modified Silica Gel Samples

R. S. FIELD[a], D. E. LEYDEN* and R. S. SHREEDHARA MURTHY

Condensed Matter Sciences Laboratory, Department of Chemistry, Colorado State University, Fort Collins, CO 80523 (U.S.A.)

(Received 18th February 1986)

SUMMARY

Calibration curves for copper(II) and iron(III) complexed with *N*-2-aminoethyl-3-aminopropyltrimethoxysilane (AEAPS) immobilized on silica gel were prepared separately by photoacoustic spectroscopy (p.a.s.) based on a response function that combines the amplitude and phase values. The concentrations of copper and iron in two-component samples are determined by obtaining the response at 600 and 400 nm, respectively, and referring to the calibration graphs. The relative errors in the concentrations determined by p.a.s. compared to atomic absorption spectrometry for copper range from —9.3 to 3.2%, while for iron the range is —52.7 to 4.5%. The large error for iron was due to its low concentration and absorptivity. With suitable chromophores and matrix, the response function extends the linear range of the calibration graph and can be used for nondestructive determination of two components.

Photoacoustic spectroscopy (p.a.s.) has been established as a technique to obtain spectra of opaque and highly light-scattering samples in the ultraviolet, visible and infrared regions. Although quantitative p.a.s. studies have been done in the u.v./visible region [1—3], the method has not found widespread use. When photoacoustic signal amplitude was used in these studies, the calibration graph had limited linear range. Consequently, only components in samples with low absorptivity could be quantified. It was necessary to dilute highly absorbing samples with a nonabsorber. This severely restricted the useful concentration range and increased sample preparation time.

Roark et al. [4] used the photoacoustic phase angle for quantitative purposes and observed a practical limit of absorptivity which was an order of magnitude larger than that obtained by using signal amplitude alone. However, for samples of low absorptivity, accurate measurement of phase was difficult because of the acoustic background and other cell absorbances. Burggraf and Leyden [5] combined the photoacoustic amplitude and phase into a single response function, taking advantage of the greater sensitivity of the phase measurements at large absorptivities. The measurement of phase

---

[a]Present address: Wyeth Laboratory, Radnor, PA 19087, U.S.A.

0003-2670/86/$03.50

values at low absorptivities was still difficult, but the contribution to the response function by the phase at low absorptivities was low. Hence, the response function extended the linear region of the calibration graphs by two orders of magnitude.

This paper describes the results obtained when the response function was used to analyze a two-component sample. Copper(II) and iron(III) complexes of *N*-2-aminoethyl-3-aminopropyltrimethoxysilane (AEAPS) immobilized on silica gel were chosen as model chromophores because neither component had significant absorptivity at the absorption maximum of the other.

EXPERIMENTAL

Instrumentation

The photoacoustic spectrometer has been described [5]. Data acquisition was done through an analog/digital converter (ADC) (Interactive Structures AI13) interfaced to a 64K Apple II+ microcomputer. Control of the monochromator stepping motor and measurement of the chopping frequency was accomplished with a 6522 VIA integrated circuit on an interface card (John Bell Engineering, 79-295) plugged into one of the interface slots of the Apple II+ computer. Computer programs were written in AppleSoft with assembly language subroutines to acquire the data, pulse the monochromator stepping motor and measure the chopping frequency. A dual-phase lock-in amplifier (Princeton Applied Research Model 5204) measured the photoacoustic signal amplitude at two phase angles (usually 0° and 90°), and a vector board option in the amplifier unit computed and output the magnitude and phase to two channels of the ADC. A chopping frequency of 176 Hz offered the best compromise between adequate sensitivity and minimum low-frequency noise and hence was used to acquire all data.

Thermometric titrations were done with a Tronac 450 isoperibol calorimeter (Tronac). A Varian AA5 atomic absorption spectrometer (Varian Associates) was used to determine the concentrations of copper and iron at 324.7 and 248.3 nm, respectively.

Sample preparation

Silica gel (10 g; 60—200 mesh, surface area 290 m^2 g^{-1}; J. T. Baker) was treated with a 5% (v/v) solution of freshly distilled *N*-2-aminoethyl-3-aminopropyltrimethoxysilane (AEAPS) in 150 ml of dry toluene for 20 min at room temperature with occasional stirring [6]. The suspension was filtered, rinsed with toluene and cured in a vacuum oven at 110°C for 6 h. Thermometric titration of the modified silica with 1 M perchloric acid indicated that the product contained 0.75 mmol of immobilized AEAPS per gram of silica.

The AEAPS-silica was mixed with a 0.1 M Cu(II) solution buffered to pH 5. The slurry was filtered after 15 min and the dark blue product was washed with distilled water and dried in a vacuum oven at 110°C for 2 h.

The Fe(III) complex was prepared by mixing the AEAPS—silica with 0.1 M iron(III) ammonium sulfate buffered to pH 3. After 30 min, the resulting yellow complex was filtered, washed with distilled water and dried in a vacuum oven for 2 h at 110°C. The AEAPS—silica samples with the coordinated metals are called here the copper— or iron—AEAPS samples.

To evaluate the capabilities of p.a.s. for quantitative applications, series of samples with decreasing concentrations of each metal were prepared by diluting the above copper— or iron—AEAPS samples with increasing amounts of unmodified silica. For each metal complex, four replicate samples were prepared at five different concentrations. The samples were mixed in a Wig-L-Bug (Crescent Dental Mfg. Co.) for 60 s without the metal ball to ensure a homogeneous mixture of the solids. Copper—AEAPS samples were mixed with iron—AEAPS samples to form a series of two-component samples of varying concentration. The magnitude and phase values for these samples were measured and combined in the response function as described before [5].

Determination of metal concentrations on the modified silica

Copper was stripped from the AEAPS—silica by mixing it with 3 M nitric acid. The suspension was filtered after 5 min and the silica was washed with distilled water. The filtrate containing the eluted copper was diluted to 10 ml and copper was quantitated by atomic absorption spectrometry (a.a.s.). The concentration of copper in the AEAPS—silica was obtained by referring to a calibration graph prepared by measuring the absorbance of standards at 324.7 nm.

A calibration curve for iron(III) was prepared by measuring the absorbance of its standard solutions at 248.3 nm by a.a.s. Iron was stripped from AEAPS—silica with 3 M nitric acid for 5 min. The slurry was then filtered, washed with water and the filtrate was diluted to 10 ml. Iron in the filtrate was determined from the calibration graph.

RESULTS AND DISCUSSION

A detailed derivation of the response function has been reported [5] and hence only the final equation is given here. The amplitude and phase data are combined to give the response function

$$C\beta\mu_s = 2^{1/2} q_n / \sin(\psi - \pi/4) \quad (1)$$

where C is a constant that depends on the thermal diffusion coefficient and thermal conductivity of the sample and reference, β is the optical absorption coefficient, μ_s is the thermal diffusion length, q_n is the photoacoustic amplitude normalized to a reference material, and ψ is calculated from

$$\psi = \phi_S - \phi_R + \pi/4 \quad (2)$$

where ϕ_S and ϕ_R are the sample and reference phases, respectively.

A perfectly opaque substance such as carbon black has generally been used to obtain the reference phase. Theoretically, a perfect reference should have a phase lag of $\pi/4$ when all the instrumental phase-lag components are removed [5]. However, this procedure may not always be reliable because of differences between the thermal properties of the reference and the sample. For example, signals from different carbon black samples were found to have different phase values. An alternative approach is to estimate the phase of a perfect absorber on the matrix under study by extrapolating the phase to a highly absorbing sample. In most modified silica samples investigated here, the phase appears to approach asymptotically to a limiting value. The limiting value can be estimated from a plot of the logarithm of the phase versus the concentration of the standard samples. For the AEAPS—silica samples used in this work, a phase angle for the reference was estimated to be 0.92°. Hence, the response values were calculated from

$$C\beta\mu_S = 2^{1/2}q_n/\sin(\phi_S - 0.92) \quad (3)$$

Determination of a single component

The normalized photoacoustic amplitude spectra of Cu(II) and Fe(III) complexes with AEAPS—silica are shown in Fig. 1. These spectra were acquired after signal averaging 1000 measurements at 2-nm intervals and normalizing to the corresponding amplitude of carbon black. The copper(II) complex has a strong absorption at 600 nm, which was shown in previous studies [7] to arise from a combination of mono- and bis-chelate forms. The iron(III) complex has an absorption edge declining from the near-ultraviolet region. In the present study, all measurements were done in the visible region to avoid changing the grating on the monochromator which may introduce errors in sample alignment.

Amplitude and phase data for silica samples containing known concentrations of copper (from a.a.s.) were obtained by signal averaging 1000 mea-

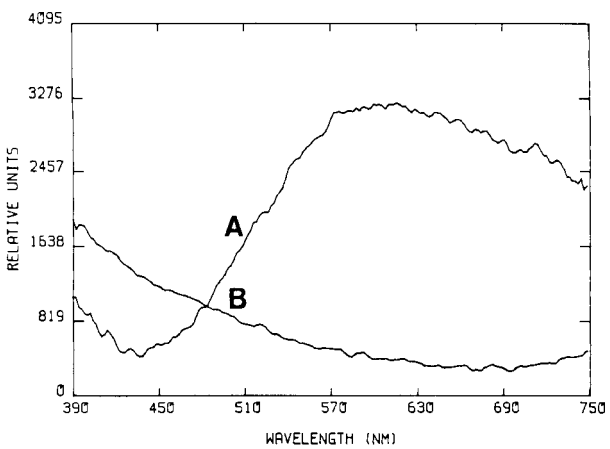

Fig. 1. Photoacoustic amplitude spectra: (A) copper—AEAPS; (B) iron—AEAPS silica.

surements at 600 nm (Fig. 2a). The amplitude plot (plot A) at 600 nm exhibits the typical nonlinearity that is often seen with calibration curves based on the amplitude data alone. The phase for the copper—AEAPS samples (plot B) follows an inverse relationship relative to amplitude. At low concentrations, it is difficult to meaure the phase accurately, while at high concentrations, the phase approaches a limiting value.

Response values were calculated from the amplitude and phase values shown in the plots for the copper—AEAPS silica samples using a reference phase angle of 0.92°. Small errors in the phase measurements at high concen-

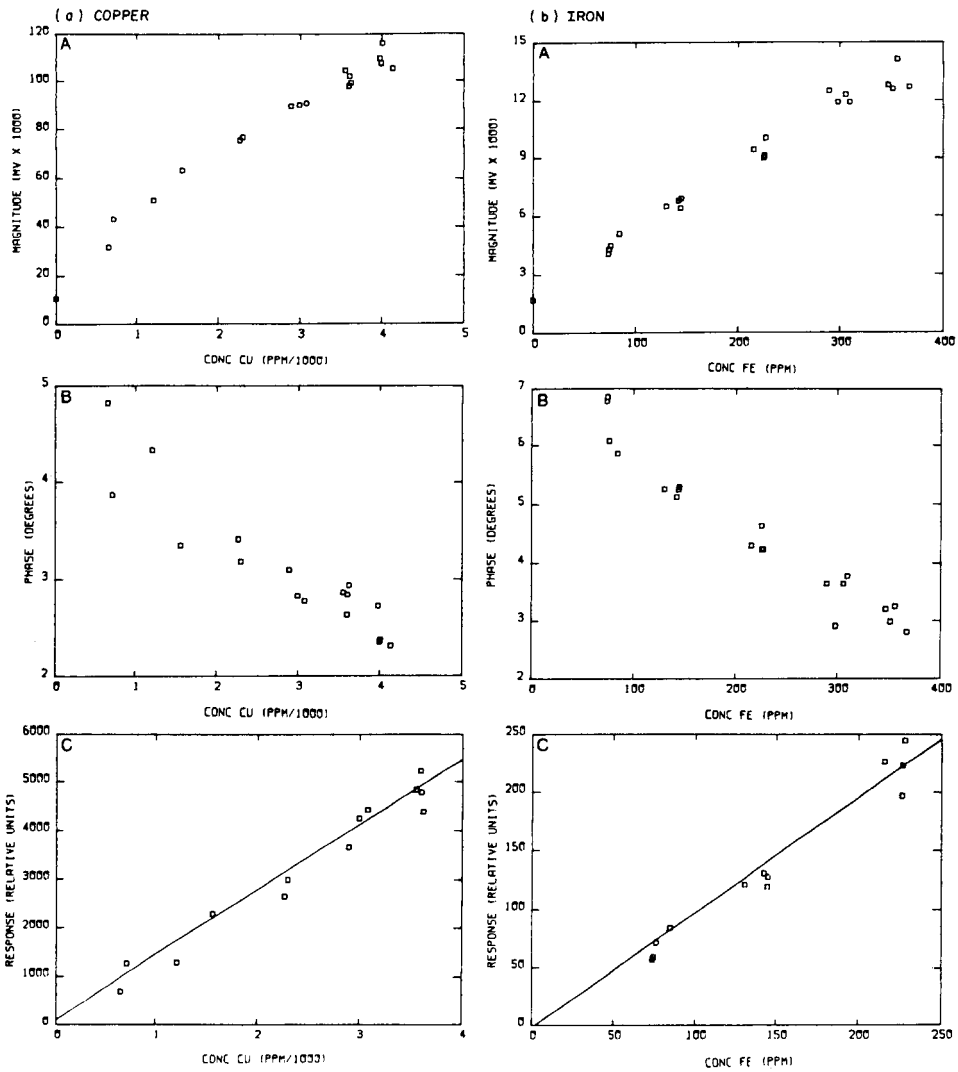

Fig. 2. Plots of photoacoustic (A) amplitude, (B) phase, and (C) response values vs. the concentration of copper or iron: (a) copper measured at 600 nm; (b) iron measured at 400 nm.

trations can cause large errors in the response function, but fortunately the most accurate phase values are obtained at high concentrations. In spite of the large scatter of the phase values at low concentrations, the phase corrections are small relative to the effect at higher concentrations. Plot C in Fig. 2(a) shows the response curve for the copper(II) complex at 600 nm. A least-squares fit gave a calibration line with a slope of 1209 ± 66, an intercept of 17 ± 177, and a correlation coefficient of 0.984.

The amplitude and phase plots for the iron(III) complex were obtained by averaging 1000 measurements at 400 nm. Plot A in Fig. 2(b) shows that the amplitude is linear up to an iron concentration of 325 $\mu g\ g^{-1}$ (ppm). Combining the amplitude and phase values for each iron—AEAPS silica sample, a response value was calculated by using the same phase reference angle as that used for copper samples. The response calibration line shown in plot C (Fig. 2b) has a slope of 1060 ± 65, an intercept of −18 ± 10, and a correlation coefficient of 0.982.

Before the copper— and iron—AEAPS silica samples were mixed for the determination of two components, it was important to know whether the dilution of the sample with either unmodified silica or iron—AEAPS silica would alter the thermal properties of the matrix. It was possible to replace the unmodified silica with iron—AEAPS silica for dilution because the latter does not absorb at 600 nm. The weight percent of the Cu(II) sample was kept constant and the diluent was changed from unmodified silica to the iron—AEAPS silica. There was no measurable difference in the amplitude or phase signal when the copper product was diluted with either unmodified silica or the iron—AEAPS silica. This implies that the thermal properties are not affected by dilution. Hence, any errors in the two-component results of the modified silica samples cannot be attributed to changes in the matrix.

Determination of two components

Simultaneous determination of two components was investigated by measuring the amplitude and phase values for a series of samples prepared by mixing different concentrations of the iron— and copper—AEAPS silica samples. At each measurement wavelength, a response value was calculated for the mixture which represented the combined signals from each absorbing component. The net signal from the two components is represented by

$$R_{400} = R_{Cu,400} + R_{Fe,400} \tag{4}$$

$$R_{600} = R_{Cu,600} + R_{Fe,600} \tag{5}$$

where R represents the response value for the indicated component at the given wavelength. Because the copper— and iron—AEAPS silica had very low absorptivities at 400 and 600 nm, respectively, accurate amplitude and phase measurements were difficult. Hence, the response terms $R_{Cu,400}$ and $R_{Fe,600}$ were neglected. The least-squares equations for the calibration lines used to

TABLE 1

Comparison of results for two components

Sample no.	Concn. of Cu ($\mu g\ g^{-1}$)		Relative error (%)	Concn. of Fe ($\mu g\ g^{-1}$)		Relative error (%)
	Found	Known		Found	Known	
1	330	350	−5.7	161	154	+4.5
2	2070	2110	−1.9	34	72	−52.7
3	600	610	−1.6	46	71	−35.2
4	680	750	−9.3	152	150	+1.3
5	1540	1520	+1.3	139	147	−5.4
6	2250	2240	+0.4	67	99	−32.3
7	2260	2190	+3.2	52	98	−46.9

calculate the concentrations of iron and copper were as follows:

$$R_{Fe,400} = 1060[Fe] - 18 \quad (6)$$

$$R_{Cu,600} = 1209[Cu] + 17 \quad (7)$$

Results for the two-component mixtures are summarized in Table 1. The percent error for the copper component was less than 10% for samples in the concentration range 300—2200 $\mu g\ g^{-1}$. The percent error for the iron component was much higher because its absorptivity was low and also the concentration of the metal was less than 160 $\mu g\ g^{-1}$ for all the samples. The difference in metal loadings was a result of their different binding capacities with the AEAPS-modified silica surface [8].

Conclusions

Although photoacoustic spectrometry will not compete with other quantitative techniques such as atomic or molecular absorption spectrometry in either sensitivity, precision or accuracy, the present work has shown that the response function is useful in extending the analyte concentration range that yields a linear calibration graph. As p.a.s. is not an absolute technique, a calibration graph must be prepared by obtaining the concentration of the analyte from another suitable technique such as a.a.s. Then rapid and non-destructive quantitation can be done by p.a.s. It can be used to determine two components in highly light-scattering samples such as metals complexed on modified silica gel. Work is in progress to extend this procedure to determine the concentration of dyes adsorbed on modified silica gel and paints.

This research was supported in part by Research Grant CHE-8210014 from the National Science Foundation.

REFERENCES

1 S. L. Castleden, C. M. Elliot, G. F. Kirkbright and D. E. M. Spillane, Anal. Chem., 51 (1980) 2152.
2 D. Hurch and T. Kuwana, Anal. Chem., 52 (1980) 646.
3 C. H. Lochmüller and D. R. Wilder, Anal. Chim. Acta, 118 (1980) 101.
4 J. C. Roark, R. A. Palmer and J. S. Hutchison, Chem. Phys. Lett., 60 (1978) 112.
5 L. W. Burggraf and D. E. Leyden, Anal. Chem., 53 (1981) 759.
6 D. E. Leyden, D. S. Kendall, L. W. Burggraf, F. J. Pern and M. DeBello, Anal. Chem., 54 (1982) 101.
7 D. E. Leyden, D. S. Kendall, L. W. Burggraf and F. J. Pern, Anal. Chim. Acta, 129 (1981) 19.
8 Fu-Jann Pern, M. S. Dissertation, University of Denver, 1980.

Analytica Chimica Acta, 186 (1986) 131—137
Elsevier Science Publishers B.V., Amsterdam — Printed in The Netherlands

FLOW-INJECTION DETERMINATION OF ADENOSINE AND INOSINE IN BLOOD PLASMA WITH IMMOBILIZED ENZYME COLUMNS CONNECTED IN SERIES AND FLUORIMETRIC DETECTION

YOHJI HAYASHI, KIYOSHI ZAITSU and YOSUKE OHKURA*

Faculty of Pharmaceutical Sciences, Kyushu University 62, Maidashi, Higashi-ku, Fukuoka 812 (Japan)

(Received 14th February 1986)

SUMMARY

A rapid and sensitive flow-injection method is described for the enzymatic determination of adenosine and inosine in human blood plasma. Teflon columns prepared by packing adenosine deaminase, purine nucleoside phosphorylase, xanthine oxidase, uricase and horseradish peroxidase immobilized chemically on controlled-pore glass beads are connected in series in that order in the flow line. Hydrogen peroxide formed in the enzymatic conversion of adenosine and inosine is measured fluorimetrically after reaction with 3-(*p*-hydroxyphenyl)propionic acid. Linear calibrations were obtained for 0.5—500 pmol of adenosine or inosine in the 20-μl sample injected. Necessary deproteination routines are outlined.

Deficiency of purine nucleoside phosphorylase, a metabolic enzyme of purine nucleosides such as inosine and guanosine, is closely associated with immunodeficiency characterized by severely defective T-cell function with normal B-cell immunity [1, 2]. Patients with this disorder show abnormally elevated concentration levels of inosine and guanosine in urine and plasma [1, 2]. Severe combined immunodeficiency, which exhibits profound defects of both cellular and humoral immune functions, is closely correlated with deficiency of adenosine deaminase, and so the levels of adenosine and deoxyadenosine in plasma and urine of immunodeficient patients are higher than those in a healthy person [3, 4].

High-performance liquid chromatography (h.p.l.c.) has been used for the simultaneous determination of adenosine, inosine and other purine metabolites in biological fluids [5—8]; the methods are not very satisfactory for the rapid assay of a large number of samples. This study aims to establish a flow-injection method for the rapid assay of adenosine and inosine in human plasma; adenosine and inosine are degraded via allantoin to hydrogen peroxide by immobilized adenosine deaminase (ADA), purine nucleoside phosphorylase (PNP), xanthine oxidase (XOD) and urate oxidase (UOD, uricase). The hydrogen peroxide is quantified by an immobilized horseradish peroxidase (HRP)-mediated reaction and 3-(*p*-hydroxyphenyl)propionic acid

0003-2670/86/$03.50

(HPPA) is used as an efficient fluorogenic substrate [9, 10]. The sequence of reactions is shown below.

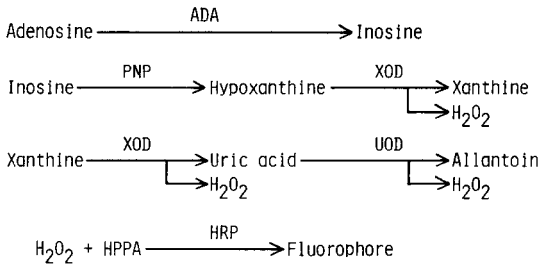

EXPERIMENTAL

Reagents

Deionized, triply-distilled water was used. HPPA was obtained from Dojindo Lab. (Kumamoto, Japan) or Otsuka Chemical (Osaka, Japan). Tris-(hydroxymethyl)aminomethane (Tris; Ultrol grade), HRP (285 purpurogallin units mg^{-1}) and UOD (grade II, 4.0 U mg^{-1}, from *candida* sp.) were from Calbiochem, Sigma, and Toyobo Biochemicals (Osaka), respectively. ADA (200 U mg^{-1}, from calf intestine, in 3.2 M ammonium sulfate suspension), PNP (19.5 U mg^{-1}, from calf spleen, in 3.2 M ammonium sulfate suspension), XOD (0.4 U mg^{-1}, from cow milk, in 3.2 M ammonium sulfate suspension, 10 mM in EDTA) and catalase (Type II, 260,000 U ml^{-1},from bovine liver, in 30% (v/v) glycerol solution containing 10% (v/v) ethanol), were obtained from Boehringer Mannheim Yamanouchi (Tokyo). Unless otherwise noted, all other chemicals were of reagent grade.

Purification of PNP

Commercial PNP contains ADA (ca. 60 mU mg^{-1}) and guanase (ca. 2.3 mU mg^{-1}) as impurities, so it was purified by gel-permeation h.p.l.c. as follows. The PNP preparation was dialyzed against 5 mM sodium phosphate buffer (pH 7.0) overnight at 4°C and concentrated to half its volume by freeze-drying. The concentrate was subjected to h.p.l.c. on a TSK gel G-3000-SW column (600 × 7.5 mm i.d.; Toyo Soda, Tokyo) using a Waters M-45 liquid chromatograph equipped with a Waters 440 absorbance detector (monitoring wavelength, 254 nm) and 50 mM sodium phosphate buffer (pH 7.0) containing 0.15 M sodium chloride as a mobile phase at a flow rate of 0.7 ml min^{-1}. The fraction which had the highest PNP activity was further dialyzed in the same way as described above and then concentrated to one fifth of its volume by freeze-drying. The concentrate was purified again in the same manner. The activities of PNP, ADA and guanase in the eluate were measured in the usual manner [11]. The activity of purified PNP was 53.1 U mg^{-1} (ADA, 2.63 mU mg^{-1}; guanase, not detected).

Preparation of immobilized enzyme glass beads and their columns

Immobilized HRP glass beads were prepared as described previously [10]. The ADA, PNP, XOD and UOD were immobilized on amino-derivatized controlled-pore glass beads (120—200 mesh, AMP-CPG 1400, mean pore size 140 nm; Electro-Nucleonics, Fairfield, U.S.A.) by the technique involving glutaraldehyde [12, 13]. The immobilized enzyme glass beads were stored at 4°C in the following conservative solutions: 3.2 M ammonium sulfate (pH 6.0) for ADA and PNP; 3.2 M ammonium sulfate (pH 8.0) 10 mM in disodium-EDTA for XOD; 50% (v/v) glycerol (pH 10.2) 50 mM in glycine and 0.13 M in sodium carbonate for UOD; and 0.1 M Tris-hydrochloric acid buffer (pH 8.5) 0.15 M in sodium chloride, 1% (w/v) in bovine serum albumin and 0.25 mM in sodium merthiolate for HRP. The activities of the immobilized enzymes were measured by published methods [10, 11]. The enzyme activities (U g^{-1} glass beads) were 17.2 (ADA), 12.2 (PNP), 2.3 (XOD), 6.9 (UOD) and 14.4 (HRP). Columns of the enzyme glass beads were prepared by packing the beads in teflon tubes (40 × 0.86 mm i.d.) as described previously [10].

Preparation of plasma sample solution

Venous blood (5 ml) obtained from a healthy volunteer was collected in a glass tube containing 50 μl of 0.2 M disodium-EDTA. The blood was immediately centrifuged for 10 min at 1000g.

The plasma (100 μl) was mixed with 100 μl of 1 M perchloric acid and centrifuged for 10 min at 1000g. To 100 μl of the supernatant liquid, 80 μl of 0.5 M potassium carbonate was added to precipitate perchlorate, and the resulting mixture was centrifuged as described above. The supernatant liquid (140 μl) was mixed with 30 μl each of 0.5 U ml^{-1} UOD solution and 40 U ml^{-1} catalase solution (both in 50 mM phosphate buffer, pH 8.0; usable for 1 week and 1 day, respectively). The mixture was incubated for 30 min at 37°C, and 30 μl of 4 M perchloric acid was added followed by 60 μl of 2 M potassium carbonate. After centrifugation for 10 min at 1000g, the supernatant liquid (210 μl) was diluted with 70 μl of 0.4 M Tris-hydrochloric acid buffer (pH 8.0) 0.6 M in sodium chloride, 0.2 M in disodium hydrogenphosphate and 40 mM in disodium-EDTA. An aliquot of the final solution (20 μl) was used for the flow-injection procedure.

Flow-injection apparatus and assay procedure

A schematic flow diagram of the flow-injection system is shown in Fig. 1. Teflon tubing (0.25 mm i.d., Gasukuro Kogyo, Tokyo) was used. The reagent solution, which was 5 mM HPPA in 0.1 M Tris-hydrochloric acid buffer (pH 8.0), 0.15 M in sodium chloride, 50 mM in disodium hydrogenphosphate and 10 mM in disodium-EDTA, and the carrier solution, which was the same as the reagent solution but without HPPA,were pumped separately with a Jasco RP-4 pump; the flow rates were both 0.25 ml min^{-1}. The plasma sample solution was injected through a Rheodyne 7125 syringe-loading sample injec-

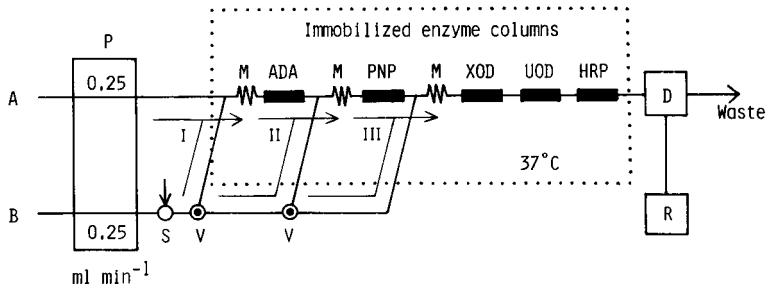

Fig. 1. Schematic diagram of the flow-injection system: (A) reagent solution; (B) carrier solution; (P) pump; (S) sample injector; (M) mixing coil; (V) three-way valve; (D) fluorescence detector; (R) recorder; (I, II, III) flow lines as described in the text.

tor valve (20-μl loop) into the carrier stream. Three T-connectors were installed in the flow line and the sample solution was passed through the ADA, PNP, XOD, UOD and HRP columns (line I), or the PNP, XOD, UOD and HRP columns (line II), or the XOD, UOD and HRP columns (line III), by operating two Kyowa Seimitsu KMM-3V three-way valves. The five enzyme columns and three mixing coils (1 m each) built in the flow line were immersed in a water bath at 37°C. The mixing coils served not only to mix the carrier solution (or sample solution) thoroughly with the reagent solution, but also to warm the mixture sufficiently before it reached the enzyme columns. The fluorescence intensity was measured at an excitation wavelength of 305 nm and an emission wavelength of 405 nm with a Shimadzu RF-530 fluorescence spectromonitor equipped with a 12-μl flow cell and a Hitachi 056 chart recorder.

For calibration, adenosine and inosine standard solutions (0.1–25 μM) were taken through the procedure (flow line I for adenosine, flow line II for inosine).

For the determination of adenosine, the sample solution was first introduced into line I, and then to line II to obtain peak heights a and b, respectively. Peak heights c and d were measured beforehand by injecting an inosine standard (2.5 μM) into lines I and II, respectively. The net peak height for adenosine was given by $a - bc/d$. The net peak height for inosine in the sample solution was calculated in a similar way from $b - ef/g$, where b and e were the peak heights for the sample obtained in lines II and III, respectively, and f and g were the peak heights observed for a hypoxanthine standard solution (2.5 μM) in lines II and III, respectively. The concentrations of adenosine and inosine were read from the calibration graphs prepared from the above values for net peak heights.

RESULTS AND DISCUSSION

When plasma was introduced without deproteination into the flow system, the inner pressure in the system increased and the flow line was damaged. In

addition, the metabolism of purines in blood is very rapid once blood has been withdrawn from the patient; purines are degraded by endogenous catabolic enzymes [5, 14, 15]. Adenosine is also avidly taken up by erythrocytes [16]. Therefore, plasma should be obtained by centrifugation as soon as blood has been withdrawn, and the plasma should be rapidly deproteinated with perchloric acid to deactivate the catabolic enzymes.

Deproteinated plasma contains not only adenosine, inosine, hypoxanthine and xanthine but also a large amount of uric acid. Uric acid in the sample greatly inhibits the fluorogenic reaction used here. Thus, it was decomposed by a UOD-mediated reaction and the resulting hydrogen peroxide was further decomposed by the addition of catalase solution. These enzymes remaining in the sample were removed by the treatment with perchloric acid. A small amount of uric acid is also produced from adenosine, inosine, hypoxanthine and xanthine in the sample solution by the enzyme reactions in the system. The resulting uric acid only slightly inhibited the fluorogenic reaction; an immobilized UOD column was placed on the flow line to eliminate the interference. Bilirubin (<130 μM) in plasma did not affect the determination of adenosine and inosine, but higher concentrations caused an apparent decrease in the recoveries of adenosine and inosine. Ascorbic acid and glucose added to plasma had no effect on the adenosine and inosine recoveries at concentrations of 280 μM and 11.1 mM, respectively. The recoveries of adenosine and inosine were unaffected by heparin and disodium-EDTA anticoagulants for blood, at the concentrations normally used.

Commercial PNP contains ADA and guanase, and so it was purified by h.p.l.c. When the purified PNP was used for the preparation of the immobilized PNP column, 5 μM adenosine and 5 μM guanine (20 μl each) injected into the system via flow line II gave peak heights corresponding to only 0.6 and 1.0% of that given by 5 μM inosine (20 μl), respectively.

Deoxyadenosine is converted to deoxyinosine by the catalysis of ADA. Deoxyinosine is further degraded to hypoxanthine in the presence of PNP, and so the presence of such deoxyribonucleosides in the sample influences the peak height for adenosine or inosine. However, deoxyadenosine is extremely labile at low pH [17]; deoxyadenosine added in plasma was decomposed almost completely during deproteination with perchloric acid. Deoxyinosine, however, was not decomposed completely by perchloric acid. Deoxyinosine has not been detected in blood samples from patients [1] or normal persons [8, 14]. Xanthosine is a poor substrate for PNP; it did not give any response in the present method at a concentration of 5 μM.

The HPPA concentration in the stream influences the fluorescence intensity produced. The most intense peak was achieved at a concentration of $\geqslant 4.0$ mM in the reagent solution, thus 5.0 mM HPPA is recommended. Disodium hydrogenphosphate (50 mM) was added to the buffer solution used for the reagent and carrier solutions because the PNP-catalyzed reaction requires inorganic orthophosphate. Disodium-EDTA was also added to the buffer solution to protect XOD from certain inhibiting metal ions.

The fluorescence from HPPA increased with increasing pH in the range

7.1—8.5. As the immobilized enzymes might be deactivated at higher pH values, pH 8.0 is recommended. The peak height increased with decreasing flow rates of the reagent and carrier solutions and the inner pressure in the system increased with increasing flow rate; 0.25 ml min^{-1} was selected for both the reagent and carrier solutions.

Because flow lines I, II and III have different inner volumes and give different peak heights even when the same inosine solution (or hypoxanthine solution) is injected to flow lines I and II (or II and III), respectively, the net peak height arising from adenosine (or inosine) should be calculated as described in the Experimental section.

Typical calibration results obtained with 4—100 pmol of adenosine (in 20 μl) are shown in Fig. 2. Calibration graphs for adenosine and inosine were linear up to 500 pmol and passed through the origin.

The correlations between the concentrations (μM) of adenosine and inosine added to plasma (X) and found by this method (Y) were linear; the regression equations were $Y = 1.01X + 0.104$ for adenosine and $Y = 1.04X + 0.390$ for inosine. The correlation coefficients were 0.999 ($n = 8$) in both instances. The ordinate intercepts in both were due to adenosine and inosine present in plasma.

Recoveries of adenosine and inosine added to plasma at concentrations of 2.5—20 μM were ca. 100%. The lower determinable limits (signal/noise ratio

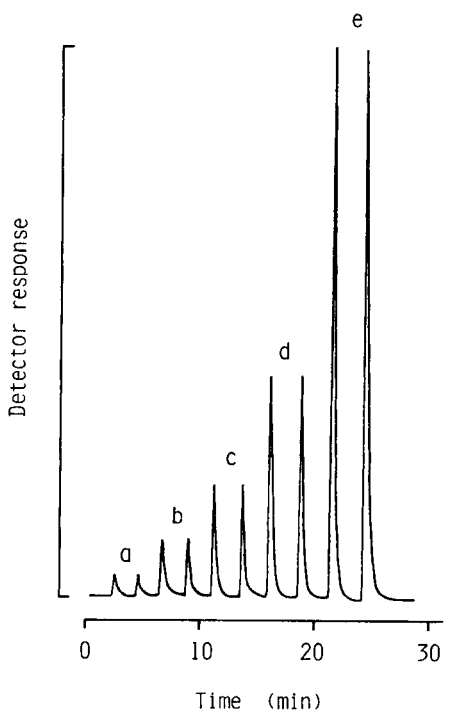

Fig. 2. Calibration peaks for adenosine. Amounts of adenosine (pmol/20 μl): (a) 4; (b) 10; (c) 20; (d) 40; (e) 100.

= 5) for adenosine and inosine were both 0.5 pmol per 20-μl injection volume. The sensitivity was similar to that of the h.p.l.c. methods with spectrophotometric detection [5—8], but a rapid sampling rate (30 h^{-1}) was possible with the proposed method. The relative standard deviations in repeated determinations of adenosine and inosine (0.13, 0.25, 0.50, 1.3, 2.5 and 5.0 μM, respectively) did not exceed 1.0% (n = 10) in each case.

To check the stability of the immobilized enzyme columns, adenosine solutions (2.5 and 5 μM) were processed 50 times a week via line I. The columns were stored at 4°C after filling with their conservative solution, when they were not required for use. The immobilized ADA, PNP, UOD and HRP columns were stable for at least 4 months; the XOD column was stable for 3 months but a 10% loss of activity was detected after 4 months.

This study provides the first flow-injection method based on immobilized enzyme columns connected in series for the determination of adenosine and inosine in blood plasma. The method is highly sensitive, rapid and precise, and could be applied in diagnosis and biomedical investigations of ADA and PNP deficiencies.

REFERENCES

1 A. Cohen, D. Doyle, D. W. Martin, Jr. and A. J. Ammann, N. Engl. J. Med., 295 (1976) 1449.
2 A. Cohen, D. W. Martin, Jr. and A. J. Ammann, J. Clin. Chem. Clin. Biochem., 14 (1976) 283.
3 R. A. Hartwick and P. R. Brown, J. Chromatogr., 143 (1977) 383.
4 J. F. Kuttesch, F. C. Schmalstieg and J. A. Nelson, J. Liq. Chromatogr., 1 (1978) 97.
5 R. A. Hartwick, A. M. Krstulovic and P. R. Brown, J. Chromatogr., 186 (1979) 659.
6 A. Leyva, J. Schornagel and H. M. Pinedo, Adv. Exp. Med. Biol., 122 (1980) 389.
7 M. Zakaria, P. R. Brown, M. P. Farnes and B. E. Barker, Clin. Chim. Acta, 126 (1982) 69.
8 J. T. Eells and R. Spector, Neurochem. Res., 8 (1983) 1451.
9 K. Zaitsu and Y. Ohkura, Anal. Biochem., 109 (1980) 109.
10 Y. Hayashi, K. Zaitsu and Y. Ohkura, Anal. Sci., 1 (1985) 65.
11 H. U. Bergmeyer, Methods of Enzymatic Analysis, 2nd edn., Academic Press, New York and London, 1974, pp. 426, 471, 490, 521, 518 and 685.
12 H. H. Weetall, in K. Mosbach (Ed.), Methods in Enzymology, Vol. XLIV, Academic Press, New York, 1976, p. 134.
13 R. Tawa, M. Kitoh, S. Hirose and K. Adachi, Chem. Pharm. Bull., 30 (1982) 615.
14 P. Slowiaczek and M. H. N. Tattersall, Anal. Biochem., 125 (1982) 6.
15 J. Ontyd and J. Schrader, J. Chromatogr., 307 (1984) 404.
16 J. Schrader, R. M. Berne and R. Rubio, Am. J. Physiol., 223 (1972) 159.
17 C. A. Koller, P. L. Stetson, L. D. Nichamin and B. S. Mitchell, Biochem. Med., 24 (1980) 179.

Analytica Chimica Acta, 186 (1986) 139—146
Elsevier Science Publishers B.V., Amsterdam — Printed in The Netherlands

FLOW-INJECTION CONFIGURATIONS FOR CHROMIUM SPECIATION WITH A SINGLE SPECTROPHOTOMETRIC DETECTOR

J. RUZ, A. RÍOS, M. D. LUQUE DE CASTRO and M. VALCÁRCEL*

Department of Analytical Chemistry, Faculty of Sciences, University of Córdoba, Córdoba (Spain)

(Received 20th December 1985)

SUMMARY

The simultaneous or sequential determination of chromium(VI) and total chromium in water by flow injection analysis, using different configurations with a double- or single-beam spectrophotometer as detector, is investigated. The method is based on reaction between chromium(VI) and 1,5-diphenylcarbazide. Chromium(III) and (VI) are distinguished by using two carrier streams, one of which contains cerium(IV) to oxidize chromium(III) to chromium(VI). The determination range is 0.2—10.0 μg Cr ml^{-1}; the r.s.d. is 0.8% for 1 μg Cr. The sampling frequency is 40 h^{-1}. A wide study of interferences is reported.

Flow injection analysis (f.i.a.) has not been widely used to distinguish different chemical forms of the same element, except for the determination of nitrite and nitrate in admixtures. The resolution of chromium(III)/(VI), iron(II)/(III) and arsenic(III)/(V) mixtures has been achieved by f.i.a.; each chemical form has been quantified separately [1] or both states have been measured simultaneously by using two optical detectors in series [2, 3], for determinations of chromium and iron, or in parallel [4, 5] for determinations of iron and arsenic, or with a single detector [6] for determination of iron. The speciation of chromium can be based on the reaction between chromium(VI) and 1,5-diphenylcarbazide (DPC) [7] in which chromium(III) does not interfere. Oxidation of chromium(III) allows the determination of the total chromium concentration. The use of detectors in series for the simultaneous determination of chromium(III) and chromium(VI) [2] involves the spectrophotometric determination of chromium(VI) with DPC and subsequent determination of the total chromium concentration by atomic absorption spectrometry. Jorgensen and Regitano [8] used the DPC reaction for the determination of chromium(VI) in natural waters and soil extracts by f.i.a. Andrade et al. [9] studied the oxidation of chromium(III) to chromium(VI) by f.i.a. in order to apply continuous flow systems to the study of chromium speciation.

In the present paper, DPC is used for the simultaneous and sequential spectrophotometric determination of chromium(VI) and total chromium. Different configurations, with one or two flow cells and spectrophotometric

0003-2670/86/$03.50

detection with a single- or double-beam spectrophotometer, are studied in order to establish the most effective configuration.

EXPERIMENTAL

Aqueous stock solutions of ammonium cerium(IV) nitrate (0.5 g Ce(IV) l^{-1}), chromium(III) chloride (100 μg Cr(III) ml^{-1}), potassium dichromate (100 μg Cr(VI) ml^{-1}) and sulfuric acid were used. 1,5-Diphenylcarbazide solution was prepared by dissolving 0.425 g of the compound in 100 ml of ethanol and diluting up 250 ml with water.

A Perkin-Elmer 575 double-beam and a Pye-Unicam SP6-500 single-beam spectrophotometer, equipped with Hellma 178.12-QS flow cells (inner volume 18 μl) were used. Gilson Minipuls-2 and Ismatec S-840 peristaltic pumps, a Tecator L-100-1 injection valve, a Rheodyne 5301 six-way valve and Tecator TM-III chemifold were also used.

Figure 1 shows the different manifolds investigated for this study of chromium speciation. These manifolds are compared below.

RESULTS AND DISCUSSION

Detection with a double-beam spectrophotometer and flow cells in series

In this configuration (Fig. 1A), the simplest investigated, the signal provided by cell 1 is related to the concentration of chromium(VI) in the sample. After the solution has passed through this cell, the oxidant, cerium(IV), is introduced to oxidize chromium(III) in reactor L_2, so that the signal provided by cell 2 is related to the total chromium concentration. However, in the presence of an excess of DPC, chromium(III) is not oxidized, and therefore this manifold cannot be used for total chromium determination.

Detection with a single- or double-beam spectrophotometer with splitting of the injected sample

In this manifold (Fig. 1B), the sample is injected into a sulfuric acid stream and at point A it is split into two streams which travel along different channels. Channel 1 merges with a DPC stream so that chromium(VI) is determined. Channel 2 first merges with a stream of cerium(IV) which oxidizes chromium(III) in reactor L_2, and then merges with another DPC stream, so that the total chromium concentration is measured.

As is shown in Fig. 2, two peaks per injected sample are obtained, their exact form depending on the detector arrangement used. When a double-beam spectrophotometer is used with one flow cell for each channel (Fig. 1B, b1), two peaks are obtained, one of which is inverted (Fig. 2a). If a single-beam spectrophotometer is used, there are two possibilities. If two cells (one in each channel) are aligned in the same optical path, double positive peaks are obtained (Fig. 2b). If there is a single cell, and a confluence of channels 1 and 2 before the cell, double peaks are again obtained (Fig. 2c).

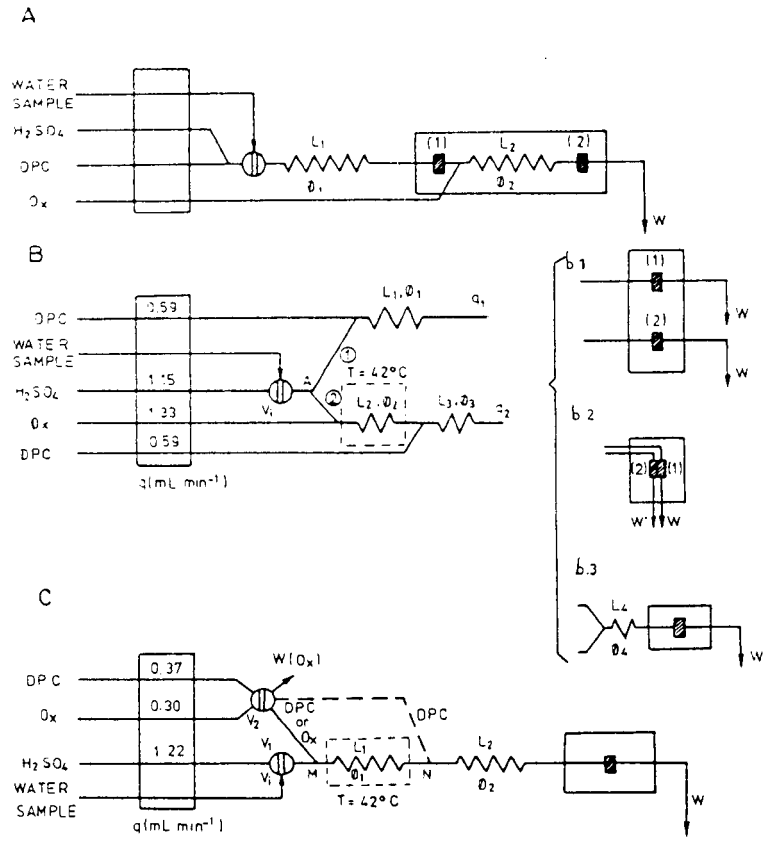

Fig. 1. Manifolds examined for chromium speciation. (A) Flow cells in series in a double-beam spectrophotometer. (B) Splitting sample into two channels with: (b1) two flow cells in parallel in a double-beam spectrophotometer; (b2) two cells in the same optical path of a single-beam spectrophotometer; (b3) stream recombination before reaching a single flow cell in a single-beam spectrophotometer. (C) A diverting valve (V_2) used for selecting the required reagent; the DPC stream represented by --- is intermittent, depending on the position of V_2.

Optimization of the flow-injection variables. Optimization was studied by the univariate method in all cases. Reproducible splitting of the sample was achieved by modifying the flow rates in channel 1, q_1, and channel 2, q_2, which in turn were a function of the lengths (L) and inner diameters (ϕ) of the reactors. The simple expression found previously [10]: $V_1/V_2 = q_1/q_2 = (L_2/L_1)/(\phi_1/\phi_2)^4$ (V_1 and V_2 being the volumes of the split sample in channels 1 and 2, respectively) is inadequate in this case, owing to the additional merging of the oxidant stream with channel 2. The optimum lengths and diameters of the reactor (for greatest peak height) were found to be: L_1 = 70 cm; ϕ_1 = 0.5 mm; L_2 = 300 cm; L_3 = 225 cm; $\phi_2 = \phi_3 = \phi_4$ = 0.7 mm. The effect of different channel lengths is shown in Fig. 3A.

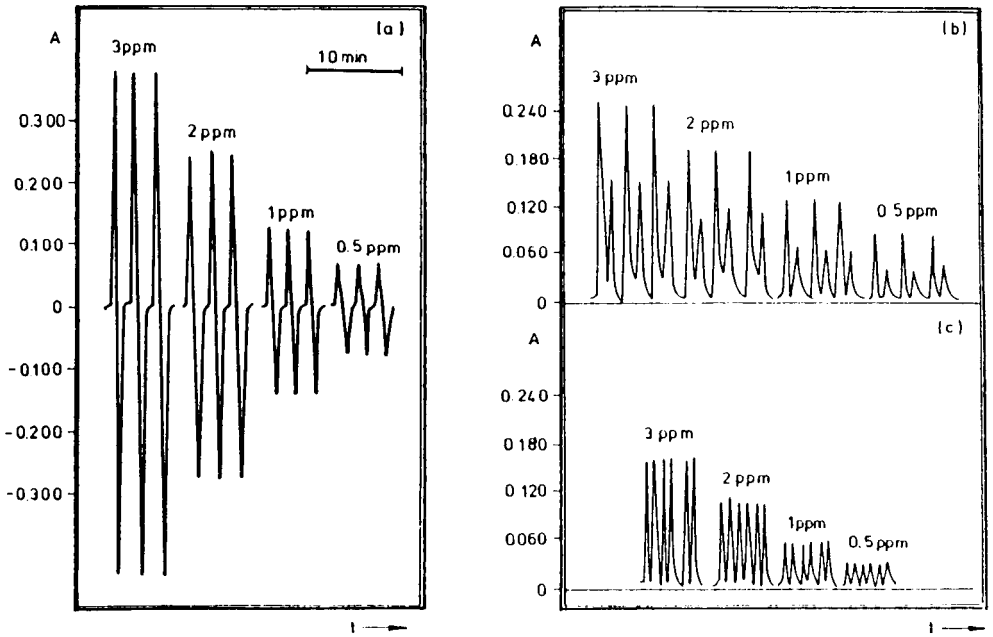

Fig. 2. Calibration peaks for chromium(VI) obtained with the different configurations: (a) B, b1; (b) B, b2; (c) B, b3.

The flow rate, q_1, should not exceed 1.7 ml min^{-1} and q_2 should not be smaller than 1.9 ml min^{-1} in order to split the sample; the optimum values were 1.5 and 2.3 ml min^{-1}, respectively (Fig. 3B). This is the flow ratio at which the straight lines in Fig. 3B coincide. An increase in the injected volume, V_i, increases the signal in both cells, but very large volumes (>300 μl), in addition to diminishing the sampling frequency, yield pairs of double peaks, because of incomplete reagent diffusion into the sample zone. The optimum sample volume is 207 μl.

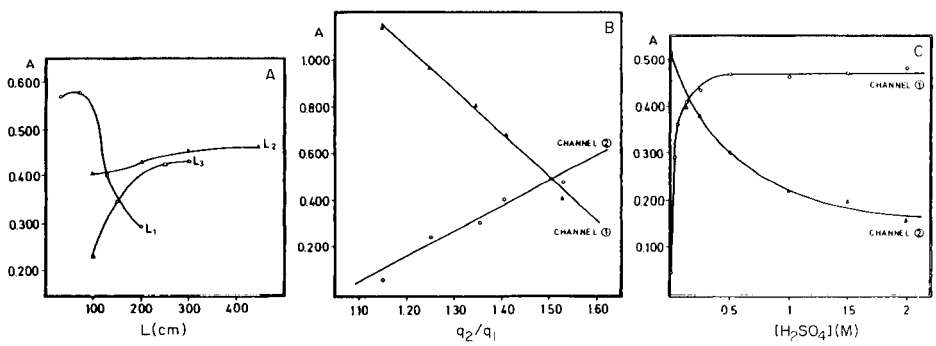

Fig. 3. Influence of different features on the relevant peak-height absorbances: (A) channel length; (B) flow rate ratio; (C) sulfuric acid concentration.

Optimization of physicochemical variables. An increase in temperature does not favour the reaction between chromium(VI) and DPC. Hence, reactors L_1, L_2 and L_4 were kept at room temperature (ca. 20°C), whilst reactor L_3 was maintained at 42°C to favour the oxidation of chromium(III). Higher temperatures caused bubble formation in the system.

The concentration of DPC ensuring complete dissolution of the reagent is 0.17% (w/v) in 40% (v/v) ethanol. An increase in the concentration of cerium(IV) dissolved in 0.15 M nitric acid increases the extent of oxidation of chromium(III), maximum signals being obtained at 0.5 g Ce l^{-1}. The concentration of sulfuric acid has a significant but different influence on the signals from each channel. Figure 3C shows that the variation of the peak-height absorbance with acid concentration is exponential in both cases. In channel 1, the signal increases with increasing concentration of sulfuric acid, which favours the progress of the indicator reaction. In channel 2, the signal decreases as the acidity increases probably because the oxidation of chromium(III) is affected by the formation of kinetically inert chromium(III)/sulphate complexes [11]. The optimum sulfuric acid concentration is considered to be 0.20 M.

Simultaneous determination of chromium(III) and chromium(VI). With any of the three possible configurations, it is necessary to obtain three calibration graphs, two for chromium(VI) (one for each peak) and one for chromium(III). In all configurations, the first peak yields the concentration of chromium(VI) originally in the sample, and the second corresponds to the total chromium concentration. The chromium(III) concentration is obtained by difference. Figure 2 shows the peaks obtained for standards used for calibration, whilst Table 1 summarizes the calibration equations and analytical parameters for each configuration.

Detection by a single-beam spectrophotometer with a diverting valve

Another manifold was also investigated (Fig. 1C). It consists of a main channel with sulfuric acid as carrier into which the sample is injected through valve V_1. Valve V_2, like V_1, is a six-way injection valve, but is used for channel selection. It allows the selected stream (DPC or oxidant) to reach point M. Initially, the oxidant stream is fed to waste by the valve whilst DPC flows to M, so that the indicator reaction can take place in reactors L_1 and L_2. Chromium(VI) is detected in this way when valve V_2 is reset so that oxidant reaches M, and the DPC stream is diverted to merge at point N whilst oxidation of chromium(III) occurs in reactor L_1. The indicator reaction takes place in L_2, and total chromium is detected. A similar use of this valve was described earlier for the simultaneous determination of pollutants in wastewaters [13].

The optimum concentrations of DPC, oxidant and sulfuric acid were the same as for the above configuration, with reactor L_1 again kept at 42°C. The optimum values of the manifold variables were: L_1 = 300 cm; L_2 = 150 cm; sulfuric acid flow rate = 1.2 ml min^{-1}; DPC flow rate = 0.4 ml min^{-1}; oxidant flow rate = 0.3 ml min^{-1}; V_i = 300 μl.

TABLE 1

Calibration parameters for chromium speciation

Manifold	Species	Channel	Calibration equation[a]	I[b]	Calibration range (μg ml^{-1})	RSD[c] (%)
1B, b1	Cr(III)	2	$A = 0.149[Cr] + 0.009$	0.998	0.2—4	0.48(1.5)
	Cr(VI)	1	$A = 0.120[Cr] + 0.010$	0.999	0.2—8	0.38(1.5)
	Cr(VI)	2	$A = 0.140[Cr] + 0.010$	0.999	0.2—8	0.38(1.5)
1B, b2	Cr(III)	2	$A = 0.040[Cr] + 0.010$	0.998	0.5—7	0.63(3.0)
	Cr(VI)	1	$A = 0.076[Cr] + 0.031$	0.995	0.5—7	0.82(3.0)
	Cr(VI)	2	$A = 0.034[Cr] + 0.033$	0.993	0.5—7	0.82(3.0)
1B, b3	Cr(III)	2	$A = 0.049[Cr] + 0.006$	0.999	0.5—11	0.30(3.0)
	Cr(VI)	1	$A = 0.054[Cr] + 0.009$	0.999	0.5—10	0.61(3.0)
	Cr(VI)	2	$A = 0.049[Cr] + 0.010$	0.999	0.5—10	0.61(3.0)
1C	Cr(III)	2	$A = 0.261[Cr] + 0.033$	0.997	0.2—2	0.21(1.0)
	Cr(VI)	1	$A = 0.352[Cr] + 0.050$	0.999	0.2—3	0.27(1.0)
	Cr(VI)	2	$A = 0.259[Cr] + 0.034$	0.999	0.2—3	0.27(1.0)

[a]Absorbance measured as peak height; [Cr] in μg ml^{-1}; 8 points. [b]Regression coefficient. [c]Relative standard deviation for triplicate injection of eleven samples at the concentration given in parentheses.

As with the above configurations, three calibration graphs are necessary for simultaneous determination of chromium(III) and chromium(VI), two for chromium(VI) (one for each position of valve V_2) and one for chromium(III). Depending on the position of valve V_2, the peak absorbance is related to the chromium(VI) or total chromium concentration in the samples. The calibration data are included in Table 1.

Comparison of procedures

A study of interferences in each procedure was made. The species tested were those commonly found in different types of waters. The maximum tolerated ratios are shown in Table 2. The determination of chromium(III) suffers from more interferences because of the inclusion of the oxidation step. Configuration Fig. 1C permits a more selective determination of both species because the sample and oxidant are not split during the determination of chromium(VI). In general, the most serious interferences are sulfide and mercury(II) ion. Nitrite, EDTA, copper(II) and manganese(II) affect only the determination of chromium(III).

The three configurations which split the sample yield similar results, but double-beam detection (Fig. 1B, b1) gives the most reproducible results. The other two configurations have the advantage that a single-beam spectrophotometer can be used for the simultaneous determination. Configuration Fig. 1C is the simplest for speciation with this chemical system. It needs no splitting of the sample (which sometimes causes problems, and increases the detection limit), and only one flow cell and one single-beam spectrophoto-

TABLE 2

Maximum tolerable weight ratios for interferences in the proposed methods for chromium speciation

Species	Tolerable ratio to chromium	Added species	
		Manifold 1B[a]	Manifold 1C[b]
Cr(III)	100[c]	PO_4^{3-}	Mg^{2+}, Zn^{2+}, Cd^{2+}, Pb^{2+}, Al^{3+}
	50	Mg^{2+}, Pb^{2+}, Fe^{3+}, Al^{3+}, Zn^{2+}, Cd^{2+}	CO_3^{2-}, Fe^{3+}
	10	NO_2^-, Mn^{2+}	PO_4^{3-}, EDTA, Hg^{2+}, Cu^{2+}
	1	CO_3^{2-}, EDTA, Cu^{2+}, Hg^{2+}	NO_2^-, S^{2-}, Mn^{2+}
	<1	S^{2-}	
Cr(VI)	100[c]	NO_2^-, CO_3^{2-}, PO_4^{3-}, EDTA, Mg^{2+}, Pb^{2+}, Al^{3+}, Cu^{2+}	NO_2^-, CO_3^{2-}, PO_4^{3-}, EDTA, Mg^{2+}, Zn^{2+}, Cd^{2+}, Pb^{2+}, Cu^{2+}
	50	Mn^{2+}, Zn^{2+}, Cd^{2+}, Fe^{3+}	Mn^{2+}, Al^{3+}
	10		Hg^{2+}, Fe^{3+}
	1	Hg^{2+}	S^{2-}
	<1	S^{2-}	

[a]For 3.0 μg ml^{-1} of chromium(III) and chromium(VI). [b]For 1.0 μg ml^{-1} of chromium(III) and chromium(VI). [c]100-Fold Cl^-, NO_3^-, SO_4^{2-}, Na^+, K^+, NH_4^+, Ca^{2+}, Ni^{2+}, Co^{2+} did not interfere in either procedure.

meter are required. This determination can be more accurately termed as sequential [14] rather than simultaneous, because two consecutive injections are necessary for the determination of the two species. The errors found for resolution of mixtures by this last configuration were the smallest, but were not significantly different from those obtained by use of the other configurations.

Conclusions

The most important advantages of flow-injection methodology in speciation studies are its simplicity, rapidity and versatility. Compared with the methods previously described for chromium speciation, the above procedures offer greater simplicity in the flow configurations. Systematic optimization of the variables led to higher sensitivity than in previous reports.

This work was supported by the CAICyT under Grant No. 2012-83.

REFERENCES

1 B. P. Bubnis, M. R. Straka and G. E. Pacey, Talanta, 30 (1983) 841.
2 T. P. Lynch, N. J. Kernoghan and J. N. Wilson, Analyst, 109 (1984) 839.
3 J. L. Burguera and M. Burguera, Anal. Chim. Acta, 161 (1984) 375.
4 T. P. Lynch, N. J. Kernoghan and J. N. Wilson, Analyst, 109 (1984) 843.
5 P. Linares, M. D. Luque de Castro and M. Valcárcel, Anal. Chem., 57 (1985) 2101.
6 A. T. Faizullah and A. Townshend, Anal. Chim. Acta, 169 (1985) 225.

7 American Public Health Association, American Water Works Association and Water Pollution Control Federation, Standard Methods for the Examination of Water and Wastewater, 4th edn., New York, 1975, p. 192.
8 S. S. Jorgensen and M. A. B. Regitano, Analyst, 105 (1980) 292.
9 J. C. Andrade, J. C. Rocha and N. Baccan, Analyst, 109 (1984) 645.
10 A. Fernández, M. A. Gómez-Nieto, M. D. Luque de Castro and M. Valcárcel, Anal. Chim. Acta, 165 (1984) 217.
11 N. Fogel, J. M. Tai and J. Yarborough, J. Am. Chem. Soc., 93 (1962) 1145.
12 J. Y. Tong and E. L. King, J. Am. Chem. Soc., 82 (1960) 3805.
13 A. Ríos, M. D. Luque de Castro and M. Valcárcel, Analyst, 110 (1985) 277.
14 M. D. Luque de Castro and M. Valcárcel, Analyst, 109 (1984) 413.

Analytica Chimica Acta, 186 (1986) 147—153
Elsevier Science Publishers B.V., Amsterdam — Printed in The Netherlands

DETERMINATION OF BISMUTH IN RIVER SEDIMENT BY ELECTROTHERMAL ATOMIC ABSORPTION SPECTROMETRY WITH LOW-TEMPERATURE ATOMIZATION IN ARGON/HYDROGEN

NI ZHE-MING*, LE XIAO-CHUN and HAN HENG-BIN
Institute of Environmental Chemistry, Academia Sinica, P.O. Box 934, Beijing (China)
(Received 29th January 1986)

SUMMARY

A method is described for the direct determination of bismuth (1—5 $\mu g\ g^{-1}$) in river sediments by graphite-furnace atomic absorption spectrometry in 90% argon/10% hydrogen with low-temperature atomization. The presence of 10% hydrogen in the argon sheath gas promotes atomization; the bismuth absorption reaches a maximum at 850—950°C, which allows better discrimination of the atomic signal from the background absorption. The use of trisodium phosphate as the matrix modifier further decreases the interference effects from the matrix components and increases the sensitivity. The results, obtained by direct calibration with aqueous standards, are in good agreement with certified values.

The use of bismuth salts in pharmaceutical preparations and the recent interest in the development and production of superalloys of bismuth and other elements with low melting points has emphasized the need for sensitive and accurate procedures for determinations of bismuth. Atomic absorption spectrometry (a.a.s.) has been used to determine bismuth in a variety of samples. Bismuth in copper has been quantified by a.a.s. with introduction of solid samples into an induction furnace [1]. Methods have been described for the determination of bismuth in environmental and biological samples such as waters, shells, marine sediments, atmospheric particulate matter, blood and urine by electrothermal a.a.s. with hydride generation [2—4].

Electrothermal a.a.s. appears to provide a convenient, rapid and sensitive method for the determination of trace bismuth in metals and alloys [5—7] as well as environmental and biological samples [8—10]. However, the volatility of bismuth often caused the metal to be lost from the graphite furnace if the charring temperature exceeded 500°C. To minimize such loss, nickel [11] or palladium [10] has been added as a thermal stabilizer in the graphite furnace prior to atomization. A much higher temperature of 1200°C could be tolerated during the charring stage in the presence of these matrix modifiers and matrix components could be removed before bismuth atomization. For the determination of volatile elements in high salt-containing materials, the use of low-temperature atomization along with matrix modifica-

0003-2670/86/$03.50

tion has been explored as a means of decreasing matrix effects [12]. Guevremont et al. [13] reported that the addition of EDTA decreased the temperature required for atomization of cadmium to far below that required to volatilize the other components of sea water, thus allowing cadmium to be determined directly by injection into the furnace. The addition of hydrogen to the argon purge gas also promoted reduction and atomization and yielded up to 100% signal enhancement for lead in soils [14]. The use of argon/hydrogen allowed lead atomization at 950°C and minimized the depressive effect of chloride on lead.

This paper describes the use of 90% argon/10% hydrogen as purge gas for the direct determination of bismuth in river sediments. In the presence of hydrogen and with the use of the maximum power heating mode of the furnace, bismuth absorbance reached a maximum plateau at 850—950°C. In this temperature range, the bulk of the inorganic salt matrix was not vaporized and the analytical signal was free from intense background absorption. In an attempt further to decrease effects of the matrix and non-specific background, the use of trisodium phosphate as matrix modifier was investigated. The results obtained for bismuth in river sediments compare favorably with the certified values.

EXPERIMENTAL

Apparatus

A Perkin-Elmer 4000 atomic absorption spectrometer operated in the automatic background mode and fitted with a HGA-400 electrothermal atomizer and a Perkin-Elmer 056 chart recorder was used. A bismuth hollow-cathode lamp (Shanghai Electro-optic Instrument Works) was operated at 8 mA. The spectral bandwidth was set at 0.7 nm. Peak-height absorbances were measured at 306.8 nm. The internal purge gas was supplied in the interrupt mode and with maximum power heating during the atomization cycle. The graphite tube was purged by argon, or 10% hydrogen in argon, at an inner flow rate of 50 ml min^{-1} during drying and charring. An Eppendorf pipette fitted with disposable polypropylene tips was used to introduce the sample solution into the graphite furnace.

Reagents

All reagents used were analytical-reagent grade. A stock solution of bismuth (1000 mg l^{-1}) was prepared by dissolving 0.1000 g of bismuth powder (99.999% purity; Koch-Light Laboratories, Colnbrook, England) in 10 ml of (1 + 1) nitric acid and diluting to volume in a 100-ml volumetric flask with demineralized water. Standard solutions were prepared by serial dilution of the above stock solution with 0.01 M nitric acid before use. Sodium phosphate solutions (0.24 M) were prepared by dissolving a suitable quantity of trisodium phosphate dodecahydrate, sodium monohydrogenphosphate or sodium dihydrogenphosphate in demineralized water.

Procedures

Sample decomposition. Accurately weigh 200 mg of river sediment into a 30-ml teflon crucible (from a pressure decomposition vessel), moisten the sample thoroughly with 0.5 ml of 0.01 M nitric acid, and add 1.5 ml each of 72% perchloric acid, concentrated nitric acid and concentrated (35%) hydrofluoric acid. Follow the procedure reported previously [15]. Dissolve the final contents of the pressure vessel by adding 2 ml of 1 M nitric acid and gently heating for a few minutes. Transfer the solution to a 25-ml volumetric flask and dilute to volume with 0.01 M nitric acid.

Bismuth determination. Inject sample solution (10 or 20 μl) and 10 μl of 0.24 M trisodium phosphate into the same location in the furnace, and use the following program: dry at 100°C for 30 s, char at 400°C for 40 s, atomize at 900°C and 1000°C each for 6 s in 90% argon/10% hydrogen and 100% argon, respectively. Evaluate the absorbance from the peak height. Finally, use a burn-out temperature of 2600°C between samples.

RESULTS AND DISCUSSION

Effect of hydrogen on the atomization and char temperatures for bismuth

A previous study showed that the addition of hydrogen to the argon purge gas decreased the atomization temperatures of lead [14]. Cadmium has been found to behave similarly, and these elements in environmental and biological samples can be determined accurately by low-temperature atomization. The effect of hydrogen was the same for bismuth. Addition of 10% hydrogen to argon enhanced the bismuth sensitivity by 20%, but a further increase in the

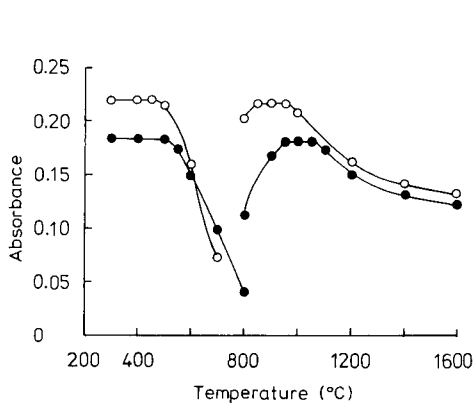

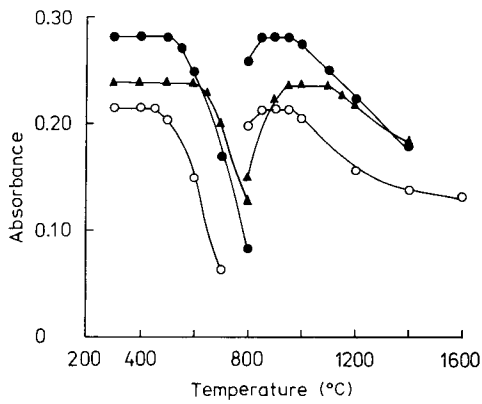

Fig. 1. Decomposition and atomization curves for bismuth (10 μl of 150 ng ml^{-1} solution): (•) in argon; (○) in 90% argon/10% hydrogen.

Fig. 2. Effect of phosphate on the decomposition and atomization curves for bismuth (10 μl of 150 ng ml^{-1} solution) in 90% argon/10% hydrogen: (○) bismuth alone; (•) bismuth with 10 μl of 0.24 M trisodium phosphate; (▲) bismuth with 10 μl of 0.24 M sodium dihydrogenphosphate.

proportion of hydrogen had no apparent effect on the signal. Comparison of bismuth atomization in argon to that in 90% argon/10% hydrogen (Fig. 1) demonstrated that hydrogen promoted the atomization of bismuth and shifted the atomization temperature to lower values. With argon as purge gas, bismuth absorbance reached a maximum at 950– 1050°C, while in 90% argon/10% hydrogen, atomization occurred between 850 and 950°C. The lower atomization temperature is advantageous because it allows better resolution of the atomic signal from the background absorption. In both argon and argon/hydrogen, the atomic absorbance of bismuth decreased with further increase in atomization temperature. The effect is probably due to the accelerated diffusional loss of atomic vapor at high temperatures.

The maximum tolerable charring temperature for bismuth in argon was 500°C when the optimum atomization temperature was maintained at 1000°C. When the argon/hydrogen mixture was used, bismuth was lost at charring temperatures above 450°C. A temperature of 400°C was chosen for charring in 90% argon/10% hydrogen.

Removal of interferences by trisodium phosphate

Preliminary experiments showed that the addition of sodium phosphate decreased the depressive effects of sample matrix on the bismuth determination. Unlike disodium hydrogenphosphate or sodium dihydrogenphosphate, both of which retard bismuth atomization and result in a higher atomization temperature, trisodium phosphate had no apparent effect on the optimum temperature range for bismuth atomization, as shown in Fig. 2. This behavior is advantageous for low-temperature atomization. Also, a great increase in bismuth sensitivity was obtained by addition of trisodium phosphate (see below). Therefore, sodium phosphate was used as a matrix modifier for the determination of bismuth. An atomization temperature of 900°C was used throughout.

To establish the amount of sodium phosphate needed for satisfactory performance, the concentration added was varied from 0.006 to 0.36 M. Bismuth sensitivity increased with increase in the trisodium phosphate concentration up to 0.06 M, which gave an absorption enhancement of 35%. For the analysis of river sediments, 10 μl of 0.24 M trisodium phosphate was added, along with 10 μl or 20 μl of sample solution, to the graphite furnace for each determination.

It has been reported that other sample components often greatly decrease the atomic absorbance of bismuth [16, 17]. This was confirmed in the present study. The chloride and perchlorate remaining after the charring-stage depressed the bismuth signal significantly. However, with addition of trisodium phosphate, the recovery of bismuth in the presence of different salts increased to $>90\%$. The data are summarized in Table 1.

Figure 3 shows the effect of sodium phosphate on the absorbance/time profile for bismuth and the background, during the analysis of a river sediment. In argon (curve a), the atomization peak was broad and absorbance

TABLE 1

Influence of added salts on the relative absorbance of bismuth

Matrix	Amount added (μg)	Relative absorbance[a]			
		Ar	Ar/H_2[b]	Ar + Na_3PO_4	Ar/H_2[b] + Na_3PO_4
—	0	1.00	1.00	1.00	1.00
$NaClO_4$	100	0.43	0.74	0.90	1.00
NaCl	100	0.81	0.94	0.90	1.00
$MgCl_2$	20	0.15	0.56	0.98	1.00
$CaCl_2$	10	0.60	0.69	0.82	0.94
$AlCl_3$	50	0.46	0.90	1.00	1.00
$CuCl_2$	1	0.56	0.40	0.95	0.95
$FeCl_3$	2	0.50	0.45	0.92	0.94
Na_2SiO_3	50	0.82	0.81	0.92	1.00

[a]For 10 μl of 150 ng ml^{-1} bismuth. [b]90% Ar/10% H_2.

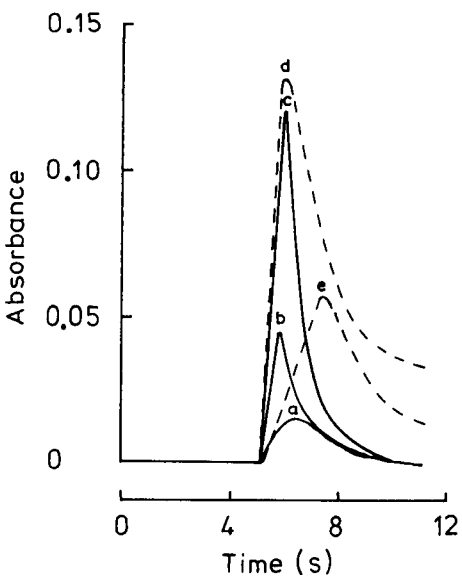

Fig. 3. Effect of trisodium phosphate on the atomic absorbance of bismuth and background absorption from river sediment: (a) Bi in Ar; (b) Bi in Ar/H_2; (c) Bi in Ar/H_2 with 10 μl of 0.24 M trisodium phosphate; (d) background absorption in Ar/H_2; (e) background absorption in Ar/H_2 with 10 μl of 0.24 M trisodium phosphate.

was small, indicating the depressive effect of the matrix on bismuth atomization. In argon/hydrogen (curve b), the matrix effect was decreased and the atomization peak became sharper. The addition of trisodium phosphate (curve c) further minimized the matrix effect and enhanced the sensitivity

greatly. Furthermore, the modifier delayed the appearance of the background absorption (curves d and e), so that a better discrimination between the bismuth peak and background scattering was obtained. This effect can probably be ascribed to the conversion of volatile matrix components to less volatile phosphates.

In order to examine the applicability of the proposed method to real samples, a recovery study was undertaken. Additions of bismuth were made to river sediment samples, which were processed by the method described above. The recovery was estimated by reference to the calibration graph constructed for aqueous bismuth standards. The results are presented in Table 2; the recoveries of 97—105% indicated that there was no matrix interference when trisodium phosphate was used as matrix modifier and argon/hydrogen as purge gas, but recoveries of <72% were obtained when pure argon was used as the sheath gas.

TABLE 2

Recovery of bismuth added to river sediments[a]

Sediment sample	Bi in sample (μg)	Bi added (μg)	Bi recovery (%)			
			Ar	Ar/H_2	Ar + Na_3PO_4	Ar/H_2 + Na_3PO_4
GSD-6	1.04	0				
		0.50	27	60	70	105
		1.0	28	67	67	100
		1.5	25	60	72	97
GSD-5	0.50	0				
		0.25	23	50	60	103
		0.50	17	42	67	100
		0.75	11	44	56	102

[a]The sample weight was 200 mg.

TABLE 3

Results for the determination of bismuth in river sediments

River sediment[a]	Bi content (μg g^{-1})[b]		
	Direct calibration	Standard addition	Certified value
GSD-2	1.6	1.6	1.6 ± 0.1
GSD-5	2.3	2.4	2.4 ± 0.2
GSD-6	5.2	5.2	5.0 ± 0.4

[a]The standard river sediments were obtained from Academia of Geological Sciences, Beijing. [b]Mean of three determinations.

Determination of bismuth in river sediments

Given these quantitative recoveries, the recommended method was applied to the direct determination of bismuth in river sediments. The results obtained by the standard addition method and by direct calibration with aqueous standards are compared with the certified values in Table 3. No difference was found in the results obtained by the two methods, and the satisfactory agreement with the certified values indicates that the method is accurate and reliable. The relative standard deviation was 3.5% for seven replicate determinations of 2.4 $\mu g\ g^{-1}$ bismuth in a river sediment.

The described method can be used for the direct determination of bismuth in river sediments without preliminary separation or preconcentration.

REFERENCES

1 A. A. Baker and J. B. Headridge, Anal. Chim. Acta, 125 (1981) 93.
2 D. S. Lee, Anal. Chem., 54 (1982) 1682.
3 K. De Doncker, R. Dumarey, R. Dams and J. Hoste, Anal. Chim. Acta, 161 (1984) 365.
4 R. C. Rooney, Analyst, 101 (1976) 749.
5 R. M. Hamner, D. L. Lechak and P. Greenberg, At. Absorpt. Newsl., 15 (1976) 122.
6 G. G. Welcher, O. H. Kriege and J. Y. Marks, Anal. Chem., 46 (1974) 1227.
7 J. E. Forrester, V. Lehecka, J. Johnston and W. L. Ott, At. Absorpt. Newsl., 18 (1979) 73.
8 R. Djudzman, E. Van den Eeckhout and P. De Moerloose, Analyst, 102 (1977) 688.
9 R. L. Bertholf and B. W. Renoe, Anal. Chim. Acta, 139 (1982) 287.
10 Jin Long-zhu and Ni. Zhe-ming, Can. J. Spectrosc., 26 (1981) 219.
11 E. S. Gladney, At. Absorpt. Newsl., 16 (1977) 114.
12 G. D. Carmack and M. A. Evenson, Anal. Chem., 51 (1979) 907.
13 R. Guevremont, R. E. Sturgeon and S. S. Berman, Anal. Chim. Acta, 115 (1980) 163.
14 Ni Zhe-ming, Han Heng-bin and Le Xiao-chun, J. Anal. At. Spectrom., 1 (1986) 131.
15 Shan Xiao-quan, Ni Zhe-ming and Zhang Li, At. Spectrosc., 5 (1984) 1.
16 T. Shimizu, Y. Kawamata, Y. Kimura, Y. Shijo and K. Kakai, Bunseki Kagaku, 31 (1982) 299.
17 K. Matsusaki, T. Yoshino and Y. Yamamoto, Anal. Chim. Acta, 167 (1985) 299.

Analytica Chimica Acta, 186 (1986) 155—162
Elsevier Science Publishers B.V., Amsterdam — Printed in The Netherlands

SPECTRAL INTERFERENCES AND BACKGROUND OVERCOMPENSATION IN INVERSE ZEEMAN-CORRECTED ATOMIC ABSORPTION SPECTROMETRY
Part 3. A Study of Eighteen Cases of Spectral Interference

G. WIBETOE and F. J. LANGMYHR*

Department of Chemistry, University of Oslo, P.O. Box 1033, Blindern, 0315 Oslo 3 (Norway)

(Received 18th February 1986)

SUMMARY

Atomic line tables were surveyed in order to select pairs of elements which have contiguous lines and so are likely to suffer from spectral interference. Spectrometric measurements of these element pairs revealed eighteen cases of spectral interference. Four of these cases occurred at the recommended wavelengths for the analyte: the 459.4-nm europium line (interference from vanadium and cesium), the 247.6-nm palladium line (interference from lead) and the 265.9-nm platinum line (interference from europium).

In conventional atomic absorption spectrometry (a.a.s.), spectral interferences caused by direct overlap of foreign atomic lines does not normally present any serious problems. However, the Zeeman splitting of the absorption lines into π- and σ-components increases the probability of encountering spectral interference.

In the two previous papers [1, 2] in this series, cases were reported of spectral interference which caused overcompensation in inverse Zeeman-corrected a.a.s. In these studies of thirty analyte elements and four matrix elements (cobalt, iron, manganese and nickel), five cases of overcompensation were revealed, all resulting from the presence of matrix element lines 0.004—0.007 nm apart from the analyte lines. In the present investigation, tables of atomic lines were surveyed first and then analyte/matrix element pairs which had lines about 0.01 nm apart or closer were examined in detail.

EXPERIMENTAL

Instruments, apparatus, reagents and solutions

The a.a.s. measurements were made with a Perkin-Elmer (P-E) model 5000/inverse Zeeman instrument and a P-E HGA-400 graphite furnace. Time-resolved absorbance data were collected and displayed with the P-E Data System 10 and the P-E 660 Printer/Plotter.

The graphite tubes were of the standard or pyrolytically-coated type; the

0003-2670/86/$03.50

atomization cells were purged with argon (>99.9% by volume). Solutions were transferred to the furnace from plastic micropipettes. The hollow-cathode lamps and electrodeless-discharge lamps were all delivered by Perkin-Elmer.

Stock solutions (10 or 1 mg ml^{-1}) of antimony, chromium(III), gold, mercury, platinum, titanium, tungsten and zirconium were of Spectrosol quality (BDH Chemicals); those of beryllium and cobalt were of Titrisol quality (Merck). Standard solutions of cesium, potassium, magnesium, rhodium, rubidium, scandium and strontium were prepared by dissolving the reagent-grade chlorides in water or a minimum amount of the appropriate acid. Barium, calcium, lithium and sodium stock solutions were prepared from reagent-grade carbonates with addition of acid, as required. The arsenic, europium and lanthanum standard solutions were prepared from the pure oxides; the silicon solution was prepared by decomposing the pure oxide with sodium carbonate. Stock solutions of the other elements were prepared from high-purity metals dissolved in minimum volumes of the appropriate acids (Suprapur, Merck).

Measurements

For the present investigation a selection of 33 electrodeless-discharge and hollow-cathode lamps was available. For the corresponding analytes, the Perkin-Elmer instrument manual was used to compile a list of all recommended wavelengths which provided a relative sensitivity of about 10 or less. Atomic line tables [3, 4] were then surveyed to find other atomic lines situated about 0.01 nm or closer to any of the above-mentioned recommended lines. In some instances, gas-fill lines and other lines, which were assumed to be contained in the bandpass of the monochromator, were also checked for adjacent lines.

Table 1 lists the analytes studied, the wavelengths and slit widths used during the measurements, and the matrix elements having adjacent lines

TABLE 1

Analyte/matrix element combinations tested for spectral interference

[The elements underlined did not show spectral interference. Matrix elements causing background overcompensation are marked with (—). All the other elements gave a positive absorbance signal, and a spectral interference cannot be excluded. Matrix elements given in brackets have lines close to the analyte lines, but were not tested. Except where mentioned, hollow-cathode lamps were used. The general furnace parameters are given in Table 2. The superscripts on the upper left of the separate elements have the following meanings: a question mark indicates that the line may be atomic or ionic (status not given in the wavelength tables); asterisks show that a spectral interference is already known [6, 7]; ne means that the matrix line is close to a neon line.]

Analyte	Wavelength (nm)	Slit width (nm)	Matrix element[a] tested	Analyte	Wavelength (nm)	Slit width (nm)	Matrix element tested
Ag	328.1	0.7	?Eu	Pb	213.6	0.2	Zr
Al	309.3	0.7	?V	Pb	261.4	0.7	Co (—), ?Sn, ?Ta
	396.2	0.7	?Mo	Pd	247.6	0.2	Co, Fe, ?Pb (—), V

TABLE 1 (*continued*)

Analyte	Wavelength (nm)	Slit width (nm)	Matrix element tested
	308.2	0.7	?Mn, *V (—)
	237.3	0.2	Ba, Co
	257.5	0.2	Zn
As[b]	193.7	0.7	Pt
Au	242.8	0.7	Pt
	267.6	0.7	V, W
B	249.7	0.7	Co (—), V
Bi	223.1	0.2	In, Ti
	227.7	0.2	?Co (—), V
Cd[b]	228.8	0.7	*As
Co	242.5	0.2	Li, (Ir), V, Zr
	241.2	0.2	Ti, V
	252.1	0.2	*In
	243.6	0.2	Ge, (Ir), Pt (—)
Cr	357.9	0.7	?V
	359.4	0.7	Rh
	360.5	0.7	Co (—), Fe, Ti
	425.4	0.7	Co, neNa, Ni, V
	427.5	0.7	neTi, Zr
Cu	324.8	0.7	?Ag, *Eu, ?Mn
	327.4	0.7	(Ir), Ti
	216.5	0.2	Pt
Eu	459.4	0.2	neCs (—), V (—)
	462.7	0.2	neCr
	466.2	0.2	neBa, neCo, Fe
Fe	248.8	0.2	Pt, Ti
	302.1	0.2	Cr
	252.7	0.2	?Mn
	372.0	0.2	Ba
Ga	287.4	0.7	(Os), Ta, ?V
	294.4	0.7	Mo, (Re), ?V
	417.2	0.7	neFe, neV
Ge[b]	265.1	0.2	?Ta
	259.2	0.2	Cu, Ta
	269.1	0.2	Ga, ?Ta
Hg	253.6	0.7	Pt
In	303.9	0.7	Ca, W
	451.1	0.7	Pt, ?Sn, neV
Mn	279.8	0.2	(Ir), neZr
	280.1	0.2	Zn
	403.1	0.2	Sc, Zr
Mo	313.3	0.7	Ba, Ta, Ti, ?V
	379.8	0.7	Ti
	319.4	0.7	Ba, V
	390.3	0.7	Cr, Fe
Ni	232.0	0.2	?Cr, V
	231.1	0.2	Co, V
	352.5	0.2	?Mn, Zr
	341.5	0.2	Co (—)
	305.1	0.2	Co, V (—)
	346.2	0.2	Co
	351.5	0.2	Zn, neZr
	276.3	0.2	Zr
	340.5	0.2	La
Pt	265.9	0.7	?Au, ?Cs, ?Eu (—), Mo
	306.5	0.7	(Ir), Ni (—)
	283.0	0.2	?W
	293.0	0.7	Fe, (?Pd)
	273.4	0.2	Cd, ?Cr, Fe (—), (Ir) ?Ta, V
	270.2	0.2	neCu, Rh
	248.7	0.2	Fe
	271.9	0.2	*Fe, Tl
Sb[b]	206.8	0.2	?Ni, Pt
	231.2	0.2	V
Se[b]	204.0	0.7	(Pd), Sb, ?Te
Si	251.6	0.2	?Mo, (Re), V
	250.7	0.7	Co (—), *V (—)
	252.8	0.2	Sb
	252.4	0.2	?Ba, ?In, Ni
	221.7	0.2	?Ba, ?Mo
Sn[b]	224.6	0.2	?Mo
	270.6	0.7	Fe
	303.4	0.2	?Ag, Cr (—), ?Fe, (Ru)
	254.6	0.7	?Mn
	300.9	0.7	Ca (—)
Sr	460.7	0.7	Au, neNi
Te	214.3	0.2	?La
Ti	365.4	0.2	Au, ?Ca, ?Mo, ?Ta, ?W
	364.3	0.2	Ca, V
	320.0	0.2	Co, ?Ta, V
	363.6	0.2	Cr, Fe, (Ir), (Ru), V
	335.5	0.2	(Ir), Rh
	375.3	0.2	Fe, (Ir), Rh
	334.2	0.2	(Ce), Co, Cr, Fe, (Ir), La, Rh
	399.9	0.2	?Ta, V
	399.0	0.2	Co, Zr
Tl[b]	276.8	0.7	?Ag, ?Bi, neCu
	377.6	0.7	Fe, V, Rh
	238.0	0.2	?Bi, Ni
V	318.4	0.7	Ba, Ca, ?Cr, ?Mo, (Ru), ?Si, ?Ti, W
	306.0	0.2	Co, Fe, ?Mo, Rb, ?Ti
	306.6	0.2	Ca, Fe, Ge, Ni, Zr
	305.6	0.2	neFe
	390.2	0.2	(Ir), La
Zn	213.9	0.2	?As, *Cu

[a]Matrix element with atomic line close to an analyte or neon emission line. [b]Electrodeless discharge lamp used.

likely to cause spectral interference. These analyte/matrix element pairs were then examined experimentally to reveal cases of overcompensation.

For this purpose, 5 μl of a 0.1% (w/v) solution of the matrix element was

TABLE 2

General furnace parameters for studying the interfering effect of the elements listed in Table 1. The Zeeman-effect background corrector, pyrolytically-coated graphite tubes and 5-μl samples were used throughout

Step	1	2	3	4[a]
Temp. (°C)	120	400	2400	2600
Ramp (s)	10	10	0	1
Hold (s)	20	20	5	4
Read (s)	—	29	—[b]	—
Int. flow	—	—	gas stop	—

[a]Clean step. [b]Read step.

pipetted into the atomization cell and the element was atomized; the general furnace parameters are given in Table 2. In those instances where background overcompensation was observed (as was evident from a negative absorbance signal), the measurements were repeated with the use of the furnace parameters recommended in the instrument manual; in some cases the element concentration was also changed. In order to avoid memory effects, a new graphite tube was used for each matrix element studied. The appropriate acids were used as blanks.

Table 3 lists revised charring and atomization temperatures for those elements which had been found to be subject to overcompensation; the other furnace parameters were the same as those given in Table 2.

Measurements were also made without Zeeman background correction (i.e., in the single-beam mode) to decide whether a positive spectral interference, i.e., caused by direct overlap of the analyte emission line with the unsplit matrix element absorption line (no magnetic field applied), could be excluded or not.

TABLE 3

Charring/atomization temperatures for elements subject to background overcompensation (the other furnace parameters were the same as those given in Table 2). Except where mentioned, pyrolytically-coated graphite tubes were used

Analyte	Temperatures (°C)		Analyte	Temperatures (°C)	
	Charring	Atomization		Charring	Atomization
Al	1500	2400	Ni	1000	2600
B	1000	2700	Pb	500	1100
Bi	500	1000	Pd	1000	2300
Co	1000	2200	Pt	1400	2500
Cr	1200	2300	Si	1400	2700
Eu[a]	1300	2600	Sn	800	2700

[a]Standard graphite tubes were used for atomization of cesium at the europium line.

RESULTS AND DISCUSSION

The results of the preliminary investigations are shown in Table 1; the effects of the matrix elements can be classified as producing (a) no signal, (b) a negative signal, or (c) a positive signal when atomized at the wavelength of the analyte tested. As is apparent from Table 1, most of the matrix elements belong to group (a), and for these elements spectral interference need not be considered. The lines of these matrix elements are probably only emission lines or very weak absorption lines.

Among the matrix elements, eighteen were found to belong to group (b), which comprises those giving a negative absorbance signal caused by a σ-component of the matrix element overlapping with the analyte emission line. In the absence of the magnetic field, the matrix absorption line may still overlap with the wing of the analyte emission line, and this causes a positive spectral interference in conventional a.a.s. Several cases of overlap of absorption with emission lines have been reported [5], even when peak-to-peak distances are as large as 0.05 nm.

As the lines of the matrix elements belonging to group (b) are all absorbing lines and, in addition, are situated less than 0.01 nm away from the analyte line, a positive spectral interference is probable in conventional a.a.s. Experiments conducted with the instrument in the single-beam mode could only establish, from the absence of a signal, that a positive spectral interference was not present. Only in two of the present cases, under the conditions where the overcompensation effect with Zeeman a.a.s. existed, could it be ascertained that a positive spectral interference did not occur; 1000 μg ml^{-1} vanadium solution measured at the 305.1-nm nickel line and 100 μg ml^{-1} lead solution measured at the palladium line gave no signal in the single-beam mode. However, at higher matrix concentrations or under other conditions, spectral interference can still be experienced. For all elements of group (b), factors which broaden, shift and/or change the profile of the peaks can also influence the interference, and the interfering effect should therefore always be established experimentally.

The total number of spectral interferences detected in the present series of investigations now adds up to 22. Only four of these seem to have been observed or described previously as possible overlapping lines in conventional a.a.s.; the eighteen new cases should therefore be added to the list of known spectral interferences in a.a.s. [6].

Table 4 gives a more detailed description of the eighteen cases of overcompensation encountered in the present study; the wavelengths of the lines believed to overlap, and the negative peak areas obtained with the recommended furnace program, are also listed. For those cases in which the matrix element solution is contaminated by the analyte, the actual negative spectral interferences will be larger than the values listed in Table 4.

Some matrix elements have an absorption line adjacent to a gas-fill line of the emission source lamp, and both lines are contained in the bandpass of

TABLE 4

Analyte/matrix element combinations subject to background overcompensation in Zeeman-corrected a.a.s.

Analyte	Line (nm)	RS[a]	Slit width[b] (nm)	Interferent	Overlapping lines (nm)			Conc.[c] (μg ml^{-1})	Peak area[d]
					Emission λ_1	Interfering λ_2	$\lambda_2-\lambda_1$		
Al	308.2	1.6	0.7	V[e]	308.2155	308.2111	−0.0044	10	−0.15
								100	−0.78
								1000	−1.07
B	249.7	1.0	0.7	Co	249.6778	249.671	−0.007	1000	−0.014
Bi	227.6	14.0	0.2	Co	227.6578	227.6532	−0.0046	1000	no sign
								1000	−1.15[f]
Co	243.6	2.9	0.2	Pt[e]	243.6657	243.6689	+0.0032	100	−0.14
								1000	−0.54
Cr	360.5	2.2	0.7	Co[e]	360.5333	360.5356	+0.0023	100	−0.07
								1000	−0.28
Eu	459.4	1.0	0.2[g]	V	459.402	459.4108	+0.009	10	−0.23
								100	−0.66
								1000	1.62[h]
Eu	459.4	1.0	0.2[g]	Cs	459.3243[i]	459.3177	−0.0066	10 000	−0.10
Ni	341.5	3.5	0.2	Co	341.4765	341.4736	−0.0029	1000	−0.067
Ni	305.1	4.5	0.2	V	305.0819	305.0890	+0.0071	100	−0.23
								1000	−0.97
Pb	261.4	10.0	0.7	Co	261.4178	261.4128	−0.0050	1000	no sign
								1000	−0.20[f]
Pd	247.6	1.0	0.2	Pb	247.6418	247.6379	−0.0039	1000	no sign
								100	−0.04[f]
								1000	−0.28[f]
Pt	265.9	1.0	0.7	Eu	265.9454	265.942	−0.003	1000	−0.21
Pt	306.5	2.1	0.7	Ni[e]	306.4712	306.4623	−0.0089	1000	−0.54
Pt	273.4	4.1	0.2	Fe[e]	273.3961	273.4004	+0.0043	1000	−0.04
Si	250.7	2.8	0.2	Co	250.6899	250.6877	−0.0022	100	−0.12
								1000	−0.67
Si	250.7	2.8	0.2	V[e]	250.6899	250.6905	+0.0006	10	−0.06
								100	−0.37
								1000	—[h]
Sn	303.4	2.3	0.2	Cr	303.4121	303.4190	+0.0069	1000	−0.24
Sn	300.9	4.1	0.7	Ca	300.9147	300.9205	+0.0058	10 000	−0.24

[a]Relative sensitivities taken from the Perkin-Elmer literature for flame a.a.s. (standard conditions). [b]Except where mentioned the recommended low slit is used. [c]Concentration of interferent; 5 μl added. [d]Except where mentioned the furnace parameters given in Table 3 are used. [e]The matrix metal solution is contaminated by the analyte element. [f]The general furnace parameters given in Table 2 are used. [g]The high slit had to be used. [h]There is a positive signal superimposed on the negative absorbance. [i]Neon emission line.

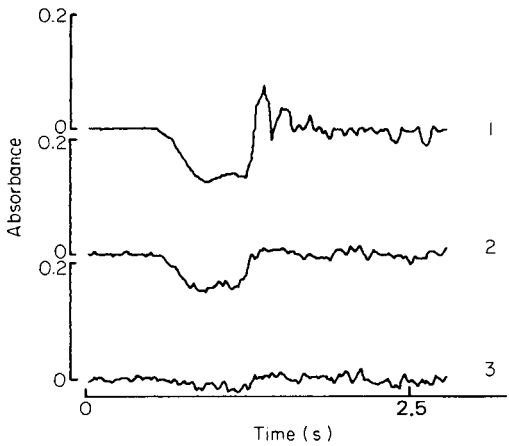

Fig. 1. Absorbance profiles of 5-μl portions of a 1% (w/v) cesium solution measured at the 459.4-nm europium line with Zeeman background correction and different slit widths. Slit widths: (1) 0.7 nm; (2) 0.2 nm; (3) 0.07 nm. For experimental conditions, see Table 3.

the monochromator/detector system. A σ-line of a matrix element may then overlap with the gas-fill emission line, this again causing overcompensation. In the present study, this type of interference probably occurred in one analyte/matrix element system. Figure 1 shows the absorbance profiles for 5-μl portions of a 1% cesium solution measured at the 459.4-nm europium line. Profiles 1 and 2, recorded at slit widths of 0.7 and 0.2 nm, respectively, show overcompensation probably caused by a σ-line of the 459.3177-nm cesium resonance line overlapping with the 459.3243-nm neon line. When the slit width was decreased to 0.07 nm, profile 3 was obtained; the two interfering lines were thus excluded from the bandpass and overcompensation was no longer observed. This type of spectral interference is not likely to cause any serious problems in practical work, but it remains a type of interference that is not normally taken into account.

Most of the present eighteen cases of overcompensation do not appear at the main lines recommended for measurement of the analyte, but some are affected, such as the 459.4-nm europium line (interference from vanadium and cesium), the 247.6-nm palladium line (interference from lead) and the 265.9-nm platinum line (interference from europium). The other cases of spectral interference encountered here occur at the less sensitive wavelengths, but these lines can also be of importance in a.a.s. Selection of absorption lines of similar or different sensitivity makes it possible to avoid interferences and to provide greater flexibility in covering different concentration ranges.

In electrothermal a.a.s., certain interferences can be avoided by taking advantage of the different volatilities of the analyte and the matrix element. In some cases, the difference in volatility even permits an element to be atomized before the other element starts to evaporate. It is also possible to utilize spectral interferences for analytical purposes, such as has been previously

described [1, 2] for the systems Hg/Co and Zn/Fe; this method may also be applicable to the element pairs Bi/Co, Pb/Co and Pd/Pb in the present investigation.

The remaining matrix elements are those belonging to group (c), i.e., the elements that gave a positive absorbance in the preliminary measurements (see Table 1). The interpretation of these results is complicated by the fact that some of the metal solutions were contaminated, and extensive work would be needed to decide whether or not a positive absorbance for a matrix element is caused by a contamination of the analyte, a positive spectral interference or both. A background overcompensation effect may be overlooked because of a contamination of the analyte. Some of the matrix elements belonging to group (c) are known to give spectral interference in conventional a.a.s. (see Table 1). For the other elements of this group, nothing definite could be concluded from the present experiments.

The present series of papers describes 22 cases of spectral interferences in inverse Zeeman-corrected a.a.s. and demonstrates that disturbances by absorbing atomic lines are more common than previously believed. Further work is required for the elucidation of other spectral interferences. Work in this field would be facilitated if highly resolved spectra of the emission sources, a data bank of current wavelengths and wavelength data, and appropriate software were available.

REFERENCES

1 G. Wibetoe and F. J. Langmyhr, Anal. Chim. Acta, 165 (1984) 87.
2 G. Wibetoe and F. J. Langmyhr, Anal. Chim. Acta, 176 (1985) 33.
3 G. R. Harrison, M.I.T. Wavelength Tables, The Technology Press, Wiley, New York, 1939.
4 P. W. J. M. Boumans, Line Coincidence Tables for Inductively Coupled Plasma Atomic Emission Spectroscopy, Pergamon Press, Oxford, 1980.
5 J. D. Norris and T. S. West, Anal. Chem., 46 (1974) 1423.
6 See, e.g., B. Welz, Atomabsorptionsspektrometrie, 3rd edn., Verlag Chemie, Weinheim, 1983.
7 T. Kantor, P. Fodor and E. Pungor, Anal. Chim. Acta, 102 (1978) 15.

Analytica Chimica Acta, 186 (1986) 163—174
Elsevier Science Publishers B.V., Amsterdam — Printed in The Netherlands

COMPUTER-BASED SYSTEM FOR CORRELATING MOLECULAR STRUCTURES WITH MASS SPECTRAL DATA

Methods for Generating Molecular Substructures and for Incorporating Fragmentation Rules

MARSHALL M. SIEGEL*, NORMAN BAUMAN and GUY T. CARTER

American Cyanamid Company, Medical Research Division, Lederle Laboratories, Pearl River, NY 10965 (U.S.A.)

(Received 23rd January 1986)

SUMMARY

The masses of ions observed in the mass spectrum of a pure compound are correlated with the masses of the molecular substructures of the compound. Three methods are described for generating molecular substructures. Each method is evaluated to establish how effectively it generates the molecular substructures and correlates the masses of the molecular substructures with the masses of the observed fragment ions. Rules for mass-spectral fragmentation processes are incorporated into the mass spectral analysis software and illustrated for retro-aldol and lactone-ester reactions occurring in the thermospray mass spectra of oligomycin antibiotics.

Recently, a computer-based method was demonstrated for correlating mass-spectral fragment-ion data with a proposed molecular structure [1]. This method uses the concept of "superatoms" to describe a proposed molecular structure. Superatoms are defined as sub-molecular units which do not undergo further fragmentation. Two types of superatoms are necessary to describe molecular structures and mass spectral processes: bonded superatoms and floating superatoms. Bonded superatoms are used to construct the proposed molecular structure, and floating superatoms, which are found anywhere in the molecule, are used to describe structural rearrangements, adduct ions and neutral losses.

In principle, nearly all ions observed in mass spectra can be constructed from connected sets of bonded superatoms and floating superatoms having the masses of the observed ions. Because many solutions are possible, the most likely set of superatoms describing the ion is postulated to be that with the fewest bond cleavages between superatoms.

To solve this problem, all the connected sets of bonded superatoms which constitute possible answers must be found and evaluated. Three methods for finding all the connected sets of superatoms were evaluated. These methods are referred to as: (1) the brute force method, (2) the bond removal method, and (3) the substructure method. The algorithms developed for implementing

0003-2670/86/$03.50

the three methods are discussed below together with their corresponding advantages and disadvantages.

An extension in the use of the mass spectral software is described which incorporates fragmentation rules to aid in interpretation of mass spectral data.

METHODS

Brute force method

The previous paper [1] described the brute force method (BFM). The masses of all combinations of both the bonded and floating superatoms were computed. Those superatom sets having the masses of the observed ions were checked for connectivity, viz., that all the bonded superatoms were connected as one substructure. If the latter criterion was met, the number of superatom bond cleavages was computed. The processing time for the method becomes very long as the number of superatoms, m, exceeds 20, because the number of superatom combinations that must be evaluated increases exponentially as the number of superatoms increases (Table 1):

$$\text{Number of superatom combinations evaluated} = \sum_{k=1}^{m} m!/[k!(m-k)!]$$

$$= 2^m - 1 \qquad (1)$$

As an order of magnitude, the processing time on a DEC PDP-10 computer is about 1 h for 25 superatoms. Most mass-spectral fragmentation processes occur with four or fewer superatom bond cleavages. The brute force method

TABLE 1

Number of superatom combinations evaluated[a]

Total number of superatoms (m) or bonds (n) in structure	Brute force method (Eqn. 1)	Bond removal method (Eqn. 2)	
		($p = 2$, $q = 3$)	($p = 2$, $q = 4$)
10	1.023×10^3	2.544×10^3	6.744×10^3
20	1.049×10^6	2.068×10^4	1.176×10^5
30	1.074×10^9	7.044×10^4	6.184×10^5
40	1.200×10^{12}	1.678×10^5	1.996×10^6
50	1.126×10^{15}	3.287×10^5	4.935×10^6
60	1.153×10^{18}	5.692×10^5	1.032×10^7
70	1.181×10^{21}	9.054×10^5	1.924×10^7
80	1.209×10^{24}	1.353×10^6	3.298×10^7

[a] m = total number of superatoms in brute force method, n = total number of bonds in bond removal method, p = number of floating superatoms, q = maximum number of bond cleavages.

produces too many solutions because most of the solutions have more than four superatom bond cleavages.

Bond removal method

The bond removal method (BRM) focuses on the superatom bonds rather than the superatoms (as in the brute force method). By focusing on the superatom bonds, the number of superatom combinations can be reduced dramatically by generating only those sets of connected superatoms with the desired number of superatom bond cleavages. The following procedure is used. First, for n superatom bonds, k of them at a time are removed, where $k = 0, \ldots, q$, q being the maximum number of bond cleavages to be considered. As the superatom bonds are systematically removed, the molecule fragments into connected superatom pieces. (The maximum number of pieces is $k + 1$ for a linear molecule.) Secondly, the masses are computed for all combinations of the molecular fragments and the floating superatoms. All the computed ion masses equal to the observed masses are acceptable solutions.

The maximum possible number of superatom combinations is

$$\{\sum_{k=0}^{q} (k+1)(n!)/[k!(n-k)!]\}\{\sum_{k'=0}^{p} p!/[k'!(p-k')!]\} \qquad (2)$$

where p is the maximum number of floating superatoms. This maximum number of combinations is relatively low (Table 1) because q is generally $\leqslant 4$ and p is generally $\leqslant 3$. (The righthand term of the above expression is equal to 2^p.) The processing time on a DEC PDP-10 is less than 5 min for 40 superatoms (37 bonded and 3 floating), 40 superatom bonds and a maximum of 3 superatom bond cleavages.

A feature of the bond removal method is that duplicate solutions are possible because similar molecular fragments are generated from different combinations of superatom bonds removed from the molecule. Sorting routines are therefore used to remove duplicate solutions. Algorithms written by Nijenhuis and Wilf [2] were used to generate all the combinations of n superatom bonds taken k at a time (subroutine NEXKSB) and to find all the connected superatom fragments (subroutine SPANFO).

Substructure method

The algorithm for the substructure method was written to generate all bonded molecular substructures efficiently and to calculate their corresponding bond cleavage numbers. This method was implemented by coding the representation of the connectivity table in a bit-map mode, i.e., if superatom i is connected to superatom j, then the ith bit of the jth word and the jth bit of the ith word are 1 and all other bits are zero. Likewise, each bonded molecular substructure is represented by a bit-mapped computer word where the kth bit corresponds to the kth superatom, and is 1 if the superatom is present

in the substructure and 0 if not. To make the calculation efficient, part of the computer word is used for the number of superatom bond cleavages. The maximum number of substructures considered is limited by the computer memory, and the maximum number of superatoms that can be evaluated is limited by the word size of the computer. For the DEC PDP-10 computer, the word consists of 36 bits and was divided into 33 bits for describing the bonded superatoms and 3 bits for describing the number of superatom bond cleavages. Therefore, this system is limited to molecules containing 33 or fewer bonded superatoms and is limited by the size of the computer memory needed for all the bit-mapped molecular substructures.

This algorithm generates all the molecular substructures by building larger sets of connected superatoms from smaller ones. Each of the superatoms making up the molecule is numbered. The algorithm does not consider a given superatom until all bonded superatom subsets are constructed from lower numbered superatoms. For example, it is assumed that all bound superatom subsets containing superatoms 1—5 have been found and superatom 6 is added to the list; the sets already found are scanned to see if they contain a superatom bound in the molecule to superatom 6 and, if so, the union of the found set and superatom 6 is added to the list. In addition, the subsets containing superatom 6 are compared to one another. If pairs of superatom sets are adjacent at superatom 6 only, then the union of the two sets is added to the list.

The above algorithm is implemented using bit-maps to represent the superatom subsets. The "aura" of a fragment ion is obtained by OR-ing together the rows in the connectivity table corresponding to the superatom numbers making up the subset. To establish if two fragments are adjacent, the bit-map word corresponding to one is AND-ed with the aura of the other. The two fragments are adjacent if and only if this result is not zero. Finally, the minimum number of bond cleavages necessary to generate this fragment can be obtained by counting the total number of 1-bits in the intersections of the bit-map representing the complementary structure (all superatoms not in the present fragment) with the rows in the connectivity table corresponding to each superatom of the fragment.

The list of acceptable connected substructure solutions is obtained by removing all substructures having bond cleavage numbers greater than the desired number and masses other than the desired value after having computed all combinations of the floating superatom masses with the masses of the substructure.

Thirty superatoms can be evaluated within 5—10 min on a DEC PDP-10 computer provided that the allocated memory is not exceeded. The high speed of this method is due to the processing of all the bit-mapped words in the computer memory.

FRAGMENTATION RULES

A further extension in the use of the mass spectral analysis algorithms as an aid in interpretation is the incorporation of mass spectrometry fragmentation rules. Because the algorithms generate all the desired combinations of superatoms, the inclusion of fragmentation rules effectively suppresses the print-out of undesirable solutions.

The use of fragmentation rules is illustrated in the analyses of thermospray (TSP) [3, 4] mass spectral data for the oligomycin A, B, C and ω antibiotics, structures I—IV, respectively. (Structures I—IV are expressed as sets of

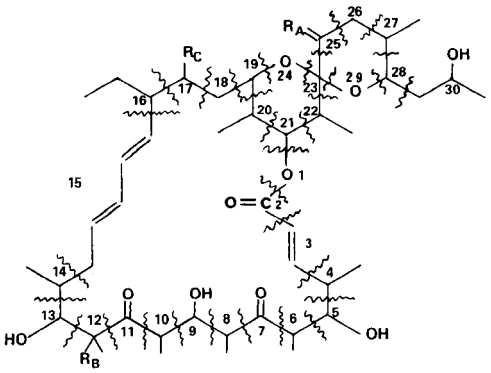

Structure	Oligomycin	R_A	R_B	R_C
I	A	2H	OH	H
II	B	O	OH	H
III	C	2H	H	H
IV	ω	2H	OH	OH

superatoms. Each superatom is demarcated by wiggly lines and numbered for each structure.) The ions observed in the TSP spectra for the different oligomycin structures are correlated, based upon the small mass differences of the structures and by their relative abundances (Table 2). The small mass differences of the correlated ions for the different oligomycins are keys to the portion of the molecule undergoing decomposition. Table 3 summarizes the rules that must be followed for structural elucidation based on the correlation of the ion masses.

Preliminary computer processing of the oligomycin data, without applying the fragmentation rules, suggested that all even-mass ions were ammonium adduct ions and that all odd-mass ions were either proton or sodium adduct ions. These observations are consistent with those on previously examined materials under thermospray conditions. The H^+ and NH_4^+ adducts originate from the 0.1 M ammonium acetate buffer used as the ionizing reagent for the thermospray process, and the Na^+ adduct arises from sodium salt impurities present in the ammonium acetate and oligomycins. In addition, computer processing of the data suggested that all the fragment ions arose from two superatom bond cleavages, the majority of which occurred between superatoms labeled 1 through 13. This is consistent with the oligomycin structures because the aliphatic and olefinic groups and the spiro-ketal ring systems are relatively stable while the oxygenated portions of the molecules are prone to undergo thermal degradation reactions. Retro-aldol reactions and reactions involving the lactone ester were expected to be responsible for the

TABLE 2

Structural assignments for positive ions observed in the thermospray mass spectra of oligomycins A, B, C and ω with molecular weights of 790, 804, 774 and 806, respectively

Proposed assignment[a]	A (790)		B (804)		C (774)		ω (806)		Proposed structure[a,b]
	m/z	%	*m/z*	%	*m/z*	%	*m/z*	%	
M + Na	813	0.4			797	3.5			
M + NH_4	808	2.5	822	1.5	792	9.5	824	12.0	
M + H	791	1.0			775	4.0			
M + NH_4 − H_2O							806	6.5	
M + H − H_2O	763	0.1	787	1.0	757	0.2			
M + NH_4 − $2H_2O$							788	1.0	
M + H − $2H_2O$					739	1.0			
M + NH_4 − $3H_2O$							770	0.1	
					719	1.0			
M + Na − {6–8} − 2H					711	2.0			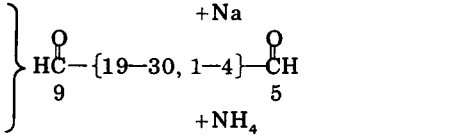
M + NH_4 − {6–8} − 2H	722	0.2	736	0.1	706[c]	10.5			
M + NH_4 − {10–12} − 2H	706	3.0	720	2.5	706[c]	10.5	722	2.5	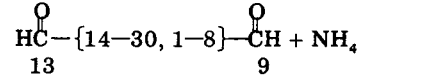
M + NH_4 − {6–9} + H − H			708	0.1					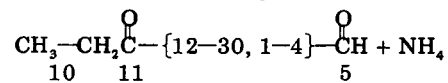
M + NH_4 − H_2O − {10–12} − 2H							704	0.2	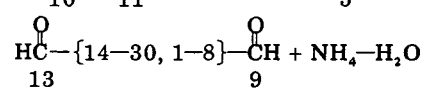
M + Na − {9–12} + H − H					683	1.5			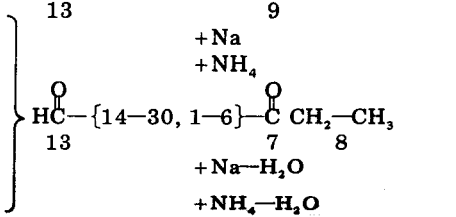
M + NH_4 − {9–12} + H − H	678	8.0	692	6.0	678	8.0	694	6.5	
M + Na − H_2O − {9–12} + H − H					665	3.0			
M + NH_4 − H_2O − {9–12} + H − H	660	11.0	674	8.5	660	12.5	676	0.5	

M + H − {8–12} + H − H[d]	633	1.0	647	0.5	633	2.0	649	0.1	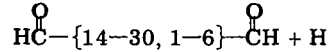
M + NH_4 − 4H_2O − {9–12} + H − H[e]	606	2.0			606	2.5			
M + Na − {6–12} − 2H	597	9.5	611	5.0	597	21.0			+Na
M + NH_4 − {6–12} − 2H	592	54.5	606	52.5	592	28.0	608	47.0	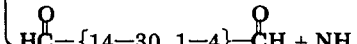
M + H − {6–12} − 2H							591	0.2	+H
	564	6.0	578	9.0	564	4.0	580	1.5	
M + H − {1–9} + H − H					533	4.0			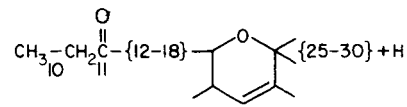
	523	0.6	537	2.0	523	1.0			
M + H − H_2O − {1–9} + H − H					515	8.5			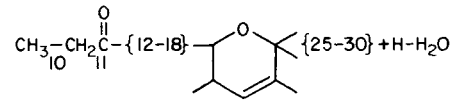
M + Na − {2–12} + H − H	487	6.0	501	11.5	487	19.5			+Na
M + NH_4 − {2–12} + H − H	482	2.0	496	100.0			498	0.2	+NH_4
M + Na − H_2O − {2–12} + H − H	469	3.0			469	4.0			+Na − H_2O
M + H − {2–12} + H − H	465	19.0	479	1.0	465	8.5	481	1.0	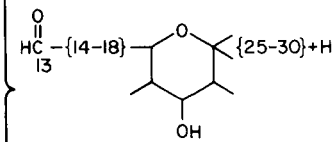
M + NH_4 − H_2O − {2–12} + H − H			478	1.5			480	3.0	+NH_4 − H_2O
M + H − H_2O − {2–12} + H − H	447	100.0	461	29.0	447	100.0	463	12.5	+H − H_2O
M + H − 2H_2O − {2–12} + H − H	429	26.0	443	25.5	429	35.0	445	4.0	+H − 2H_2O
M + H − 3H_2O − {2–12} + H − H	411	6.0	425	3.0	411	6.0	427	1.5	+H − 3H_2O
			399	5.5	399	2.0			
H + {1–12} + 2H	(329	4.0)[e]			329	10.0			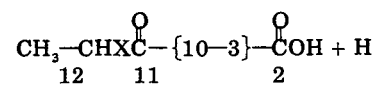

TABLE 2 (continued)

Proposed assignment[a]	A (790)		B (804)		C (774)		ω (806)		Proposed structure[a,b]
	m/z	%	*m/z*	%	*m/z*	%	*m/z*	%	
NH_4 + {5—12} + H — H[d]	262	2.0	262	1.5			262	2.5	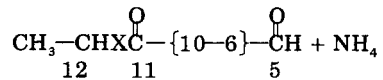
Na + {6—12} + 2H	239	3.0	239	5.0	223	4.0	239	3.0	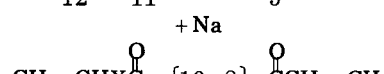
NH_4 + {6—12} + 2H	234	9.0	234	7.0	218	9.5	234	100.0	
NH_4 + {1—8} + 2H							232	11.0	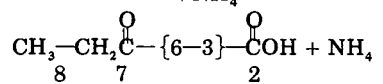
H — H_2O + {1—9} + H — H	225	9.0			225	11.0	225	16.0	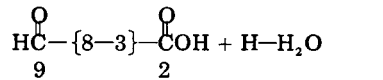
H + {6—12} + 2H			217	6.5	201	6.5			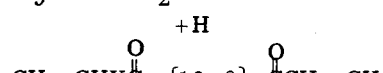
NH_4 — H_2O + {6—12} + 2H							216	57.0	
H — $2H_2O$ + {1—9} + H — H	207	5.5							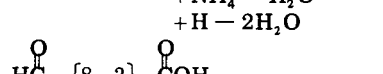
NH_4 — $3H_2O$ + {1—9} + H — H							206	8.0	
H — H_2O + {6—12} + 2H	199	19.5	199	20.5			199	39.5	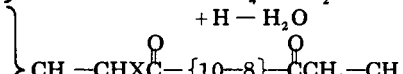
H — $2H_2O$ + {6—12} + 2H	181	6.5	181	5.5			181	40.5	

NH_4 + {9—12} + H — H	148	1.5	148	2.0			148	5.0	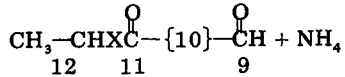
{1—5} + H — H[e]	128	3.5	128	6.0	128	8.0			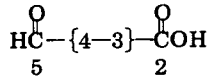

[a]The numbers within braces correspond to the superatom numbers in structures I—IV. [b]The subscripted numbers in the proposed structures correspond to the superatom numbers in structures I—IV. X = OH for oligomycins A, B and ω, but H for oligomycin C. [c]Degenerate solutions. [d]Proposed assignment does not follow the retro-aldol reaction. [e]Assignment uncertain.

TABLE 3

Structural correlations for small mass differences in ions observed in thermospray mass spectra of oligomycin A with oligomycins B, C and ω

Ions correlated in TSP mass spectra of oligomycins A and X	Mass difference in correlated ions Δ[a] (daltons)	Structural relationship between oligomycins A and X: superatoms absent or present in both fragment ions
B	0	25 absent
C	0	12 absent
ω	0	17 absent
B	−14	25 present
C	16	12 present
ω	−16	17 present

[a] Δ is the mass of oligomycin A ion minus mass of oligomycin X ion.

observed TSP degradation reactions because these types of fragmentation processes were used previously to rationalize electron-impact ionization mass spectra of oligomycins [5, 6].

The following thermally-induced processes were proposed to account for the ions observed in the TSP spectra: (a) retro-aldol and lactone ester reactions followed by (b) chemical ionization of the reaction products with the formation of proton, ammonium or sodium adduct ions. The retro-aldol reaction results in the cleavage of a bond which is α to a hydroxyl group and β to a carbonyl group, and, in the loss (gain) of a hydrogen atom at the alcohol (carbonyl) group:

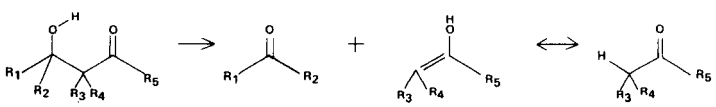

The lactone ester reacts either by elimination, yielding an olefin and carboxylic acid, or by hydrolysis, yielding an alcohol and carboxylic acid:

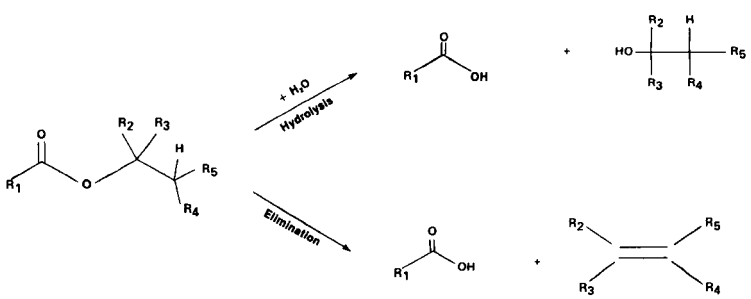

These reaction processes were evaluated by writing an algorithm into the mass spectral evaluation routine for finding only those combinations of superatoms in which the superatom on one side of the cleavage is present

and on the other side is absent, and at the same time adjusting the mass of the combination of superatoms for the gain (loss) of 1 dalton because of hydrogen transfer. Because there are four possible sites for retro-aldol reactions in the oligomycins, only eight lines of code (all logical IF statements) are necessary for describing those combinations of superatoms satisfying the retro-aldol conditions. Likewise, for the two lactone ester cleavages, four lines of code are necessary. Table 2 lists the unique solutions obtained with the aid of the mass spectral evaluation program. Note that nearly all of the ions are due to double retro-aldol reactions or one retro-aldol and one lactone cleavage and that the fragment ions either gain or lose two hydrogen atoms or gain and then lose a hydrogen atom.

It is a simple matter to incorporate other fragmentation rules into the software. Another option is to write a post-evaluation program to select from all the possible superatom combinations those satisfying the fragmentation rules.

Conclusions

The brute force method inefficiently generates all connected superatom substructures. For large numbers of superatoms ($\geqslant 25$), the processing time is excessive (>1 h). The substructure method is a more efficient method for obtaining the connected superatom substructures because it operates in the bit-mapped mode but it is limited by computer word size and computer memory. The bond removal method has been found to be the most efficient method for generating all the connected superatom substructures because it is fast, utilizes minimal amounts of computer memory and is not limited by the numbers of superatoms studied.

The bond removal method, incorporating mass spectral fragmentation rules, has been used almost exclusively in solving a variety of structural elucidation/correlation problems in this laboratory. These applications have been principally to aid in the interpretation of mass spectra and daughter-ion mass spectra of natural and semi-synthetic antibiotics. The spectra were acquired in a variety of ionization modes (fast atom bombardment, TSP, chemical ionization, electron impact) as nominal and exact mass data.

The FORTRAN listings are available upon request from the authors.

The authors greatly appreciate the constructive comments of Kevin Haraki in developing the algorithms, the work of Steven Greenhouse in making the algorithms compatible with the DEC VAX family of computers, Robert Isensee and Debra Beck for the thermospray data, and the helpful editorial comments of Marilyn Englander.

REFERENCES

1 M. M. Siegel, Anal. Chim. Acta, 174 (1985) 61.
2 A. Nijenhuis and H. S. Wilf, Combinatorial Algorithms, Academic Press, New York, 1980, Chaps. 3 and 14.

3 C. R. Blakley and M. L. Vestal, Anal. Chem., 55 (1983) 750.
4 M. L. Vestal and G. J. Fergusson, Anal. Chem., 57 (1985) 2373.
5 W. F. Prouty, R. M. Thompson, H. K. Schnoes and F. M. Strong, Biochem. Biophys. Res. Commun., 44 (1971) 619.
6 G. T. Carter, Dissertation, University of Wisconsin, Madison, 1976. University Microfilms, Ann Arbor, Michigan.

Analytica Chimica Acta, 186 (1986) 175—183
Elsevier Science Publishers B.V., Amsterdam — Printed in The Netherlands

MULTI-INDUCTIVE COMPONENT ANALYSIS, A NEW APPROACH IN PATTERN RECOGNITION

H. STEIGSTRA and A. P. JANSEN

Laboratory for Clinical Chemistry, Sint Radboud Hospital, Geert Grooteplein 8, 6500 HB Nijmegen (The Netherlands)

G. KATEMAN*

Department of Analytical Chemistry, Catholic University of Nijmegen, Toernooiveld, 6525 ED Nijmegen (The Netherlands)

(Received 20th December 1985)

SUMMARY

A powerful transformation technique in pattern recognition is presented as an alternative to principal component analysis. Its properties include automatic feature selection, presentation of physically interpretable results, and elucidation of hidden relationships between variables. The mathematics of the transformation is described. Numerical examples are given for an artificially generated data set and for the ARCH data set on metals in obsidian rocks.

Principal components analysis (PCA) is commonly used in various scientific disciplines. It offers the possibility of ordering information in large data sets by reducing the number of descriptive variables. This reduction is achieved by rotating the data set, so as to concentrate the variance into the most important eigenvectors. Interpretation of data sets with large numbers of variables is then done by projecting the data set on these eigenvectors. Clusters or trends can be visualized without detailed examination of the originally large data set. Although PCA is an attractive way of ordering a complex data set, there are some serious disadvantages. The most important are the very abstract presentation of the transformed information and the fact that no reduction of the number of physical variables is accomplished. Moreover, as a consequence of the optimization to a maximum variance, linear combinations of variables that do not distinguish between clusters may be produced. The application of experimental factors such as variance or Fisher weighting may help to minimize this effect. A new transformation technique, multi-inductive component analysis (MICA), has been developed; it has the same dimension-reducing power as PCA, but without the disadvantages mentioned. It is a powerful tool in the selection of the most important variables and in the study of their physical relationships.

0003-2670/86/$03.50

MULTI-INDUCTIVE COMPONENT ANALYSIS

A standardized data set $\vec{Z}$ with m vectors in n-dimensional space is considered. The purpose is to transform this data set into a new data set $\vec{U}$ in the n-dimensional space with the following properties: (a) the transformed variables are not correlated; and (b) the first transformed variable contains the greatest amount of variance in the original data set and each successive new variable contains the next greatest amount of the residual variance.

A linear transformation was considered:

$$\vec{U} = \mathbf{V}\,\vec{Z} \tag{1}$$

where $\mathbf{V}$ is the $(n*n)$ transformation matrix. The approach of PCA is to maximize the variance of the first transformed variable u_1, described by

$$\text{var}\,[u_1] = (1/m) \sum_{i=1}^{m} u_{1i}^2 \tag{2}$$

Afterwards, the successive transformed variables are calculated by optimizing the residual variances. The solution of this problem leads to the well known eigenvector decomposition or Karhunen-Loeve transformation [1, 2] and is equivalent to a multidimensional rotation of the data set. In the transformation of the original data set (Eqn. 1), the back-transformation of the transformed data set is $\vec{Z} = \mathbf{V}^{-1}\,\vec{U}$. To simplify the notations, $\mathbf{V}^{-1}$ is replaced by $\mathbf{P}$, which is the inverse of the operation $\mathbf{V}$; thus $\vec{Z} = \mathbf{P}\,\vec{U}$. Each element in Z is determined by this equation and is similar to the following set of equations:

$$z_{ik} = p_{1i}\,u_{1k} + p_{2i}\,u_{2k} + \ldots + p_{ni}\,u_{nk} \tag{3}$$

with $i = 1 \ldots n$ and $k = 1 \ldots m$. The elements of the inverse transformation matrix $\mathbf{P}$ are calculated by using the expected values of the cross-correlation of the original and transformed variables:

$$E[z_{ik}\,z_{jk}] = C_{ij} \tag{4}$$

$$E[u_{ik}^2] = 1 \text{ and } E[u_{ik}u_{jk}] = 0 \quad i \neq j \tag{5}$$

where C_{ij} is the cross-correlation between variables i and j. Substitution of Eqn. 3 into Eqn. 4 leads to

$$E[(p_{1i}\,u_{1k} + p_{2i}\,u_{2k} + \ldots + p_{ni}\,u_{nk})\,(p_{1j}\,u_{1k} + p_{2j}\,u_{2k} + \ldots + p_{nj}u_{nk})] = C_{ij}$$

With use of Eqn. 5, this equation can be simplified, resulting in

$$\sum_{k=1}^{n} p_{ki}\,p_{kj} = C_{ij} \quad (\text{with } i \text{ and } j = 1 \ldots n) \tag{6}$$

As the number of coefficients in Eqn. 6 is n^2, while the number of independent equations is only $n(n + 1)/2$, some condition is needed. A straightforward condition is to require orthogonality of the transformation matrix, e.g., $v_i\ v_j = 0$ with $i \neq j$. This condition actually means a rotation of the

data set and leads to a solution similar to PCA. Another possible condition is minimization of the number of linear combinations to be made. This is done by assigning a zero value to each element in the inverse transformation matrix **P** above the diagonal; thus $p_{ij} = 0$ for $i > j$, and the final solution for the inverse transformation matrix is then

$$p_{ij} = [C_{ij} - \sum_{k=1}^{i-1} p_{ki}\, p_{kj}]/p_{ii} \tag{7}$$

for $i \leqslant j$. These coefficients can be calculated without the use of iterative procedures and so the calculations are easily programmed. The transformation matrix **V**, which describes how the transformed (mutually independent) variables are composed from physical variables, can be calculated by inverting the matrix **P**. In the MICA approach, however, the inverse transformation matrix **P** is always used; it describes how the physical variables are composed from independent variables. With this interpretation, a clear view is obtained of the relationships between the variables under investigation.

Sequence of the variables

In contrast to PCA, the result of the described transformation is dependent on the sequence of the original variables. The first transformed variable has the same physical meaning as the first original variable and contributes in linear combinations with the remaining $(n - 1)$ transformed variables to all the original variables; the second transformed variable is a linear combination of the first and second original variables and contributes in linear combinations to the last $(n - 1)$ original variables, etc. Thus, each transformed variable induces variance in a number of untransformed variables, depending on the index of the variable. In this approach, variance is determined only by the correlation matrix and the sequence of the variables; thus the only way to maximize this variance is to optimize the sequence of the variables. The sequence is established one by one, starting with the first variable. When this variable is selected, the sequence of the remaining variables does not influence the induced variance. If no resequencing of variables is applied, the induced variance of the transformed variable is given by

$$\mathrm{var}_i = \sum_{j=i}^{n} \mathrm{var}\,[p_{ij}\, u_i] = \sum_{j=i}^{n} p_{ij}^2 \tag{8}$$

When variable selection is applied, each permutation of variables i and l, where $l \geqslant i$, has to be examined, whereafter the MICA transformation is performed and the induced variance, according to Eqn. 8, can be calculated. To save calculation time, it is not necessary to do the complete transformation; only the coefficients p_{kj} with $k < i$ and $j \leqslant n$ have to be calculated. The induced variance can then be expressed as a function of coefficients that have already been calculated:

$$\text{var}_{il} = \left\{ \sum_{j=i}^{n} [C_{il} - \sum_{k=1}^{i-1} p_{kl}\, p_{kj}]^2 - 1 + p_{il}^2 \right\} / p_{il}^2 \qquad (9)$$

with $p_{il}^2 = 1 - \Sigma_{k=1}^{i-1} p_{kl}^2$. Ultimately, the permutation that results in maximum induced variance will be performed.

Interpretation

The inverse transformation matrix in MICA allows a much more powerful interpretation than the eigenmatrix does in PCA. This is mainly because of the narrow affinity of the correlation matrix. The columns of the inducing matrix contain information about the contribution of independent variables to each physical variable. For example, inducing component i induces variance in the physical variables $i \ldots n$. The amount of induced variance is defined by the squares of the coefficients in column i and the total induced variance equals the sum of these squares. A high induced variance is an indication of a physical relationship between variables and is comparable with the eigenvalue obtained with PCA. As the optimization of the variance is a secondary goal with MICA, this variance may be slightly lower than the eigenvalues.

The rows of the induction matrix define how the physical variables are composed from the inducing components. Physical variable i has contributions to the inducing components $1 \ldots i$ and the sum of the squares of each row is always unity. The closer the diagonal element of row i is to unity, the stronger the relation between this physical variable and inducing component i. Generally, the diagonal elements have decreasing values when the inducing component number is increasing. Consequently, the first inducing components will have the strongest relation to the original physical variables.

RESULTS AND DISCUSSION

Multi-inductive component analysis provides a powerful new technique for studies of large data sets. Whereas PCA only reduces the dimensionality of the experimental space, MICA selects those physical variables that give the best description of the relations between all physical variables under investigation. Consequently, the reduction of the dimensionality of the experimental space is the same, but this reduction is coupled with an equal reduction in the number of physical variables. As a result of the transformation, the most important transformed variables can be identified with the corresponding physical variables. Applications of MICA seem possible in all disciplines where many physical properties are measured in the hope that one or more will discriminate between clusters.

For illustration, an artificial data set with random numbers was generated according to the algorithm

X = random number
$Y = 0.200^* X + 0.98^*$ random number
$A = 0.998^* X + 0.05^*$ random number

$B = 0.998^* X + 0.05^*$ random number
$C = 0.998^* X + 0.05^*$ random number
$D = 0.707^* X + 0.707^* Y$

The correlation matrix is shown in Table 1A. After PCA has been applied, it appears that 99.9% of the total variance is represented by the first two eigenvectors. The sixth eigenvector has an eigenvalue of zero, because variable D is a linear combination of variable X and Y, and has therefore been removed (see Table 1B); but PCA does not indicate which linear combination causes the redundancy of the last principal component. Table 1C shows the coeffic-

TABLE 1

Three different methods of characterization of the data set obtained with the described algorithm. Part A is the correlation matrix; Part B is the eigenmatrix derived from the correlation matrix in Part A; Part C represents the inducing matrix obtained with MICA

A

Physical variable	Physical variable					
	X	*Y*	*A*	*B*	*C*	*D*
X	1.000					
Y	0.213	1.000				
A	0.998	0.215	1.000			
B	0.998	0.218	0.997	1.000		
C	0.998	0.214	0.997	0.997	1.000	
D	0.740	0.815	0.740	0.742	0.739	1.000

B

Eigenvalue (%)	Eigenmatrix						
	X	*Y*	*A*	*B*	*C*	*D*	
79.0	−0.449	−0.199	−0.449	−0.449	−0.449	−0.397	99.9%
20.9	−0.187	0.813	−0.185	−0.183	−0.186	−0.449	
0.06	−0.003	0.003	−0.170	−0.606	−0.777	0.000	
0.06	0.089	−0.024	0.756	−0.580	−0.287	0.036	
0.02	0.751	−0.205	−0.405	−0.248	−0.278	0.302	

C

Physical variable	Inducing components					
	*X**	*Y**	*A**	*B**	*C**	*D**
X	1.000		99.9%			
Y	0.213	0.977				
B	0.998	0.005	0.062			
C	0.998	0.001	0.006	0.061		
A	0.998	0.003	0.002	0.000	0.055	
D	0.740	0.673	0.000	0.000	0.000	0.000
Variance (%)	76.4	23.5	0.07	0.07	0.05	0.00

ients obtained with MICA. The original variables are resequenced according to the given algorithm, but appear to remain in the same sequence as they were in before resequencing. This means that X^* induces the most variance in the data set (and has the greatest correlation to the other variables); Y^* is the variable that induces the next greatest variance and so on. X^* and Y^* induce together 99.9% variance in the data set. As X^* equals X and Y^* is a linear combination of X and Y, 99.9% of the total variance is described by X and Y only. However, the relation between the variables becomes apparent in Table 1C, especially the linear dependence of D on X and Y. The high correlations of A, B and C with X (the values 0.998) and the small independent noise components (the values 0.062, 0.061 and 0.055 on the diagonal) are shown clearly. If a presentation of 99.9% of the information by the first

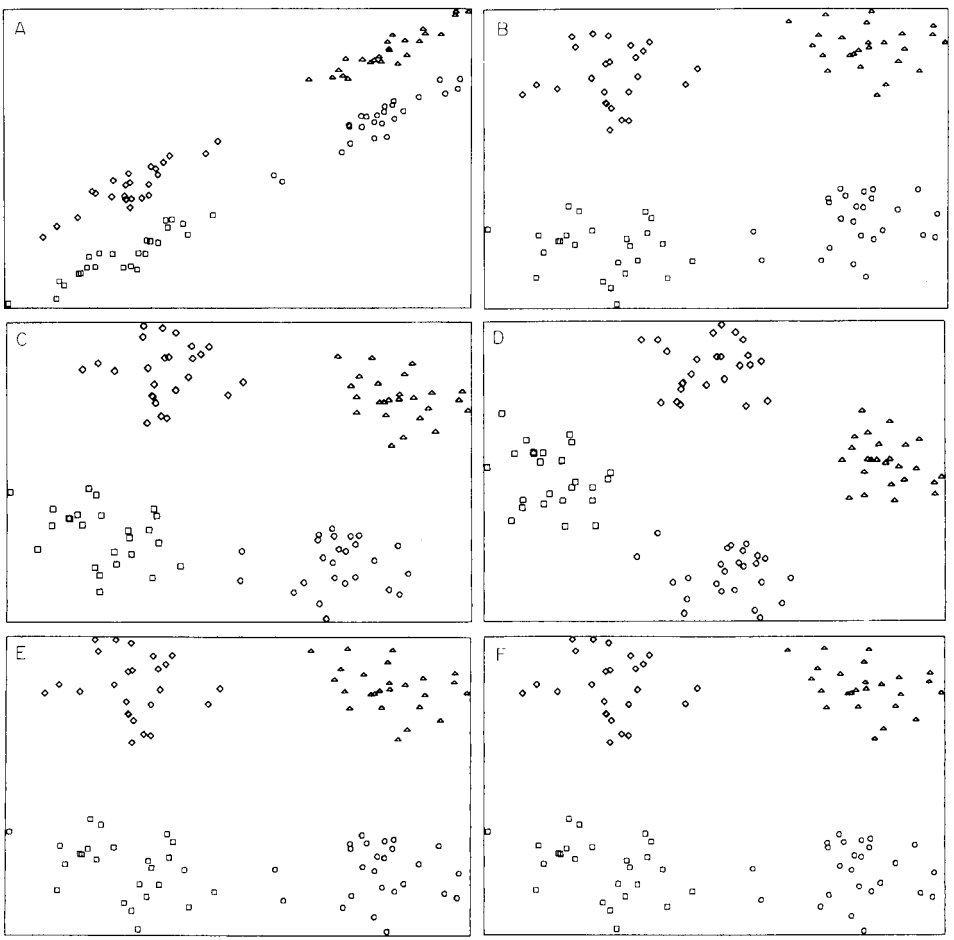

Fig. 1. Transformation results of two data sets (A and B) with correlation coefficients of 0.9 and 0.1, respectively. C and D are the corresponding transformation results from PCA; E and F are the results from MICA.

two transformed variables is satisfactory, only the determination of X and Y is required. When PCA is used, all six variables have to be known to perform the transformation.

Figure 1 illustrates the difference in projection between PCA and MICA for two different data sets, each consisting of two variables and subdivided into four clusters. The two (simulated) data sets have different correlation coefficients, 0.9 (Fig. 1A) and 0.1 (Fig. 1B). The eigenvector plots of these two data sets (Fig. 1C and D) are essentially the same as a rotation of the original data sets over an angle of 45°. The two axes of the eigenvector plots (*PC 1* and *PC 2*) are now purely artificial and the relations to the original variables X and Y have been completely lost. Projections made with MICA (Fig. 1E and F) are closely related to the original variables X and Y: variable X does not change at all, while the resemblance between Y and the second inducing component depends on the correlation between X and Y. In Fig. 1F (correlation coefficient 0.1) this axis differs only slightly from the original variable Y and remains physically interpretable, in contrast to the eigenvector plots, where the axes cannot be identified with the original variables.

As a practical illustration, the ARCH data set [3] was analysed. This data set consists of elemental concentrations of ten metals in 63 obsidian samples from four sites near San Francisco. Figure 2A, B shows the relationships between the original variables Fe, Ba and Ca. Figure 2C, D shows the eigenvector plots of the first versus the second and the first versus the third principal component. These plots represent 75 and 64% of the variance, respectively. Although the four clusters in Fig. 2C are well separated, this plot gives no information on the contribution of each element to that separation and provides no reduction of the number of elements required for the separation. Also, relationships between the elements and the principal components are difficult to find. A useful technique in the determination of the separating power of each variable is the use of Fisher weighting, which showed here that the four most important elements are Fe, Ti, Ba and Ca. Figure 2E, F shows the MICA projections of the three most important transformed variables. These plots represent 67 and 60% of the total variance and are linear combinations of the elements Fe, Ba and Ca. The contribution of titanium (having a high Fisher weight) appears to be determined at 90% by these 3 elements, which makes it one of the redundant elements. The MICA projection of inducing component 1 (Fe) to inducing component 3 (Ba − 0.51Fe + 0.15Ca) gives a very good separation between the clusters, while the resemblance between the transformed variables and the original elements is remarkable.

Conclusions

The MICA technique gives a new aspect to pattern recognition. It combines several requirements in one approach: (1) creation of new variables representing maximum variance of the original data; (2) selection of the physical variables that are mostly representative for the total variance; (3)

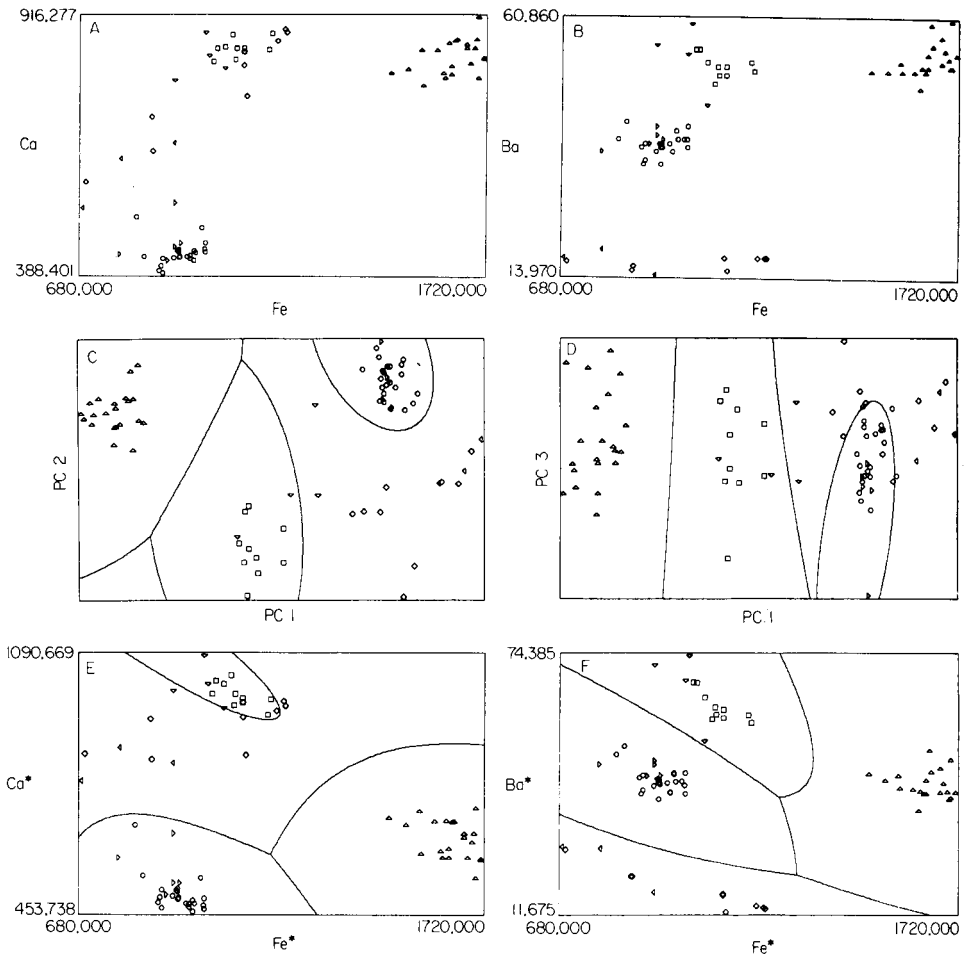

Fig. 2. Projection of the ARCH data set. (A, B) Plots of the three most important (Fe, Ca, Ba) of ten variables, selected with MICA. (C, D) Eigenvector plots of the first three eigenvectors. (E, F) Projections made with MICA of the first three inducing components (Fe*, Ca*, and Ba*), corresponding to A and B, respectively. Location of samples: (□) Mount Konocti; (◇) Borax Lake; (○) Glass Mountain; (△) Anadel; (◁) unknown; (▷) unknown; (▽) unknown. The unknowns served as test sets.

retention of physical information and its visualization; (4) elucidation of hidden relationships between physical variables.

In many applications, the use of MICA will be preferable to the use of PCA. Only in those applications where an absolute maximum variance in a minimum number of artificial variables is required will PCA be more effective.

As the algorithm of MICA is very simple, the software implementation is very easy. A software package (SOLOMON) has been developed in which MICA is used for modelling classification and will be reported at a later date.

With this program, much better classification results are obtained than with programs such as SIMCA [4].

This study was conducted with the support of the Stichting Kwaliteitsbewaking Klinisch Chemische Ziekenhuis Laboratoria.

REFERENCES

1. B. R. Kowalski and C. F. Bender, J. Am. Chem. Soc., 95 (1973) 686.
2 K. Fukunaga and W. L. G. Koontz, IEEE Trans. Comput., C-19 (1970) 311.
3 D. F. Stevenson, F. H. Stross and R. F. Heizer, Archaeometry, 13 (1971) 17.
4 S. Wold, Pattern Recognition, 8 (1976) 127.

Analytica Chimica Acta, 186 (1986) 185—193
Elsevier Science Publishers B.V., Amsterdam — Printed in The Netherlands

MODELLING AND GRAPHIC INTERPRETATION OF RESPONSE SURFACES IN CHEMICAL ANALYSIS

OLGA GROSSMANN

Akademie der Wissenschaften der DDR, Zentralinstitut für Festkörperphysik und Werkstofforschung, DDR-8027 Dresden (German Democratic Republic)

(Received 31st December 1985)

SUMMARY

The complicated effects of several factors on an analytical signal can be studied comprehensively only by an experimental design in which the additive and non-additive effects of these factors are included in one experimental run, with simultaneous variation of the values of all factors. From the law of mass action, it is shown that systems in which the analytical signal is produced by a species formed during a chemical reaction (i.e., for spectrophotometry) can be described by a model based on quasi-linear regressions with squares and products of variables. The regression coefficients can be evaluated by means of factorial designs at three levels. Interpretation of results in the case of two or three independent variables is simplified by using a graphic method in which the complex effects of factors on the dependent variable are represented as an empirical response surface. In the case of regression with three independent variables, the response surface is four-dimensional; its dimensionality is reduced to three by several three-dimensional representations. The shapes of the response surfaces described by the response functions and the adequacy of the models are discussed.

Establishment of the optimum conditions for a chemical analysis requires consideration of the influence of many different factors on the analytical signal (e.g., the concentrations of sample components, salts and reagents in the solution, the pH value and the reaction time). Experimental design is needed for comprehensive investigation of those effects. A study of the interaction of other sample components with the component to be determined will be considered here for comparison of the classical one-variable-at-a-time approach and the method of experimental design. Quantitative evaluation of the influence of sample composition on the analytical signal, i.e., evaluation of one source of systematic errors, is important in ensuring accurate results.

Estimation of the effects of all the sample components on the analytical signal was discussed by Neiman [1]. A sample containing M_i ($i = 1, 2, \ldots R$) elements will be considered, where M_1 is the element to be determined. The influence of elements M_2—M_R on the analytical signal, A, of M_1 is usually studied by the one-variable-at-a-time method, e.g., signal A of M_1 is measured first in the absence (A_0) and then in the presence (A_i) of a definite amount of element M_i, keeping the concentration of all the other elements

0003-2670/86/$03.50

constant; only rarely is the influence of M_i tested at several concentrations of M_1. If the signal of M_1 is not changed, then it is assumed that M_i does not affect the determination of M_1. This conclusion is correct only if the statistical estimation at a defined probability level is done by the t-test [2]:

$$t = [|\bar{A}_0 - \bar{A}_i|/\bar{s}]\ [n_0 n_i/(n_0 + n_i)]^{1/2} < t_{\mathrm{Tab}}\ (P, f)$$

$$\bar{s}^2 = (s_0^2 f_0 + s_i^2 f_i)/(f_0 + f_i); f = n_0 + n_i - 2$$

If the first equation is valid over the whole concentration range of M_i, then use of probability P indicates that M_i does not interfere with the determination of M_1. Estimates of the effects of elements M_2—M_R on the signal of M_1 in this manner give correct conclusions only when the effects of elements M_2—M_R are additive, i.e., these elements do not interact with each other. If there is interaction, the one-variable-at-a-time method leads to erroneous conclusions.

Experimental design is effective in solving such problems. By means of simultaneous variation of all the investigated variables in one run of experiments, it is possible to estimate which factors affect the analytical signal and to what extent, and whether or not the effects are additive. The theoretical and practical aspects of experimental design have been discussed comprehensively [3—9]. A vital part of the application of experimental design is formulation of a mathematical model (response function) which will describe adequately the empirical relationship between the dependent variable and several continuous independent variables (factors).

In the present paper, the demands of the mathematical model

$$y = f(x_1, x_2, \ldots x_R)$$

will be discussed for cases in which the analytical signal A is produced by a species formed in the course of a chemical reaction. That can mean the formation of a coloured complex in solution (spectrophotometry) or the generation of free atoms after thermal dissociation of compounds in a hot flame (atomic absorption spectrometry). Other sample components can affect the formation of those species. The simultaneous variation of independent variables over a limited experimental region (factor space) is done by orthogonal design (see, e.g., [3, 4]). The above $y = f(x)$ function describes a response surface in a $(R + 1)$-dimensional space. Graphic representation of the empirical response surface by means of experimental results illustrates the effects of factors which appear as coefficients in the regression.

APPROXIMATION OF EMPIRICAL RELATIONSHIP BETWEEN THE ANALYTICAL SIGNAL AND THE CONCENTRATION OF COMPONENTS BY MEANS OF QUASI-LINEAR REGRESSION

The existence of an unambiguous connection between the analytically useful signal y of an element and its concentration, $y = f(C_M)$, in the given sample is a prerequisite for any quantitative method, be it based on titrimetry,

polarography, spectrophotometry, fluorimetry or another technique. In inorganic analysis, spectrophotometry is usually based on a coloured complex formed by association of n ligand molecules L^{l-} and metal ion M^{m+}

$$M^{m+} + nL^{l-} \rightleftharpoons ML_n^{(m-ln)+}$$

The existence of complexes with less than n ligand molecules in the solution must be considered. The individual stability constant of complexes ML_i (in the following, the charges of complexes will be neglected) can be calculated from the law of mass action: $k_i = [ML_i]/[ML_{i-1}]\ [L]$ and the overall stability constant is $\beta_n = k_1\ k_2 \ldots k_n = [ML_n]/[M]\ [L]^n$. From this,

$$[ML_n] = \alpha y = \beta_n\ [M]\ [L]^n \qquad (1)$$

where y is the signal related to ML_n, and α is the proportionality factor. From the relationship $y = f\ (C_M)$, the total concentrations of components must be brought into connection with the equilibrium concentration of ML_n. If the sum of the concentrations of bound metal and ligand can be calculated:

$X = [ML] + [ML_2] + \ldots + [ML_n]$ and $Y = [ML] + 2\ [ML_2] + \ldots + n\ [ML_n]$,

it follows that

$[M] = C_M - X$ and $[L]^n = (C_L - Y)^n$.

Then, from Eqn. 1,

$$y = (\beta_n/\alpha)\ (C_M - X)\ (C_L - Y)^n \qquad (2)$$

In addition to the formation of the analytically useful ML_n, other reactions between metal ion M^{m+} and other components of the solution can affect the equilibrium of the required metal/ligand reaction. Such reactions must be considered in the overall equilibrium equation, but frequently some of them are unknown. It is then impossible to calculate explicitly the correlation between the analytical signal (response value), y, and the concentration of the reaction components in a given system.

Equations similar to Eqn. 2 are nonlinear and therefore their solution towards $[ML_n]$ is impossible. Not only the linear members, but also the products and powers of independent variables can influence the analytical signal. A quasi-linear regression (linear in coefficients b but not in variables x_i) of the type

$$y = b_0 + \sum_{i=1}^{R} b_i x_i + \sum_{i \neq j=1}^{R} b_{ij} x_i x_j + \sum_{i=1}^{R} b_{ii} x_i^2 \qquad (3)$$

(where $x_1, x_2, \ldots, x_R$ are factors related to C_M, C_L, $C_{M_2}, \ldots, t$) can be considered as a suitable model for describing chemical systems in which several reactions affect the formation of the species producing the analytical signal. To explore such relationships over a limited region of factor space, a factorial design at three levels must be applied without any mixing of variables [10]. The regression with quadratic terms adequately describes chemical systems

in most cases. The inclusion of terms with higher power into the regression on increasing the number of levels in the design requires a considerable increase in the number of experiments, m ($m = R^k$ where k is the number of levels). However, the increase in information is often small in comparison with the increase of experimental effort. For this reason, these regressions are rarely applied as models.

A model which describes the chemical system formulated as a quasi-linear regression, is necessarily a mathematical approximation. The laws of kinetics and thermodynamics which govern the motion and state of the system are contained in the model, only vaguely rather than explicitly. Estimates of which factors are important can be made only from prior information or from preliminary experiments. This information determines the size and the construction of design. The changes of the response value y from observation to observation during experimental testing of the design result from the action and interaction of all the laws governing the chemical system. But the results obtained by means of experimental design are inadequate for conclusions to be drawn about the true algebraic form of the relationships between all the factors in the system.

Of course, under certain conditions, a particular law can be chosen in order to prove its mode of action. For example, if it can be assumed that only one reaction takes place in a given system, then the stoichiometric coefficients (e.g., in the above M/L reaction) can be examined. The logarithmic form of Eqn. 1 is

$$\log y = \log (\beta_n/\alpha) + \log [\mathrm{M}] + n \log [\mathrm{L}],$$

and the coefficients of this regression are also the stoichiometric coefficients of the reaction.

REGRESSION AND PRESENTATION OF RESPONSE SURFACES FOR THE FACTORIAL DESIGN WITH TWO AND THREE FACTORS AT THREE LEVELS

A factorial design at three levels enables all the coefficients in the regression Eqn. 3 to be determined. Their calculation is done by the least-squares method [4, 9]. Estimates of the statistical significance of coefficients are obtained by the t-test, and the adequacy of the applied model with the empirical relationship is proved by the F-test.

The experimental examination based on a design with two factors at three levels (Table 1) in coded factor space (Fig. 1) makes it possible to estimate the regression coefficients:

$$y = b_0 + b_1x_1 + b_2x_2 + b_{11}x_1^2 + b_{22}x_2^2 + b_{12}x_1x_2 \qquad (4)$$

In the following treatment, $\bar{y}$ represents the experimental response and $\hat{y}$ the response calculated from the empirical polynomial.

If all the actions and interactions of the two factors represented by the coefficients of the empirical polynomial are known, then a conclusion about

TABLE 1

Factorial design with two factors at three levels

No.	n_j	x_1	x_2	$\bar{y}$	No.	n_j	x_1	x_2	$\bar{y}$
1	n	+1	+1	$\bar{y}_1$	6	n	0	+1	$\bar{y}_6$
2	n	+1	−1	$\bar{y}_2$	7	n	0	−1	$\bar{y}_7$
3	n	−1	+1	$\bar{y}_3$	8	n	+1	0	$\bar{y}_8$
4	n	−1	−1	$\bar{y}_4$	9	n	−1	0	$\bar{y}_9$
5	m	0	0	$\bar{y}_5$					

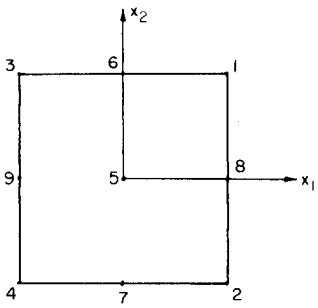

Fig. 1. Coded factor space and the arrangement of observations for factorial design with two factors. The experimental factor space is coded to the design factor space with zero in the centre and equal distances from the centre to each space corner with edge length $l = 2$.

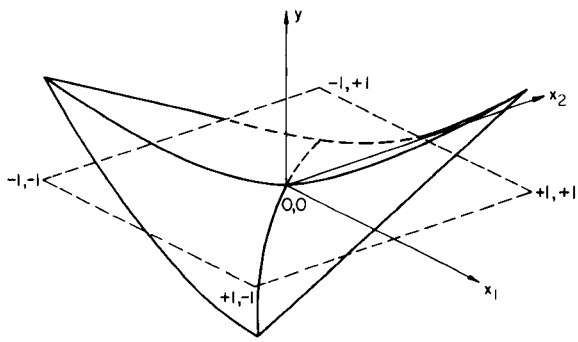

Fig. 2. Shape of response surface for the response function $y = x_1^2 + 3x_1x_2$.

the shape of the response surface can be reached. If only the linear terms in the empirical polynomial are actually valid, then the response surface will be a plane lying under an angle to the x_1 x_2 plane which depends on the values of coefficients b_1 and b_2. If the quadratic terms and/or x_1x_2 term are valid, then the shape of the surface will be nonlinear. Thus, if b_{11} and/or b_{22} are positive, the surface will show a minimum; if b_{11} and/or b_{22} are negative, the surface will have a maximum; and if b_{11} is negative and b_{22} is positive (or reserved), or b_{12} only is valid, a saddle-shaped surface will be obtained. If several terms are present in the empirical regression, then the response surface will be of mixed form, but this form will be decisively governed by the term with the highest coefficient.

Because the experimental points (observations) are put into the design in those positions where all the independent variables take the value +1, 0 or −1, the terms with higher odd powers appear in the regression as linear terms and the terms with higher even powers appear as quadratic terms. For this reason, the quadratic regression represents a good approximation of higher-order polynomials.

The dominant shape of the response surface can be recognized from the form of the diagonals which connect the points $\bar{y}_1$, $\bar{y}_5$, $\bar{y}_4$ and $\bar{y}_2$, $\bar{y}_5$, $\bar{y}_3$ (Table 1, Fig. 1). For this purpose, only observations 1—5 in the design of Table 1 need to be obtained experimentally. Statistical estimates of the significance of the differences between the $\bar{y}$ values must be done by means of the t-test (see above). If the diagonals are linear, then the response surface will be a plane, and can be comprehensively described by observations 1—5 (Table 1). If the diagonals are nonlinear, so that the response surface is also nonlinear, then the next corner points of the factor space can be connected, if the observations at the middle of the edges are obtained experimentally (points 6—9 in Table 1). Only in this case is it possible to produce a perspective graphic of this response surface. This graphic can be useful by delineating the ranges on the response surface which are appropriate for solution of the problem involved. This empirical response surface can be compared with the polynomial surface $\hat{y}(x_1, x_2)$. In this way, the adequacy of the model can also be estimated. Examples of graphic representation of the response surfaces are given in Figs. 2 and 3.

A further possibility for estimating the adequacy of the model by the empirical relationship is provided by consideration of the shape of lines which connect the $\bar{y}$ values along the edges of the factor space. The two lines of the opposite edges [e.g., the lines connecting the points (+1, +1), (+1, 0), (+1, −1) and (−1, +1), (−1, 0), (−1, −1)] will show the same basic shape if the quadratic regression describes adequately the empirical relationship; examples are given in Table 2. If these lines do not show the same basic shape (e.g., if one is concave and the other convex), then different mathematical relationships must be valid within the factor space. This means that, in different areas of the factor space, the empirical relationship must be approximated by different polynomials. In such cases, the calculated polynomial provides an inadequate description of the empirical relationship. If a better approximation is demanded, then the factorial space must be separated into

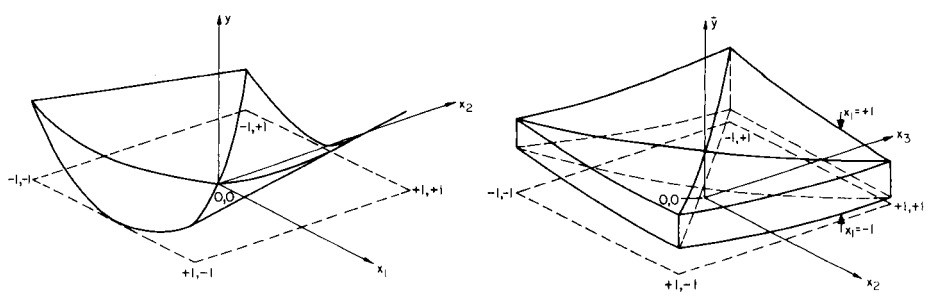

Fig. 3. Shape of response surface for the response function $y = 3x_1^2 + x_1x_2$.

Fig. 4. Shape of response space for the response function $y = f(x_1, x_2, x_3)$ with the condition $x_1 = \pm 1$.

TABLE 2

Form of diagonals and of side lines of response surfaces adequately described by quadratic polynomials

Coefficients present in the polynomial	Shape of lines			Shape of response surface
	Diagonals	Parallel side lines		
		1st pair	2nd pair	
b_1, b_2	Straight	Straight	Straight	Plane
b_{12}	One convex, one concave	Straight	Straight	Minimax
b_{11} or b_{22} positive or negative	Concave or convex	Straight	Concave or convex	Stationary minimum or maximum
b_{11} and b_{22} positive	Concave	Concave	Concave	Minimum
b_{11} and b_{22} negative	Convex	Convex	Convex	Maximum
b_{11} positive and b_{22} negative[a]	Concave and convex[a]	Convex or concave	Concave or convex	Saddle-shaped

[a] Or vice versa.

several areas which have to be investigated separately. Representation of the response surface by the experimental values, $\bar{y}$, gives only a rough picture of the real response surface if the factors interaction are not additive and if the function changes within the factorial space. In order to obtain the real picture, additional experiments are required. But here it is necessary to consider carefully the experimental effort against the possible increase in information.

A design with three factors at three levels (Table 3, observations 1—15) enables the coefficients in the following polynomial to be calculated:

$$y = b_0 + b_1x_1 + b_2x_2 + b_3x_3 + b_{11}x_1^2 + b_{22}x_2^2 + b_{33}x_3^2 + b_{12}x_1x_2 + \\ + b_{13}x_1x_3 + b_{23}x_2x_3 \qquad (5)$$

The response surface described by the function with three independent variables lies in a four-dimensional space and therefore cannot be presented. But if one of the independent variables, x_i, assumes a constant value ($x_i = +1$ or -1) and if this constant is put into the regression $y = f(x_1, x_2, x_3)$, then the three following pairs of functions are obtained: $y_{1+} = f_{1+}(x_2, x_3)$, $(x_1 = +1)$; $y_{1-} = f_{1-}(x_2, x_3)$, $(x_1 = -1)$; $y_{2+} = f_{2+}(x_1, x_3)$, $(x_2 = +1)$; $y_{2-} = f_{2-}(x_1, x_3)$, $(x_2 = -1)$; $y_{3+} = f_{3+}(x_1, x_2)$, $(x_3 = +1)$; $y_{3-} = f_{3-}(x_1, x_2)$, $(x_3 = -1)$.

If these operations are adapted to the polynomial (Eqn. 5), then the following three pairs of polynomials are obtained:

TABLE 3

Factorial design with three factors at three levels

No.	x_1	x_2	x_3	No.	x_1	x_2	x_3
1	+1	+1	+1	16	+1	+1	0
2	+1	+1	−1	17	+1	−1	0
3	+1	−1	+1	18	−1	+1	0
4	+1	−1	−1	19	−1	−1	0
5	−1	+1	+1	20	+1	0	+1
6	−1	+1	−1	21	+1	0	−1
7	−1	−1	+1	22	−1	0	+1
8	−1	−1	−1	23	−1	0	−1
9	+1	0	0	24	0	+1	+1
10	−1	0	0	25	0	+1	−1
11	0	+1	0	26	0	−1	+1
12	0	−1	0	27	0	−1	−1
13	0	0	+1				
14	0	0	−1				
15	0	0	0				

$$y_{1+} = (b_0 + b_1 + b_{11}) + (b_2 + b_{12})x_2 + (b_3 + b_{13})x_3 + b_{22}x_2^2 + b_{33}x_3^2 + \\ + b_{23}x_2x_3 \quad (6)$$

$$y_{1-} = (b_0 - b_1 + b_{11}) + (b_2 - b_{12})x_2 + (b_3 - b_{13})x_3 + b_{22}x_2^2 + b_{33}x_3^2 + \\ + b_{23}x_2x_3 \quad (7)$$

$$y_{2+} = (b_0 + b_2 + b_{22}) + (b_1 + b_{12})x_1 + (b_3 + b_{23})x_3 + b_{11}x_1^2 + b_{33}x_3^2 + \\ + b_{13}x_1x_3 \quad (8)$$

$$y_{2-} = (b_0 - b_2 + b_{22}) + (b_1 - b_{12})x_1 + (b_3 - b_{23})x_3 + b_{11}x_1^2 + b_{33}x_3^2 + \\ + b_{13}x_1x_3 \quad (9)$$

$$y_{3+} = (b_0 + b_3 + b_{33}) + (b_1 + b_{13})x_1 + (b_2 + b_{23})x_2 + b_{11}x_1^2 + b_{22}x_2^2 + \\ + b_{12}x_1x_2 \quad (10)$$

$$y_{3-} = (b_0 - b_3 + b_{33}) + (b_1 - b_{13})x_1 + (b_2 - b_{23})x_2 + b_{11}x_1^2 + b_{22}x_2^2 + \\ + b_{12}x_1x_2 \quad (11)$$

Each of these polynomials describes a response surface in three-dimensional space. Observations 1—4 and 9 in the design in Table 3 ($x_1 = +1$) enable the contours and the curvature of one empirical response surface to be represented and compared with the response surface resulting from Eqn. 6. Observations 5—8 and 10 ($x_1 = -1$) enable the position of the corresponding surface (Eqn. 7) to be outlined. When these response surfaces have been visualized, the next corner points can be connected by straight lines provided that coefficients b_i and b_{ij} in the polynomial differ from zero. If coefficients b_{ii} or

b_{ii} and b_{ij} are present in the polynomial, then the four corner points are no longer sufficient for recognizing the shape of the response surface. The design in Table 3 must then be expanded by observations 16–27.

The two corresponding response surfaces (Eqns. 6 and 7), with the four planes delineating the factor space and parallel to the y-axis, form a space within which the response values y will lie if the factors x_1, x_2 and x_3 are varied between +1 and −1. The distances between the corresponding response surfaces reflect the influence of the variable being kept constant ($x_i = \pm 1$). Figure 4 shows, as an example, a response space for the function $y_{\pm 1} = f(x_2, x_3)$ with $x_1 = \pm 1$. The same considerations are valid for the two other pairs of response functions (Eqns. 8–11).

In this way, the response surface lying in a four-dimensional space can be reduced to three different response surfaces in three-dimensional space ($y_{\pm 1}$, x_2, x_3), ($y_{\pm 2}, x_1, x_3$) and ($y_{\pm 3}, x_1, x_2$). In the case of a response function with four independent variables, the response surface lies in a five-dimensional space. In order to reduce its dimensionality to three, representation of twelve three-dimensional spaces is required. The number of observations then increases to $3^4 = 81$. If prior information suggests that more than three independent variables may be affecting the data, it is reasonable first to study the ranking order of factors by means of fractional factorial design, and then to arrange the variables so as to obtain maximum information about conditions in a given system.

Practical applications of the proposed method will be discussed in a subsequent paper.

REFERENCES

1 E. Ya. Neiman, Zh. Anal. Khim., 25 (1980) 1647.
2 K. Doerffel, Statistik in der Analytischen Chemie, VEB Deutscher Verlag für Grundstoffindustrie, Leipzig, 1982, p. 129.
3 V. V. Nalimov and N. A. Chernova, Statisticheskie Metody Planirovaniga Ekstremalnykh Eksperimentov, Nauka, Moscow, 1965.
4 G. E. P. Box, W. Hunter and J. S. Hunter, Statistics for Experimenters, Wiley, New York, 1978.
5 N. L. Johnson and F. C. Leone, Statistics and Experimental Design in Engineering and the Physical Sciences, Vol. II, Wiley, New York, 1977.
6 A. M. Ginberg, J. W. Granowski, N. J. Fedotowa and W. S. Kalmuzki, Optimierung Technologischer Prozesse in Galvanotechnik, VEB Verlag Technik, Berlin, 1979.
7 E. Scheffler, Einführung in die Praxis der Statistischen Versuchsplanung, VEB Deutscher Verlag für Grundstoffindustrie, Leipzig, 1974.
8 S. M. Ermakov (Ed.), Matematicheskaja Teoriya Planirovaniya Eksperimenta, Nauka, Moscow, 1983.
9 R. A. Fisher, The Design of Experiments, Oliver and Boyd, Edinburgh, 1960.
10 R. M. De Baun, Technometrics, 1 (1959) 1.

Analytica Chimica Acta, 186 (1986) 195—203
Elsevier Science Publishers B.V., Amsterdam — Printed in The Netherlands

APPLICATION OF THE k_0 STANDARDIZATION METHOD IN REACTOR NEUTRON ACTIVATION ANALYSIS OF STANDARD STEELS AND FLY ASH

A. DEMETER

Central Research Institute for Chemistry, Hungarian Academy of Sciences, P.O. Box 17, H-1525 Budapest (Hungary)

(Received 30th January 1986)

SUMMARY

The method of k_0 standardization is suitable for routine multi-element determinations by reactor neutron activation. Investigation of NBS steel standards showed the systematic error of the method to be less than 3%. Numerical evaluation of the spectra was found to be fast and convenient. Fourteen elements in the steel samples were determined; for nine, the standard deviation was less than 4%. Thirty seven elements were determined in NBS SRM-1663a Coal Fly Ash; agreement with certified values was again very good.

The analysis of industrial materials by activation methods has become of greater interest recently, but steel samples are rarely analyzed by reactor neutron activation analysis (n.a.a.). Activated steel samples have high activity which makes measurements more difficult. Three types of application have been reported. First, the total analysis of steels was done by chemical separation after irradiation [1, 2]; about sixteen elements could be determined. Special microcomponents of steels were also determined with or without chemical separation [3, 4]. The third field of interest was the composition of individual microspheres [5, 6]. Somewhat later, two papers [7, 8] dealt with measurements of eleven elements in iron and spectral iron samples by reactor n.a.a.

The aim of the present work was to study the possibilities of applying modern reactor n.a.a. methods to the analysis of steel matrices. Another purpose was to optimize the measurement parameters (weight and time), and to check the k_0 standardization method for industrial samples. These steel measurements are suitable for industrial purposes because the types of steels examined are used in the construction of nuclear power plants, and some easily measurable microcomponents (As, Co, Cu, Mn, Sb, Ta, W, etc.) can play an important role in the transport of radioactivity or can cause radiation damage. The experimental possibilities and detailed descriptions of the k_0 method have been described elsewhere [9, 10].

0003-2670/86/$03.50

EXPERIMENTAL

The k_0 standardization method includes the measurement of three co-irradiated comparator isotopes (^{198}Au, ^{95}Zr, ^{97}Zr) to monitor the specific count rate of the comparator, $A_{sp}(^{198}\text{Au})$, and to evaluate the subcadmium to epicadmium neutron flux ratio (f) and the α parameter, which characterizes the epithermal flux deviation from the E^{-1} law (neutron flux $\approx E^{-(1+\alpha)}$). The concentration of element x (c_x) in the sample is determined by counting the γ-photons at one line (x_i) emitted by the isotope formed, and can be calculated as follows:

$$c_x = [A_{sp}(x_i)/A_{sp}(\text{Au})k_{0,\text{Au}}(x_i)]\,[f + Q_{0,\text{Au}}(\alpha)/f + Q_{0,x}(\alpha)]\,[\epsilon_p(411.8\text{ keV})/\epsilon_p(x_i)]$$

where A_{sp} is the specific count rate calculated from the peak area, the irradiation time, the decay time, the measuring time, the half-life of the isotope formed (or half-lives in more complicated cases of activation depending on the decay mechanism), and the weights of the comparator and sample. The $k_{0,\text{Au}}(x_i)$ value is an experimentally measured composite nuclear constant, which can be calculated (less accurately) from nuclear data in the literature:

$$k_{0,\text{Au}}(x_i) = M_{\text{Au}}\theta_x\sigma_{0,x}\gamma_{x_i}/M_x\theta_{\text{Au}}\sigma_{0,\text{Au}}\gamma_{\text{Au}}$$

where M is the atomic mass, θ is the isotopic abundance, σ_0 is the 2200 ms^{-1} (n, γ) cross-section, and γ is the absolute γ-intensity at the measured peak; $Q_0(\alpha)$ denotes the experimentally measured ratio of the resonance integral to the thermal cross-section corrected with the α parameter; ϵ_p shows the full-energy peak detection efficiency.

Irradiation conditions and counting

Samples were irradiated in the WWRM reactor at the Central Research Institute for Physics, Budapest. The conditions of irradiation and measurement together with the parameters of neutron fluxes are summarized in Table 1. The samples were 200-μm discs with a diameter of 5 mm. Fly ash samples were handled according to recommended procedures and were then covered by filter paper or aluminium foil for short or long irradiations, respectively.

The comparators were 3 μg of gold (15 μg cm^{-2}) in an aluminium pellet and a zirconium foil. Gold standards were prepared very carefully from gold nitrate with an overall imprecision of better than 0.5%. Burn-up and neutron shielding corrections were made when required.

A Ge(Li) Canberra system with a 4096-channel analyzer was used for counting. The resolution of the detector was 1.72 keV at the 1332.5-keV γ-peak of ^{60}Co. The differential nonlinearity of the analyzer was 0.65%. The distance between the sample and the detector was 15 cm; true coincidence correction was not used. Dead-time correction was done by the pulser

TABLE 1

Summary of conditions for irradiation and measurement used in the reactor n.a.a. determinations

Sample	NBS 1163A		NBS 408a		NBS 442	
Irradiation type	short	long	short	long	short	long
Sample weight (mg)	10	10	10	20	3	20
Number of samples	5	5	5	5	5	5
Irradiation time (min)	5	540	5	540	5	540
Decay time a	3 min	2 d	3 min	1 d	3 min	1 d
b	5 min	6 d	20 min		20 min	
c	20 min	6 mos.[a]		1—2 mos.		1—2 mos.
d		10 mos.				
Measuring time a	10 s	1 h	10 min	1 h	10 min	1 h
b	10 min	2 h	60 min		60 min	
c		2 d		2 d		2 d
d		2 d				
Subcadmium neutron flux			3.1—4.8 × 10^{13} ns^{-1} cm^{-2}			
Subcadmium to epicadmium flux ratio			32	20		
Subcadmium to fast neutron flux ratio			5.6	3.2		
α			0.015	0.005		

[a]Months.

method. (At high count rates, a BNC DB-2 random pulser was used but at low rates a BNC PB-4 pulser was applied.) No pile-up correction was applied.

Evaluation of data

The spectra were deconvoluted by the Hypermet program [11] run on a R40 (IBM 360) computer. The concentrations of elements were evaluated by another program called SPECTRUM written for a TPA-1140 (PDP 11-40) computer. The final concentrations and precisions were calculated from independent parallel data (c_i) and their known random error σ_i (derived mainly from Poisson statistics of radiation) in the following way:

$$\bar{c} = \sum_i c_i(\sigma_i^2 + \sigma^2)^{-1} / \sum_i (\sigma_i^2 + \sigma^2)^{-1}$$

$$s^2(\bar{c}) = \{\sum_i [(c - \bar{c})^2(\sigma_i^2 + \sigma^2)^{-1}]\} / [n(n-2) \sum (\sigma_i^2 + \sigma^2)^{-1}]$$

$$+ \sum_{i=k_0, Q_0, \lambda} (\partial c / \partial(i))^2 s^2(i)$$

where σ^2 is an unknown variance which could originate from various sources, e.g., in inhomogeneity of the sample. σ^2 was calculated with the help of the equation:

$$[\sum_i (\sigma_i^2 + \sigma^2)^{-1}]^{-1} = [\sum_i (c_i - \bar{c})^2(\sigma_i^2 + \sigma^2)^{-1}] / (n-2) \sum_i (\sigma_i^2 + \sigma^2)^{-1}$$

If iterative calculation gave a negative variance, the left side of the equation was used with the value of $\sigma^2 = 0$ for further calculation. The procedure will be presented in more detail in a subsequent publication. In the Tables, standard deviations of the sample mean values are given at 95% significance level.

RESULTS AND DISCUSSION

NBS spectrographic Steel standards

On application of a short irradiation time, most of the activity came from the ^{56}Mn isotope. For this reason, two measurements were made, one as early as possible to measure the activity of isotopes with short half-lives (^{28}Al, ^{66}Cu, ^{50}Ti, ^{51}V), and another to measure the activity of the ^{65}Ni isotope with a longer measuring time to obtain better counting statistics. In the case of long irradiations, the two measurements were as follows: the first was made after one day when the ^{56}Mn activity had decreased by a factor of one thousand and was then lower than that of ^{76}As and ^{187}W; the second was done after one month when the highest activity was produced by ^{60}Co and ^{51}Cr isotopes. Interferences caused by fast neutrons could be neglected and there were no problems from spectral interferences.

The analysis of stainless steel samples gave the concentrations of eight elements (As, Co, Cr, Fe, Mn, Mo, V, W) with an error of 1—4%. In the case of four elements (Cu, Ni, Sb, Ta), uncertainties were higher (5—20%), and the results obtained for Au, Al and Ga could be taken only as approximate values. Errors for the carbon steel sample were 1—4% for As, Co, Cr, Cu, Fe, Mn, Mo, Sb, W, and 5—20% for Al, Au, Ga and V; the concentration of nickel had a high standard deviation. Significant inhomogeneity was found in the case of Al, Au and Ga. As can be seen in Fig. 1 and Table 2, excellent agreement was found with the certified values of the NBS reference materials.

When the long irradiation was used, the ^{58}Co isotope from ^{58}Ni$(n, p)^{58}$Co by fast neutron activation could be easily measured at 810.8 keV. Application of the ^{54}Mn isotope from ^{54}Fe$(n, p)^{54}$Mn as an internal comparator for the fast neutron flux, which facilitated measuring the concentration of nickel, eliminated the second measurement needed with the short irradiation time. An experimental value for k_0, ^{54}Mn(^{58}Co) was obtained which was almost independent of irradiation conditions and showed no change for several months. This k_0 value was calculated from

$$k_0 = [A_{sp}(^{58}\text{Co})/A_{sp}(^{54}\text{Mn})]\,[\epsilon_p(834.8\ \text{keV})/\epsilon_p(810.8\ \text{keV})]$$

where the A_{sp} values were found from the activity of co-irradiated iron and nickel foils. In the case of ^{58}Co, a high burn-up effect was observed and had to be taken into consideration in deriving the $A_{sp}(^{58}\text{Co})$ value. This k_0 value depends on the shape of the fast neutron spectrum of the reactor, and must therefore be evaluated in each laboratory.

By using the proposed comparator method, the lowest measurable quantities of nearly 30 elements can be calculated easily without additional

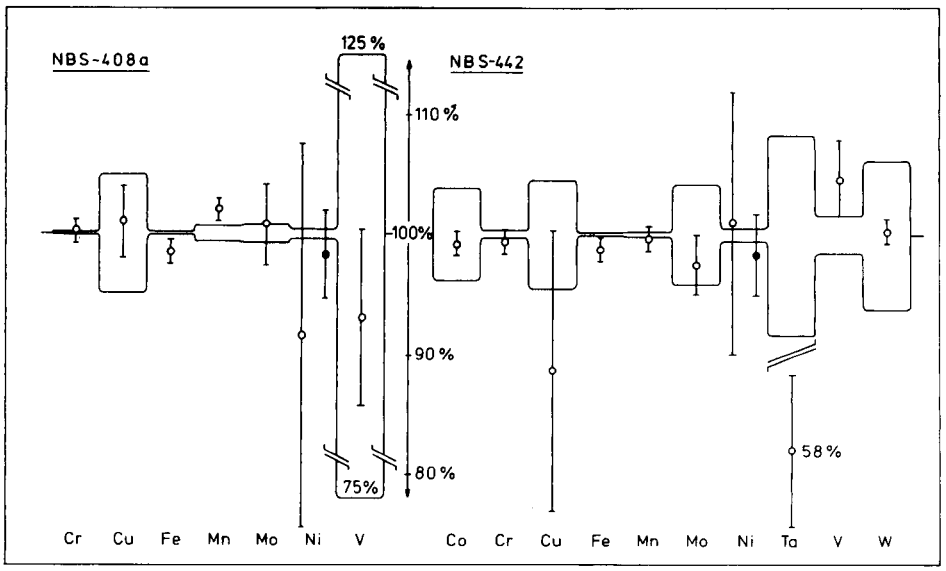

Fig. 1. Comparison of results for the NBS 408a and NBS 442 steel samples, showing the ratios of results from this work to the NBS values taken as 100%. The symmetrical rectangles around 100% show the uncertainties of NBS data; the bars indicate the errors of the present measurements (95% significance level). The full points denote data for nickel from the reaction $^{58}Ni(n, p)^{58}Co$.

TABLE 2

Concentrations of elements in the NBS 408a Spectrographic Steel and NBS 442 Spectrographic Stainless Steel

Element	Mean concentration of element (%)			
	NBS 408a		NBS 442	
	This work[a]	Certified[b]	This work[a]	Certified[b]
Al	0.0265(19)		0.0058(40)	
As	0.00971(1.0)		0.00765(2.0)	
Au	0.00001(12)		0.000012(21)	
Co	0.0198(1.0)		0.129(1.0)	0.13
Cr	0.0656(1.0)	0.655	16.0(1.0)	16.1
Cu	0.101(3.0)	0.10	0.0975(12)	0.11
Fe	95.5(1.0)	~96.9	69.7(1.0)	~70.5
Ga	0.00171(6.0)		0.0077(60)	
Mg	<0.18		<1.1	
Mn	0.775(1.0)	0.76	2.87(1.0)	2.88
Mo	0.0655(3.4)	0.065	0.117(2.5)	0.12
Nb	<0.12		<0.6	0.032
Ni (n, γ)	1.1(19)	1.20	10.0(11)	9.9
Ni (n, p)	1.18(3.7)	1.20	9.74(3.4)	9.9
Sb	0.00143(2.0)		0.00037(16)	
Ta	<0.0002		0.00035(6.3)	0.0006
Ti	<0.05		<0.16	0.002
V	0.00186(7.4)	0.002	0.0335(3.2)	0.032
W	0.000825(3.2)		0.0802(1.0)	0.08

[a]With relative standard deviation (%) in parentheses. [b]Certificates of Analysis, Spectrographic Steel Standards 401 to 430, and Spectrographic Stainless Steel Standards 442 to 444, Office of Standard Reference Materials, National Bureau of Standards, U.S. Department of Commerce, Washington, DC, 1965.

experimental work. As can be seen in Table 2, calculations were done only for some elements (Mg, Nb, Ta, Ti) although they could be done for other elements as well.

Epicadmium n.a.a. of steels did not show any benefits compared to reactor n.a.a.

NBS SRM-1663a Coal Fly Ash

Some corrections had to be made for the reaction of fast neutrons and ^{235}U fission products [12]. Several spectral interferences were observed. The correct area of an investigated peak "a", $N(a)$, which suffered interference from a peak "b" emitted by another isotope was calculated from

$$N(a) = N(a + b) - N(c)k_{0,Au}(b)\epsilon_p(b)/k_{0,Au}(c)\epsilon_p(c)$$

where "c" is a readily measurable peak from the interfering isotope. If the k_0 values were not available, the appropriate γ-ray nuclear data were used [13]. The most important interferences and the correction factors are shown in Table 3. The interfering effects of microcomponents of covering materials (Ag, Au, Ce, Co, Cr, Sb, Sc, Zn from Pierce P00008-m5N3 aluminium foil; Al, Cl, Mn, Na, from Whatman 41 filter paper) were taken into consideration.

In all, 37 elements were determined, eleven of which were not given by

TABLE 3

Spectral interferences

Isotope	Energy (keV)	Interfering isotope	Interfering energy (keV)	Reference energy (keV)	$\frac{k_{0,Au}(b)\epsilon_p(b)}{k_{0,Au}(c)\epsilon_p(c)}$
^{170}Tm	84.3	^{182}Ta	84.6	1221.4	0.576
^{75}Se	136.0	^{181}Hf	133.0	482.0	1.535
	264.0	^{182}Ta	264.1	1221.4	0.591
^{141}Ce	145.4	^{59}Fe	142.6	1099.2	0.117
		^{175}Yb	144.8	396.3	0.118
		^{233}Pa	145.4	311.9	0.024
^{51}Cr	320.1	^{147}Nd	319.2	91.1	0.040
				531.0	0.225
		^{233}Pa	320.0	311.9	3.7×10^{-4}
		^{177m}Lu	319.0	208.4	0.103
				378.5	0.431
^{175}Yb	396.3	^{233}Pa	398.6	311.9	0.029
		^{147}Nd	398.2	531.0	0.089
^{122}Sb	564.1	^{134}Cs	563.3	604.7	0.088
		^{152}Eu	564.0	1408.1	0.057
^{65}Zn	1115.5	^{160}Tb	1115.1	879.4	0.041
^{46}Sc	1120.5	^{182}Ta	1121.3	1221.4	1.390
^{154}Eu	1274.5	^{160}Tb	1271.9	879.4	0.176

TABLE 4

Concentration of elements in NBS SRM-1663A standard

Element	Mean concentration of element ($\mu g\ g^{-1}$ unless % indicated)[a]						
	This work	n[b]	Xilei [13][c]	Certified[d]	Garcia [14][c]	Vogt [15][c,e]	Failey [16][e]
Ag	14.1(28)	7					
Al (%)	14.4(1.9)	5		(14)	14.2(2.2)[f]	14.0(1.4)[f]	14.0(1.4)[f]
As	145(6.2)	14	151.7(0.3)[f]	145(10.3)		146(1.4)	
Ba (%)	0.149(7.6)	11	0.136(1.5)	(0.15)	0.15(6.0)		
Br	2.36(30)	4					
Ca (%)	1.17(11)	5		1.11(0.9)	1.12(6.9)	1.29(6.3)	1.2(17)
Ce	161(1.6)	8	155(0.6)	180(12.5)	183(10.8)	185(2.7)	
Co	43.8(3.1)	32	45.0(0.4)	46(5.5)	46.2(3.8)	45.9(1.5)	
Cr	204(4.0)	5	198(0.5)	196(3.1)	197(6.5)	198(0.5)	
Cs	11.0(5.6)	13	10.1(1.0)	(11)	10.6(10.4)	11.2(4.5)	
Dy	15.2(3.6)	22			16.6(7.7)		
Eu	3.6(7.0)	6	4.1(4.9)	(4)	2.98(11.2)	4.0(5.0)	
Fe (%)	9.0(1.3)	28	9.56(0.5)	9.40(1.1)	9.50(3.2)	9.50(1.6)	9.7(2.1)
Ga	65.2(3.0)	21	58.0(1.0)	(58)			
Hf	7.15(5.4)	10	7.15(2.5)	(7.6)	7.78(10.9)	7.6(2.6)	
In	0.177(5.8)	13					
K (%)	1.84(3.8)	15	1.92(2.6)	1.88(3.2)	1.84(7.4)	1.92(2.1)	1.97(2.0)
La	78.3(1.3)	67	81.7(0.4)		100(23)	90.2(1.0)	
Mg (%)	0.53(18)	4		0.455(2.2)	0.45(11)		
Mn	180(1.8)	28		(190)	191(2.3)	189(1.1)	190(7.9)
Na (%)	0.172(2.3)	27	0.175(0.6)	0.17(5.9)	0.172(2.8)	0.174(4.0)	0.21(29)
Nd	83.7(24)	8	91.0(4.4)				65.6(8.2)
Rb	139(14)	5	137.0(4.4)	131(1.5)	130(2.0)		
Sb	6.2(6.8)	5	6.7(1.5)	(7)	7.8(20)	6.9(4.3)	
Sc	38.0(1.0)	29	40.4(0.5)	(40)	40.6(3.2)	40.3(2.0)	
Se	9.6(5.7)	12	10.3(1.0)	10.3(5.8)			
Sm	15.9(2.7)	9	15.5(0.6)		20(22)	16.6(1.8)	16.0(1.3)
Sr	840(7.0)	6	857(1.0)	830(3.6)	819(6.7)		
Ta	1.94(7.3)	21	1.91(2.0)		2.0(23)		
Tb	2.44(7.6)	14	2.54(2.0)		2.3(29)		
Th	24.7(3.2)	23	24.3(1.2)	24.7(1.2)	24.8(6.5)	24.7(4.9)	
Ti (%)	0.857(4.5)	7		(0.8)	0.806(4.6)	0.832(0.9)	0.84(1.2)
Tm	2.0(25)	3					
U	10.5(9.4)	16	10.1(1.0)	10.2(1.0)	10.2(2.1)	10.4(4.8)	
V	309(7.7)	7		(300)	301(2.6)	289(1.0)	360(11.1)
W	6.2(19)	9	6.0(1.7)				
Yb	7.5(5.9)	19	7.7(1.3)		10(18)		
Zn	231(25)	6		220(4.5)	220(23)		

[a]Relative standard deviation (%) in parentheses. [b]Number of averaged data. [c]Instrumental n.a.a. [d]Certificate of Analysis, National Bureau of Standards, Washington, DC, 1979. Values in parentheses are only tentative. [e]Prompt-gamma activation analysis. [f]Probably 1σ standard deviation.

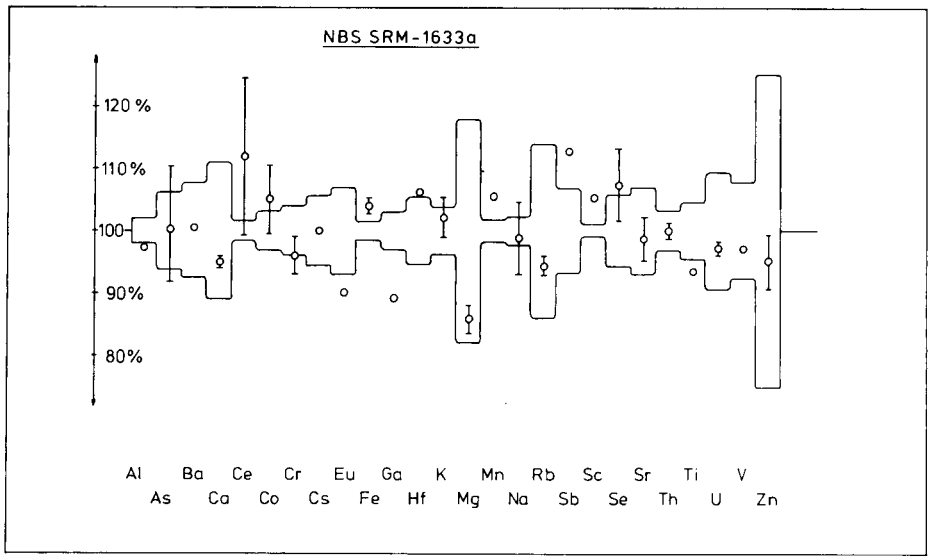

Fig. 2. Comparison of results for the NBS SRM-1633a Coal Fly Ash sample, showing the ratio of NBS data to the results from this work which are taken as 100%. The symmetrical rectangles around 100% show the uncertainties of the present data at 95% significance level. The bars indicate the uncertainties given by NBS; points without bars are data supplied by NBS as information values only.

NBS. The values obtained were in good agreement with the data certified by NBS (Fig. 2 and Table 4). Significant differences were found for only four elements: Ce (12.5/2%), Ga (12.4/3%), Fe (−3.7/1.3%), Mn (−5.2/1.8%). Corrections for spectral interference (^{59}Fe) were difficult in the case of cerium. In the present measurements, the concentrations of iron were systematically lower than the NBS reference values. In view of this, the k_0 value of ^{59}Fe was remeasured both in Budapest and in the Institute for Nuclear Science, State University, Ghent, Belgium; slight but definite differences were found for the k_0 values, possibly owing to under-estimation of the $Q_0 = I_0/\sigma$ value. The k_0 values of ^{51}Cr, ^{181}Hf and ^{46}Sc were measured again and with the use of these data [10], the concentrations of chromium, hafnium and scandium were closer to the NBS certified values.

The author expresses his appreciation to Mr. A. Simonits and Mr. F. De Corte for their helpful cooperation. The technical assistance of Miss S. Upor, Mrs. L. Gál and Miss M. Béres is gratefully acknowledged.

REFERENCES

1 B. A. Thompson and P. D. LaFleur, Anal. Chem., 41 (1969) 852.
2 W. J. Ross, Anal. Chem., 36 (1964) 1114.
3 N. N. Dogadkin, O. I. Kychinskaya, V. I. Tustanovsky and Yu. V. Yakovlev, J. Radioanal. Chem., 29 (1976) 251.

4 R. A. Nadkarni and B. C. Haldar, Talanta, 16 (1969) 116.
5 P. A. Benson and C. E. Gleit, Anal. Chem., 35 (1963) 1029.
6 I. J. Gruverman and W. A. Henninger, Anal. Chem., 34 (1962) 1680.
7 C. De Wispelaere, J. P. Op De Beeck and J. Hoste, Anal. Chim. Acta, 64 (1973) 321.
8 C. De Wispelaere, J. P. Op De Beeck and J. Hoste, Anal. Chem., 45 (1973) 547.
9 A. Simonits, L. Moens, F. De Corte, A. Wispelaere, A. Elek and J. Hoste, J. Radioanal. Chem., 60 (1980) 461.
10 F. De Corte, L. Moens and A. Simonits, Bull. Soc. Chim. Belg., 90(4) (1981) 317.
11 G. W. Phillips and K. W. Marlow, Program HYPERMET for automatic analysis of γ-ray spectra, NRL Memorandum Report 3198, 1976.
12 L. Xilei, Ph.D. thesis, Institute for Nuclear Sciences, Rijksuniversiteit Gent, 1981.
13 L. Xilei, F. De Corte, L. Moens, A. Simonits and J. Hoste, J. Radioanal. Chem., 81/2 (1984) 333.
14 S. R. Garcia, W. K. Hensley, M. M. Minor, M. M. Denton and M. A. Fuka, in R. H. Filby, B. S. Carpenter, R. C. Ragaini (Eds.), Atomic and Nuclear Methods in Fossil Energy Research, Plenum, New York, 1982, p. 133.
15 J. R. Vogt and S. C. Schlegel, J. Radioanal. Chem., 88/2 (1985) 379.
16 M. P. Failey, D. L. Anderson, W. H. Zoller, G. E. Gordon and R. M. Lindstrom, Anal. Chem., 51 (1979) 2209.

Analytica Chimica Acta, 186 (1986) 205—212
Elsevier Science Publishers B.V., Amsterdam — Printed in The Netherlands

THE USE OF A ROBUST RESISTANT REGRESSION METHOD FOR PERSONAL MONITOR VALIDATION WITH DECAY OF TRAPPED MATERIALS DURING STORAGE

JOHN M. THOMPSON

Department of Chemistry, University of Birmingham, P.O. Box 363, Birmingham B15 2TT (Great Britain)

(Received 20th February 1986)

SUMMARY

The stability of trapped materials stored in thermally desorbable monitors is not essential. When monitors are stored in defined conditions and the decay is well characterized, a decay curve and a corresponding correction curve with 95% confidence envelopes can be established. Even if "wild" or outlier data are present, the robust and resistant regression methods described and illustrated enable reasonable curves and confidence envelopes to be obtained. The methods are applied to validation of the Simtec Adsorba Type CM ethylene oxide monitor stored at 4°C after diffusive sampling of 2 ppm (3.6 mg m^{-3}) ethylene oxide for 4 h. The monitors are shown to comply with the U.S. OSHA requirements for up to eleven days of storage.

Laboratory validation of the storage stability of active or passive adsorptive monitors has been concerned with the assumed need for no decay of trapped materials during storage. If, however, the decay can be properly characterized and storage conditions defined, then it should be possible to design experiments to obtain data from which a decay curve and the corresponding correction factor can be obtained as functions of time. From such data, it should be possible to define envelopes around the decay and correction factor curves within particular confidence limits.

The assumption of storage stability has normally been the hypothesis under test. For example, Taylor et al. [1] on behalf of the National Institute of Occupational Safety and Health (NIOSH), suggested a requirement for the sample to be stable for at least five days, so that the sample could be shipped back to a central laboratory for analysis. They proposed a protocol to test that requirement. Recently, the U.K. Health and Safety Executive [2] suggested storing samples for two weeks and comparing them with samples analysed immediately, as part of a protocol for validation of passive samplers. Cox and Brown [3] used this approach in validation of a passive monitor for nitrous oxide; but they observed a loss of 27% during storage for two weeks and suggested that it was preferable to analyse the monitors as soon as possible after exposure. Qazi and Ketcham [4] stored activated

0003-2670/86/$03.50

carbon tubes loaded with ethylene oxide for 2, 5 and 7 days at room temperature and also under refrigeration (the exact temperatures were not specified); means of three determinations at each storage time and temperature were calculated for two different types of activated carbon. The means were compared without application of any formal statistical tests. From their examination of the data, Qazi and Ketcham [4] suggested that the activated carbon tubes for ethylene oxide should be stored refrigerated and analysed within seven days of exposure.

In this paper, it is proposed that it is preferable to accept that, with some monitors, losses of trapped materials during storage are inevitable and that these losses can be properly characterized under standardized storage conditions. A method of statistical analysis of the decay data is proposed which enables a decay curve to be defined and, from that, a correction factor curve to be calculated. The statistical methodology also enables confidence limits to be defined and calculated for these curves. The use of the methodology is illustrated with the laboratory validation of a passively-sampled, thermally-desorbable monitor for ethylene oxide.

Most workers, when analysing such data, would be inclined to use standard statistical techniques, such as least-squares regression. If the data relate to an obviously exponential decay process, the regression would be applied to the logarithmically transformed data. However, the presence of even one outlier in the set of data will affect the reliability of the regression [5], if it is done by a parametric method such as the Gaussian least-squares regression. In the statistical protocol forming Appendix A of the NIOSH Validation Tests [1], the use of Bartlett's test is recommended to test for homogeneity of variances for pooling of results. Davies and Goldsmith [6] urge caution in the interpretation of this test, unless there is sufficient evidence of normal distribution. The test protocol of Taylor et al. [1] does not provide sufficient evidence of normal distribution for that assumption to be made [5]. Busch, in Taylor et al. [1], further suggests the use of Grubbs' test [7] for identification of, and subsequent rejection of, an outlier. The number of actual outliers in the experimental data set will be unknown. Grubbs' test for one outlier is reasonably satisfactory, if it is known a priori that only a single outlier is present and if it can be assumed that the underlying distribution is Gaussian [8]. If, in fact, more than one outlier is present and/or the actual number of outliers is unknown, then such single outlier tests can actually fail to detect any outliers at all [8]. Multiple outlier tests have been derived, but must be used with great care if the user is not to be misled in their interpretation [8].

The distribution from which the data are sampled might actually be a contaminated or mixed distribution, but such contamination can be difficult to demonstrate without collection of very large amounts of data [5]. Thus, the method or group of methods used for the data evaluation should be both resistant and robust in some reasonable measure. Resistance in a statistical procedure implies insensitivity to localised misbehaviour of the data [9].

Robustness relates to insensitivity to departures from assumptions that may have been made about the underlying distribution [9]. The approach described below is an attempt to bring together a set of procedures such that data can be analysed even in the presence of "rogue" or "wild" data and yet enable sensible, predictive models to be derived from validation experiments.

EXPERIMENTAL

Monitor exposure

The Simtec Adsorba monitors used in these experiments are based on those described by Thompson et al. [10]. A chamber for exposure of the monitors was made as follows. Simtec Adsorba monitor holders were fixed into an acrylic cylindrical chamber (200 mm long, 90-mm diameter) and arranged in a spiral fashion around the cylinder. The gas mixture entered the bottom of the chamber and flowed around a baffle. It was exhausted through a T-piece connector at the top of the cylinder. The use of a T-piece enabled gas samples for quality control to be taken, whilst exhausting most of the gas to a suitable scavenger. The equivalence of the various sampling positions and hence the homogeneity of the gas mixture in the chamber were established by measuring the concentration at each sample position. No significant differences were found between sample positions.

Humidified ethylene oxide atmospheres were generated by using a Kin-Tek 570C precision gas standards generator and a Kin-Tek ethylene oxide permeation tube. Simtec Adsorba Type CM ethylene oxide monitors (Thorn-EMI Electronics, Simtec Division, Bulwell, Nottingham NG6 8UX, England) were placed in the holders on the chamber. The ethylene oxide concentration generated was 2 ppm (3.6 mg m^{-3}) and this atmosphere was sampled for 4 h. The exposed monitors were capped and then stored in air-tight screw-capped cans at 4°C for 1, 2, 4, 5, 6, 7, 10 and 15 days prior to analysis. Some monitors were also exposed and analysed immediately.

Thermal desorption and gas chromatography

The ethylene oxide was desorbed thermally at 130°C by using a Simtec Desorba desorption oven coupled via a six-port sampling valve to a Pye-Unicam 304 gas chromatograph fitted with a flame ionization detector. The chromatographic conditions were as follows: 1/8 in. by 3 ft. stainless steel column packed with Porapak Q (50—80 mesh); oxygen-free nitrogen carrier gas at 60 ml min^{-1}; the oven temperature programme was 50°C for 2 min, 25°C min^{-1} to 130°C, 130°C for 1 min, 50°C min^{-1} to 200°C, and hold at 200°C for 5 min.

RESULTS AND DISCUSSION

The percentage recovery, and the natural logarithm of the percentage recovery, of ethylene oxide versus the number of days of storage at 4°C, are

shown in Table 1. Initial tests with this monitor indicated an exponential decay of stored ethylene oxide. It is likely that the decay is the result of a reaction with co-adsorbed water vapour, the concentration of the latter being vastly in excess of the ethylene oxide concentration. In effect, there is a pseudo-first-order reaction involving ethylene oxide and water on the charcoal surface. Thus it is not unreasonable to use an exponential decay model for the loss of ethylene oxide during storage. It is also apparent even from a cursory examination of the data in Table 1 that wild or outlier data do occur surprisingly often. This is despite very careful control of experimental conditions by a skilled operator.

In the statistical procedures described below for data analysis, all the data are accepted for the assessment, even though some may appear uncomfortably "wild". The procedures do not weight outliers more heavily than non-outliers but make use of them in assessing the confidence envelope. In the least-squares approach to regression, outliers are weighted more heavily than datum points close to the regression line.

The regression coefficient calculation is based on Sen's extension [11] of Theil's rank-invariant regression analysis [12] and is based on the use of Kendall's tau. The Kendall tau statistic is a measure of association between sampled pairs of observations. It is based on the order (ranks) of the observations, not on their absolute values. The distribution of tau does not depend on the distributions of the two variables for which a relationship is being estimated (i.e., on whether they are distributed in a Gaussian or other fashion). Kendall's tau is a relative measure of the discrepancy between the actual observed order of the Y's and the order that would result from perfectly ordered observations [13, 14]. So, in making a regression estimate based on ranks as described below, Kendall's tau may be used to estimate the level of confidence in the regression coefficient so derived.

Theil [12] proposed a simple point estimator of the regression coefficient, viz., the median of the $\binom{n}{2}$ slopes $(Y_j - Y_i)/(t_j - t_i)$, $1 < i < j < n$, where in this case the Y_i or Y_j is an individual recovery coefficient for a particular storage time t_i or t_j and n is the number of pairs of observations (Y_i, t_i). Sen's procedure [11] is analogous to Theil's but is based on weaker assumptions and does not require $t_1, \ldots, t_n$ all to be distinct. Thus it enables the experimenter to use individual observations as in the experiments here, where several observations were made for each storage time. The number of observations at each storage time need not be the same. If N is the number of non-zero differences $t_j - t_i$ $(1 \leqslant i < j \leqslant n)$, Sen's proposed estimator of the regression coefficient is the median of the N slopes $(Y_j - Y_i)/(t_j - t_i)$ for which $t_j \neq t_i$. Sen [11] demonstrated that this is an unbiased regression coefficient estimator. Sen also derived a method of estimating the confidence interval about the regression coefficient based on Kendall's tau.

To obtain the upper and lower estimators of the regression coefficient β^*, defined as

TABLE 1

Percentage recovery of ethylene oxide from Simtec Adsorba Type CM ethylene oxide monitors after diffusive sampling of 2 ppm for 4 h and storage at 4°C

Storage time (days)	Recovery (%)	Logarithm[a]	Storage time (days)	Recovery (%)	Logarithm[a]	Storage time (days)	Recovery (%)	Logarithm[a]
0	52.9	3.9864	2	42.6	3.7519	7	24.2	3.1864
	57.3	4.0483		47.0	3.8501		27.3	3.3069
	58.8	4.0741		41.2	3.7184		31.8	3.4595
	64.1	4.1604		33.8	3.5205		25.6	3.2426
	58.7	4.0724		40.0	3.6889		30.3	3.4112
	46.0	3.8286		40.0	3.6889		28.8	3.3604
	46.0	3.8286	4	33.8	3.5205	10	33.3	3.5056
	55.5	4.0164		29.2	3.3742		25.0	3.2189
	46.0	3.8286		36.2	3.6082		26.7	3.2847
	69.8	4.2456					25.0	3.2189
	57.8	4.0570	5	61.7	4.1223		31.6	3.4532
	64.1	4.1604		30.9	3.4308		39.7	3.6814
	59.4	4.0843		36.4	3.5946		23.5	3.1570
	56.2	4.0289		37.9	3.6350		28.3	3.3429
	64.1	4.1604		25.8	3.2504		25.4	3.2347
1	52.2	3.9551	6	28.3	3.3429		31.3	3.4436
	49.2	3.8959		30.0	3.4012		8.3	2.1163
	46.3	3.8351		36.7	3.6028	15	33.3	3.5056
	71.4	4.2683		30.0	3.4012		31.8	3.4595
	52.4	3.9589					30.3	3.4112
	49.2	3.8959					31.8	3.4595
							30.3	3.4112
							28.8	3.3604

[a]Natural logarithm of percentage recovery.

$$\beta^* = \begin{cases} X_{(M+1)} & N = 2M + 1 \\ 1/2(X_{(M)} + X_{(M+1)}) & N = 2M \end{cases}$$

where, in this case, the X values are from the N slopes already calculated. Sen [11] defined $N^* = [N(\frac{n}{2})]^{1/2} U_n^*$ and $M_i = 1/2[N + (-1)^i N^*]$ for $i = 1, 2$ where U_n^* is defined by $P[-U_n^* \leqslant U_n(\beta) \leqslant U_n^* | \beta] = 1 - \epsilon_n$ and $0 < \epsilon_n < 1$.

Sen [12] showed that one can obtain values of U_n^* by using the table of Kendall's tau. For the data shown in Table 1, the value of U_n^* is calculated approximately as follows [15]: $U_n^* = Z[2(2n + 1)]^{1/2}/3[n(n - 1)]^{1/2}$, where Z is the standardized normal value which corresponds to $1/2\epsilon_n$. For values of $n < 30$, U_n^* may be approximated by the value of Kendall's tau (Table J [13]).

For this particular set of data, the calculation proceeds as follows. For the number of pairs of Y, t values, $n = 62$, and number of slopes $N = 1652$, and for 95% confidence, $p = 0.025 = 1/2\epsilon_n$ and $Z = 1.96$, thus $U_n^* = 1.96[2(2 \times 62 + 5)]^{1/2}/3(62 \times 63)^{1/2} = 0.1679$ and $N^* = [N(\frac{n}{2})]^{1/2} U_n^* = [1652(\frac{62}{2})]^{1/2} \times 0.1679 = 297$. The upper and lower confidence limits can be found by calculating the ranks of the relevant slopes: $M_1 = 1/2(N - N^*) = 1/2(1652 - 297) = 677.5$ and $M_2 = 1/2(N + N^*) = 974.5$. The corresponding values of the slopes are as follows: median = −0.0656, upper confidence limit = −0.0802, and lower confidence limit = −0.0486.

By applying the method of Theil [12], the intercept of the regression function can be calculated as follows: for each i, $Y_i = \ln$(percentage recovery) $= \beta^* t_i + a_i$, where β^* is the median regression coefficient, t_i is the time in days and a_i is the intercept for each Y_i, t_i pair. The intercept values, a_i, for each (Y_i, t_i) pair are found from $a_i = Y_i - \beta^* t_i$. The median of all the n values of a_i is the intercept, a^*, for the regression: $Y = \beta^* t + a^*$ hence $a^* = 3.9615$.

The 95% confidence interval on the intercept value can be calculated by the robust method described by Iglewicz [15]:

$$a^* \pm [t_{n-1}(d_f)/1.075\, n^{1/2}] = 3.9615 \pm 0.0624$$

where t_{n-1} is Student's t value for $n - 1$ at $p = 0.05$, and d_f is the fourth spread (= upper fourth − lower fourth). The upper and lower fourths are identified from their rank values. The depth of the upper fourth from the top of the list of ranked intercepts and of the lower fourth from the bottom of that list is calculated [16] from: depth of fourth = [(depth of median) + 1]/2, where the depth of the median is its rank.

Finally, three equations are obtained, one defining the regression itself, $Y = 3.9615 - 0.0656t$, and two for the confidence envelope,

$$Y = 3.8991 - 0.0802t \quad \text{and} \quad Y = 4.0239 - 0.0486t.$$

From these curves, the correction factors can be derived as a function of storage time after exposure as listed in Table 2. Examination of the percentage relative deviations from the correction factors listed in Table 2 shows

TABLE 2

The correction factor with its 95% upper and lower confidence limits as a function of storage time for the ethylene oxide monitor (cf. Table 1)

Storage time (days)	Correction factor	95% upper confidence limit	Relative deviation from correction factor (%)	95% lower confidence limit	Relative deviation from correction factor (%)
0	1.905	2.024	6.2	1.789	6.1
1	2.033	2.193	7.9	1.876	7.7
2	2.169	2.381	9.8	1.972	9.1
3	2.315	2.577	11.3	2.070	10.6
4	2.475	2.793	12.8	2.174	12.2
5	2.646	3.021	14.2	2.278	13.9
6	2.825	3.279	16.1	2.392	15.3
7	3.012	3.546	17.7	2.513	16.6
8	3.215	3.846	19.6	2.639	17.9
9	3.436	4.167	21.3	2.770	19.4
10	3.663	4.525	23.5	2.907	20.6
11	3.922	4.902	25.0	3.049	22.3
12	4.184	5.291	26.5	3.205	23.4
13	4.464	5.747	28.7	3.367	24.6
14	4.762	6.211	30.4	3.534	25.8
15	5.102	6.757	32.4	3.704	27.4

that the behaviour of the monitor for up to eleven days of storage at 4° C is within the accuracy requirements of the U.S. OSHA, that the 95% confidence limits should be less than or equal to ±25% [17].

The author is grateful to David John, University of Aston in Birmingham and Dr. Rajadurai Sithamparanadarajah, Institute of Naval Medicine, Gosport for the supply of the ethylene oxide data with which the regression methods have been illustrated.

REFERENCES

1 D. G. Taylor, R. E. Kupel and J. M. Bryant, Documentation of the NIOSH Validation Tests, U.S. Department of Health, Education and Welfare, NIOSH, Publication No. 77-185, 1977.
2 U.K. Health and Safety Executive, Protocol for Assessing the Performance of a Diffusive Sampler, MDHS 27, 1983.
3 P. C. Cox and R. H. Brown, Am. Ind. Hyg. Assoc. J., 38 (1984) 635.
4 A. H. Qazi and N. H. Ketcham, Am. Ind. Hyg. Assoc. J., 38 (1977) 635.
5 F. Mosteller and J. W. Tukey, Data Analysis and Regression. A Second Course in Statistics, Addison-Wesley, Reading, MA, 1977.
6 O. L. Davies and P. L. Goldsmith, Statistical Methods in Research and Production, Longman, London, 1977, Appendix 6E.
7 F. E. Grubbs, Ann. Math. Stat., 21 (1950) 27.
8 D. M. Hawkins, Identification of Outliers, Chapman and Hall, London, 1980, Chaps. 3 and 5.

9 D. C. Hoaglin, F. Mosteller and J. W. Tukey (Eds.), Understanding Robust and Exploratory Data Analysis, Wiley, New York, 1983, pp. 1—5.
10 J. M. Thompson, R. Sithamparanadarajah and W. I. Stephen, U.K. Patent No. GB2078128B, 1984.
11 P. K. Sen, J. Am. Stat. Assoc., 63 (1968) 1379.
12 H. Theil, Ned. Akad. Wetensch. Proc., 53 (1950) 386, 521 and 1397.
13 J. D. Gibbons, Nonparametric Methods for Quantitative Analysis, Holt, Rinehart and Winston, New York, 1976, Chap. 7 and p. 420.
14 W. J. Conover, Practical Nonparametric Statistics, 2nd edn., Wiley, New York, 1980, pp. 256—260 and 263—271.
15 B. Iglewicz, in D. G. Hoaglin, F. Mosteller and J. W. Tukey (Eds.), Understanding Robust and Exploratory Data Analysis, Wiley, New York, 1983, Chap. 12.
16 D. C. Hoaglin, in D. G. Hoaglin, F. Mosteller and J. W. Tukey (Eds.), Understanding Robust and Exploratory Data Analysis, Wiley, New York, 1983, Chap. 2.
17 N. A. Leidel, K. A. Busch and J. A. Lynch, Occupational Exposure Sampling Strategy Manual, U.S. D.H.E.W. (NIOSH) publication no. 77-173, 1977.

Analytica Chimica Acta, 186 (1986) 213—221
Elsevier Science Publishers B.V., Amsterdam — Printed in the Netherlands

ACID-BASE EQUILIBRIA IN TERNARY WATER/METHANOL/DIOXANE SOLVENT SYSTEMS
Determination of pK_a Values of Some Aliphatic Monocarboxylic Acids

G. PAPANASTASIOU*, I. ZIOGAS and I. MOUMTZIS

Laboratory of Physical Chemistry, Department of Chemistry, Faculty of Science, University of Thessaloniki, 540-06 Thessaloniki (Greece)

(Received 22nd January 1986)

SUMMARY

The thermodynamic acidity constants of n-butanoic, n-pentanoic, n-hexanoic, and n-heptanoic acids were determined at 25°C in ternary water/dioxane/methanol mixtures. The results obtained show that the composite medium effect, expressed by a parameter $b = dpK'/du$ (u being a variable expressing the solvent composition), depends on the ratio of the organic co-solvent concentrations. In the ternary mixtures, superposition of the various effects detected in the corresponding binary solvents (water/dioxane and water/methanol) enables simple interpolation formulae to be used to estimate the pK_a values in solutions with any ratio of the three solvents.

In the progress of investigations concerning the mechanism of various organic additives used as growth inhibitors during the electrolytic deposition of various metals, it has been shown [1, 2] that the inhibiting effect of tartaric acid, which is among the most effective growth inhibitors, clearly depends on the degree of dissociation of this acid. Because of these results, it was decided to extend investigation to mixed water/organic solvent systems, where the introduction of one or more organic solvents could make it possible to change the degree of dissociation of the organic additive.

In a first attempt, the dissociation of tartaric and succinic acids were examined comparatively in binary and ternary water/organic solvent systems [3, 4]. These studies indicated that the behaviour of these acids in the various ternary solvent systems resulted from the superposition of the various medium effects detected in the corresponding binary systems. Simple equations were suggested which allowed prediction of the thermodynamic pK_a values of the above-mentioned acids in any ternary solvent system.

However, it remained uncertain if this behaviour is a particular property of tartaric and succinic acids or a general property, characterizing other categories of organic acids, e.g., the monocarboxylic ones. It should be noted that these acids are added very often to various plating baths [5]. In an attempt to solve this problem, a study was undertaken concerning the dissociation of four monocarboxylic acids, i.e., n-butanoic (butyric), n-pentanoic

0003-2670/86/$03.50

(valeric), n-hexanoic (caproic) and n-heptanoic (oenanthic) acids with the general formula $CH_3—(CH_2)_{n-1}—COOH$, in various ternary water/methanol/dioxane systems. The criterion for choosing these acids was a previous finding [6] that monocarboxylic aliphatic acids with $n \geqslant 3$ show similar behaviour when they are ionized in mixed solvents. Consequently, these acids were selected with the expectation that the resulting conclusions could probably be extended over all the higher members of the aliphatic series of monocarboxylic acids. The higher members of this acid series have very small solubilities in water at room temperature, so that any results relating to their dissociation in mixed solvent systems, in which their solubilities increase, become particularly interesting.

The thermodynamic pK_a values estimated here can also be used in various analytical determinations or applications in the corresponding media, e.g., preparation of buffer solutions etc. In particular, the possibility of predicting the pK_a values of the acids under investigation in any ternary water/methanol/dioxane system, by means of the values proposed below, should be of value. The dissociation of these acids in ternary solvents seems not to have been investigated previously.

EXPERIMENTAL

Reagents

Conductivity water (conductance = $1.0 \times 10^{-6}\ \Omega^{-1}\ cm^{-1}$) was used throughout. 1,4-Dioxane was purified by refluxing with sodium for several days and redistilling; the whole procedure was repeated until the sodium remained bright after several hours. Absolute methanol was distilled once and the first and last 10% fractions were rejected. Reagent-grade acids (Fluka) were used without further purification; their purity was checked by potentiometric titration. All the sodium hydroxide solutions were prepared in the corresponding medium from stock solutions of known concentration (Merck, Titrisol).

Measurements

The pK_a values of the acids (HA_n) studied were determined by means of potentiometric titration using a cell (I) with liquid junction;

Glass electrode	0.01 m soln. of HA_n in partly aq. solvent	Conc. KCl (aq)	Conc. KCl (aq)	Hg_2Cl_2, Hg	(I)

The electrode pair (Beckman 39004, type E-2 glass electrode/Ingold, type 303-NS-EK saturated calomel electrode) was connected to a Beckman Research pH-meter with an accuracy of 0.002 pH units on the instrument scale.

Temperature was controlled at 25 ± 0.01°C by means of a Haake Ultrathermostat NBS. A nitrogen atmosphere was maintained above the working solution to avoid any contact with atmospheric carbon dioxide. All acid solutions, of a concentration 0.01 M, were prepared by weighing just before use.

The titrant, 0.1 M sodium hydroxide prepared in the appropriate mixed solvent, was added to the working solution from a Metrohm piston burette (Dosimat) with a readability of 0.005 ml. About 15 pH measurements were made during each titration, approximately between 20% and 80% of neutralization.

The electrode system was standardized against the aqueous buffer solutions recommended by the National Bureau of Standards [7]. The glass electrode used was confirmed to have a Nernstian pH response. In order to determine, in each mixed solvent system, the α_H^* values (where α_H^* stands for the hydrogen ion activity, referred to the standard state in the corresponding medium), the pH-meter readings (pH) were converted to $p\alpha_H^*$ values by the introduction of a correction term δ (= pH $-$ $p\alpha_H^*$). All these conversions were made by using δ values reported previously [8].

RESULTS AND DISCUSSION

Table 1 summarizes the composition of all the ternary systems studied here and also gives the corresponding values of the mole fractions of dioxane (X_1) and methanol (X_2). Three series of ternary solvents were used. The following linear relationships (where the corresponding linear correlation coefficient was very close to unity) were found.

$$\begin{aligned} &\text{Series A: } X_1 = 0.2034\, X_2 \\ &\qquad \text{B: } X_1 = 1.1075\, X_2 \\ &\qquad \text{C: } X_1 = 0.08106 - 0.5213\, X_2 \end{aligned} \tag{1}$$

The thermodynamic pK_a values were calculated by means of an iterative autocorrelation method [6]. This method also allowed for the evaluation of the mean ionic size, $\mathring{d}$ (minimum approach distance of two ions), corresponding to each series, the values of which are given in the Table. The pK_a values, with a standard deviation of $s \leqslant 0.01$, presented in Table 1 were calculated from experimental data derived from at least three titration curves.

The influence of the composition of the medium on the dissociation equilibria of the acids was first investigated. It was assumed that all these effects could be expressed eventually by means of simple equations, giving the pK_a dependence on a single appropriately chosen variable of the solution which would be related to the solvent composition. Initially, the dielectric constant D of the solvent was used as such a variable. Thus, graphs such as $pK_a = f(1/D)$ were plotted. It was assumed from the literature [9—13], that in water-rich mixtures the proton probably occurs as a hydronium ion, regardless of the nature of the organic co-solvents. Consequently, the ionization reaction is

$$HA_n + H_2O \rightleftharpoons H_3O^+ + A_n^-$$

The acidity constant of this reaction explicitly includes the activity of water α_{H_2O} [10, 11] $K_a' = K_a/\alpha_{H_2O}$, where α_{H_2O} can be approximated by its concentration, C_{H_2O} [9, 12, 13].

TABLE 1

Thermodynamic pK_a values of aliphatic monocarboxylic acids $CH_3-(CH_2)_{n-1}-COOH$ in various ternary water/dioxane/methanol systems at 25°C

Solvent (% v/v)[a]		X_1	X_2	Density (g ml^{-1})	C_{H_2O} (mol l^{-1})	D[b]	pK_a			
Diox.	MeOH						$n=3$	$n=4$	$n=5$	$n=6$
Series A ($\mathring{a}$ = 3.2 ± 0.1 Å)										
3	7	0.0067	0.0329	0.9898	50.176	73.64	4.98	5.02	5.04	5.06
6	14	0.0142	0.0698	0.9832	45.042	68.65	5.21	5.23	5.24	5.26
9	21	0.0227	0.1118	0.9765	39.903	63.55	5.45	5.49	5.51	5.52
12	28	0.0325	0.1599	0.9684	34.686	57.86	5.73	5.78	5.79	5.81
15	35	0.0440	0.2163	0.9586	29.375	52.26	6.05	6.08	6.12	6.12
Series B ($\mathring{a}$ = 3.5 ± 0.1 Å)										
7	3	0.0158	0.0142	0.9990	50.153	71.58	5.07	5.09	5.11	5.11
14	6	0.0339	0.0306	1.0010	44.964	64.56	5.33	5.40	5.38	5.40
21	9	0.0551	0.0497	1.0026	39.752	57.42	5.66	5.71	5.73	5.73
28	12	0.0802	0.0724	1.0025	34.446	50.08	6.05	6.11	6.11	6.13
35	15	0.1107	0.0999	1.0013	29.079	42.81	6.45	6.52	6.54	6.56
Series C ($\mathring{a}$ = 3.7 ± 0.1 Å)										
5	25	0.0125	0.1315	0.9679	39.959	65.40	5.39	5.42	5.46	5.48
10	20	0.0254	0.1069	0.9785	39.881	62.82	5.47	5.50	5.54	5.55
15	15	0.0386	0.0814	0.9895	39.825	60.32	5.55	5.60	5.62	5.65
20	10	0.0523	0.0551	1.0002	39.725	57.96	5.65	5.68	5.72	5.74
25	5	0.0665	0.0280	1.0107	39.669	55.60	5.74	5.77	5.81	5.83

[a]The statement that the ternary solvent is % v/v means that, e.g., 3 ml of dioxane and 7 ml of methanol were diluted to 100 ml with water. [b]Taken from ref. 16.

The theoretical basis of the graphs $pK'_a = f(1/D)$ is the following equation, advanced by Wynne-Jones [9, 14]:

$$dpK'_a/d(1/D) = (e^2/2kT \ln 10)\,\phi \qquad (2)$$

where ϕ is the reciprocal of the harmonic mean radius of the ions taking part in the above equilibrium. Equation 2 predicts a linear relationship between pK'_a and $1/D$ in all cases for which the pK'_a changes, after a change of medium, which can be attributed to phenomena of an electrostatic nature. It is assumed that all the non-electrostatic solute/solvent interactions remain constant, regardless of the solvent composition. In each series of ternary mixtures, examination of the plots of pK'_a vs. $1/D$ showed that all the acids studied here behaved completely analogously to tartaric and succinic acids in the corresponding media [4]. Thus, in all cases and for $D > 43$, the expected linear relationship between pK'_a and $1/D$ was observed; some examples are given in Fig. 1. It is also observed that for each of the acids studied, the corresponding graph $pK'_a = f(1/D)$ yields straight lines of different slope for each series of solvent mixtures, but the values of these slopes, $dpK'_a/d(1/D)$, corresponding to the various acids, are found to be practically equal to one

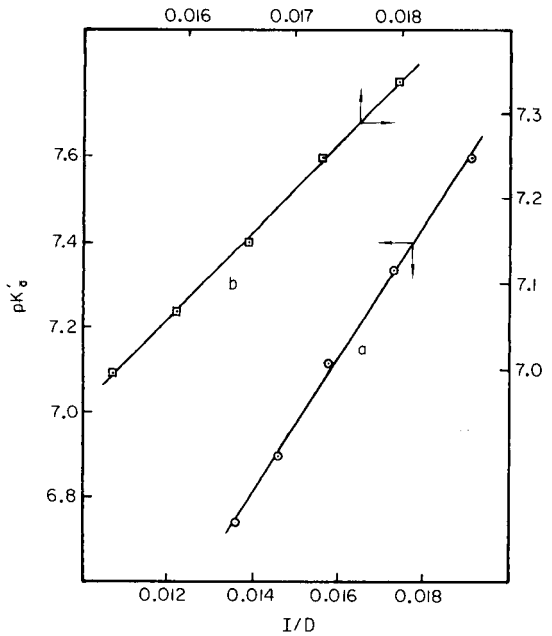

Fig. 1. Variation of pK'_a as a function of $1/D$ in two series of ternary water/dioxane/methanol solvents: (a) n-hexanoic acid in series A; (b) n-butanoic acid in series C.

another in each series of the ternary solvents. All these findings for the monocarboxylic acids studied can be interpreted on the assumption that the non-electrostatic solute/solvent interactions change from one solvent series to another.

Although the equations of the linear relations $pK'_a = f(1/D)$ found by the method of least squares (with $r > 0.998$) are very useful interpolation formulae, their practical applications may be regarded as quite limited. The use of these equations requires data on the dielectric constants, which are not always available, especially for ternary mixtures. This made it necessary to examine the pK'_a variations as a function of the mole fractions, X_1 and X_2, of the organic co-solvents in each series of the ternary mixtures used, i.e., $pK'_a = f(X_1, X_2)$. This function represents a 3-dimensional system in which the functions $pK'_a = f(X_1)$ and $pK'_a = f(X_2)$ are orthogonal projections of the corresponding 3-dimensional curves. In all cases, these projections were straight lines, as shown by the examples in Fig. 2. However, the linear Eqns. 1, of the general form $X_1 = X_1^0 + mX_2$, clearly represent the orthogonal projections of the same space curves on the coordinates X_1OX_2. From these equations, for each series of ternary systems, the linear relationship can be represented as

$$pK'_a = a + b\,u \qquad (3)$$

where $u = [(X'_1)^2 + X_2^2]^{1/2}$ and $X'_1 = X_1 - X_1^0$, X_1^0 being the X_1-intercept of the linear Eqns. in (1).

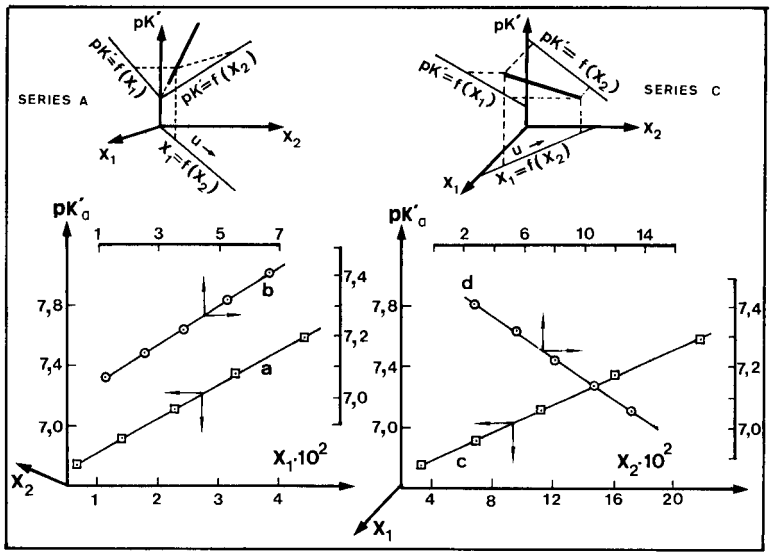

Fig. 2. Graphs of orthogonal projections $pK'_a = f(X_1)$ and $pK'_a = f(X_2)$ for ternary water/dioxane/methanol solvents: (a) and (c) n-heptanoic acid in series A; (b) and (d) n-hexanoic acid in series C.

The linear relationship between pK'_a and u was found to be true in all cases; correlation coefficients were always better than 0.9991. Equation 3 is valid not only for the ternary mixtures but also for any binary solvent system. In the latter case, linear relationships between pK'_a and the mole fraction X_j of the corresponding organic cosolvent j were observed, because in the binary solvent systems, variable u is the same as X_j.

These derivations were justified by determining, by exactly the same method, the thermodynamic pK_a values of all the acids used in the corresponding binary solvent systems, i.e., water/methanol and water/dioxane. The values obtained are listed in Table 2. Systematic pK_a determinations of these acids in these binary solvent systems are not available in the literature for comparison, but the present data are in good agreement with the pK_a values for n-butanoic acid in certain water/methanol mixtures (20 and 40% (v/v) in methanol) reported by Bacarella et al. [15]. For all the acids studied, the pK_a vs. X_j plots were fairly linear ($r > 0.9991$) for percentages up to 40% (v/v) in dioxane and up to 50% (v/v) in methanol. Further, in each binary system, the b ($= dpK'_a/dX_j$) values corresponding to the various acids were practically equal to one another (see Table 3). But the b values were about five times greater for the water/dioxane systems than for the water/methanol systems. Clearly, the solvent effect expressed by parameter b depends markedly on the nature of the organic solvent.

In the ternary systems, the values of parameter b again differed greatly, (Table 3). In an attempt to explain these variations, the electrostatic part of the medium effect was introduced (cf. Eqn. 2):

TABLE 2

Thermodynamic pK_a values of aliphatic monocarboxylic acids $CH_3-(CH_2)_{n-1}-COOH$ in various water/dioxane and water/methanol systems at 25°C

Organic solvent (% v/v)	X_j	Density[a] ($g\,ml^{-1}$)	C_{H_2O} ($mol\,l^{-1}$)	D[a]	pK_a			
					$n=3$	$n=4$	$n=5$	$n=6$
Water/dioxane ($\mathring{a}$ = 3.7 ± 0.1 Å)								
10	0.0227	1.0060	50.142	70.25	5.10	5.13	5.18	5.18
20	0.0493	1.0145	44.914	61.73	5.43	5.46	5.51	5.49
30	0.0811	1.0217	39.613	53.18	5.82	5.85	5.93	5.91
40	0.1197	1.0286	34.296	44.71	6.32	6.35	6.40	6.40
50	0.1680	1.0335	28.868	36.22	6.86	6.90	6.96	6.95
Water/methanol ($\mathring{a}$ = 2.9 ± 0.1 Å)								
10	0.0467	0.9827	50.180	75.13	4.98	4.99	5.02	5.00
20	0.0983	0.9694	45.077	71.72	5.14	5.15	5.17	5.17
30	0.1555	0.9570	40.019	67.79	5.32	5.34	5.36	5.35
40	0.2199	0.9425	34.845	63.40	5.55	5.57	5.59	5.57
50	0.2936	0.9257	29.549	60.05	5.78	5.79	5.82	5.81

[a]Taken from ref. 3 for water/dioxane solvent systems and from ref. 16 for water/methanol solvent systems.

$$b = dpK'_a/du = [dpK'_a/d(1/D)]\,[d(1/D)/du]\,.$$

The electrostatic term is expected to remain fairly constant in all these binary or ternary solvent systems, as is the non-electrostatic part of the medium effect. Thus, the second term $d(1/D)/du$, defined here as β, must depend strongly on the nature of the solvent components, and possibly on some association between the components of the solvent. In previous studies [16, 17] of ternary water/methanol/dioxane mixtures, the formation of polar associates ($CH_3OH \cdot 2H_2O$, $C_4H_8O_2 \cdot 3H_2O$) was detected at concentration ratios which differed markedly in the various series of solvents. These associates could change the term β. Calculation of β from plots of $1/D$ vs. $f(u)$, which were linear ($r > 0.999$), showed that β assumes completely different values in the three series of the ternary mixtures (Table 3). The changes in the values of parameter b for the different acids in different series of solvents can thus be attributed to changes in β. Parameter b can be used to indicate the electrostatic part of the medium effect as well as all possible interactions between the various substances present.

In order to correlate the behaviour of the acids studied in the various ternary mixtures with their behaviour in the corresponding binary solvents, it was assumed that the ternary solvent systems involve some interference with the effects detected in the corresponding binary mixtures. On the basis of the expression $pK'_a = f(X_1, X_2)$, this can be expressed as

$$b = dpK'/du = (\partial pK'/\partial X_1)(dX_1/du) + (\partial pK'/\partial X_2)(dX_2/du) \qquad (4)$$

The partial derivatives, $b_1 = \partial pK'_a/\partial X_1$ and $b_2 = \partial pK'_a/\partial X_2$, obviously repre-

TABLE 3

Experimental and calculated b (= dpK'_a/du) values with their standard deviations in various ternary water/dioxane/methanol systems for $CH_3—(CH_2)_{n-1}—COOH$

Solvent[a]	m	β	n-Butanoic		n-Pentanoic		n-Hexanoic		n-Heptanoic	
			Exp. b	Calc. b	Exp. b	Calc. b	Exp. b	Calc. b	Exp. b	Calc. b
H_2O/-dioxane		0.084	10.85 ± 0.14	—	10.85 ± 0.13	—	10.93 ± 0.13	—	10.96 ± 0.16	—
A	0.2034	0.0297	4.46 ± 0.07	4.46 ± 0.05	4.47 ± 0.09	4.46 ± 0.09	4.57 ± 0.07	4.48 ± 0.08	4.48 ± 0.08	4.49 ± 0.05
B	1.1075	0.0735	9.45 ± 0.16	9.62 ± 0.13	9.77 ± 0.21	9.63 ± 0.14	9.71 ± 0.15	9.69 ± 0.14	9.85 ± 0.05	9.71 ± 0.13
C	−0.5213	−0.0233	−2.99 ± 0.05	−2.94 ± 0.03	−2.98 ± 0.07	−2.93 ± 0.01	−2.99 ± 0.05	−2.97 ± 0.01	−3.02 ± 0.07	−2.98 ± 0.06
H_2O/-MeOH		0.0138	2.34 ± 0.04	—	2.35 ± 0.06	—	2.35 ± 0.06	—	2.35 ± 0.02	—

[a]See Table 1 for A, B and C.

sent the values of parameter b corresponding to the binary solvent systems (water/dioxane and water/methanol), respectively.

Simple calculation [4] combining Eqns. 3 and 4 with $X_1 = X_1^0 + mX_2$ leads to the relation

$$b = (mb_1 + b_2)/(m^2 + 1)^{1/2} \quad (5)$$

By means of Eqn. 5 and the b_1 and b_2 values of the binary systems water/dioxane and water/methanol, respectively, the values of parameter b were calculated in all cases. These values are listed in Table 3 compared with the experimental b values, and it can be seen that there is excellent agreement. These observations confirm the proposal that the behaviour of the acids studied in the various series of ternary mixtures results from the superposition of their behaviour in the corresponding binary solvents. This study extends the conclusions derived from previous work in relation to the behaviour of tartaric and succinic acids, to a homologous series of aliphatic monocarboxylic acids.

Finally, it is useful to emphasize the practical value of Eqns. 3 and 5. These equations are useful interpolation formulae, permitting prediction of the pK_a of the acid in any ternary solvent from the mole fractions of the organic co-solvents, without knowledge of the dielectric constant of the solvent. Thus, Eqn. 5, by means of the known b_1 and b_2 values, makes it possible to estimate the b values in any series of ternary mixtures defined by the value of parameter m. Then, given only one point on the corresponding linear graph $pK_a' = f(u)$, it is possible to predict the pK_a' values in any ternary mixture of the same series.

REFERENCES

1 J. Amblard, M. Froment, C. Georgoulis and G. Papanastasiou, Surf. Technol., 6 (1978) 409.
2 G. Papanastasiou, D. Jannakoudakis, J. Amblard and M. Froment, J. Appl. Electrochem., 15 (1985) 71.
3 G. Papanastasiou, I. Ziogas and D. Jannakoudakis, Chimika Chronika, in press.
4 G. Papanastasiou and I. Ziogas, Bull. Soc. Chim. Fr. I, (1985) 725.
5 F. Lowenheim, Modern Electroplating, Wiley, New York, 1974, p. 710.
6 G. Papanastasiou, G. Stalidis and D. Jannakoudakis, Bull. Soc. Chim. Fr. I, (1984) 255.
7 R. G. Bates, J. Res. Natl. Bur. Stand., Sect. A:66 (1962) 179.
8 G. Papanastasiou, I. Ziogas and D. Jannakoudakis, Anal. Chim. Acta, 173 (1985) 281.
9 E. J. King, Acid-Base Equilibria, Pergamon Press, Oxford, 1965, pp. 204, 254, 261.
10 H. S. Dunsmore and J. C. Speakman, Trans. Faraday Soc., 50 (1954) 236.
11 M. Yasuda, Bull. Chem. Soc. Jpn., 32 (1959) 429.
12 R. Reynaud, Bull. Soc. Chim. Fr. I, (1967) 4605; (1968) 3945.
13 E. Roletto and V. Zelano, J. Chim. Phys., 74 (1977) 1126.
14 W. F. K. Wynne-Jones, Proc. Roy. Soc. London, Ser. A:140 (1933) 440.
15 A. L. Bacarella, E. Grunwald, H. P. Marshall and E. L. Purlee, J. Org. Chem., 20 (1955) 747.
16 D. Jannakoudakis, G. Papanastasiou and I. Moumtzis, Chimika Chronika, New Series, 2 (1973) 73.
17 D. Jannakoudakis, G. Papanastasiou and P. G. Mavridis, J. Chim. Phys., 73 (1976) 156.

Analytica Chimica Acta, 186 (1986) 223—232
Elsevier Science Publishers B.V., Amsterdam — Printed in The Netherlands

SPECTROPHOTOMETRIC TITRATION OF MIXTURES OF NAPHTHALENE SULFONATES BASED ON THEIR ELECTRON-DONOR PROPERTIES IN WATER/ACETONE SOLUTIONS

V. V. KUZNETSOV, MOHAMED BENAMOR and O. M. PETRUKHIN*
D. I. Mendeleev Institute of Chemical Technology, 125047 Moscow A-47 (U.S.S.R.)
(Received 17th December 1985)

SUMMARY

Naphthalene sulfonates form neutral outer-sphere complexes with aquated barium ions which are relatively stable in water/acetone solutions. Such reactions are used in the spectrophotometric titration of binary mixtures of substituted napthhthalene sulfonates in the submilligram range with 1×10^{-2} M barium chloride and thymolphthalein complexone as indicator.

Substituted naphthalene sulfonates are widely used in the synthesis of intermediate products, azo dyes and pigments. Their manufacturing technology [1, 2] makes it necessary to analyze mixtures of sulfonates, including isomers, as well as mixtures of sulfonates with sulfates. Current methods of analysis for aromatic sulfonic acids, including titrimetric methods [3, 4] are generally not very selective. The use of separation methods [3, 5, 6] is effective but such separations are not possible for all sulfonates.

Analytical methods based on the use of the electron-donor properties of the aromatic sulfo group, as in spectrophotometric titrations [7] can be simpler and effective. Coordination of aromatic sulfonates in the outer sphere of the aquated barium ion, already coordinatively saturated in its Werner coordination sphere, produces relatively stable complexes. This allows spectrophotometric titrations with an indicator to be used to determine sulfonates of benzene [7], anthraquinone [8] and napthhthalenes [9]. Titration of naphthalene, hydroxynaphthalene and aminonaphthalene sulfonates in acidic water/acetone solutions with barium salts [9] is not always possible, especially in determining those sulfonates conjugated with weak bases, because of the influence exerted by the other substituents of the naphthalene ring. In this case, greater opportunities are provided by working with weakly alkaline solutions, as is described in this paper.

EXPERIMENTAL

Reagents, solutions and apparatus

The salts of sulfonates (pure grade; Reakhim) were purified by recrystallization from aqueous ethanol. The concentration of the initial solutions was

0003-2670/86/$03.50

established by potentiometric titration with alkali after conversion of the sulfonates to the free acids on a KU-2 cation-exchanger in the H^+-form. The titrant was prepared from barium chloride dihydrate used as a primary standard. The titrant was added from a precision piston-type microburette with 0.3-μl reproducibility. A pH of 8—10 was maintained with a borate buffer. Thymolphthalein complexone (Lachema) was used as the barium indicator. Acetone (specially pure grade; Reakhim), was used without additional purification. Unless otherwise specified, the chemicals were c.p. (chemically pure) grade.

The stability constants of the complexes were evaluated from the relative change in the potential of a Hg/HgEDTA electrode [10] in a circuit also involving a SCE. The ionic strength was kept constant with sodium perchlorate.

Spectrophotometric titrations were done with a SF-16 single-beam spectrophotometer, in a 17-ml cuvette with an optical path length of 3 cm. Prior to titration, the optical zero was set with respect to the initial solution by adjusting the slit.

Procedure

A 5-ml portion of solution containing 0.1—1 mg of sulfonates was transferred to the cuvette, and 1 ml of pH 9 buffer solution, 0.5 ml of 0.5% thymolphthalein complexone solution, 8 ml of acetone and 2.5 ml of distilled water were added. The mixture was titrated with standard 10^{-3}—0.1 M barium chloride at 630 nm (the absorbance maximum of the barium complex with the indicator).

RESULTS AND DISCUSSION

The semi-polar nature of the S—O bond in the sulfo group attached to the aromatic ring [11] causes the group to have electron-donor properties and act as a monodentate ligand. Many aromatic sulfo acids are strong acids, so their anions can exist in solution over a broad pH range. Some aminonaphthalene sulfo acids, however, have quite high pK_a values [12]; therefore, in order to ensure that all naphthalene sulfo acids are present as sulfonates, it is best to use weakly alkaline solutions. This eliminates undesirable side-reactions caused by protonation of substituted naphthalene sulfonates.

The dependence of the overall stability constant, $\log \beta_2$, of naphthalene sulfonate complexes with aqua ions of some metals on the hydrolysis constants (pK_n) of the metal ions [13] is given in Fig. 1, which shows that in the barium/zinc/lead series, the smallest tendency to hydrolysis corresponds to greatest complex stability, as exemplified by barium. Similar dependences were observed for other sulfonates. Therefore, barium ions were selected for the spectrophotometric titration of the naphthalene sulfonates [9].

Table 1 shows the values of the stability constants for the aquated barium ion complexes with different naphthalene sulfonates. The data show that, in general, the introduction of electron-donor or electron-acceptor substituents

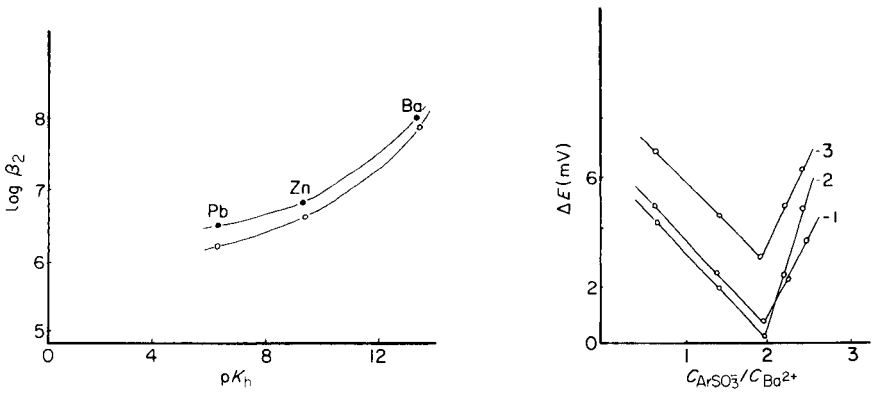

Fig. 1. Correlation of the stability constants of the metal complexes with the hydrolysis constants of the metal ions: (○) naphthalene-1-sulfonate; (●) naphthalene-2-sulfonate.

Fig. 2. Isomolar potential diagram for $C_{Ba^{2+}} + C_{ArSO_3^-} = 1 \times 10^{-5}$ M: (1) 5-aminonaphthalene-2-sulfonate; (2) 8-aminonaphthalene-2-sulfonate; (3) 4-hydroxynaphthalene-1-sulfonate.

into the naphthalene ring results in an increase in stability of the complex in comparison to the unsubstituted naphthalene sulfonates. However, in water the rate of the complexation reactions is decreased, as shown by the time needed for the required indicator electrode potential to be reached.

The above shortcomings (low stability constants, low rates) are easily overcome by using water/acetone solutions; increasing amounts of acetone added to water increased the stability of all the complexes investigated (Table 1), and equilibrium was attained rapidly. The difference in the stepwise stability constants (K_1 and K_2) is small, which in practice results in the formation only of the neutral complex, $ArSO_3^-$: Ba^{2+} = 2:1. This is shown in Fig. 2, and is in agreement with previous data [7—9].

The interaction of naphthalene sulfonates with barium ions in aqueous acetone is thus seen to satisfy the requirements for the reactions used in titrimetry [13]. When an individual sulfonate is titrated, the recorded titration curve has only one break, corresponding to the quantity of sulfonate in solution. Typical examples of such curves are given in Fig. 3, curves 1 and 2. The shapes of the curves are in good agreement with theory, corresponding specifically to the case where there is a small difference in the stability constants of the metal ion complexes with the titrant ion and the indicator [14]. The stability constant of the barium complex with an indicator, using the same potentiometric procedure as above, was found to be log β = 5.35 ($\mu \rightarrow 0$). The best relationship between the stability constants is in ca. 50% (v/v) acetone, which gives satisfactory titration reproducibility (Table 2). The substituted naphthalene sulfonates give more clearly defined breaks on the titration curves, as would be expected from the data in Table 1.

TABLE 1

Stability constants of naphthalene sulfonate complexes with barium ($\mu \rightarrow 0$, 25°C)

Ligand	Acetone (% v/v)	Log K_1	Log K_2	Log β_2	$-\Delta G_t^\circ$ (kJ mol^{-1})
Naphthalene-2-sulfonate	0	3.10	3.55	6.65	
	30	3.80	3.90	7.70	5.98
	50	4.05	3.93	7.98	7.58
	70	4.26	3.94	8.20	8.83
	90	4.46	3.93	8.39	9.92
Naphthalene-1-sulfonate	0	2.96	3.45	6.40	
	30	3.60	3.85	7.15	4.27
	50	3.96	3.89	7.85	8.26
	70	4.15	3.90	8.05	9.40
	90	4.30	3.88	8.18	10.14
1-Bromonaphthalene-2-sulfonate	0	3.30	3.40	6.70	
	30	3.78	3.96	7.74	5.39
	50	4.18	4.00	8.18	8.43
	70	4.32	3.98	8.30	9.12
	90	4.50	3.99	8.49	10.20
4-Hydroxy-naphthalene-1-sulfonate	0	3.36	3.52	6.88	
	30	4.01	4.13	8.14	7.18
	50	4.26	4.18	8.44	8.89
	70	4.45	4.19	8.64	10.03
	90	4.53	4.17	8.70	10.37
6-Hydroxy-naphthalene-2-sulfonate	0	3.40	3.56	6.96	
	30	4.04	4.12	8.16	6.85
	50	4.31	4.16	8.47	8.60
	70	4.49	4.16	8.65	9.63
	90	4.60	4.17	8.77	10.31
5-Aminonaphthalene-2-sulfonate	0	3.46	3.50	6.96	
	30	4.07	4.12	8.19	7.01
	50	4.35	4.15	8.50	8.78
	70	4.53	4.14	8.67	9.75
	90	4.65	4.15	8.80	10.49
8-Aminonaphthalene-2-sulfonate	0	3.60	3.52	7.12	
	30	4.12	4.10	8.22	6.28
	50	4.46	4.12	8.58	8.33
	70	4.60	4.13	8.73	9.18
	90	4.72	4.11	8.85	9.87
8-Acetylamino-naphthalene-1-sulfonate	0	2.93	3.08	6.01	
	50	4.20	3.96	8.16	12.25
	70	4.30	4.01	8.31	13.11
	90	4.40	4.02	8.42	13.73
7-Amino-4-hydroxy-naphthalene-2-sulfonate	0	3.40	3.12	6.52	
	50	4.85	4.11	8.96	13.90
	70	5.10	4.12	9.22	15.39
	90	5.46	4.12	9.58	17.44
6-Amino-4-hydroxy-naphthalene-2-sulfonate	0	3.20	3.13	6.33	
	50	4.52	4.11	8.63	13.11
	70	4.66	4.11	8.77	13.91
	90	4.82	4.12	8.94	14.87

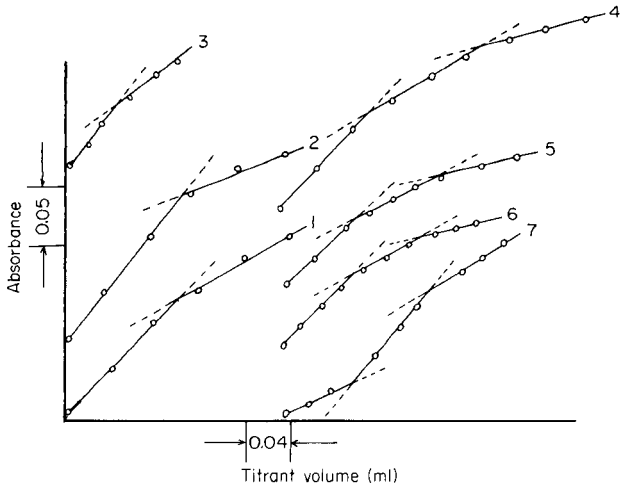

Fig. 3. Typical spectrophotometric titration curves for naphthalene sulfonates in 50% (v/v) acetone: (1) 8-aminonaphthalene-1-sulphonate, 0.35 mg; (2) 8-tolylaminonaphthalene-1-sulfonate, 0.62 mg; (3) 8-phenylaminonaphthalene-1-sulfonate, 0.27 mg; (4) 7-amino-4-hydroxynaphthalene-2- + plus 6-amino-4-hydroxynaphthalene-2-sulfonate plus 7-amino-1-hydroxynaphthalene-3-sulfonate, 0.24 mg + 0.48 mg; (5) 5-aminonaphthalene-2- plus 8-aminonaphthalene-2-sulfonate, 0.20 mg + 0.43 mg; (6) naphthalene-2- plus 1-bromonaphthalene-2-sulfonate, 0.22 mg + 0.49 mg; (7) sulfate plus 8-acetylaminonaphthalene-1-sulfonate, 0.048 mg + 0.52 mg. (Titrant 1×10^{-2} M $BaCl_2$.)

Negative values for the transfer energies ΔG_t^0 given in Table 1, calculated from $\Delta G_t^0 = RT \ln (\beta_w \beta_s^{-1})$, where β_w and β_s are the overall stability constants of the complexes in water and aqueous acetone, respectively, are indicative of the stabilization of outer-sphere complexes in a water/organic solution. In all the investigated cases, the dependence of ΔG_t^0 on the difference between the inverse values of the dielectric constants of aqueous acetone and water was nonlinear, which shows that both electrostatic and non-electrostatic interactions contribute to ΔG_t^0. Their nature apparently depends on the electron density distribution in the sulfonate ion, which generally should also be indicated by the difference between the stability of the complexes of different sulfonates.

From Table 1, the dependence on acetone concentration of the stepwise stability constants of the complexes is seen to be different. The value of $\log K_1$ increases monotonically throughout the whole range of acetone concentrations, whereas $\log K_2$ reaches its maximum value in 30% acetone. The $\log K_2$ values are also seen to be practically the same for the complexes of all sulfonates. By taking the labile nature of aquated barium ions into account, the experimental facts can be explained by the following complex-formation equilibria [15]:

$$Ba(OH_2)_6^{2+} + ArSO_3^- \overset{K_1}{\rightleftharpoons} [Ba(OH_2)_6]O_3SAr^+ + ArSO_3^- \overset{K_2}{\rightleftharpoons} [Ba(OH_2)_6](O_3SAr)_2$$

$$[Ba(OH_2)_{6-n}O_3SAr]^+ + nH_2O$$

TABLE 2

Results for determination of substituted naphthalene sulfonates

Sulfonate	Added (mg)	Found (mg)	S.d.[a]
5-Aminonaphthalene-2-	0.89	0.86	0.04
	0.45	0.46	0.01
8-Aminonaphthalene-2-	0.66	0.64	0.02
	0.22	0.23	0.04
8-Acetylaminonaphthalene-1-	0.53	0.54	0.02
8-Tolylaminonaphthalene-1-	1.00	0.96	0.04
	0.63	0.62	0.02
8-Phenylaminonaphthalene-1-	0.30	0.29	0.03
8-Aminonaphthalene-1-	0.86	0.82	0.05
	0.34	0.35	0.03
7-Amino-4-hydroxynaphthalene-2-	0.48	0.47	0.02
	0.25	0.24	0.04
6-Amino-4-hydroxynaphthalene-2-	0.48	0.49	0.02
	0.12	0.13	0.07
Scarlet acid[a]	1.08	1.03	0.04
	0.54	0.55	0.02
6-Phenylamino-4-hydroxynaphthalene-2-	0.63	0.62	0.02
	0.16	0.12	0.03
7-Hydroxynaphthalene-1,3-	0.69	0.70	0.01
	0.35	0.33	0.04
1-Bromonaphthalene-2-	0.28	0.29	0.03
5-Aminonaphthalene-2- + 8-amino-naphthalene-2-	0.22 + 0.45	0.20 + 0.43	0.05; 0.04
	0.12 + 0.22	0.10 + 0.24	0.06; 0.04
8-Phenylaminonaphthalene-1- + 8-acetylaminonaphthalene-1-	0.29 + 0.53	0.27 + 0.54	0.06; 0.02
8-Phenylaminonaphthalene-1- + 8-aminonaphthalene-1-	0.29 + 0.34	0.28 + 0.32	0.04; 0.05
8-Aminonaphthalene-1- + 8-phenyl-aminonaphthalene-1-	0.17 + 0.63	0.18 + 0.61	0.06; 0.03
8-Tolylaminonaphthalene-1- + 8-acetylaminonaphthalene-1-	0.31 + 0.53	0.33 + 0.52	0.06; 0.02
Sulfate + 8-acetylaminonaphthalene-1-	0.049 + 0.53	0.048 + 0.52	0.02; 0.02
7-Amino-4-hydroxynaphthalene-2- + 6-amino-4-hydroxynaphthalene-2-	0.24 + 0.48	0.26 + 0.46	0.07; 0.04
6-Amino-4-hydroxynaphthalene-2- + 6-phenylamino-4-hydroxynaph-thalene-2-	0.24 + 0.63	0.23 + 0.61	0.04; 0.03
6-Amino-4-hydroxynaphthalene-2- + 7-hydroxynaphthalene-1,3-	0.48 + 0.69	0.47 + 0.71	0.02; 0.03
Sulfate + 6-amino-4-hydroxynaph-thalene-2-	0.097 + 0.96	0.097 + 0.93	0.01; 0.03
Naphthalene-2- + 1-bromonaph-thalene-2-	0.21 + 0.50	0.22 + 0.49	0.04; 0.02

[a]Standard deviation of three results.

From this scheme, the outer-sphere coordination of the first ligand is seen to be accompanied by transformation of the monoligand outer-sphere complex into an inner-sphere complex. The overall equilibrium is described by the stability constant K_1, and the reaction is accompanied by displacement of water molecules from the aquated barium ion coordination sphere. The stability constant K_2, describing the insertion of the second ligand into the outer sphere, does not, however, depend on water concentration. Thus as, the addition of acetone to water decreases the water concentration, it is clear why $\log K_1$, and not $\log K_2$, varies with acetone concentration.

The predominance of outer-sphere coordination in the complexing at the first stage can be estimated based on the formal adherence of this equilibrium to Fuoss' ion-association theory [16]. For the investigated sulfonates, the value of Bjerrum's parameter a, found from the slope of the straight line describing the dependence of $\log K_1$ on the inverse dielectric constant of the medium, was 0.525 ± 0.02 nm. The physical meaning of Bjerrum's parameter is represented by the sum of the radii of the interacting ions. The charge of the sulfonate ion is localized exclusively on the sulfo group. The length of the S—O bond (ca. 0.14 nm [11]), therefore, can be equated to the sulfo-group radius. The sum of the S—O bond length and the barium ionic radius (0.135 nm) is ca. 0.28 nm, which is nearly half the experimental value of a. The correspondence of theory and practice greatly improves if the separation of barium and sulfonate ions by water is taken into account. For a barium ion—water distance of 0.275 nm, calculated as given by Marcus [17], the value of a becomes 0.555 nm, which is close to the experimental value. This confirms the assumption of the predominance of outer-sphere interaction in the first stage of complexing.

For sulfonates in which the π-electron density is shifted by electron-donating amino and hydroxyl groups, information on the outer-sphere interaction can be obtained from the interpretation of electron spectroscopy data. As an example, Fig. 4 presents the absorption spectra of 7-amino-4-hydroxynaphthalene-2-sulfonate (J-sulphonate) and its complex with aquated barium ions in acidic and alkaline media, in water and 50% ethanol. The latter solvent was chosen in preference to acetone because of the absence of ultraviolet absorption above 200 nm. From Fig. 4, it can be seen that in aqueous ethanol at an apparent pH of 3.5, barium causes changes in the sulfonate spectra, coinciding with the effect of OH ionization in an alkaline medium (curves 4 and 5). This is clearly seen if the absorption bands in the 220—260 and 270—320 nm regions are compared. The spectra have the same characteristic features at apparent pH values of 9 and 3.5. The state of the sulfonate ion in the complex, therefore, is close to its ionized state in water/organic solution. This indicates outer-sphere complexing of aquated barium ions with the sulfonate in accordance with the above scheme, and makes it possible to assume a considerable ionic contribution to the chemical bond in the outer sphere. Similar spectral data were also obtained for 6-amino-4-hydroxynaphthalene-2-sulfonate (γ-sulfonate), 8-acetylaminonaphthalene-

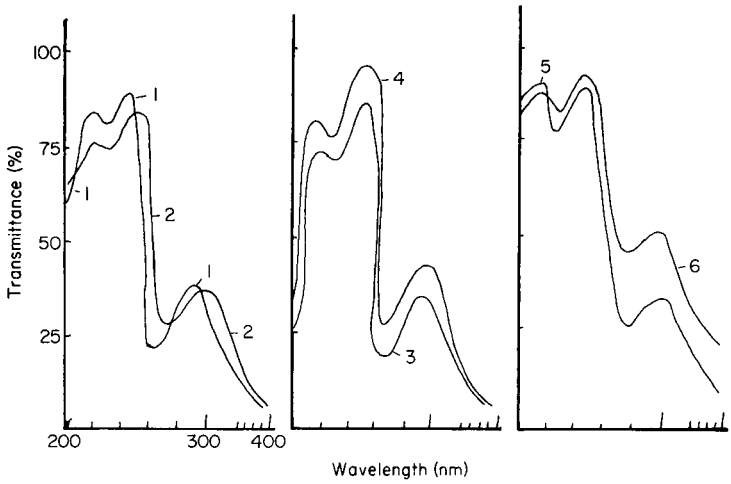

Fig. 4. Absorption spectra: (1—3, 5) 6-Amino-4-hydroxynaphthalene-2-sulfonate; (4, 6) its complexes with barium ion. Medium: (1, 2) water; (3—6) 50% (v/v) ethanol. pH: (1, 3, 4) 3.5; (2, 5, 6) 9.

1-sulfonate, 5-aminonaphthalene-2-sulfonate and its 8,2-analogue (Cleve's acids).

The selective character of a spectrophotometric titration makes it possible to use very small differences in the stability of complexes for achieving analytical selectivity. Even when mixtures of sulfonates with very similar properties are titrated, two breaks are recorded on the titration curves, corresponding to successive titration of the two components. Typical examples are given in Fig. 3 (curves 4—7). The possibilities of the method should be stressed for the analysis of the mixtures of isomers differing only in the position of substituents in the naphthalene ring (e.g., the J- and γ-sulphonates, or the anions of Cleve's acids) as well as its suitability for the analysis of the mixtures of sulfonates obtained as a result of the preparation of one from the other [1], e.g., naphthalene-2-sulphonate and 1-bromonaphthalene-2-sulfonate, etc. (Fig. 3, curves 4—6) and others. In such cases, the reproducibility (Table 2) is satisfactory. There is no information in the literature on the possibility of such a rapid analysis of binary mixtures of these sulfonates.

It is also easy to analyze a mixture of a sulfate and any naphthalene sulfonate (Table 2). Because of the different stabilities of their outer-sphere complexes with aquated barium ions, two clearly defined breaks are recorded on the titration curve (Fig. 3, curve 7).

The use of the electron-donor properties of the different naphthalene sulfonates in spectrophotometric titrations with indicators thus makes it possible to develop a system of simple yet novel analytical methods. Similar results can also be obtained in other water/organic solutions, characterized by a positive deviation from ideality [18]. It is this deviation from ideality that

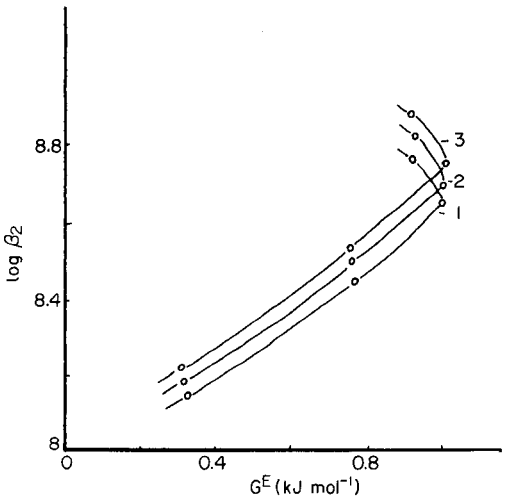

Fig. 5. Correlation of the stability of barium complexes with Gibbs free energy: (1) 6-hydroxynaphthalene-2-sulfonate; (2) 5-aminonaphthalene-2-sulfonate; (3) 8-aminonaphthalene-2-sulfonate.

proves to be responsible for the stabilization of the outer-sphere complexes in these solutions. Indicative of this is the log β_2 correlation with the Gibbs free energy (G^E) of the mixing of water and acetone, shown as an example for certain systems in Fig. 5. The curves correspond to the so-called isosolvate point observed for acetone when its content in the binary system is $\gtrsim$90% (v/v) [19]. The isosolvate region, within which occur the above equilibria involving aquated barium ions complexing with substituted sulfonates, is the region suitable for analytical use.

REFERENCES

1 L. S. Efros and M. V. Gorelik, The Chemistry and Technology of Intermediate Products, Khimiya, Leningrad, 1980, p. 156.
2 N. Donaldson, The Chemistry and Technology of Naphthalene Compounds, Edward Arnold, London, 1957.
3 Kuo Mao-Sung and H. A. Mottola, Crit. Rev. Anal. Chim., 9 (1980) 297.
4 K. Vytras, T. Kalous and Z. Kalabova, Anal. Chim. Acta, 141 (1982) 163.
5 J. Kroupa and O. Cerny, Chem. Prum., 34 (1984) 354.
6 G. Kaoprzak, W. Kups and J. M. Kulawinek, Biul. Inf. Barwn. Srodki Pomoch., 28 (1984) 9.
7 V. V. Kuznetsov and M. S. Liaufer, Zh. Anal. Khim., 36 (1981) 755.
8 V. V. Kuznetsov and M. S. Liaufer, Zh. Anal. Khim., 35 (1980) 747.
9 V. V. Kuznetsov and M. S. Liaufer, Zh. Anal. Khim., 38 (1983) 2210; 39 (1984) 111; Zavod. Lab., 47 (1981) No. 3, 10.
10 C. N. Reilley and R. W. Schmid, Anal. Chem., 30 (1958) 947.
11 Oae Sigeru, The Chemistry of Sulfur Organic Compounds, Khimiya, Moscow, 1975, pp. 448, 451.
12 R. K. Freier, Aqueous Solutions, Vol. 1, Data for Inorganic and Organic Compounds, Walter de Gruyter, Berlin, 1976, p. 315.

13 A. Berka, J. Sevcik and R. A. Chalmers, Talanta, 19 (1972) 747.
14 R. Kucharkowski and B. Pietsch, Fresenius Z. Anal. Chem., 314 (1983) 451.
15 Yu. A. Makashev and V. Ye. Mironov, Usp. Khim., 69 (1980) 1188.
16 J. E. Gordon, The Organic Chemistry of Electrolyte Solutions, Wiley, New York, 1975.
17 Y. Marcus, J. Solution Chem., 12 (1983) 271.
18 V. P. Belousov and M. Yu. Panov, Thermodynamics of Nonelectrolyte Water Solutions, Khimiya, Leningrad, 1983, p. 136.
19 M. Ulrich, W. Geiger and V. Gutmann, Monatsh. Chem., 108 (1977) 489.

Analytica Chimica Acta, 186 (1986) 233—245
Elsevier Science Publishers B.V., Amsterdam — Printed in The Netherlands

THE CHROMATOGRAPHIC INTERACTION AND SEPARATION OF METAL IONS WITH 8-QUINOLINOL STATIONARY PHASES IN SEVERAL AQUEOUS ELUENTS

CHARLES H. RISNER and JOHN R. JEZOREK*

Department of Chemistry, University of North Carolina at Greensboro, Greensboro, NC 27412 (U.S.A.)

(Received 9th January 1986)

SUMMARY

Several 8-quinolinol silica gel (QSG) columns were used, with metal-uptake capacities of 10—156 μmol g^{-1}. Various transition and heavy metal ions were used as analytes in nitrate, sulfate, phosphate, citrate, tartrate, oxalate, phthalate, and maleate mobile phases. Metal-ion retention increased with column capacity and pH. Optimum capacity factors were obtained on columns of intermediate capacity (27 and 46 μmol g^{-1}). Retention times decreased with an increase in eluent buffer concentration, typically by half with a doubling of buffer. Evidence is presented for the occurrence of mobile-phase complexation of analyte ions by eluent buffer species. Multiple or split peaks were often observed when the analyte solvent differed from the mobile phase. Chromatographic separation of up to six metals on the QSG columns is demonstrated in tartrate and maleate mobile phases.

The need to determine metal ion concentrations at low levels in complex matrices in the health and environmental areas is increasing. Use of high-performance liquid chromatography (h.p.l.c.) for these types of samples is increasing. Thus far, cation-exchange (ion-chromatographic) methods have been most commonly applied [1, 2]. These methods often require the use of a metal-complexing additive in the buffered eluent to produce a range of effective metal-ion charges so that the lack of selectivity of the ion-exchange material can be overcome. A less common approach has been to preform neutral chelates of the metal ions in the sample mixture and to effect separation on reversed-phase columns [3]. A somewhat more direct approach, essentially a hybrid of these two methods, is to effect selectivity by immobilizing the chelating agent on the stationary phase itself [4, 5]. In this way, pretreatment of the sample solution is generally not necessary and simpler mobile phases can be used because selectivity is designed into the stationary phase.

An obvious choice for the chelating agent is 8-quinolinol (8-hydroxyquinoline, oxine), a very general complexing agent which reacts with over sixty metal ions. Differences in formation constants have long been exploited for metal-ion separations, primarily by liquid—liquid extraction [6], and as

0003-2670/86/$3.50

early as 1939 an attempt was made to use columns packed with solid 8-quinolinol to separate metal ions, but changes in the solubility of the material with pH foiled this effort [7]. The remedy, of course, is to bind the ligand covalently to some inert substrate. Several organic materials have been used as supports for 8-quinolinol, such as styrene—divinylbenzene copolymers [8], resorcinol or phenol—formaldehyde resins [9], or polyacrylates [10]. Silicate materials such as controlled-pore glass [11] and silica gel [12, 13] have also been widely used. Immobilized 8-quinolinol has been used primarily for metal-ion preconcentration [14], removal of interfering metal ions [13], or the column separation of mixtures of two or at most three metal ions [8—10, 13]. No true h.p.l.c. separations have been demonstrated. Jezorek and Freiser [15] used modern h.p.l.c. equipment but the 8-quinolinol was bound to rather large-diameter silica (37—74 μm) and columns were dry-packed. However, that work demonstrated the promise of silica-bound 8-quinolinol (QSG) for metal-ion separation and the need for more study of this stationary phase.

This report gives the results of further work with QSG phases. The effects of ligand coverage, pH, and concentration of several common acid eluents on transition- and heavy-metal retention and resolution are presented. The phenomenon of multiple or split peaks for metal ions is discussed, and several separations of metal mixtures are illustrated. Small-particle (10 μm) silica and modern packing techniques were used to produce columns of relatively high efficiency for metal-ion separations.

EXPERIMENTAL

Apparatus

The chromatographic system consisted of a Spectra-Physics SP-8000 liquid chromatograph fitted with a 50-μl sample loop, and a Kratos/Schoeffel Model SF 770 detector operated at 510 nm.

Stationary phases were packed into glass-lined stainless-steel tubing (25 cm × 4 mm Scientific Glass Engineering) in the upward direction [16] at about 5000 psi with a Haskel Model 26980-4 pneumatic pump, using methanol as both slurry and packing solvent. The precolumn (8.5 cm × 4 mm) was dry-packed with relatively high capacity QSG [17].

The post-column derivatization system has been described [1, 18]. Briefly, the derivatizing reagent, 4-(2-pyridylazo)resorcinol (PAR), or ZnEDTA/PAR was pumped at about 1 ml min^{-1} from an air- or nitrogen-pressurized plastic reservoir to a mixing T-joint, where it was blended with the column effluent. The metal-PAR complex was detected at 510 nm.

Reagents and solutions

Water used in the preparation of mobile phases and sample solutions was first distilled and then passed through either a Nanopure system (Barnstead, Boston, MA), a Gelman Water I system, or a mixed-bed ion-exchange cartridge and redistilled. All water, aqueous mobile phases, and samples were passed through 0.45-μm cellulose acetate membrane filters before use.

Metal-ion solutions (10^{-4} M) were prepared from the metal perchlorate salt or from atomic-absorption standards, and were adjusted to pH 2.0 with nitric acid.

The 4-(2-pyridylazo)resorcinol (PAR; Baker or Eastman) was used as received. The zinc-EDTA reagent was from Riedel de Haën. The PAR and PAR/ZnEDTA solutions were generally 3×10^{-5} M, 0.05 M in ammonium nitrate, adjusted to about pH 10.5 with aqueous ammonia.

The 3-aminopropyltriethoxysilane and Trisil Z (20% v/v solution of trimethylsilylimidazole in pyridine) were from Pierce Chemical and the trimethylchlorosilane from PCR Research Chemicals (Gainesville, FL). All silanes were kept under refrigeration.

The stationary-phase support was Polygosil 60/10 (Macherey-Nagel; particle size 10 μm with 60 Å pores and 500 $m^2\ g^{-1}$ surface area). The pre-column silica support was Adsorbosil (Applied Science, now Alltech; 10 μm particle size with 70 Å pores and 480 $m^2\ g^{-1}$ surface area). The silica column (SI-10A; Brownlee Labs) used in the calcium/magnesium separation studies was packed with Lichrosorb Si-100 (10 μm particle size with 100 Å pores, and 300 $m^2\ g^{-1}$ surface area). All these silicas have irregular microparticles.

Toluene, dimethylformamide (DMF), and chloroform used in the syntheses were dried over 4 Å molecular sieves. Buffers used as mobile phases were prepared by "titrating" equimolar solutions of the conjugate acid by the base, or vice versa, until the desired pH was obtained.

Syntheses

The QSG phases were prepared essentially as described by Fulcher et al. [19], based on the method of Hill [13] and Sugawara et al. [11]. Aminopropyl silica gel (APSG) was prepared in 2% (v/v) solutions of the silane in toluene instead of the usual 5—10%, in order to obtain low-to-moderate coverage. One preparation of APSG included the usual refluxing of the silane/toluene solution for 2.5 h, the second only warm conditions (ca. 35°) for 4 h to minimize coverage by the silane. After preparation of the nitrobenzamide silica gel (NBSG), both batches of modified silica were endcapped with trimethylchlorosilane in refluxing toluene to deactivate residual silanol groups.

Silanol groups on a Polygosil bare silica column and a QSG-27 column (27 μmol g^{-1} capacity) were trimethylsilyl-endcapped in situ with a 5% (v/v) solution of trimethylsilylimidazole in dry DMF. Each column was preconditioned with 200 ml of methanol and 150 ml of dry DMF, and then silylated by circulating the endcapping solution through the column at 1 ml min^{-1} for 16 h at room temperature. The hydroxyl group on the 8-quinolinol moiety of the QSG-27 column was first protected by loading the column with iron(III). This was done by pumping a 5×10^{-3} M iron(III) solution in pH 2.2 nitric acid through the column at 1 ml min^{-1} to a positive thiocyanate test, and then pumping for an additional 30 min. Following the capping procedure, the iron(III) was removed from the QSG-27 column with 0.1 M nitric acid to a negative thiocyanate test.

Portions of the QSG-27 and QSG-10 originally prepared from the two batches of APSG were reduced to the aminobenzamide form (ABSG) in boiling sodium dithionite solution as previously described [19]. New QSG phases (QSG-156 and QSG-46) were then prepared from these ABSG materials in the same manner as in the initial synthesis.

Capacity determinations

Batch metal-uptake capacities of the APSG and QSG were evaluated as previously described [19]. Briefly, Cu(II) was loaded on 100—200 mg of the material, the solid was filtered off and washed with water, and the extracted Cu(II) was stripped off with 0.1 M hydrochloric acid. The amount of extracted Cu(II) was determined by atomic absorption spectrometry.

Capacities of QSG-27, QSG-156, and QSG-46 were also evaluated by an on-column breakthrough procedure. A 5×10^{-3} M iron(III) solution in pH 2.2 nitric acid was pumped through the column to a positive visual thiocyanate test or until a detector, which monitored at 450 nm the column effluent blended with 0.01 M potassium thiocyanate, exhibited a deflection from the baseline. The columns were flushed with 0.1 M nitric acid prior to the breakthrough procedure in order to ensure that all chelation sites were open. Results from the batch Cu(II) uptake and Fe(III) breakthrough procedures were in good agreement. The values for the four QSG phases used here (10, 27, 46 and 156 μmol g^{-1}) are based on the batch copper-uptake results in order to conform to past practice of reporting stationary-phase capacities [15, 17, 19].

General chromatographic conditions

Chromatograms were generally run at ambient temperature with a flow rate of 1 ml min^{-1}. All mobile phases were degassed with helium before use. Prior to sample injection, columns were equilibrated with eluent for at least 1 h at 1 ml min^{-1}. Columns were considered to be equilibrated when the acidity of the effluent matched that of the entering mobile phase to ± 0.02 pH units, when a stable baseline was obtained, and when two successive injections of sample yielded the same retention time.

The PAR flow rate generally matched that of the mobile phase, 1 ml min^{-1}. The detector was set at 510 nm at, usually, 0.4 absorbance for full scale.

RESULTS AND DISCUSSION

Stationary phase preparation

As mentioned above, much of the work with polymer- or silica-bound chelating agents, especially bound 8-quinolinol, has been concerned with metal preconcentration, so that high ligand coverage has been sought. This is not necessarily desirable for liquid chromatographic purposes, however, as band broadening can occur because of mass-transfer limitations [20]. Therefore, in order to study the effect of ligand coverage, two preparations of the

precursor aminopropyl silica gel (APSG) were made, one under refluxing conditions to effect moderate silylation, and the second under less vigorous conditions at about 35° C to minimize surface coverage. Amine ligand coverage of the first batch was 282 μmol g^{-1} and that of the second was 180 μmol g^{-1}, based on Cu(II) uptakes of .141 and 90 μmol g^{-1} respectively and 1:2 metal/ligand stoichiometry [21]. These two batches of APSG yielded QSG phases with ligand coverages of 27 and 10 μmol g^{-1}. These surprisingly low values were traced to the use of sodium dithionite from an old bottle which had apparently become oxidized. Portions of each of these batches of QSG were therefore reacted in dithionite solution prepared from fresh reagent (which reduced both unreacted NBSG and the original azo bonds), and the diazotization and 8-quinolinol coupling steps were repeated. Metal-uptake values of these reformed QSG phases were 156 and 46 μmol g^{-1}. It was thus possible to examine four different QSG phases, with capacities of 10, 27, 46, and 156 μmol g^{-1}, the first two having been obtained unexpectedly. Sodium dithionite reagent is oxidized readily. A quick qualitative test of its potency is to use it to reduce the azo bond of some surplus QSG; the brick-red color should fade to tan or beige within a few minutes in warm aqueous 2—5% sodium dithionite solution [19], and the dithionite should be discarded if this does not happen.

Columns of QSG used in this and other studies have proven very stable [17] though they are somewhat light-sensitive. Some brick-red QSG was exposed to light and air for about two weeks, and the surface gradually lost much of its color. The material below the surface layer, however, retained its original color. When QSG is kept in the dark, even though exposed to air, it does not fade.

The fall-off in capacity from APSG to QSG is attributed to steric limitations caused by partial closure of the pores as the surface becomes modified and to the inherent bulk of the 8-quinolinol itself [19, 22, 23].

Clearly, the ultimate coverage by 8-quinolinol can be controlled by intentionally varying the amount of the original silane and also of the sodium dithionite in the reduction of NBSG to ABSG. It has been shown that the unreacted nitro groups cause minimal metal-ion retention [24]. Therefore, it would appear that QSG phases of the desired capacity can be tailor-made, with high coverage for weakly interacting ions, low coverage for strongly interacting ions, and intermediate coverage for general-purpose columns. Furthermore, for a given QSG column, the extent of ligand coverage can be changed by reducing the azo bond back to the ABSG stage, reforming the diazonium-salt silica gel, and using an appropriate 8-quinolinol concentration to control the extent of coupling with the diazonium salt. All these reactions should be done in situ to obviate the need to open the column. We are currently developing these procedures.

Retention as related to capacity

Retention data for several metals on the four QSG phases in pH 2 nitric acid eluent confirmed the expectation that the greater the coverage by

bound 8-quinolinol, the more extensive the interaction with metal ions. At pH 2 (probably as low a pH as should be routinely used to avoid damage to columns or pumps), retention times on the QSG-156 column were too long to be useful, and late eluting peaks were very broad and badly tailed. But little or no retention was observed for any of the probe ions on QSG-10 at this pH. It appears that QSG-46 exhibits the most useful range of capacity factors (k') in this particular mobile phase. Capacity factors of 0, 0.3, 0.4, 1.8 and 5.6 were obtained for divalent ions of manganese, cadmium, lead, zinc and cobalt, respectively. While this ligand coverage (0.046 mmol g^{-1}) is very low compared to commercial ion-exchange phases, which typically exhibit capacities of 1 mmol g^{-1} or larger, chemical complexing interactions with this chelating phase are probably much stronger than coulombic interaction with ion-exchange phases. It is of interest that Fritz et al. [2] demonstrated effective separation of metals on ion-exchange phases of capacity comparable to the QSG phases reported here.

Evidence that the metal-ion retention observed on the QSG phases in pH 2 nitric acid eluent is due primarily to interaction with the 8-quinolinol moiety was needed. Therefore, several probe ions were injected onto a Polygosil-60-10 silica column and also onto the same column after it had been trimethylsilyl-endcapped in situ. Little or no retention of any of the metals was observed on either column up to about pH 3. Although slight retention was observed above pH 3, that on the QSG columns was much greater, implying little effect of residual silanols. Even if some residual silanols do remain on the QSG phases after end-capping, it is likely that the bulky 8-quinolinol appendage will shield the surface. Furthermore, as most of the work reported here was done at pH < 3.0, silanol interaction is believed to have been minimal, and most of the retention can be attributed to interaction with 8-quinolinol.

Column void volumes, based on essentially unretained manganese(II), were lower for the QSG (1.6 ml) than for the silica and capped silica columns (2.4 ml). This is probably due to partial filling of the pores of the substrate by the large 8-quinolinol and its backbone appendage, resulting in a decreased void volume [19, 22, 23].

Mobile phase effects

Several aqueous acids were used as eluents, including nitric acid, hydrogen sulfate, and phosphoric, phthalic, maleic, citric, tartaric, and oxalic acids. The unprotonated anions of all of these, save nitric, exhibit some interaction with the metal ions used as probes in this study, but in all cases the formation constants of the metal/anion complex in homogeneous solution are from 10^3—10^5 smaller than those of the metal ion with 8-quinolinol.

When the concentration of the acid in the mobile phase was decreased, retention of the metal ions increased. Some data for zinc(II) are given in Table 1, along with the pK_a values of the acids. These trends were not unexpected, and can be attributed to two effects. First, the effective formation constant of the metal ion with the bound 8-quinolinol is greater at high

TABLE 1

Retention volume for zinc(II) on a QSG-46 column in several acid eluents as a function of pH. The eluent concentrations are given in parentheses. The acid pK_{a1} values are also given

pH	V_R (ml) and eluent concentrations (M)							
	HNO_3	H_3PO_4	HSO_4^-	Tartaric	Phthalic	Maleic	Citric	Oxalic
2.00	3.40 (1×10^{-2})	3.40 (2.5×10^{-2})	3.30 (2×10^{-2})	3.26 (8.3×10^{-2})	— —	2.76 (1.8×10^{-2})	3.83 (1.1×10^{-1})	>20 (1×10^{-2})
2.25	4.40 (5.6×10^{-3})	4.40 (1×10^{-2})	3.60 (7.6×10^{-3})	4.13 (4×10^{-2})	6.30 (3×10^{-2})	4.63 (1×10^{-2})	5.72 (4.8×10^{-2})	>20 (6×10^{-3})
2.35	5.60 (4.4×10^{-3})	6.20 (7.4×10^{-3})	3.78 (5.8×10^{-3})	5.42 (2.6×10^{-2})	7.45 (1.8×10^{-2})	6.35 (6.8×10^{-3})	8.93 (2.9×10^{-2})	>20 (4.6×10^{-3})
2.55	— —	— —	— —	10.8 (1.2×10^{-2})	15.3 (1.0×10^{-2})	3.5 (3.8×10^{-3})	16.3 (1.4×10^{-2})	>20 (3.1×10^{-3})
pK_{a1}	—	2.14	1.92	3.04	2.95	1.92	3.12	1.27

pH values as deprotonation of both the heterocyclic nitrogen ($pK_a \approx 3.3$) [12, 15] and the phenol group must occur in order to allow chelation. Secondly, competition for the metal ions by the anions of the mobile-phase acids also decreases, permitting greater interaction with the stationary phase.

Capacity factors for several metals as a function of pH are shown in Fig. 1 for the 0.01 M tartrate system on the QSG-46 column. Again, increasing retention with increasing pH was observed despite the more extensive mobile-phase competition provided by the tartrate dianion. The very large k' values manifest strong interaction with the QSG phase. Co(II) is completely retained above pH 2.7, and Zn(II) above pH 3.3. All peaks were broad and tailed at the higher k' values.

The elution order of the metal ions in all the mobile phases studied was generally observed to be Mn < Cd < Pb < Zn < Co < Ni. This order is essentially the same as that of the 1:1 formation constants of the metals with 8-quinolinol, as observed previously [15]. Interestingly, a reversal in the retention order of Cd(II) and Pb(II) was observed in both tartrate and oxalate mobile phases with a pH increase. In both eluents, cadmium eluted before lead at lower pH values. Near pH 3.5 in tartrate and 2.2 in oxalate the two metals co-eluted, and at higher pH values lead eluted before cadmium, probably because of the stronger complexation of lead(II) than cadmium(II) by oxalate and tartrate at higher pH values. The reversal occurred in each eluent system when the ratio of the monoprotonated to the diprotonated species was about 3:1. Also, because of the more stable lead/oxalate complex, Pb(II) was much less highly retained in oxalate than in tartrate medium, exhibiting $k' \approx 5$ in 0.01 M oxalate and $k' \approx 25$ in 0.01 M tartrate at pH 3.5. When the eluent concentration was increased at a given pH, retention volumes decreased in all cases. For example, retention of Zn(II) at pH 2.55 decreased from 15

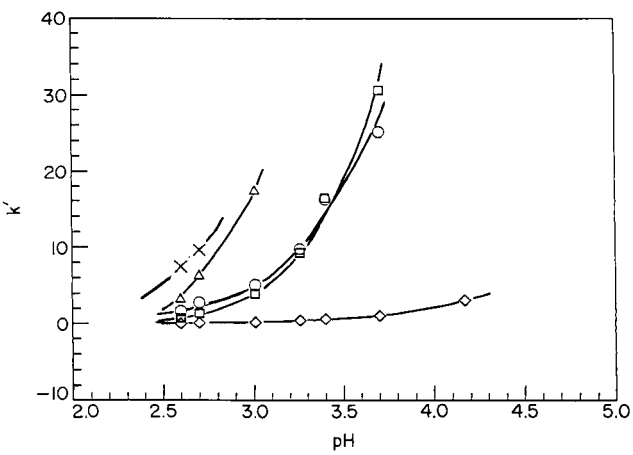

Fig. 1. Capacity factors as functions of pH in 0.01 M tartrate mobile phase on a QSG-46 column: (◇) Mn(II); (□) Cd; (○) Pb; (△) Zn; (×) Co.

to 10 min with an increase in hydrogen sulfate concentration from 0.01 to 0.02 M. In any case, in the pH range 2—4 used with the moderate capacity phases (QSG-27 and QSG-46), and for eluent acid concentrations about 10^{-2} M, the relative mobile phase strength appears to be oxalic < citric < phthalic < tartaric < maleic for most metals, although there were several exceptions to this order.

Clearly, both pH and concentration of the complexing anion are instrumental in determining the retention of these metal ions, as are the pK_a of the weak acid and stability constants of the complexes of the metal with the anion and 8-quinolinol. However, other effects may also be involved. For example, some of these organic acids may adsorb on or otherwise interact with the organic backbone of the stationary phase, changing the complexing properties of both the stationary phase and the adsorbed species (see below). Nevertheless, for comparison purposes, a mixture of Cd(II), Pb(II), and Zn(II) was run on QSG-46 at pH 2.35 with each of the mobile-phase additives discussed above. The results are shown in Fig. 2. Qualitatively, the differences in the chromatograms in the various acid eluents are striking, and make clear the necessity of careful screening of eluents for metal-ion separations. Reduction in peak size in some chromatograms is probably due to incomplete

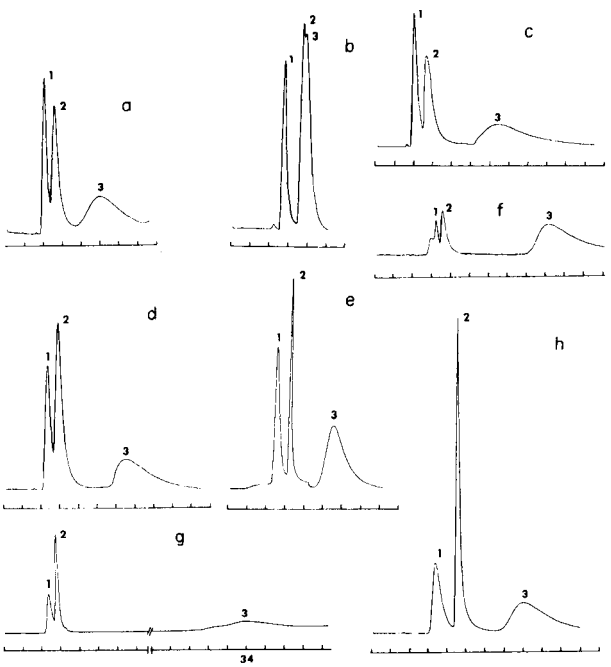

Fig. 2. Chromatograms on a QSG-46 column. Peaks: (1) Cd; (2) Pb; (3) Zn. Eluent (at pH 2.35): (a) 4.4 × 10^{-3} M HNO_3; (b) 5.8 × 10^{-3} M HSO_4^-; (c) 7.4 × 10^{-3} M H_3PO_4; (d) 6.8 × 10^{-3} M maleic acid; (e) 2.6 × 10^{-2} M tartaric acid; (f) 2.9 × 10^{-2} M citric acid; (g) 4.6 × 10^{-3} M oxalic acid; (h) 1.8 × 10^{-2} M phthalic acid. All divisions are 1 min except those of (g), which are 2 min. All sensitivities were the same, 0.4 AFS.

formation of the PAR/metal complex because of nonlability of some of the metal/acid anion species.

Peak splitting and other anomalies

Further evidence of mobile-phase additive interaction with analyte species is the widespread incidence of split peaks observed here and in another study [24]. While factors such as sample impurities and stationary phase inhomogeneity can result in split peaks, the main cause for most reported peak splitting appears to be chemical, i.e., the existence of two or more forms of the substance of interest in the mobile phase [25]. Several cases of split peaks have been reported for the reversed-phase separation of metal chelates, and attributed to partial equilibrium dissociation of these complexes to produce two or more mobile-phase species [25, 26].

In this work, split peaks were observed when metal ion solutions, 10^{-3} M in pH 3 nitric acid, were diluted to 10^{-4} M in a solvent different from the mobile phase. An analogous situation has been reported for reversed-phase work in which sample and mobile-phase polarity differed [27]. Even when the dilution was done with mobile phase, injections made immediately resulted in split peaks. However, when the diluted sample solution was allowed to stand for several hours and then injected, only one, symmetrical peak was observed. Apparently, slow metal/ligand substitution reactions are involved with different ligands in the aqueous phase. Although most metal ions tested exhibited occasional split peaks, Pb(II) and to a slightly lesser extent Cd(II) gave multiple or split peaks most frequently. Further evidence of these slow kinetics of metal/complex conversion are seen in Fig. 3(a), where Pb(II) in nitric acid exhibited a badly split peak when injected into oxalate mobile phase at 2.0 ml min^{-1}. At lower flow rates, the ratio of the early to the later peak decreased as more time on the column permitted

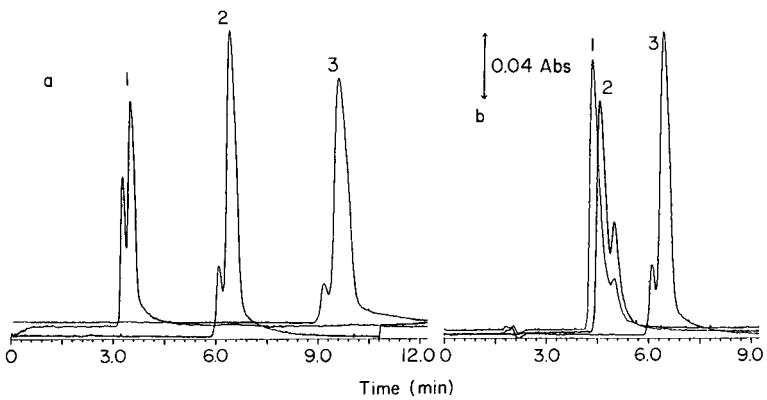

Fig. 3. Elution of Pb(II) in 0.01 M nitric acid solvent by 0.01 M oxalate eluent at pH 2.63 on a QSG-46 column. (a) As a function of flow rate: (1) 2 ml min^{-1}; (2) 1 ml min^{-1}; and (3) 0.5 ml min^{-1}. (b) As a function of temperature: (1) 60°; (2) 45°; and (3) 34°C.

greater conversion to the (presumably) more stable oxalate complex of Pb(II). When the same experiment was run at constant flow rate but different temperatures, the later peak increased and the earlier peak decreased at lower temperatures (Fig. 3b).

The only situation in which split peaks were observed when the metal ion solvent and eluent were the same was on bare silica or TMS-capped silica stationary phases. The cause most probably was the existence of silica surface sites of different activity or mass-transfer kinetics. That no splitting was observed on QSG columns under these conditions is additional indirect evidence that interaction with the residual silanols is blocked by the QSG appendage or that, at least, the very active sites have been modified and the less active sites remaining do not interact significantly with the metal-ion analytes.

In Table 1, it is seen that retention times for zinc(II) in oxalate eluent are greater than in nitric acid medium at the same pH. These results are somewhat unexpected, as complexing by nitrate presumably is minimal and interaction with the bound 8-quinolinol should be at a maximum. Similar results were also found for the other complexing eluents used but to a lesser extent. Although it would seem that the more extensive the mobile-phase complexation of the metal, the less interaction there would be with the stationary phase, the longer retention in oxalic acid implies rather strong attraction of the metal complex for the QSG stationary phase. Either the metal complex itself adsorbs on the surface or the complexing acid or its anion does so and takes part in subsequent complexation. These possibilities are not unlike those now postulated to occur in so-called ion-pairing chromatography via dispersion interactions with reversed-phase columns. Indeed, the QSG phase exhibits multiple sites at which dispersion, hydrogen bonding, π—π, and polar interactions can occur. Furthermore, below a pH of about 3.6, the stationary phase is highly protonated [12] and the anions of the complexing acids may adsorb on the surface as the counter-ion, and interact with metal ions in the mobile phase. Work is in progress to describe more clearly the mechanisms of metal ion interaction with QSG stationary phases.

Separations of metal ions

Mixtures of several metal ions were separated on Porasil-based QSG [15] but the large-diameter material resulted in rather broad peaks, and fairly long retention times were exhibited under gradient conditions. The smaller-size QSG and more efficient packing methods used here permitted the isocratic separation of several metal ions with good efficiency, as shown in Fig. 4 for the QSG-46 column in tartrate medium. The very broad cobalt(II) peak is probably due to poor mass-transfer kinetics between the QSG stationary phase and tartrate mobile phase. Jezorek and Freiser [15] also encountered broad cobalt(II), and nickel(II), peaks and used a pH gradient to improve sharpness. In the present study, a combined pH/buffer concentration gradient was found to produce better results than a simple pH gradient. Figure 5

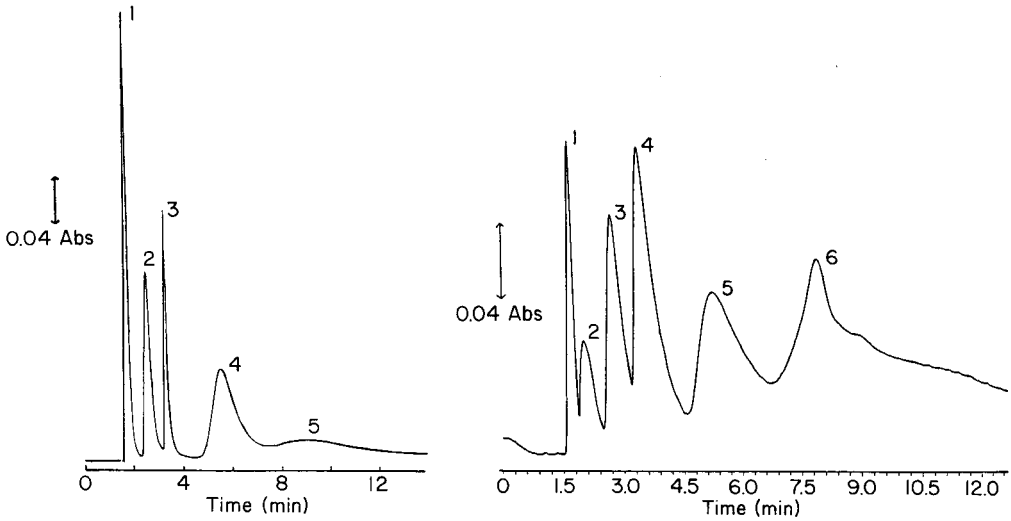

Fig. 4. Isocratic separation with 2.6×10^{-2} M tartaric acid at pH 2.35 on a QSG-46 column. Peaks: (1) Mn(II); (2) Cd(II); (3) Pb(II); (4) Zn(II); (5) Co(II).

Fig. 5. Separation of metals on a QSG-46 column with a 20-min linear gradient from 0.01 to 0.1 M maleate buffer, pH 2.37 to 2.04. Detection with 1×10^{-4} M PAR/ZnEDTA reagent. Peaks: (1) Mn(II); (2) Tl(I); (3) Cd(II); (4) Pb(II); (5) Zn(II); (6) Co(II).

shows the elution of six metal ions with a maleic acid/maleate gradient from 0.01 to 0.1 M on the QSG-46 column and the PAR/ZnEDTA post-column derivatization system.

It also proved possible to separate a Ca(II)/Mg(II) mixture on this column with a tartrate/tartaric acid gradient from pH 7 to pH 2.3. No separation was obtained when the gradient was begun with water instead of the tartrate, nor was resolution obtained on a Lichrosorb Si-100 silica column under the same conditions. Apparently, the tartrate system and the QSG both play a role in the separation, although the exact mechanism is unknown.

Based on these and earlier results [18], it would appear that silica-bound 8-quinolinol can be an effective stationary phase for efficient separation of transition and heavy metals, particularly when relatively lightly loaded. Phases with 20—50 μmol g^{-1} capacity appear to be most effective in terms of resolution and speed of separation, while common mobile-phase additives such as tartrate, maleate, hydrogensulfate and nitric acid can be used for elution and separation. More study is clearly needed to establish the exact role of the buffer anions and the causes of peak splitting and peak broadening, but there does seem to be a place for QSG phases in metal-ion separations.

The authors acknowledge The Research Corporation, The North Carolina Board of Science and Technology, and the University of North Carolina at Greensboro Research Council for support of this work. We also thank R. J. Reynolds Company for some chromatographic equipment used.

REFERENCES

1 S. Elchuck and R. M. Cassidy, Anal. Chem., 51 (1979) 1434.
2 J. S. Fritz, D. T. Gjerde and R. M. Becker, Anal. Chem., 52 (1980) 1519.
3 R. C. Gurira and P. W. Carr, J. Chromatogr. Sci., 20 (1982) 461.
4 K. T. DenBleyker, J. K. Arbogast and T. R. Sweet, Chromatographia, 17 (1983) 449.
5 R. J. Phillips and J. S. Fritz, Anal. Chem., 50 (1978) 1504.
6 G. H. Morrison and H. Freiser, Solvent Extraction in Analytical Chemistry, Wiley, New York, 1957, p. 162.
7 H. Erlenmeyer and H. Dahn, Helv. Chim. Acta, 22 (1939) 1369.
8 J. R. Parrish, Anal. Chem., 54 (1982) 1890.
9 F. Vernon and K. M. Nyo, J. Inorg. Nucl. Chem., 40 (1978) 887.
10 J. R. Parrish, Anal. Chem., 49 (1977) 1189.
11 K. F. Sugawara, H. H. Weetall and G. D. Schucker, Anal. Chem., 46 (1974) 489.
12 M. A. Marshall and H. A. Mottola, Anal. Chem., 55 (1983) 2089.
13 J. M. Hill, J. Chromatogr., 76 (1973) 455.
14 M. A. Marshall and H. A. Mottola, Anal. Chem., 57 (1985) 729.
15 J. R. Jezorek and H. Freiser, Anal. Chem., 51 (1979) 366.
16 G. J. Manius and R. J. Tscherne, Am. Lab., 13 (1981) 138.
17 G. J. Shahwan and J. R. Jezorek, J. Chromatogr., 256 (1983) 39.
18 J. R. Jezorek, K. H. Faltynski and J. W. Finch, J. Chem. Educ., 63 (1986) 354.
19 C. Fulcher, M. A. Crowell, R. Bayliss, K. B. Holland and J. R. Jezorek, Anal. Chim. Acta, 129 (1981) 29.
20 C. H. Lochmüller and C. W. Amoss, J. Chromatogr., 108 (1975) 85.
21 J. R. Jezorek, C. Fulcher, M. A. Crowell, R. Bayliss, B. Greenwood and J. Lyon, Anal. Chim. Acta, 131 (1981) 223.
22 J. R. Jezorek, K. H. Faltynski, L. G. Blackburn, P. J. Henderson and H. D. Medina, Talanta, 32 (1985) 763.
23 M. A. Marshall and H. A. Mottola, Anal. Chem., 57 (1985) 375.
24 K. H. Faltynski and J. R. Jezorek, Chromatographia, 22 (1986) 5.
25 G. K. C. Low, A. M. Duffield and Pr. R. Haddad, Chromatographia, 15 (1982) 289.
26 R. A. Keller and J. C. Giddings, J. Chromatogr., 3 (1960) 205.
27 P. K. Tseng and L. B. Rogers, J. Chromatogr. Sci., 16 (1978) 436.

Analytica Chimica Acta, 186 (1986) 247—259
Elsevier Science Publishers B.V., Amsterdam — Printed in The Netherlands

COUPLING OF NARROW-BORE LIQUID CHROMATOGRAPHY TO THIN-LAYER CHROMATOGRAPHY
Part 1. Interfacing

J. W. HOFSTRAAT*, M. ENGELSMA, R. J. VAN DE NESSE, C. GOOIJER, N. H. VELTHORST and U. A. TH. BRINKMAN

Department of General and Analytical Chemistry, Free University, De Boelelaan 1083, 1081 HV Amsterdam (The Netherlands)

(Received 25th February 1986)

SUMMARY

The coupling of liquid chromatography (l.c.) on narrow-bore columns to thin-layer chromatography (t.l.c.) is described. The effluent from a l.c. column can be deposited on a t.l.c. plate after a normal-phase or reversed-phase separation without serious loss of chromatographic information. Both silica and alkyl-modified silica plates can be used for storage. The interface is a fused silica capillary which connects the column outlet to the spray jet assembly of a Linomat applicator for t.l.c. The stored chromatogram can serve as starting point for a new separation, but also allows the use of detection principles which are normally not compatible with l.c. The chromatography of some polynuclear aromatic hydrocarbons is used to illustrate the possibilities of the combinations.

Column liquid chromatography (l.c.) is well established as a means of solving many problems in organic trace analysis but, with the increasing complexity of analytical work, does not meet all the demands for selectivity and sensitivity. A means of extending the potential of l.c. would be to combine it with thin-layer chromatography (t.l.c.). The essential aim is to deposit the effluent from the l.c. column on a t.l.c. plate without significant loss of chromatographic information, so that the chromatogram would be preserved after the l.c. separation and so available for further separation and/or investigation. A severe impediment to the on-line coupling of l.c. and t.l.c. has been the relatively large inner diameter (3—4.6 mm) of most commercial columns with their correspondingly high flow rates. This necessitates splitting of the effluent to reduce the amount of liquid reaching the t.l.c. plate and causes a severe loss in sensitivity. For miniaturized column l.c., where smaller internal diameters (0.7—1.0 mm) and lower flow rates are utilized, the barrier to successful on-line coupling should be much lower.

The coupling of column l.c. to t.l.c. can be useful for different purposes: (1) separation efficiency may be increased by combining two different separations, e.g., reversed-phase l.c. followed by silica adsorption t.l.c.; (2) detection modes which are incompatible with l.c. or require special experimental conditions can be applied, e.g., spectroscopic techniques such as

0003-2670/86/$03.50

fluorescence line-narrowing [1], phosphorescence [2, 3] and surface-sensitized spectroscopy [4, 5], which generally require immobilized analytes. Also, storage of the chromatogram may be useful in improving the feasibility of relatively slow detection techniques like i.r. spectroscopy and two-dimensional fluorescence and absorption spectroscopy.

The present paper is concerned with the coupling of both normal-phase and reversed-phase narrow-bore column l.c. to t.l.c. The interface used is a slightly modified Camag applicator for t.l.c. The effect of flow rate, t.l.c. material and R_f value (for the combination of t.l.c. material and eluent concerned) on the chromatographic integrity of the stored chromatogram is examined. The application of fluorescence line-narrowing and two-dimensional fluorescence emission and excitation spectroscopy will be discussed in a later paper.

EXPERIMENTAL

Chromatography

A schematic diagram of the chromatographic set-up and the interface is shown in Fig. 1. A Gilson (Villers le Bel, France) 302 pump and a home-made injection valve with an internal loop of 0.57 μl were used. For normal-phase separations, a 100 × 0.7-mm i.d. column was packed with 5-μm LiChrosorb SI-60 (Merck) from a slurry in n-hexane. The eluent was n-hexane. For reversed-phase separations, a 100 × 0.7-mm i.d. column was packed with 5-μm Spherisorb ODS (Phase Separations) using a slurry in methanol. Methanol/water (9:1, v/v) was used for elution. Flows were varied between 20 and 40 μl min^{-1}. In some experiments, a Kratos (Ramsey, NJ) Spectroflow 757 u.v. absorbance detector was included in the chromatographic set-up to check the performance.

The l.c. effluent was led through a 30 cm × 100-μm i.d. fused silica capillary attached to either the outlet of the l.c. column or the outlet of the u.v. absorbance detector. Subsequently, it was sprayed on a t.l.c. plate through a Camag (Muttenz, Switzerland) Linomat III spray-jet assembly. The spray-jet assembly ensures efficient application of the l.c. effluent and (partial) removal

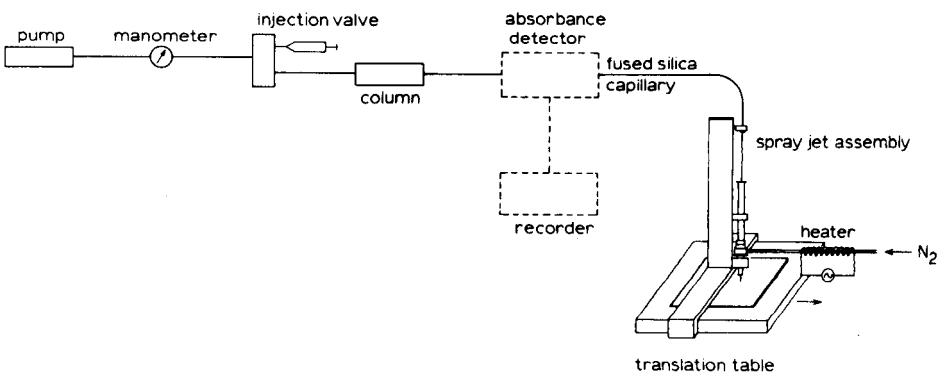

Fig. 1. Schematic diagram of the chromatographic set-up and the interface.

of volatile constituents of the mobile phase by means of a nitrogen flow applied around the tip of the capillary. In the present set-up, it was also possible to heat the nitrogen.

The t.l.c. plates used as a storage device were either precoated silica plates (DC Alufolien Kieselgel 60-H; Merck) or plates precoated with a C_{18}-modified silica (KC_{18} plates; Whatman). The plates were placed on the translation table of the Linomat. By replacing a capacitor in the instrument, the conventional speed range of the table was reduced by a factor of 50 to the range of 0.36—1.8 cm min^{-1}.

The plates were scanned with a Carl Zeiss (Oberkochen) spectrophotometer with densitometer attachment, operated in the fluorescence mode. A 390-nm cut-off filter was placed before the photomultiplier to detect total emission above 390 nm. Both a mercury lamp (λ_{ex} = 254 nm) and a deuterium lamp (λ_{ex} = 280 and 306 nm) were used for excitation, the former lamp providing the highest sensitivity. The spatial resolution was 0.1—0.7 mm in the direction of the scan and 4.1 mm perpendicular to the scan direction. For scans perpendicular to the deposition direction, the t.l.c. plate was turned 90°. Chromatograms were recorded on a Kipp & Zonen (Delft, The Netherlands) BD-8 recorder.

Chemicals

The polynuclear aromatic hydrocarbons (PAH) used as model compounds were pyrene (EGA-Chemie, Steinheim, F.R.G.), tetracene (Eastman Kodak) benz[k]fluoranthene (Joint Research Centre of the European Economic Communities, Petten, The Netherlands; reference compound) and chrysene (Materials Limited, Englewood Cliffs, NJ); they were used as received. Benzene, n-hexane and absolute methanol (all Baker; analyzed reagents) were used as solvents. In the l.c. separation, the eluents were prepared from n-hexane (Baker; HPLC quality, distilled from sodium), absolute methanol (Baker; analyzed reagent) and demineralized water. The eluents were deaerated before use.

RESULTS AND DISCUSSION

For the l.c./t.l.c. coupling, the crucial aspect is the maintenance of the chromatographic integrity during the storage process. The influence of several experimental parameters was studied most extensively by means of normal-phase l.c. (n.p.l.c.) coupled to a silica t.l.c. plate. Some experiments were also done to explore the possibilities of n.p.l.c. coupled to C_{18}-silica plates and reversed-phase l.c. (r.p.l.c.) coupled to both silica and C_{18}-silica plates.

Several factors are expected to influence the storage process. First, the volatility of the eluent depends mainly on the eluent used, but can be influenced by varying the flow of nitrogen supplied to the spray jet; the nitrogen can be heated to increase the evaporation of the effluent if required. Secondly,

TABLE 1

R_f values for some PAHs in t.l.c.[a]

Compound	R_f value on			
	Silica		C_{18}-silica	
	n-Hexane	Methanol/water[b]	n-Hexane	Methanol/water[b]
Pyrene	0.31	0.77	0.63	0.35
Chrysene	0.22	0.74	0.55	0.29
Benz[k]fluoranthene	0.17	0.71	0.49	0.23

[a]With development over 5 cm on all plates. [b]9:1, v/v.

TABLE 2

Flow rate of eluent for combinations of t.l.c. plates and eluents

Eluent	Time (s) for migration over			
	2 cm		4 cm	
	Silica	C_{18}-silica	Silica	C_{18}-silica
n-Hexane	95	30	450	130
Methanol/water (9:1, v/v)	205	75	750	260

the retention behaviour of the combination of solute and effluent on the t.l.c. plate will be important, the main parameters being the R_f value of the solute and the migration speed of the effluent on the t.l.c. plate. Summaries of the values relevant to this investigation are presented in Table 1 (R_f values) and Table 2 (migration velocities). Thirdly, the flow of the eluent in the l.c. system and the Linomat table speed together govern the amount of effluent deposited per unit surface area of the t.l.c. plate. This amount of effluent per unit surface area is not only important with respect to the sorption possibilities of the t.l.c. plate; it also seems to be the main factor governing the resolution attainable in the storage process.

Normal-phase l.c. coupled to silica t.l.c.

The combination of normal-phase l.c. and silica t.l.c. was expected to be the most suitable because n-hexane is a rather volatile eluent and because the retention behaviour of the PAHs used as model compounds indicates that migration will be limited once they have been applied to the t.l.c. plate. Therefore, this combination was investigated with particular attention to the influence of the l.c. flow rate and the Linomat table speed on the storage process.

The model compounds were well separated within a reasonable time (<10 min) in the present l.c. set-up at flow rates of 20—40 μl min^{-1}. The chromatograms were recorded with an absorbance detector incorporated in

TABLE 3

Comparison of chromatographic data for normal-phase l.c. separation and silica t.l.c. storage for pyrene (Pyr), tetracene (Tet) and benz[k]fluoranthene (B[k]F) at several flow rates and table speeds

Liquid chromatography							Thin-layer chromatography								
Flow rate (μl min^{-1})	Retention time (s)			Band width (FWHM[a], s)			Table speed (mm min^{-1})	Band width[b] (FWHM, mm)			$\Delta\sigma_{1/2}^2$[c] (10^2 s^2)			Trace width[d] (FWHM, mm)		
	Pyr	Tet	B[k]F	Pyr	Tet	B[k]F		Pyr	Tet	B[k]F	Pyr	Tet	B[k]F	Pyr	Tet	B[k]F
20	236	300	350	9.5	11	13	5.1	1.4	1.3	1.2	1.8	1.1	0.3	1.1	0.7	0.8
30	166	212	249	6.5	8.0	9.0	3.7	0.9	0.8	0.8	1.7	1.0	0.9	1.3	1.1	1.1
30	161	207	243	7.0	8.0	9.0	6.9	1.5	1.4	1.3	1.2	0.8	0.5	1.2	0.9	0.9
30	157	197	233	7.0	7.5	8.5	13.7	2.2	2.3	2.4	0.4	0.4	0.4	1.2	0.8	0.9
40	116	145	169	5.5	6.0	6.5	10.2	1.7	1.5	1.6	0.7	0.4	0.5	1.3	0.9	1.0

[a]Full width at half maximum. [b]Corrected for the spatial resolution of the Zeiss densitometer; see text. [c]$\Delta\sigma_{1/2}^2$ denotes the difference between the squared band widths (FWHM) in seconds obtained in the l.c. and t.l.c. experiments. [d]The data were obtained by scanning the densitometer perpendicularly across the trace with spatial resolution of 0.7 mm in the direction of the scan and 4.1 mm perpendicular to this direction.

the chromatographic system directly after the separation column. Relevant data are shown in Table 3. Pyrene, tetracene and benz[k]fluoranthene are eluted in that order with retention times varying from 2 to 6 min. The peaks in the chromatogram have band widths from 6 to 7 s at 40 μl min^{-1} up to 13 s at 20 μl min^{-1}. Benzene was added as an unretained solute and was found to elute in 75, 104 and 154 s for flow rates of 40, 30 and 20 μl min^{-1}, respectively. Benzene cannot be detected on the t.l.c. plate because of its volatility.

After having passed the absorbance detector, the separated compounds were applied on the silica t.l.c. plates. The effluent was sprayed on the plate while a normal nitrogen pressure of 2 bar was applied around the tip. The nitrogen was not heated. Flow rates of 20—40 μl min^{-1} and Linomat table speeds of 3.7—13.7 mm min^{-1} were used. The stored thin-layer chromatograms were scanned with the densitometer at a spatial resolution of 0.7 mm in the direction of the scan. In the following paragraphs, the shapes of the spots of the deposited compounds in the deposition direction as well as perpendicular to this direction will be discussed. For the scans in the direction of deposition (along the trace) the term "band width" is used, while for scans perpendicular to the deposition direction (across the trace) the term trace width is used. The results are summarized in Table 3. The band widths recorded with the densitometer were corrected for the spatial resolution of the apparatus by using the procedures described by Neuman [6]. The extra contribution to the band width produced by spreading in the interface and during deposition is denoted as $\Delta\sigma^2_{1/2}$. Because of the peculiar shape of the spots perpendicular to the deposition direction, no correction could be made for the trace width with Neuman's procedure [6]. Therefore, the values for the trace widths in Table 3 are higher than the actual values, as the relatively large spatial resolution (0.7 mm) of the densitometer will also contribute to the observed width. The relative values, however, are not influenced by the spatial resolution. Scans recorded at a higher spatial resolution, so that the peculiar shape of the spots becomes clear, are discussed below. All data in Table 3 are the result of averaging over at least two experiments.

Two parameters were varied in this coupling experiment. First, storage was done at constant flow (30 μl min^{-1}) and variable table speed. The results indicated the lowest effect of depositon at high table speeds. At 13.7 mm min^{-1}, a $\Delta\sigma^2_{1/2}$ of only 40—50 s^2 was found for the three model compounds. Secondly, both the flow rate and the table speed were varied, so as to keep the amount of effluent deposited per mm of t.l.c. plate constant. Again, the use of higher table speed seemed to produce a smaller $\Delta\sigma^2_{1/2}$, which was rather unexpected. High table speeds have the disadvantage of producing more expanded spots on the plate. This may be detrimental to the detection limits, especially if laser radiation, which can be focussed down to very small spot sizes [7], is used for detection.

The retention behaviour of the model compounds in l.c. is important because band widths increase with retention time. For instance, at a flow rate of

20 μl min^{-1}, the band width of pyrene is 10 s (FWHM) and that of benz[k]-fluoranthene 13 s. However, in the stored thin-layer chromatogram, the band width for pyrene is 1.4 mm but for the later eluting benz[k]fluoranthene it is 1.2 mm. Only at the highest table speeds does the compound with the longest retention time also have the widest band. This behaviour can be attributed to the differences in retention behaviour of the three model compounds on the t.l.c. plate (see Table 1).

An example of the results obtained for a l.c. separation at a flow rate of 30 μl min^{-1} with subsequent deposition on a silica plate moving at 13.7 mm min^{-1} is shown in Fig. 2; Fig. 2(a) shows the n.p.l.c. chromatogram obtained with the absorbance detector and Fig. 2(b) is the corresponding stored thin-layer chromatogram. The retention times obtained for the stored chromatogram (189, 232 and 267 s for pyrene, tetracene and benz[k]fluoranthene, respectively) are approximately 30 s longer than those measured in the l.c. experiment. This implies a dead volume of about 15 μl between the absorbance detector and the t.l.c. plate. The main contribution to this dead volume undoubtedly comes from the outlet of the absorbance detector. Of course, the extra dead volume will affect the band widths observed on the plate.

The influence of migration of the deposited compounds on the t.l.c. plate becomes clear when their trace widths are compared (Table 3). Pyrene invariably has a wider trace than tetracene and benz[k]fluoranthene. Figure 3(a) shows the scan perpendicular to the trace obtained for benz[k]fluoranthene for the l.c./t.l.c. data shown in Fig. 2; at the spatial resolution of the densitometer used (0.7 mm), the band width is 1 mm. At the much higher spatial resolution of 0.1 mm, the scan depicted in Fig. 3(b) was obtained; the width of this cross scan is 0.7 mm (where the maximum is taken to be the maximal intensity value of the lobes). The typical form of the high-resolution scan perpendicular to (but not along) the trace is due to the migrational behaviour of the solute on the t.l.c. plate (see below).

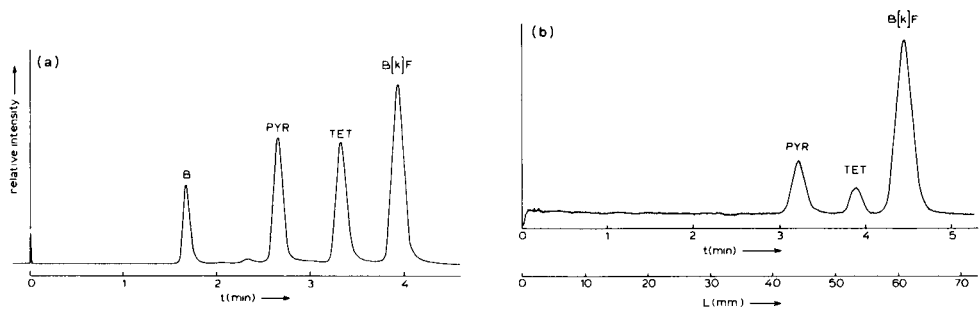

Fig. 2. Normal-phase l.c. coupled to silica t.l.c. for a mixture containing benzene (B), 5.0 × 10^{-5} M (5.7 ng) pyrene, 1.0 × 10^{-4} M (13 ng) tetracene and 2.5 × 10^{-5} M (3.5 ng) benz[k]fluoranthene. The l.c. flow rate was 30 μl min^{-1} and the Linomat table-speed was 13.7 mm min^{-1}. (a) N.p.l.c. chromatogram with absorption detection (250 nm); (b) stored thin-layer chromatogram with fluorescence detection (deuterium lamp excitation, λ_{ex} = 280 nm, λ_{em} > 390 nm; spatial resolution 0.7 × 4.1 mm).

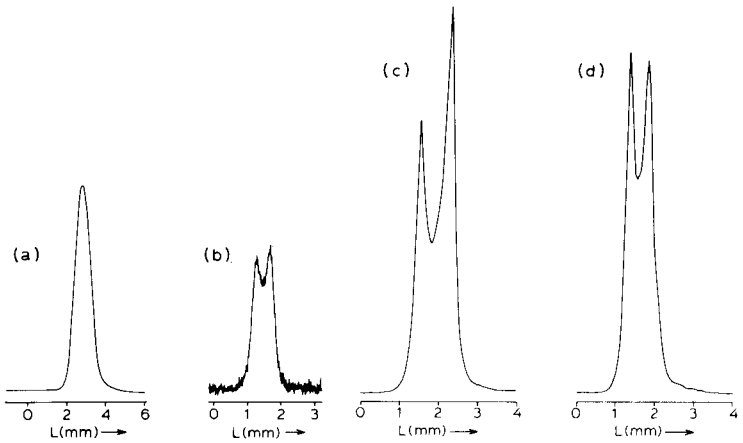

Fig. 3. Scan across the trace for benz[k]fluoranthene (2.5×10^{-5} M, 3.5 ng) deposited on t.l.c. plate. (a) Storage on silica plate; scanned at a spatial resolution of 0.7 × 4.1 mm; (b) storage on silica plate; scanned at a spatial resolution of 0.1 × 4.1 mm; (c) storage on C_{18}-modified silica plate with unheated 2-bar nitrogen flow applied to the Linomat spray-jet assembly; scanned at a spatial resolution of 0.1 × 4.1 mm; (d) storage on C_{18}-modified silica plate with heated 2-bar nitrogen flow; scanned at a spatial resolution of 0.1 × 4.1 mm. Conditions: l.c. flow rate 30 μl min^{-1}; table speed 13.7 mm min^{-1}; fluorescence detection with deuterium lamp excitation (λ_{ex} = 306 nm, λ_{em} > 390 nm).

Normal-phase l.c. coupled to C_{18}-modified silica t.l.c.

The coupling of n.p.l.c. (n-hexane eluent) to C_{18}-modified silica plates for the model compounds used here was expected to be somewhat less successful than that to bare silica because the PAHs have higher R_f values on modified plates (Table 1). Moreover, Table 2 shows that the eluent flow rate is about three times faster on C_{18}-modified silica. This coupling was investigated for benz[k]fluoranthene; the l.c. flow rate was 30 μl min^{-1} and the table speed was 13.7 mm min^{-1}. The band width along the trace was little affected by the change of t.l.c. material; under identical conditions, the band width increased by <10% on changing from deposition on silica to C_{18}-modified silica (from 2.4 to 2.6 mm). When the nitrogen flow fed to the spray jet was heated, this increase was even smaller. The absolute decrease in band width attributable to heating is only ca. 5%; when silica plates were used, it was almost negligible.

The effect of the different migrational behaviour of the compounds on the C_{18}-modified plates became more obvious when the scans across the trace were studied.

Figure 3(c, d) shows scans across the trace for benz[k]fluoranthene deposited on a C_{18}-modified plate; at the spatial resolution of 0.1 mm, no correction of the observed band shape was necessary. Without heating of the nitrogen, a relatively broad (ca. 1.1 mm wide) bifurcated band was obtained (Fig. 3c). Heating of the nitrogen decreased the the width to ca. 0.8 mm (Fig. 3d) compared to a width of 0.7 mm for the silica plate. The bifurcated

peak (Fig. 3d) suggests a stronger effect of migration of the deposited components on the C_{18}-modified material (cf. Fig. 3b). The effect of heating on the cross scans for the unmodified silica plates was insignificant, which suggests that the deposition process was not then influenced very much by further increase in solvent volatility.

It is emphasized that the typical bifurcated peak shape observed for the scans perpendicular to the trace was not observed for scans in the direction of deposition. Of course, the effluent also migrates along the trace after deposition but the manner in which it is applied is completely different (continuous deposition). In the latter case, the application is apparently mainly determined by the distribution of the solutes in the column effluent, which is generally of Gaussian shape.

Reversed-phase l.c. coupled to silica and C_{18}-modified silica t.l.c.

In r.p.l.c. generally, a water-containing eluent is used, and so more problems are to be expected in the coupling to t.l.c. than with n.p.l.c. However, reversed-phase h.p.l.c. appears to be more suitable for the separation of PAHs [8]. To explore such coupling, a separation on a C_{18} column with methanol/water (9:1, v/v) as eluent was combined with normal-phase and reversed-phase t.l.c. plates. The model compound tetracene was replaced by chrysene because tetracene is not very soluble in the eluent.

A typical result obtained for immobilization of the r.p.l.c. column effluent on a silica plate is shown in Fig. 4. The l.c. retention times of pyrene, chrysene and benz[k]fluoranthene are 363, 449 and 653 s, respectively, and the peaks are well resolved with band widths of 2.7, 3.2 and 4.0 mm on the plate, corresponding to 24, 28 and 35 s. These band widths are 2—3 times greater than those obtained with the n.p.l.c. coupling discussed above (Table 3), but part of this increase is due to a corresponding increase of the retention times in r.p.l.c. Only a small reduction of band width was achieved when C_{18}-

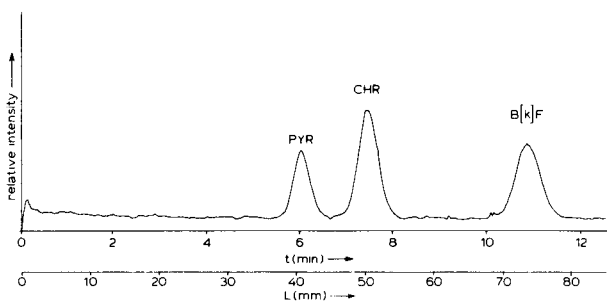

Fig. 4. Reversed-phase l.c. coupled to silica t.l.c. The chromatogram obtained for a 20 μl min^{-1} flow rate was deposited on the plate moving at 6.9 mm min^{-1}. The mixture contained 1.0×10^{-4} M (11 ng) pyrene, 1.0×10^{-4} M (13 ng) chrysene (CHR) and 1.0×10^{-5} M (1.4 ng) benz[k]fluoranthene. Fluorescence detection with mercury arc excitation (λ_{ex} = 254 nm, λ_{em} > 390 nm); spatial resolution 0.2 × 4.1 mm; heated 2-bar nitrogen flow applied.

modified silica plates were used for storage. Under the same experimental conditions as for Fig. 4, the band widths were 2.5, 3.0 and 4.0 mm. As all peaks were of Gaussian form in the direction of deposition, the band shapes of the stored chromatogram must depend mainly on how the column effluent is applied on the t.l.c. plate (i.e., continuously). This statement is supported by the fact that heating of the nitrogen flow hardly influenced the deposition process; only a negligible reduction of the band widths (<5%) was observed.

Again, a more sensitive test of the migrational behaviour of the compounds on the t.l.c. plate was found to be the scan across the trace. A good example of the influence of the R_f value is shown in Fig. 5, where scans perpendicular to the trace are depicted for deposition of a r.p.l.c. column effluent on C_{18}-modified silica. Pyrene, with the highest R_f value (Table 1), exhibits the strongest influence of migration on the t.l.c. plate; the distance between the maxima of the two lobes is 1.3 mm and the FWHM of the total band is

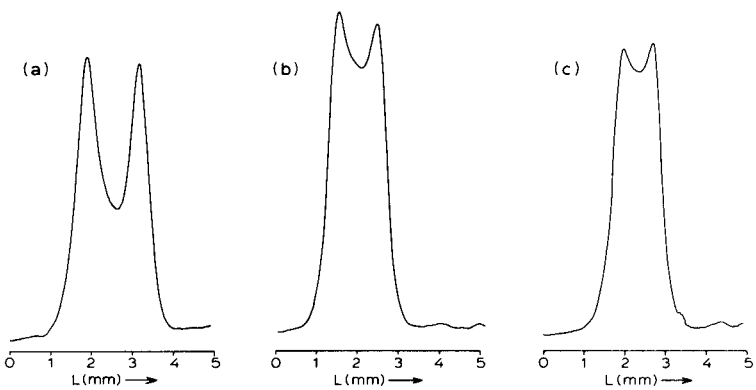

Fig. 5. Scans across the trace for r.p.l.c. coupled to C_{18}-modified silica t.l.c.: (a) pyrene (11 ng); (b) chrysene (13 ng); (c) benz[k]fluoranthene (1.4 ng). Conditions: flow rate 20 μl min^{-1}; Linomat table speed 6.9 mm min^{-1}; concentrations, nitrogen flow and detection circumstances as in Fig. 4.

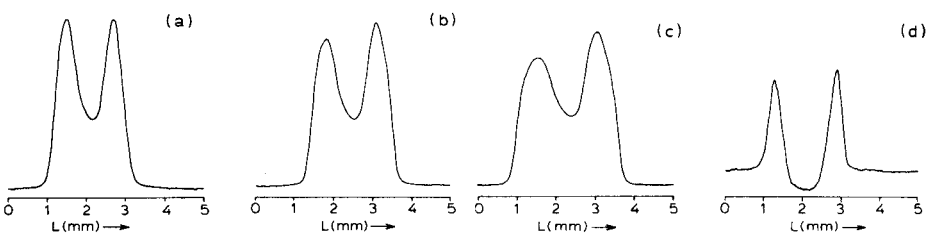

Fig. 6. Scans across the trace for r.p.l.c. coupled to silica t.l.c.: (a) 10^{-5} M (1.4 ng) benz[k]fluoranthene deposited with an unheated 2-bar nitrogen flow; (b) as (a) but with a 1-bar nitrogen flow; (c) as (a) but with a 0.5-bar nitrogen flow; (d) eluent blank (methanol/water 9:1, v/v) deposited with an unheated 2-bar nitrogen flow [this scan was recorded at twice the sensitivity used for (a—c)]. Other conditions as for Fig. 5.

almost 2.0 mm. For benz[k]fluoranthene with the lowest R_f value, these values are 0.8 and 1.3 mm, respectively, indicating a much less pronounced migration effect. Chrysene (0.9 mm between the maxima of the lobes and 1.5 mm FWHM) occupies an intermediate position.

Comparison of Figs. 5(c) and 6(a) illustrates the difference of deposition on C_{18}-modified and bare silica plates; the R_f values of the model compounds on bare silica plates are much higher than those on C_{18}-modified silica (see Table 1). This is also obvious from the cross scans: Fig. 6(a) shows a bifurcated peak with a distance of 1.2 mm between the maxima of the lobes and a FWHM of 1.8 mm, much higher values than those found in Fig. 5(c). This is interesting because the migration on modified plates is about three times faster (Table 2). Apparently the R_f values and not the eluent flow rates are decisive. Methanol evaporates much faster than water, so that the percentage of water in the eluent increases during and after application; this increase sharply reduces the eluent flow rate on both types of plate and the R_f values of the model compounds will also be affected.

Finally, the influence of the pressure of the nitrogen gas on the deposition process was investigated (Fig. 6). Optimal removal of the eluent was obtained when higher nitrogen pressures were used (1—2 bar at the nitrogen cylinder outlet; the actual pressure at the spray jet assembly will be much lower because of the pressure drop over the narrow tubing). At a pressure of 0.5 bar, peak broadening was considerable (Fig. 6c); the band width of 2.5 mm is almost 1.5 times the width obtained at 2 bar.

Figure 6(d) shows a scan obtained when only methanol/water was applied on the silica plate. Obviously, some elution of impurities occurs at the surface of the t.l.c. plate. Investigation of this effect at different nitrogen pressures indicated that mechanical damage of the plate does not contribute appreciably to the band shape observed. Repeated elution with methanol/water did not remove the behaviour shown in Fig. 6(d). This blank elution effect could not be discerned in the scan of the deposited model compound (see Fig. 6a).

CONCLUSIONS

The results of this exploratory study indicate that coupling of narrow-bore l.c. and t.l.c. can be accomplished without serious detraction from the chromatographic integrity of the initial l.c. separation. Interfacing can be done with a slightly modified Linomat applicator for t.l.c. Storage of the l.c. effluent is possible for both normal-phase and reversed-phase l.c. The deposition of the analytes on the t.l.c. plate is strongly influenced by their R_f values for the particular combination of plate material and effluent used, the migration behaviour of the eluent on the plate and, most importantly, the volatility of the effluent. Best results are obtained for highly volatile effluents that exhibit minimal migration on the plate. The ways in which these three factors affect the storage process for the l.c./t.l.c. combinations investigated here are summarized in Table 4. Clearly, the best conditions are obtained for deposi-

TABLE 4

Survey of the factors that affect the l.c./t.l.c. coupling[a]

Factor	N.p.l.c. coupled to		R.p.l.c. coupled to	
	Silica	C_{18}-silica	Silica	C_{18}-silica
Volatility of eluent	+	+	−	−
R_f values (PAHs)	+	−	−	+
Migration speed	0	−	+	0

[a]The influence of the factors is ranked from beneficial (+) via intermediate (0) to detrimental (−) to the particular coupling.

tion of normal-phase l.c. eluents on silica t.l.c. plates. However, even for the worst combination, i.e., r.p.l.c./silica t.l.c., the chromatogram remains quite well resolved. It should be emphasized that the data in Table 4 are valid only for the materials used here. For instance, n-hexane served as eluent in the n.p.l.c. experiment; the use of tri- or tetra-chloromethane as eluent or modifier would strongly influence the ease of eluent removal. In the r.p.l.c. experiment, the use of acetonitrile/water instead of methanol/water would facilitate eluent removal. Eluent changes will obviously affect the R_f values of the analytes and the eluent flow rate.

The storage process can also be influenced by varying the amount of effluent stored per unit surface area of the t.l.c. plate, which can be varied via the l.c. flow rate or the Linomat table speed. An optimum has to be found because small amounts of effluent per mm^2 of plate are favourable from the storage point of view but unfavourable for sensitive detection. The nitrogen flow applied to the spray jet assembly can also be used to change the deposition conditions.

Although the t.l.c. plate coupled to the column system can serve as the stationary phase in a second separation, the more important applications of the present system seem to lie in the area of enhanced detection potential. Two examples, related to two-dimensional fluorescence emission and excitation spectroscopy and low-temperature fluorescence line-narrowing spectroscopy of compounds stored on t.l.c. plates, will be discussed in a subsequent paper.

We thank Dr. R. E. Kaiser and Mr. R. Rieder (Institut für Chromatografie, Bad Dürkheim, F.R.G.) for their kind assistance in solving initial coupling problems, and Merck Nederland (Amsterdam, The Netherlands) for the loan of a Linomat III applicator.

REFERENCES

1 J. W. Hofstraat, H. J. M. Jansen, G. Ph. Hoornweg, C. Gooijer and N. H. Velthorst, Anal. Chim. Acta, 170 (1985) 61.

2 J. N. Miller, Trends Anal. Chem., 1 (1981) 31 (and references therein).
3 S. L. McCall and J. D. Winefordner, Anal. Chem., 55 (1983) 391.
4 P. G. Seybold, D. A. Hinckley and T. A. Heinrichs, Anal. Chem., 55 (1983) 1994.
5 C. D. Tran, J. Chromatogr., 292 (1984) 432.
6 M. N. Neuman, Spectrochim. Acta, Part A, 41 (1985) 1163.
7 M. K. L. Bicking, R. N. Kniseley and H. J. Svec, Anal. Chem., 55 (1983) 200.
8 M. L. Lee, M. Novotny and K. D. Bartle, Analytical Chemistry of Polycyclic Aromatic Compounds, Academic Press, New York, 1981.

Analytica Chimica Acta, 186 (1986) 261—266
Elsevier Science Publishers B.V., Amsterdam — Printed in The Netherlands

Short Communication

SEPARATION OF TRACE ELEMENTS FROM HIGH-PURITY METALS BY SIMULTANEOUS ELECTROLYTIC DISSOLUTION AND ELECTRODEPOSITION OF THE MATRIX ON A MERCURY CATHODE

Part 1. Determination of Aluminium in Iron by Electrothermal Atomic Absorption Spectrometry

MASATAKA HIRAIDE[1,a], PETER TSCHÖPEL[1] and GÜNTHER TÖLG[1,2]

[1]*Max-Planck-Institut of Metal Research, Bunsen-Kirchhoff-Str. 13, D-4600 Dortmund I (Federal Republic of Germany)*
[2]*Institute of Spectrochemistry and Applied Spectroscopy, Bunsen-Kirchhoff-Str. 11, D-4600 Dortmund 1 (Federal Republic of Germany)*

(Received 21st January 1986)

Summary. High-purity iron is effectively dissolved by anodic oxidation and the resulting matrix ions are immediately deposited on a flowing mercury cathode from 2 ml of sodium acetate/potassium chloride electrolyte. Aluminium (>5 ng) in this electrolyte was determined by direct injection into a graphite furnace for atomic absorption spectrometry. The high-purity iron was found to contain 0.34 (±0.03) $\mu g\ g^{-1}$ aluminium.

In the determination of metallic impurities in high-purity materials, analytical results are frequently falsified very considerably by systematic errors. Because there is no certain method to recognize and avoid these errors, it is necessary to check the results of each analysis by one or two independent methods. However, the methods that can be applied in extreme trace analysis are narrowly restricted by these systematic errors. One means of decreasing errors caused by blank values is the use of an electric current as reagent.

In this communication, a procedure is described which involves electrolytic sample dissolution (anodic oxidation for metals) combined with the electrolytic deposition of matrix elements. Both steps should be done simultaneously in the smallest possible dissolution volume (high analyte concentration), in a quartz vessel (low blank values) with the smallest possible surface area (low adsorption losses). In order to prepare the sample for analysis whilst excluding as far as possible the risk of contamination, cleaning of surfaces by electrolytic etching should be included in the same procedure. The procedure was tested on the determination of aluminium in iron. The

[a]Present address: Faculty of Engineering, Nagoya University, Chikusa-ku, Nagoya 464, Japan.

0003-2670/86/$03.50

results are discussed below. Further investigations concerning the determination of extremely low concentrations of other elements in iron, and in other matrices (noble metals, copper, nickel, cobalt) are in progress. Dissolution of the metal sample and removal of the matrix element are done simultaneously by electrolysis [1—3], in which the sample is used as the anode. The resulting matrix ions are deposited on a flowing mercury cathode. Graphite-furnace atomic absorption spectrometry (a.a.s.) is used for the determination of the impurities at ng g^{-1} levels.

In the present investigation, the electrolyte volume was decreased to 2 ml (a tenth of conventional amounts) to give higher concentrations of the trace elements. During electrolysis with diluted sulphuric or perchloric acid as electrolyte, the pH of the solution increased rapidly, which caused the precipitation of hydrated iron oxide. When a more acidic electrolyte was used, numerous tiny hydrogen bubbles were generated from the mercury cathode. These problems were overcome by using an acetate buffer solution containing potassium chloride and flowing mercury.

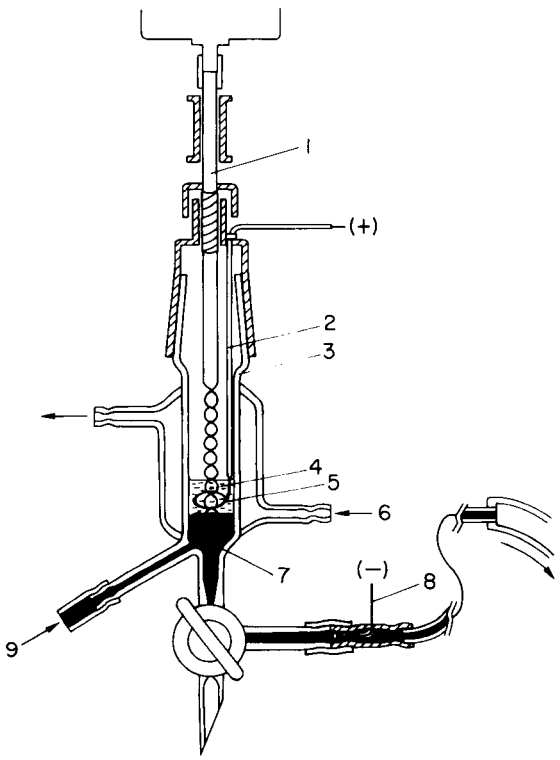

Fig. 1. Electrolysis cell: (1) quartz stirrer; (2) connecting lead, covered with polyethylene; (3) quartz vessel; (4) electrolyte, 2 ml; (5) sample; (6) cooling water inlet; (7) mercury; (8) platinum wire; (9) mercury inlet from peristaltic pump (0.1 ml min^{-1}).

Experimental

Apparatus. The quartz glass electrolysis cell is shown in Fig. 1. The capillary tube increased the velocity of mercury, to avoid back-diffusion of iron. The level of mercury was kept constant by the siphoning effect at the final polyethylene tube. All parts of the apparatus which were likely to cause contamination were made of quartz and were cleaned with nitric acid vapour followed by steam [4, 5] or by soaking in 7 M nitric acid. A peristaltic pump (Gilson Miniplus 2) was used to maintain the mercury flow at 0.1 ml min^{-1}.

A Perkin-Elmer Zeeman System 5000 atomic absorption spectrometer equipped with a HGA-500 graphite-furnace programmer and an AS-40 autosampler were used. A class 100 laminar-flow clean bench was used throughout the procedure, except during weighing of samples and a.a.s. measurements.

Reagents. The electrolyte (pH 3.5) was prepared from 25 ml of a mixture (10:1) of 1 M acetic acid and 1 M sodium acetate (Suprapur; Merck) and 5 ml of 1 M potassium chloride (Suprapur, Merck), diluted with water to 100 ml. Thrice-distilled mercury (100 ml) was further purified by shaking it vigorously with 200 ml of 0.7 M nitric acid for 10 min in a 500-ml PTFE bottle, followed by washing twice with 300 ml of water for 10 min. An iron wire (1-mm diameter, certified content of aluminium <1 $\mu g\ g^{-1}$; Johnson Matthey Chemicals) was used as a high-purity iron sample after etching the surface with 1 M nitric acid. A standard aluminium solution (2 mg ml^{-1}) was prepared in 0.1 M hydrochloric acid from a commercial standard solution (Titrisol, Merck) and diluted to the appropriate concentrations with 0.1 M hydrochloric acid immediately before use. Water purified by ion-exchange followed by double distillation in a quartz still was used. The reagents used were of analytical-reagent grade unless otherwise stated.

Procedure. Mercury is pumped into the electrolysis cell and the Pyrex glass cover which holds the polyethylene-covered positive lead connected to the weighed sample is inserted (Fig. 1). The tip of the stirring rod is immersed into the mercury and the electrolyte and mercury are stirred. Cooling water (20°C) is circulated at 1 l min^{-1}. A current of 0.15 A is passed through the solution to dissolve the sample and the dissolved iron is deposited on the mercury cathode. After the electrolysis, the stirrer and pump are switched off and the stopcock is opened to discard the mercury containing the iron. The thin sample is replaced by a platinum wire, fresh mercury is fed in, and the electrolysis is continued for 10 min as before so as to deposit the iron remaining in the solution. Again the stirrer and pump are stopped, the mercury is removed rapidly through the stopcock and the electrolyte is collected. The residual sample is weighed. A 40-μl portion of the solution is transferred to the graphite furnace for the a.a.s. determination (309.3 nm; drying 150°C, 30 s; decomposition 1000°C, 30 s; atomization 2700°C, 5 s). The measurements are repeated five times and the average absorbance is used to calculate the aluminium content. The sample weight dissolved is calculated from the weights before and after electrolysis.

Results and discussion

Several electrolytes were examined; an acetate buffer solution (pH 3.5) containing some potassium chloride was found to be the most suitable, because hydrated iron oxide did not precipitate during the electrolysis and a reasonable electric current (0.15 A) was obtained without bubble generation. Decreasing the electrolyte volume was desirable to increase the sensitivity, but sample handling became difficult at less than 2 ml.

Although an electrolysis cell of large diameter provided a large surface area for the mercury cathode, the iron sample was liable to contact the mercury, because of oscillation of the mercury level. The best inner diameter of the electrolysis cell was therefore 15 mm. For stirring the electrolyte and mercury, a conventional magnetic stirrer was useless, because the stirring bar floated on the mercury surface and attached easily to the iron sample. The use of ultrasonics (35 kHz) was not successful, because some mercury was dispersed and remained as tiny particles in the electrolyte. A quartz stirrer was satisfactory.

Sample dissolution and deposition of the iron were done as in the recommended procedure. The shape of the sample was such as to maximize the surface area near the mercury cathode (Fig. 1). The electrolyte was colourless and clear throughout the electrolysis. The second electrolysis with a platinum anode was necessary because a few milligrams of iron(II) remained in the aqueous phase. In this electrolysis, the electrolyte immediately became reddish-brown owing to oxidation of iron(II) at the anode. A precipitate of hydrated iron(III) oxide was not formed. After a few minutes, the solution became colourless again. The volume and pH of the electrolyte did not change during the electrolysis. Table 1 shows that the iron sample was dissolved with a current efficiency near 100% and the concentration of the remaining iron in the electrolyte was less than 5 $\mu g\ ml^{-1}$ (determined by flame a.a.s. at 248.3 nm).

Any element having a more negative deposition potential than iron can be expected to remain quantitatively in the electrolyte during electrolysis. As an example, the recovery of aluminium was examined as follows. The iron

TABLE 1

Efficiency of electrolysis

Electrolysis[a] time (min)	Iron dissolved (mg)	Iron remaining in electrolyte[b] (μg)	Electrolysis[a] time (min)	Iron dissolved (mg)	Iron remaining in electrolyte[b] (μg)
30	75	1.0	70	179	10.0
30	77	1.2	80	205	8.6
30	78	0.8	80	206	8.0
50	130	2.4			

[a] At 0.15 A. [b] After the second 10-min electrolysis.

TABLE 2

Recovery of aluminium after electrolysis

Al added (ng)	10	10	20	20	50	100
Al found[a] (ng)	10	11	19	21	50	106
Al recovered (%)	100	110	95	105	100	106

[a]Corrected for 13 ng (the average of 12, 12, 13, 14 and 15 ng) released from the iron sample.

TABLE 3

Determination of aluminium in high-purity iron

Sample dissolved (mg)	Al found (ng)	Al in sample ($\mu g\ g^{-1}$)	Sample dissolved (mg)	Al found (ng)	Al in sample ($\mu g\ g^{-1}$)
77	26	0.34	184[a]	114	0.35
94	29	0.31	213	69	0.32
130[a]	99	0.38	213	72	0.34
154	48	0.31			Av. 0.34

[a]50 ng of Al was also added.

sample was immersed into the electrolyte containing 10—100 ng of aluminium and electrolysis was done for only 15 min, in order to minimize the quantity of aluminium released from the iron sample. After the second electrolysis for 10 min, aluminium in the electrolyte was determined. The calibration graph constructed from the results obtained for 2-ml electrolyte solutions containing different amounts of aluminium was linear up to at least 200 ng with a maximum deviation of 5 ng, and passed through the origin; 20 μg of iron did not interfere with the determination, but 30 μg of iron suppressed the absorbances by 20%. Contamination with aluminium in the reagents, apparatus and environment was negligible (<5 ng). As shown in Table 2, aluminium added to the electrolyte remained nearly completely in the aqueous phase.

By increasing the electrolysis time to 80 min, the aluminium in the high-purity iron sample could be determined. The results are shown in Table 3.

This simple electrolysis technique offers a procedure for the sensitive and reliable determination of aluminium at the ng g^{-1} range by using milligram amounts of sample, and it can also be applied to other impurities having similar deposition potentials to aluminium, e.g. lanthanides, Be, Mg, B, Si, P, Zr, Nb, Ta and W.

REFERENCES

1 R. C. Chirnside, H. J. Cluley and P. M. C. Proffitt, Analyst, 82 (1957) 18.
2 R. C. Rooney, Analyst, 83 (1958) 546.
3 A. Mizuike, Enrichment Techniques for Inorganic Trace Analysis, Springer, Berlin, 1983, p. 67.
4 P. Tschöpel, L. Kotz, W. Schulz, M. Veber and G. Tölg, Fresenius Z. Anal. Chem., 302 (1980) 1.
5 P. Tschöpel, Pure Appl. Chem., 54 (1982) 913.

Analytica Chimica Acta, 186 (1986) 267—272
Elsevier Science Publishers B.V., Amsterdam — Printed in The Netherlands

Short Communication

INDUCTIVELY-COUPLED PLASMA ATOMIC EMISSION SPECTROMETRIC DETERMINATION OF BORON BASED ON GENERATION OF METHYL BORATE

TAKAHIRO KUMAMARU*[a] and HIROSHI MATSUO

Division of Interdisciplinary Studies of Natural Sciences, Faculty of Integrated Arts and Sciences, Hiroshima University, 1-1-89 Higashisenda-machi, Naka-ku, Hiroshima 730 (Japan)

YASUAKI OKAMOTO, MANABU YAMAMOTO and YUROKU YAMAMOTO

Department of Chemistry, Faculty of Science, Hiroshima University, 1-1-89 Higashisenda-machi, Naka-ku, Hiroshima 730 (Japan)

(Received 3rd January 1986)

Summary. Boron is converted to methyl borate, distilled and condensed, and selectively volatilized at 50°C into the plasma without interference from methanol, which quenches the plasma. The 3σ detection limit is 40 ng ml^{-1} boron, the calibration graph is linear up to 10 $\mu g\ ml^{-1}$ and the r.s.d. is 3.0% for 2.0 $\mu g\ ml^{-1}$ ($n = 10$). Boron is determined in plant-tissue and steel standards.

Atomic absorption spectrometry is not very sensitive for boron, even if a nitrous oxide/acetylene flame is used, because of the large dissociation energy of the B—O bond [1]. The sensitivity can be increased by an order of magnitude by introducing gaseous methyl borate, produced by reaction of borate with sulphuric acid/methanol, into a nitrous oxide/acetylene flame [2]. Several methods for the flame emission spectrophotometric determination of boron have been developed by measuring the green BO_2 emission. Such determinations were first discussed by Stahl [3], who prepared methyl borate from boric acid and introduced the volatile product into a Bunsen flame. Belcher et al. [4] successfully applied the principle to the determination of boron by molecular emission cavity analysis.

The present work is concerned with the application of inductively-coupled plasma atomic emission spectrometry (i.c.p./a.e.s.) to the determination of boron. The most sensitive atomic emission line is B I 249.773 nm [5]. However, traces of boron in steel could not be determined accurately by direct aspiration of the sample solution, because the Fe II 249.771 nm and Fe I 249.653 nm lines interfered [6], the former iron line giving a response equivalent to 1.2 $\mu g\ B\ g^{-1}$. Therefore, to analyze such samples, separation of boron from the matrix was necessary. Volatilization of boron as methyl

[a]Present address: Department of Chemistry, Faculty of Science, Hiroshima University.

0003-2670/86/$03.50

borate was chosen for investigation. The vapour could not be introduced directly into the plasma, however, because the methanol which is also volatilized quenches the plasma. Ishii et al. [6] adapted a distillation procedure [7] in which the distillate was passed into a sodium hydroxide solution and the resulting borate solution was evaporated completely to remove methanol.

In this study, methyl borate was distilled and condensed, and the direct introduction of methyl borate vapour from the distillate into the plasma was investigated, advantage being taken of the slight difference in boiling points between methyl borate (55—56°C) and methanol (64.7°C). The methyl borate evaporated first and was introduced into the plasma. The emission peak signal of boron could be measured just before methanol vapour reached the plasma. This technique was applied to the determination of boron in steel and plant-tissue standards.

Experimental

Apparatus. A Kyoto Koken (Kyoto) Model UOP-1S inductively-coupled plasma atomic emission derivative spectrometer was used with a glass concentric nebulizer. The spectrometer had a modified Czerny-Turner configuration and incorporated an echelle grating and an oscillating quartz-refractor plate, by which the second-derivative emission spectrum or intensity was measured and fed to a strip-chart recorder [8].

In the system for generating methyl borate, connections were made with 5-mm i.d. silicone rubber tubing. Teflon decomposition vessels (Uniseal, Haifa, Israel) were used for the mineralization of plant tissue.

Reagents. All the reagents used were of analytical-reagent grade. Pure water (Miniclear Model DC-610 system, Organo, Tokyo) was used. A stock solution (1000 μg ml^{-1}) of boron was prepared by dissolving 2.86 g of boric acid in 500 ml of water. Methanol/sulphuric acid (2 + 1) was prepared by mixing methanol and sulphuric acid and heating in a water bath (90°C) for ca. 30 min to expel traces of contaminating boron as methyl borate. The solution was stored at −15°C.

Procedure for boron determination. Precooled methanol/sulphuric acid (30 ml) and a stirring bar were transferred to a precooled quartz round-bottomed 100-ml flask and 5 ml of aqueous sample solution containing about 50 μg of boron was added. The flask was connected immediately to a Liebig condenser (150 mm long) which was attached to the collection vessel (see Fig. 1) placed in an ice bath. The distillation flask was heated at 90°C in a water bath over a magnetic stirrer for 30 min and the generated methyl borate was collected. After the distillation, the collection vessel, still in the ice bath, was detached from the condenser and purged for ca. 5 min with argon flowing at 0.4 l min^{-1}. The collection vessel was then connected to a four-way stop-cock, set in the by-pass position, and heated in a water bath at 50°C for 120 s (Fig. 1). The stop-cock was turned to the 'sweep' position and the generated methyl borate vapour was introduced into the i.c.p. The

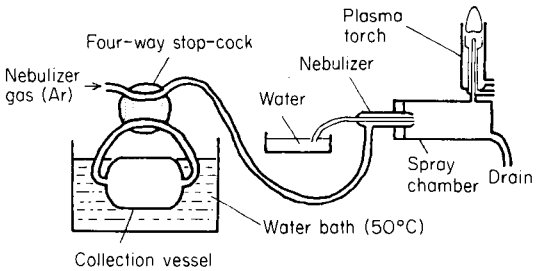

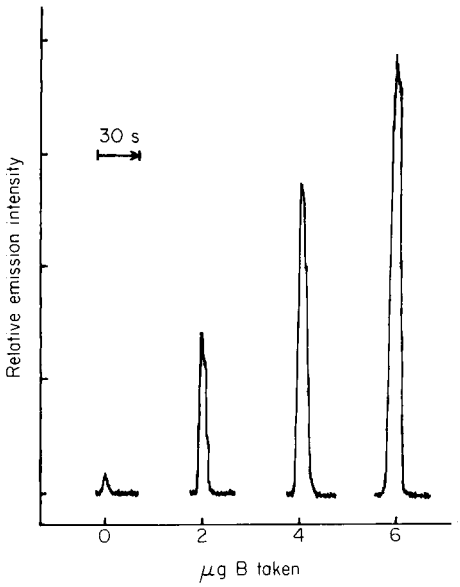

Fig. 1. Apparatus for introducing methyl borate into the plasma.

Fig. 2. Emission-time responses for various amounts of boron. The time axis represents the time from starting to turning the stop-cock to the 'sweep' position. The stated amounts of boron are those added initially to the distillation flask.

peak-height intensity was measured. The stop-cock was turned to the by-pass position immediately after the maximum signal had been obtained. To stabilize the plasma, pure water was always introduced through the nebulizer into the plasma.

Analysis of plant tissue. A 0.5-g sample was weighed accurately into the teflon decomposition vessel and 5 ml of concentrated nitric acid and 1 ml of concentrated perchloric acid (60%) were added. The vessel was then sealed in the usual manner and heated at 150°C for 10 h in an air oven. After cooling to room temperature, the vessel was opened, 2 ml of sulphuric acid was added and the vessel was heated on a hot plate to evaporate nitric acid, until white fumes of perchloric acid were obtained. After the solution had cooled to room temperature, it was transferred to a 25-ml volumetric flask and diluted to volume with water.

Analysis of steel [7]. A 1-g sample was weighed accurately into a 200-ml quartz beaker, 10 ml of aqua regia was added and the beaker was heated to dissolve the sample completely. A 10-ml portion of sulphuric acid/phosphoric acid/water (1 + 3 + 4) was added and the mixture was heated on the hot plate to white fumes of sulphuric acid. After the solution had cooled to room temperature, it was transferred to a 50-ml volumetric flask and diluted to volume with water.

Results and discussion

The r.f. power used was 1.0 kW, which was the same as that needed for aqueous solutions. The reflected power was kept near to zero by an auto-tuning system on the spectrometer. The optimal nebulizer gas flow rate was 0.4 l min^{-1}, which was slightly lower than that for aqueous solutions. Optimal auxiliary gas and plasma gas flow-rates were 0.6 and 12 l min^{-1}, respectively, which were slightly higher than for aqueous solutions. The most sensitive observation height was 15 mm above the load coil, which was the lowest position that could be used. The other operating conditions of the i.c.p. spectrometer are summarized in Table 1.

The emission peak for boron was suppressed by a small amount of methanol, and the plasma itself was quenched when a large amount of methanol was introduced into it. Therefore, the effect of the quantity of methanolic distillate in the collection vessel was investigated. Ishii et al. [6] used a volume ratio of sulphuric acid to methanol of 0.063, as given by the Japanese Industrial Standard [7]. Muraki and Hiiro [9], however, reported that the optimum volume ratio was 0.4 for a spectrophotometric determination based on curcumin. A ratio of 0.5 was adopted in this work in order to minimize the distillation of methanol. Under the conditions used, including a distillation period of 30 min, the amount of distillate, which consisted almost entirely of methanol, was ca. 0.7 ml. Provided that the volume was 1 ml, no interference was observed under the recommended conditions.

TABLE 1

Operating conditions for the i.c.p. spectrometer

Slit width	100—2000 μm	Wavelength modulation	8
Gain	2	Response	1
Applied voltage	800 V	Analytical line	B I 249.773 nm

TABLE 2

Effect of volatilization conditions on emission intensity for 10 μg of boron

Heating temp. (°C)	Heating time (s)	Relative intensity
50	30	48
	60	50
	90	75
	120	88
55	60	35
	90	44
	120	78
60	60	77
	90	100
	120	81

With other variables held constant, the effect of heating time and temperature on the evaporation step were investigated. The results (Table 2) showed that the most sensitive boron emission was obtained by evaporating at 60°C for 90 s, but this caused the plasma to become unstable because methanol was evaporated at almost the same time as methyl borate. However, at 50°C for 120 s, methyl borate evaporated first, followed ca. 10 s later by methanol. Such conditions were acceptable, allowing time to disconnect the vaporization system before too much methanol was transferred into the plasma.

The plasma was also quenched by air. Therefore the air in the collection vessel was displaced by argon prior to the vaporization of methyl borate. An argon flow rate of 0.4 l min^{-1} with the collection vessel and the purge argon ice-cooled beforehand to prevent evaporation of methyl borate, gave no loss of borate over 1 h. To expel air from the collection vessel, a 5-min purge was enough.

When the reagent and sample solutions were transferred to the distillation flask, methyl borate was formed and some was lost, unless precooled distillation flask and reagent solutions were used. The distillation flask was precooled in the ice bath and the reagent solutions were stored at −15°C. These precautions gave a 33% increase in sensitivity compared with that achieved without precooling.

Under the optimal operating conditions, a linear calibration graph was obtained for 0—10 $\mu g\ ml^{-1}$ boron. Typical response curves are shown in Fig. 2. The emission peak of the reagent blank shown in Fig. 2 probably originated from residual boron in the sulphuric acid used. The 3σ detection limit was 40 ng ml^{-1}. The relative standard deviation for 10 replicate measurements of 2.0 $\mu g\ ml^{-1}$ boron was 3.0%.

Interference from iron was removed by the proposed procedure, even when iron was present in a 20 000-fold amount (by weight) compared to boron. Other elements which have lines near the B I 249.773-nm line are tantalum (249.777 nm), germanium (249.796 nm) and tungsten (249.796 nm). These elements also did not interfere.

The accuracy of the present method was established by analyzing two

TABLE 3

Determination of boron in standard reference materials

	Boron ($\mu g\ g^{-1}$)	
	Found[a]	Certified
NBS SRM 348 (High-temperature alloy steel)	31.6 ± 1.6	31
NIES No. 1 (Pepperbush)	44.6 ± 2.2	(48)[b]

[a]Mean ± av. dev., 3 results. [b] Not certified, but given for information.

standard reference materials, Pepperbush (The National Institude for Environmental Studies, Environmental Agency of Japan) and an alloy steel (NBS). The results obtained are shown in Table 3. The data are in good agreement with the certified values.

REFERENCES

1 B. Welz, Atomic Absorption Spectroscopy, Verlag Chemie, Weinheim, 1976, p. 98.
2 Y. Yamamoto, T. Kumamaru, Y. Hayashi and Y. Kochi, The 22nd Annual Meeting of the Japan Society for Analytical Chemistry, Fukuoka, Japan, November 1973, Abst. No. 1A20 (unpublished).
3 W. Stahl, Fresenius Z. Anal. Chem., 83 (1930) 268; 101 (1935) 342, 348.
4 R. Belcher, S. A. Ghonaim and A. Townshend, Anal. Chim. Acta, 71 (1974) 255. M. Burguera and A. Townshend, Anal. Chim. Acta, 127 (1981) 227.
5 P. W. J. M. Boumans, Line Coincidence Tables for Inductively-coupled Plasma Atomic Emission Spectrophotometry, Vol. 1, Pergamon Press, Oxford, 1980.
6 T. Ishii, Y. Ishibashi and C. Takeuchi, Trans. Iron Steel Inst. Jpn., 24 (1984) 498.
7 Japanese Industrial Standard, G 1227 (1980).
8 H. Ishii and K. Satoh, Talanta, 29 (1982) 243. J. Xu, H. Kawaguchi and A. Mizuike, Appl. Spectrosc., 37 (1983) 123.
9 I. Muraki and K. Hiiro, Nippon Kagaku Zasshi, 78 (1957) 850.

Analytica Chimica Acta, 186 (1986) 273—277
Elsevier Science Publishers B.V., Amsterdam — Printed in The Netherlands

Short Communication

DETERMINATION OF LEAD IN THE URINE OF EXPOSED AND UNEXPOSED ADULTS BY EXTRACTION AND FLOW-INJECTION/ ATOMIC ABSORPTION SPECTROMETRY

JOSÉ LUIS BURGUERA* and MARCELA BURGUERA*

Departamento de Química, Facultad de Ciencias, Universidad de Los Andes, Apartado 542, Mérida 5101-A (Venezuela)

LUIS LA CRUZ O. and OLGA RAQUEL NARANJO

Departamento de Farmacología y Toxicología, Facultad de Medicina, Universidad de Los Andes, Mérida 5101-A (Venezuela)

(Received 17th February 1986)

Summary. Lead is extracted from urine with ammonium pyrrolidine dithiocarbamate into methyl isobutyl ketone, and 20 μl of the extract is injected into a water carrier stream in a flow-injection/atomic absorption system. The procedure is simple, quick, accurate and reproducible. Recoveries are 96—105%. The mean urine lead contents of 20 unexposed and 20 printing-press lead exposed workers was found to be 39.0 ± 8.3 and 71.7 ± 26.3 μg Pb l^{-1}, respectively.

Lead finds many uses in lead smelters, paints, soldering, manufacture of storage batteries, cables, ceramics, typesetting and in motor fuel, causing widespread environmental contamination. The principal route of entry of the metal into the body is oral [1] although pulmonary or skin absorption is also of importance [2]. Lead is gradually excreted, predominantly in faeces and urine [3]. Recent emphasis has shifted to the use of erythrocyte protoporphyrin as a more physiologically significant laboratory procedure for detecting increased body lead concentration [4—6], but blood lead values continue to be important both as confirmatory and conjunctive information useful in the diagnosis and treatment of lead poisoning [7—9]. Urine lead levels correlate with blood lead levels when lead is in the normal range [10] and there is a similar correlation for elevated blood lead levels [11]. These correlations, however, are only statistically valid; individual urine analyses cannot be used to predict blood lead values unless, of course, the lead excretion is very high, i.e., over 150 μg/day.

Spectrophotometric and electrochemical methods for the determination of lead in urine [12] have limitations. Electrothermal atomic absorption techniques [13, 14] also have problems, such as the need for sample pretreatment, interference effects, non-specific absorption and loss of lead by volatilization either as halide or as organically-bound lead. Although the determination of lead in urine by atomic absorption spectrometry (a.a.s.) in

0003-2670/86/$03.50

a flame may require wet digestion [15] or extraction in an organic solvent [16], it offers simplicity and precision, and is faster than the other methods.

Recently, flow-injection analysis (f.i.a.) [17] has had great impact in many areas of analysis, because of its high precision and high sampling rate. This communication describes a combination of f.i.a. with a.a.s. for the determination of lead in urine after extraction. The lead content of the urine of workers on a printing press and of non-occupationally exposed adult males is measured.

Experimental

Instrumental. The flow-injection a.a.s. system used was essentially the same as that described by Fukamachí and Ishibashi [18]. The peristaltic pump (Sage 375-A) was furnished with Solvaflex pump tubes. The injector was a rotary valve (Rheodyne, model 7125) with a 20-μl loop. Teflon tubing (25 cm long, 1.0 mm i.d.) was used to connect the valve to the nebulizer of the spectrometer. A Varian model 1475-BD atomic absorption spectrometer was used with a Varian model 9176 chart recorder. The flame was air (8.5 l min^{-1})/acetylene (1.2 l min^{-1}). A lead hollow-cathode lamp was operated at 5.0 mA, and lead was measured at 217.0 nm with a spectral slit-width of 1.0 nm. The centrifuge was capable of a speed of 3500 rpm. The tubes for phase mixing were shaken mechanically. All glassware was precleaned in dilute nitric acid and water.

Reagents and standards. All reagents were of analytical grade unless otherwise stated, and all water was double-distilled and deionized. A 1000 mg Pb l^{-1} standard stock solution was prepared by dissolving exactly 0.5 g of lead metal strip (99.9%) in (1 + 1) nitric acid and diluting to exactly 0.5 l. More dilute standard solutions were prepared daily from the stock solution by dilution with water.

Sample collection. To obtain an indication of the amount of lead excreted each day, 24-h urine specimens were collected. This was done by issuing each individual with two 1-l acid-washed polypropylene bottles. Sampling commenced at the start of the morning shift. The first urine sample was discarded and every subsequent sample was collected for the next 24 h. At the end of this time, the contents of the two bottles were combined and acetic acid was added to give a final acid concentration of 1—3% (v/v). Unless this was done, there was a danger that the urine would slowly decompose and precipitate calcium phosphate, which might coprecipitate some of the lead. The stabilized samples were stored in a refrigerator.

Methods and recommended procedure. Direct analysis of urine for lead by a.a.s. is difficult because the high inorganic content of the urine interferes [19]. Therefore, the modified procedure of Davidow et al. [20] was used, in which the addition of Triton X-100 was unnecessary. This procedure is based on extraction of the lead from urine into methyl isobutyl ketone (MIBK) after addition of ammonium pyrrolidinedithiocarbamate (APDC).

The recommended procedure is as follows. A 5-ml portion of urine on

standard lead solution is added to 1 ml of aqueous 5% (w/v) APDC solution and shaken vigorously for 1 min. Then MIBK (exactly 1 ml) is added, and the mixture is shaken for 1 min and centrifuged for 5 min. The upper, lead-containing layer is removed, and 20 μl is injected into the flow system (flow rate 3.8 ml min^{-1}). The peak absorbance is measured.

Results and discussion

Analytical characteristics of the method. The precision of the method was measured by analysing four urine samples each day for 30 days and 10 consecutive times in one day. The results (Table 1) show satisfactory precision; day-to-day variation was consistent with the within-day variation over 30 days, showing that the repeatability of the method is good and that urine samples are stable as far as their lead content is concerned. To check the accuracy of the procedure, ten specimens of urine were also determined spectrophotometrically [21]. The results (Table 2) show good agreement with the proposed method.

Recoveries of lead in urine were investigated by adding known amounts of the metal to a low-lead (30 $\mu g\ l^{-1}$) pooled urine sample to give lead concen-

TABLE 1

Variation in estimates of lead in four urine specimens

Sample	Mean Pb found (30 tests)[a] ($\mu g\ l^{-1}$)	Mean Pb found (10 tests)[b] ($\mu g\ l^{-1}$)
1	50 ± 2 (4)	51 ± 2 (4)
2	44 ± 1 (2)	44 ± 1 (2)
3	33 ± 1 (3)	34 ± 1 (3)
4	40 ± 2 (5)	41 ± 1 (2)

[a]Mean of 30 daily determinations with standard deviation and relative standard deviation in parentheses. [b]Mean of 10 determinations on one day.

TABLE 2

Comparison of results obtained for lead in urine by the new method and by spectrophotometry [21]

Sample	Lead conc. ($\mu g\ l^{-1}$)[a]		Sample	Lead conc. ($\mu g\ l^{-1}$)[a]	
	This method	Spectrophot.		This method	Spectrophot.
1	33	34	6	39	40
2	46	48	7	45	46
3	50	49	8	44	44
4	50	50	9	33	32
5	44	43	10	46	46

[a]Mean of 4 determinations.

TABLE 3

Determination of lead in urine from unexposed and exposed workers

Unexposed group[a]				Exposed group[b]			
Sample no.	Pb conc. ($\mu g\ l^{-1}$)	Sample no.	Pb conc. ($\mu g\ l^{-1}$)	Sample no.	Pb conc. ($\mu g\ l^{-1}$)	Sample no.	Pb conc. ($\mu g\ l^{-1}$)
1	21	11	45	1	43	11	84
2	25	12	50	2	22	12	82
3	33	13	50	3	42	13	84
4	45	14	39	4	42	14	89
5	42	15	44	5	40	15	89
6	39	16	42	6	50	16	90
7	44	17	46	7	59	17	91
8	40	18	39	8	52	18	95
9	33	19	33	9	71	19	110
10	46	20	25	10	80	20	119
		MEAN:	39 SD: 8			MEAN	72 SD: 26

[a]25—50 years old, mean 38 years. [b]24—54 years old, mean 36 years; samples 1—6 are from workers with 3—10 years exposure to lead; samples 7—20 are from workers with 10—25 years exposure to lead.

trations in the range 60—90 $\mu g\ l^{-1}$. The results obtained indicated recoveries from 96 to 105%. The detection limit (3 × s.d. of blank) estimated for lead in the working standards was 10 $\mu g\ l^{-1}$. The calibration graphs were linear over the range 15—200 $\mu g\ l^{-1}$ lead.

The results of lead determinations in the urine of unexposed and printing-press workers are presented in Table 3. They show that levels of urinary lead in the unexposed population are all $\leqslant 50\ \mu g\ l^{-1}$, and that exposure to lead generally causes a significant increase in the value. The results for the unexposed population are in good agreement with those previously published [22, 23] and also compare well with the mean of 35 $\mu g\ l^{-1}$ obtained in a survey of the inhabitants of 16 countries [24]. In lead-exposed workers, only in six cases were values lower than 52 μg Pb l^{-1}. Thus, 70% of the exposed workers had urine lead levels of 52 $\mu g\ l^{-1}$ or higher. The amount of lead excreted by the printing-press workers may indicate excessive exposure to lead. However the clinical suspicion of plumbism must be confirmed by the application of chemical and other tests before treatment is started. The relationships between urine, blood and hair lead content, and between lead and other metal levels (Cd, Fe, Mn, Zn and Cu), should be studied as well as metabolic changes involving increased excretion of δ-aminolevulinic acid, coproporphyrins and erythrocyte δ-aminolevulinic acid dehydrase [25]. Investigations are in progress in order to incorporate the extraction system into the flow-injection a.a.s. procedure.

REFERENCES

1 National Research Council, Biological Effects of Atmospheric Pollutants: Lead, Airborne Lead in Perspective, National Academy of Science, Washington, 1972.
2 S. Chandra-Rastogi and J. Clausen, Toxicology, 6 (1976) 371.
3 E. I. Underwood (Ed.), Trace Elements in Human and Animal Nutrition, 4th edn., Academic Press, New York, 1977, pp. 410—423.
4 A. A. Lamola, M. Joselow and T. Yamane, Clin. Chem., 21 (1975) 93.
5 J. R. Reigart and N. H. Whitlock, Pediatrics, 57 (1976) 54.
6 T. L. Hanna, D. N. Dietzler and C. H. Smith, Clin. Chem., 22 (1976) 161.
7 R. K. Roschnik, Analyst, 98 (1973) 596.
8 S. K. Giri, C. K. Shields, D. Littlejohn and J. M. Ottaway, Analyst, 108 (1983) 810.
9 J. R. Behari, Int. J. Environ. Anal. Chem., 10 (1981) 149.
10 J. Teisinger, Cas. Lek. Cesk., 105 (1966) 810.
11 S. Selander and K. Cramer, Br. J. Ind. Med., 27 (1979) 28.
12 See, e.g., D. Bryce-Smith, Trends in Anal. Chem., 1 (1982) 199.
13 J. Hodges and D. Skelding, Analyst, 106 (1981) 299.
14 G. Grossi, S. Piazzi, D. Perugini and M. Paolini, J. Res. Lab. Med., 8 (1981) 179.
15 P. M. Eller and J. C. Haartz, Am. Ind. Hyg. Assoc. J., 7 (1977) 116.
16 M. T. Volosin, N. P. Kubask and H. E. Sine, Clin. Chem., 21 (1975) 1986.
17 J. Růžička and E. H. Hansen, Flow Injection Analysis, Wiley, New York, 1981.
18 K. Fukamachi and N. Ishibashi, Anal. Chim. Acta, 119 (1980) 383.
19 A. A. Brown and A. Taylor, Analyst, 110 (1985) 579.
20 B. Davidow, B. Searle and W. Chan, in I. Sunshine (Ed.) Methodology for Analytical Toxicology, CRC Press, Boca Raton, FL, 1975, pp. 207—209.
21 J. Cholak, D. M. Hubbard and R. E. Burkey, Anal. Chem., 20 (1948) 671.
22 C. Long (Ed.), Biochemists' Handbook, Van Nostrand, Princeton, NJ, 1961, p. 363.
23 P. L. Altman and S. Dittmer (Eds.), Blood and Other Body Fluids, Fed. Am. Soc. Exp. Biol., Bethesda, MD, 1971, p. 363.
24 L. J. Goldwater and A. W. Hoover, Arch. Environ. Health, 15 (1967) 60.
25 T. M. Roberts, T. C. Hutchinson, J. Paciga, A. Chattopadhyay, R. E. Jervis, J. VanLoon and K. K. Parkinson, Science, 186 (1972) 1120.

Analytica Chimica Acta, 186 (1986) 279—282
Elsevier Science Publishers B.V., Amsterdam — Printed in The Netherlands

Short Communication

DETERMINATION OF FLUORIDE AND TIN IN FLUORIDE-DOPED TIN OXIDE FILMS ON GLASS

K. E. NIETERING and C. F. MASON
Glass Division, Ford Motor Company, Dearborn, MI 48121 (U.S.A.)
R. O. CARTER III*
Research Staff, Ford Motor Company, Dearborn, MI 48121 (U.S.A.)
(Received 27th January 1986)

Summary. Time-consuming fusion and pyrohydrolysis methods for quantifying fluoride and tin in fluoride-doped tin oxide films on glass are replaced by a simple electrolytic reduction for sample preparation. The unusual conductivity of these films enables solutions to be produced in which fluoride can be quantified by ion chromatography. Tin is quantified in the original sample by x-ray fluorescence spectrometry. Electrolytic reduction and the fusion/pyrohydrolysis methods are compared for films with Sn/F ratios of 10—40 (71—183 $\mu g\ cm^{-2}$ tin and 0.54—2.8 $\mu g\ cm^{-2}$ fluoride). The Sn/F ratios and precision are similar for the two methods. The older method only yields the tin/fluoride ratio; the electrolytic method gives results as mass per unit area and requires much less time per sample.

Tin(IV) oxide films are commonly used glass coatings in applications for which high optical transmission and good chemical and mechanical durability are required. When doped with fluoride (up to 5 atom%), these films become electrically conductive and infrared (heat) reflective. Fluorine-doped tin(IV) oxide films ($<1\ \mu m$) are now pyrolytically applied to architectural glass to improve the R-value (thermal resistance) of glass. The infrared reflectivity of SnO_2/F films depends on thickness, crystallinity, grain orientation, and dopant level. The active dopant level is commonly found by modeling infrared reflectance spectra with the classical Drude "free carrier" model [1]. Comparing dopant levels to actual chemical concentration is important for optimizing production parameters. However, actual fluoride concentrations have been difficult to obtain because of the chemical inertness of the tin(IV) oxide, which is not attacked at room temperature by concentrated nitric, sulfuric, hydrochloric or hydrofluoric acid, or by concentrated bases such as ammonium, sodium and potassium hydroxide.

The first method used in this laboratory for the determination of fluoride was the pyrohydrolysis of tin(IV) oxide [2], coupled with fusion of tin(IV) oxide for the determination of tin. Both these methods of sample decomposition suffer from the need to grind the SnO_2/F film off the glass substrate to obtain enough sample for proper handling. High temperatures (up to 1100°C)

0003-2670/86/$03.50

are also required. Tin/fluoride ratios were found for tin(IV) oxide films (<1 μm) on soda-lime glass. Only ratios could be measured because one could never be certain of the quantitative removal of the film by grinding. Quantitation was by atomic absorption spectrometry for tin and ion chromatography for fluorine.

In this communication, the pyrohydrolysis/fusion method is compared to a new method of sample preparation based on the electrochemical reduction of tin(IV) oxide. The conductivity (<100 ohm sq^{-1}) of these doped tin(IV) oxide films permits the passage of current to an electrolyte/film interface, where reduction of the oxide can occur. The tin content is quantified via x-ray fluorescence prior to film decomposition. Ion chromatography increases the speed of the fluoride determination.

Experimental

A variable-potential power supply (Oriel Model C-72-50) was used at 100 V without current control, because the electrode system was not well defined and changed as the sample reduction proceeded. Float glass coated with fluoride-doped tin(IV) oxide was cut into discs of 4.44-cm (1.75-in) diameter. These were cleaned with detergent and water. The power supply was attached to the sample through a cadmium-plated steel clip. The clip was also attached to the arm of a Sage Instruments Model 341A syringe pump. The pump provided a smooth and constant immersion rate of 0.25 cm min^{-1} of the sample into the carbonate (0.0013 M sodium carbonate/0.0033 N sodium hydrogencarbonate) electrolyte. Sample and electrolyte were contained in a cuvette constructed to minimize the volume of the electrolyte, which was usually 10 ml. Reduction was done with the film as the cathode and a platinum wire as the anode, with a current of 150—300 mA.

Tin was quantified in the solid samples with a Siemens SRS 200 x-ray fluorescence spectrometer equipped with a LiF crystal. Peak areas were compared to those of standards to evaluate the amount of tin present. Fluoride was detected by conductivity on a Dionex 2010i ion chromatograph, equipped with an AS3 anion-separator column and a 50-μl sample-injection loop. The eluent and electrolyte buffer were the same. A 2.0-mg l^{-1} sodium fluoride standard was processed with each set of samples.

For the pyrohydrolysis/fusion method, the SnO_2/F film was removed by grinding off the top layer of a 10 × 10-cm sample with a β-alumina-impregnated core drill. Two 0.1-g portions of this powder were used for fluoride and tin determinations. The fluoride was liberated from the matrix by pyrohydrolysis in the manner of Nardozzi and Lewis [2]. The tungstic acid/glass powder mixture, held in a ceramic boat, was heated in a tube furnace for 30 min at 1100°C. The liberated hydrogen fluoride gas was trapped in 15 ml of the carbonate buffer, described above, to which 20 μl of 30% (w/v) sodium hydroxide had been added. The resulting solution was diluted in the buffer to 25 ml. Fluoride was then quantified by ion chromatography.

Tin was quantified by atomic absorption spectrometry (a.a.s.) with a nitrous oxide/acetylene burner in an IL 751 AA/AE spectrometer and a Westinghouse single-element tin hollow-cathode lamp, operated at 235.5 nm. The tin oxide was fused by heating the powder to 1000°C for 30 min with 1 g of a mixture of 66.1 g of potassium carbonate and 87.7 g of boric acid. The clear melt was cooled and reacted with 100 ml of (1 + 9) hydrochloric acid. A reference tin solution was prepared in the expected concentration range from a standardized solution obtained from Anderson Laboratories (Ft. Worth, TX).

Results and discussion

Five different SnO_2/F films were applied to soda-lime glass. Four samples were prepared from each of these films. One set of duplicate samples was used to determine the fluoride concentration by pyrohydrolysis [2]/ion chromatography and tin concentration by fusion/a.a.s. Tin was quantified in the remaining two sets by x-ray fluorescence and fluoride was quantified by electrolytic reduction/ion chromatography. The use of fusion/pyrohydrolysis resulted in a Sn/F ratio as indicated earlier. This result is adequate for the purpose of film production control. The use of x-ray fluorescence/electrolytic reduction provides results in terms of mass per unit area which could be of interest in other applications.

The Sn/F ratios are presented in Table 1 along with results from x-ray fluorescence and electrolytic reduction. Variations in the duplicate samples as well as in technique yielded results with some scatter, as indicated by the ranges shown in Table 1 for the mean Sn/F ratios. In general, the agreement between the two methods was excellent. Averaged Sn/F ratios are within 6% of each other for the two methods. Total sample processing time for the ten samples by the fusion/pyrohydrolysis method was about 16 h; this consisted of 11 h for sample preparation and 5 h for quantitation. The x-ray fluorescence/electrolytic reduction technique reduced the total time spent to 7.5 h, which included 4 h for sample preparation and 3.5 h for quantitation. The relative time savings could be improved at small cost if parallel electrolytic reduction apparatus were used.

TABLE 1

Tin and fluoride results for duplicate sets of fluoride-doped tin oxide film on float glass

Sample	Electrolytic reduction			Fusion/pyrohydrolysis
	Sn ($\mu g\ cm^{-2}$)	F ($\mu g\ cm^{-2}$)	Sn/F (mole ratio)	Sn/F (mole ratio)
A	71.2 ± 0.9	0.597 ± 0.008	41.8 ± 1.0	40.6 ± 1.1
B	183 ± 2	2.81 ± 0.04	17.0 ± 1.0	16.6 ± 0.6
C	156 ± 2	1.94 ± 0.02	12.9 ± 0.3	12.8 ± 0.3
D	73.8 ± 0.7	0.698 ± 0.009	10.5 ± 0.1	10.9 ± 0.3
E	143 ± 1	0.543 ± 0.007	19.1 ± 0.1	18.0 ± 1.1

An alkaline electrolyte must be used for the reduction of the fluoride-doped tin oxide films to assure the retention of fluorine as fluoride ion. An acidic electrolyte (dilute hydrochloric acid) was tested, but the conductive film was incompletely removed and arcing was noted along the film/electrolyte/air interface, perhaps because of hydrogen produced in the acidic medium by the high over-potential. Also, strong acid solutions interfered with the ion-chromatographic detection of fluoride.

The electrolyte selected for the electrolytic reduction was the buffered carbonate eluent in the ion-chromatographic procedure. With this buffer, no hydrogen fluoride or fluorostannate complexes were formed because the reduced tin remained as the metal while the oxide was progressively reduced. The tin could be easily recovered later if needed for quantitation. In order to avoid the formation of an over-layer of tin which would inhibit, if not passivate, the reduction of the oxide, the sample was slowly lowered into the electrolyte at a constant rate. Generally, 100 V was used to maintain rapid dissolution at the interface. Small bubbles emanated from both electrodes. It is assumed that oxygen is produced at the anode and carbon dioxide is produced where the film enters the solution. The heat produced by the passage of the current in the resistive film can be so intense as to crack the glass; this heat is probably responsible for evolving carbon dioxide from the electrolyte. As the sample is slowly immersed, the film is decomposed in the region where the electrolyte is drawn up the sample. The tin metal is produced as a black powder which flakes off, accumulating on the bottom of the cuvette. Upon completion of the decomposition, the glass substrate is clean and the fluoride is dissolved in the clear colorless solution, the volume of which is minimized by the shape of the cuvette. Tin and fluoride were quantified as described above. If required, the accumulated tin in the cuvette could be dissolved in hydrochloric acid and quantified by a.a.s. or plasma emission spectrometry.

Conclusions

There are four distinct advantages of the electrolytic reduction method over the fusion/pyrohydrolysis methods. The time per sample is reduced; all procedures are done at room temperature; no further solutions are needed, if the electrolyte is readily available; and no grinding is necessary, so that contamination is avoided. The resulting solutions are quite concentrated and free of most interferences.

REFERENCES

1. P. Drude, Ann. Phys. (Leipzig), 14 (1904) 936.
2 M. J. Nardozzi and L. L. Lewis, Anal. Chem., 33 (1961) 1261.

Analytica Chimica Acta, 186 (1986) 283—287
Elsevier Science Publishers B.V., Amsterdam — Printed in The Netherlands

Short Communication

LIQUID—LIQUID EXTRACTION AND DETERMINATION OF URANIUM(VI) WITH 2,6-DIACETYLPYRIDINE BIS(BENZOYLHYDRAZONE)

ANTONELLA CASOLI, ALESSANDRO MANGIA*, GIOVANNI MORI and GIOVANNI PREDIERI

Istituto di Chimica Generale ed Inorganica, Università di Parma, Via M. D'Azeglio 85, 43100 Parma (Italy)

(Received 29th January 1986)

Summary. 2,6-Diacetylpyridine bis(benzoylhydrazone) (H_2DPBH) is proposed as a ligand for the extraction of uranium(VI). Complete extraction from aqueous solutions into dichloromethane is achieved with a ligand/metal mole ratio of <2 for 10^{-5}—10^{-4} M uranyl ion. Potentiometric measurements indicate that the extracted species is UO_2(DPBH). Uranium can be determined in the extract by spectrophotometric measurements at 420 nm and by differential pulse polarography (E_p = −0.67 V) with tetraethylammonium bromide as supporting electrolyte. For both methods, the detection limit is about 2×10^{-6} M in the extract.

Because of their donor properties in coordinating metals, and their ability to behave as polydentate ligands in neutral and deprotonated forms, aroylhydrazones are attractive ligands from the structural and analytical point of view. Aroylhydrazones have been widely used for the extraction of metals from aqueous phases [1–3] and for spectrophotometric determination of metals [4—7]. The use of bis(aroylhydrazones) has also been reported, e.g., for spectrophotometric determinations of calcium, tin and titanium [8, 9]. The chelating properties of these ligands towards several divalent cations have been studied [10—14] and the structures of some complexes have been determined in the solid state [10, 11, 13, 14]. In these complexes, the bis(aroylhydrazones) tend to act as pentadentate ligands in a roughly planar arrangement. This feature, along with the possibility of chelate formation in the deprotonated form, makes 2,6-diacetylpyridine bis(benzoylhydrazone) (H_2DPBH) particularly suitable for the extraction of divalent cations, and of uranyl ion in particular, as neutral complexes. Recently, the extraction of antimony(III) with this ligand from acidic aqueous solutions into 3-methylbutan-1-ol was reported; the SbL and SbL_2 species were extracted [15].

In the present work, H_2DPBH is used for the extraction of uranyl ion from aqueous solutions and for its determination by visible spectrophotometry and polarography. Extraction of uranium is still a relevant problem in both the technological and analytical aspects [16—19]. In the extractions,

0003-2670/86/$03.50

the concentration of the ligand was kept as low as possible, with a maximum concentration ratio of ligand to metal of 10:1, with a view to using the ligand in column chromatography as a modifier of the mobile phases or bonded to the stationary phase.

Experimental

Preparation of the ligand and of the uranyl complex. 1,6-Diacetylpyridine bis(benzoylhydrazone) was prepared as described previously [14]. The product, recrystallized from methanol, was characterized by elemental data, melting point, i.r., n.m.r. and mass spectra. The uranyl complex was synthesized from uranyl acetate in water (1 mmol) and H_2DPBH in methanol (molar ratio 1:1) by heating under reflux. On cooling, the uranyl complex separated as yellow crystals. The elemental data and the spectral properties (i.r., n.m.r.) agreed with the formula of the neutral complex, UO_2DPBH.

Dichloromethane (HPLC grade; Carlo Erba, Milan) and twice-distilled water were used. Other reagents were of analytical grade (Carlo Erba).

Extraction procedure. Aqueous solutions of the metal ion (typically 2 ml) were equilibrated with an equal volume of a dichloromethane solution of the ligand. A Vortex stirrer was used. The concentration of the metal ion was 10^{-4}—10^{-5} M with a stoichiometric metal/ligand ratio from 1:1 to 1:10. For each metal at the different concentrations, a blank extraction was done without the ligand.

Determination of the metals. Extractions of the metals, except for uranium, were checked by means of atomic absorption (Perkin-Elmer model 303 spectrometer) or atomic emission (Leeman PlasmaSpec I spectrometer) spectrometry. The extraction yields for uranium were evaluated after quantifying uranium in both the aqueous and dichloromethane phases by the spectrophotometric Arsenazo-III method [20]. For this purpose the uranyl ion was back-extracted from dichloromethane into 6 M hydrochloric acid prior to spectrophotometry.

Differential-pulse polarographic determinations of uranyl ion in the aqueous phase were done in 25 ml of 2 M acetic acid/2 M sodium acetate; the reduction occurred at —0.41 V vs. Ag/AgCl (3 M KCl) (pulse amplitude —25 mV). For the organic phase, the supporting electrolyte was tetraethylammonium bromide (0.2 M) in dichloromethane. The cell was cooled to 14°C to prevent evaporation of the solvent. The scan rate was 6.25 mV s^{-1} and the reduction peak was at —0.67 V.

Results and discussion

The solid uranyl complex with H_2DPBH was obtained as yellow crystals. The elemental data and spectral (i.r., n.m.r.) behaviour showed that the complex is the neutral UO_2DPBH, with the ligand dianion acting as a pentadentate chelating agent to give a stoichiometric 1:1 metal/ligand ratio.

For the extraction of uranium, dichloromethane was used as solvent. In this solvent, the solubilities of H_2DPBH and its uranyl complex are 2×10^{-3} and

5×10^{-3} M, respectively. The u.v.-visible spectra of the ligand and of the complex are shown in Fig. 1. At 420 nm, the molar absorptivity of the complex is 1.1×10^4 l mol^{-1} cm^{-1}, whereas the absorption of the free ligand is negligible up to 10^{-3} M. The effect of the concentration of the ligand in the dichloromethane phase on the extraction of uranyl ion (10^{-4} M) is shown in Fig. 2. It is worth noting that complete extraction was obtained with a very low concentration of ligand; even after 1 min of stirring, only a 1.6:1 ligand/metal ratio was needed.

The nature of the extracted species was deduced from potentiometric measurements. Unbuffered aqueous solutions of uranyl nitrate were extracted with H_2DPBH. The residual concentrations of uranyl ion were measured polarographically and the aqueous phases were titrated with sodium hydroxide. Two protons were released into the aqueous phase for each extracted uranyl ion. This was also true for extractions in which the ligand/extracted metal ratio was <2, thus it can be deduced that the two protons are displaced by the uranyl ion from one molecule of H_2DPBH, forming a neutral 1:1 complex. The chemical and steric characteristics of the ligand suggest deprotonation of both NH-groups and formation of the UO_2DPBH monomer, as in the solid phase.

The extraction of uranium as a neutral complex is confirmed by the fact that the extraction yield was independent of the nature of the anion. The same percent extraction (95%) was obtained from unbuffered solutions (10^{-4} M) of uranyl acetate, nitrate or sulfate into 1.5×10^{-4} M H_2DPBH in dichloromethane. To verify the effect of ionic strength, 10^{-4} M uranyl (as

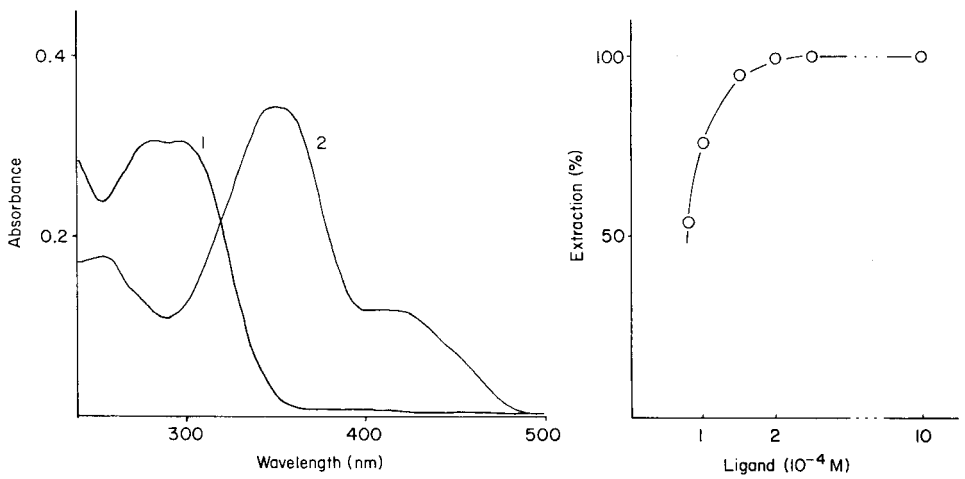

Fig. 1. U.v.-visible spectra: (1) H_2DPBH; (2) its uranyl complex (both at 10^{-5} M) in dichloromethane.

Fig. 2. Dependence of the extraction percentage of uranium (aqueous 10^{-4} M uranyl acetate) on the concentration of ligand in dichloromethane.

acetate) was extracted in presence of 2 M sodium nitrate or chloride with 1.5×10^{-4} M H_2DPBH; again the percentage extraction was about 95%.

Interference study. The extraction of other metals (10^{-4} M) was checked for ligand/metal ratios of 10:1. Iron(III), chromium(III) and aluminium(III) were not extracted, probably owing to the difficulty of forming neutral complexes. The divalent ions Co, Ni, Mn, Cd, Fe, Zn, Ca, Mg, Ba and Sr were not extracted when the ligand/metal ratio was 2:1, but with a ligand/metal ratio of 10:1, appreciable extractions of Co, Ni, Mn, Zn and particularly Ca were obtained (Table 1). For these metal ions, the extraction yields depended on the anion used. This behaviour could be related to the fact that on a preparative scale [14], neutral chelates M(DPBH) (M = Mn, Co, Ni, Zn) were obtained from the metal acetates, whereas complexes with the formula $M(H_2DPBH)Cl_2$ were obtained from the metal chlorides. A different behaviour was observed in the extraction of copper, which was completely extracted with a ligand/metal ratio of 1.2:1. The simultaneous extraction of mixtures of uranium with Co, Ni, Zn, Ca or Cu ions was examined for aqueous solutions containing uranium (5×10^{-5} M) and the other metal (5×10^{-4} M) with dichloromethane solutions of the ligand (1×10^{-3} M). The results indicated that copper ion was the only one which competed effectively in the uranium extraction, which was lowered to 30%. The presence of the other metals did not influence the extraction under these conditions. The interference of copper was overcome by adding EDTA as masking agent; the above extraction, with 5×10^{-4} M EDTA added, gave complete extraction of uranium and 5% extraction of copper.

Determination of uranium. The results of the extractions and the spectral and polarographic behaviour of the complex suggested the use of the ligand not only for the extraction of uranium for technical purposes, but also for its determination by spectrophotometry or polarography. For measurements at 420 nm of the complex dissolved in dichloromethane, the absorbance vs. concentration dependence in the range 10^{-5}—10^{-4} M was given by the equation $y = 1.104(4) \times 10^4 x$; the intercept did not differ significantly from zero (t-test). When uranyl acetate (1.5—6.0×10^{-5} M) was extracted into 5×10^{-4} M H_2DPBH in dichloromethane (triplicate extractions at four concentrations), the absorbance vs. concentration dependence fitted the equation $y = 1.13(8) \times 10^4 x$, again with zero intercept. Comparison of these slopes by a t-test showed that the two curves did not differ significantly at the 99.5%

TABLE 1

Percentage extraction of divalent metal ions (10^{-4} M) with H_2DPBH (10^{-3} M)

Metal	Co	Ni	Mn	Zn	Ca
E (%)	19.5[a]	45[a]	9[a]	30[a]	70[b]
	0[b]	0[c]	2[d]	15[b]	—

[a] As acetate. [b] As chloride. [c] As nitrate. [d] As sulfate.

confidence level (t = 0.118, m = 12). Thus, in the examined concentration range, the extraction does not affect the determination. The detection limit [21] was 1.9×10^{-6} M.

For the polarographic determination, the calibration plot was linear in the concentration range 8×10^{-6}—4.5×10^{-5} M, when a standard solution of the complex in dichloromethane was used with peak measurement at −0.67 V; the detection limit was about 1.7×10^{-6} M but could be lowered by concentrating the dichloromethane phase after extraction.

The use of 2,6-diacetylpyridine bis(benzoylhydrazone) and other bishydrazones for the determination of uranium in real samples is being studied.

This work was financially supported by the Ministero della Pubblica Istruzione, Italy.

REFERENCES

1 A. K. De, S. M. Kopkar and R. A. Chalmers, Solvent Extraction of Metals, Van Nostrand Reinhold, New York, 1970.
2 M. Gallego, M. Garcia-Vargas and M. Valcarcel, Microchem. J., 27 (1982) 328.
3 M. Garcia-Vargas, M. P. Hernandez-Artiga and J. A. Perez-Bustamante, Anal. Chim. Acta, 157 (1984) 363.
4 M. Gallego, M. Garcia-Vargas, F. Pino and M. Valcarcel, Microchem. J., 23 (1978) 353.
5 A. G. Asuero and M. M. Rodriguez, Analyst, 105 (1980) 203.
6 M. Garcia-Vargas, M. Gallego and M. de la Guardia, Analyst, 105 (1980) 965.
7 M. Garcia-Vargas, J. M. Bautista and P. de Toro, Microchem. J., 26 (1981) 557.
8 M. Lever, Anal. Chim. Acta, 65 (1973) 311.
9 M. Silva and M. Valcarcel, Microchem. J., 25 (1980) 117, 289; Analyst, 105 (1980) 193.
10 A. Mangia, C. Pelizzi and G. Pelizzi, Acta Crystallogr., Sect. B, 30 (1974) 2146.
11 M. Nardelli, C. Pelizzi and G. Pelizzi, Transition Met. Chem., 2 (1977) 35.
12 G. Paolucci and G. Marangoni, Inorg. Chim. Acta, 27 (1977) L5.
13 G. Paolucci, G. Marangoni, G. Bandoli and D. A. Clemente, J. Chem. Soc., Dalton Trans., (1980) 1304.
14 C. Lorenzini, C. Pelizzi, G. Pelizzi and G. Predieri, J. Chem. Soc., Dalton Trans., (1983) 721, 2155.
15 M. Garcia-Vargas, C. Belizon, M. Milla and J. N. Perez-Bustamante, Analyst, 110 (1985) 51.
16 I. Tabushi, Y. Kobuke, K. Ando, M. Kishimoto and E. Ohara, J. Am. Chem. Soc., 102 (1980) 5948.
17 G. M. Gasparini and G. Grossi, Sep. Sci. Technol., 15 (1980) 825.
18 L. Zhu and H. Freiser, Anal. Chim. Acta, 146 (1983) 237.
19 J. Aznarez, F. Palacios and J. C. Vidal, Analyst, 108 (1983) 1392.
20 B. W. Budesinsky, Microchem. J., 22 (1977) 50.
21 J. D. Winefordner and G. L. Long, Anal. Chem., 55 (1983) 712A.

Analytica Chimica Acta, 186 (1986) 289—294
Elsevier Science Publishers B.V., Amsterdam — Printed in The Netherlands

Short Communication

SPECTROPHOTOMETRIC FLOW-INJECTION DETERMINATION OF NITRATE BASED ON REDUCTION WITH TITANIUM(III) CHLORIDE

A. AL-WEHAID and ALAN TOWNSHEND*
Chemistry Department, University of Hull, Hull HU6 7RX (Great Britain)
(Received 27th January 1986)

Summary. Nitrate (0.02—5 μg N ml^{-1}) is determined by injection into a water carrier which merges with a 6% (w/v) titanium(III) chloride stream. The nitrite formed is reacted with sulphanilamide and *N*-(1-naphthyl)ethylenediamine, and the resulting azo compound is quantified spectrophotometrically at 530 nm. Of the common ions, only copper(II) interferes; it is removed by an on-line cation-exchange minicolumn. The method is applied to potable waters.

Numerous methods have been proposed for the determination of nitrate. Direct spectrophotometric methods have been based on either u.v. spectrophotometric measurement of nitrate itself [1], or measurement after reaction with brucine [1, 2], chromotropic acid [1, 2], methylene blue [3], 2,4-xylenol [1, 2, 4] or other reagents. Indirect spectrophotometric methods are based mainly on reduction of nitrate to nitrite followed by diazotization and coupling. These methods utilize either a homogeneous reduction process (e.g., with hydrazine [1, 2, 5]) or heterogeneous reduction with zinc, amalgamated zinc [1, 6], cadmium [1, 2, 7, 8], amalgamated cadmium [2], copperized cadmium [1, 8, 9, 10, 11] and copperized cadmium silver [12].

The health hazards associated with cadmium and its salts are well known [13], therefore the use of other reductants would be preferable. Chavdarova [14], for example, used electrolytically generated titanium(III) to reduce nitrate in a coulometric titration. It seemed likely, therefore, that titanium(III) could also be used in a spectrophotometric procedure.

In flow injection analysis, columns of various solid reductants [8—11, 15] have been used for nitrate reduction. The only soluble reductant to have been used is hydrazine [5], which requires copper ions to catalyze the reaction; zinc ions were also added, apparently to suppress interferences. The hydrazine method required very long (8-m) reaction coils, both for reduction and colour development. In an attempt to speed up the method, titanium(III) was examined as a reductant prior to spectrophotometric measurement of nitrite by diazotization and coupling. The development of this procedure is described below.

0003-2670/86/$03.50

Experimental

Apparatus. Two different flow-injection manifolds were evaluated (Fig. 1). In both, an Ismatec Mini-S 820 peristaltic pump was used, and nitrate, or titanium(III), was introduced via a Rheodyne RH-5020 injection valve. The reduction and colour development coils (A and B, respectively) were of 0.5 mm i.d. teflon tubing, as was the remainder of the manifold tubing. The absorbance of the azo dye produced was measured at 530 nm with a Cecil CE-373 spectrophotometer provided with a 18-μl flow cell and attached to a chart recorder. A Hewlett-Packard 8451A diode array spectrophotometer was used for the direct u.v. measurements of nitrate in water samples.

Solutions. All reagents were of analytical grade and distilled/deionized water was used. Titanium(III) chloride solutions were prepared by dilution with water of a 15% (w/v) stock solution (BDH Chemicals). The stock and diluted solutions were kept under helium (or nitrogen), as titanium(III) is oxidized by air, and were stored in the dark when not in use. The colour-forming reagent was prepared daily by dissolving 5 g of sulphanilamide (Hopkin and Williams) and 0.125 g of *N*-(1-naphthyl)ethylenediamine dihydrochloride (Koch-Light Laboratories) in 100 ml of 1.5 M hydrochloric acid and diluting to 250 ml with water. This solution was stored at 4°C.

A nitrate stock solution (1000 μg N ml^{-1}) was prepared by dissolving 6.068 g of sodium nitrate in water and diluting to exactly 1 l; a little chloroform was added to suppress growth of microorganisms, and the solution was stored at 4°C. Working standards were prepared by appropriate dilutions with water to cover the range 0.0—5 μg N ml^{-1}. Hull tap-water samples were analyzed immediately after collection.

Results and discussion

This work developed in three stages. First, the manifold in Fig. 1(a) was used; the nitrate samples were introduced into a stream of titanium(III) chloride. Reduction took place in coil A, and the nitrite formed merged with the colour-forming reagent. The conditions were optimized to achieve the greatest absorbance. A 2% (w/v) titanium(III) chloride solution gave the highest peaks. When coil A was <100 cm long, the reduction time was insufficient to give a good yield of nitrite. For coils >100 cm, nitrite itself was significantly reduced. This effect was clear when nitrite samples were injected, as the absorbance decreased continuously as the length of coil A increased, and

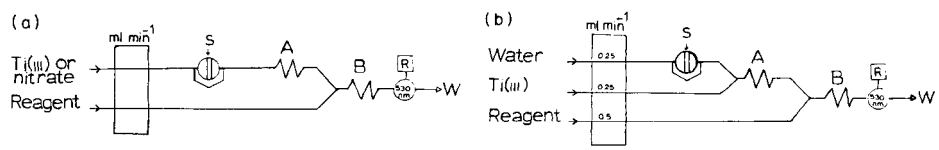

Fig. 1. Manifolds used: (a) for pumping titanium(III) and injecting nitrate, or vice versa; (b) for nitrate injected into water. S, sample injected; A, reduction coil; B, colour development coil; R, recorder; W, waste.

maximum absorbance was obtained when coil A was removed. A 100-cm coil is therefore recommended for nitrate determination with this manifold. The colour-forming coil B, gave less absorbance when its length exceeded 150 cm, owing to further reduction by titanium(III) chloride.

Titanium(III) chloride solutions are violet, and absorb light in the same range as the pink azo dye (Fig. 2). When very dilute samples of nitrate ($\leqslant 2$ μg N ml^{-1} in 40 μl) were injected into the titanium(III) chloride stream, negative peaks were obtained owing to the dilution of the titanium(III) chloride. This problem was avoided by injecting the titanium(III) chloride into a stream of nitrate solution, with the same manifold, but it was replaced by a residual positive peak caused by the excess of titanium(III) chloride.

Various ways of preventing the remaining titanium(III) chloride from interfering in this way were examined. An oxidizing agent was sought that would oxidize titanium(III) but not nitrite and would not affect the chromogenic reaction for nitrite. However, all those reagents tested [iron(III), copper(II), hydrogen peroxide, methylene blue] either did not oxidize titanium(III) or also affected the azo-dye formation. The use of a cation-exchange resin to trap titanium(III) was also evaluated. A small column (2 cm long, 2 mm i.d.) filled with a strong acid cation-exchange resin (Dowex 50W-X8, H^+ form, 200—400 mesh) was inserted after coil A. Unfortunately, although titanium(III) was retained by the column, nitrite was not eluted from it either. A modified manifold, therefore, was used. Nitrate solutions were injected into a stream of water (Fig. 1b), which later merged with the titanium(III) solution. This eliminated the undesirable effects. Conditions were optimized for that manifold. Titanium(III) chloride concentrations from 2% to 15% were evaluated. The results obtained (Fig. 3) showed that within the range 6—10% the sensitivity was constant and maximal. At higher concentrations the peak height decreased owing to further reduction of nitrite. Therefore, 6% titanium(III) chloride was used in all further experiments. The effects of the coil lengths for reduction and colour development were

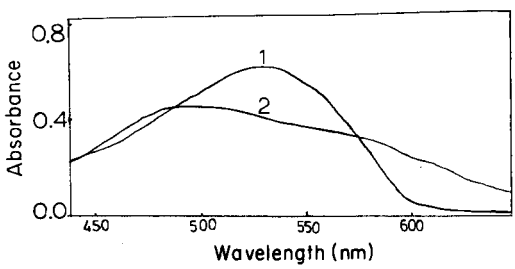

Fig. 2. Absorption spectra: (1) azo dye product (5 μg N ml^{-1}); (2) titanium(III) chloride (1% w/w).

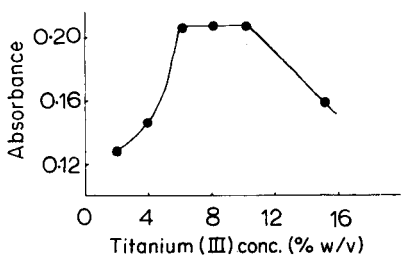

Fig. 3. Effect of titanium(III) chloride concentration on peak-maximum absorbance of 40 μl of 10 μg N ml^{-1} nitrate. (Coils A and B were 50 and 150 cm, respectively; sample, reductant and reagent channels were 0.35 ml min^{-1} each.)

TABLE 1

Effect of coil lengths for reduction and colour development on peak-height absorbance (40 μl of 30 μg N ml^{-1} nitrate solution injected; reductant and reagent flow rates were 0.25 ml min^{-1} each.)

Coil A length[a] (cm)	Absorbance	Coil B length[b] (cm)	Absorbance
4	0.55	100	0.46
50	0.60	150	0.60
100	0.55	200	0.52

[a]Coil B = 150 cm. [b]Coil A = 50 cm.

TABLE 2

Effect of reduction and reagent flow rates on peak height absorbance (Reduction and colour-development coil lengths were 50 and 150 cm, respectively; 20 μl of 30 μg N ml^{-1} nitrate solutions were injected.)

Reductant flow rate[a] (ml min^{-1})	Absorbance	Reagent flow rate[b] (ml min^{-1})	Absorbance
0.13	0.42	0.25	0.35
0.25	0.46	0.50	0.42
0.50	0.30	0.70	0.33

[a]Reagent flow rate, 0.5 ml min^{-1}. [b]Reductant flow rate, 0.35 ml min^{-1}.

also investigated. The results are shown in Table 1. A 50-cm reduction coil gave the greatest peak height; a longer coil gave a smaller peak owing to further reduction of nitrite. Colour development was greatest in a coil of length 150 cm. Variation of reductant flow rate (Table 2) also showed the need to balance maximum reduction of nitrate and minimum reduction of nitrite; a flow rate of 0.25 ml min^{-1} gave the greatest peak height in this respect. Similarly, a compromise was needed for the flow rate of the colour-forming reagent; maximal delivery of reagent, with reasonable time for the reaction and minimal dispersion, was achieved at 0.5 ml min^{-1}.

The calibration peaks for nitrate standards in the range 1—5 μg N ml^{-1} are shown in Fig. 4. The calibration graph was linear up to at least 5 μg N ml^{-1} with a correlation coefficient (5 points) of 0.9999. The least-squares calibration equation is: peak height absorbance = 7.68×10^{-3} [N] -1.28×10^{-3}, where the nitrate concentration is in μg N ml^{-1}. The detection limit (2 $\times$ blank noise) was 0.02 μg N ml^{-1}, and the sample throughput was 30 h^{-1}.

The following species showed negligible interference at the 100 μg ml^{-1} level on nitrate at 10 μg N ml^{-1}: acetate, citrate, iodate, urea, carbonate, dichromate, chloride, sulphate, aluminium, iron(III), calcium, zinc, sodium and potassium. Copper depressed the peak height even at 1 μg ml^{-1}. Such a large depressive effect by copper has not previously been reported when other

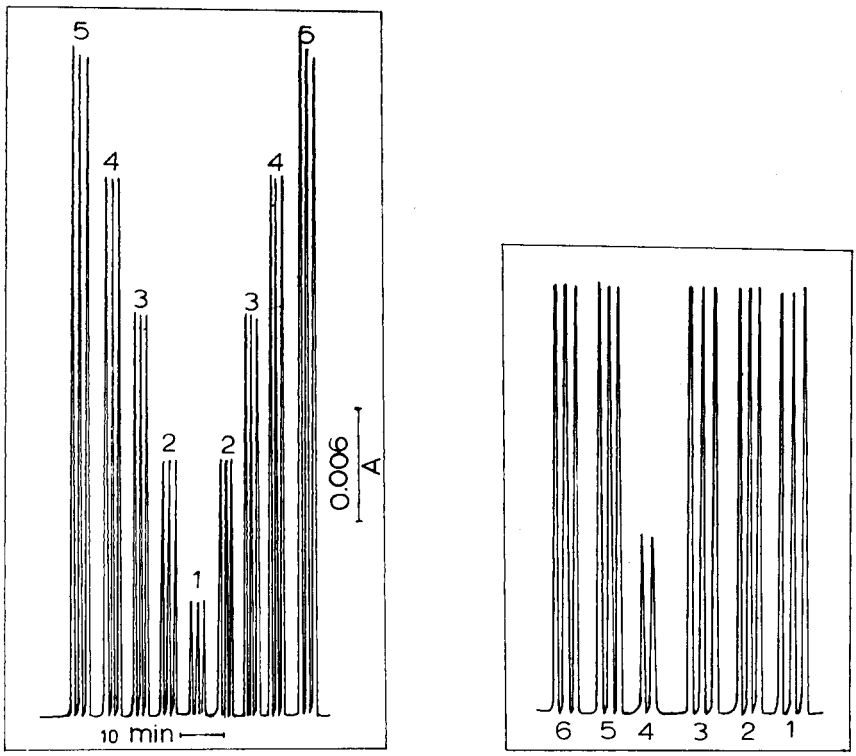

Fig. 4. Peaks obtained by injecting triplicate nitrate standards at concentrations of 1—5 μg N ml^{-1}.

Fig. 5. Signals obtained for 200 μg N ml^{-1} nitrate solutions containing different amounts of copper(II) with a cation-exchange column on-line (scales as in Fig. 4): (1, 6) 0; (2) 10; (3) 20; (4) 20 (no column); (5) 30 μg ml^{-1} copper(II).

reductants were used. This effect was investigated in detail. Copper ions did not affect the diazotization and coupling reaction, even at high concentration ($\geqslant$1000 μg ml^{-1}), as was shown by injection of 2 μg N ml^{-1} nitrite solutions containing different copper concentrations, without the titanium(III) chloride solution. In addition, such small copper concentrations had a negligible effect on the titanium(III) chloride concentration. It would seem, therefore, that copper ions inhibit the reaction between nitrate and titanium(III) chloride.

Copper ions can be completely removed before the sample meets the reductant by passing the water stream through a small column (3 cm long, 2 mm i.d.) filled with the same strong acid cation-exchange resin as used above Figure 5 shows the signals obtained for 20 μg N ml^{-1} nitrate solutions mixed with various amounts of copper. It shows that the depressive effect of copper was completely eliminated up to at least 30 μg ml^{-1}.

The procedure was applied to a sample of Hull tap water. The value obtained

was 8.3 μg N ml^{-1} as nitrate (3 identical results). The same tap water was analyzed by u.v. spectrophotometry with deionized water as a reference, at 234 nm; the value obtained was 8.5 μg N ml^{-1} as nitrate.

REFERENCES

1 F. D. Snell, Photometric and Fluorimetric Methods of Analysis, Nonmetals, Wiley-Interscience, New York, 1981, pp. 544—576.
2 Z. Marczenko, Spectrophotometric Determination of Elements, Ellis Horwood, Chichester, 1976, pp. 397—399.
3 H. Ciesielski, G. Sorgnet, M. Catone and P. Vancayzeele, Analusis, 6 (1978) 38.
4 G. Norwitz, J. Farino and P. N. Keliher, Anal. Chim. Acta, 105 (1979) 335.
5 B. C. Madsen, Anal. Chim. Acta, 124 (1981) 437.
6 S. J. Bajic and B. Jaselskis, Talanta, 32 (1985) 115.
7 J. H. Margeson, J. C. Suggs and M. R. Midgett, Anal. Chem., 52 (1980) 1955.
8 M. A. Koupparis, K. M. Walczak and H. V. Malmstadt, Anal. Chim. Acta, 142 (1982) 119.
9 L. Anderson, Anal. Chim. Acta, 110 (1979) 123.
10 M. F. Giné, B. F. Reis, A. E. G. Zagatto, F. J. Krug and A. O. Jacintho, Anal. Chim. Acta, 155 (1983) 131 (and references therein).
11 J. F. Van Staden, Anal. Chim. Acta, 138 (1982) 403.
12 R. B. Willis, Anal. Chem., 52 (1980) 1376.
13 E. Berman, Toxic Metals and Their Analysis, Heyden, London, 1980, pp. 66—68.
14 R. Chavdarova, Dokl. Bolg. Akad. Nauk, 26 (1973) 227.
15 J. Růžička and E. H. Hansen, Flow Injection Analysis, Wiley-Interscience, New York, 1981, pp. 80—81.

Analytica Chimica Acta, 186 (1986) 295—299
Elsevier Science Publishers B.V., Amsterdam — Printed in The Netherlands

Short Communication

POLAROGRAPHIC STUDY OF 1-METHYL-5-*o*-CHLOROPHENYL-7-ETHYL-1,2-DIHYDRO-3H-THIENO[2,3-e],[1,4]-DIAZEPIN-2-ONE (CLOTIAZEPAM)

R. M. ALONSO ROJAS

Departamento de Química, Facultad de Ciencias, Universidad del Pais Vasco, 48080 Bilbao (Spain)

L. HERNANDEZ-HERNANDEZ*

Departamento de Química Analítica, Facultad de Ciencias, Universidad Autónoma de Madrid, 28049 Madrid (Spain)

(Received 18th June 1985)

Summary. The electroreduction of 1-methyl-5-*o*-chlorophenyl-7-ethyl-1,2-dihydro-3H-thieno[2,3-e],[1,4]-diazepin-2-one (Clotiazepam) is investigated by different polarographic techniques. The electrochemical reaction involves a 2-electron exchange in both acidic and alkaline media. The reduction process is irreversible and the current is diffusion-controlled. With differential pulse polarography, the linear response range is 6.5×10^{-7}—1.10×10^{-5} M, with a relative standard deviation of 1.2% at the 2.6×10^{-6} M level. The method is applied to the determination of Clotiazepam in tablets after simple dissolution in 0.1 M sulphuric acid.

Since the introduction of Librium, chlordiazepoxide hydrochloride, in 1960, many 1,4-benzodiazepine derivatives have been investigated as tranquillizers, antidepressants and sedatives [1]. 1-Methyl-5-*o*-chlorophenyl-7-ethyl-1,2-dihydro-3H-thieno-[2,3-e],[1,4]-diazepin-2-one (Clotiazepam) belongs to a more recent series, thienodiazepines, which differ from benzodiazepines only in having a thiophene nucleus bound to the diazepinic ring instead of a benzene nucleus. Nakanishi et al. [2] studied the pharmacological properties of this compound and showed that its properties were similar to those of benzodiazepines. It is a well tolerated and excellent tranquillizer.

Numerous papers have described electrochemical studies of 1,4-benzodiazepines [3—6], but thienodiazepines do not seem to have been studied. Accordingly, a study of the electrochemical behaviour of Clotiazepam by means of different polarographic techniques [7] was conducted. A method for quantifying the drug by differential pulse polarography is reported.

Experimental

Apparatus. A Princeton Applied Research Corporation (PAR) model 174 polarographic analyzer was used with a PAR model 303 SMDE cell and a

0003-2670/86/$03.50

Houston Omnigraphic X-Y recorder. The three-electrode cell (capacity 10.0 ml) was fitted with a dropping mercury electrode (DME, capillary internal diameter 0.015 mm), a Ag/AgCl/KCl (saturated) reference electrode and a platinum wire auxiliary electrode.

The sampled d.c. and differential-pulse polarographic modes were applied. For the latter, the pulse amplitude was 25 mV and the drop time 0.5 s. Scans were recorded from −0.60 to −1.90 V (vs. Ag/AgCl electrode) at a scan rate of 5 mV s^{-1} with a full range of 1.5 V.

For cyclic voltammetry, an AMEL model 448 oscillographic polarograph was used with a hanging mercury drop electrode, a saturated calomel reference electrode and a platinum auxiliary electrode. For the controlled-potential coulometric measurements, a mercury pool electrode was used. All experiments were done at 20 ± 1° C. Dissolved oxygen was removed from solutions by bubbling oxygen-free nitrogen through the cell for 8 min.

A Radiometer pHM64 digital pH-voltmeter was used with a combined glass/calomel electrode (GK-2301-C).

Reagents. The stock solution of Clotiazepam (Esteve Laboratories, Barcelona) was 3.13 × 10^{-3} M in methanol. It was stored in the dark under refrigeration. All reagents used were of analytical grade (Merck). A stock Britton-Robinson buffer solution (pH about 2) composed of boric acid, phosphoric acid and acetic acid (all 0.04 M) was prepared. Buffer solutions of different pH were then prepared by addition of 0.2 M sodium hydroxide to this stock solution to give the required pH on a pH-meter.

Results and discussion

The effect of pH on the current/voltage peaks in differential pulse polarography (d.p.p.) was investigated by recording polarograms for 2.51 × 10^{-5} M Clotiazepam in Britton-Robinson buffers (Fig. 1). Clotiazepam produces one

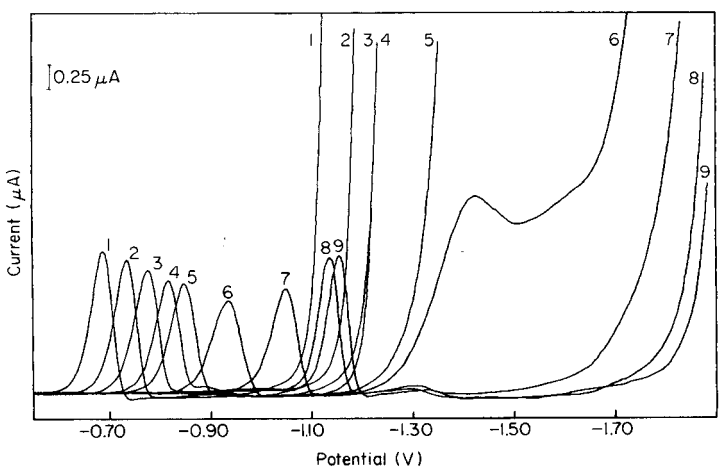

Fig. 1. Differential pulse polarograms of Clotiazepam (2.51 × 10^{-5} M) at different pH values: (1) 0.95; (2) 1.92; (3) 2.80; (4) 4.05; (5) 4.69; (6) 5.98; (7) 7.07; (8) 9.18; (9) 10.35.

well-defined peak in the pH range 1—11 and a second peak at about pH 6, the latter appearing to be catalytic in origin. The peak potential, E_p, is shifted linearly to more negative potentials as the pH is increased, indicating that hydrogen ions are involved in the reduction. The plot of E_p vs. pH (Fig. 2) shows three linear portions; the first break at pH 4.40 corresponds to the spectroscopic pK_a (4.25 at ionic strength 0.1 M [8]) and the second break at pH 8.35 corresponds to the pK_1' value [9]. In the first linear portion (pH 1.0—4.4), the E_p peak potential can be expressed by the equation, $E_p = -0.69 - 0.03$ pH; in the second portion (pH 4.4- 8.35) $E_p = -0.49 - 0.08$ pH, whereas the third portion is pH-independent, the peak current also being pH-dependent. The highest currents are obtained for acidic media (pH $\leqslant$ 2) and at pH > 8.0.

The reversibility of the electrode process was studied by sampled d.c. polarography, differential pulse polarography and cyclic voltammetry, the criteria depending on the technique chosen. The αn values (average 1.7) obtained from the plot log $(i_d - i)/i$ vs. E [10] in sampled d.c. polarography, the peak half-widths (average $w_{1/2}$ = 55 mV) in d.p.p. [11] and the criteria of Birke et al. in d.p.p. [12] demonstrated the irreversibility of the reduction process, as did the absence of an anodic peak, the asymmetric form of the wave and the increase of peak potential as a function of scan rate (v) in cyclic voltammetry [13]. Figure 3 shows the cyclic voltammograms at pH 2.00.

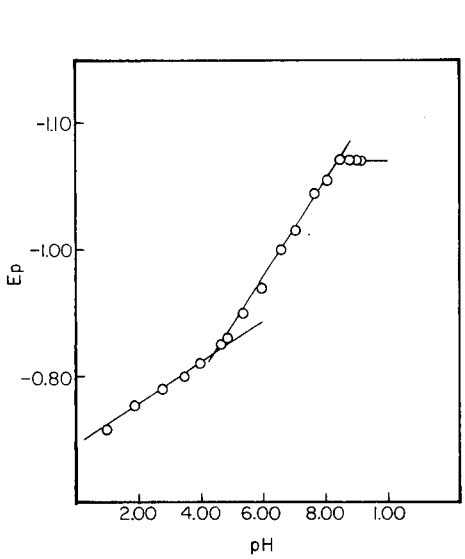

Fig. 2. Influence of pH on the peak potentials of Clotiazepam. Conditions as for Fig. 1.

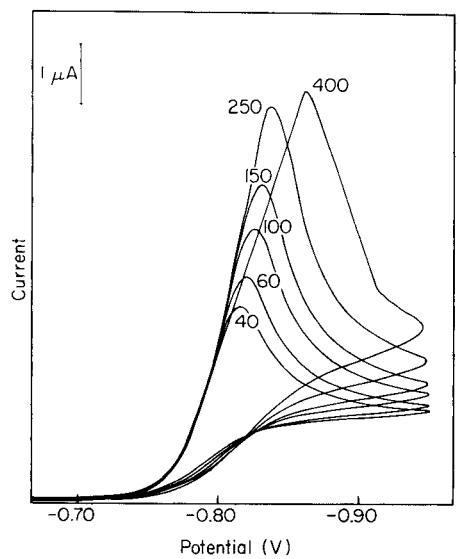

Fig. 3. Cyclic voltammograms of Clotiazepam at pH 2.0 at the scan rates (mV s^{-1}) indicated on the peaks.

The reduction process was diffusion-controlled in the media studied; this was deduced from the linear dependence of peak current on the concentration of Clotiazepam in d.p.p. and from the linear $i = f(v^{1/2})$ relation in linear sweep voltammetry [7]. Two electrons were involved in the reduction process, as found by microcoulometry, for the whole pH range studied. From the number of electrons and the slopes of the plot E_p vs. pH, the number of protons for each linear portion of the plot can be calculated as 1 for the first portion and 2 for the second portion. Accordingly, the following scheme can be proposed for the Clotiazepam reduction.

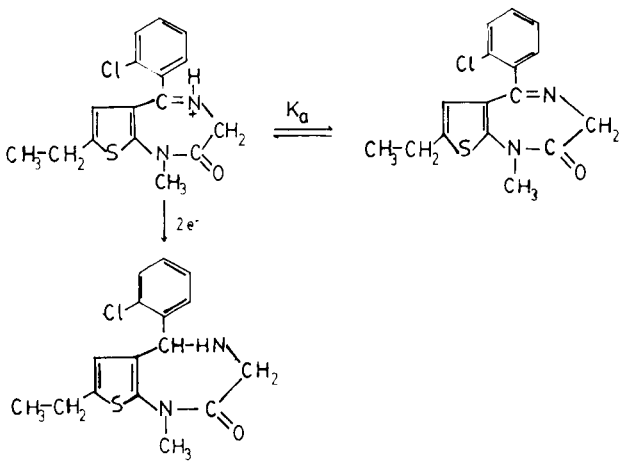

In this scheme, the unprotonated molecule is not reduced in the available pH range and only the protonated form is electroactive at the DME. This scheme is similar to others reported for 1,4-benzodiazepines such as Diazepam [4].

Application to the analysis of tablets. On the basis of the above experiments, a differential-pulse polarographic method of quantifying Clotiazepam was developed. The stock solutions of Clotiazepam were found to be stable with time for at least a week. Calibrations graphs were prepared by using a series of solutions diluted with the appropriate Britton-Robinson (BR) buffer. The optimum concentration range for the Clotiazepam determination at pH 1.89 was 6.50×10^{-7}—1.10×10^{-5} M; the slope of the calibration graph in this medium was 0.0477×10^6 μA M^{-1} with a standard deviation of 0.0026.

The Clotiazepam-containing tablets, Distensan, were found to disintegrate very quickly in dilute sulphuric acid; because polarograms of the compound recorded at pH $\leqslant$ 2 exhibited a well-defined peak with higher peak current than in other media, 0.1 M sulphuric acid was used as supporting electrolyte. Accordingly, the tablets were simply stirred with 0.1 M sulphuric acid for 5 min and the solution was made up to 100 ml with the same acid. Standard additions were used to quantify the content of Clotiazepam in tablets because there was no prior separation of excipient, thus avoiding extraction of the

drug and possible losses involved in filtration of the excipient. The results obtained for the determination in tablets gave a mean value of 10.0 (±0.1) mg/tablet (n = 5; nominal content 10.0 mg).

The proposed method is very simple and has satisfactory accuracy for the determination of Clotiazepam in tablets. Moreover, because removal of the insoluble matter is omitted and there is no need to change the pH of the medium, the method is also more rapid than spectrophotometric procedures.

REFERENCES

1 C. Bellantuono, V. Reggi, G. Tognani and S. Garattini, Drugs, 19 (1980) 195.
2 M. Nakanishi, T. Tsumagari, Y. Takigawa, S. Shuto, T. Kenjo and T. Fukuda, Arzneim. Forsch., 22 (1972) 1905.
3 B. Z. Senkowski, M. S. Levin, J. R. Urbigkit and E. G. Wollish, Anal. Chem., 36 (1964) 1991.
4 J. M. Clifford and W. F. Smyth, Z. Anal. Chem., 264 (1973) 149.
5 M. A. Brooks, Bioelectrochem. Bioenerg., 10 (1983) 37.
6 H. Oelschager, Bioelectrochem. Bioenerg., 10 (1983) 25.
7 A. J. Bard and L. R. Faulkner, Electrochemical Methods. Fundamentals and Applications, Wiley, New York, 1980.
8 R. M. Alonso, L. Hernandez and M. A. Fernandez-Arciniega, Quim. Anal., in press.
9 P. Zuman and C. L. Perrin, Organic Polarography, Wiley, New York, 1969.
10 L. Meites, Polarographic Techniques, Interscience, New York, 1955.
11 A. M. Bond, Modern Polarographic Methods in Analytical Chemistry, Dekker, New York, 1980.
12 R. L. Birke, K. Myung-Hoon and M. Strassfeld, Anal. Chem., 53 (1981) 852.
13 P. Delahay, New Instrumental Methods in Electrochemistry, Interscience, New York, 1954.

Analytica Chimica Acta, 186 (1986) 301—305
Elsevier Science Publishers B.V., Amsterdam — Printed in The Netherlands

Short Communication

COMPARATIVE STUDY OF POTENTIOMETRIC AND AMPEROMETRIC TISSUE-BASED ELECTRODES FOR OXALATE

TEKUM FONONG

Department of Chemistry, Illinois State University, Normal, IL 61761 (U.S.A.)

(Received 4th December 1985)

Summary. Acetone-precipitated pulp from banana skins is physically entrapped at the tip of a carbon dioxide gas-sensor and on a hydrogen peroxide sensor probe to determine oxalate potentiometrically and amperometrically in aqueous solution and in urine. The enzyme present in the tissue is oxalate oxidase. The potentiometric response has a slope of 47—50 mV/decade for 1×10^{-4} M—2×10^{-3} M oxalate with a detection limit of 2×10^{-5} M. The amperometric response is linear for 2×10^{-5}—3×10^{-4} M oxalate with a detection limit of 2×10^{-6} M. Average recoveries of oxalate added to aqueous samples were 96.2% and 98.0%, and average relative standard deviations were 3.8% and 3.6% for the potentiometric and amperometric systems, respectively. Oxalate was determined in six control urine samples, with relative errors of about 2.5%, by both electrode systems after a simple clean-up.

The determination of oxalate in urine is of clinical importance in the diagnosis of urinary tract stones and hyperoxaluric acid syndromes. Several methods exist for determinations of oxalate in urine [1—9]. Usually, isolation of oxalate from the urine by precipitation, extraction, or ion-exchange is needed before assay of oxalate, or a derivative, by titrimetry, colorimetry, fluorimetry or gas-liquid chromatography; ^{14}C-oxalic acid is often used as a recovery marker.

Several enzymatic methods for determining oxalate have been reported [10—18]. These methods utilize either oxalate decarboxylase (E.C. 4.1.1.2.) which converts oxalate to formate and carbon dioxide, or oxalate oxidase (E.C. 1.2.3.4) which converts oxalate stoichiometrically to hydrogen peroxide and carbon dioxide:

$$\text{oxalate} + O_2 \rightarrow H_2O_2 + 2\ CO_2$$

The enzymatic methods are normally preferred because they are simple and fast (requiring minimal sample pretreatment). In the enzymatic method reported here, oxalate oxidase present in the pulp of banana peel [19] is utilized. This method should be attractive because of the inexpensive source of the enzyme, its easy availability and its stability.

Potentiometric measurement of the carbon dioxide or amperometric determination of hydrogen peroxide formed in the above reaction can be

0003-2670/86/$03.50

used to quantify oxalate. Oxalate oxidase is preferable to oxalate decarboxylase for potentiometric measurements because two moles of carbon dioxide are produced compared to one mole in the case of oxalate decarboxylase. Moreover, commercially available oxalate decarboxylase has been reported to exhibit low specific activity, requiring further purification [18].

Experimental

Apparatus. An Orion 95-02 carbon dioxide gas-sensing electrode and a YSI Model 2510 Oxidase Probe (Yellow Springs Instrument Co., Yellow Springs, OH) were used to construct the tissue-based electrodes. A Fisher Scientific Accumet Ionalyzer Model 750 meter was used with a Fisher Model 4512BF strip-chart recorder for potential measurements. A YSI Model 25 oxidase meter was used with the recorder for current measurements. All the measurements were made in a glass cell thermostated at 30.0 ± 0.1°C with a constant-temperature circulator (Fisher Model 80).

Reagents. Ripe bananas were purchased locally and the pulp from the peel was used as the source of oxalate oxidase. Chelex-100 chelating resin (100—200 mesh; Na^+-form; Bio-Rad Labs., Richmond, CA) was used. Disodium oxalate, glycylglycine, and oxalate urine control-N (Cat. No. 0-6627, Lot 55F-6134) were all from Sigma Chemical Co. Collagen membrane was obtained from YSI and cellulose acetate membrane was prepared by established procedures. Buffer solutions of 0.10 M concentration were prepared in distilled/deionized (Millipore) water. The recommended buffer is 0.10 M glycylglycine adjusted to pH 4.0 with hydrochloric acid.

Procedure. Ripe banana peel (40 g) was homogenized in a Warren blender, diluted with 100 ml of pH 4.00 phosphate buffer and then filtered through cheesecloth to remove fibrous material. The acetone-precipitation procedure described by Rhagavan and Devasagayam [19] was used. The precipitated pulp was used as the source of crude enzyme. The presence of oxalate oxidase in the pulp was verified by adding about 2 g of the pulp to 2.00 ml of pH 4.00 buffer in which the concentration of oxalate was 1×10^{-3} M. Both carbon dioxide and hydrogen peroxide were detected.

About 500 mg of the pulp was placed on the gas-permeable membrane of the carbon dioxide gas-sensor. A dialysis membrane was placed over it and held with an O-ring. A similar entrapment procedure was used with the hydrogen peroxide probe, except that an ultrafine cellulose acetate membrane was first placed over the probe so that the pulp was held between this membrane and a covering collagen membrane. The assembled electrodes were conditioned in pH 4.00 buffer for at least 1 h or until a steady baseline potential or current was obtained.

Pretreatment of urine samples. To 5 ml of reconstituted oxalate urine control was added 0.5 ml of 5×10^{-4} M iron(III) chloride in 3 M hydrochloric acid. The sample was heated at 60°C for 15 min. After cooling to room temperature, the solution was passed through a Chelex-100 (Na^+-form) column (10 mm i.d., 200 mm long). The pH of the eluted solution was

adjusted to 6 with sodium hydroxide and then 0.5 ml of 0.25 M EDTA was added. The sample was adjusted to pH 4 before oxalate was quantified.

Results and discussion

The maximum enzyme activity in the assembled electrode system was found at pH 4.0 (Fig. 1). Buffers of pH <4.00 were prepared from glycyl-glycine/hydrochloric acid mixtures. The rate of carbon dioxide production from 10 ml of buffer solution containing 1×10^{-3} M disodium oxalate was measured and plotted as a function of pH. The pH of 4.0 is compatible with the CO_2 gas-sensor. The stability of the assembled electrodes was studied by checking calibration curves for oxalate daily for ten days; the assembled electrodes were stored at 0°C in pH 4.00 buffer when not in use. A typical calibration curve for oxalate by the potentiometric method is shown in Fig. 2; the fading response at $>5 \times 10^{-3}$ M oxalate could be due to saturation of the oxidase or to insufficient oxygen concentration around the enzyme. At 25°C, the slope was 47 mV/decade in the concentration range 1×10^{-4}—5×10^{-3} M, whereas at 30°C the slope was 50 mV/decade with a detection limit of 2×10^{-5} M. After the tenth day of study, the slope of the calibration curve dropped to 43 mV/decade at 30°C.

The amperometric calibration curve was linear in the concentration range of 2—30 mg l^{-1} (2×10^{-5}—3×10^{-4} M), defined by the equation y (μA) = (2.79 ± 0.02)x (mg l^{-1}) — 1.23 ± 0.25 μA with $r = 0.999$ and $S_{yx} = 0.30$ μA. The ultrafine cellulose acetate membrane prevents reducing agents likely to be present in the sample solution from reaching the hydrogen peroxide sensor. The amperometric procedure offers a lower limit of detection for oxalate (5×10^{-6} M) than the potentiometric method, probably because the Model 25 oxidase meter has two modes of operation and in the variable sensitivity mode, currents as low as 0.2 nA can be measured accurately.

The measurement times varied depending on the amount of pulp at the electrode surface. It took about 1 h to obtain a calibration curve when more than 500 mg of the pulp was entrapped. This is obviously a diffusion problem

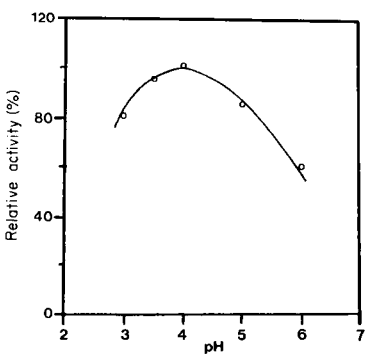

Fig. 1. pH profile of the banana-pulp electrode for oxalate at 30° C.

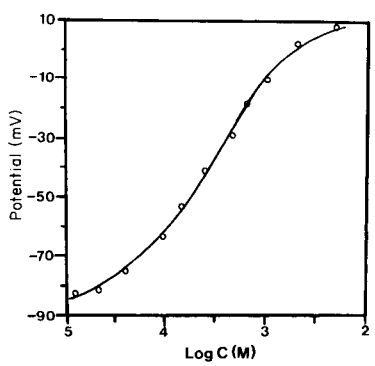

Fig. 2. Typical potentiometric calibration curve for oxalate at pH 4.00 and 30°C.

because of the crude source of the enzyme. With 500 mg of pulp, it took about 10 min to obtain a steady-state potential in a sample containing 2×10^{-5} M oxalate and about 3 min for 5×10^{-4} M oxalate.

The precision of oxalate measurements with the two tissue-based electrodes was evaluated. The results (Table 1) show the utility of both methods for oxalate in aqueous samples. Recoveries of oxalate in aqueous samples in both procedures were good. For oxalate concentrations of 5.8—100 mg l^{-1}, the recovery ranged from 94 to 98% with an average of 96% by potentiometry, and from 96 to 101% with an average of 98% by amperometry.

Urine contains inhibitors of oxalate oxidase, including divalent cations and ascorbic acid. Pretreatment of urine with iron(III) chloride in hydrochloric acid oxidizes ascorbic acid and dissolves any calcium or magnesium oxalate; EDTA binds Ca^{2+} and Mg^{2+}. The cation-exchange column removes Fe^{3+} and other urinary enzyme inhibitors. Only oxalate was converted to products; no other carboxylic acids tested interfered significantly with the determination of oxalate.

Six urine control samples containing oxalate (as oxalic acid) in the range 18—31 mg l^{-1}, with an assigned mean value of 23 mg l^{-1}, were tested with the two tissue-based electrodes. The lyophilized urine samples were reconstituted according to the manufacturer's instructions. Half of the samples were tested directly after reconstitution (18—31 mg l^{-1} oxalic acid) while the others were diluted (1 + 1) with 0.2 M glycylglycine buffer, pH 4.0 (9—15.5 mg l^{-1} oxalic acid). One sample was evaluated each day for six days. Values in the range 17.2—28.4 mg l^{-1} (as oxalic acid) were obtained, with mean values of 21.5 mg l^{-1} (potentiometric method) and 24.3 mg l^{-1} (amperometric method).

These tissue-based electrodes appear suitable for the clinical determination of urinary oxalate. While both the potentiometric and amperometric electrodes are stable, the amperometric system has a much lower limit of detection and it could be the method of choice for very low concentrations of oxalate.

TABLE 1

Imprecision and relative errors for random oxalate assays at 30°C by the potentiometric and amperometric procedures

Oxalate concentration (mg l^{-1})			Relative error (%)		Imprecision[a]	
Added	Found		Pot.	Amp.	Pot.	Amp.
	Pot.	Amp.				
2.7	—	2.9	—	+7.4	—	±6.0
5.4	5.0	5.1	−7.4	−5.6	±5.2	±3.0
12.2	11.9	12.4	−2.5	+1.6	±2.8	±2.5
25.8	25.3	25.5	−1.9	−1.2	±2.1	±1.8
59.6	60.2	60.2	+1.7	+1.0	±1.7	±1.5
126.6	128.0	—	+1.1	—	±1.1	—

[a]RSD calculated from twelve repetitions for each sample.

REFERENCES

1 R. Bias, N. Potezny, R. Krishnan and H. M. James, Proc. Aust. Biochem. Soc., 23 (1980) 21.
2 J. Costello, M. Hatch and B. Bourke, J. Lab. Clin. Med., 87 (1984) 903.
3 G. G. Mayer, D. Markow and F. Karp, Clin. Chem., 9 (1963) 334.
4 G. Charransol, C. Barthelemy and P. Desgrez, J. Chromatogr., 145 (1978) 452.
5 T. D. R. Hockaday, R. W. Frederick, J. R. Clayton and L. H. Smith, J. Lab. Clin. Med., 65 (1965) 677.
6 W. G. Robertson and A. Rutherford, Scand. J. Urol. Nephrol. Suppl., 53 (1980) 85.
7 P. M. Zabremski and A. Hodgkinson, Biochem. J., 96 (1965) 717.
8 A. Hodgkinson and A. Williams, Clin. Chim. Acta, 36 (1972) 127.
9 E. F. Dempsey, A. P. Forbes, R. A. Melick and P. H. Henneman, Metabolism, 9 (1960) 52.
10 A. Hodgkinson, Oxalic Acid in Biology and Medicine, Academic Press, London, 1978.
11 G. Kohlbecker and M. Butz, J. Clin. Chem. Clin. Biochem., 19 (1981) 1103.
12 M. Hatch, E. Bourke and J. Costello, Clin. Chem., 23 (1977) 76.
13 M. F. Laker, A. F. Hofmann and B. J. D. Meeuse, Clin. Chem., 26 (1980) 827.
14 T. Hopner and J. Knappe, in H. U. Bergmeyer (Ed.), Methods of Enzymatic Analysis, 2nd edn., Academic Press, New York, 1974, p. 1551.
15 D. M. Obzansky and K. E. Richardson, Clin. Chem., 29 (1983) 1815.
16 F. Winquist, B. Danielsson, J.-Y. Malpote, L. Persson and M.-B. Larson, Anal. Lett., 18 (1985) 573.
17 P. Vadgama, W. Sheldon, J. M. Guy, A. K. Covington and M. F. Laker, Clin. Chim. Acta, 142 (1984) 193.
18 R. K. Kobos and T. A. Ramsey, Anal. Chim. Acta, 121 (1980) 111.
19 K. G. Rhagavan and T. P. A. Devasagayam, Clin. Chem., 31 (1985) 649.

Analytica Chimica Acta, 186 (1986) 307—311
Elsevier Science Publishers B.V., Amsterdam — Printed in The Netherlands

Short Communication

CALCIUM-SELECTIVE ELECTRODES BASED ON NONCYCLIC POLYETHER DIAMIDES

TATSUHIRO OKADA*, HIDEKI SUGIHARA and KAZUHISA HIRATANI
Industrial Products Research Institute, M.I.T.I., Yatabe, Tsukuba, Ibaraki 305 (Japan)
(Received 25th February 1986)

Summary. Calcium-selective neutral carriers based on *o*-phenylene derivatives are described. Aliphatic substituents of intermediate chain length (n-C_8H_{17}) on the amide nitrogen favor calcium selectivity. Structure/selectivity relationships and the effects of different plasticizers and polymeric supports are reported.

Monitoring of calcium ion activity in blood serum is regarded as important during surgical treatment and for various diagnostic applications. Many calcium-selective electrodes have been proposed for fast direct measurements of calcium ion. Such electrodes have been based on ion-exchange liquid membranes [1, 2], and on neutral carriers in the membrane [3—7], the latter being of great present interest. Many types of calcium-selective neutral carriers, e.g., cyclic diamides [3, 4], noncyclic diamides [5, 6], bicyclic amide derivatives [7], have been reported. Most of these are characterized by ether oxygen and amide groups as the binding sites in the compounds.

Noncyclic compounds have been synthesized as catechol derivatives and studied as selective ion carriers in liquid-membrane transport [8, 9] and poly(vinyl chloride) (PVC) ion-selective electrodes [10]. In this communication, diamide derivatives which show calcium selectivity are synthesized and evaluated for use in calcium-selective electrodes. The dependence of the selectivity of the electrode on the structure of the compounds and on the membrane composition is discussed.

Experimental

Synthesis of carriers. 1,2-Dihydroxy-4-t-butylbenzene in dimethylformamide was treated with 2 equivalents of ethyl chloroacetate in the presence of 2 equivalents of potassium t-butoxide under nitrogen at 70°C. The resultant diesters were converted to the dicarboxylic acids by hydrolysis. The dicarboxylic acids were treated with excess of thionyl chloride in benzene at 60°C, to give the bis-carboxylic acid chlorides which were obtained. The diamides were prepared from these bis-chlorides by acylation with 2 equivalents of the appropriate amine in dichloromethane under nitrogen at —20°C. The crude product was purified by column chromatography on silica gel, and recrystallized from n-hexane/benzene (1/3). The carriers synthesized are listed in Table 1.

0003-2670/86/$03.50

TABLE 1

The diamides studied

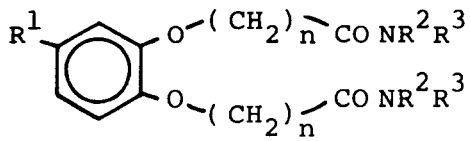

Carrier	R^1	n	R^2	R^3
I	t-Bu	1	H	n-$C_{16}H_{33}$
II	t-Bu	1	H	n-C_8H_{17}
III	H	1	H	n-C_8H_{17}
IV	t-Bu	1	CH_3	n-C_7H_{15}
V	t-Bu	1	H	C_6H_4(*o*-$COOC_2H_5$)
VI	H	1	H	C_6H_4(*o*-$COOC_2H_5$)
VII	t-Bu	3	H	n-$C_{16}H_{33}$

Preparation of membrane and e.m.f. measurements. The carrier (5—10 mg), plasticizer (250 mg), poly(vinyl chloride) (100 mg) and potassium tetrakis-(*p*-chlorophenyl)-borate (KTCPB) (3 mg) as a lipophilic additive were dissolved in 4 ml of tetrahydrofuran (THF). The mixture was poured into a Petri dish (42 mm diameter) and THF was evaporated slowly at room temperature. Homogeneous membranes of ca. 0.2 mm thickness were obtained. The plasticizers used were *o*-nitrophenyl octyl ether (NPOE), di-n-octylphenyl phosphonate (DOPP), bis-(2-ethylhexyl)sebacate (DOS) and trioctyl phosphate (TOP). In some cases, membranes were prepared with triacetyl cellulose, or a polyester/polyether copolymer (Toyobo Co.; P40H with bulk resistance 2×10^{12} Ω cm, dielectric constant 5.8, m.p. 172°C, density 1.12) or poly-1,3-butadiene instead of PVC.

A disk (5-mm diameter) of the membrane was cut out and mounted on an Orion model 92 electrode body for e.m.f. measurements. The electrochemical cell was Ag/AgCl/10^{-3} M $CaCl_2$//membrane//test solution/10^{-1} M NH_4NO_3/sat. KCl/AgCl/Ag.

All solutions were prepared from analytical-grade chlorides of alkali and alkaline-earth metals and deionized water (specific conductivity $<5 \times 10^{-7}$ Ω^{-1} cm^{-1}).

Potentiometric selectivity coefficients, K_{ij}^{pot}, of ion i over ion j were evaluated by the separate solutions method [11].

Results and discussion

The calibration graphs obtained for the PVC membrane based on carrier II with NPOE as solvent mediator are shown in Fig. 1. The responses at low ionic activity showed some hysteresis but near-Nernstian response was obtained by conditioning the membrane for >10 h in 10^{-3} M calcium chloride.

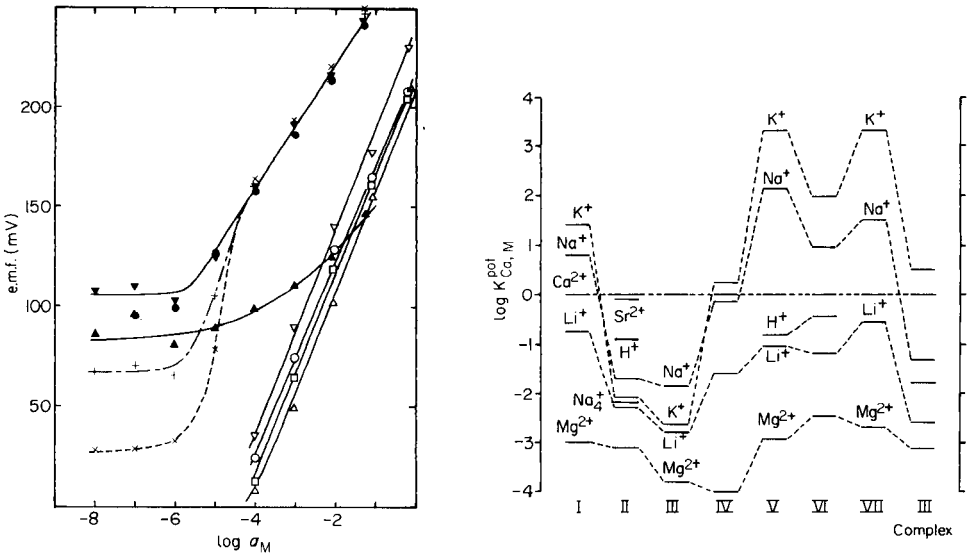

Fig. 1. Calibration graphs for a PVC membrane electrode based on carrier II with NPOE plasticizer: (△) Li^+; (▽) Na^+; (○) K^+; (□) NH_4^+; (▲) Mg^{2+}; (●) Sr^{2+}; (×), (+) Ca^{2+} for membranes with insufficient conditioning; (▼) Ca^{2+} for membrane immersed for 15 h in 10^{-3} M $CaCl_2$.

Fig. 2. Selectivity coefficients log $K^{pot}_{Ca,M}$ for PVC/NPOE membranes containing carriers I—VII and a mixture (2:2:1) of carrier III, KTCPB and Ca^{2+}.

Stirring solutions of low ionic activity shifted the e.m.f. value mostly to more positive potentials, indicating rather slow complexation at the membrane/solution interface.

Figure 2 summarizes the logarithmic selectivity coefficients for calcium over other ions for PVC membranes based on the series of carriers with NPOE as solvent mediator. The selectivity changed greatly depending on the end substituents of the carriers. Carriers with n-C_8H_{17} groups exhibited the best calcium selectivity; the calcium selectivity disappeared for carriers with longer chains, branched chains or aromatic substituents. Replacing the methylene group of the binding sites by trimethylene group as in carrier VII caused serious loss of calcium selectivity. Removal of the t-butyl group from the *o*-phenylene moiety slightly improved the electrode characteristics. The complexing ability of carriers for ions, as well as their mobility and lipophilicity can be greatly affected by substituent groups in the carriers [12]. Some of these factors probably counteracted each other. The best fit of the carrier structure to the calcium ion seems to be achieved in carriers II and III.

The plasticizer for PVC membranes can exert a remarkable effect on the ion selectivity [12, 13]. When DOPP was used as the plasticizer instead of NPOE, the calcium selectivity was greatly decreased and, indeed, the membrane became highly selective for lithium (Fig. 3a). The use of DOS or TOP as plasticizer also diminished the calcium selectivity (Fig. 3b). For mixed

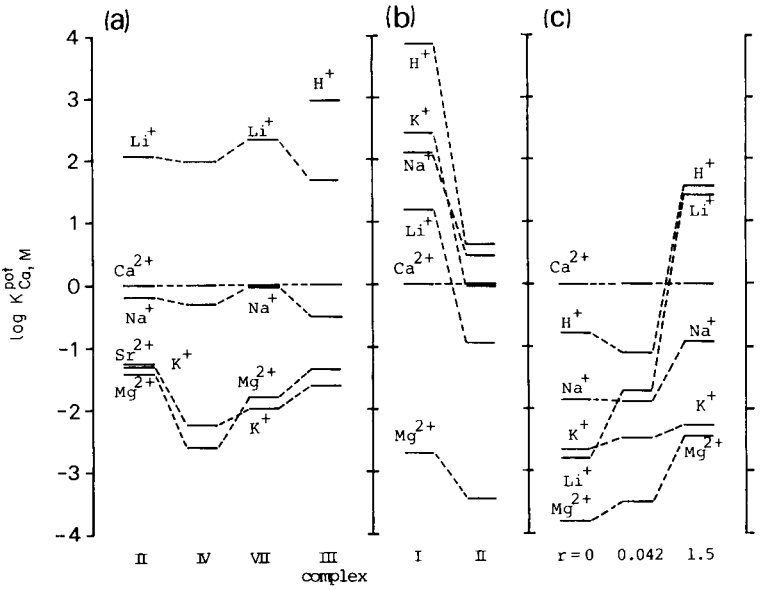

Fig. 3. Selectivity coefficients of PVC membranes containing different plasticizers: (a) carriers II, IV and VII and a mixture (2:2:1) of carrier III, KTCPB and Ca^{2+} with DOPP; (b) carriers I and II with DOS; (c) carrier III with mixed DOPP/NPOE (*r* is the weight ratio of DOPP to NPOE).

plasticizers (DOPP/NPOE), increasing the amount of DOPP diminished the calcium selectivity of carrier III (Fig. 3c); similar data were obtained for carrier II. A membrane based on a mixture of carrier III, KTCPB and calcium ion in a mole ratio of 2:2:1 was prepared with the hope of improving the calcium selectivity [3, 4, 14]. Figures 2 and 3 shows that this membrane was unsuccessful.

The polymer used and the conditions of membrane preparation also influence the ion selectivity, as shown in Fig. 4 for carrier III. Of the polymers tested, poly-1,3-butadiene produced a membrane with less calcium selectivity than other polymers, although the differences were not large; decreased polarity of the membrane may be the reason [12, 13]. A change in solvent had a poor effect on selectivity (Fig. 4, line D).

Conclusions

The main features of the structure/calcium selectivity relationship of these *o*-phenylene-based diamide carriers can be summarized as follows: (1) good coordination sites for calcium ion are formed by the ether oxygen and the amide oxygen when these are separated by two carbon atoms; (2) aliphatic substituents of intermediate chain length (n-C_8H_{17}) on the amide nitrogen favor selectivity for calcium; and (3) omission of a t-butyl group in the *o*-phenylene moiety improves the characteristics of the carrier. The t-butyl

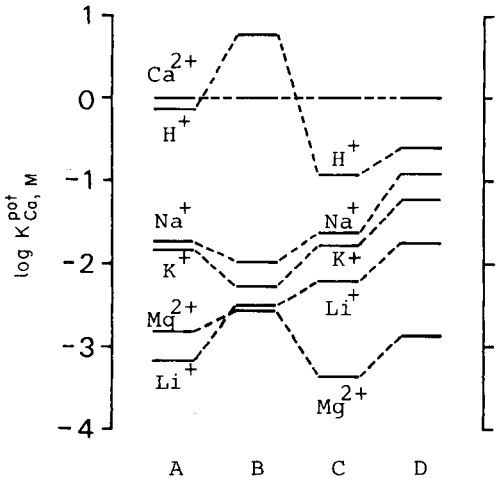

Fig. 4. Selectivity coefficients for different membrane materials containing carrier III with NPOE plasticizer: (A) triacetyl cellulose membrane; (B) polyester/polyether copolymer membrane; (C) poly-1,3-butadiene membrane; (D) PVC membrane cast from cyclohexanone solution.

group may decrease the binding ability and/or the mobility of the carrier. It should be noted that point 1 is valid for other types of calcium-selective neutral carriers [3—7].

REFERENCES

1 A. Craggs, G. J. Moody and J. D. R. Thomas, Analyst, 104 (1979) 412.
2 J. Růžička, E. H. Hansen and J. Chr. Tjell, Anal. Chim. Acta, 67 (1973) 155.
3 J. Petránek and O. Ryba, Collect. Czech. Chem. Commun., 45 (1980) 1567.
4 J. Petránek and O. Ryba, Anal. Chim. Acta, 128 (1981) 129.
5 W. Simon, D. Ammann, M. Oehme and W. E. Morf, Ann. N.Y. Acad. Sci., 307 (1978) 52.
6 P. Anker, E. Wieland, D. Ammann, R. E. Dohner, R. Asper and W. Simon, Anal. Chem., 53 (1981) 1970.
7 K. Kimura, K. Kumami, S. Kitazawa and T. Shono, Anal. Chem., 56 (1984) 2369.
8 K. Hiratani, K. Taguchi, H. Sugihara and K. Iio, Bull. Chem. Soc. Jpn., 57 (1984) 1976.
9 K. Taguchi, K. Hiratani, H. Sugihara and K. Iio, Chem. Lett., (1984) 1457.
10 H. Sugihara, T. Okada and K. Hiratani, J. Chem. Soc. Chem. Commun., (1985) 957.
11 K. Srinivasan and G. A. Rechnitz, Anal. Chem., 41 (1969) 1203.
12 W. E. Morf and W. Simon, in H. Freiser (Ed.), Ion-Selective Electrodes in Analytical Chemistry, Vol. 1, Plenum Press, New York, 1981, Ch. 3.
13 D. Ammann, W. E. Morf, P. Anker, P. C. Meier, E. Pretsch and W. Simon, Ion-Sel. Electrode Rev., 5 (1983) 3.
14 W. E. Morf, D. Ammann, R. Bissig, E. Pretsch and W. Simon, Progress in Macrocyclic Chemistry, Vol. 1, Wiley, New York, 1979, p. 1.

Analytica Chimica Acta, 186 (1986) 313—318
Elsevier Science Publishers B.V., Amsterdam — Printed in The Netherlands

Short Communication

EQUILIBRIUM STUDY ON THE MASKING OF ALUMINUM ION IN THE DETERMINATION OF FLUORIDE WITH ION-SELECTIVE ELECTRODES

AKIO YUCHI*, KAZUHIRO UEDA, HIROKO WADA and GENKICHI NAKAGAWA

Laboratory of Analytical Chemistry, Nagoya Institute of Technology, Gokiso-cho, Showa-ku, Nagoya 466 (Japan)

(Received 5th November 1985)

Summary. The complexation equilibria between aluminum, a masking agent (DCyTA, EDTA and citrate) and fluoride were studied. Mixed ligand complexes of aluminum, fluoride and the masking agent are generally formed. Citrate is more effective for masking aluminum than DCyTA or EDTA because of the lower conditional formation constants of the mixed ligand complexes. Higher pH, such as 7, and increased dilution of the sample solution are recommended for samples containing large amounts of aluminum.

Fluoride ion-selective electrodes are widely used in the determination of fluoride because of their excellent selectivity. Some samples, however, contain appreciable amounts of metal ions such as aluminum, iron and magnesium, which interfere with the determination of total fluoride because of complex formation. Aluminum shows the most serious interference among the common metals. As separation methods complicate the normal simple use of ion-selective electrodes, direct potentiometry is very advantageous whenever possible.

Various masking reagents (L, charges are omitted for clarity) have been compared [1]. The reaction usually assumed for masking aluminum to release fluoride is

$$AlF_n + (L)' \rightleftharpoons (AlL)' + n\ F^- \qquad (1)$$

but the calculated recovery of fluoride from Eqn. 1 did not agree with experimental values [2]. This communication deals with the equilibria in systems consisting of aluminum, a masking reagent and fluoride, and provides some guidance for masking aluminum.

Experimental

Reagents. Aluminum stock solution (ca. 1×10^{-2} M) was prepared by dissolving the nitrate in 10^{-2} M nitric acid, and standardized by back-titration of excess of EDTA with a standard copper(II) solution and 1-(2-pyridylazo)-2-naphthol indicator [3]. Potassium fluoride was dried for 24 h at 110°C. Fluoride solutions were stored in polyethylene containers. Citric acid, EDTA, 1,2-diaminocyclohexanetetracetic acid (DCyTA) and 2-(*N*-morpholino)-

0003-2670/86/$03.50

ethanesulfonic acid (MES) were used as received. Potassium nitrate was recrystallized twice. Carbonate-free potassium hydroxide solution [4] was used.

Measurement. A fluoride ion-selective electrode (Denki Kagaku Keiki Co.; DKK type 7200) was used with a saturated calomel reference electrode having a porous teflon junction (DKK type 4400). The electrode showed Nernstian response between 10^{-6} and 10^{-2} M fluoride. The pH was measured with a fluoride-resistant glass electrode (Ohkura Electric Co.; GP-1200). These electrodes were calibrated with 1.00×10^{-2} M fluoride and 1.00×10^{-2} M nitric acid of ionic strength 0.1 M (KNO_3), before and after each series of measurements. The sample solution was placed in a polyethylene beaker thermostated at 25.0 ± 0.5°C, and the e.m.f. for $-\log[H^+]$ and $-\log[F^-]$ was read with a DKK ion-meter (IOC-10) to 0.1 mV.

Series of solutions containing various amounts of aluminum ion, a ligand and fluoride were prepared. The pH was adjusted to the desired value with MES and potassium hydroxide, and the ionic strength was kept at 0.1 M with potassium nitrate. After standing overnight, $-\log[H^+]$ and $-\log[F^-]$ were measured.

Calculations. From the $-\log[H^+]$ and $-\log[F^-]$ values for each experimental point, the average number of fluoride ions bound in the aluminum complexes $\bar{n}_{obs}$, was calculated from

$$\bar{n}_{obs} = (C_F - [F^-] - [HF] - [HF_2^-])/C_{Al}$$

(C_F and C_{Al} are the concentrations of these ions taken initially). In the Al—F system, $\bar{n}_{calc}$ was given by

$$\bar{n}_{calc} = \Sigma n[AlF_n]/C_{Al}$$

whereas in the Al—L—F system,

$$\bar{n}_{calc} = (\Sigma n[AlF_n] + \Sigma m[AlH_kLF_m])/C_{Al}$$

which was calculated with the $[Al^{3+}]$ and [L] values that satisfied the following equations simultaneously: $C_{Al} = f([Al^{3+}], [L])$ and $C_L = g([Al^{3+}], [L])$. The stability constants were refined to give the minimum error square sum about $\bar{n}$: $U = \Sigma (\bar{n}_{calc} - \bar{n}_{obs})^2$.

Results

Complexation of aluminum with fluoride. The complexation equilibria between aluminum ion and fluoride have been studied [5, 6]. To avoid hydrolysis of aluminum, only acidic media are relevant. In this study, the ratio of the total concentrations of fluoride to aluminum was kept at definite values ranging from 0.5 to 6.5, and the free fluoride concentration (pF) was measured as a function of pH (Fig. 1). If aluminum formed soluble mixed ligand complexes such as $AlF_m(OH)_n$, pF would change with pH. Figure 1 shows that pF was unchanged until hydrated aluminum oxide started to precipitate, releasing fluoride at higher pH. Species such as $AlF_m(OH)_n$ clearly do not exist in appreciable amounts under these conditions.

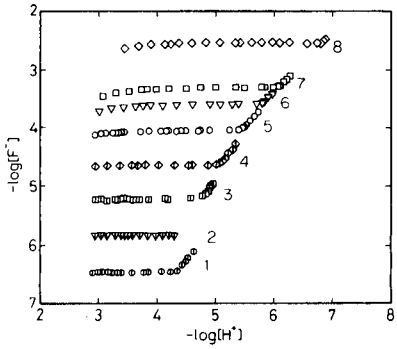

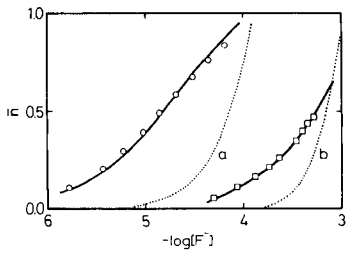

Fig. 1. The $-\log[F^-]$ vs. $-\log[H^+]$ relation for Al—F systems with $C_{Al} = 1.009 \times 10^{-3}$ M. C_F ($\times 10^{-3}$ M): (1) 0.4994; (2) 0.9925; (3) 1.500; (4) 1.989; (5) 2.481; (6) 2.995; (7) 3.474; (8) 6.493.

Fig. 2. $\bar{n}$ vs. $-\log[F^-]$ for Al—F—aminopolycarboxylate systems ($C_{Al} = 1.009 \times 10^{-3}$ M; $C_L = 1.100 \times 10^{-3}$ M). Ligand: (○) EDTA; (□) DCyTA. (···) Calculated curve assuming no mixed ligand complex formation for EDTA (a) and DCyTA (b); (—) calculated curve with constants obtained.

From the pF values of the plateaux of the curves in Fig. 1, $\bar{n}$ was calculated and the successive formation constants of the aluminum-fluoride complexes were evaluated. The constants obtained were $\log K_1 = 6.40$, $\log K_2 = 5.24$, $\log K_3 = 3.86$ and $\log K_4 = 2.75$ (0.1 M KNO_3, 25°C), which is in good agreement with literature values for the same medium (6.45, 5.21, 3.79 and 3.18, respectively [6]).

Mixed complexes of aluminum with a masking reagent and fluoride. The possible formation of mixed complexes of aluminum with a masking reagent and fluoride was examined. Citrate, DCyTA and EDTA were used as the

TABLE 1

Stability constants of aluminum complexes used for the calculations (25°C, 0.1 M KNO_3)

Ligand	Type[a]	Equilibrium	log K	Ref.
EDTA	H_4L	[AlL]/[Al] [L]	16.5	7
		[AlHL]/[AlL] [H]	3.4	
		[AlL]/[AlL(OH)] [H]	5.8[b]	
DCyTA	H_4L	[AlL]/[Al] [L]	18.9	7
		[AlHL]/[AlL] [H]	3.4	
		[AlL]/[AlL(OH)] [H]	7.5[b]	
Citric acid	H_3L	[AlL]/[Al] [L]	7.98	8
		[AlHL]/[AlL] [H]	2.94	
		[AlL]/[AlH_{-1} L] [H]	3.31	

[a]Logarithmic acidity constants of the ligands used for the calculation: 10.34, 6.24, 2.75 and 2.07 for EDTA; 11.43, 5.93, 3.41 and 2.39 for DCyTA; 5.71, 4.39 and 3.03 for citric acid. [b]Calculated with $\log K_w = -13.78$.

masking reagents; their complexation equilibria with aluminum have been well characterized (Table 1) [7, 8].

With EDTA and DCyTA, the pH of the solution containing 10^{-3} M aluminum and 1.1×10^{-3} M ligand was adjusted so that AlL was formed, and various amounts of fluoride were added. The $\bar{n}$ vs. $-\log[F^-]$ diagrams for these systems are given in Fig. 2. If only AlF_n, AlL, AlHL and AlLOH were formed, the function would be as shown by the dotted lines. The deviations of the experimental points suggest the presence of mixed ligand complexes; $AlL + F^- \rightleftharpoons AlLF$. The stability constants, K(AlLF), were refined as described under Experimental. For EDTA and DCyTA, the log K(AlLF) values were 4.95 and 3.14, respectively. The solid lines in Fig. 2 are the curves calculated with these constants.

The equilibria in aluminum—citrate systems are rather complicated. The distribution of each species was calculated and the data are shown as a function of pH for $C_L = 10^{-2}$ M or 2×10^{-3} M in Fig. 3A. Various species of the general formula AlH_kL form depending on pH and the concentration of citrate. The reactions of these species with fluoride were studied at the various pH values indicated by arrows in Fig. 3A. The $\bar{n}$ vs. $-\log[F^-]$ plots depend strongly on pH (Fig. 3B). The experimental points show systematic deviation from the curves calculated on the assumption that mixed ligand complexes are not formed. Various mixed ligand complexes with the general form AlH_kLF_m were then considered. It was found that both AlHL and AlL form mixed ligand complexes AlHLF, AlLF and $AlLF_2$, but $AlH_{-1}L$ does not. The refined stability constants were found to be log K(AlHLF) = 5.7, log K(AlLF) = 4.5 and log K($AlLF_2$) = 3.9.

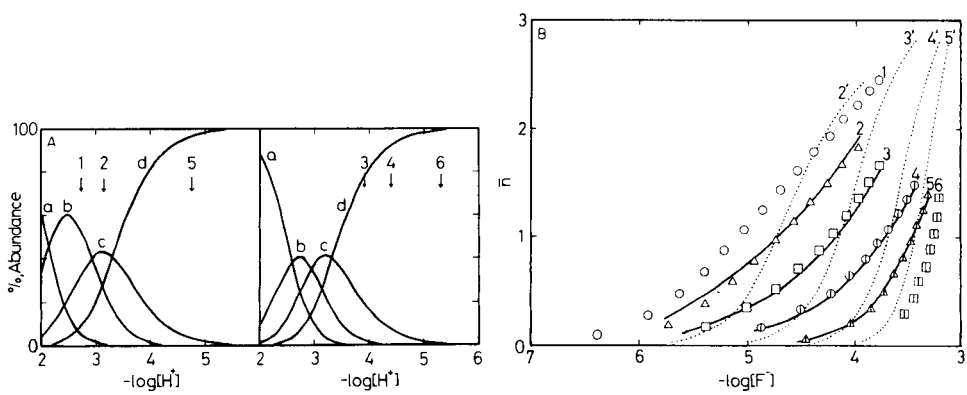

Fig. 3. (A) Distribution of species for the Al—citrate system with $C_{Al} = 10^{-3}$ M and $C_L = 10^{-2}$ M (left) or 2×10^{-3} M (right). Species: (a) Al^{3+}; (b) $AlHL^+$; (c) AlL; (d) $AlH_{-1}L^-$. ($AlH_{-1}L$ denotes any species formed by deprotonation from AlL.) The numbers in (A) correspond to the experimental conditions in (B). (B) $\bar{n}$ vs. $-\log[H^+]$ for the Al—citrate—F system: (···) calculated curves, assuming no mixed ligand complex formation; (—) calculated curves with the constants obtained.

Discussion

EDTA and DCyTA. When aluminum is to be masked with DCyTA or EDTA, the reactions are $AlF_n + L \rightleftharpoons AlLF + (n-1)F^-$ and $AlLF \rightleftharpoons AlL + F^-$. The recoveries of fluoride depend on the positions of these equilibria. When excess of masking reagent is added at pH around 6 and the total concentration of fluoride is less than 10^{-3} M, the first equilibrium is completely shifted to the right. The release of the last fluoride left in AlLF depends on the formation constant of the mixed ligand complex and the concentrations of aluminum and fluoride.

It is well known that DCyTA is superior to EDTA for masking aluminum [9]. This was first ascribed to the larger formation constant of the aluminum—DCyTA complex, but it was later shown that the conditional formation constants of both complexes are about the same between pH 6 and 9 [10]. The advantage of DCyTA should be ascribed to the smaller formation constant of the mixed ligand complex.

Citrate. The formation of $AlH_{-1}L$ is favored even in acidic solutions (Fig. 3A) and this complex does not form mixed ligand complexes with fluoride, i.e., the conditional formation constant of mixed ligand complexes is small when formation of $AlH_{-1}L$ is taken into account (Fig. 3B). Thus, on the addition of citrate, fluoride is released from aluminum complexes despite the smaller conditional formation constant of aluminum complexes [K'(AlDCyTA) = $10^{13.2}$ and K'(Alcit.) = $10^{7.8}$ at pH 6] and the larger formation constants of the mixed ligand complexes with citrate. The reactions are

$$AlF_n + L \rightleftharpoons AlLF_2 + (n-2)F^-$$

$$AlLF_2 \rightleftharpoons AlLF + F^-;\ AlLF \rightleftharpoons AlH_{-1}L + H^+ + F^-$$

The actual recoveries with citrate are a little higher than those calculated [2]. Kauranen [11] also found that higher concentrations of citrate give better recoveries.

Tolerable amount of aluminum. From the formation constants of AlF_n, AlH_kL and AlH_kLF_m, the interference by aluminum can be predicted for any total concentrations of aluminum and fluoride. The recoveries of fluoride are shown as a function of total concentration of aluminum for various fluoride concentration levels in Fig. 4. For this potentiometric determination, fluoride must be in the free ionic form, e.g., $(\Sigma n[AlF_n] + \Sigma m[AlH_kLF_m])/C_F < 0.01$. Table 2 shows the tolerable amounts of aluminum calculated for 99% recovery of fluoride when DCyTA or citrate is used as masking reagent. Citrate is clearly a much more effective masking reagent for aluminum than CDTA, and the masking abilities of citrate are markedly enhanced by increasing pH (Fig. 4B—C and Table 2). The ratio of the tolerable amount of aluminum to fluoride is increased with decreasing total fluoride concentration. When samples containing large amounts of aluminum are to be analyzed, the stepwise dilution method is highly desirable [2], so long as the final fluoride concentration is within the linear dynamic range of the electrode. These

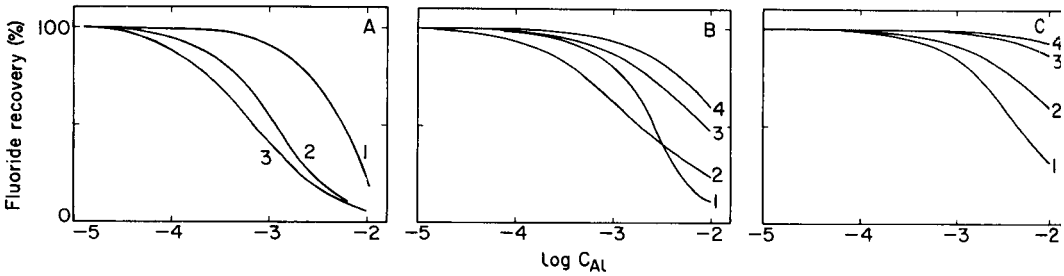

Fig. 4. Calculated percent recovery of fluoride vs. log C_{Al} in masking aluminum. Masking reagent: (A) DCyTA at pH 6; (B) citrate at pH 6; (C) citrate at pH 7. C_F: (1) 10^{-2}; (2) 10^{-3}; (3) 10^{-4}; (4) 10^{-5} M. C_L = 0.1 M.

TABLE 2

Calculated tolerance limits for aluminum and the ratio to total fluoride in the presence of masking reagents[a]

C_F (M)	Tolerance limit for aluminum					
	DCyTA (pH 6)		Citrate (pH 6)		Citrate (pH 7)	
	(M)	C_{Al}/C_F	(M)	C_{Al}/C_F	(M)	C_{Al}/C_F
10^{-2}	1.0×10^{-4}	0.01	5×10^{-5}	0.005	6×10^{-5}	0.006
10^{-3}	1.6×10^{-5}	0.016	1.6×10^{-5}	0.016	1.0×10^{-4}	0.1
10^{-4}	6×10^{-6}	0.06	6×10^{-5}	0.6	6×10^{-4}	6.0
10^{-5}	6×10^{-6}	0.6	1.3×10^{-4}	13.0	1.3×10^{-3}	130.0

[a]For 99% recovery of fluoride at pH 6.0 and with C_L = 0.1 M.

findings explain the experimental results presented in previous work [1, 2, 9–12].

The authors gratefully acknowledge a Grant-in-Aid for Scientific Research from the Ministry of Education, Science and Culture (No. 61127007).

REFERENCES

1 K. Nicholson and E. J. Duff, Anal. Lett., 14 (1981) 493 (and references therein).
2 N. Shiraishi, Y. Murata, G. Nakagawa and K. Kodama, Anal. Lett., 6 (1973) 893.
3 S. Murate, G. Nakagawa and K. Kodama, Jpn. Analyst, 23 (1974) 242.
4 J. E. Powell and M. A. Hiller, J. Chem. Educ., 34 (1957) 330.
5 E. W. Baumann, J. Inorg. Nucl. Chem., 31 (1969) 3155.
6 R. P. Agarwal and E. C. Moreno, Talanta, 18 (1971) 873.
7 D. A. Aikens and F. J. Bahbah, Anal. Chem., 39 (1967) 646.
8 R. J. Motekaitis and A. E. Martell, Inorg. Chem., 23 (1984) 18.
9 J. E. Harwood, Water Res., 3 (1969) 273.
10 B. Vickery and M. L. Vickery, Analyst, 101 (1976) 445.
11 P. Kauranen, Anal. Lett., 10 (1977) 451.
12 S. Tanikawa, H. Kirihara, N. Shiraishi, G. Nakagawa and K. Kodama, Anal. Lett., 8 (1975) 879.

Analytica Chimica Acta, 186 (1986) 319—323
Elsevier Science Publishers B.V., Amsterdam — Printed in The Netherlands

Short Communication

COVALENT BINDING OF HUMAN SERUM ALBUMIN AND OVALBUMIN BY CHLORAMINE-T AND CHEMICAL MODIFICATION OF THE PROTEINS

JEFFREY C. EVANS*, SIMON K. JACKSON and CHRISTOPHER C. ROWLANDS
Chemistry Department, University College, Cardiff (Great Britain)
MARTIN D. BARRATT
Environmental Safety Laboratory, Unilever Research, Colworth House, Sharnbrook, Bedford (Great Britain)

(Received 17th February 1986)

Summary. The covalent binding of ^{35}S-chloramine-T to human serum albumin (HSA) and ovalbumin is described. At pH 6.5, up to 24 chloramine-T molecules were found to be covalently bound per molecule of HSA; with ovalbumin the binding was only 5—7 molecules per protein molecule. Binding was accompanied by extensive modification of methionine, cysteine, histidine, tyrosine and lysine. Three new peaks appeared in the amino acid profiles of the modified proteins; two were identified as 1-aminoadipic acid (oxidation of lysine) and 3-chlorotyrosine. The most likely sites for covalent binding are lysine residues.

Chloramine-T (*N*-chloro-*p*-toluene sulphonamide, sodium salt) is a powerful disinfectant used in cleaning floors and other surfaces in abattoirs, kitchens, operating theatres, breweries, etc. The development of asthmatic symptoms in a number of factory workers has been shown to be due to occupational exposure to chloramine-T [1, 2]. Sera from these patients were found to contain specific IgE antibodies which were shown to be directed against several different proteins treated with chloramine-T [3]. Radioimmunoassay inhibition studies of chloramine-T and several structurally-related compounds indicated that the antigenic determinant was formed at least in part by the *p*-toluenesulphonyl group of the chloramine-T molecule [3]. The reaction of chloramine-T with proteins is therefore important to the immunologist and clinical chemist from the viewpoint of antigen formation. It is also of interest to the biochemist because chloramine-T has been used as a reagent for the radio-iodination of proteins for over twenty years [4].

This communication describes the reaction of chloramine-T with human serum albumin (HSA) and ovalbumin. The stoichiometry of conjugate formation was measured by means of ^{35}S-labelled chloramine-T and the extent of modification of different amino acid residues was monitored by analysis for amino acids.

0003-2670/86/$03.50

Experimental

Materials. Human serum albumin (fraction V, fatty-acid free), chlorotyrosine, methionine sulphoxide and homocysteic acid (Sigma Chemical Co.) were used. The ^{35}S-chloramine-T was synthesised from ^{35}S-chlorosulphonic acid (Amersham International) by published methods [5]. It was found to be pure by thin-layer chromatography (Polygram Silica G; 95% ethanol) and by isotope dilution analysis. Its specific activity at the commencement of the binding studies was 0.30 μCi mg^{-1}.

Methods. Liquid scintillation counting was done with a Packard Prias PLD liquid scintillation spectrometer. Beckman Ready-Solv EP scintillant (3 ml) was added to 0.1- or 0.2-ml aliquots of the samples to be counted. Protein concentrations were determined by the method of Bradford [6] (Bio-Rad protein assay) with the appropriate proteins as standards. Samples for amino acid analysis (done with a Rank-Hilger Chromaspek ion-exchange chromatograph) were hydrolysed for 18 h at 110°C in 6 M hydrochloric acid in sealed tubes under nitrogen. The 2 M hydrochloric acid hydrolysate of the HSA/chloramine-T conjugate was chromatographed on a column of Sephadex LH-20 (80 cm × 1.6 cm diameter) with 30% methanol as eluent; 10-ml fractions were collected. The presence of amino acids in the fractions was detected with ninhydrin [7].

Preparation of conjugates. ^{35}S-Chloramine-T (5 or 10 mg) was added to a solution of the protein (10 mg) in 0.05 M sodium phosphate (pH 6.5) or distilled water (1 ml). The pH of the mixture was adjusted to 6.5 with a few drops of 2 M hydrochloric acid; the mixture was stirred overnight. The protein solution was then passed through a column of Sephadex G-10 in 0.05 M ammonium hydrogencarbonate to remove unreacted chloramine-T, after which it was freeze-dried.

Chloramine-T (10 mg) with protein (10 mg) in 0.05 M sodium phosphate pH 8.5 (1 ml), was irradiated for 30 min in a quartz cuvette by a Hanovia medium-pressure mercury arc lamp fitted with Schott UG-5 (2 mm, u.v.-transmitting) and WG-310 (1 mm) filters giving 58% transmission at 313 nm.

Results and discussion

The mole ratios of ^{35}S-chloramine-T bound to HSA and ovalbumin under the conditions used, and the amino acid contents of the modified proteins are shown in Tables 1 and 2. Up to 24 chloramine-T molecules were covalently bound per molecule of HSA; with ovalbumin the binding was considerably less (5—7 chloramine-T molecules per protein molecule).

The extent of binding of chloramine-T to HSA and ovalbumin was greater in water at pH 6.5 than in 0.1 M sodium phosphate at pH 6.5, owing to the lower solubility of chloramine-T in the latter. Raising the pH to 8.5 also decreased the extent of binding of chloramine-T. Irradiation of chloramine-T in the presence of proteins at pH 8.5 increased the extent of binding.

The binding of chloramine-T to HSA and ovalbumin was accompanied by extensive modification of certain amino acid side-chains and the appearance

TABLE 1

Amino acid mole ratios and chloramine-T (CAT) content of HSA/chloramine-T conjugates (analyses based on 585 residues)

	Control	5 mg CAT H_2O, pH 6.5	10 mg CAT H_2O, pH 6.5	10 mg CAT buffer, pH 6.5[a]	10 mg CAT buffer, pH 8.5[a] irradiated
Mole ratio CAT/protein	—	9.0	24.2	12.2	8.6
ASP (53)[b]	49.1	50.3	58.4	57.0	63.7
THR (28)	27.2	41.2	34.8	33.3	32.5
SER (24)	23.2	30.1	28.1	27.1	26.6
GLU (82)	83.7	58.0	82.5	94.6	95.9
PRO (24)	29.0	25.9	30.1	30.9	27.7
GLY (12)	8.9	10.5	11.5	11.9	14.0
ALA (62)	56.6	59.7	62.7	66.8	69.2
½ CYS (35)	16.5	6.0	5.9	5.5	1.6
VAL (41)	37.5	50.7	48.3	45.2	44.9
MET (6)	5.5	1.7	1.1	1.1	2.0
ILEU (8)	6.9	10.1	11.0	9.1	9.4
LEU (61)	59.6	72.5	71.1	69.1	66.6
TYR (18)	15.1	8.0	1.1	3.9	6.3
PHE (31)	30.8	38.4	42.6	38.7	33.1
HIS (16)	15.8	19.3	4.3	9.0	14.0
LYS (59)	56.3	38.5	29.1	28.8	30.8
ARG (24)	24.1	27.2	28.7	26.3	26.9
Peak 1 (unidentified)[c]	0.0	21.6	12.2	6.6	4.4
1-Aminoadipic acid	0.0	14.0	25.9	22.9	16.9
3-Chlorotyrosine	0.0	5.9	2.0	3.1	3.3

[a]Sodium phosphate buffer. [b]Amino acid mole ratios from Meloun et al. [8]. [c]Measured as leucine.

of three additional ninhydrin-positive peaks in the amino acid analysis. In all of the protein samples treated with chloramine-T, whether at pH 6.5 or with u.v. irradiation, the levels of cysteine, methionine, tyrosine, histidine and lysine were consistently less than the control values.

The three extra peaks found in the analyses of the proteins after treatment with chloramine-T are presumed to have been formed by chemical modification of some of the amino acids listed above. Two of the three extra peaks were identified by their elution positions in ion-exchange chromatography. 3-Chlorotyrosine, which was eluted between phenylalanine and histidine, is formed by reaction of tyrosine with chlorine from the decomposition of chloramine-T. 1-Aminoadipic acid, which was eluted between proline and glycine, is very probably formed by oxidation of some of the lysine residues by chloramine-T. The third extra peak, which was eluted between aspartic acid and threonine, has not been identified. From its elution position, it is acidic or at least polar in character; it could not be matched up with cysteic acid, methionine sulphoxide or methionine sulphone, or homocysteic acid, all of which are oxidation products of cysteine or methionine.

In an attempt to identify the site or sites of binding of chloramine-T on proteins, a sample of HSA/chloramine-T conjugate was hydrolysed in 6 M

TABLE 2

Amino acid mole ratios and chloramine-T (CAT) content of ovalbumin/chloramine-T conjugates (analyses based on 387 residues)

	Control	5 mg CAT H_2O, pH 6.5	10 mg CAT H_2O, pH 6.5	10 mg CAT buffer, pH 6.5[a]	10 mg CAT buffer, pH 8.5[a] irradiated
Mole ratio CAT/protein	—	5.4	7.2	6.4	5.8
ASP (32)[b]	35.0	38.1	36.6	35.6	35.8
THR (15)	16.8	17.8	18.4	17.8	18.9
SER (38)	35.1	32.9	35.0	34.1	36.3
GLU (52)	54.4	53.4	57.1	55.3	51.9
PRO (15)	N.D.	16.5	16.7	17.1	18.0
GLY (19)	20.4	22.2	20.8	19.8	19.5
ALA (35)	37.3	36.7	38.1	37.9	36.2
½ CYS (6)	3.5	1.3	0.8	0.0	0.0
VAL (32)	29.3	31.3	31.4	32.8	32.5
MET (15)	14.9	3.5	1.4	3.1	10.1
ILEU (24)	23.0	24.1	4.1	25.3	24.9
LEU (31)	34.9	35.1	35.4	35.3	34.4
TYR (10)	12.9	4.3	1.5	2.2	5.0
PHE (19)	21.9	22.1	23.7	23.1	20.6
HIS (7)	7.8	6.3	3.5	4.3	7.0
LYS (20)	21.9	8.9	12.3	11.2	12.3
ARG (15)	16.4	16.3	16.0	15.9	15.6
Peak 1 (unidentified)[c]	0.0	4.9	6.6	7.9	0.0
1-Aminoadipic acid	0.0	8.5	3.8	4.9	3.5
3-Chlorotyrosine	0.0	6.4	6.0	5.9	6.5

[a]Sodium phosphate buffer. [b]Amino acid mole ratios from Smith and Back [9]. [c]Measured as leucine.

hydrochloric acid (18 h) and chromatographed on Sephadex LH-20 with 30% methanol as eluent. The results are shown in Fig. 1. Most of the ninhydrin-positive material was eluted between fractions 17 and 22; a single radioactive peak was eluted in fractions 26–28. The radioactive peak was collected, examined for amino acids and found to contain phenylalanine and tyrosine, but no other ninhydrin-positive material. The radioactive component of the peak was not identified. This result indicates that the chemical linkage between chloramine-T and proteins is not stable to acid hydrolysis. The most likely residues for covalent binding of chloramine-T are lysines; these are the only chemically suitable sites for reaction which are present in sufficient numbers to fit the observed stoichiometry. (When chloramine-T was added to poly-L-lysine solution at pH 6.5, an insoluble precipitate thought to be a poly-L-lysine salt of chloramine-T was formed and no covalent binding between chloramine-T and poly-L-lysine was observed.)

The mechanism of binding of chloramine-T to proteins at pH 6.5 and on irradiation probably involves free radicals. Electron spin resonance spin trapping studies have demonstrated the generation of free radicals from chloramine-T both at pH 6.5 and on u.v.-irradiation [10].

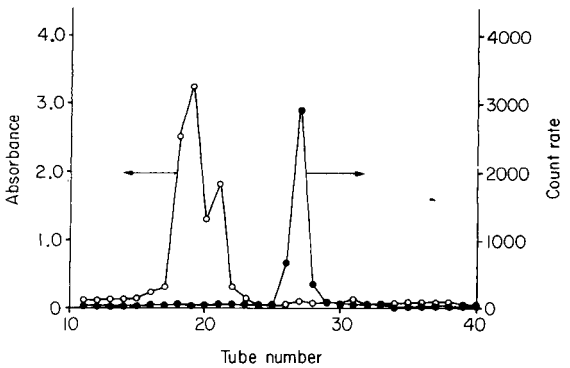

Fig. 1. Elution profile of acid hydrolysate of HSA/chloramine-T conjugate on Sephadex LH-20 in 30% methanol: (○) absorbance at 570 nm (ninhydrin); (●) count rate (dpm).

Chloramine-T has been used extensively as a reagent for the radio-iodination of proteins. In view of the results described above, it is clear that in addition to the incorporation of iodine into tyrosine residues, a reaction similar to the chlorination of tyrosine described above, other quite extensive modification of amino acid side-chains as well as covalent binding of chloramine-T itself to protein can occur. The use of this reagent for radio-iodination of proteins should thus be approached with caution.

The authors thank Mr. C. T. James for synthesising the ^{35}S-labelled chloramine-T, Mr. A. J. Marks for the amino acid analyses and SERC for awarding one of us (S. K. J.) a CASE studentship.

REFERENCES

1 J. H. Dijkman, P. H. Vooren and J. A. Kramps, Int. Arch. Allergy Appl. Immunol., 64 (1981) 422.
2 M. S. Bourne, M. L. H. Flindt and J. Miles Walker, Br. Med. J., 2 (1979) 10.
3 J. A. Kramps, A. W. van Toorenbergen, P. H. Vooren and J. H. Dijkman, Int. Arch. Allergy Appl. Immunol., 64 (1981) 428.
4 W. M. Hunter and F. C. Greenwood, Nature, 194 (1962) 495.
5 A. I. Vogel, Practical Organic Chemistry, Longmans, Green, London, 1962, pp. 822—824.
6 M. Bradford, Anal. Biochem., 72 (1976) 248.
7 P. S. Diamond and R. F. Denman, Laboratory Techniques in Chemistry and Biochemistry, Butterworths, London, 1966, p. 426.
8 B. Meloun, L. Moravek and V. Kostka, FEBS Lett., 58 (1975) 134.
9 M. B. Smith and J. F. Back, Aust. J. Biol. Sci., 23 (1970) 1211.
10 J. C. Evans, S. K. Jackson, C. C. Rowlands and M. D. Barratt, Tetrahedron, 41(22) (1985) 5191, 5195.

Analytica Chimica Acta, 186 (1986) 325—329
Elsevier Science Publishers B.V., Amsterdam — Printed in The Netherlands

Short Communication

BEST ESTIMATES FROM INTERLABORATORY DATA

BRIAN LISTER
British Geological Survey, Geochemistry Directorate, London WC1X 8NG (Great Britain)
(Received 23rd January 1986)

Summary. The arithmetic mean has long been accepted as the best estimate of a true value in the evaluation of replicate data. Other estimates, such as the median, are rarely used. Problems in the evaluation of interlaboratory data received in the certification of reference materials are used to illustrate the fallibility of the mean and the value of different types of robust estimate such as the Gastwirth median.

A recent paper by Pszonicki [1] advocated the use of the median in the evaluation of reference materials. This is a welcome advance from the general acceptance by analytical chemists of the mean as a best estimate of a true value. The British Geological Survey (Institute of Geological Sciences as it then was) produced its first series of reference materials in 1976 [2]. Within the 20 ore and concentrate samples, a total of 55 elemental concentrations received recommended or more tentative probable values. In that compilation, after elimination of outliers, the mean was generally used as the best estimate. However, in one case, that of tantalum in a columbite (IGS 33), the median was preferred and in another, that of silver in a lead-zinc concentrate (IGS 28), it was recognised that no conventional estimate yielded a satisfactory result. Since 1976, during appraisal of thousands of results received in the certification of further reference materials, the writer has come to accept that the mean is unreliable, particularly if data are few in number or are a poor approximation to a normal distribution. Indeed, even when data are within the 5% significance levels for a normal distribution, the mean may still be unsatisfactory. In the case of the tantalum data referred to above, when discrepant data were removed by recognised methods [3, 4], the remaining data formed an acceptable normal distribution, yet the mean was 4.285% and the median, 4.37%, a considerable difference.

The median or middle result of ordered data is the simplest of many so-called "robust" estimates, i.e., estimates that are less affected by aberrant data. Brief reference may be made to the median, but details of these estimates are rarely found in elementary statistical texts. There is also the problem of communication; it takes years for developments published in statistical journals to percolate through to other disciplines. Details of a particularly useful estimate, the Gastwirth median, for example were published 20 years

0003-2670/86/$03.50

ago [5] and the results of a seminar at which some 60 robust estimates were assessed were published in 1972 [6]. An up-to-date book on robust estimates is only now available [7].

The seminar [6] is particularly important because the six statisticians who participated examined each estimate for different numbers of data (n = 5, 10, 20 and 40). The most appropriate estimate was found to depend on the number of data and also on the amount of trouble that a worker was prepared to take. For example, the median can be used for any number of data but, with little more calculation, the Gastwirth median is generally better for $n > 20$. Other useful estimates are the 25% trimmed mean and Hampel's M-estimates, although here a computer becomes essential. One emphatic conclusion was that without some form of rejection procedure for discrepant data, the worst estimate was the arithmetic mean [6]. Some of these robust estimates are described briefly below.

The Gastwirth median (GM) consists of 0.4 of the median added to 0.3 of the results lying one third of the way in from the highest and the lowest. Hampel's M-estimates make use of ψ functions, the plots of which are line segments [6—8]; version 12A has been used most frequently. The 25% trimmed mean is simply the average after elimination of the highest 25% and lowest 25% of the data. For the dominant cluster mode (DCM) [9], data are eliminated at four standard deviations from the mean and the mean and standard deviation are re-calculated. Results are then removed at three standard deviations and the process is continued iteratively using smaller factors until only a few data remain; these are then averaged. This estimate appears to give realistic evaluations with skewed data in particular, but the process is laborious without a computer.

One valuable way of examining replicate data is to plot them sequentially from the lowest to the highest as S-shaped distribution curves. The advantage of this method over other ways of visual presentation is that the data are not processed in any arbitrary way but are merely ordered. Anomalies in the form of outliers or other inconsistencies in a set of data are immediately apparent. The data presented below attempt to illustrate several of these points.

Examples

In the following examples, data were ordered and plotted sequentially. Figure 1 illustrates the 53 data from twelve laboratories for tantalum in the reference material, IGS 33. In the original data processing, the three lowest results were removed, after which the distribution was within the 5% significance levels for normal distribution (Table 1, column 3). However, the unsatisfactory, skewed nature of the distribution is shown by the great difference between mean and median. As stated above, the median was preferred. Other suspect data are apparent in Fig. 1 (five high and ten low); the fourth column of Table 1 shows estimates after their removal. The distribution is now almost normal and there is much closer agreement between

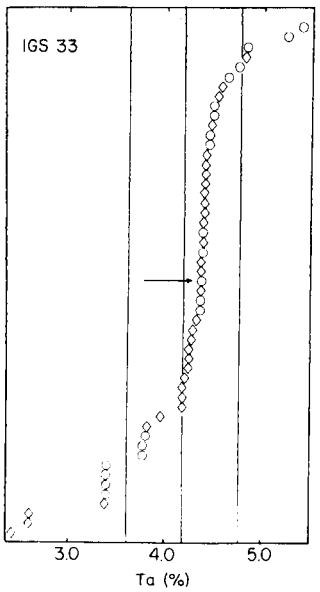

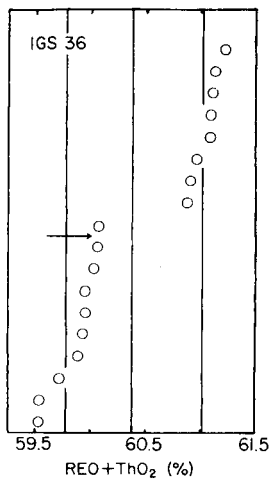

Fig. 1. Tantalum in columbite, IGS 33: (○) gravimetry; (◇) x-ray fluorescence spectrometry. The abscissa represents concentration and the ordinate the number of data. Vertical lines represent the mean and one standard deviation either side of it; an arrow points to the median.

Fig. 2. Rare earth oxides and thorium dioxide in monazite, IGS 36, by a gravimetric method. Explanation as for Fig. 1.

TABLE 1

Tantalum in IGS 33[a]

n	53	50	35
Arithmetic mean, $\bar{x}$	4.19	4.29	4.37
s	0.58	0.42	0.11
Coefficient of skewness[b], $\sqrt{b_1}$	−1.22	−0.33	0.11
Coefficient of kurtosis[c], b_2	5.05	4.02	2.95
Median	4.37	4.37	4.39
Gastwirth median	4.34	4.34	4.38
M-estimate, 12A	4.37	4.37	4.39
Trimmed mean (25%)	4.33	4.35	4.38
Dominant cluster mode	4.40	4.40	4.40

[a] n, number of results; s, standard deviation. [b] Zero in a normal distribution. [c] 3 in a normal distribution.

different estimates. The greater consistency of robust estimates should be noted compared with the mean when the data are reduced from 53 to 35. The maximum variation within the robust estimates is 0.07 whereas the mean varies by 0.18. Because of the negatively skewed nature of the data,

some form of mode is probably the best estimate and in a recent re-evaluation of BGS reference materials, the dominant cluster result of 4.40% was used.

The original data for rare-earth oxides and thorium dioxide in a monazite, IGS 36, are shown in Fig. 2. There are two groups of data and the mean falls between them. Later additional data lay within this gap and so resolved the anomaly but, as shown in the figure, the mean is meaningless as indeed is any other estimate. A distribution of this type with a big gap in the middle is particularly liable to be missed if there is blind reliance on a computer printout.

Figure 3 shows the results of calcium in SOIL-5 from twelve laboratories [10]. The originators gave a mean of 2.20% for information only. These data fall, to some extent, into the gap-in-the-middle category and so the mean is misleading. Figure 3 shows clearly that there is a group of data from five laboratories within the range 2.34—2.52%, which were obtained by three different methods of analysis. The probability of this grouping having occurred by chance is very small and an estimate of around 2.50% (e.g., the median of 2.4975) would be much better than the mean.

Discussion

The three examples cited illustrate the fallibility of the mean and also the dangers of not examining data in some visual way. Of alternatives to the

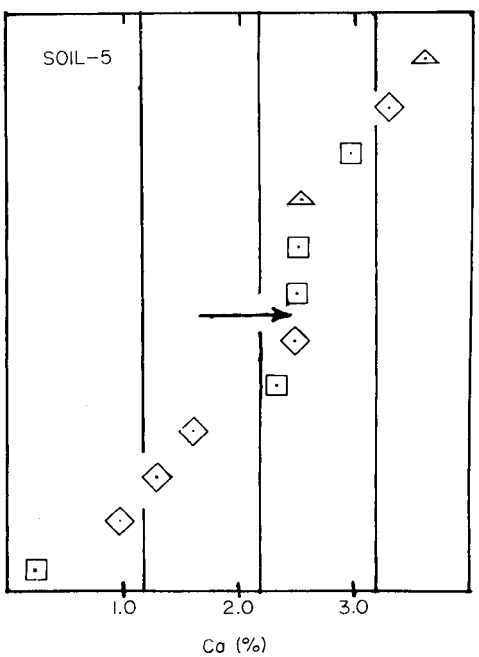

Fig. 3. Calcium in SOIL-5: (□) neutron activation analysis; (◇) x-ray fluorescence spectrometry; (△) atomic absorption spectrometry. Explanation as for Fig. 1.

mean, the median is simple to locate now that computer ordering of data is routine. Confidence intervals, if required, can be calculated by using the binomial distribution or its normal approximation [11]. The Gastwirth median is to be preferred for $n > 20$ and for all n there are many other estimates that may be tried besides the M-estimates and the 25% trimmed mean described. It is disturbing that the British Standards Institution prints the following statement in BS 2846, Part 1, App. A, 1975: "average or arithmetic mean... It is the most commonly used, and generally the most satisfactory, measure of the centre of a distribution". Whereas the first part of the statement is probably true, the second is very far from correct.

This paper is published with the approval of the Director, British Geological Survey (NERC).

REFERENCES

1 L. Pszonicki, Anal. Chim. Acta, 176 (1985) 213.
2 B. Lister, Trans. Inst. Min. Metall., Sect. B, 86 (1977) B133; Geostand. Newsl., 2 (1978) 157.
3 F. Grubbs, Technometrics, 11 (1969) 1.
4 V. Barnett and T. Lewis, Outliers in Statistical Data, Wiley, Chichester, 1978.
5 J. Gastwirth, J. Am. Stat. Assoc., 61 (1966) 929.
6 D. F. Andrews, P. J. Bickel, F. R. Hampel, P. J. Huber, W. H. Rogers and J. W. Tukey, Robust Estimates of Location: Survey and Advances, Princeton University Press, Princeton, 1972.
7 F. R. Hampel, P. J. Rousseeuw, E. M. Ronchetti and W. A. Stahel, Robust Statistics, Wiley, New York, 1986.
8 B. Lister, Geostand. Newsl., 8 (1984) 171.
9 P. J. Ellis, I. Copolowitz and T. W. Steele, Geostand. Newsl., 1 (1977) 123.
10 R. Dybczíński, A. Tugsavul and O. Suschny, Geostand. Newsl., 3 (1979) 61.
11 A. M. Mood and F. A. Graybill, Introduction to the Theory of Statistics, McGraw-Hill, New York, 1963, p. 407.

Analytica Chimica Acta, 186 (1986) 331—335
Elsevier Science Publishers B.V., Amsterdam — Printed in The Netherlands

Short Communication

SENSITIVE SPECTROPHOTOMETRIC DETERMINATION OF PALLADIUM WITH TIN(II) CHLORIDE AND RHODAMINE-6G AFTER FLOTATION

K. KALINOWSKI and Z. MARCZENKO*
Department of Analytical Chemistry, Technical University, 00-664 Warsaw (Poland)
(Received 4th December 1985)

Summary. Palladium is determined by reaction with tin(II) chloride and rhodamine-6G in hydrochloric acid medium, flotation of the ion-association complex, $[(R6G^+)_2Pd(SnCl_3^-)_4] \cdot [(R6G^+)(SnCl_3^-)]$ with di-isopropyl ether, and dissolution in acetone for spectrophotometry. The molar absorptivity is 2.84×10^5 l mol^{-1} cm^{-1} at 530 nm; Beer's law is obeyed in the range 0.05—0.35 μg Pd ml^{-1}. Other platinum metals and silver interfere. Traces of palladium in silver metal are determined after extraction of palladium with dimethylglyoxime in chloroform.

Flotation-spectrophotometric methods for the determination of platinum metals and gold, based on sparingly soluble ion-associates of anionic complexes of these metals with basic dyes, provide molar absorptivities of $2—10 \times 10^5$ l mol^{-1} cm^{-1} [1—5]. The flotation separation of the ion-associates involves shaking an aqueous pseudosolution containing a sparingly soluble hydrophobic compound with an appropriate less dense solvent. The sparingly soluble ion-associate usually contains a multivalent anionic complex of the metal combined with more than one hydrophobic monovalent cation of the dye. Sometimes, the floatable compound is not a simple ion-associate but an adduct with salt molecules of the dye used. Normally, the precipitate separated by flotation is washed to remove the free dye and dissolved in a polar organic solvent for spectrophotometric measurements.

In hydrochloric acid medium, and in the presence of tin(II), palladium, like other platinum metals, forms multivalent cluster compounds which give sparingly soluble floatable ion-associates with some basic dyes. This communication deals with the flotation and spectrophotometric determination of palladium with tin(II) chloride and rhodamine-6G.

Experimental

Reagents. Palladium standard solution (1 mg Pd ml^{-1}) was prepared by dissolving a suitable amount of palladium(II) chloride in water containing 10 ml of concentrated hydrochloric acid and diluting to volume with water in a 500-ml volumetric flask. The solution was standardized gravimetrically with dimethylglyoxime. Working solutions were prepared by suitable dilution with 2 M hydrochloric acid.

0003-2670/86/$03.50

Rhodamine-6G (R6G) was used as an aqueous 1×10^{-3} M (ca. 0.05% w/v) solution. The dye was purified by dissolving in ethanol and precipitating with a five-fold volume of diethyl ether. Other basic dyes were used as 1×10^{-3} M solutions of analytical-reagent grade chemicals.

Tin(II) chloride dihydrate was used as a 10% (w/v) solution in 2 M hydrochloric acid. The radioisotope (OPiDI Świerk) used was ^{113}Sn as tin(II) chloride in 6 M hydrochloric acid.

Apparatus. A Specord u.v.-visible recording spectrophotometer and a VSU-2P spectrophotometer were used with 1-cm cells.

Recommended procedure. Evaporate to dryness the acidic (HCl) test solution containing up to 4 μg of palladium, on a boiling water bath. Add 2 ml of the tin(II) solution, dilute to 10—20 ml with 1.5 M HCl, and transfer the solution to a separatory funnel. Add 1 ml of rhodamine-6G solution and 5 ml of di-isopropyl ether and shake for 30 s. Open the separatory funnel from the top, allow the phases to separate, and slowly discard the aqueous layer. Wash the ether phase and the separated precipitate by shaking with three 10-ml portions of 1.5 M HCl for 30 s each. Carefully remove the aqueous and organic layers and dissolve the precipitate adhering to the wall in acetone. Transfer the solution to a 10-ml volumetric flask, dilute to the mark with acetone, and measure the absorbance at 530 nm against a reagent blank prepared in the same way.

For the preparation of the calibration graph, apply the same procedure to suitable portions of the palladium standard solution.

Analysis of silver. Dissolve the silver sample (ca. 1.5 g) in concentrated nitric acid (about 8 ml), transfer the solution to the separatory funnel and dilute with water to 50 ml. Add 2 ml of a methanolic 1% (w/v) solution of dimethylglyoxime (DMG), leave the mixture for about 10 min, and then extract the Pd-DMG complex with two 5-ml portions of chloroform. Evaporate the combined extracts to dryness, digest with 3 ml of hydrochloric acid and 2 ml of nitric acid (both concentrated) and evaporate to dryness again. Dissolve the residue in 1.5 M HCl and then apply the above procedure.

Results and discussion

Formation and flotation of palladium compounds. In hydrochloric acid medium, palladium(II) forms anionic complexes with $SnCl_3^-$ and chloride [6]. Palladium complexes with tin(II) halides have not been investigated as extensively as similar compounds of other platinum metals [7]. Shlenskaya et al. [6] proved the existence of three complexes in solution, depending on the reagent concentrations and especially on the Sn(II):Pd mole ratio. Undoubtedly, mixed complexes of the type $[PdCl_{4-i}(SnCl_3)_i]^{2-}$ are formed. These complexes of palladium, unlike those of some other platinum metals, form quickly at room temperature.

Palladium complexes with tin(II) and chloride, formed in about 1.5 M HCl and with a 200-fold molar excess of tin(II) relative to palladium react with some basic dyes to form sparingly soluble ion-associates that accumulate

on the wall of the separatory funnel after shaking with any solvent of low polarity. Preliminary investigations showed that rhodamine-6G was the most promising dye. Aqueous pseudosolutions containing 0.4—4 M hydrochloric acid were shaken with benzene, toluene, cyclohexane, amyl acetates, butyl and amyl alcohols, MIBK, and amyl or propyl ethers (all lighter than water). The sparingly soluble compounds were floated with propyl and amyl ethers and amyl acetates. In the case of propyl ethers, the maximum absorbance of the acetonic solution of the precipitate (measured against the reagent blank) was obtained in the acidity range 1—1.5 M (Fig. 1a,b). With amyl ethers or acetates, responses were worse although the absorbances of the blanks were markedly lower than in the case of propyl ethers (Fig. 1c—e); isoamyl acetate behaved similarly to n-amyl acetate. With cyclohexane (as in the system with rhodium [5]), only the ion-associate of rhodamine 6G with $SnCl_3^-$ was floated when the aqueous phase was more than 1.5 M in hydrochloric acid (Fig. 1f). The other organic solvents tested partly floated and partly dissolved the ion-associate.

Studies of the analytical application of the system to the determination of palladium were limited to the use of di-isopropyl ether. With this solvent, the optimum hydrochloric acid concentration is 1—1.5 M (Fig. 1b). Regardless of the phase volume ratio during flotation, separation of palladium is practically complete. Shaking times should be 30 s or more. The molar excess of the dye with respect to palladium should be $\geqslant 50:1$, to ensure total separation of palladium.

The ion-associate of rhodamine-6G with $SnCl_3^-$ is co-precipitated and co-floated with the palladium compound. The latter is more stable; when the precipitate is washed, the rhodamine-6G/$SnCl_3^-$ complex decomposes and the

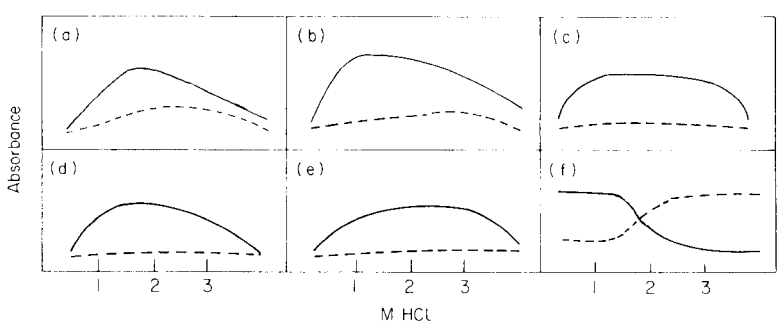

Fig. 1. The effect of hydrochloric acid concentration on the absorbance of acetonic solutions of the compound. Organic solvent: (a) di-n-propyl ether; (b) di-isopropyl ether; (c) di-n-amyl ether; (d) di-isoamyl ether; (e) n-amyl acetate; (f) cyclohexane. (—) Absorbance of the solution measured against the blank, (- - -) absorbance of the blank measured against acetone.

freed dye passes to the aqueous solution. It was shown that washing the precipitate with three portions of 1.5 M hydrochloric acid was adequate to remove the unwanted complex.

The concentration of tin(II) in the initial aqueous solution should be in the range 0.02—0.04 M. At lower concentrations, the final absorbances were small; at higher concentrations, the blank increased significantly. Because of the instability of tin(II) in solution, the effect of tin(IV) was examined. Tin(IV), present as $SnCl_6^{2-}$ in the hydrochloric acid medium [8], also forms an ion-associate with rhodamine-6G, which can be floated by shaking with di-isopropyl ether. It is relatively unstable, however, and a single washing with 1.5 M HCl is enough to cause its total decomposition. Experiments proved that palladium cannot be floated in the presence of tin(IV) only, which means that chlorostannate(IV) does not form an anionic complex with palladium. In order to obtain reproducible results, it is necessary to introduce a tin solution of an approximately stable Sn(II)/Sn(IV) ratio. A solution of tin(II) chloride in 2 M hydrochloric acid that has been stored for about a week without special precautions contains about 2/3 of tin(II). Such a solution was used in the experiments described here.

Composition of the floated compounds. The molar ratio of palladium to rhodamine-6G in the separated and washed compound was evaluated by comparing the absorbances of acetonic solutions of the precipitates from a known amount of palladium with those of acetonic solutions of the same amount of dye. The molar ratio was 1:3. This result was confirmed by the Bent and French logarithmic method [9].

In order to establish the ratio of tin to palladium atoms in the floated compound, tin was determined radiometrically by using the ^{113}Sn radioisotope, and spectrophotometrically with phenylfluorone [10]. Both methods gave a mean Pd:Sn value of ca. 1:5. Given the general formula of the palladium complexes formed in presence of tin(II) in dilute hydrochloric acid (see above) and assuming that the palladium(II) is maintained under the conditions used, the following formula seems reasonable for the adduct formed: $[(R6G^+)_2Pd(SnCl_3^-)_4] \cdot [(R6G^+)(SnCl_3^-)]$. This adduct can be obtained reproducibly by washing the precipitate with three portions of 1.5 M HCl (30 s in each case). After a single washing, the Pd:Sn(II) mole ratio in the separated compound is about 1:7, which may indicate the existence of another adduct, but it is too unstable for analytical purposes.

Determination of palladium. The reactions discussed above provide a very sensitive flotation-spectrophotometric determination of palladium. Beer's law is obeyed in the range 0.05—0.35 μg Pd ml^{-1}; the molar absorptivity (ϵ) is 2.84×10^5 l mol^{-1} cm^{-1} (specific absorptivity $a = \epsilon$/atomic mass $\times$ 1000 = 2.7). The precision and accuracy of the method were verified for standard solutions of palladium (Table 1).

Under the conditions used, the other platinum metals also form floatable compounds. For applications, therefore, a selective separation of palladium is needed, e.g., with dimethylglyoxime [11]. This separation is also needed

TABLE 1

Statistical evaluation of the results obtained by the proposed method

Palladium (μg)		Standard deviation[a]	Relative standard deviation (%)	Confidence limits (μg)[b]
Added	Found			
1.00	1.02	0.09	8.0	1.02 ± 0.08
2.00	1.98	0.08	4.1	1.98 ± 0.07
3.00	3.04	0.08	2.5	3.04 ± 0.07

[a]For seven determinations. [b]Probability level = 0.95.

TABLE 2

Determination of the traces of palladium in silver metal (1.5 g)

Palladium (μg)		Standard deviation (μg)[a]	Confidence limits[b]	
Added	Found		(μg)	($\times 10^{-4}$%)
—	2.91	0.62	2.91 ± 0.82	2.0 ± 0.6
2.50	2.67	0.16	2.67 ± 0.18	1.9 ± 0.1

[a,b]See Table 1.

to avoid interference from silver, which is precipitated as silver chloride. On this basis, the proposed method was applied to determine traces of palladium in silver metal after dissolution and separation as described under Experimental. The results (Table 2) show the good precision of the method applied.

This work was supported by Research Program MR-I-32.

REFERENCES

1 Z. Marczenko, Crit. Rev. Anal. Chem., 11 (1981) 195; Pure Appl. Chem., 57 (1985) 849.
2 Z. Marczenko and K. Kalinowski, Anal. Chim. Acta, 144 (1982) 173; Mikrochim. Acta, II (1983) 169; Anal. Chim. Acta, 153 (1983) 219.
3 Z. Marczenko, M. Balcerzak and H. Pasek, Mikrochim. Acta, II (1982) 371.
4 Z. Marczenko and K. Jankowski, Talanta, 32 (1985) 291; Anal. Chim. Acta, 176 (1985) 185.
5 K. Kalinowski and Z. Marczenko, Mikrochim. Acta, I (1985) 167.
6 V. I. Shlenskaya, A. A. Biryukov and L. N. Moryakova, Zh. Neorg. Khim., 14 (1969) 496.
7 S. I. Ginzburg, N. A. Ezerskaya, I. V. Prokof'eva, N. V. Fedorenko, V. I. Shlenskaya and N. K. Belskii, Analytical Chemistry of Platinum Metals, Izd. Nauka, Moscow, 1972.
8 C. I. Browne, R. P. Craig and N. Davidson, J. Am. Chem. Soc., 73 (1951) 1946.
9 H. Bent and C. French, J. Am. Chem. Soc., 63 (1941) 568.
10 Z. Marczenko, Separation and Spectrophotometric Determination of Elements, Ellis Horwood, Chichester, 1986.
11 R. S. Young, Analyst, 76 (1951) 49.

Analytica Chimica Acta, 186 (1986) 337—354
Elsevier Science Publishers B.V., Amsterdam — Printed in The Netherlands

Book Reviews

Philip K. Hopke, *Receptor Modeling in Environmental Chemistry.* Wiley, New York, 1985. pp. vii + 319. Price £86.75.

The term "receptor modeling" will not be familiar to the majority of analytical chemists. It is defined by Professor Hopke in his Preface as "... the way of referring to the class of methods where the properties of a sample are used to infer the origin of its components". This is a highly topical subject with a major effort being made towards quantifying the contribution of individual sources to levels of pollutants in the environment. The book concentrates upon source apportionment for airborne particulate matter, although the mathematical techniques described could be applied to systems other than the atmosphere.

After a brief introduction, the book reviews in considerable detail the physico-chemical procedures available for characterising airborne particles in a manner which will indicate their source. These include both microscopic (light and electron) methods and macroscopic procedures such as x-ray powder diffraction. The major part of the book deals with mathematical receptor models where elemental analyses of source material and ambient air particulates may be used to quantify individual source contributions to the latter. These include chemical mass balance, principal components and factor analysis, which are not for mathematical faint hearts. Included as an Appendix are 47 very valuable pages of source profiles selected from the literature.

Professor Hopke is an acknowledged authority in this field and has produced a most readable and informative book, which will be essential reading to all with a serious interest in the field.

R. M. Harrison

K. R. Spurny (Ed.), *Physical and Chemical Characterization of Individual Airborne Particles.* Horwood, Chichester, 1986 (ISBN 0-85312-793). pp. xi + 418. Price £55.00.

The field of aerosol science is currently experiencing a considerable upsurge of interest. Whilst earlier focusses of attention have been in the areas of physical properties and respiratory deposition and hazards, perhaps the major focus is now upon techniques for chemical characterization of aerosols. Chemical composition has major implications in evaluating toxic hazards associated with aerosol inhalation, in source-apportionment of pollutant particles and in understanding atmospheric chemical processes pertinent to environmental problems such as acid rain.

Much of the work carried out on chemical characterization of aerosols

involves collection of a rather large sample of particles, usually by filtration, and subsequent bulk chemical analysis for major, minor or trace elemental and ionic components. Such an approach has the major drawback of reflecting the averaged composition of the entire sample whilst ignoring the compositional differences between individual particles within a mixture. This book, comprising 21 chapters by various authors, focusses upon the techniques available for chemical characterisation of individual particles. These include electron probe microanalysis, laser microprobe mass analysis (LAMMA) and secondary ion mass spectrometry, amongst others. The majority of these techniques when applied to aerosol analysis are at the research stage and chapters have been contributed by the research groups which are carrying out the pioneering work. Additional chapters outline basic aerosol science principles, and cover some of the techniques for physical characterization of aerosol particles.

This is a highly specialised book which will be of great value to those interested in the more sophisticated techniques of aerosol characterization. It is unlikely, however, to stimulate the interest of a wider community of workers in analytical chemistry, environmental science and occupational hygiene to whom it undoubtedly bears relevance.

R. M. Harrison

Wayne R. Wolf (Ed.), *Biological Reference Materials: Availability, Uses and Need for Validation of Nutrient Measurement.* Wiley-Interscience, New York, 1985 (ISBN 0-471-80636-6). pp. xv + 425. Price £69.50.

The value of a reference material for validating analytical results is well understood. The need for biological reference materials is particularly great, and developments in this area have been so rapid as to justify this complete book. Essentially, it is a record of a symposium held at the FACSS meeting in Philadelphia in September 1983. It is arranged in six Parts. The first deals with available (or soon to be available) certified materials, covering kale (H. J. M. Bowen), NBS and IAEA materials, and food and marine biological reference materials. Part 2 covers "homogeneous and well-characterized materials", and includes the preparation of a daily diet reference material, a bovine serum pool, maize and beef muscle reference materials, and a discussion of ISPRA's activities in candidate biological reference material production. A third section deals with quality control materials for nutrient analysis, followed by a fourth section on environmental sample banking. Part 5 is a resumé of an open discussion held at the end of the symposium, and Part 6 is a reproduction of NBS Special Publication no. 635 — Reference Materials for Organic Nutrient Content.

The 16 papers and discussion by internationally-known authors give a valuable insight into the preparation and philosophy of reference materials, as well as detailing the availability and future availability of such materials,

their contents and uses. The growing demand for, and production of reference samples containing organic compounds is recognized, and the need for specimen banking, and the effects of storage are discussed in detail. Overall, the book provides an impressive account of the amount of effort that is being expended in meeting the rapidly increasing demand for an equally rapidly increasing range of reference materials, not only for nutrient measurements, but for all areas of analytical chemistry.

Alan Townshend

H. Oechsner (Ed.), *Thin Film and Depth Profile Analysis, Vol. 37* in the series, *Topics in Current Physics.* Springer, Berlin, 1984 (ISBN 3-540-13320-8). pp. 205. Price DM 72.00.

The characterization of thin films and solid interfaces and the determination of concentration profiles are most important tasks in materials characterization. As a consequence, the physical techniques for surface and interface analysis play a key role in the development of high technology materials. This book contains state-of-the-art reviews of the most important techniques presented at a seminar in Bad Honeff in 1984. The following topics are covered: Requirements for Thin Film and In-Depth Analysis (H. Oechsner); Application of Beam and Diffraction Techniques to Thin Film and Surface Micro-Analysis (H. W. Werner); Depth Profile and Interface Analysis of Thin Films by AES and XPS (H. J. Mathieu); Secondary Neutral Mass Spectrometry and its Application to Depth Profile and Interface Analysis (H. Oechsner); In Situ Laser Measurements of Sputter Rates During SIMS/AES In-Depth Profiling (J. E. Kempf, H. H. Wagner); Physical Limitations to Sputter Profiling at Interfaces (J. Kirschner, H. W. Etzkorn); Depth Resolution and Quantitative Evaluation of AES Sputtering Profiles (S. Hofmann, M. Sanz); Theory of Recoil Mixing in Solids (U. Littmark, W. O. Hofer).

As is evident from the titles of the contributions and the expertise of the authors, emphasis is placed on the physical processes of sputtering and signal generation. But also, the analytical information content of the various methods and applications to important problems of materials characterization are presented. The individual chapters are written at a top international level, precisely and clearly produced, and very informative. This book can therefore be regarded as a very important source of information for everyone concerned with surface and interface characterization. The strongly physical approach provides an excellent basis for an in-depth understanding of sputtering and its associated processes (such as mixing, diffusion, etc.) and signal generation. In fact, I consider this volume as one of the best pieces of basic literature in this field. The only slight criticism I have as an analytical chemist concerns the rather short presentation of SIMS, which in my opinion is one of the most powerful techniques of surface and interface analysis, especially in view of the high performance instrumentation available for a few years. Nevertheless, an excellent book, highly recommended.

M. Grasserbauer

Hans Jörg Hediger, *Quantitative Spektroskopie.* Hüthig Verlag, Heidelberg, 1985 (ISBN 3-7785-0874-1). pp. 160. Price DM 48.

This book is a collection of altogether 126 alphabetically ordered key-words which, with the scope of the associated contents, hardly meet the title of the book. The majority of the listed terms characterize i.r. and u.v./visible spectroscopy; for the wide field of atomic spectroscopic methods, for instance, only 12 key-words can be found. Further, many definitions and references are missing which, in such a comprehensively titled book, should be treated.

The reviewer was very surprised not to find a single key-word in the book dealing with Raman-, mass-, magnetic resonance-, or x-ray spectroscopy, and other methods of varied importance in the determination of concentrations are not discussed. On the other hand, the rather exotic photoacoustic spectroscopy is treated in detail. Also, the apparently arbitrary inclusion of 12 determination procedures for different substances as key-words is of small significance, the less so because in the preface of the book the author explicitly refuses any responsibility for their reliability.

Inconsistencies can be found in the assignment of key-words to the contents. In some cases, practically identical terms are allocated to different texts and listed separately. In other cases important terms, which are illustrated by the whole subject matter of the book, are missing. Important information is sometimes hidden under unlikely key-words; the optical function of prisms and gratings can only be found under "Dispersionsglied".

In their detail and information content, the texts assigned to the key-words are to be viewed very differently. In some cases, inadmissible generalized statements, e.g. on sensitivity or on possible interferences, can be found which may lead to erroneous conclusions. Finally, the explanations of the book dealing with data gathering and processing, and with the estimation of analytical procedures and results, are only of limited use.

Altogether, the reviewer hesitates to name larger groups of possible users to whom he could recommend this, not even cheap book as profitable reading.

E. Jackwerth

Joanna Sadlej, *Semi-empirical Methods of Quantum Chemistry.* Horwood, Chichester, 1985. pp. xiv + 386. Price £42.50.

This is the English edition of a book first published in Polish in 1976. The author has revised and updated the Polish edition to include work published up to the end of 1978. Her subject is the use of semi-empirical methods in the application of SCF LCAO MO theory to chemical problems. A variety of such methods have been developed over the past twenty years, and have been made available for general use through the Quantum Chemistry Program

Exchange at the University of Indiana. They have the advantage that they require less computer time than nonempirical methods, and are capable of giving results for larger molecules. Their disadvantage lies in the uncertain nature of the approximations that are used. The author's aim is to provide an account of these methods for chemists with no more than a basic training in quantum chemistry who would like to use them in their work.

After a brief introduction, she begins with a short account of SCF LCAO MO theory and of the various approximations to it, and parameterizations of it, that the semi-empirical methods employ (Chaps. 2—4). She then describes the application of these methods to the calculation of molecular properties, conformational analysis, chemical reactivity, interpretation of molecular spectra, hydrogen-bonding, and the electronic structure of biologically-active molecules (Chaps. 5—10). Her exposition is clear, and has the great merit of bringing together the different methods that have been suggested, treating them in a consistent and coherent way. She is also careful to stress the limitations of each method, as well as its usefulness. The early chapters are not easy, however, and may prove a barrier to some of those for whom the author is writing. The book is spoilt by a number of typographical errors, and, more seriously, by the long delay in publication.

P. G. Nelson

Gary J. Long (Ed.), *Mössbauer Spectroscopy Applied to Inorganic Chemistry, Vol. 1.* Plenum Press, New York and London, 1984. pp. xviii + 667. Price $92.50.

This book had been seized upon by my postgraduate students and was extensively used in my laboratory before I was invited to review it. It is a pleasure to be able to review a book which I have already found to be of great value both to my research activities and supervision of postgraduates, and to my undergraduate teaching. Mössbauer Spectroscopy is a well-established laboratory technique finding a diverse range of applications in many subject disciplines. The chosen area of application in inorganic chemistry may at first sight appear unnecessarily limiting, but this is far from the case, as an inspection of the wealth of topics covered soon reveals. Indeed, it is interesting to note that the contributors include six chemists, six physicists and a materials scientist. All have international reputations in their specialist fields, and have combined to give a thorough and up-to-date overview.

The first four chapters are concerned with: historical background, basic concepts, spectrometers and calibration, and data reduction and refinement. These combine to give the reader a sound basis in current Mössbauer methodology. The next three chapters deal in considerable detail with isomeric shift, quadrupole interaction and magnetic systems. The remainder of the book focuses upon specific applications in inorganic chemistry, and it is the nature of these eleven chapters that give the book its unique flavour. It is impossible

within the confines of this review to adequately describe the range and depth of the material covered. This extends from relaxation phenomena to one-dimensional magnetism, and includes tin, iron and gold chemistry. The book is well written, has been extremely well presented and, although rather expensive, gives good value; it should soon become a standard text adopted by all Mössbauer laboratories.

John Brooks

J. C. Berridge, *Techniques for the Automated Optimisation of HPLC Separation.* Wiley, Chichester, 1985 (ISBN 0-471-90861-4). £22.00.

The selection of the optimum mobile and stationary phases to achieve the complete separation of a complex mixture in HPLC has been a mixture of experience and trial and error, because of the large number of variables available to the operator. However, as John Berridge points out, it is this wide versatility that makes HPLC such a powerful technique, and over the past few years numerous methods have been reported which try to rationalise this optimisation process and to adapt it to unattended operation.

This valuable book by Berridge has brought these methods together and evaluated them, giving both their strengths and weaknesses. Although many of the concepts are also valuable for chromatographers attempting manual optimisation, the emphasis is on the ability to automate the procedures both for the selection of the separation conditions and the control of the chromatograph.

After a brief description of the HPLC hardware required for automated operation, the different criteria used to establish the success of the optimisation process, such as chromatographic response functions, are compared. The different approaches to optimisation are then discussed in detail. These begin with the use of simple but limited methods for the selection of a single isocratic mobile phase, based on stepwise trials or a gradient elution run. A pragmatic approach is briefly discussed in which the retentions are predicted from the properties of the analytes and relationships derived from a limited set of experimental data. The next three chapters describe alternative methods to determine response maps of the separation conditions. Statistically based experiments are discussed first, in which a small set of possible elution conditions is selected, frequently based on Synder solvent triangles. After all the corresponding chromatograms have been measured, the results are evaluated, either by modelling or visual examination, to determine the optimum values. This section also includes the "brute force" approach of a multi-step measurement of all possible combinations of conditions. An alternative chemometric method based on window diagrams is considered. These give a visual representation based on extensive modelling from which alternative suitable conditions can be identified and compared.

Probably the most useful part of the book is the detailed description of

directed search methods. These include the simplex and modified simplex approaches, in which the results of each trial chromatogram are used to select the conditions for the next trial. Although the simplex technique has been reported frequently, the limitations of the research paper have often previously restricted a full explanation of its operation or the underlying rules. In a second section, iterative methods are described but, although they give rapid results, they can be harder to automate. Finally, the author describes the potential of expert systems and the application of post-separation techniques such as diode array spectrometry for the identification of analytes.

The book is very readable and the author usefully concludes each section with a summary of the advantages and disadvantages of the particular method. He notes that frequently in commercial systems the algorithm or software being used to select the optimum conditions is inaccessible or hidden, and in the appendices provides a number of BASIC routines to carry out typical procedures. Throughout the book, the author has illustrated the different techniques using the separation of a standard six-component test mixture. However, this usage is not well explained and the composition of the mixture is given only in an appendix. Overall, this book is a valuable (and for once reasonably priced) addition to the chromatographic literature which clarified much of the often conflicting claims of reported techniques.

Roger M. Smith

C. J. Holloway (Ed.), *Analytical and Preparative Isotachophoresis.* Walter de Gruyter, Berlin, New York, 1984. DM 170.00.

This book presents the proceedings of the 3rd International Symposium on Isotachophoresis which was held at Goslar, Germany in June 1982.

The book is divided into six sections, as follows. (1) Instrumental, Theoretical and Fundamental Aspects of Isotachophoretic Separations. (2) Applications of Isotachophoresis in the areas of Quality and Environmental Control and Food Chemistry. (3) Isotachophoretic Analysis of Low Molecular Weight Metabolites: Biochemical and Biological Applications. (4) Isotachophoretic Analysis of Low Molecular Weight Metabolites: Clinical Applications. (5) The Isotachophoretic Separation and Analysis of Proteins. (6) Preparative Isotachophoresis.

The introduction to this volume is by A. J. P. Martin, who may be named as the Father of isotachophoresis as he is of chromatography, and it is instructive to read his comments.

As the sections given above indicate, the papers comprising the bulk of this book give information on the various applications to which this powerful method of separation and analysis have been applied.

It is clear from the contents that isotachophoresis is uniquely suitable for the separation of charged species compared with the accepted methodologies

of liquid chromatography. While this book does not give information on all that can be achieved by isotachophoresis, it provides stimulating reading for those workers in the field of clinical chemistry, biochemistry and related subjects, to say nothing of workers interested in possibly the more mundane subjects of simple anion and cation analysis of waters and trade effluents, to which the technique is particularly suited, although not specifically mentioned in this volume.

While this book deals principally with research topics, the information provided should stimulate workers in related research fields to investigate the potential of isotachophoresis for their analytical problems, where it could well provide the solution to erstwhile intractable analyses.

C. F. Simpson

Gary D. Christian, *Analytical Chemistry, 4th edn.* Wiley, New York, 1986 (ISBN 0-471-8874-6). pp. xvii + 676. Price £38.85.

The fourth edition of this textbook has been extensively revised and now includes chapters on fundamental analytical principles, classical techniques, instrumental techniques and applications to specific types of samples. The emphasis is on a practical approach, with details of 44 experiments given at the back of the book.

The material presented is appropriate for introductory undergraduate courses, and, like other recent publications in this area, is very clearly presented. There are several worked examples in each chapter, important concepts are highlighted in boxes and key-words are in boldface type. There are very few photographs, however, and those that are included look somewhat dated.

The contents of the first sixteen chapters are fairly predictable. An introduction outlines the "Analytical Approach" and is followed by chapters dealing with laboratory technique, data handling, chemical equilibria and gravimetric analysis. Various volumetric procedures are presented in detail and each of the major areas of instrumental analysis is also covered.

What distinguishes this particular book from others of its kind are the last five chapters, which discuss laboratory automation, kinetic methods, clinical chemistry, drug analysis and environmental analysis. These applications chapters provide interesting and useful background information for the reader and put the contents of preceding chapters into a practical context. They also highlight the importance of sampling and sample treatment procedures when faced with "real" analytical problems. Coverage of the role of enzymes in analysis and sections on immunoassays and flow injection analysis are also welcome additions.

P. J. Worsfold

M. A. Sharaf, D. L. Illman and B. R. Kowalski, *Chemometrics.* Wiley, New York (ISBN 0-471-83106-9). pp. xi + 332. Price £51.00.

The authors' intention in writing this book is to provide "the first systematic broad-based attempt to offer analytical chemists, chemical engineers and advanced students the mathematical and statistical tools needed to extract vital and often hidden information from considerable amounts of chemical data". This is an ambitious task, and so the general format of each chapter is to provide a detailed introduction to each topic and supply references and suggestions for further readings. The latter are well described by brief abstracts to enable the correct text to be selected. The chapters are arranged in the logical sequence of sampling a system, designing an experiment, signal detection and enhancement, and then moving to data analysis techniques such as calibration, resolution, and a comprehensive pattern recognition section.

The early chapters on sampling and experimental design contain descriptions of conventional statistical theory which are, although very well written, a little too condensed for the reviewer. However, the examples were very well chosen. The detection and manipulation chapter is very good for a beginner like myself but I would have appreciated some exercises to test my understanding. The calibration chapter is excellent; starting with simple inverse regression, leading through the standard addition method to multicomponent analysis and generalized standard addition. The chapter on signal resolution is hard going and I felt compelled to leave that until I have a specific application! Over a third of the book is devoted to pattern recognition methods, and here a logical and well written sequence introduces preprocessing and display, unsupervised and supervised learning, SIMCA and partial least squares. There are examples from the literature and simple worked examples. It is very nice to see it all in a unified notation!

This is a well written and illustrated book and there must be very few chemists, chemometricians and statisticians who would not learn something new from a thorough reading. However, it may not teach you much about your particular area of chemometric expertise. The major gap is the failure to review the current software available, because this is how these techniques are picked up by the research community.

To summarize, it is a useful book to have somewhere in your organization but at the price it cannot be recommended as a course text.

H. J. H. MacFie

D. P. Woodruff and T. A. Delchar, *Modern Techniques of Surface Science.* Cambridge University Press, Cambridge, 1986 (ISBN 0-521-30602-7). pp. x + 453. Price £50.00.

This book is the 11th item of the series entitled Cambridge Solid State Science Series, edited by R. W. Cahn, University of Cambridge, E. A. Davis,

University of Leicester, and I. M. Ward of the University of Leeds. It is significant that one of the authors of the present volume of the series, D. P. Woodruff, was also the author of the very first volume of the series on "The Solid-Liquid Interface".

The authors of the book attempted the difficult task of describing the physical basis and some applications of a considerable, but sometimes related, number of techniques used in the characterization of surfaces. After a short general introduction on the surface and ultra-high vacuum, the techniques covered are grouped together in eight chapters treating, in sequence, surface crystallography and electron diffraction, electron spectroscopies, incident ion techniques, desorption spectroscopies, high field techniques, work function techniques, atomic and molecular beam scattering and, finally, vibrational spectroscopies. Considering that each of these chapters covers several individual methodologies, it is clear that the authors could not go in detail on any of the ca. 20 distinct methods covered. Nevertheless, their aim of describing physical principles, instrumentation, and strengths and limitations of all these techniques is adequately fulfilled. An exhaustive survey characteristic of a scientific review was not attempted. In fact, this would not have been feasible in view of the enormous literature now available. Nevertheless, it is a pity that with a few exceptions most of the literature listed dates from before 1980, and especially that most of the further reading information provided at the end of each chapter lists older, and sometimes difficult to find, material.

Even so, the clear writing style, very good illustrations and breadth of coverage makes this book highly recommendable as an advanced level textbook for the many research workers who are involved with surface characterization, and even for researchers outside this field who need some detailed knowledge on the plethora of methods (usually identified by esoterically sounding acronyms) utilised in surface analysis and characterization.

F. Adams

A. Darbre (Ed.), *Practical Protein Chemistry — A Handbook.* Wiley, New York, 1986. pp. xix + 620. Price £52.00.

This large handbook contains a collection of forty years of experience in bench practice, and associated theory, in separating and sequencing proteins of diverse structure and biological function. This is of inestimable value to workers in the field. This book consists of twenty-one chapters. Chapters 1—9 cover analytical approaches to preparation of protein chains and their controlled hydrolysis, including the problems of disulphide bonds arising from cystine. These include affinity chromatography of proteins, HPLC separations (including amino acids) and peptide mapping. Analytical methods are discussed by the editor in Chap. 8. Chapters 10 and 11, by Greg Winter, are

on manual sequence strategy and the Dansyl-Edman reaction. Chapter 12 is on practical methods for solid-phase sequence analysis, followed by the analysis of phenylthiohydantoin amino acids (Chap. 13) and analysis of polypeptides using 4-dimethylaminoazobenzene-4′-isothiocyanate (Chap. 14). Chapter 15 deals with current techniques for automated liquid-phase sequence analysis, followed by newer methods, solid- and liquid-phase (Chap. 16). Chapter 17 is on microsequencing analysis using a gas-liquid solid-phase peptide and protein sequencer. Carboxy terminal sequencing analysis is described in Chap. 18. The book concludes with more detailed consideration of physical methods, with the application of electron-impact mass spectrometry in the structural analysis of peptides and proteins (Chap. 19) and x-ray crystallography and electron microscopy (Chap. 20).

Not to be missed is the most penetrating discussion by Dr. B. Robson of the Medical School at the University of Manchester on "The Prediction of Peptide and Protein Structure", in Chapter 21. It is still remarkably difficult to make accurate predictions about the native tertiary structure of a protein molecule from its primary structure (the sequence of amino acid residues). There are innumerable folding possibilities and even computer predictions cannot solve this problem as yet. Attempts to make such predictions are alluded to and the "current state-of-the-art" is appraised in the final pages. There follows a valuable index.

Most of the problems of identifying the final structure of a protein, i.e., after post-translational modification in the cell, cannot be solved by gene (DNA) sequencing alone. The success of x-ray crystallographic methods, when appropriate crystals can be grown, do not obviate, as yet, the need for protein sequencing techniques. Professor B. S. Hartley, in a foreword to the book, compares in outline the contributions of the protein chemist with that made by the genetic engineer and by the x-ray crystallographer. The contributions of each are invaluable, and clearly are complementary and interactive, in the solving of protein folding, and in the understanding of enzyme catalysis.

Alan Wiseman

J. Angerer and K. H. Schaller (Eds.), *Analyses of Hazardous Substances in Biological Materials, Vol. 1.* VCH, Weinheim, 1985 (ISBN 3-527-26095-1). pp. 222.

This volume has been compiled by the Working Group on "Analytical Chemistry", which was established by the Commission for the Investigation of Health Hazards of Chemical Compounds in the Work Area in 1969. The mandate of this Commission, which is part of the German Science Foundation, is to establish maximum concentrations at the work place (MAK values) and biological tolerance values (BAT values) in the Federal Republic of Germany.

The emphasis of the Commission's work is clearly seen in the contents of this volume, which includes detailed analytical methods for fifteen inorganic (beryllium, bromide, cadmium, cobalt, lead, nickel and thallium) and organic (aromatic amines, benzene derivatives, carboxyhaemoglobin, chlorobenzenes, chlorophenols (methyl)hippuric acids, phenol and trichloroacetic acid) species in either blood or urine.

The introductory material for each method includes a method evaluation, reliability criteria, and toxicological and industrial information. The nub of each section is a detailed description of the various preparatory and analytical steps involved, together with information on precision, accuracy, detection limits and interferences.

This book is therefore designed specifically for people using analytical techniques in the field of biological monitoring, with emphasis on the determination of carcinogenic substances and their metabolites. As such it is a useful publication and the information is logically and clearly presented.

Paul Worsfold

A. L. Burlingame and Neal Castagnoli, Jr. (Eds.), *Mass Spectrometry in the Health and Life Sciences.* Elsevier, Amsterdam, 1985 (ISBN 0-444-42562-4). pp. xxiv + 638. Price US$ 133.25/Dfl 360.00.

There can be no doubt that mass spectrometry, with its various ionization techniques, is playing a large and increasingly important role in the understanding of biological processes. It has been particularly useful, especially in combination with the various chromatographic techniques, for detection and identification of biochemically relevant small molecules. Its value for looking at large molecules (peptides, proteins, glucuronides, lipids etc.) has been greatly enhanced by modern developments in mass spectrometry, and it is these developments and applications that form the basis of the papers in this 24th volume in the Analytical Chemistry Symposia series. The papers were presented at a symposium held in San Francisco in September 1984, on the occasion of the opening of the Mass Spectrometry Facility in the Pharmaceutical Chemistry Department, University of California.

The topics covered range from peptides, porphyrins and metal complexes to measurement of the structure of proteins and glycolipids. Steroid conjugates, nucleic acids and glucuronides are also dealt with, and applications to studies of various disease states are given. Uses, too, of the various ionization techniques are included. Overall, this is a very extensive and useful account of the power of modern mass spectrometry in solving biochemical problems, and gives an exciting account of the directions in which the subject is developing. The camera-ready presentation, including the illustrations, is clear, and the information presented will be of great value to all mass spectrometrists and to all scientists working the area of molecular identification in biological systems.

Karl Pfleger, Hans Maurer and Armin Weber, *Mass Spectral and GC Data of Drugs, Poisons and their Metabolites.* Verlag Chemie, Weinheim, 1985 (ISBN 3-527-26303-9). Part I pp. xxx + 208. Part II pp. xi + 744. Price (both parts) DM 480.

There is no better technique than gas chromatography/mass spectrometry (g.c./m.s.) currently available either for the rapid identification of drugs or poisons, or for monitoring their metabolic products. Yet such details that are available on this subject are scattered amongst the literature of chemistry, toxicology, pharmacy, etc. For these reasons, Professor Pfleger and his colleagues have spent much of their careers obtaining and collating g.c./m.s. data on such compounds. The outcome is the present two volumes, designed for easy and rapid access to the data, so as to allow swift analyte identification.

The first volume (Part I) contains some introductory information (30 pp.) on sample treatment, the conditions used for obtaining and storing the chromatographic and mass spectral data reported, and an example of the procedure by which a drug might be identified. There are also useful small sections on correlations between structure and fragmentation patterns and on artifact formation. The remainder comprises three tables. The first is an alphabetical list of >1700 compounds under consideration, together with their g.c. retention indices (OV-101), derivatives and fragment ions. The second lists the same information in order of increasing magnitude of retention index. Table III lists the compounds in order of increasing mass number, and also categorizes the compounds (preservative, vasoconstrictor, desinficient(?), etc.).

The second volume (Part II) is almost entirely devoted to the reproduction of >3300 mass spectra and structural formulae, followed by a compound index for the spectra, and a table of CAS systematic names and registry numbers.

There can be no doubt of the great value of this reference collection. It provides, for the first time, a comprehensive set of retention indices and mass spectra organized to allow a rapid search for and identification of biologically active compounds. The presentation is of a high quality, and the reproduction of the spectra is very clear. All reputable toxicological laboratories should have access to this collection, and it should quickly earn its keep.

Alan Townshend

S. Kotrlý and L. Šůcha, *Handbook of Chemical Equilibria in Analytical Chemistry, Ellis Horwood Series in Analytical Chemistry.* Horwood/Wiley, 1985 (ISBN 0-85312-107-9). pp. 414. Price £45.00.

In the sixties and seventies, many instrumental techniques favourably competed with classical wet-chemical techniques and this led to the mis-

understanding that knowledge of equilibria was no longer essential for getting good analytical results. Such simplifications last until the limitations of an instrumental technique become obvious.

Techniques such as AAS and ICP-AES require analytes present in more or less aqueous solutions. Even for ICP-AES it turns out that signal—analyte relations are seldomly completely matrix-independent. In many cases, the problems could be understood by considering the states of the analytes in solution. A thorough knowledge of solution chemistry is indispensible in these cases. The same holds for accurate classical techniques in use for certification of reference materials.

In general it can be stated that solution chemistry is one of the undeniable bases of analytical chemistry and will remain so for at least two decades. For practical application in specific cases, both the newcomer in this field and those not daily working with equilibria are usually discouraged by the complexity and the extent of the calculations. Moreover, literature data of equilibrium constants are often unreliable.

It is the merit of Kotrlý and Šůcha's work to have provided the potential user first with a critical compilation of reliable data and secondly with a clear method for the construction of logarithmic diagrams for protonation, complexation, solubility and redox equilibria, and predominance-area diagrams. The method is simple, effective and reliable enough for practical use.

In chapters 1—4, the various definitions of equilibrium constants are elucidated, the influence of temperature and ionic strength extensively discussed (with useful tables added) and instructions given for plotting the diagrams when studying simultaneous equilibria. Chapters 5—11 contain an extensive compilation of data conscientiously checked against the original literature, the authors' experience and common sense (sometimes leading to recalculations). Practical side reaction values are tabulated, evaluated from previously given data. Finally, some typical examples are presented, illustrating the approach which should be followed when problems have to be solved in analytical chemistry, electrochemistry, biochemistry and many other fields.

The book is most valuable, well-printed, reasonably priced and obviously meticulously checked on printing errors. The index is adequate and the contents listing good. The text is clear and is not only a well-written, easily readable introduction for newcomers and undergraduate students, but also valuable for more-experienced researchers. The book is recommended to all chemists dealing with "solution chemistry". It should find a place not only in academic and industrial libraries, but also on the bench in the laboratory.

Hans Kragten

Phyllis R. Brown (Ed.), *HPLC in Nucleic Acids Research: Methods and Applications, Chromatographic Science Series, Vol. 28.* Marcel Dekker, Inc., New York and Basel, 1984 (ISBN 0-8247-7236-9). pp. 424. Price $71.50.

With the ever growing interest in genetic engineering, nucleotide and nucleoside synthesis, and effecting metabolic controls there is a definite need for a text, usable as a practical laboratory guide, which also provides an up-to-date, concise and easily digestable review of separative methods in the field of nucleic acid research. In many respects this book fulfils these requirements.

The book's contents are suitably arranged in three parts: overview, methodology and applications. The subsections are logically set out, providing a basis at each stage for progression to the next and allowing information to be readily accessible. As an overview, Part I is somewhat limited since it attempts to cover whole subject areas in just a few sentences. This provides the informed (perhaps?) with merely an elementary reminder and the uninitiated with rather a bare skeletal outline. The methodology of nucleic acid chemistry presented in Part II still tries to cover large topic areas too briefly, with the result that only the basics of each technique are described. However, most subject areas are well supported by a useful list of references. Since the title of the book implies an emphasis on specialism, it would have perhaps been better to assume a basic understanding of the more commonly known methods and give, for example, a more detailed description of the chromatographic methods. The applications outlined in Part III should prove very useful to workers in the areas the book hopes to attract. Many helpful practical tips are given and the range of examples chosen is comprehensive, well documented and related to problems of current interest in the field. A minor criticism is that there is some repetition of the general techniques outlined in Part II. Maybe the book is taking too much on in too short a space to satisfy both the novice and experienced researcher, but despite this it is likely to prove a useful asset to those working in the field of nucleic acids research.

G. Mackenzie
R. W. Humble

E. Stahl and W. Schild, *Isolierung und Characterisierung von Naturstoffen.* G. Fischer, Stuttgart, 1986 (ISBN 3-437-30511-5). pp. x + 180. Price DM 39.80.

This excellent small text book is divided into two sections: (1) Methods and (2) Isolation and Characterisation of Natural Products. The methods section comprises outlines of extraction procedures, chromatography (all main methods but with detailed emphasis on adsorption thin-layer methods), sublimation and spectroscopic methods (u.v.-visible, infrared), including

microtechniques. Detailed procedures are provided for the isolation and characterisation of some 53 natural products, of which the structures are given along with infrared spectra and tabulated information on their main features and origin.

Overall, this is a scholarly, well presented book of major interest to teachers of natural product pharmacy and organic chemistry, but not without considerable value to analytical chemists concerned with characterisation of materials of plant origin. It is in many ways a companion volume to H. Wagner, S. Bladt and E. M. Zgainski's "Plant Drug Analysis. A Thin Layer Chromatography Atlas", reviewed earlier this year.

D. Thorburn Burns

H.-H. Perkampus, *UV-VIS-Spektroskopie und ihre Anwendungen.* Springer-Verlag, Berlin, Heidelberg, New York and Tokyo, 1986 (ISBN 3-540-15467-1 and 0-387-15467-1). pp. viii + 208. Price DM 148.

This volume of the series "Anleitungen für die Chemishe Laboratoriumspraxis" deals with the oldest branch of molecular spectroscopy, u.v.-visible spectroscopy. Despite the title of the series, this volume emphasises theoretical aspects of the subject, providing a sound exposition at the advanced undergraduate level of classical methods and more recent developments such as photo-acoustic, stopped flow and relaxation methods. The general approach is exact and rigorous. Sections of special merit, neglected in many undergraduate instrumental analysis texts, are those on measurement of equilibrium constants, kinetic methods and the discussion of band shapes. Overall, this is a useful piece of scholarship which would repay careful translation and serious reduction in price. It is extremely expensive even for library purchase.

D. Thorburn Burns

Maximum Concentrations at the Workplace and Biological Tolerance Values for Working Materials 1985, Verlag Chemie, Weinheim, 1985 (ISBN 3-527-27340-9). pp. xiv + 80. Price DM 24.

This is the latest annual update of Report No. XIX of the Commission for the Investigation of Health Hazards of Chemical Compounds in the Work Area. Since the 1983 edition (reviewed in this journal in Vol. 181, p. 293) there has been a significant increase in the number of chemicals and materials covered. Discussion of teratogenic effects has been expanded, and a small new section on Carcinogenic Working Material has been included. Of particular interest is the appendix on compounds currently being considered for inclusion in the 1986 edition.

Harald Schutz, *Dünnschichtchromatographische Suchanalyse für 1,4-Benzodiazepine in Harn, Blut und Mageninhalt.* VCH, Weinheim, 1986 (ISBN 3-527-27350-6). pp. x + 130.

This is the sixth monograph in the series published by the Senatskommission für Klinisch-Toxikologische Analytic. It does, however, contain much more information than the title suggests. As well as giving full details of the t.l.c. separation of 62 1,4-benzodiazepines and their metabolites, including drawings of the chromatograms obtained with various solvents, there are structural and elemental formulae of the drugs, CAS registry numbers, metabolic pathways and proprietary names. Pharmacokinetic and dynamic aspects are summarized, clinical and toxicological information is provided and other analytical procedures are referred to. The monograph concludes with 146 references and a subject index.

W. Fresenius, H. Günzler, W. Huber, I. Lüderwald, G. Tölg and H. Wisser (Eds.), *Analytiker-Taschenbuch, Band 6.* Springer, Berlin, 1986 (ISBN 3-540-15037-4). pp. xi + 351. Price DM 118.00.

This sixth volume of what are genuine "pocket-books" is another mixed bag. It begins with articles on reference materials, computerized systems and correlation functions. There follow sections on IR spectra of polymers and on-line HPLC/MS, and on trace analysis (absorptive preconcentration, gas analysis and biological samples), skin pigmentation and HPLC of amino acids and proteins. The final section consists mainly of SI units. There is a subject index, and an index of authors for Vols. 1—6. Each article contains a fund of information, and is extensively referenced.

Peter Hallpap and Dietmar Stadermann, *Stereochemie Organisch-Chemischer Reaktionen.* Fischer Verlag, Stuttgart, 1985 (ISBN 3-437-20315-0). pp. 167. Price DM 18.80.

This small (18½ × 11 cm) book classifies and describes the essence of stereochemical effects in organic reactions. It discusses steric effects on various types of reactions, the different types of effects that can occur and the means of controlling them, thus leading to stereoselectivity and stereospecificity in reactions. The book concludes with a brief discussion of the quantitative treatment of steric effects. There are 63 references, mostly reasonably recent, and a subject index.

Verein Deutscher Ingenieure, Kommission Reinhaltung der Luft, *VDI-Handbuch Reinhaltung der Luft, Band 5.*

The Commission has recently issued the following further Guidelines: They are all bilingual (German/English).

— VDI 2462 Part 7: Measurement of Gaseous Emissions. Measurement of the Sulfur Trioxide Concentration. 2-Propanol Method.

— VDI 2462 Part 8: Measurement of Gaseous Emissions. Measurement of the Sulfur Dioxide Concentration. H_2O_2-Thorin Method.

— VDI 2468 Part 7: Gaseous Air Pollution Measurement. Measurement of Peroxyacetyl Nitrate (PAN).

— VDI 2468 Part 8: Gaseous Air Pollution Measurement. Preparation of PAN Calibration Gas. Calibration of a PAN Analyzer.

— VDI 3494 Part 3: Gaseous Air Pollution Measurement. Determination of Vinyl Chloride. Automated Gas Chromatographic Method (A.I.R. Instruments Model 755 GC).

— VDI 2267 Part 11: Determination of Suspended Particulates in Ambient Air. Measurement of the Mass Concentration of Lead by Energy Dispersive X-Ray Fluorescence Analysis.

— VDI 2456 Part 8: Gaseous Emission Measurement. Determination of the Total of Nitrogen Monoxide and Nitrogen Dioxide. Sodium Salicylate Method.

— VDI 3482 Part 1: Gaseous Air Pollution Measurement. Gas Chromatographic Determination of Organic Compounds. Fundamentals.

— VDI 3494 Part 2: Gaseous Air Pollution Measurement: Determination of Vinyl Chloride Concentrations. Gas Chromatographic Determination by Separation Column Switch-Over for Live Chromatography.

Further information can be obtained from the VDI-Commission on Air Pollution Prevention, PO Box 1139, D-4000 Düsseldorf-1, Federal Republic of Germany.

ANALYTICA CHIMICA ACTA, VOL. 186 (1986)

AUTHOR INDEX

(Continued from inside back cover)

 0003-2670/86/$03.50

Printed in The Netherlands

Completely Revised

nstrumental Liquid Chromatography

**Practical Manual on High-Performance
quid Chromatography Methods**

cond, completely revised edition

N.A. PARRIS, E.I. du Pont de Nemours Company, Biomedical Products Depart-nt, Research and Development Division, perimental Station Laboratory lmington, DE, USA

urnal of Chromatography Library 27

is extensively revised and up-to-date ok is an essential tool for the HPLC user the laboratory. It first appeared in 1976, is twice reprinted and was described in boratory Practice as "one of the more eful and successful texts on HPLC . . . a st readable book packed with valuable ormation and advice . . . strongly re-mmended."

actically orientated, it is an easy-to-low guide containing the minimum sential theoretical background. The jority of the material is based on actical experience and highlights details ich may have important operational lue for laboratory workers. It helps the LC user to select the most appropriate trumentation, injectors, columns etc.

plications of liquid chromatography are scribed with reference to the potential of technique for qualitative, quantitative d trace analysis as well as for the pre-rative application. Numerous applica-ns from the literature are tabulated and oss-referenced to sections concerned th the optimization procedures of the rticular methods. The format of the ori-al edition proved so successful that it s remained unchanged, but some 45% of material is either new or completely vised in order to bring the column hnology and applications data up-to-te.

"The style . . . is clear. The subject is placed in perspective by comparisons with other separation techniques and should provide a good reference book for all involved in practical LC," (Laboratory Practice).

"Overall the book is well written, and, because of its practical emphasis, it is highly recommended for both the aspiring and experienced chromatographer," (J. Am. Chem. Soc.).

1984 xiv + 432 pages. Price: US $ 83.25 / Dfl. 225.00 (including postage).
ISBN 0-444-42061-4

ELSEVIER SCIENCE PUBLISHERS

P.O. Box 211, 1000 AE Amsterdam,
The Netherlands
P.O. Box 1663, Grand Central Station,
New York, NY 10163, USA

ATOMIC ABSORPTION SPECTROMETRY

edited by
J. E. CANTLE
VG Isotopes Ltd., Winsford, Great Britain

Techniques and Instrumentation in Analytical Chemistry Vol. 5

Atomic absorption spectroscopy is now established as one of the most useful tools for analysing trace metals in samples which may be taken into solution. It has wide applicability, is inexpensive and can be used with confidence by a wide range of analysts. The rapid growth and advancement of electrothermal atomisation methods and their subsequent automation has consolidated the technique's position by extending the dynamic analytical range down to concentration levels that other techniques cannot reach.

The topic is treated here in a very practical manner and the book is mainly concerned with real-life analyses for practising instrument users. The book is invaluable to those working in all laboratories where the technique is used as the methods described can be interpreted to fit all suppliers' hardware.

Of interest to those working in: Analytical Chemistry, Spectroscopy, Geochemistry, Agricultural and Environmental Chemistry

1982 xvi + 448 pages
US $ 83.25 / Dfl. 225.00
ISBN 0-444-42015-0

ELSEVIER

P.O. Box 330,
1000 AH Amsterdam,
The Netherlands.

P.O. Box 1663,
Grand Central Stat
New York, NY 1016

The Dutch guilder price is definitive. US $ prices are subject to exchange rate fluctuations

ontinued from outside back cover)

(Continued on p. 358)

CONTENTS

(Abstracted, Indexed in: Anal. Abstr.; Biol. Abstr.; Chem. Abstr.; Curr. Contents Phys. Chem. Earth Sci.; Life Sci.; Index Med.; Mass Spectrom. Bull.; Sci. Citation Index; Excerpta Med.)

(Continued on inside back